BEHAVIOUR CHARACTERISTICS

OF

CONCRETE MASONRY

By

AHMAD A.A. HAMID, B.Sc., M.Sc.

A Thesis

Submitted to the School of Graduate Studies

in Partial Fulfilment of the Requirements

for the Degree

Doctor of Philosophy

McMaster University

September, 1978

To my Grandfathers

"The Ancient Egyptians"

who

built the most outstanding masonry

structure in the history of Man.

BEHAVIOUR CHARACTERISTICS

OF

CONCRETE MASONRY

DOCTOR OF PHILOSOPHY (1978)
(Civil Engineering)

MCMASTER UNIVERSITY
Hamilton, Ontario

TITLE: Behaviour Characteristics of Concrete Masonry

AUTHOR: Ahmad Ahmad Abdel Hamid, B.Sc. (Ain Shams University)

M.Sc. (Ain Shams University)

SUPERVISORS: Dr. R.G. Drysdale
Dr. A.C. Heidebrecht

NUMBER OF PAGES: xxiii, 445

ACKNOWLEDGEMENTS

The author wishes to express his sincere gratitude to Dr. R.G. Drysdale and Dr. A.C. Heidebrecht for their guidance, encouragement, and supervision during the course of this study. The valuable comments offered by Dr. Drysdale during the experimental program and the effort he expended in reviewing the manuscript are greatly appreciated.

Appreciation is extended to the other committee members, Dr. W.K. Tso and Dr. P.S. Nicholson for their valuable suggestions.

The author wishes to thank his friends, Rennier Vanderkeyl for his help during the testing program and Essam Allam for his help in drafting the figures. Thanks are due to Mrs. Betty Petro and Miss Marlene Fletcher for their concerned work in typing the manuscript.

Acknowledgement is due to McMaster University and the National Research Council of Canada for financial support. The author appreciates the contribution of masons's time and equipment made available through the Ontario Masonry Industry Promotion fund and also thanks to General Concrete Ltd. for providing the concrete blocks.

Finally, a special note of deep appreciation is due to my parents for their help and encouragement without which this thesis would have been difficult to complete.

ABSTRACT

The lack of understanding the behaviour of concrete masonry and the complex interaction existing between its components (block, mortar, and grout) at failure may be the cause of the continued use of the code's working stress method. This approach could underestimate the potentials of masonry as a construction material. It is the main objective of this investigation to provide a better understanding of concrete masonry behaviour under different in-plane load conditions (compression, tension, shear and biaxial stresses) considering the anisotropic nature of masonry as a composite material. This understanding was gained through a combined experimental and analytical investigation.

In the experimental study, 323 masonry assemblages were tested under compression normal and parallel to the bed joints, splitting tension at different orientations from the bed joints, shear along the bed joint with different levels of precompression, and off-axis compression and tension to produce biaxial states of stresses along the bed and head joints. The test material variables were mortar type, grout strength, and bed joint reinforcement.

Analytical strength formulas, based on a "strength" approach, are proposed to express, in quantitative terms, the assemblage compressive strength normal to the bed joints, tensile

strength normal, diagonal, and parallel to the bed joints, and shear strength along the bed joint with and without precompression. The applicability of the failure theories for both isotropic and composite materials to masonry were examined. Failure criteria are proposed to predict the strength and the failure mode of concrete masonry under biaxial stresses taking into account the anisotropic nature of masonry as a brittle composite material. Design code provisions (CSA S 304) for plain masonry are reviewed.

TABLE OF CONTENTS

LIST OF TABLES

LIST OF FIGURES

CHAPTER 1

INTRODUCTION

1.1 General

Although masonry structures have been built since the earliest days of man, it has only been in relatively recent times that masonry structures have been designed based upon engineering principles. Stone and brick masonry structures were designed and built without steel reinforcing to support gravity loads. These gravity loads stabilized the structure against any lateral forces due to wind or seismic action. Recently, reinforced concrete masonry has been introduced to provide structures with sufficient deformation capabilities necessary to resist the lateral dynamic forces of wind and earthquakes. Hence, design practice has incorporated more and more the feature of filling the cores in hollow masonry walls with grout to simply be able to anchor the reinforcing vertical steel and/or to share the compression, tension or shear stresses.

While there is considerable information describing the behaviour of brickwork under different load conditions, relatively little is known about blockwork structures[21,33,45]. In fact, there is very little information concerning the basic behaviour chharacteristics and the failure mechanism for ungrouted and

grouted concrete masonry even under simple compression, tension or shear stresses.

Because of the lack of information concerning the effect of grouting on the strength characteristics of concrete masonry, typical masonry codes[12,27] assign design values for grouted masonry similar to solid masonry provided that the grout strength is at least equal to that of the units. Introducing grout as a third component with a specified strength and deformation characteristics could affect the assemblage behaviour, as the grouted cores provide continuity in a direction normal to the bed joints. It seems logical that the contribution of the grouted cores towards increasing masonry strength would vary in accordance with the different modes of failure associated with different combinations of normal and shear stresses acting along the critical bed and head joint directions. It seems likely that the code[12] approach needs to be reviewed.

Most experimental determinations of the strengths of materials are based on uniaxial stress states. However, the practical application of masonry involves at least a biaxial if not a triaxial state of stress. Thus, a logical method of using uniaxial strength information in the analysis of multiaxial loading is required. Failure theories for isotropic materials have been used[8,49,58] to express the failure criteria of masonry which is characterized by its anisotropic nature of behaviour. No failure criterion is available for masonry which accounts for the

directional variation of its strength characteristics as a composite material.

1.2 Objectives and Scope

A survey of the available literature revealed a need for research on the strength and deformational characteristics of ungrouted and grouted concrete masonry under different load conditions (compression, tension, shear, and biaxial stresses). To meet this objective, the experimental and analytical investigations reported in this dissertation were initiated.

Because there has not been much research done on this subject, it was decided that the most effective way to approach the problem and to present the information was to fully investigate each strength characteristic separately. Therefore, the specific strength characteristics presented in this dissertation, will in general have their individual introductions with reviews of relevent literature, details of experimental study, analytical interpretations, reviews of the code[12] provisions, and related conclusions.

In the experimental study, a total of 323 masonry assemblages (both grouted and ungrouted) were built using standard 6 inch concrete blocks and tested under axial compression normal and parallel to the bed joints, splitting tension at different orientations from the bed joints, shear along with different levels of precompression, and off-axis compression and tension to

produce biaxial states of stresses along the bed and head joints.

Analytical simplified formulas, based on a "strength" approach, have been proposed to express in quantitative terms, the assemblage strength characteristics in the principal material directions (normal and parallel to the bed joints) in terms of the strength and geometric characteristics of its components (block, mortar, and grout). Formulas to predict the compressive strength normal to the bed joint, tensile strength normal diagonal and parallel to the bed joint, and shear strength along the bed joint with or without precompression are proposed. The applicability of the failure theories for both isotropic and composite materials to masonry were examined. Proposed failure criteria for concrete masonry (either grouted or ungrouted) under biaxial stresses are suggested.

To help the reader follow the organization of the material in this dissertation, the following outline is presented: Chapter 2 contains the common information on the properties of the component materials (block, mortar, grout, and joint reinforcement) which will be referred in Chapters 3 to 6. Chapters 3, 4 and 5 contain information on the behaviour characteristics of masonry under compression, tension, and shear, respectively. In Chapter 6, the behaviour of concrete masonry under biaxial stresses is studied. Chapter 7 provides a summary of the investigation and presents the overall conclusions.

1.3 Nomenclature

Each symbol used in the text is explained where it first appears. However, a summary of frequently used symbols is also presented below for convenience. In some cases, more than one symbol have been used to describe a parameter. This was done in order to retain the previous authors' notations for those items which are taken from other references.

A_g	gross cross-section area
A_{gr}	cross-section area of the grout
A_n	net cross-section area of the block
A_{nm}	maximum net area of the block in the bed direction
a	nominal length of half block
b	nominal height of the block
d	height or diameter of the specimen
E_a	assemblage's modulus of elasticity
E_b	secant modulus of elasticity of the block in compression at 50% the ultimate stress
E_{bs}	secant modulus of elasticity of the shell (block and mortar) in compression at 50% the ultimate stress
E_g	secant modulus of elasticity of grout in compression at 50% the ultimate stress
F_{xc}, F_{yc}, F_{zc}	compressive strength characteristics of masonry in the principal material directions x, y, and z, respectively

F_{xt}, F_{yt}, F_{zt} tensile strength characteristics of masonry in the principal material directions x, y, and z, respectively.

F_{sxy} shear strength characteristic of masonry in the principal material plane xy

f'_{mn} compressive strength of masonry (hollow, grouted, or solid) normal to the bed joint

$f'_{m\theta}$ compressive strength of masonry (either grouted or ungrouted) under load having an orientation, θ, from the bed joint

f'_{mg} compressive strength of grouted masonry under load oriented at any direction from the bed joint

f'_{mgn} compressive strength of grouted masonry normal to the bed joint

f'_{mgp} compressive strength of grouted masonry parallel to the bed joint.

f'_{mu} compressive strength of ungrouted masonry under load oriented at any direction from bed joint

f'_{mun} compressive strength of ungrouted masonry normal to the bed joint

f'_{mup} compressive strength of ungrouted masonry parallel to the bed joint

$f_{t\theta}$ tensile strength of masonry under load having an orientation, θ, from the bed joint

f_{td} diagonal tensile strength of masonry (under

	tensile load oriented at 45° from the bed joint)
f_{tn}	tensile strength of masonry normal to the bed joint
f_{tp}	tensile strength of masonry parallel to the bed joint
GM	medium strength grout
GS	strong strength grout
GW	weak strength grout
h	height of masonry prism
N, S	types of mortars as specified in ASTM standard C-270[1].
n	modular ratio, E_{bs}/E_g
t	thickness of masonry wall or prism
t_b	height of masonry unit
t_m	thickness of mortar joint
t_s	thickness of masonry unit's shell in a horizontal cross-section (parallel to the bed joint)
α	joint thickness to block height ratio, t_m/t_b
η_h	minimum net to gross area ratio of the block in a horizontal cross-section (parallel to the bed direction), A_n/A_g
η_{hm}	maximum net to gross area ratio of the block in the top horizontal section (parallel to the bed direction)
η_v	net to gross area ratio of the block in a vertical

	cross-section crossing the face shells just beside the intermediate web
	angle of the applied load (tension or compression) with respect to the bed joint direction
μ	coefficient of friction
ν_b, ν_m, ν_g	Poisson's ratios for block, mortar, and grout, respectively
σ_{cb}	compressive strength of block as calculated from half blocks, hard capped, and tested flatwise under axial compression
σ_{cg}	unconfined compressive strength of grout as calculated from block moulded prisms
σ_{cm}	unconfined compressive strength of mortar as calculated from air cured mortar cubes
σ_n	compressive stress normal to the bed joint
σ_{tbl}	tensile strength of the block as calculated from the splitting tension test
σ_{tbm}	tensile bond strength of the mortar
σ_{sbm}	shear bond strength of the mortar
σ_x	stress parallel to the bed joint
σ_{xb}	lateral tensile stress acting on the block in a direction parallel to the bed joint
σ_{xm}	lateral compressive stresses acting on the mortar joints of axially loaded masonry assemblages (confining lateral stresses)

σ_y	stress normal to the bed joint
σ_{yb}, σ_{ym}	compressive stress acting on the shell (block and mortar) of axially loaded grouted masonry assemblages in a direction normal to the bed joint
σ_{yg}	compressive stress acting on the grouted cores of axially loaded grouted masonry assemblages in a direction normal to the bed joint
τ_a	shear strength of masonry along the bed joint under shear along with normal compressive stress normal to the bed joint
τ_g	shear strength of the grouted cores under shear and normal compressive stress acting along the bed joint
τ_{mb}	shear strength of a mortar bed joint under zero normal compressive stress (precompression)
τ_{mh}	shear strength of mortar head joint
τ_{xyb}	shear strength of masonry along the bed joint under shear and normal compressive stresses
τ_{xyh}	shear strength of masonry along the head joint under shear and normal compressive stress.

CHAPTER 2

MATERIALS

2.1 General

Grouted or ungrouted concrete masonry is a multiphase material which cannot be adequately understood on a fundamental level unless the structural properties of the individual component materials are fully defined and understood. It is the objective of this chapter to investigate and document the physical and mechanical properties of the component masonry materials: block, mortar, and grout.

2.2 Masonry Materials

All of the masonry materials used in the construction of the assemblages of this experimental program were commercially available and were similar to those commonly used in building construction.

2.2.1 Concrete Blocks

2.2.1.1 Physical Properties: Autoclaved concrete masonry units were used throughout the test program and most were the standard 6 inch block having 2 cores as shown in Fig. 2.1(a). This type of block had nominal dimensions of 8x6x16-inch. The average net cross-sectional area of this type of block, based on measurements

(a) Standard 2 Core Block

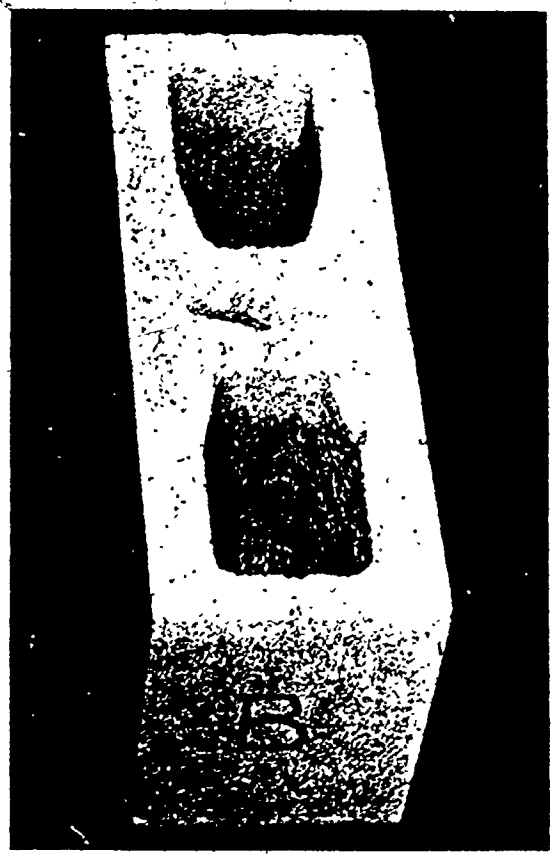

(b) Kerfed 2 Core Block

Fig. 2.1 MASONRY BLOCKS USED IN ASSEMBLAGES CONSTRUCTION

of five specimens, was 52.1 in^2. This resulted in a net to gross area ratio of 0.59.

The initial rate of absorption (IRA) of a block is defined according to ASTM Standard C-67[1] as the amount of water initially absorbed by a dry unit when it is partially immersed in water to a depth of 1/8 inch for a period of one minute. The average IRA based on tests of five specimens was 36.3 gm/min./30 in^2 with a coefficient of variation of 8.4%. The average density of the unit based on weighing five dry specimens was 125 lb/ft^3 with a coefficient of variation of 1.5%.

Another type of block, shown in Fig. 1(b), was also used in this program to provide half blocks. This kerfed block has the same outside dimensions and similar physical properties as the standard block. The cross-sectional dimensions of the two block types are shown in Fig. 2.2.

2.2.1.2 Compressive Characteristics of Blocks: The compressive strength of a masonry block is appreciably affected by its shape or geometry and type of capping material. These two factors interact to modify the stress pattern in the block under test and may lead to different unit compressive strengths. If a homogeneous isotropic material is tested in compression between platens or capping material, the effect of end conditions must be considered. If the platen or capping material has a higher elastic modulus than the test specimen, some confining or compresssive stresses are induced in the end regions of the test specimen. For a higher

(a) Horizontal Cross-Section of a Standard Block

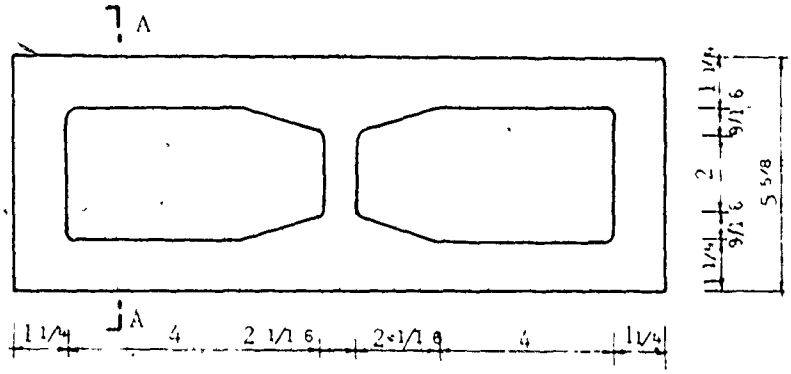

(b) Horizontal Cross-Section of a Kerfed Block

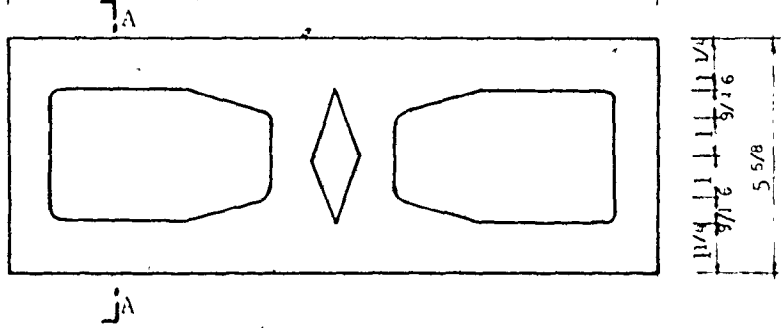

(c) Vertical Cross-Section (A-A) of a Block

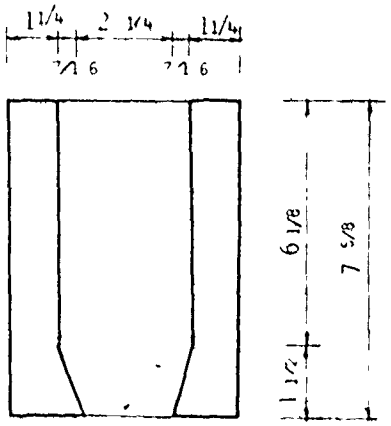

Note: All dimensions in inches (1 in = 25.4mm)

Fig. 2.2 DIMENSIONS OF BLOCKS

modulus of elasticity of the capping and for higher friction between the test specimen and the platens, the greater will be the modification of the stress system by introducing lateral confinement which increases the load required for failure. This is the effect of "platen restraint". When platens or capping of lower elastic modulus are used, the test specimen is subjected to tensile stresses arising from the greater lateral strains of the platens or capping. For concrete block masonry, which is substantially weaker in tension than in compression, these tensile strains can lead to a considerable reduction in the load necessary for failure. In the presence of platen restraint, the smaller aspect ratio of a block results in a greater influence of the platen restraint and consequently higher load for failure.

There is no universally accepted method of testing the block units to determine the compressive strength of the material as an absolute value. The recommended methods available provide only a measure or a "standard" indicator for the compressive strength. However, they can be used as quality control tests. The ASTM Standard C-140[1] recommends that a full size unit be tested flatwise to obtain a measure of the block compessive strnegth. However, it is reported[33] that the National Bureau of Standards has recommended that the compressive strength of a half block tested flatwise provides a good basis for judging the behaviour of masonry wall under axial compression.

In this investigation, half blocks cut from kerfed blocks

were selected as the type of test specimen (having higher aspect ratio than a full block) in order to reduce the effect of the platen restraint, which can cause an erroneously high measure of the material compressive strength. The half blocks were tested under axial compression as shown in Fig. 2.3. The following capping materials were used:

1. Hard capping: A gypsum-cement compound as specified in ASTM Standard C-140[1] was adopted here and was also used later for compression tests of masonry assemblages.

2. Soft capping: A mortar mix consisting of 1 part cement, 0.5 parts lime, and 3.75 parts sand was used. It has a cylinder (3-inch diameter by 6-inch high) compressive strength of 1650 psi after 3 days of air curing.

The effect of capping material on the strength and deformational characteristics (stress-strain relationships) of half block units was investigated. Two inch long electrical resistance strain gauges and mechanical gauge points (using a 4 inch gauge length) were mounted on both faces of the half block as shown in Fig. 2.3, so that the deformations in the vertical and horizontal directions could be measured. A Huggenourger strain indicator having a precision of 1×10^{-5} in/in was used to mechanically measure the deformations between the gauge points. To improve the accuracy of the measurements, they were repeated until two successive readings were the same. The stress-strain curve for the specimens capped with the gypsum-cement compound is

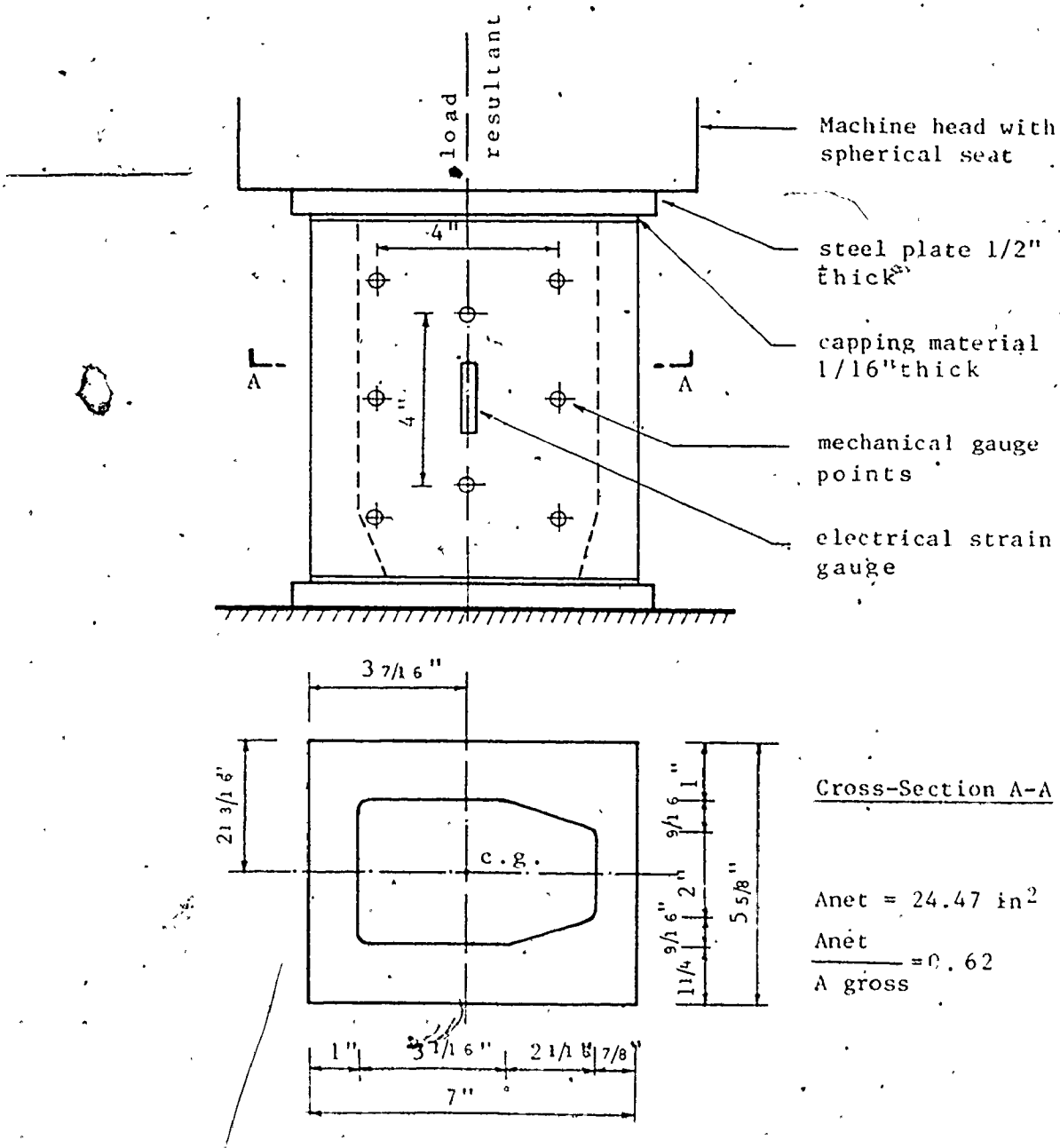

Note: 1 inch = 25.4 mm

Fig. 2.3 HALF BLOCK UNDER AXIAL COMPRESSION

shown in Fig. 2.4. The plotted strain values were the average of eight readings (two for each of four specimens) using the mechanical gauges, whereas they were the average of two readings (both faces of one specimen) using the electrical strain gauges. As can be seen, very good agreement between the mechanical and electrical measurements was achieved. The inelastic behaviour of the concrete block under axial compression is illustrated in Fig. 2.4. Using the method of least squares, a best-fit curve of the data yields the following relationship between the stress, σ (psi), and the corresponding strain, ε:

$$\sigma = (3.029\ \varepsilon - 1550\ \varepsilon^2 + 39400\ \varepsilon^3 - 38500000\ \varepsilon^4) \times 10^6 \quad (2.1)$$

For comparison, the deformations of the half blocks under axial compression, for both hard and soft capping, are presented in Fig. 2.5. For vertical strains, no significant difference existed between hard and soft capped specimens in the early stages of loading. However, at higher stress levels, the soft capped specimens showed higher deformations. Comparison of the lateral strains shows that the soft capped specimens exhibited much higher lateral tension strains compared with the hard capped specimens. It is apparent that the soft capped specimens were subjected to lateral tensile stresses arising from the greater lateral strains of the weaker and more flexible capping. These tensile stresses caused a premature splitting failure of the specimen as can be seen from comparison of the cracking patterns at failure shown in

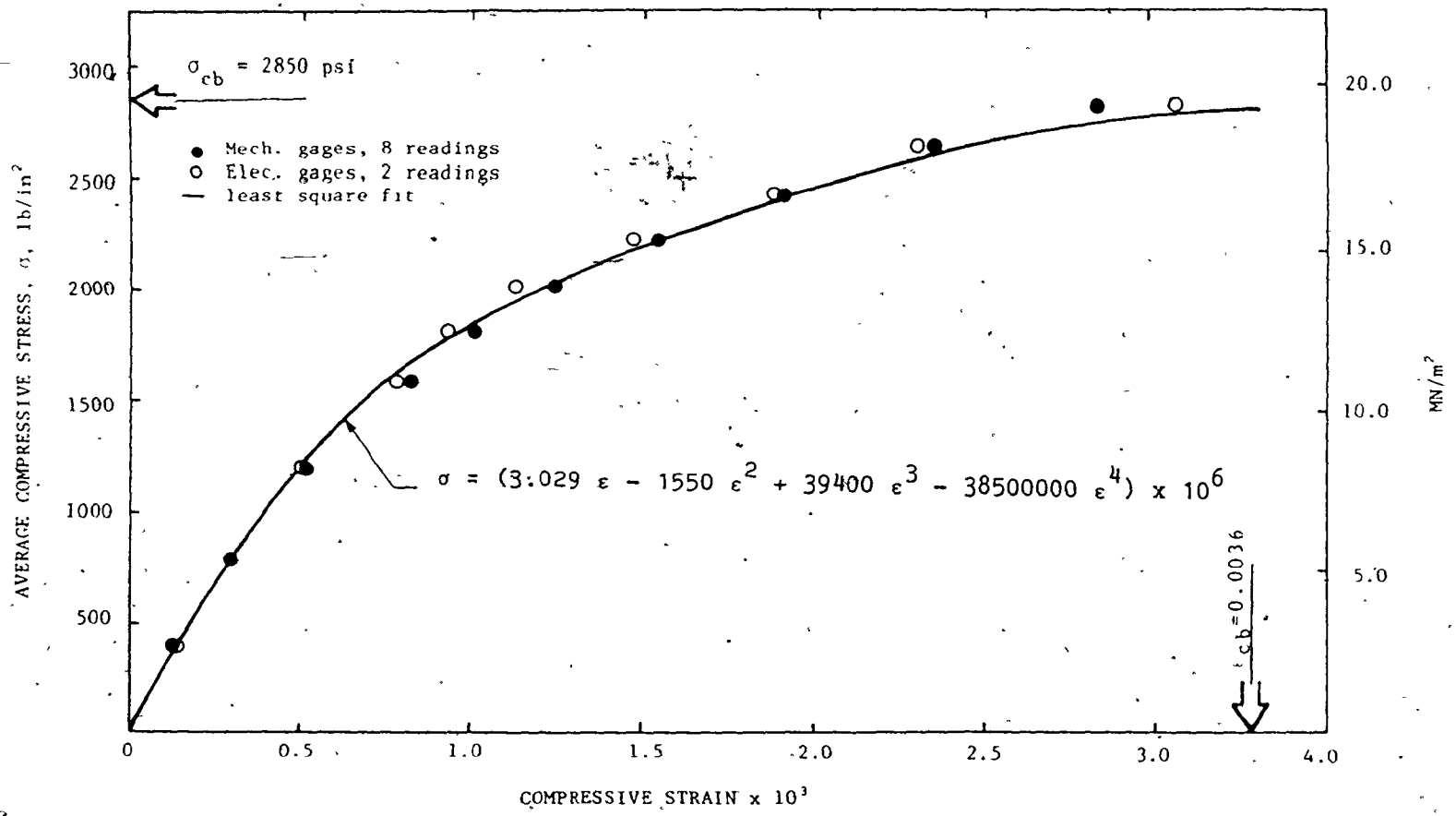

Fig. 2.4 STRESS-STRAIN CURVE OF HALF BLOCKS UNDER AXIAL COMPRESSION

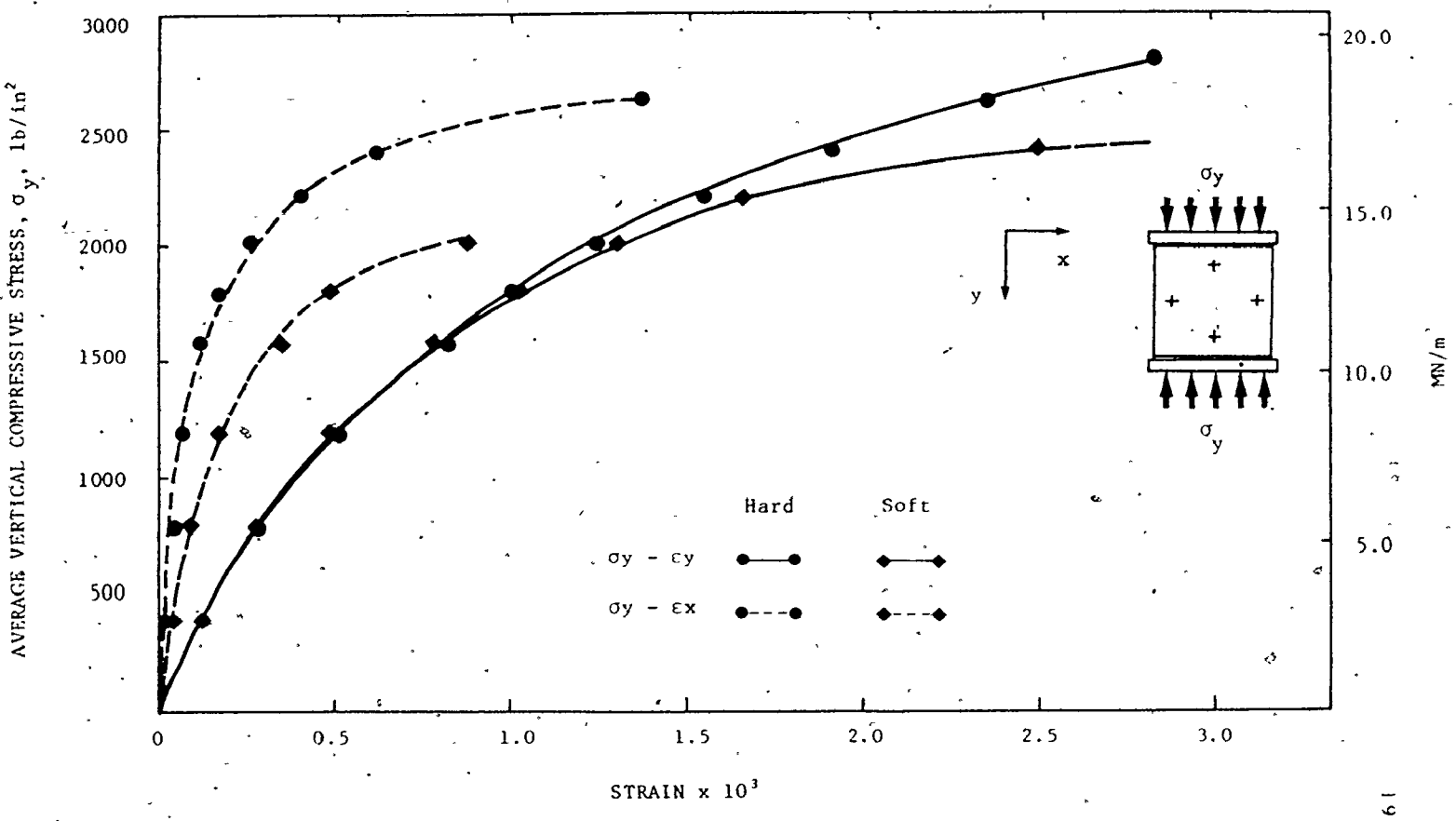

Fig. 2.5 EFFECT OF CAPPING MATERIAL ON THE BEHAVIOUR OF HALF UNIT BLOCKS UNDER AXIAL COMPRESSION

Figs. 2.6 and 2.7. The compressive strength results for the half blocks tested using both hard and soft capping are presented in Table 2.1. An average capacity reduction of 16% resulted from using soft capping rather than hard capping. The results also indicate that the harder the capping material, the less the variability of the test results.

Full blocks were tested endwise under axial compression using another hard capping material, sulphur. The compressive strengths of the specimens are listed in Table 2.1. The strengths of blocks tested endwise (having a higher aspect ratio) were nearly the same as those obtained from half blocks tested flatwise which may indicate that the end restraint effect on the half blocks tested flatwise and using hard capping did not have a significant influence on the block strength. It seems that the half blocks, hard capped, and tested under axial compression can provide a good measure of the block material characteristics under axial compression. Therefore, the results of the hard capped half blocks are adopted to represent the strength and deformation characteristics (stress-strain relationships) of the concrete blocks under axial compression and will be used throughout this investigation.

2.2.1.3 Tensile Characteristics of Blocks: The evaluation of the block tensile strength is of prime importance since it is usually the governing parameter influencing the assemblage strength under axial compression and diagonal tension. The tensile strength of

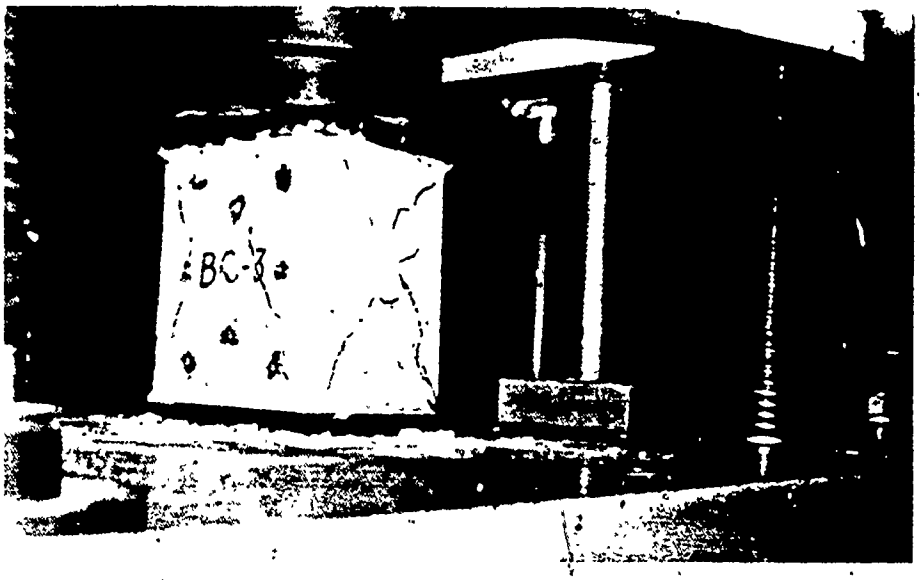

Fig. 2.6 FAILURE OF HARD CAPPED HALF BLOCK UNDER AXIAL COMPRESSION

Fig. 2.7 FAILURE OF SOFT CAPPED HALF BLOCK UNDER AXIAL COMPRESSION

TABLE 2.1

COMPRESSIVE STRENGTH OF CONCRETE BLOCKS

Test Type	Capping Material	Individual Strength[a] (psi)	Mean (psi)	C.O.V.[b] (%)
half blocks, flatwise	Hard Capping, (gypsum-cement)	2820 2960 3000 2660 2830 2840	2850	4.2
	Soft Capping, (mortar)	2820 2250 2130 2430 2400	2410	10.8
full block, endwise	Hard Capping, (sulphur)	2950 2930 3440 2800 2920	3010	8.2

NOTE: 1 psi = 6.9×10^{-3} MN/m^2

a - based on net area
b - coefficient of variation

concrete blocks, as a result of being a brittle material, is very sensitive to the stress fields developed by different test techniques. Apparently, there is no universal method or standard test to determine the block tensile strength[33]. The ASTM standard C-67[1] modulus of rupture test is recommended for the determination of the tensile strength of brick units. In this investigation, four different methods were used to evaluate and compare the tensile strength of concrete blocks under different load conditions:

1 - Axial Tension: For this test a full block was tested in axial tension by attaching loading mechanism to both ends. Each steel loading mechanism consisted of a threaded bar which was attached to a reinforced channel which rested on the end and which in turn had angles bolted to it, extending along the faces of the block as shown in Figs. 2.8 and 2.9. An epoxy cement (Coma Dur-Gel, a compound of two components added together using 1:1 volume ratio) was used to bond the angles and the plate reinforcing the channel to the faces and end of the block, respectively. The mechanical connection could be adjusted to assure proper alignment of the specimen in order to minimize the eccentricity of the applied load. This experimental technique is similar to that adopted by the California Masonry Technical Committee as part of their standards for the California Quality Control Specifications[33]. Electrical resistance strain gauges having 2 inch gauge lengths were mounted on both faces of the

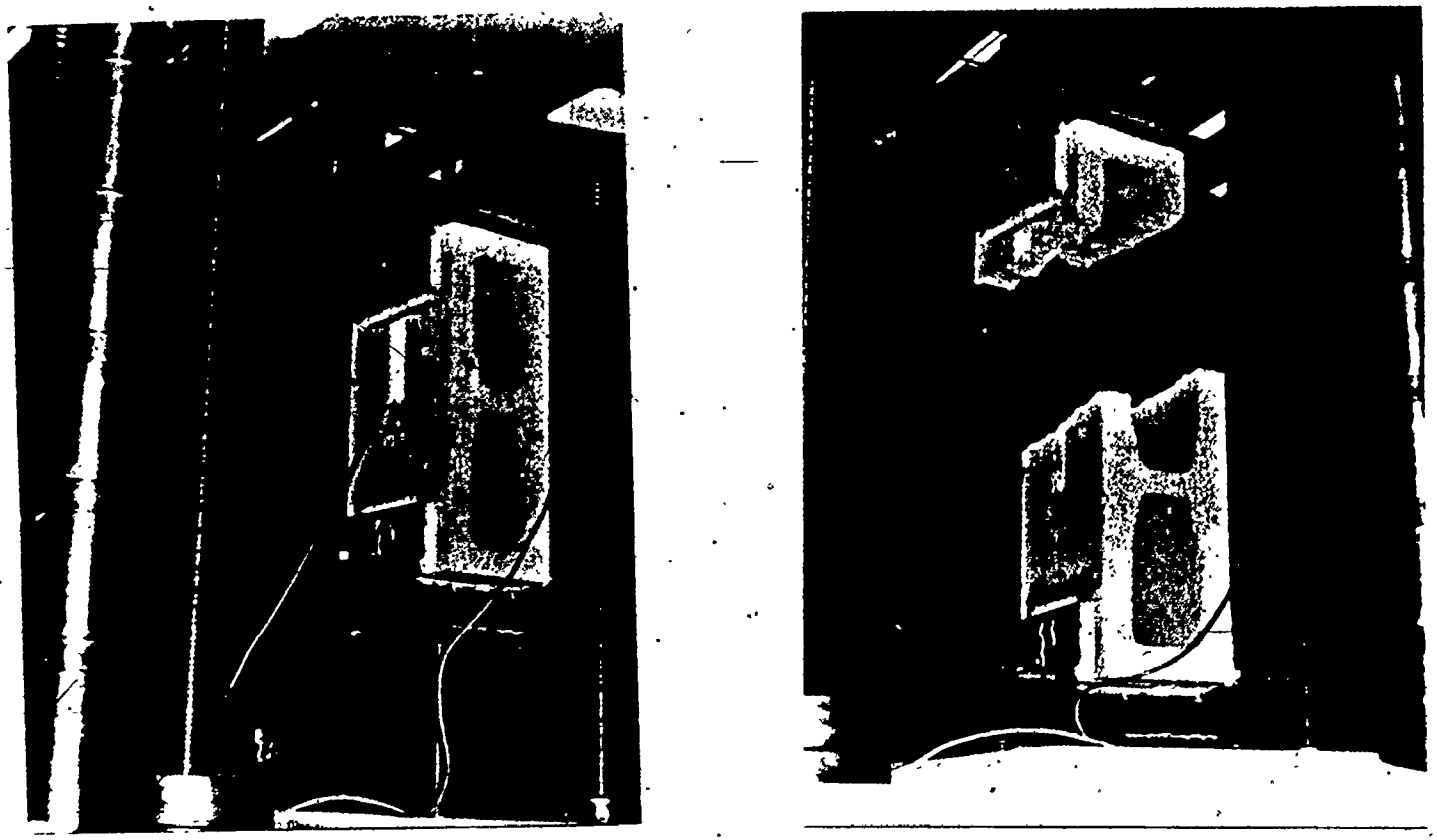

(a) Prior to Loading

(b) After Failure

Fig. 2.8 AXIAL TENSION TEST OF FULL CONCRETE BLOCK

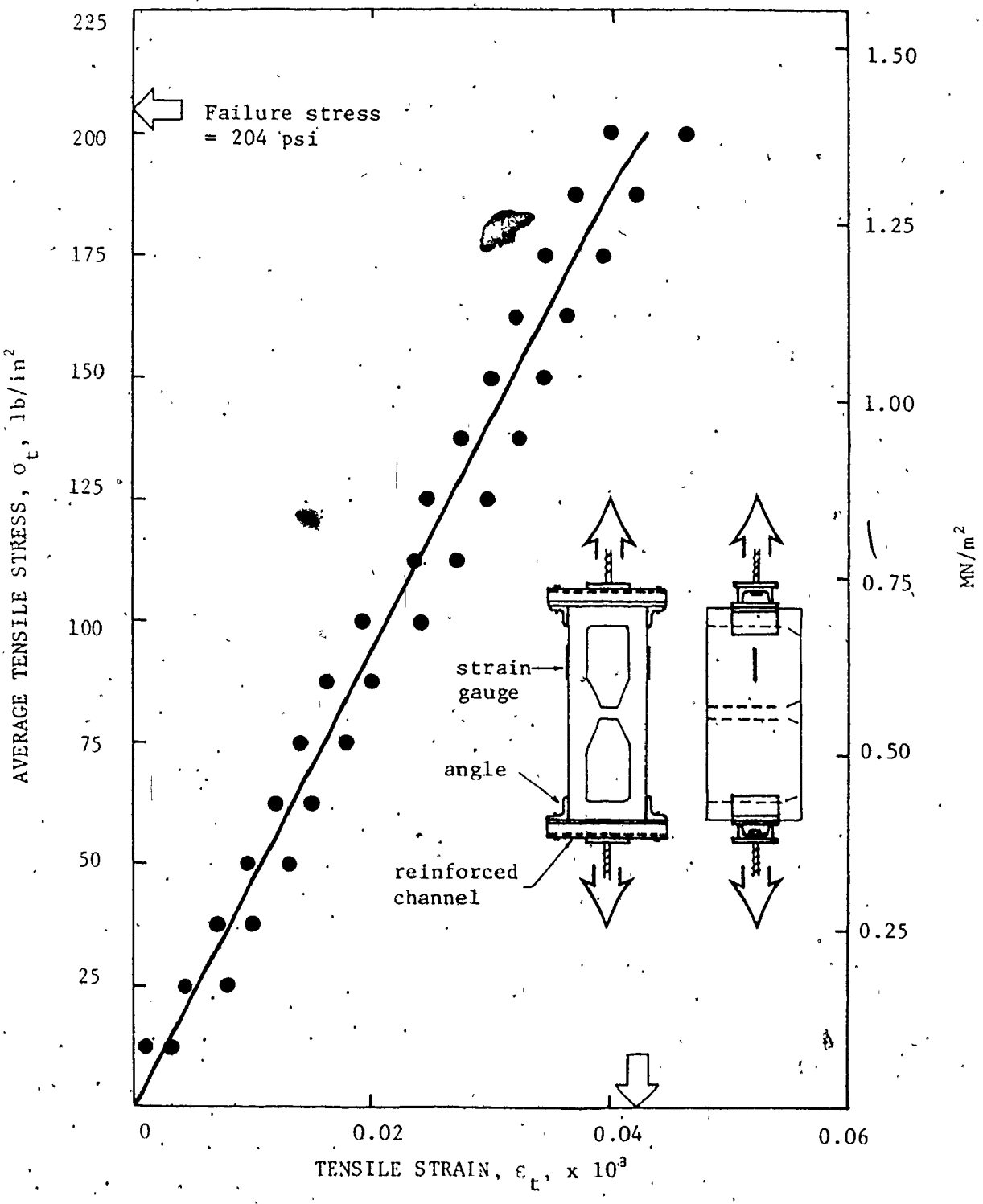

Fig. 2.9 STRESS-STRAIN RELATIONSHIP OF CONCRETE BLOCK UNDER AXIAL TENSION

specimen to measure the elongation during loading. The stress-strain curve which was obtained from one test specimen is plotted in Fig. 2.9.

2 - Eccentric Tension: Using the technique described above, the tensile load was applied at the kern point of the minimum section to produce a triangular strain distribution over the block cross-section. Electrical resistance strain gauges with 2 inch gauge lengths were mounted on the sides of the block to measure the extreme fibre strains. Fig. 2.10 shows the test set-up and the failure condition under eccentric loading. The stress-strain curves obtained for the maximum and minimum tension fibres are shown in Fig. 2.11.

3 - Flexural Tension: A beam was formed by gluing two blocks end-to-end using an epoxy cement (Colma-Dur-Gel). The beam was simply supported with a span to depth ratio of 3.8 and was tested with two point loads applied at the central webs of each block as shown in Fig. 2.12(a). The dimensions are shown in the sketch in Fig. 2.13. As shown in Fig. 2.12(b) the beam failed by flexure in the minimum face shell region in the pure bending zone of the one of the blocks. Failure had never occurred in the joint connecting the two blocks for any of these tests. This experimental technique has the advantage over the modulus of rupture test, using a single unit, in that it provides a flexural member of longer span to depth ratio which minimizes the influence of shear and therefore gives a better measure of the flexural

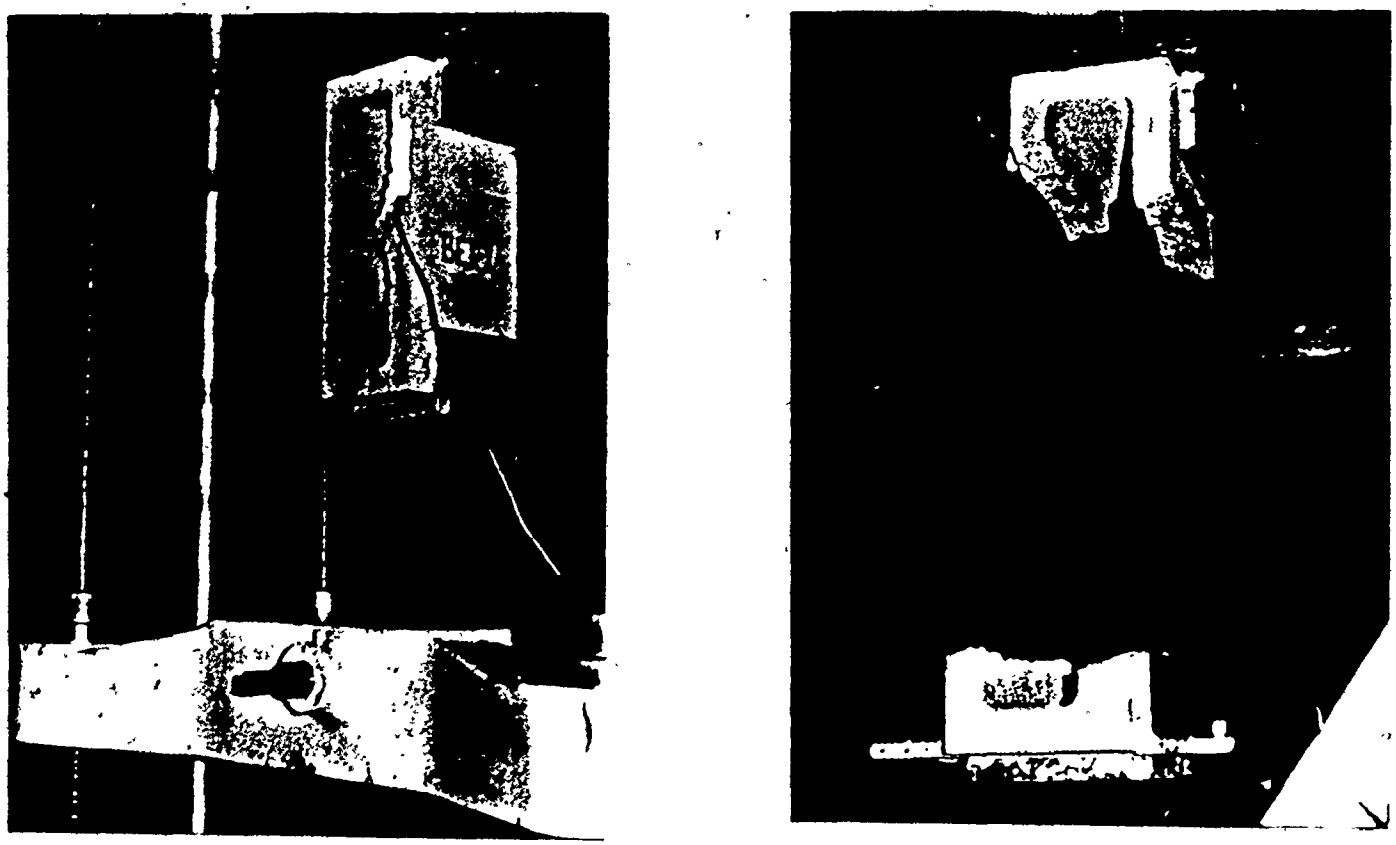

(a) Prior to Loading

(b) After Failure

Fig. 2.10 ECCENTRIC TENSION TEST OF FULL CONCRETE BLOCK

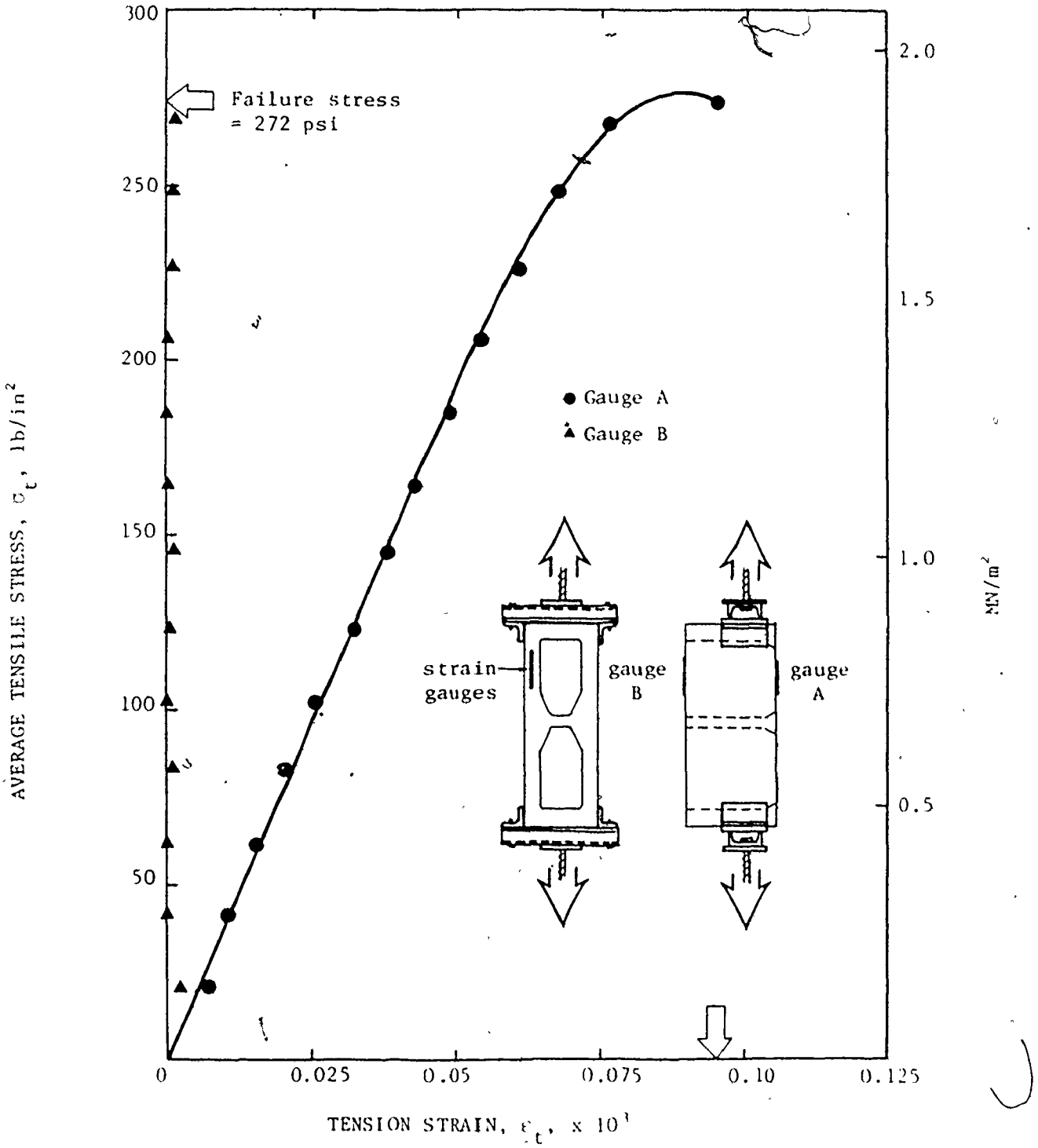

Fig. 2.11 STRESS-STRAIN RELATIONSHIP OF CONCRETE BLOCK UNDER ECCENTRIC TENSION

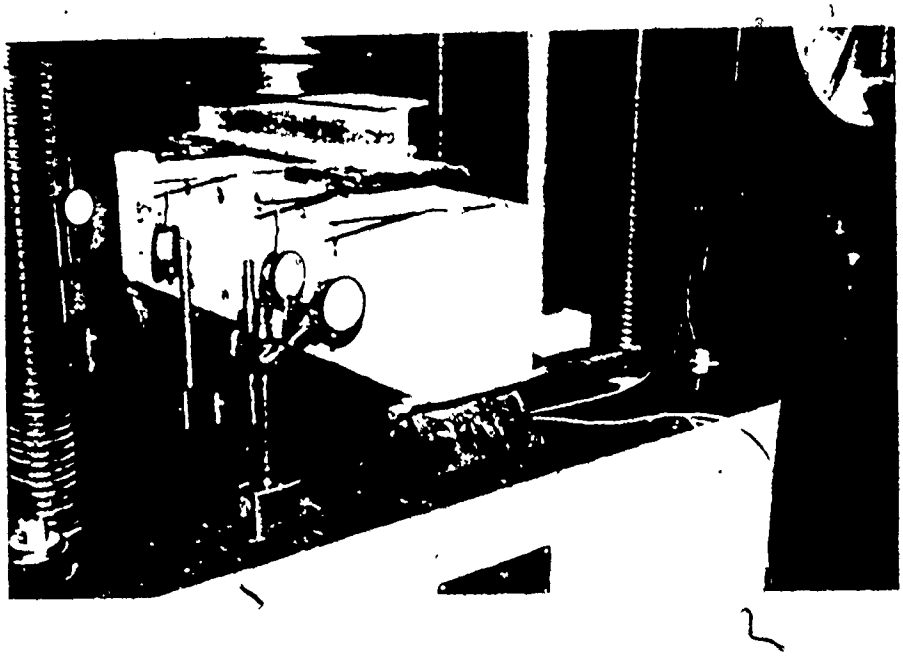

(a) Prior to Loading

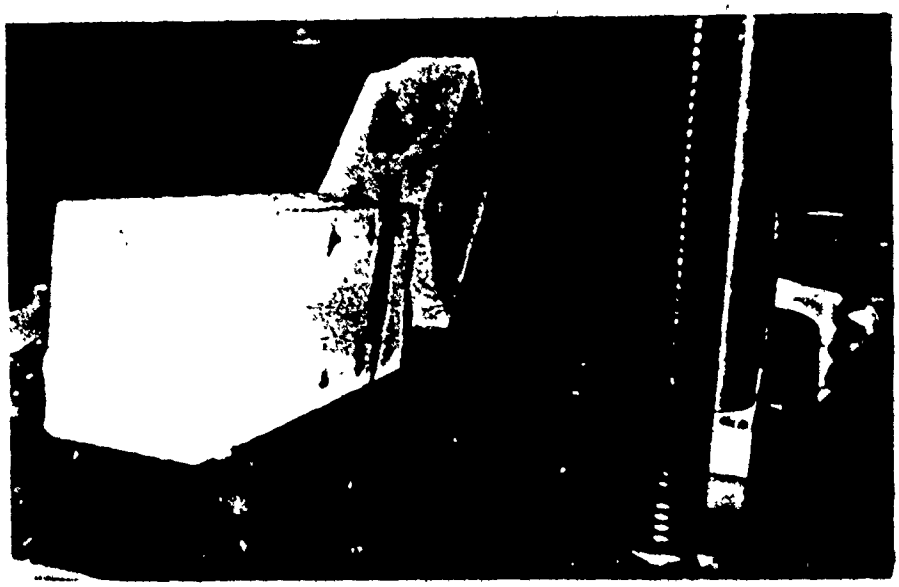

(b) After Failure

Fig. 2.12 FLEXURAL TENSION TEST OF CONCRETE BLOCKS

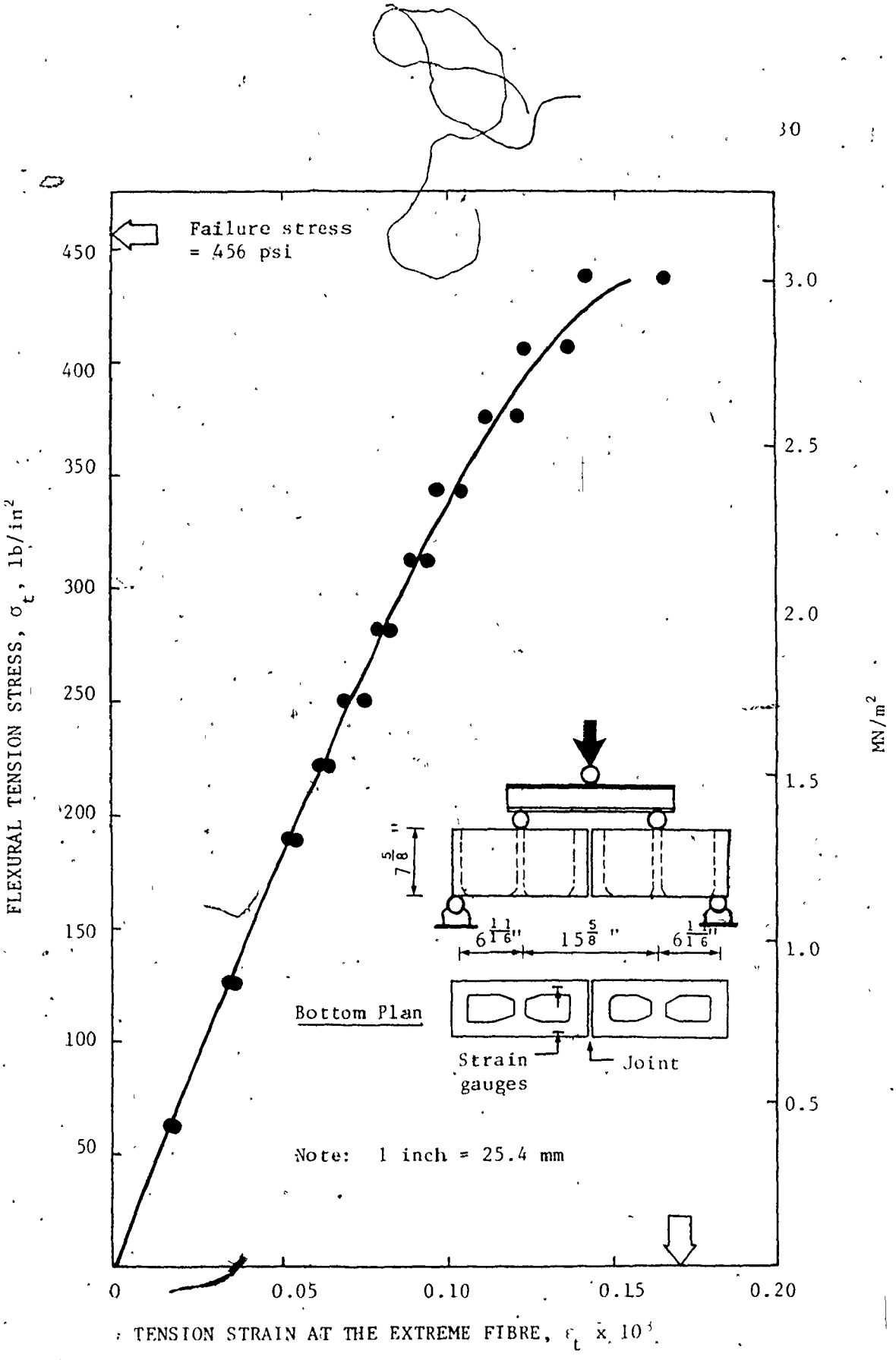

Fig. 2.13 STRESS-STRAIN RELATIONSHIP OF CONCRETE BLOCK UNDER FLEXURAL TENSION

tensile strength of concrete blocks. The stress-strain curve, based on electrical resistance strain gauge measurements, is shown in Fig. 2.13.

4 - Splitting Tension: Half blocks were tested under opposite compressive line loads crossing the face shells as shown in Fig. 2.14(a). The load was applied through 3/8 inch diameter bars. Plywood strips (1/2 in. wide by 1/4 in. thick) were used between the bars and the blocks to eliminate the stress concentration along the applied line loads. The mode of failure was splitting along the loaded plane as shown in Fig. 2.14(b). This test technique is similar to the indirect tensile test for concrete cylinders[57] and the induced transverse tensile stresses are similar. The tensile strength of the block, σ_{tbl}, was calculated using the following relationship adopted by Self[48]:

$$\sigma_{tbl} = \frac{2P}{\pi A_n} \qquad \ldots\ldots (2.2)$$

where P is the splitting load and A_n is the sectional area of the splitting plane (the net sectional area). Use of this relationship have been analyzed and is discussed in more detail in Appendix B.

To be able to statistically analyze the results, five repetitions for each of the above-mentioned test methods were adopted. The tensile strength results for all these tests are listed in Table 2.2. It is obvious that the tensile strength of

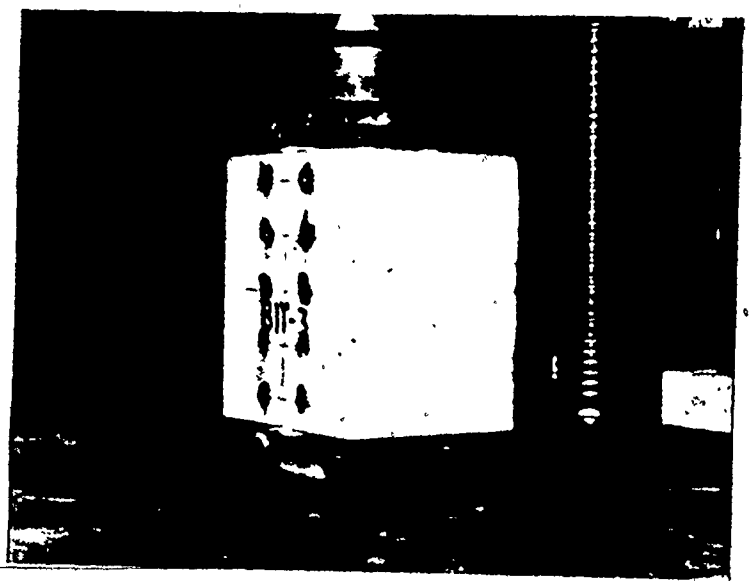

(a) Prior to Loading

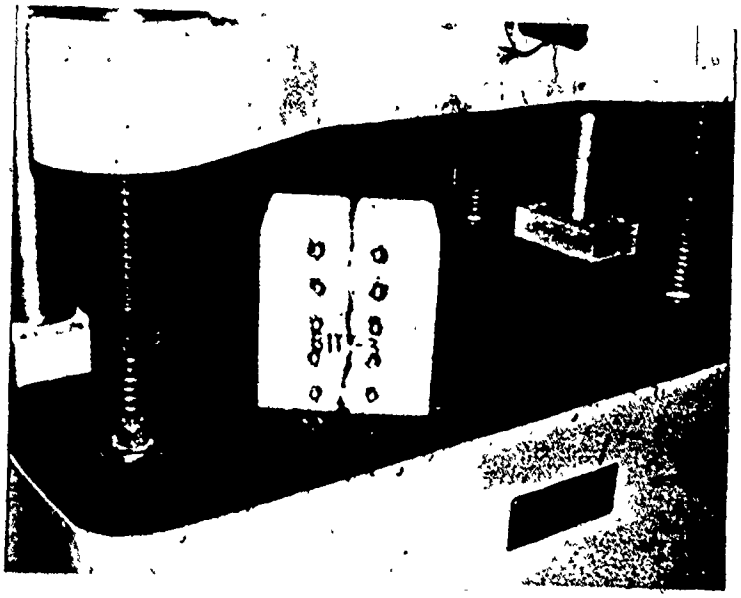

(b) After Failure

Fig. 2.14 SPLITTING TENSION TEST OF HALF CONCRETE BLOCK

TABLE 2.2

BLOCK TENSILE STRENGTH

Test Type	Individual Strength[a] (psi)	Mean (psi)	C.O.V.[b] (%)	$\frac{\sigma_t}{\sqrt{\sigma_{cb}}}$
Axial tension	188 153 204 191 183	184	10.2	3.5
Eccentric tension	272 299 230 270 265	267	9.3	5.0
Flexural tension	495 394 441 425 456	442	8.5	8.3
Splitting tension	221 231 175 240 244	218	11.6	4.1

NOTE: 1 psi = 6.9×10^{-3} MN/m^2

a - based on net area
b - coefficient of variation

the block varied appreciably with the test type. The strengths ranged from four to eight times the square root of the block compressive strength, σ_{cb}, as determined from the half block compression test.

The results, presented in Fig. 2.15, show that the loading condition, and consequently the strain gradient, has a pronounced effect on the tensile strength of concrete blocks. Higher strain gradients resulted in higher tensile strengths. The strength under flexural tension, having the maximum strain gradient, was approximately double that under axial tension which has no strain gradient. This phenomenon, which is known to be valid for normal concrete[40], is attributed to the fact that under zero strain gradient the entire volume of the specimen is subjected to maximum stress so that the probability of a weak element occurring in a zone of maximum stress is high. Also, under a strain gradient condition, the maximum fibre stress reached is higher than in the case of no strain gradient because the less highly stressed material is at an energy level below that necessary for the formation of a new crack surface. Thus the propagation of micro-cracks is restricted[40].

A comparison of the stress-strain relationships, for the different test types, indicates that the maximum strain at the onset of failure increases with the increase in the strain gradient.

The block tensile strength seems to be directly

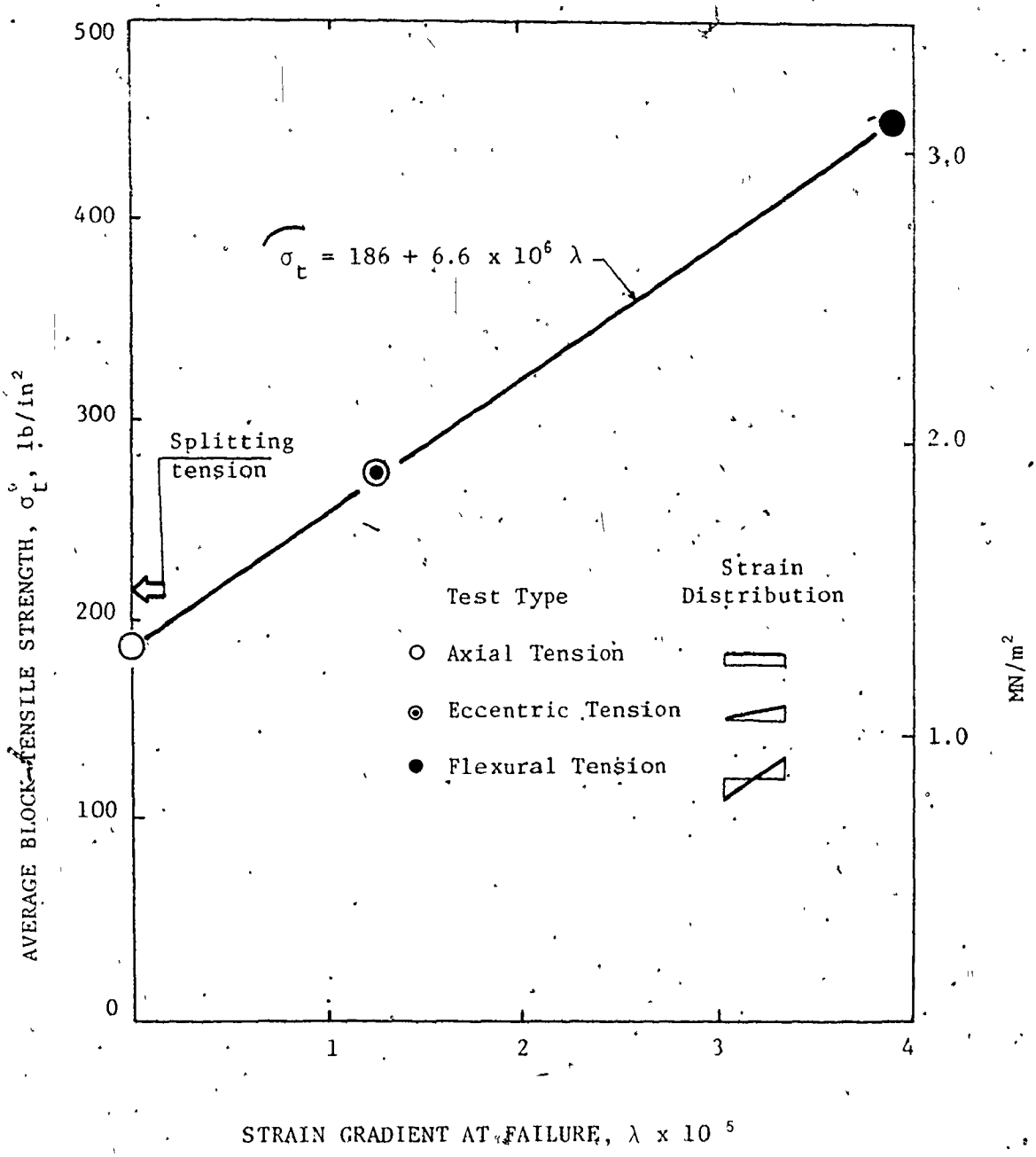

Fig. 2.15 EFFECT OF STRAIN GRADIENT ON THE TENSILE STRENGTH OF CONCRETE BLOCKS

proportional to the strain gradient, λ, as shown in Fig. 2.15. Using a linear regression analysis, the block tensile strength, σ_t (psi), can be expressed as:

$$\sigma_t = 186 + (6.6 \times 10^6)\ \lambda \qquad \ldots\ (2.3)$$

This empirical formula can be rewritten in a general form as:

$$\sigma_t \simeq \sigma_{to} + 2\ \lambda\ E_t \qquad \ldots\ (2.4)$$

where σ_{to} is the tensile strength under no strain gradient, E_t is the modulus of elasticity as calculated from the flexural tension test, and λ is the strain gradient at the critical section at failure.

The splitting tensile test is adopted to represent the block tensile strength in the current investigation because it is a reliable measure of the tensile strength and from a practical viewpoint is an easy test to perform[9]. The direct tension test unavoidably incorporates local stress concentrations at the webs, and the preparation and testing are comparatively complicated processes. The flexural test is easier than the axial tension test, but gives results considerably in excess of a realistic tensile strength for actual masonry assemblages, which usually have lower strain gradients than those which result using this test method. In addition, the failure of a block under a splitting load is similar to the failure of the blocks in a masonry wall under axial compression (splitting failure mode). This similarity of failure modes is another advantage of using the splitting test, rather than the other test techniques, as the

standard for determining the block tensile strength. The splitting test has been adopted by other investigators as a measure of the tensile strength of either brick[9,45] or block[9,48] masonry units.

2.2.2 Mortar

The cements and sand were provided by local suppliers in Ontario. Portland Cement type 10 and lime (masonary hydrate) were used as the cemetitous materials. The available masonry sand, the sieve analysis of which is shown as curve A in Fig. 2.16, did not meet the requirements of ASTM Standard C-144[1], since it contains a too high percentage of fines. To meet the specification, two sand types ordinarily used for concrete were sieved and the parts which passed through the No. 8 sieve were used as masonry sands. The grading of the resulting sands are shown in Fig. 2.16 as curves B and C. Two types S mortar and one type N mortar (ASTM C-270[1]) were used in the current program to build the test specimens. Their proportions by volume, with the weights shown in brackets, are listed in Table 2.3. For better control, the proportions were actually measured by weight rather than by volume. The water contents were established by the mason's requirements for suitable workability. These water contents provided mortars of initial flows ranging from 110 to 120 percent which comply with the ASTM C-270[1] requirements. The water-cement ratio was controlled for a particular mortar type

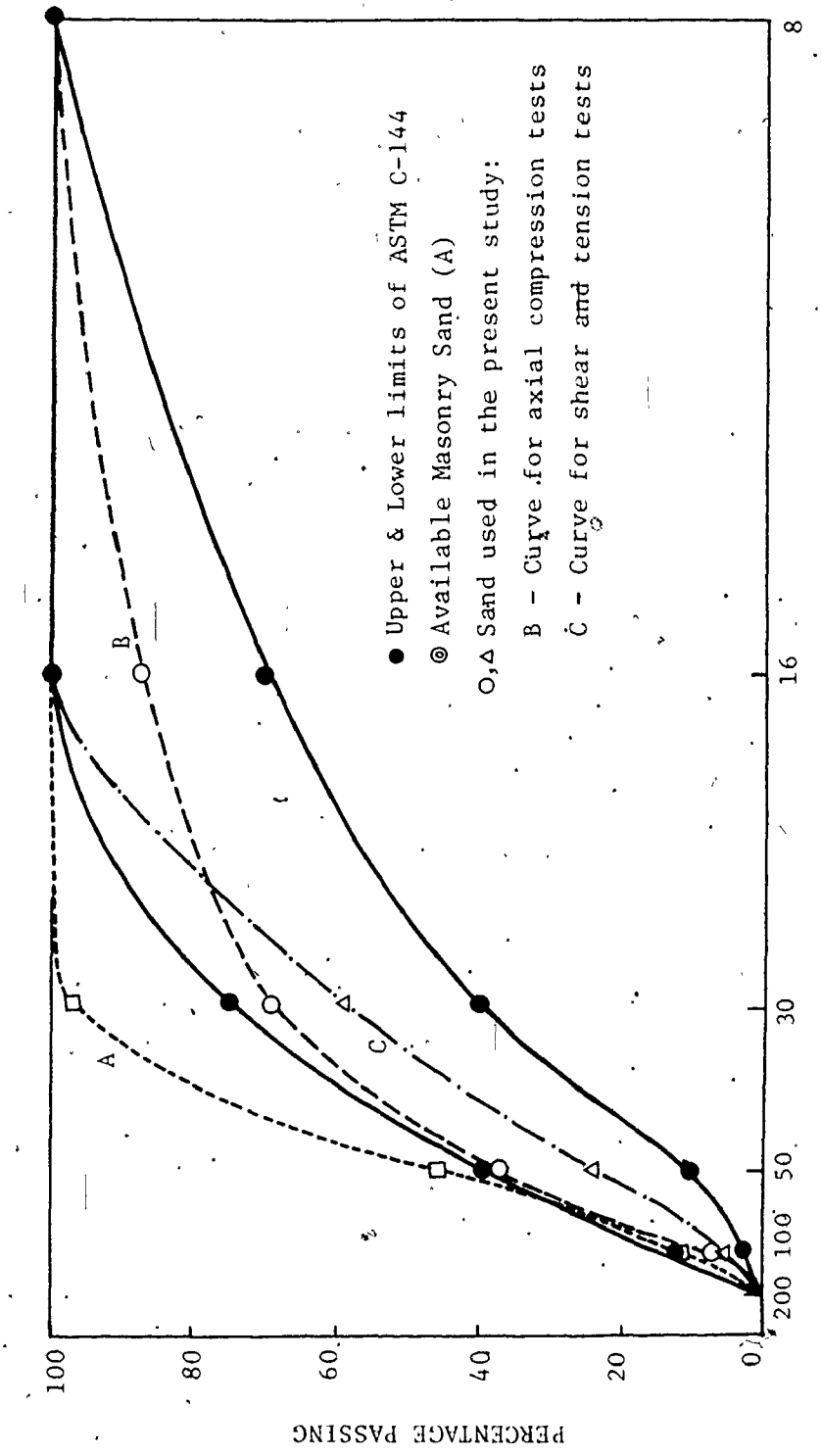

Fig. 2.16 SIEVE ANALYSIS OF SAND FOR MASONRY MORTAR

with only slight variations due to one possible retempering. Any mortar not used within a half hour was thrown out to avoid variations resulting from the need for exeeessive retempering.

TABLE 2.3

MORTAR MIXES

Mortar type	Proportions by volume (weight) cement	lime	sand	water
S_1	1	0.5 (0.21)	4.0 (4.24)	(0.9)[a]
S_2	1	0.5 (0.21)	3.375 (3.58)	(0.75)[a]
N	1	1.25 (0.53)	6.75 (7.16)	(1.53)[a]

a - average values of the different batches used throughout the program

Two inch mortar cubes and 3 inch diameter by 6 inch high mortar cylinders were cast in nonabsorbent moulds during the contruction of the assemblages. These control specimens were air cured in the laboratory under the same conditions and tested at approximately the same age as the corresponding assemblages. For the sake of comparison in the first series of experiments (axial compression tests of prisms), mortar cubes were made or cured in two different ways in addition to the air cured cubes. One set

was water cured and the other was made by spreading the mortar on masonry blocks to a thickness of 1/2 in. to 5/8 in. and allowing it to stand for one minute before placing in the moulds[7] after which they were air cured. Table 2.4 presents the compressive strengths of the mortar cubes for three different methods. The results show that water curing the mortar cubes caused an increase of about 83% in the compressive strength over the air cured cubes. Spreading the mortar on the block before moulding increased the mortar strength by about 17% over the air cured mortars. In the actual masonry assemblages water is removed from the mortar due to the suction exerted by the masonry blocks. The suction varies depending upon the water absorption of the unit, the rate of absorption, and the capillary suction force[50]. In some cases where the absorption of the unit is very small, practically no water may be removed from the mortar which could be represented by water curing. In other cases where the absorption of the unit is high, most of the water would be removed which could be represented by air curing after spreading the mortar on the block. The strength of the mortar depends upon the water to cement ratio after absorption by the blocks and also upon the curing conditions after the mortar has hardened. The state of the mortar in the assemblage is not adequately represented by any of these methods. However, although it is a common practice to adopt water curing as a standard method, the technique of spreading the mortar on the units before moulding and then air curing seems to be the best to

simulate the strength of the mortar in the assemblage. In the current program, air cured mortar cubes were adopted as the standard control specimen.

TABLE 2.4

COMPRESSIVE STRENGTHS OF MORTAR CUBES[a]

Mortar type	Air cured (psi)		Water cured (psi)
	(1)[b]	(2)[c]	
S_1	2130	2560	3950
N	830	950	1500

NOTE: 1 psi = 6.9×10^{-3} MN/m^2

a - a minimum of 3 cubes per batch was adopted
b - air cured cubes cast in nonabsorbent moulds
c - mortar spreaded on blocks before moulding

The tensile bond strength of the mortar, which is an important characteristic influencing masonry capacity under loads which produce tension and/or shear stresses, is not a unique function of its compressive strength[7]. The bond value is mainly affected by the physical properties of the block (surface roughness and IRA) and the mortar (initial flow and water retentivity). For any mortar mix, the more fluid and more plastic the mortar is, the greater is the bond strength. In the current program, the tensile splitting of masonry couplets were adopted to determine the mortar tensile bond strength. This test consisted

of two half blocks with mortar placed between them in either the bed or head joint as shown in Fig. 2.17. Upon completion of the construction of the half blocks with mortar in the bed joint, two half blocks were placed on the top block to provide some weight on the bed joint, simulating the self weight of the upper courses in the wall. The head joint was also laid horizontally but no extra weight was added. For testing, the two half blocks were turned so that the mortar joint was vertical and a wooden strip was placed over the top and bottom of the mortar joint as shown in Fig. 2.17. A compression line load was applied thereby inducing transverse tensile stresses which resulted in splitting along an interface between the mortar and the block. The tensile bond strength, σ_{tbm}, is calculated using the following previously discussed (see Section 2.2.1.3) relationship:

$$\sigma_{tbm} = \frac{2P}{\pi A} \qquad \ldots\ldots (2.5)$$

where P is the splitting load and A is the sectional area at the splitting plane (at the block-mortar interface).

A direct tension test similar to the direct tensile test technique for the block was also tried as an alternative test technique to determine the tensile bond strength of masonry couplets. However, because of the high variability of the test results and relatively time consuming nature of this test, it was not used as a control test.

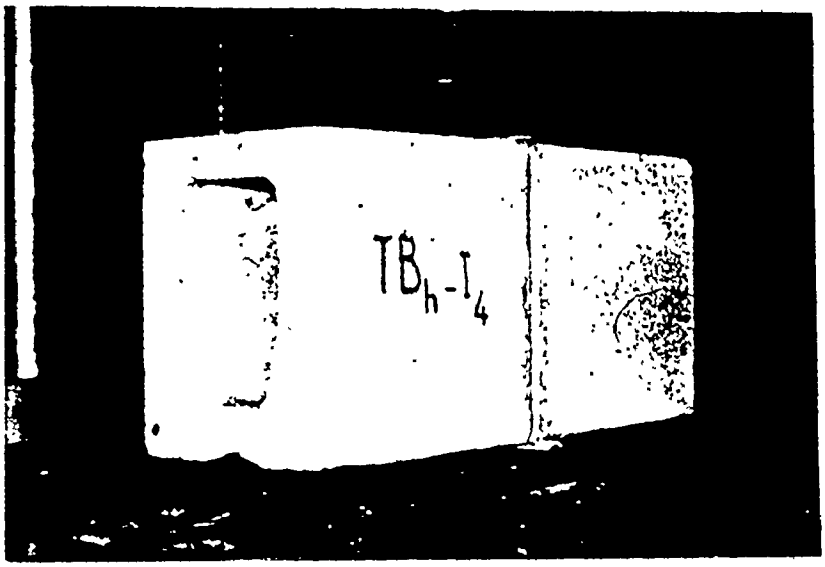

(a) Bed Joint

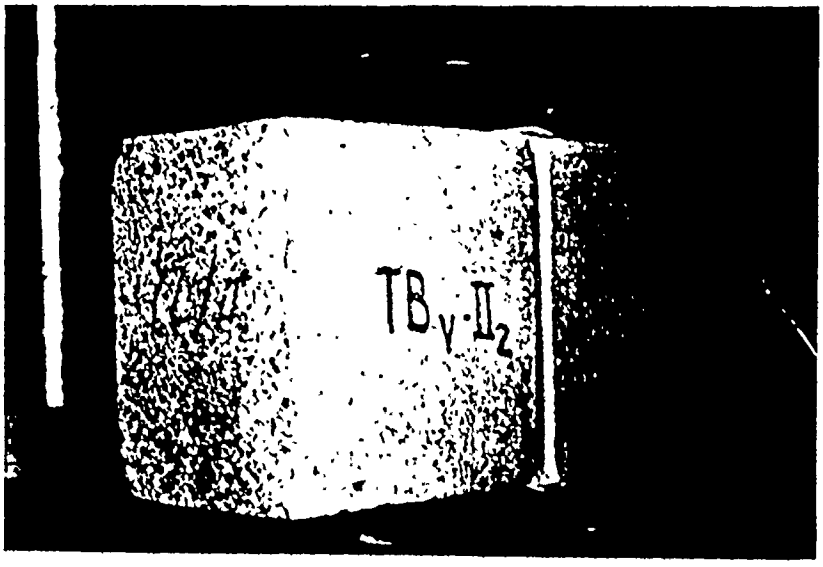

(b) Head Joint

Fig.2.17 SPLITTING TESTS OF MASONRY COUPLETS

2.2.3 Grout

The following three different types of grout were used in this investigation: 1) weak grout (GW), 2) medium grout (GM), and 3) strong grout (GS). Three different mixes of type GM grout were considered. All of the latter satisfy the specifications ASTM C-476[1], whereas the two mixes, GW and GS, do not satisfy the specifications. The latter were desighed to obtain a wider range of grout strengths. In Table 2.5, the proportions of the different mixes are given by volume and by weight as indicated in brackets. The gradation of the sand and gravel used in the mixes are shown in Figs. 2.18 and 2.19, respectively. The gradings generally meet the specifications of ASTM Standard C-404[1]. The water-cement ratios were established to give about a 10 inch slump thus assuring a fluid grout which could be poured into the cores without requiring vibration.

The following two types of control specimens were used for the grout; 1) air cured 3 inch diameter by 6 inch high cylinders and 2) block moulded prisms using paper towels as a seperator, as shown in the photograph in Fig. 2.20, so that the water would pass into the blocks. The prism dimensions were 2 1/2 x 5 5/8 x 7 5/8-in. which gives nearly the same surface area to volume ratio as the cell in the block. The prisms were left moulded between the blocks and air cured till the time of testing. The compressive strength of the grout converted to an equivalent strength of cylinder of a height to diameter ratio of two, was determined from

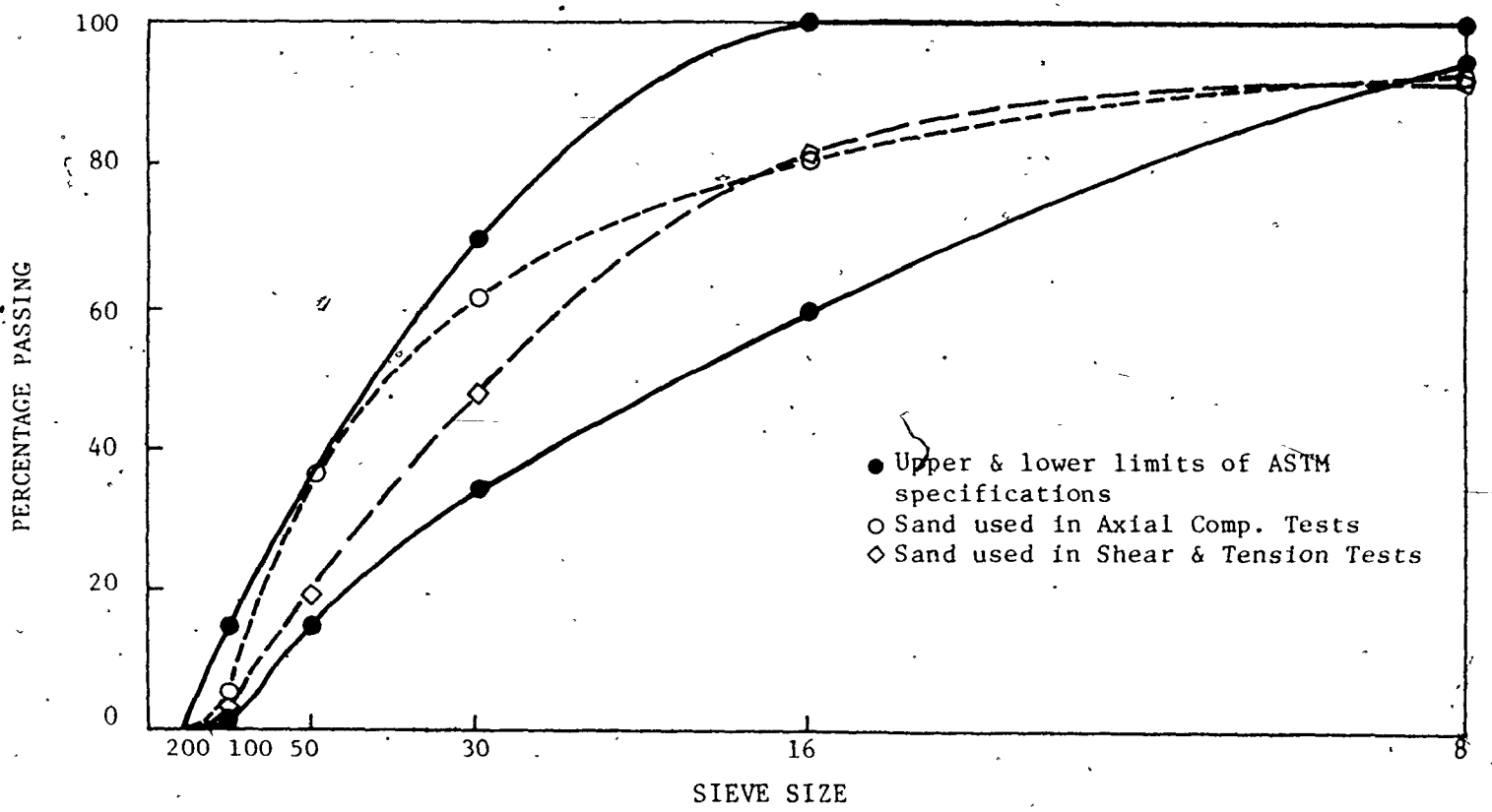

Fig. 2.18 SIEVE ANALYSIS OF SAND FOR GROUT

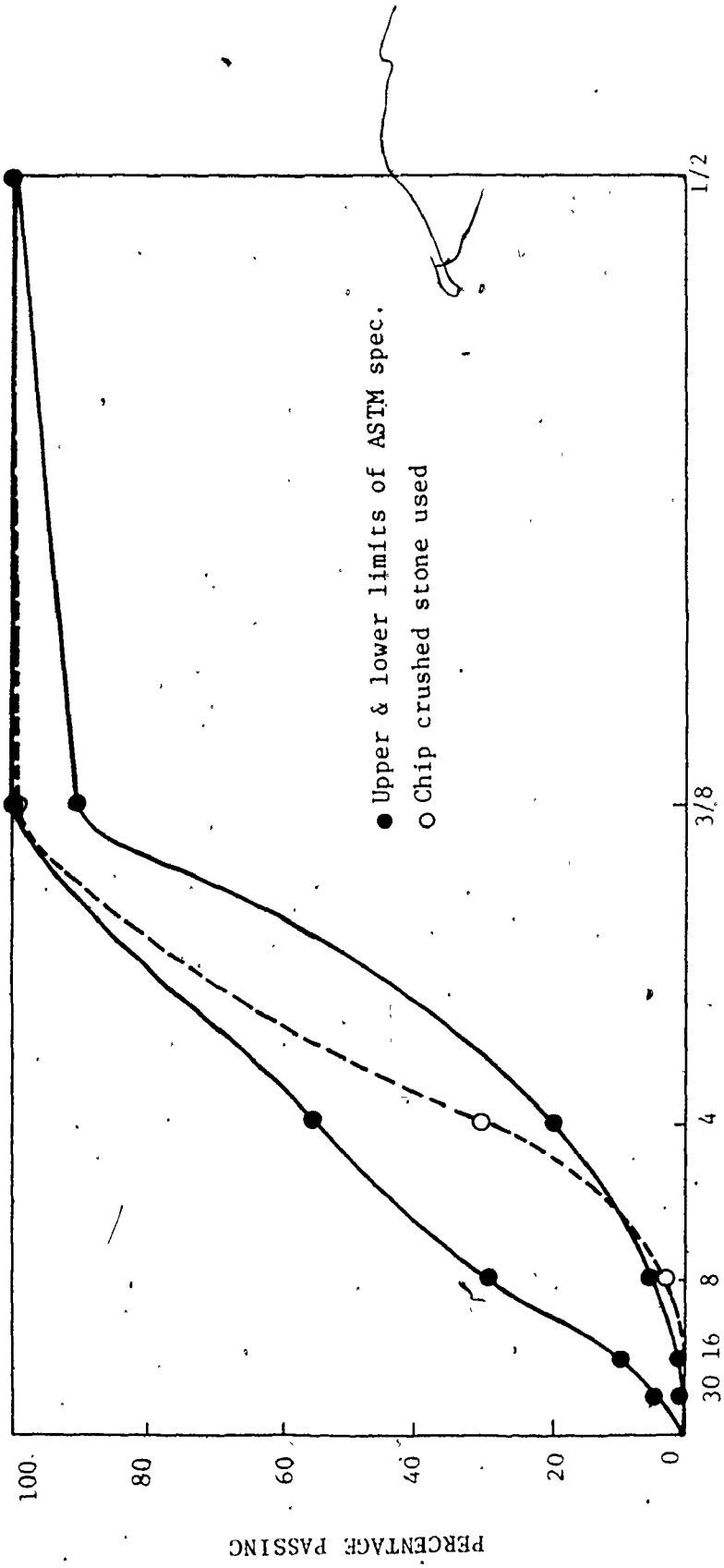

Fig. 2.19 SIEVE ANALYSIS OF AGGREGATE FOR COARSE GROUT

Fig.2.20 BLOCK MOULDING OF GROUT PRISMS

the prism strength using the following empirical formula adopted for concrete[39]:

$$\frac{Ps}{P'} = 0.85\ (0.56 + 0.697\ \frac{d}{(\frac{V}{6h} + h)}) \qquad \ldots\ (2.6)$$

where Ps = cylinder compressive strength

P' = prism compressive strength

d = the maximum lateral dimension of the prism

h = height of the prism

V = volume of the prism

TABLE 2.5

GROUT MIXES

Grout Type	Proportions by Volume (Weight)				
	cement	lime	sand	gravel	water
GW	1		5 (5.95)		(1.08)[a]
GM_1	1	0.1 (0.044)	3.3 (3.55)		(0.70)[a]
GM_2	1	0.1 (0.044)	3.0 (3.22)		(0.66)[a]
GM_3	1	0.1 (0.044)	2.475 (2.66)		(0.60)[a]
GS	1		1 (1.11)	1 (0.9)	(0.43)[a]

a - average values of the different batches used throughout the program

A comparison study was conducted to investigate the effect of block moulding on the grout compressive strength. The 3 inch diameter by 6 inch high cylinders were adopted as a reference for comparison. The results are represented in Fig. 2.21 in which each point represents the ratio between the average of three prism tests and three cylinder tests. The prism strength had been reduced to take into account the effect of the geometry on the compressive strength using Equation (2.6). It can be seen that for mixes of high water to cement ratios (w/c), such as mix GW, block moulding had a significant influence in producing higher strength grout. This could be attributed to the decrease of w/c ratio due to water absorbed by the block. For mixes of low w/c ratio, such as GS, there was no significant difference between the compressive strengths of the air cured cylinders and the block moulded prisms. The grout strengths calculated from the block moulded prisms, σ_{cg}, are used in the current investigation as being representative of the grout strength in the block.

2.2.4 Joint Reinforcement

To study the effect of joint reinforcement on the behaviour of concrete masonry assemblages, horizontal steel was embedded in the mortar bed joint of some specimens. Standard Dur-O-Wal Steel[14], ladur type, (see Fig. 2.22(a)), having a total area of 0.036 in^2 for both side rods, was used in some tension and shear specimens. For the compression specimens, the cross members were

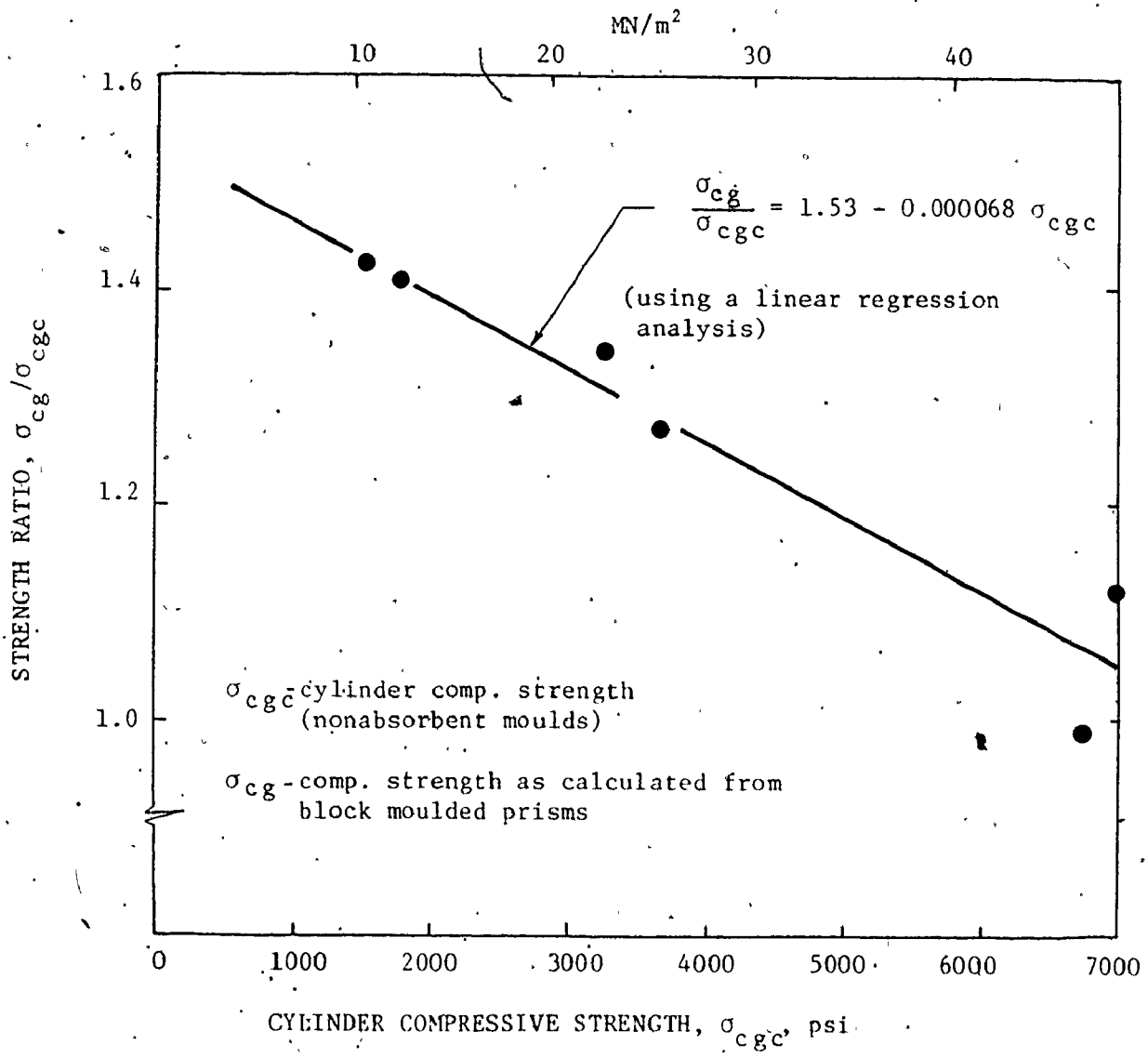

Fig. 2.21 EFFECT OF METHOD OF MOULDING ON THE GROUT COMPRESSIVE STRENGTH

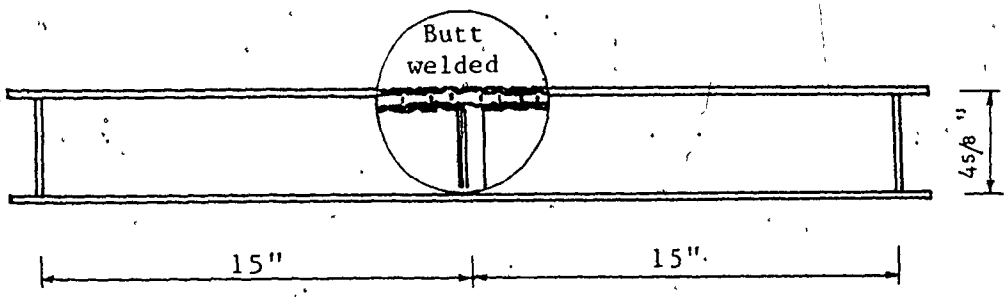

a. Joint reinforcement for tension and shear specimens (No. 9 Gauge Wire)

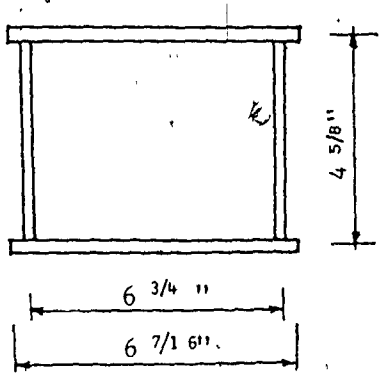

b. Adjusted Dur-O-Wal for compression prisms

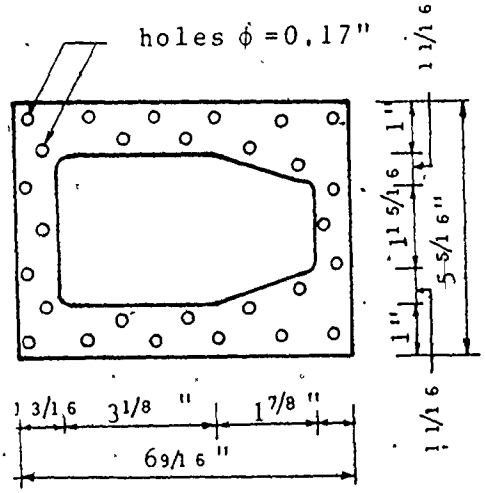

c. Confining steel plate for compression prisms

Fig. 2.22 DETAILS OF JOINT REINFORCEMENT

adjusted to fit the prism dimensions as shown in Fig. 2.22(b). Confining plates of 0.11 inch thick were also used to reinforce the joints of some prisms under axial compression. Holes were drilled in the steel plates to provide mechanical interlocking at the interface with the mortar. Details of the confining plate are shown in Fig. 2.22(c).

2.3 Summary and Conclusions

In this chapter the material properties of the block, mortar, and grout are presented and discussed. Information about the strength and deformation characteristics of the component materials, which will be used in the succeeding chapters, are also presented.

The following are the major conclusions which have been drawn from the tests of the material properties described in this chapter:

1 - The type of capping material affects the compressive strength of the block as well as its mode of failure. Softer capping material results in less compressive capacity of the block. Soft capping changes the mode of the failure from a shear mode of failure, using hard capping, to a splitting mode of failure. Also, the variation in the compressive strengths of identical specimens is higher when soft capping is used.

2 - The compressive strength of half blocks tested flatwise and full blocks tested endwise are nearly the same.

3 - The loading condition and, consequently, the strain graident has a pronounced effect ont he tensile strength of the block. Higher strain gradients result in higher tensile strengths. A direct proportionality is proposed.

4 - The proposed technique to test masonry blocks under flexural tension has the advantage over the modulus of rupture tests, recommended in ASTM C-67 Standard for brick, in that it provides a flexural member of larger span to depth ratio which minimizes the effect of shear and therefore gives a better measure of the flexural tensile strength of the block.

5 - The splitting tension test provides a reliable, easy to perform, and representative measure of the block tensile strength.

6 - As a result of the testing, it is apparent that masonry codes should specify the loading conditions and the unit geometry when specifying the strength of the masonry units.

7 - The method of making or curing significantly affects the mortar strength. However, although it is a common practice to adopt water curing as a standard method, the technique of spreading the mortar on the blocks before moulding and then air curing seems to be more representative of the mortar in the assemblage.

8 - The method of moulding the grout affects the strength of the control specimens, especially for those mixes having high water to cement ratios. Grout prisms moulded between masonry blocks and having the same surface to volume ratio as that of the

cells in the blocks are representative of the grout in the assemblages.

CHAPTER 3

AXIAL COMPRESSION OF CONCRETE MASONRY

3.1 Introduction

A principal use of masonry is to transfer gravity loads to the foundation and as such the axial load bearing capacity of masonry walls has been the subject of experimental research for many years. The need to establish compressive allowable stresses for design codes has often motivated compression testing of masonry specimens where the allowable stresses in tension and shear may also be expressed as functions of the compressive strength, f'_m[12,27]. The effects of varying the material properties, slenderness ratio, and geometric characteristics of the test specimens on the compressive strength of brick masonry walls have been investigated and reported in the brick masonry literature[17,31,33,47].

While there is considerable information describing the behaviour of brickwork under axial compression, relatively little is known about blockwork structures[20,21,32,44]. In fact, there is very little information concerning the basic behaviour characteristics and the failure mechanism for ungrouted and grouted concrete masonry under axial compression. It has been reported[21,33] that insufficient information is available in current literature to knowledgably comment on the behaviour of

grouted masonry under axial compression. However, a few investigations were carried out to test block masonry walls under axial and eccentric compression loads[10,13,20,45]. These studies dealt with the overall behaviour of the walls without much emphasis on the influence of the material properties and the basic strength and deformation characteristics of masonry as a composite media.

Because of the multitude of parameters influencing the compressive strength of masonry, each experimental study has been constrained by economic necessity to studying limited ranges of parameters. Notwithstanding the fact that little correlation exists among the various studies, several useful observations have resulted from a literature review of the experimental phases of brickwork research. These have helped to gain a better understanding of the problem associated with the behaviour of masonry under axial compression.

The first observation was that the traditional treatment of brickwork as a homogenous material is far from reality, and that in brickwork one is dealing with a two phase assemblage of brick and mortar for which the carrying capacity under compressive stress will be determined by the interaction of strength properties of its constituent materials.

Secondly, it was observed that a masonry panel axially loaded to failure exhibits vertical cracks in the masonry units. This vertical splitting mode of failure is related to the

different deformation characteristics of the masonry units and the mortar joints. In most masonry assemblages, the modulus of elasticity of the mortar (one or two million psi) is lower than that of the brick (about four to six million psi) or concrete block (about two to four million psi). Therefore, its unrestrained lateral deformation is substantially greater than that of the brick or the concrete block, assuming that the Poisson's ratios are similar. Because the masonry unit at the mortar interface must undergo the same lateral expansion as the mortar, due to the friction and bond, the lateral expansion of the mortar is restrained, thereby producing tensile strain in the masonry units. This observation is considered to be the most important aspect for the understanding of the failure mechanism of masonry assemblages in compression, and has become the central concept in attempts[15,24,31] to derive an analytical solution of the problem of the brickwork under axial compression.

Is has also been found that the compressive strengths of masonry assemblages are only moderately dependent on the mortar strength for practical ranges and its is more dependent on the tensile strength of the masonry units[9,31,47]. Less apparent, however, is the observation that a higher compression capacity is achieved if the mortar thickness to masonry unit height ratio is kept to a minimum[15,31,33].

To what extent these findings are applicable to grouted masonry is not yet known and hence further investigation is

needed. For grouted masonry, one is dealing with a three phase material wherein the continuity provided by grouting the cores could have a significant effect on the assemblage behaviour. Other parameters involved in the behaviour of grouted masonry, which are not applicable to ungrouted masonry, are:

1 - the grout strength and deformational characteristics relative to those of the blocks and the mortars,

2 - the core area governed by the net to gross area ratio of the block, and

3 - the core shape.

In the absence of an analytical solution, empirical relationship derived from experimental results, have been put forward[17] to show the variation of the masonry compressive strength with given parameters. These relationships are generally limited in scope and in application to include other ranges of parameters. There is a need for analytical solutions which can account for the multitude of parameters contributing to the compressive strength of masonry.

Several attempts have been made to analytically determine, in quantitative forms, the compressive strength of solid brick masonry prisms. Hilsdorf[24] and Khoo[31] developed their analytical models on the basis of stress analysis considerations wherein the strengths of the component materials governed. Francis et al[15] suggested an alternative failure mechanism based on strain considerations. These models are not applicable

to grouted masonry as they only deal with a two phase material composed of solid brick and mortar.

Because of the lack of either analytical or experimental information concerning the effect of grouting on the compression capacity of conrete masonry, typical masonry codes[12,27] assign compressive design values for grouted masonry equal or greater than those for solid masonry provided that the grout strength is at least equal to that of the units. Introducing grout as a third component with specified strength and deformation characteristics may significantly change the assemblage behaviour and therefore this code approach needs to be reviewed.

It is the objective in this chapter to investigate the effect of the strength and deformation characteristics of the block, mortar, and grout on the assemblage behaviour under axial compression. To analytically express the failure mechanism of ungrouted and grouted masonry under axial compression is also an aim. The code[12] provisions concerning grouted masonry will be reviewed and evaluated utilizing the results of the current investigation.

3.2 Experimental Study

An experimental program has been conducted to study the effect of the strength and geometric parameters on the behavioural characteristics of ungrouted and grouted masonry assemblages. A total of 150 full size specimens have been tested under axial

compression.

The following are the main points of interest during the course of experimentation:

1 - Failure loads

2 - Crack patterns and failure modes

3 - Deformations in both the vertical and horizontal directions to establish stress-strain relationships.

3.2.1 Test Specimens

Present working stress design methods are based upon a knowledge of the masonry compressive strength, f'_m. In practice, f'_m is often determined from tables relating the strengths of the component mortars and the masonry units. However, because tests of masonry prisms usually result in higher values of f'_m, it is economically feasible to use prism tests for gauging the strength of the masonry in a wall. In the current program, prism tests were adopted to examine the behaviour of masonry under axial compression.

It is the standard practice[10,45,48] to compute f'_m on the basis of 2-course prisms laid in stack bond (Fig. 3.1) and capped with high strength gypsum plaster according to ASTM C-140[1]. The North American codes[12,27] not only allow the 2-course prism test but also encourage it by adopting universal correction factors for prism geometry. These correction factors, shown graphically in Fig. 3.2, purport to enable conversion of the strength of a prism

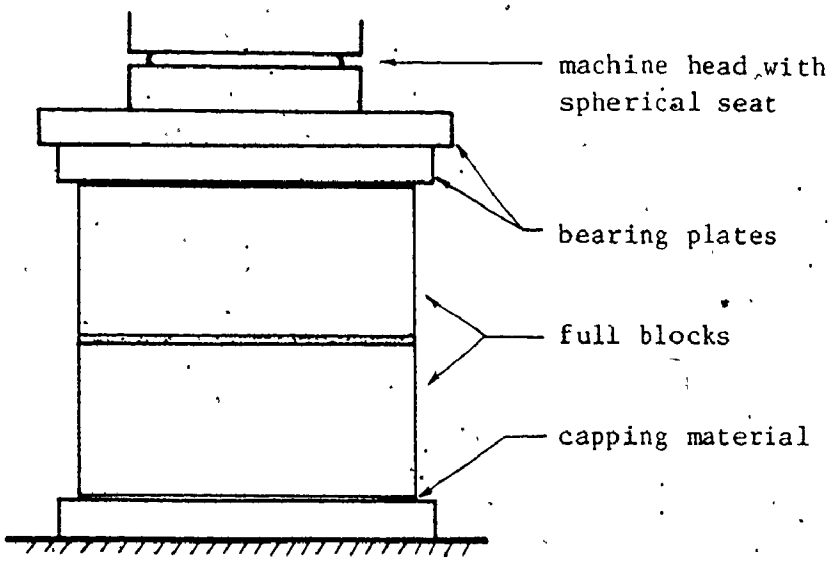

Fig. 3.1 2-COURSE PRISM UNDER AXIAL COMPRESSION.

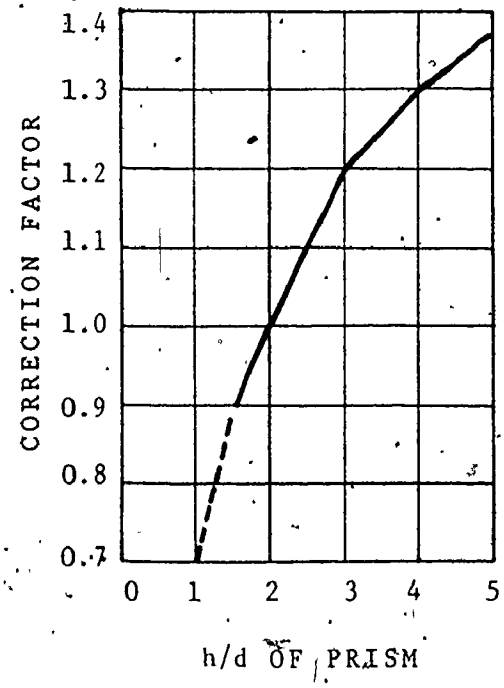

Fig. 3.2 UBC CORRECTION FACTOR VERSUS h/t OF PRISM[27].

of a particular geometry to that of a standard 2-course prism having h/t = 2.0 (h and t denote prism height and least lateral dimension, respectively). This assignment of the conversion factor presumes the existence of a strong correlation between prisms of h/t = 2.0 and full scale masonry.

As a preliminary program to select the proper shape of the prism to be used throughout this investigation, three 2-course prisms were constructed and tested under axial compression using gypsum as a capping material, (see Fig. 3.1). A shear mode of failure, shown in Fig. 3.3, was obtained, whereas the observed failure mode of the masonry wall is vertical tensile splitting. The reason for this shear failure is that with rigid platens, short specimens are subjected to lateral compressive stresses created by the friction restraint at the loading platens. Hence, the specimen will be under a triaxial compression state of stresses which causes a shear mode of failure and an increase in the apparent compressive strength[5,9,18]. This behaviour indicates that the 2-course prism is not representative of a masonry wall under axial compression, as a prime criterion to satisfy in any test specimen is that the "correct" failure mode occurs and that in fact the specimen is being subjected to a condition that represents the prototype behaviour[56]. Therefore, it was decided to adopt a 3-course prism for the current program in order to reduce the influence of the end restraint.

Using 3-course prisms may be appropriate since the middle

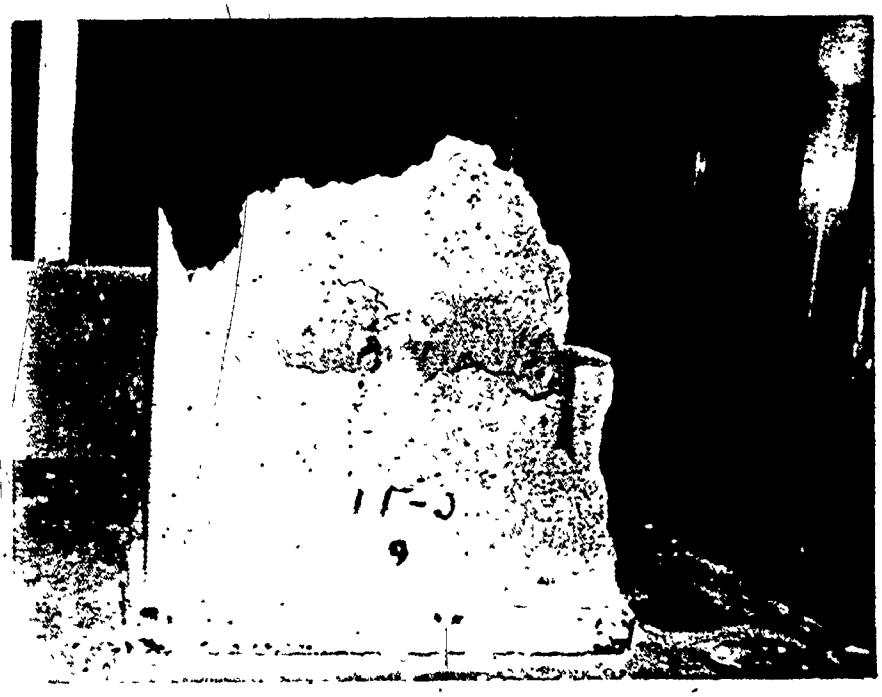

Fig. 3.3 A TYPICAL SHEAR MODE OF FAILURE OF 2-COURSE PRISMS UNDER AXIAL COMPRESSION

block should be free from the end restraint which produces artifical stresses. Intuitively, if one considers the effect of the platens to be confined to a 45° inclined pyramidal zone, then in a prism consisting of three half blocks, the central block and its two adjacent mortar beds will be free from any end effects and probably a splitting failure would be initiated in the central zone. The 3-course prism was adopted by Williams[59] using solid masonry cubic units, and more recently, 3-course prisms composed of full concrete blocks have been adopted by Hegemier et al[21] for axial compression tests. The latter indicated that the 2-course prisms (couplets) laid in stack bond and capped according to ASTM C-140[1] can lead to an overestimate of the masonry compression capacity, f'_m.

3.2.2 Control Specimens

Control specimens were made along with the masonry prisms and were air cured in the laboratory under the same conditions as the prisms. Two inch cubes and 3x6-in cylinders, using 3 per each batch, were adopted as the control specimens to represent the nominal compressive strengths of the mortars used in the prisms. For grout, two types of control specimens were considered; 3x6-in cylinders cast in nonabsorbent moulds and 2 1/2 x 5 5/8 x7 5/8-in. block moulded prisms (see Section 2.2.3 for details of block moulded prisms). The latter is representative of the grout in the assemblage. The grout cylinders and prisms were capped using

gypsum-cement compound and tested under axial compression. Fig. 3.4 shows a grout prism after failure.

For investigating the influence of the core geometries for various core shapes (Section 3.2.3.3), grout prisms were also obtained by splitting the block into halves. The inner surface of the core was covered with paper towels as a porous separator, and hence a block mould was formed by clamping the two halves of the blocks together as shown in Fig. 3.5. Grout was poured into the moulds and at the time of testing the two halves were easily taken apart. The resulting grout, shown in Fig. 3.6, were capped using sulpher compound and tested under axial compression. Fig. 3.7 shows one of these control specimens before testing. Three specimens per batch were tested at approximately the average time of testing the corresponding assemblages.

The proposed technique of block moulding by splitting the blocks seems to be appropriate as it allows the water to pass through from the grout into the blocks under the same condition as for the assemblages. In addition, the technique has the advantage of simplicity and ease of preparation in the laboratory.

3.2.3 Experimental Details and Testing Procedure

Two groups of variables are considered in the current experimental program. The first of these is concerned with the strength characteristics of the component materials such as grout strength, mortar type, and joint reinforcement. The second group

Fig. 3.4 GROUT PRISM TESTED UNDER AXIAL COMPRESSION

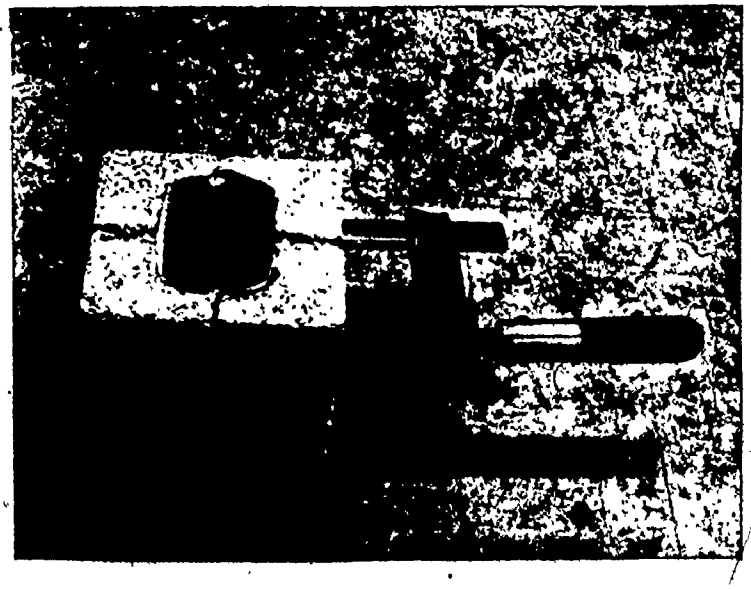

Fig. 3.5 BLOCK MOULDING FOR GROUT CONTROL SPECIMENS FOR DIFFERENT CORE GEOMETRIES (GROUP C2-3)

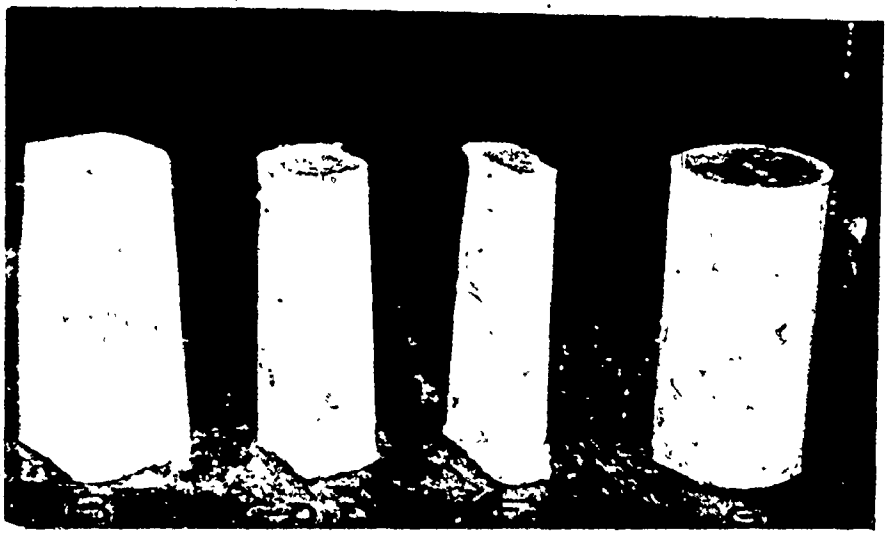

Fig. 3.6 GROUT CONTROL SPECIMENS FOR DIFFERENT BLOCK GEOMETRIES (GROUP C2-3)

Fig. 3.7 A GROUT SPECIMEN UNDER AXIAL COMPRESSION

is concerned with the geometric characteristics of the assemblage. These factors comprise bond type, joint thickness, and core geometry. For each factor, most of the practical ranges are covered.

The effect of grouting, which is of a prime concern in the current program, is investigated through a comparison study between the behaviour of grouted prisms and similar ungrouted specimens.

3.2.3.1 Group C1: Strength Parameters: A total of 57 prisms were constructed in stack bond, using 3 half blocks, to study the effect of the grout strength, mortar type, and joint reinforcement on the behaviour of ungrouted and grouted concrete masonry under axial compression. Using an electrical table saw, the half blocks were obtained by cutting the kerfed units (type B, Fig. 2.1) along lines 7 inches from the ends in order to obtain a cross section with its centroid nearly coinciding with its centre. The half blocks used in the construction of the prisms were identical to those used in determining the block compressive strength (see Fig. 2.3 for details of the cross-section).

The prisms were built by an experienced mason adopting flush mortar joints of nominal 3/8 inch thickness. Care was taken to ensure that the units were laid horizontally. Excess mortar around the joints was cleaned from the cores a few minutes after laying the blocks. The grout was poured after 24 hours and was well puddled using a steel rod. At the age of 28 to 42 days, the

prisms were capped using a gypsum-cement compound (ASTM C-140[1]) and after 24 hours they were tested under axial compression. The test set-up is shown in Fig. 3.8. The load was applied at the centroid of the net area of the ungrouted prisms and at the centre of the gross area of the grouted prisms.

Mechanical gauge points were mounted on both faces of the prisms using a 4 inch gauge length, so that the deformations in the vertical direction (across the top and bottom joints and on the middle block) and in the horizontal direction could be measured. The arrangement of the gauge points is shown in Fig. 3.8. The gauge lengths were constructed along the height of the central block and the two adjacent mortar joints which are free from the confining lateral stresses produced from the platen restraint. Strain measurements were taken at regular load increments up to about 90% of the failure load. Each test took about half an hour.

The first group comprised three series of tests, each concerned with different levels of one parameter where the other parameters were kept constant.

Series C1-1: The effect of the mortar type on the behaviour of ungrouted and grouted masonry prisms under axial compression was studied in this series. Two mixes of the S mortar (S_1 and S_2) and one type N mortar mix were adopted for both ungrouted and grouted specimens. Medium grout, GM_1, was used in this series. The properties of the mortar and grout mixes were

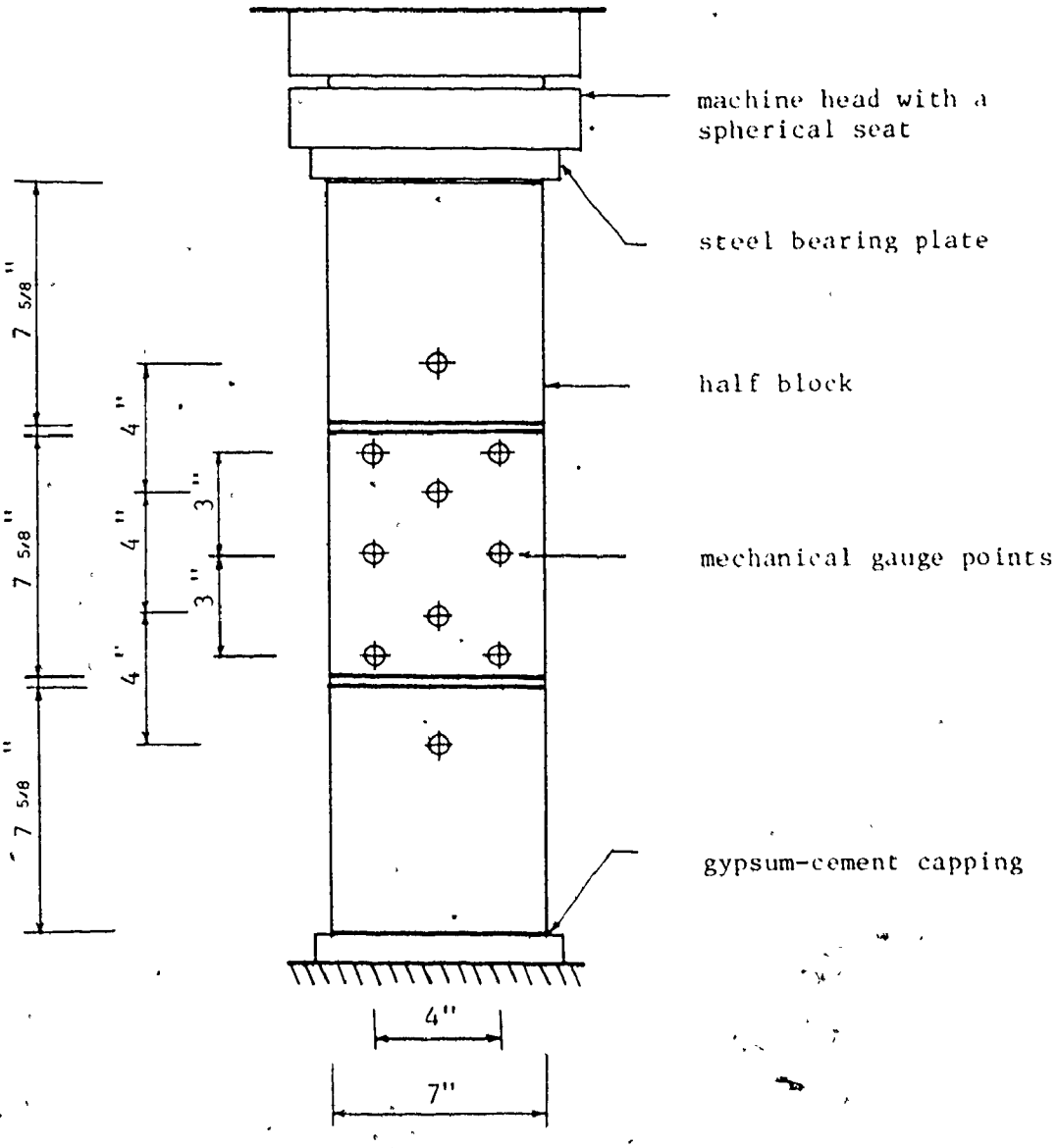

Fig. 3.8 COMPRESSION TEST SET-UP FOR THE 3-HALF BLOCKS PRISM

presented in Chapter 2.

Series C1-2: This series was designed to study the effect of the grout strength on the behaviour characteristics of grouted masonry under axial compression. Five different grout mixes as listed in Table 2.5 were adopted to provide a wide range of grout strengths. Type S_1 mortar was adopted for all the specimens in this series.

Series C1-3: This series was initiated to investigate the effect of joint reinforcement on the compression capacity of ungrouted prisms (of type S_1 mortar) and grouted prisms (of type S_1 mortar and GM_1 grout). The two types of joint reinforcement considered were Dur-O-Wal steel and confining steel plates as described in Section 2.2.4. The mason spread a layer of mortar and then emedded the reinforcement in it by applying a slight pressure (see Fig. 3.9). Another thin layer of mortar was added on top of the first one before placing the next course. In the case of the confining plates, the total mortar joint thickness with the plates was about 1/2 inch thick. (As shown in detail "A" in Fig. 3.26, the mortar itself was kept in the nominal 3/8 inch thickness adopted for unreinforced prisms).

3.2.3.2 Group C2: Geometric Parameters: This group of specimens comprises three series each concerned with one parameter. Type S_1 mortar and GM_1 grout were used for this and kept unchanged throughout.

Series C2.1: Thirty prisms (3-course) were constructed to

Fig.3.9 CONFINING STEEL PLATES AS JOINT REINFORCEMENT

investigate the effect of the head joints (perpends) on the behaviour of ungrouted and grouted masonry under axial compression. Three different bond types, as shown in Fig. 3.10, were adopted. Type B represents a running bond whereas type C represents a stack bond. Type A was considered for comparison purpose for the case of no head joints.

Half blocks were obtained by splitting kerfed units (Type B; Fig. 2.1) through the central webs, and the edges were chipped off by the mason according to site practice. The chipped sides faced the inside and contacted the vertical mortar joints. Full bed and head joints were employed. Flush joints at both sides of the prism were adopted. The specimens were capped with gypsum-cement compound.

The test set-up is shown in Fig. 3.11. The bearing plates consisted of solid 16x8x11/2-in steel sections. Additional bearing plates were provided at top to ensure a uniform transmission of compressive stresses along the prism cross section. A spherical seat was used between the top bearing plate and the load cell in order to permit rotation at the top of the prism and thus eliminate artificial restraint stresses. Loads were applied using a 200 kip hand operated jack and were measured using a calibrated load cell installed between the jack and the spherical seat.

Mechanical gauge points were mounted on both faces of the prisms as shown in Fig. 3.10, so that the deformations in the

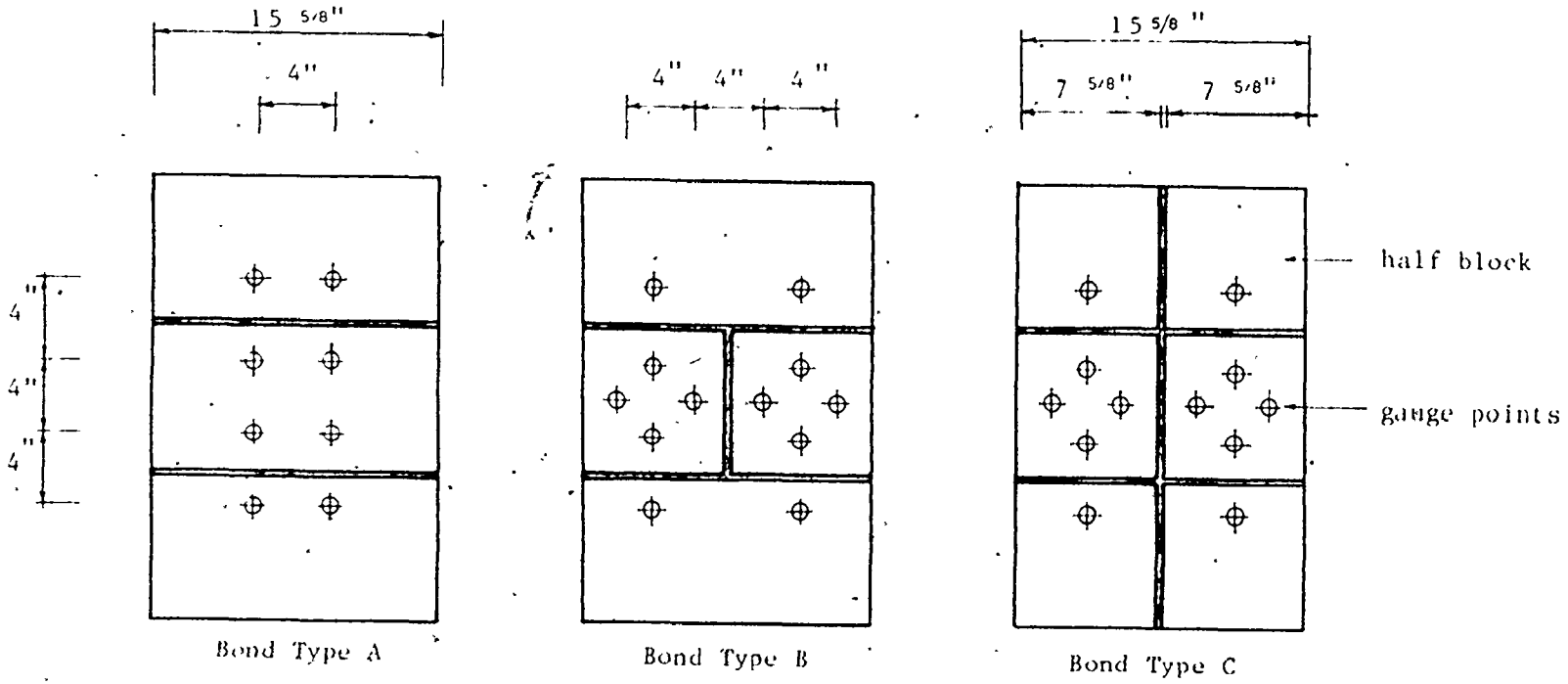

Fig. 3.10 BOND TYPES AND DEMEC POINTS ARRANGEMENTS FOR AXIALLY LOADED PRISMS (SERIES C2-1)

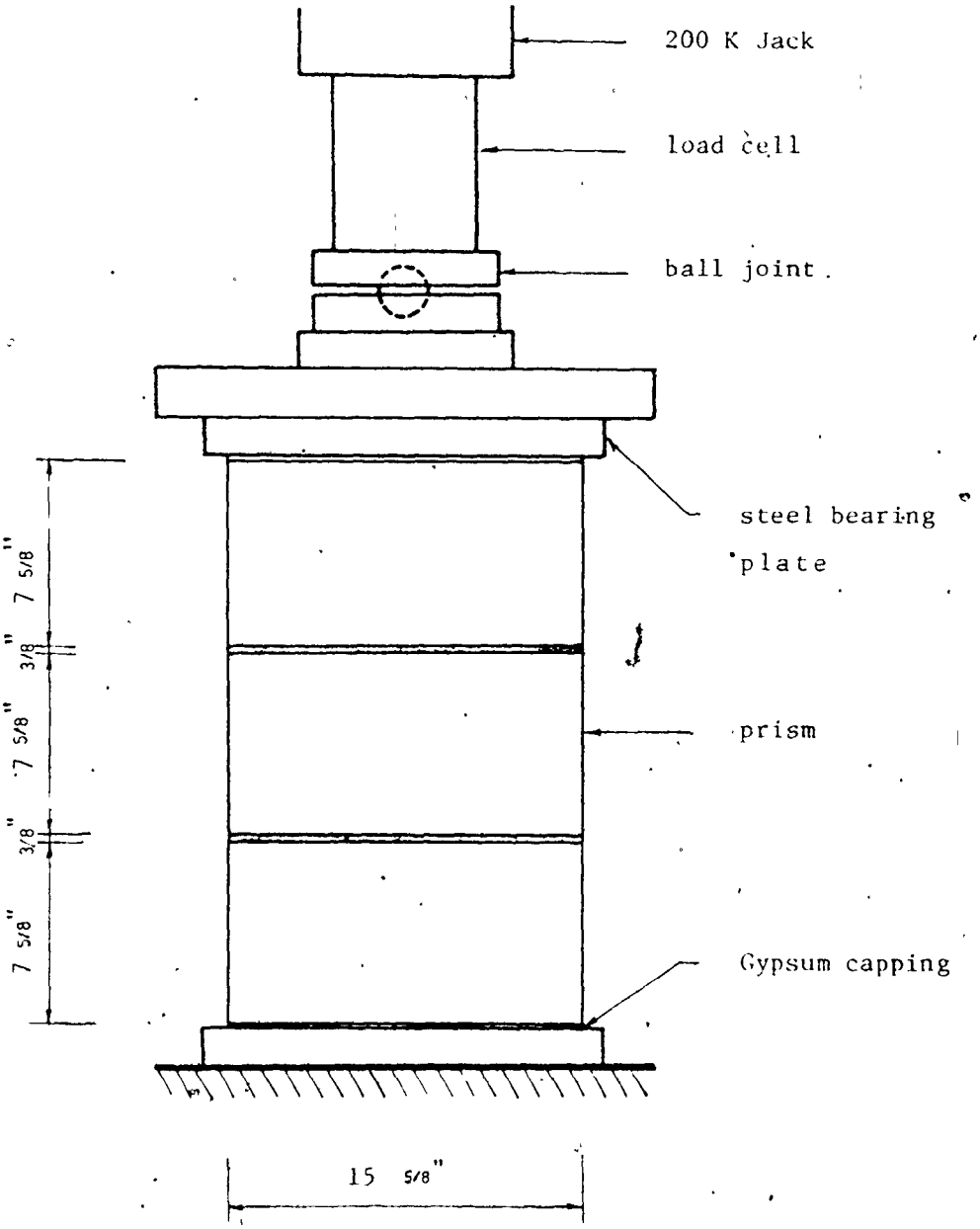

Fig. 3.11 COMPRESSION TEST SET-UP FOR 3-FULL BLOCKS PRISM

vertical direction (across the top and bottom joints and on the middle block) and in the horizontal direction (on the intermediate blocks and across the vertical joint) could be measured. Strain measurements were taken at regular load increments up to about 90% of the failure load.

Series C2-2: Fourteen prisms were tested under axial compression to investigate the effect of the joint thickness on the compression capacity and the deformation characteristics of ungrouted and grouted concrete masonry. The prisms were constructed in stack bond using 3 saw-cut half blocks shown as type B in Figs. 3.12 and 3.13. These units have different mechanical and physical characteristics from those used in the previous two series. The block dimensions are shown in Fig. 3.12. The average compressive strength from five specimens, tested flatwise and capped with sulphur, was 4670 psi (C.O.V. = 6.9%). The splitting tensile strength, based on testing five specimens, was 410 psi (C.O.V. = 4.1%).

The 3 joint thicknesses adopted were zero, 3/8 inch, and 3/4 inch. It was not feasible to achieve a full polished contact area between the two adjacent blocks, in the case for the zero mortar joint thickness. To eliminate any stress concentrations and to alleviate the difficulty of getting the blocks perfectly cut at right angles for vertical alignment, it was decided to use a very thin cement paste layer between the unit to approximately represent the case of zero joint thickness (the cube compressive

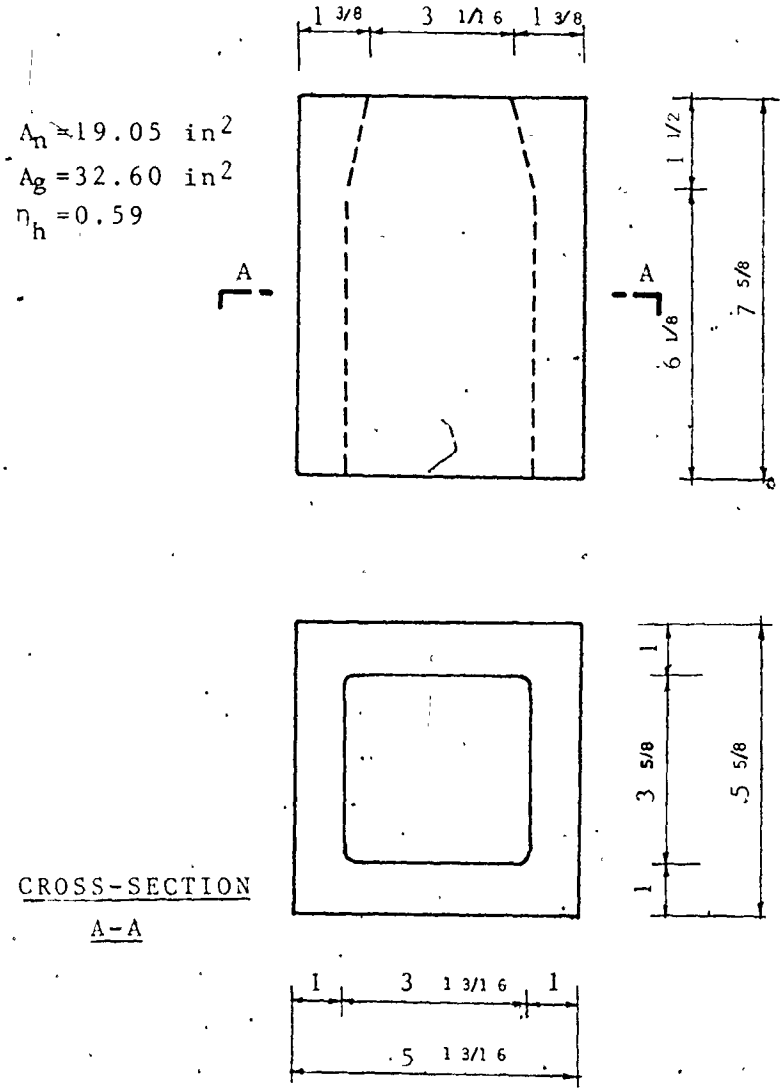

Note:All dimensions are in inches (1 in=25.4 mm)

Fig. 3.12 DIMENSIONS OF BLOCKS USED IN SERIES C2-2 (BLOCK TYPE B)

strength of the cement paste after 28 days in air curing was 6580 psi).

The ends of the prisms were capped using a sulphur compound. The mechanical gauge points arrangements and the test set-up were similar to those of series C1-1 as shown in Fig. 3.8.

Series C2-3: Six different shapes of blocks, shown in Fig. 3.13 as types A, C, D, E, F and G were used to study the effect of the core geometry on the compressive strength and the deformation characteristics of ungrouted and grouted masonry. The blocks were saw-cut by the supplier from different block types.

The following three different features of core geometry were investigated:

1. The core shape, circular and rectangular.
2. The shell thickness to width ratio for units with rectangular cores.
3. The net to gross area ratio for units with rectangular cores. Also, solid units were compared with hollow units having circular central holes.

To be able to analyze the results on a statistical basis, test repetition was considered. The basis for determining the number of replicates per each test type are discussed in Appendix A.

3.2.4 Results and Discussion of the Experimental Program.

3.2.4.1 Group C1: The experimental results of this group, which

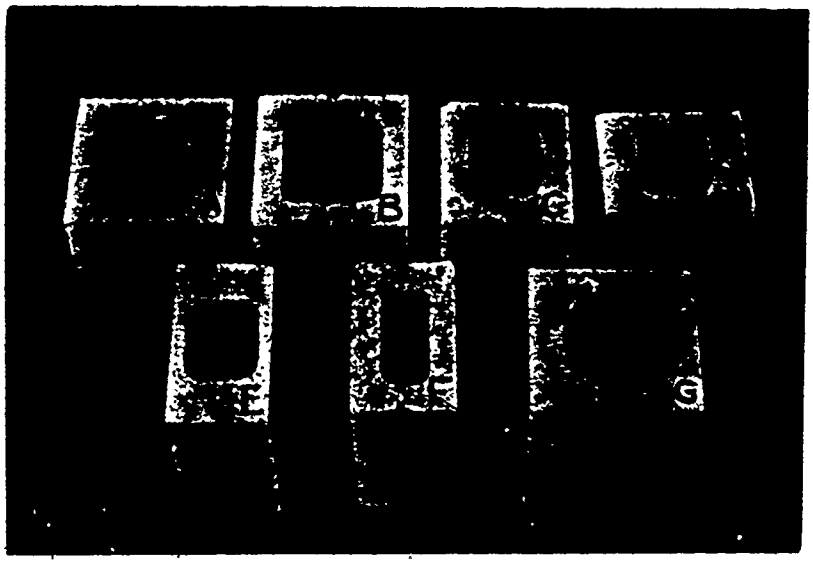

Type	Dimensions				Compressive Strength[c]	
	An[a]	Ag[a]	n	ts/w[b]	Mean (psi)	C.O.V. (%)
A	--	32.4	--	--	2370	12.7
B	19.05	32.6	0.59	0.18	4670	6.9
C	18.4	26.2	0.70	0.22	3190	3.9
D	17.0	24.8	0.69	0.16	3080	6.0
E	13.7	21.4	0.63	0.13	2920	5.4
F	15.5	21.0	0.73	0.18	2900	5.9
G	19.8	32.4	0.61	0.14	2270	8.0

Note: 1 in^2 = 645.2mm^2, 1 psi = 6.9×10^{-3} MN/m^2

a - Areas expressed in in^2
b - Minimum shell thickness to width ratio
c - Average of 5 tests

Fig. 3.12 Properties of Blocks Used in Series C2-2 and C2-3

concern the effect of the strength parameters on the behaviour of masonry prisms under axial compression, will be discussed under the following headings:

a) Modes of Failure: In Fig. 3.14, photographs of typical failures of ungrouted prisms (types S_1 and N mortars) are shown. In both cases, a splitting mode of failure originated in the central block away from the effect of the platen restraint. This behaviour is similar to the failure of solid brick masonry under axial compression, where the differential deformational characteristics of the masonry units and the mortar joints produces tensile strains in the units causing splitting failure under a tension-compression state of stress.

A somewhat similar mode of failure occurred for grouted prisms. Similar typical modes of failure are displayed in Fig. 3.15 for three prisms having weak, medium and strong grout. The consistent failure mode could be characterized as tensile splitting of the outer shells (blocks) and compression failure of the grout cores. It is suggested that the high lateral inelastic deformations of both the mortar and the grout at high stress levels are the cause of the splitting failure of the shells. The failures also originated in the central blocks free from the end confining effects. In many cases it was possible to recover the grout core intact after extensive splitting of the shell had occurred (see the photograph in Fig. 3.37). In addition, the grouted prisms showed a more gradual failure compared to the

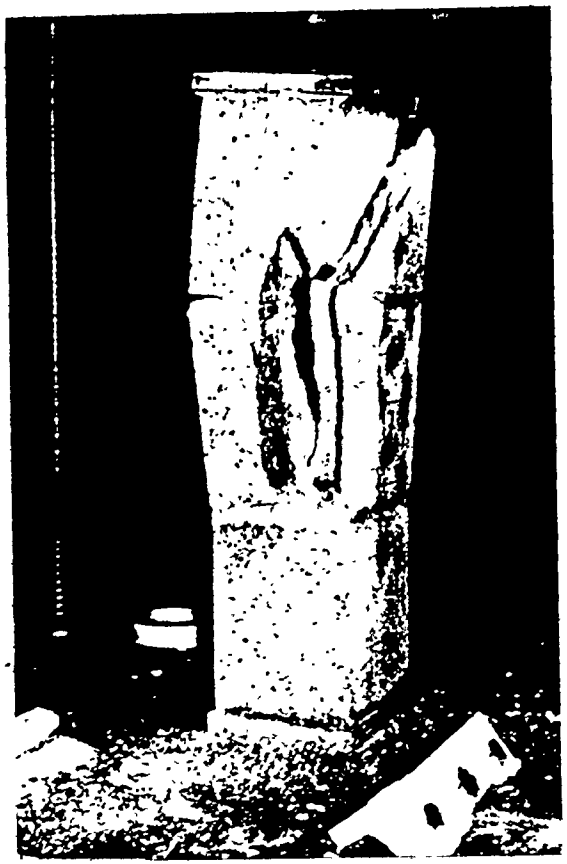

(a) Type S_1 Mortar

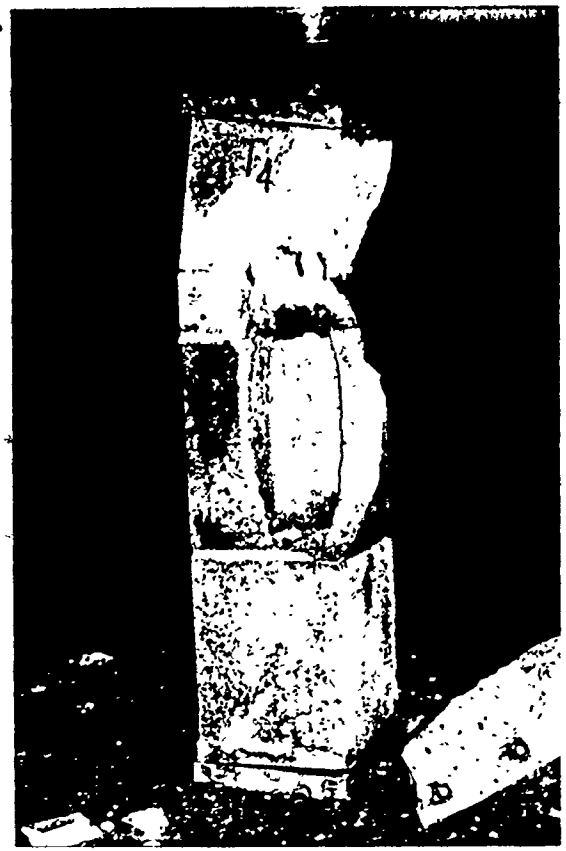

(b) Type N Mortar

Fig. 3.14 SPLITTING FAILURE OF UNGROUTED PRISMS UNDER AXIAL COMPRESSION

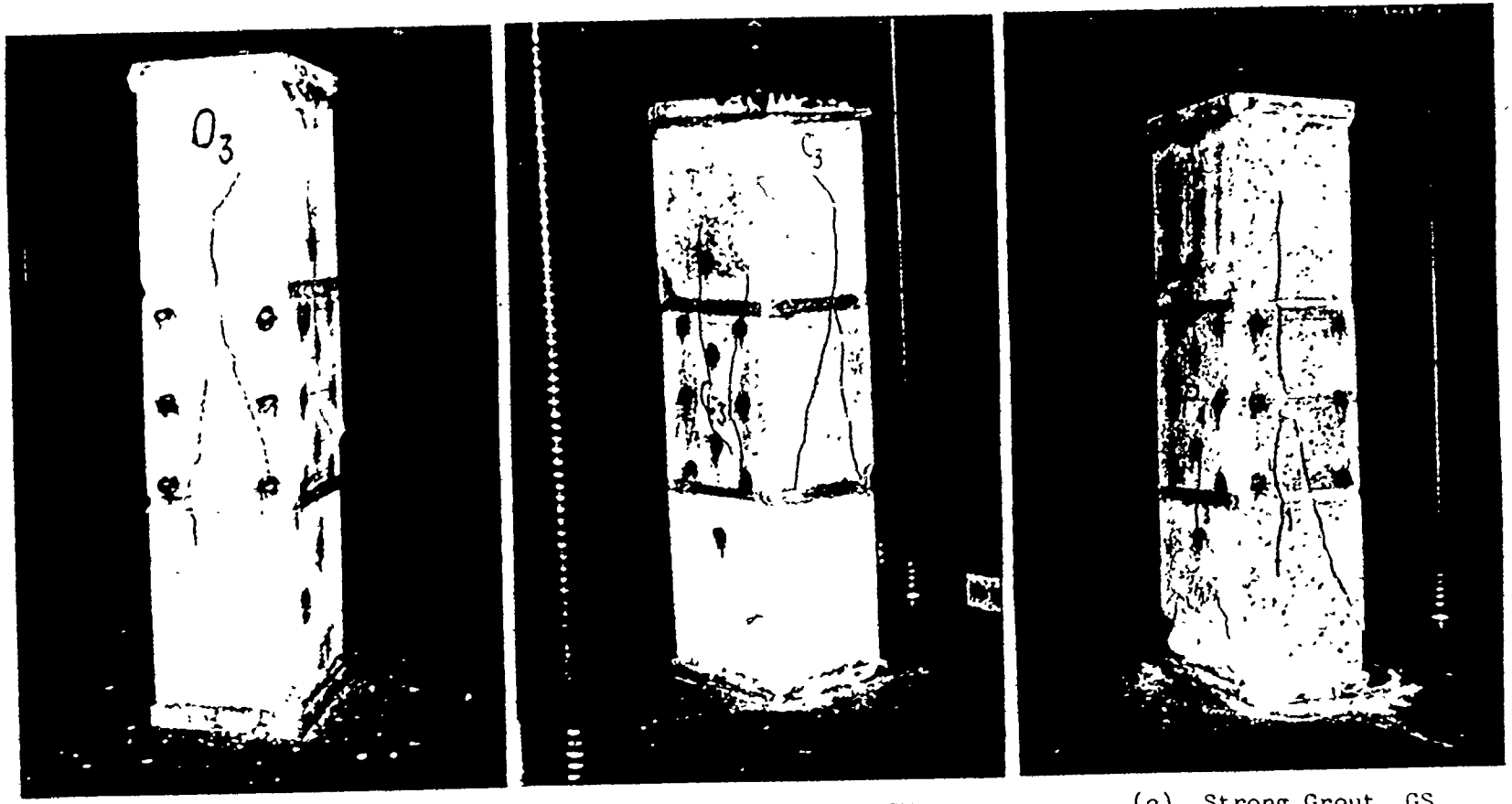

(a) Weak Grout, GW (b) Medium Grout, GM_1 (c) Strong Grout, GS

Fig. 3.15 SPLITTING FAILURE OF GROUTED PRISMS UNDER AXIAL COMPRESSION

ungrouted prisms which was sudden and explosive. [It is worth noting that the the desired failure by splitting originating in the central block was achieved thereby justifying the adoption of the chosen shape of specimen (3-course prism).]

Providing Dur-O-Wal Steel embedded in the mortar joints did not change the failure mode for either the ungrouted or the grouted prisms. The splitting mode was exhibited as shown in Fig. 3.16. Ungrouted prisms reinforced with confining steel plates behaved differently. Near failure, spalling of the outer shells of the mortar layers were observed and finally the prisms failed in shear. This shear mode of failure, shown in Fig. 3.17(a), could be attributed to the change of the stress field as the confining plates (of much higher steel percentage than the Dur-O-Wal Steel) helped to confine the lateral expansion of the mortar and consequently eliminated the lateral tensile stresses imposed on the shell which caused the splitting failure. The confining plates did not change the splitting failure mode for grouted prisms as shown in Fig. 3.17(b). This indicates that the degree of confinement provided was not enough to eliminate all the high lateral tension imposed on the shell by the expansion of the grout.

b) Effect of Grouted Cores on the Prism Compressive Strength: The compressive strengths of the prisms were calculated on the basis of the net area, A_n, for ungrouted prisms and on the basis of the gross area, A_g, for the grouted prisms.

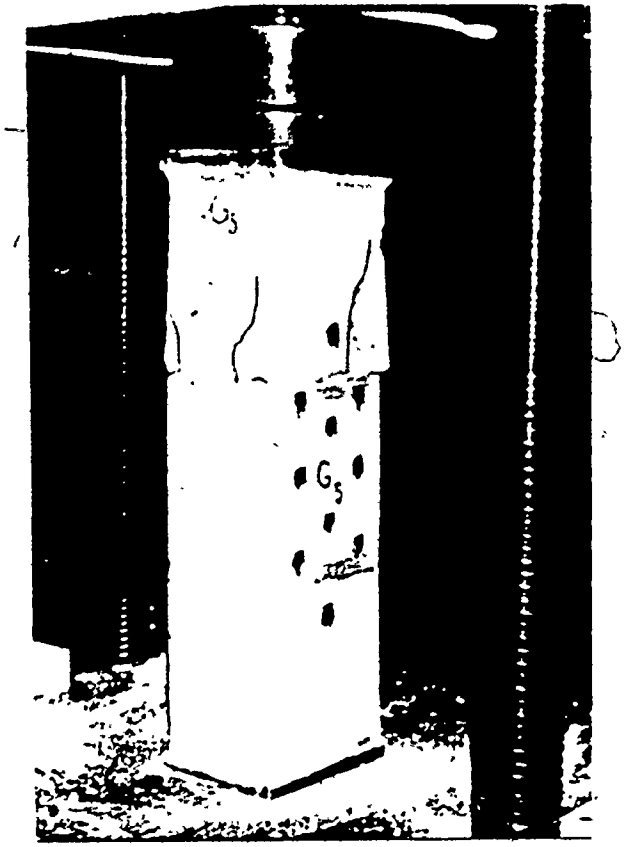

(a) Ungrouted Prism

(b) Grouted Prism

Fig. 3.16 FAILURES OF UNGROUTED AND GROUTED PRISMS REINFORCED WITH DUR-O-WAL STEEL

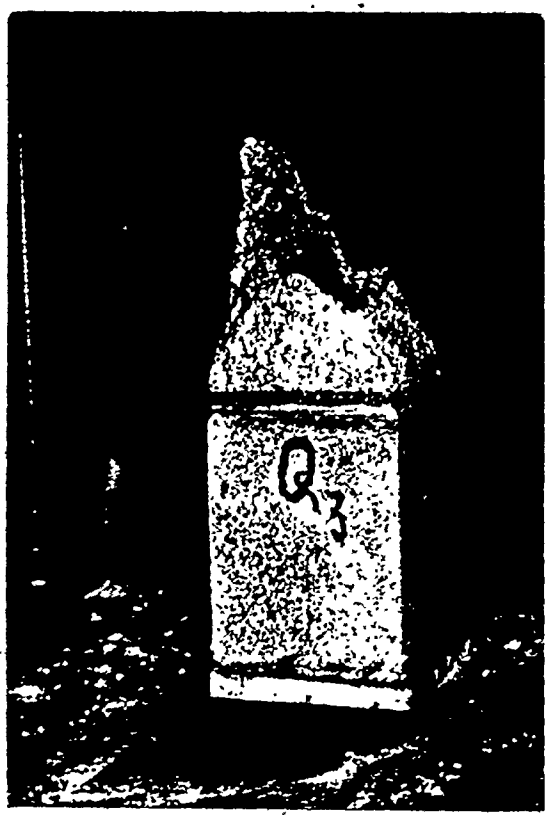

(a) Ungrouted Prism

(b) Grouted Prism

Fig. 3.17 FAILURES OF UNGROUTED AND GROUTED PRISMS REINFORCED WITH CONFINING PLATES

The results of the ungrouted and grouted prisms tests and their corresponding control specimens are listed in Tables 3.1 and 3.2, respectively.

TABLE 3.1

RESULTS OF COMPRESSION TESTS OF UNGROUTED PRISMS

Mortar Type	Mortar Strength[a] (psi)	Compressive Strength of Prisms[b]		
		Individual (psi)	Mean (psi)	C.O.V. (%)
S_1	2130	2310 2260 2430 2440 2440	2380	3.6
S_2	2640	2390 2290 2450 2290	2360	3.3
N	830	2100 2250 2190 2390	2230	5.5

NOTE: 1 psi = 6.9×10^{-3} MN/m^2

a - Compressive strength of air cured 2-in. mortar cubes
b - Based on the net area.

TABLE 3.2
RESULTS OF COMPRESSION TESTS OF GROUTED PRISMS

Grout Type	Mortar Type	Grout Strength[a] (psi)	Mortar Strength (psi)	Compressive Strength of prisms[b]		
				Individual (psi)	Mean (psi)	C.O.V. (%)
GM_1	S_1	1790	2060	1510 1550 2010 1450 1670	1640	13.6
GM_1	S_2	2050	2640	1770 1780 1670 1780	1750	3.0
GM_1	N	2050	830	1500 1600 1430 1510	1510	3.3
GM_2	S_1	2500	2290	1820 1860 2060 1760 1780	1860	6.4
GM_3	S_1	3630	1960	2110 1960 1780 1900	1940	7.2
GW	S_1	2040	1960	1770 1780 1670 1780	1750	3.0
GS	S_1	5550	1970	1980 2310 2280 2240	2200	6.9

NOTE: 1 psi = 6.9×10^{-3} MN/m^2

a - Unconfined compressive strength of grout as calculated from block moulded prisms

b - Based on the gross areas.

Fig. 3.18 shows the results of grouted prism strengths in terms of the compressive strength of the grout (calculated from block moulded prism strength) for the S_1 mortar. The most striking feature to be noted is that compressive strengths of the grouted prisms were all less than the strength of the ungrouted prism, f'_{mun}, which is also indicated in the figure, even for grouts having higher strengths than the block. Apparently, little increase in prism strength was achieved with large increases in grout strength. This indicates that the strength superposition concept highly overestimates the compression capacity especially for high strength grout. In fact, if the individual strength of ungrouted masonry, f'_{mun}, and the grout, σ_{cg}, are linearly combined as shown by the dashed line in Fig. 3.18, the extent to which superposition is not valid is even more obvious. This finding contradicts the commonly held opinion that design strength values may be efficiently increased by increasing the grout strength.

It is suggested that at high stresses in the grout, the resulting inelastic deformations in the horizontal direction (due to the development of microcracking) produce high bilateral tensile stresses in the outer shell as it tends to confine the grout. These tensile stresses in combination with the vertical compressive stress could be the cause of a premature splitting failure of the block under a state of biaxial compression-tension stress. (See the analytical investigation in Section 3.3.3). In fact, comparing the stress-strain relationship for the grout,

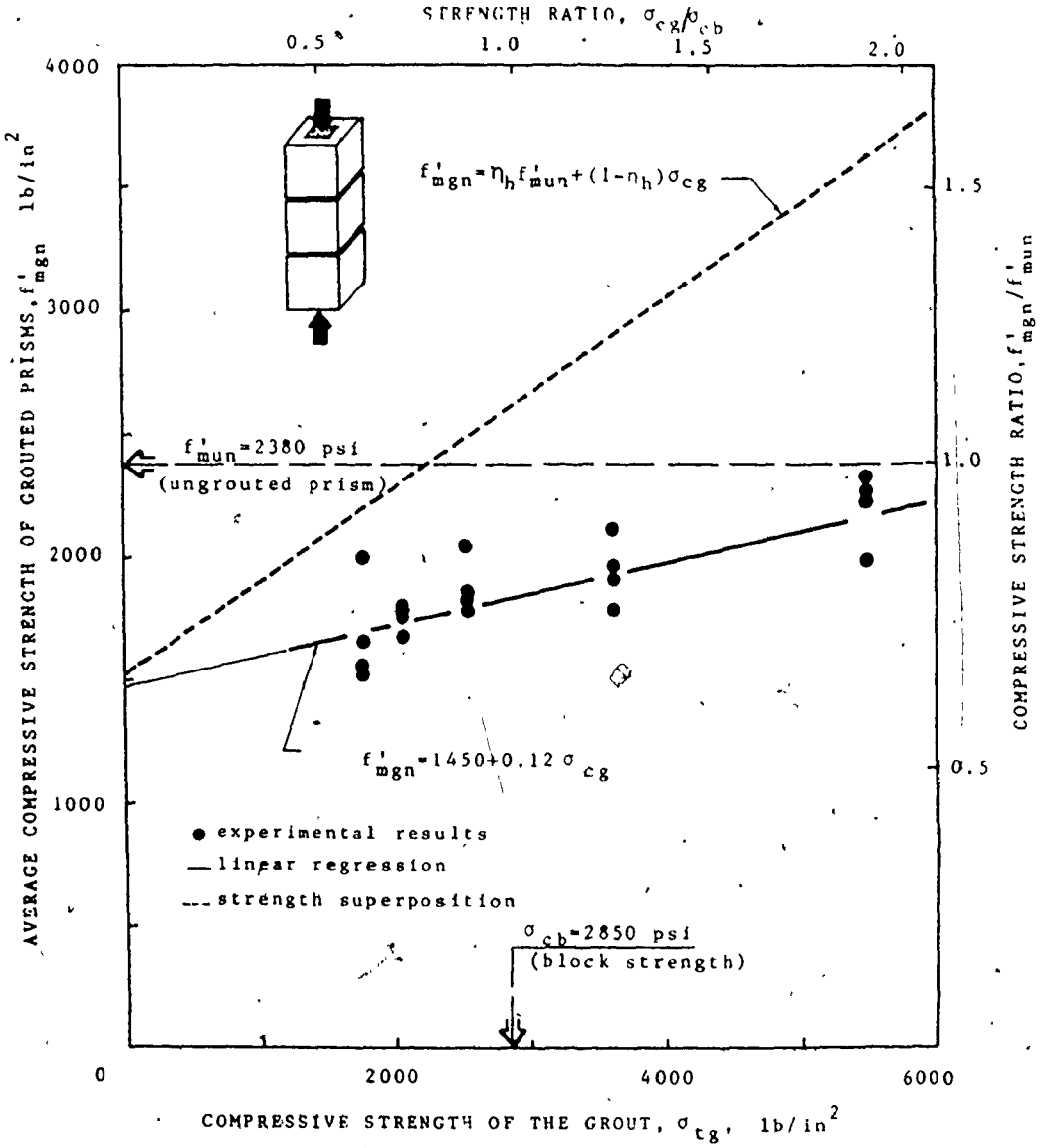

Fig. 3.18 GROUTED PRISM STRENGTH VERSUS GROUT STRENGTH (TYPE S_1 MORTAR)

presented in Fig. 3.19, and that for the block, shown in Fig. 2.4, illustrates this behaviour more clearly. At any strain level, the load will be shared by the shell and the grouted cores in proportion to their axial stiffness (compatibility of deformation in the vertical direction). At a strain nearly equals to 0.002 in/in the grout would reach its unconfined strength, at which high lateral deformations occur. At such a strain level, the block is capable of accommodating more load, as its strain at maximum stress is 0.0036 in/in, and hence it acts to confine the grout. Failure occurs when the blocks are no longer capable of confining the grout (and the mortar as well). This study of the deformation characteristics of the block and the grout indicates that matching the components' strengths to achieve higher strength of the composite is not efficient and it is more appropriate to match the strain at the ultimate load for the components. Under this condition, the ultimate stress of each component would be developed simultaneously. Consequently, the full efficiency of the components could be achieved and the superposition of the components' strengths will then be valid.

Using a linear regression analysis, the compressive strength of the grouted prisms, f'_{mgn}, (in psi) can be expressed in terms of the grout strength, σ_{cg}, as:

$$f'_{mgn} = 1450 + 0.12\ \sigma_{cg} \qquad \ldots\ (3.1)$$

This empirical relationship was developed using the data of the

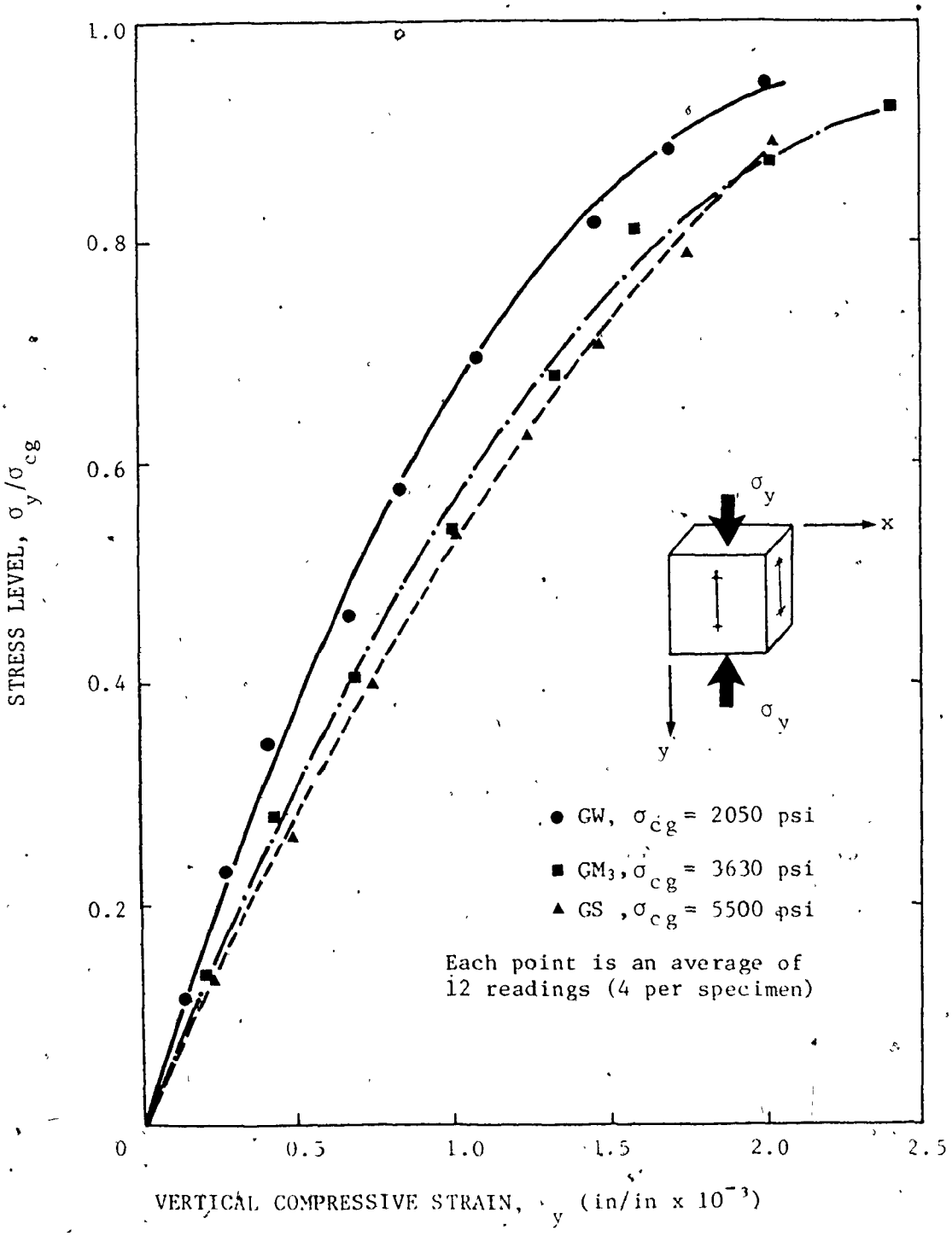

Fig. 3.19 STRESS-STRAIN RELATIONSHIPS OF DIFFERENT BLOCK MOULDED GROUT PRISMS UNDER AXIAL COMPRESSION

grouted prisms. However, the strength of the ungrouted prism could also predicted by the same expression when $\sigma_{cg} = 0$ on the basis of the gross area. This confirms the proposed formula which can be expressed in a normalized form as:

$$\frac{f'_{mgn}}{f'_{mun}} = 0.61 + 0.143 \frac{\sigma_{cg}}{\sigma_{cb}} \qquad \ldots\ (3.2\text{-a})$$

considering that the net to gross area ratio of the block, η_h, equals 0.62, the above equation can be rewritten in the form:

$$\frac{f'_{mgn}}{f'_{mun}} = \eta_h + 0.143 \frac{\sigma_{cg}}{\sigma_{cb}} \qquad \ldots\ (3.2\text{-b})$$

Equation (3.2-b) indicates that the reduction in the compressive strength associated with grouting is a function of the net to the gross area ratio, η_h, which is a geometric characteristic of the block. If one considers f'_{mgn}/f'_{mun} as an efficiency coefficient, then it can be seen that higher grout strengths and/or higher η_h, ratios result in higher efficiency coefficients.

It has to be noted that Equation (3.1) was obtained using one block size and a single strength of concrete block. However, as long as the components materials are of the same ranges of strengths and geometric characteristics used in this investigation, Equation (3.2) could be used as an empirical

equation to assess the compressive strength of grouted concrete masonry.

c) Effects of Mortar Type on the Prism Compressive Strength: Fig. 3.20 shows the variation of the compressive strength of ungrouted and grouted prism for different strengths of mortar cubes. The results indicate that the mortar strength (within the range considered for types S and N) has little effect on the compressive strength of either ungrouted or grouted prisms.

This trend of little increase in the ungrouted prism strength with high increases in mortar strength is different from that observed for brick masonry under axial compression. The results of a structural Clay Research Foundation Study[54] show that the prism strength using type S mortar is reduced by about 29% using type N mortar. This difference in behaviour between block and brick masonry (from the viewpoint of the effect of the mortar strength) could be attributed to the fact that it is the mortar strength relative to that of the masonry unit which affects the assemblage compression capacity and not the absolute value of the mortar strength[31,47,48]. The lower the mortar-masonry unit strength ratio is, the less is the compressive strength[33]. It is evident that the difference in the deformational characteristics of the mortar and the units, which may be taken more or less as a function of the strength ratio, creates tensile lateral stresses in the units which govern the failure

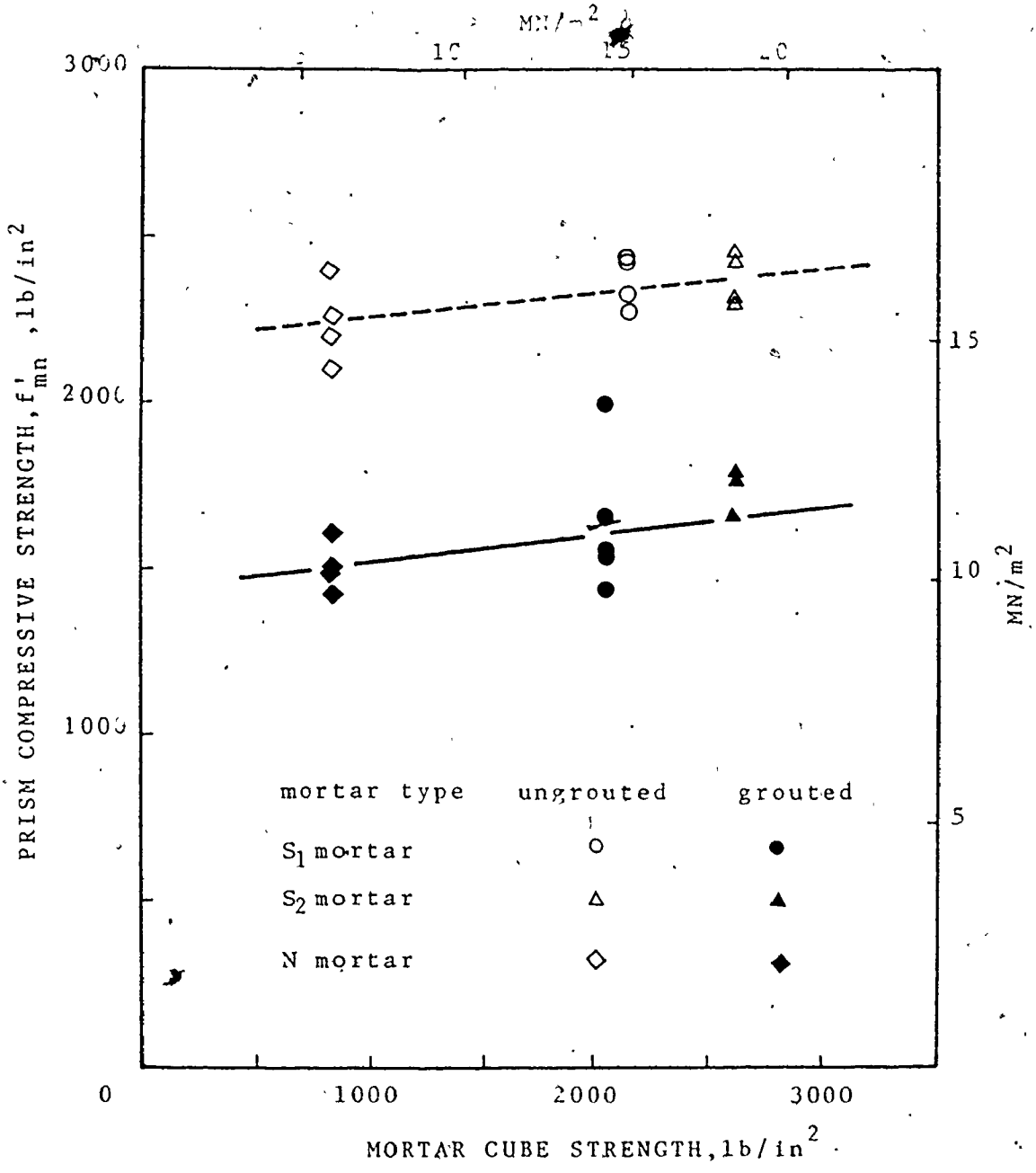

Fig. 3.20 PRISM COMPRESSIVE STRENGTH VERSUS MORTAR STRENGTH

condition[24,31,33]. Because brick units are much stronger than the blocks (about 2-6 times), it is expected that the mortar strength would more efficiently influence the compressive strength of brickwork.

Williams's[56] experimental results of solid concrete masonry prisms showed little increase in the prism strength with high increases in the mortar strength. This confirms the behaviour shown from the current results.

d) Effect of Joint Reinforcement on the Prism Compressive Strength: The test results for ungrouted and grouted reinforced prisms are presented in Table 3.3. The contribution of the reinforcement towards the increase in the prism compressive strength is indicated as an efficiency coefficient which is the compressive strength of the reinforced prism to that of a similar unreinforced specimen.

It is shown that the Dur-O-Wal steel did not provide a significant contribution towards increasing the capacities of either the ungrouted or grouted prisms. It is felt that the percentage of steel (0.08%) was so small that it could not help in confining the lateral deformations of the mortar and the grout. Williams[56] came to a similar conclusion as a result of testing solid block masonry prisms having joint reinforced with a wire mesh type of reinforcement.

Confining plates showed a considerable contribution towards

TABLE 3.3

TEST RESULTS OF REINFORCED PRISMS UNDER AXIAL COMPRESSION
(SERIES C1-3)

Type of Reinf.	Prism Type	Mortar Strength[a] (psi)	Grout Strength[b] (psi)	Prism Compressive Strength			Eff. Coeff.[c]
				Indv. (psi)	Mean (psi)	C.O.V. (%)	
Dur-O-Wal Steel	ungrouted	1860		2400 2450 2420	2420	1.1	1.02
	Grouted, GM_1	1860	1940	1840 1660 1700	1730	5.2	1.05
Confining plates	ungrouted	1960		2740 2490 2530 2500	2570	4.6	1.08
	Grouted, GM_1	1860	1940	2070 1830 1900 1920	1030	5.2	1.18

NOTE: 1 psi = 6.9×10^{-3} MN/m^2

a - Compressive strength of air cured 2-in mortar cubes
b - Unconfined compressive strength of grout as calculated from block moulded prisms
c - Efficiency coefficient calculated as the ratio of the compressive strength of the reinforced prism to that of a similar unreinforced specimen

the increase of the compressive strength. Higher efficiency was shown in the case of grouted prisms compared to that achieved for ungrouted specimens (an efficiency coefficient of 1.18 was achieved for grouted prisms versus 1.08 for ungrouted specimens). It seems that the confining plates helped to confine the lateral deformations of the mortar and grout as is evidented from the change of the mode of failure from splitting to shear failure. The elimination of the tensile strains imposed on the blocks in the case of unreinforced specimens was the major factor in increasing the compression capacity. The higher efficiency shown in the case of grouted prisms indicates that the confining plates not only helped to confine the mortar joint, but also contributed in confining the grout.

Of passing interest is the correlation between the mode of failure and the compression capacity of ungrouted masonry prisms. Those exhibiting a shear mode of failure (as in case of confining plates) showed higher compression capacity whereas for those exhibiting a splitting failure (as in case of Dur-O-Wal Steel), no significant contribution towards the increase in the capacity was achieved.

Priestley and Brigeman[44] included confining steel plates in the bottom few mortar courses at the end of brick masonry walls tested under slow cyclic lateral loading. The steel plates helped to confine the crushing zone and thus, eliminated the vertical tension cracks in the brick. This behaviour is somewhat similar

to that obtained in the current program with axially loaded prisms reinforced with confining plates.

e) Deformational Characteristics: The relationships for stress to vertical strain and to lateral strain for the compression prisms are shown in Figs. 3.21 and 3.22, respectively. It can be seen that the grouted prisms had less axial stiffness and exhibited larger tension strains compared to the ungrouted prisms. This behaviour is especially noticeable at high stress levels. Since the loading conditions assures that uniform axial strains are imposed on both the outer shell and the grouted core, it would usually be considered that the compression load would be shared in proportion to their axial stiffnesses. Compared to the test results of the ungrouted prism, the prism with weak grout, GW, (σ_{cg} = 2040 psi) exhibited large lateral strains at lower stress levels. A large increase in the grout strength (σ_{cg} = 5500 psi), using strong grout, GS, resulted in a vertical stress-strain behaviour (σ_y - ε_y) approaching that of the ungrouted prism. Therefore, it might be assumed that the axial strength of the outer shell is near to being developed and is the controlling factor. However, when the corresponding lateral strains are reviewed, Fig. 3.22, a different behaviour is very apparent. At stresses above approximately 40% of the strength of the ungrouted prisms, the grouted prisms exhibited comparatively large lateral strains. Although it was usually difficult to differentiate between the failure modes for the ungrouted and grouted prisms

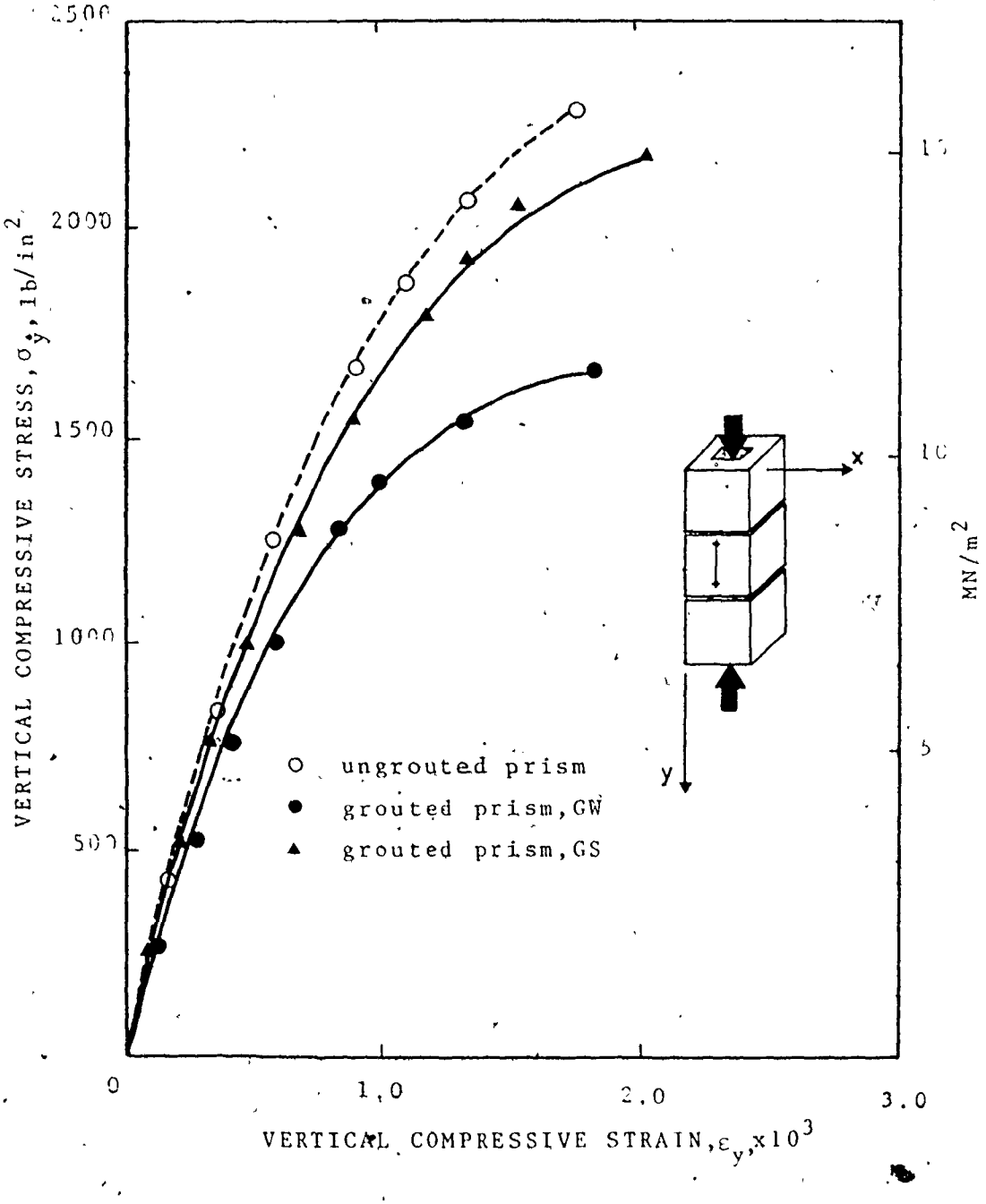

Fig. 3.21 STRESS-VERTICAL STRAIN RELATIONSHIPS FOR AXIALLY LOADED PRISMS

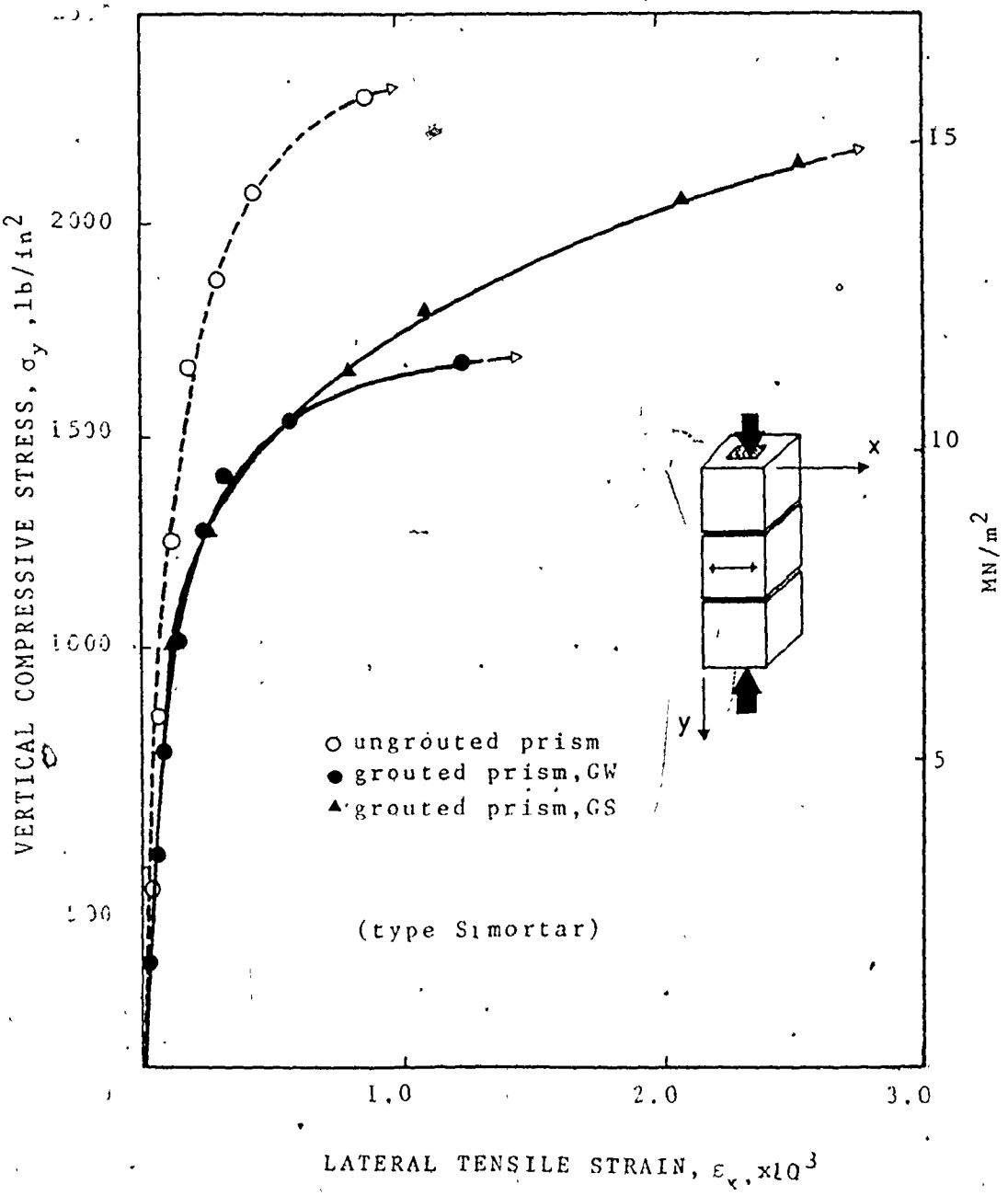

Fig. 3.22 STRESS-LATERAL STRAIN RELATIONSHIPS FOR AXIALLY LOADED PRISMS

(both exhibited a splitting mode of failure), these lateral strain measurements provide a key to understanding the failure mechanism.

As discussed before, the high inelastic deformations of the grouted cores when approaching their unconfined strength produced high bilateral tensile stresses in the outer shell as it tended to confine the grout. These tensile stresses in combination with the vertical compressive stresses caused a premature splitting failure of the block under a compression-tension state of stress. This phenomenon will be a central concept in proposing a failure criterion for grouted masonry under axial compression (see section 3.3.3.4).

Figures 3.23 and 3.24 show the different stress-strain relationships for deformations measured on the block compared to those measured across the joint for ungrouted and grouted prisms for types S_1 and N mortars, respectively. For ungrouted prisms, the vertical strains measured across the joint using a 4 inch gauge length were greater than corresponding strains taken within the height of the central block. However, for grouted prisms, these strains were quite close. It would seem that the continuity provided by the grout reduces the significance of the characteristics of the mortar joint on the behaviour of grouted masonry under axial compression. From a comparison of the results for the two mortar types, it can be seen that the same trend is evident. Figures 3.23 and 3.24 also indicate that for ungrouted prisms, the difference for deformation across the joint compared

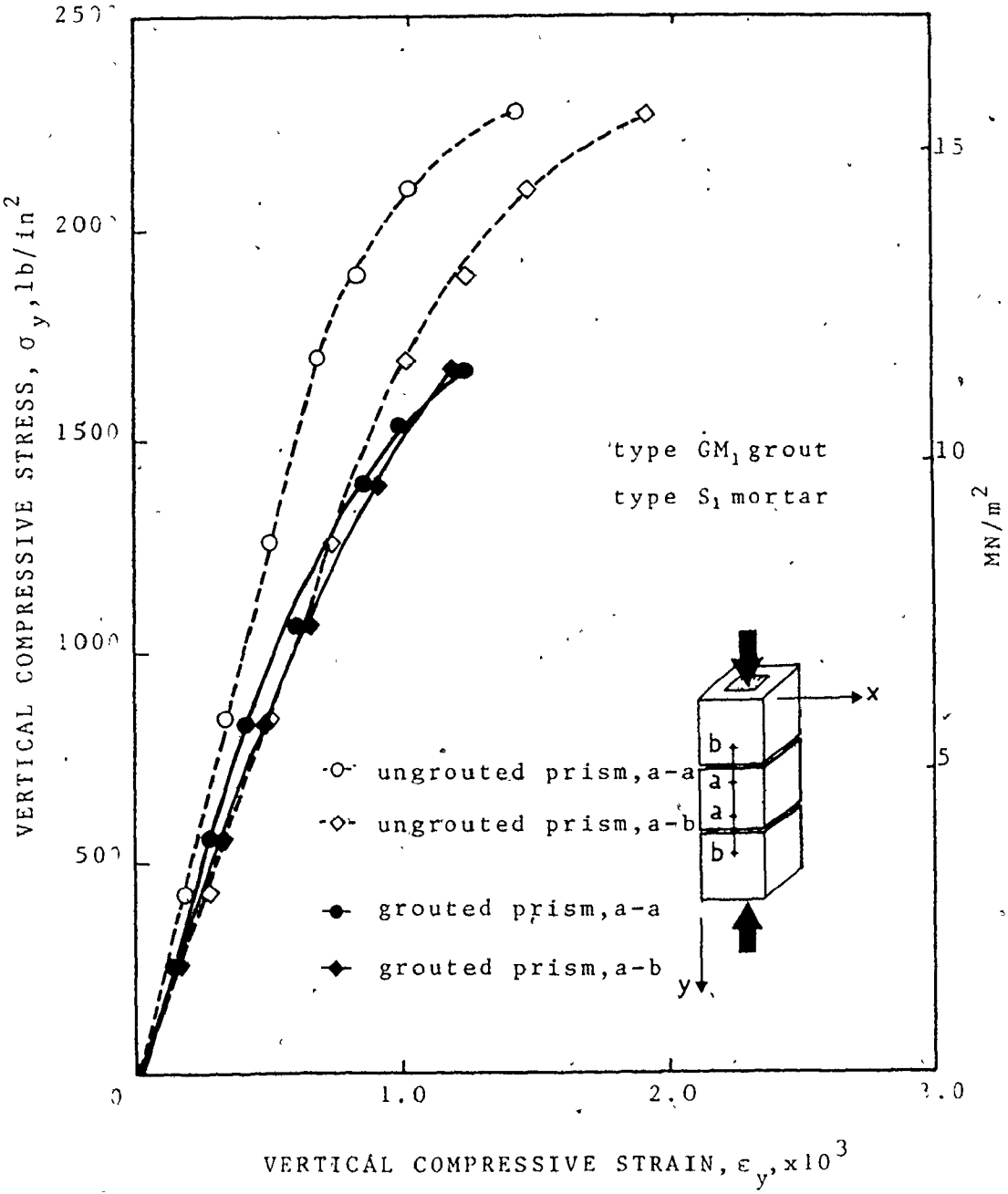

Fig. 3.23 DEFORMATIONS ON BLOCKS AND ACROSS THE JOINTS OF AXIALLY LOADED PRISMS (TYPE S_1 MORTAR)

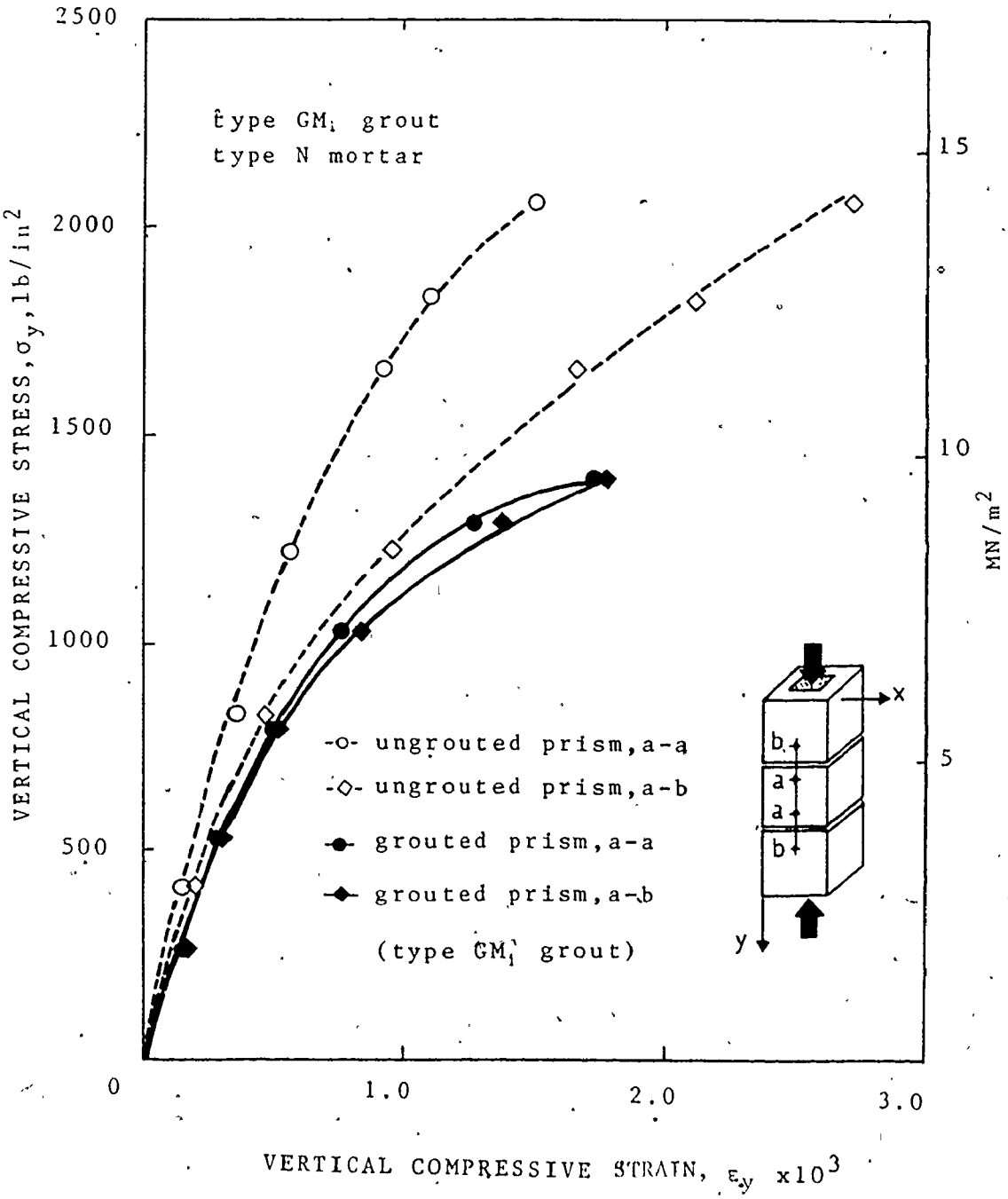

Fig. 3.24 DEFORMATIONS ON BLOCKS AND ACROSS THE JOINTS OF AXIALLY LOADED PRISMS (TYPE N MORTAR)

to that on the block are higher for type N mortar than for type S_1 mortar.

From the deformations measured across the joint and on the block presented in Fig. 3.23, the deformation within the mortar joint could be determined assuming that the superposition of deformations is valid. Referring to the sketch shown in Fig. 3.23, the deformation within the joint, Δ_m, can be expressed as:

$$\Delta_m = \Delta_{b-a} - \Delta_{a-a} \left(\frac{1-t_m}{1}\right) \quad \ldots\ldots (3.3)$$

where Δ_{b-a} is the deformation measured across the joint, Δ_{a-a} is the deformation measured on the block, and 1 is the gauge length (4 inches). The mortar compressive strain, ε_m, is

$$\varepsilon_m = \frac{\Delta_m}{t_m} = \frac{\Delta_{b-a} - \Delta_{a-a}\left(\frac{1-t_m}{1}\right)}{t_m} \quad \ldots\ldots (3.4)$$

The resulting stress-strain curves for the S_1 and N mortar joints are shown in Figs. 3.25 and 3.26. It is interesting to observe that the mortar strain at failure exceeded its maximum strain under uniaxial compression determined from testing mortar cylinders. (The strain at failure of mortar cylinders ranges from 0.002 to 0.003 in/in[2,31]). This is attributed to the fact that higher deformations could be accommodated under a triaxial compression state of stress which is the case for mortar joints in

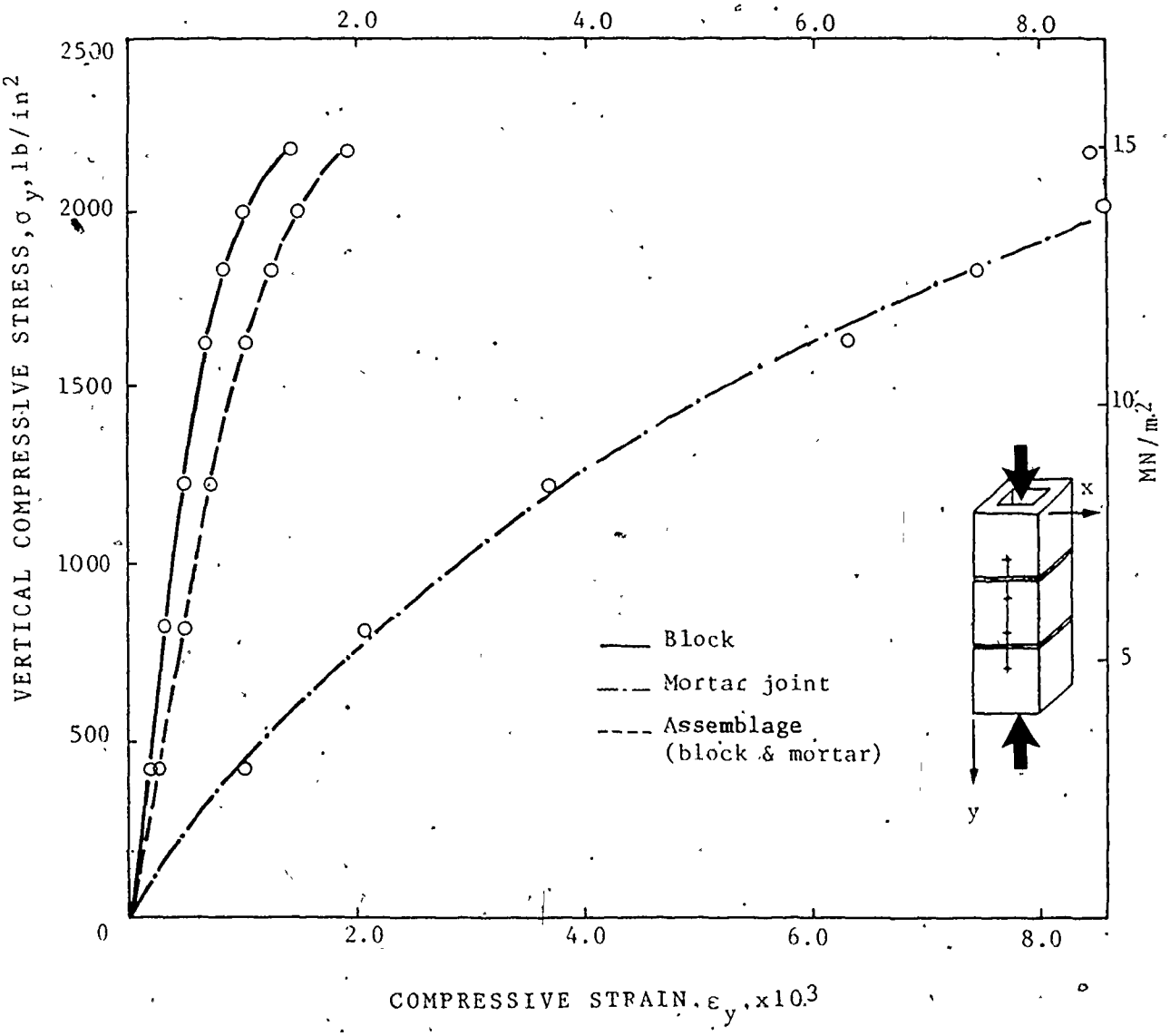

Fig. 3.25 STRESS-STRAIN RELATIONSHIPS OF UNGROUTED MASONRY UNDER AXIAL COMPRESSION (Type S_1 mortar)

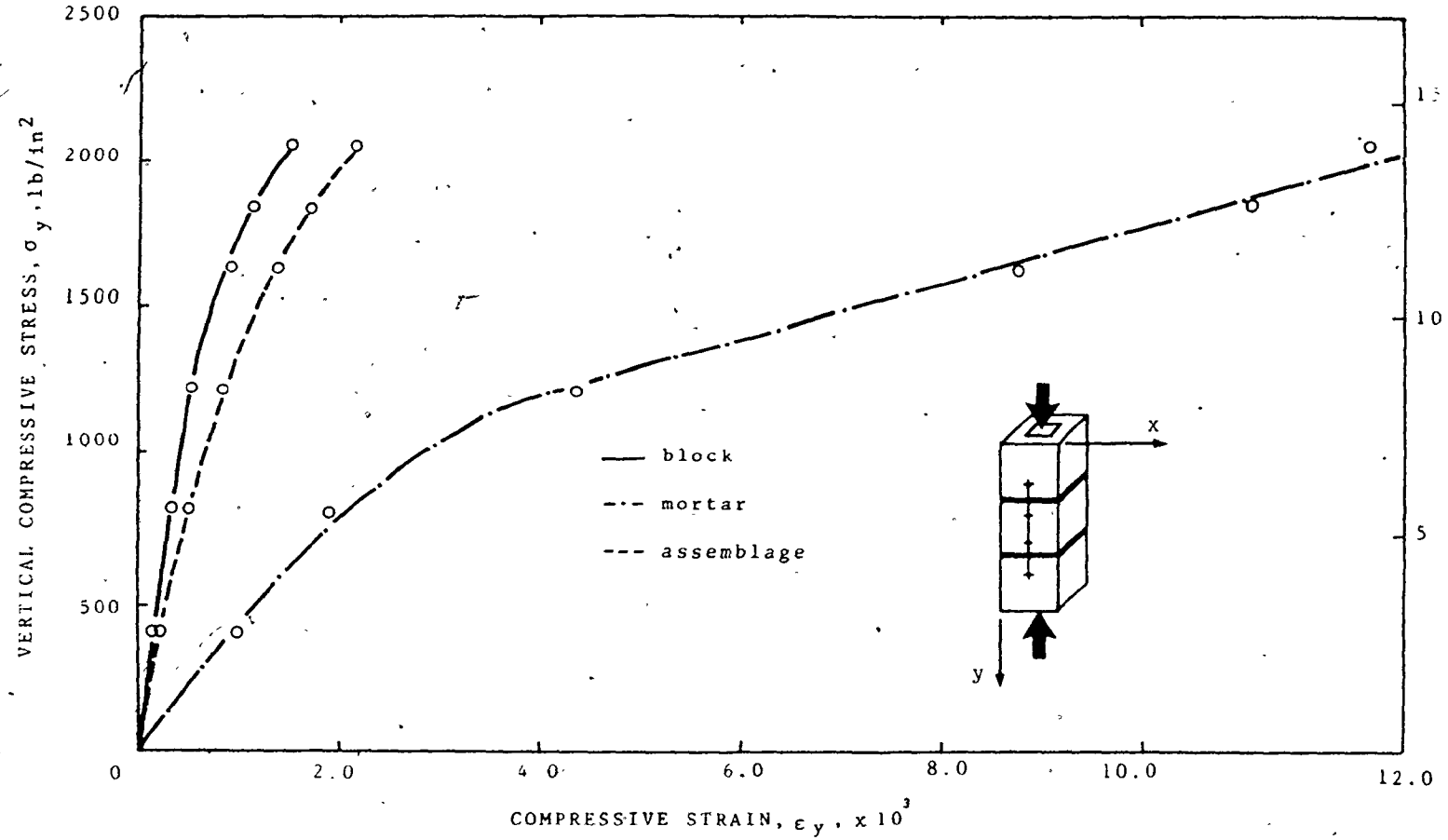

Fig. 3.26 STRESS-STRAIN RELATIONSHIPS OF UNGROUTED MASONRY PRISMS UNDER AXIAL COMPRESSION (TYPE N MORTAR)

axailly loaded masonry assemblages. It is also shown that the joint stiffness, at high stress levels, did not reduce stubstantially as is the case under uniaxial compression. Nearly constant stiffness was exhibited from about 0.6 of the ultimate stress to failure. The confining stresses imposed on the mortar joints, as described previously, help to increase the mortar stiffness.

From the mortar joint deformation, ε_m (as calculated from Equation (3.4)) and the block deformation, ε_b (as determined directly from strain measurements on blocks), the assemblage strain, ε_a, can be calculated as,

$$\varepsilon_a = \frac{\varepsilon_m \cdot t_m + \varepsilon_b \cdot t_b}{t_m + t_b} \qquad \ldots\ldots (3.5)$$

The resulting stress-strain relationships for ungrouted masonry prisms are shown, respectively, in Figs. 3.25 and 3.26 for types S_1 and N mortar.

Fig. 3.27 shows the variation of the modulus of elasticity compared to the compressive strength for ungrouted and grouted prisms for types S_1 and N mortar. The modulus of elasticity is based on the secant modulus at 50% of the strength. It is shown that there is no direct correlation between the modulus of elasticity and the compressive strength as the parameters affecting these two characteristics are not the same. At failure, the interactions of the blocks, mortar, and grout associated with

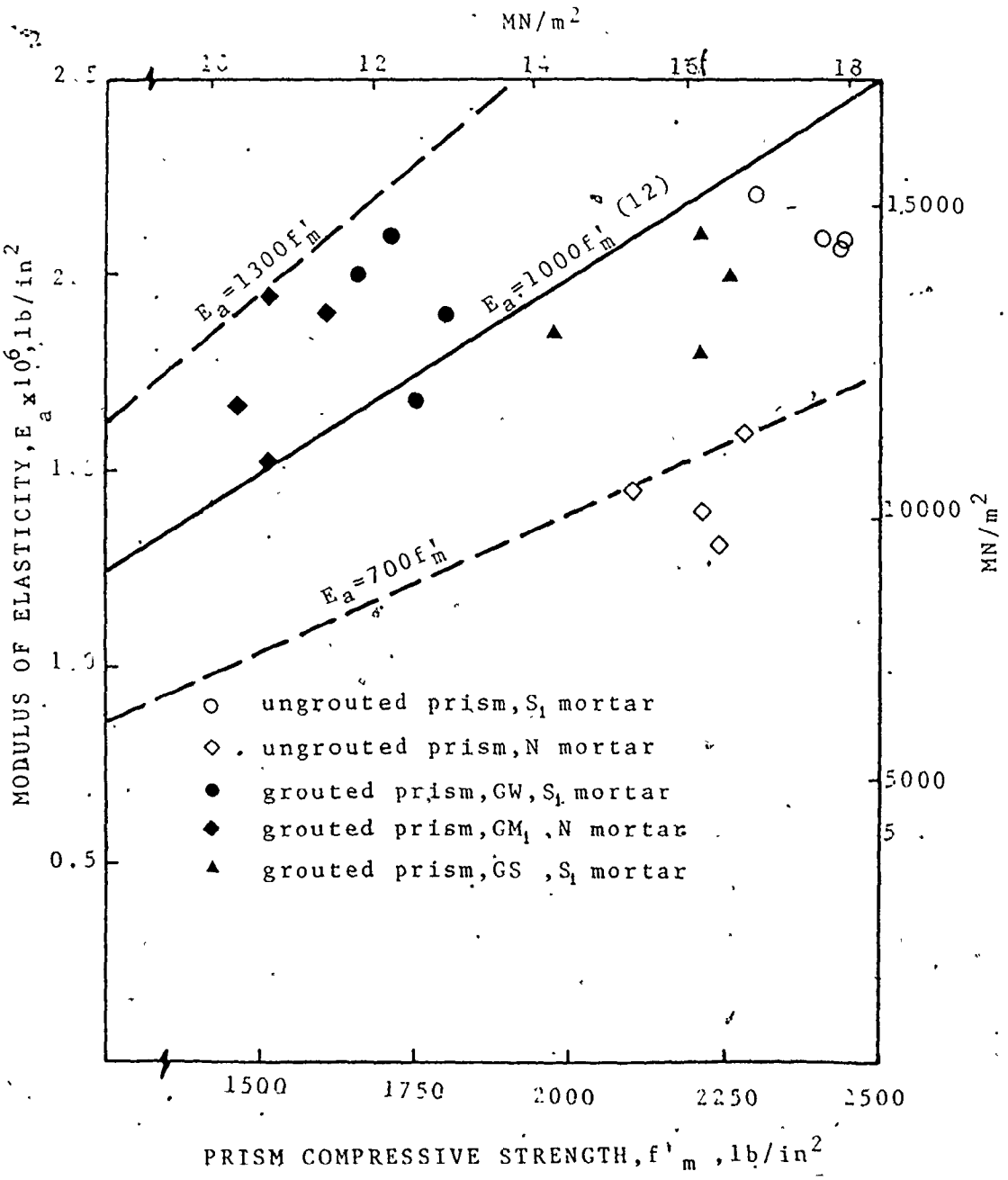

Fig. 3.27 MODULUS OF ELASTICITY VERSUS COMPRESSIVE STRENGTH OF PRISMS

the high inelastic deformations create complex states of stress which are different from those at early stages of loading. For example, the mortar shifts from uniaxial compression at low stress levels (assuming that Poisson's ratio of the block and the mortar is the same) to triaxial compression at high stress levels exceeding its unconfined compressive strength. While it is possible to get a strong correlation between the strength and the stiffness for isotropic homogeneous material, it is rather difficult to achieve this correlation for an anisotropic nonhomogeneous material such as masonry, which has two or three component materials of different deformation characteristics. Fig. 3.27 shows that the formula $E_a = 1000\ f'_m$, currently recommended by the codes[12,27] significantly overestimates the elastic modulus of ungrouted masonry constructed with type N mortar. (It was shown previously that while the mortar type significantly influence the deformation characteristics, it was of no pronounced effect on the compressive strength). For type S_1 mortar the formula seems to overestimate the stiffness for ungrouted masonry and for grouted masonry of high strength grout, while it underestimates the stiffness of grouted masonry having low strength grout. As discussed before, the weak grout causes a premature splitting failure and a reduction of the compressive strength while, under low stress levels where the applied stress does not exceed its compressive strength, it has relatively less effect in reducing the structure's stiffness. Fig. 3.27 also

shows that the formulas $E_a = 700\ f'_m$ and $E_a = 1300\ f'_m$ give lower and upper limits of the experimental results, respectively.

Fig. 3.28 shows the effect of confining plates on the deformation characteristics of ungrouted and grouted prisms under axial compression. The stress-lateral strain relationships show that confining plates significantly reduced the lateral tension strains imposed on the block due to the lateral restraint of the plates, especially at high stress levels. Its effect was more significant in the case of grouted prisms where the lateral expansion of the grout causes higher tension to be imposed on the block. Because the concrete block is a brittle material, it is highly sensitive to the tension stresses and thereby less tension results in higher compression loading to cause failure. This indicates the the confining plates would be more efficient in increasing the compressive strength in the case of grouted masonry. This explanation of deformational behaviour is consistent with the compressive strength results presented in Table 3.3.

3.2.4.2 Group C2: This group comprises three different series, each concerned with one geometric parameter. The results of each series will be discussed in the following three sections:

a) Series C2-1: Effect of Bond Type: The test results for this series and their corresponding control specimens are listed in Table 3.4. Comparison of the compressive strengths of the prisms indicates that there is no significant effect of the bond type on the prism compression capacity for ungrouted and grouted

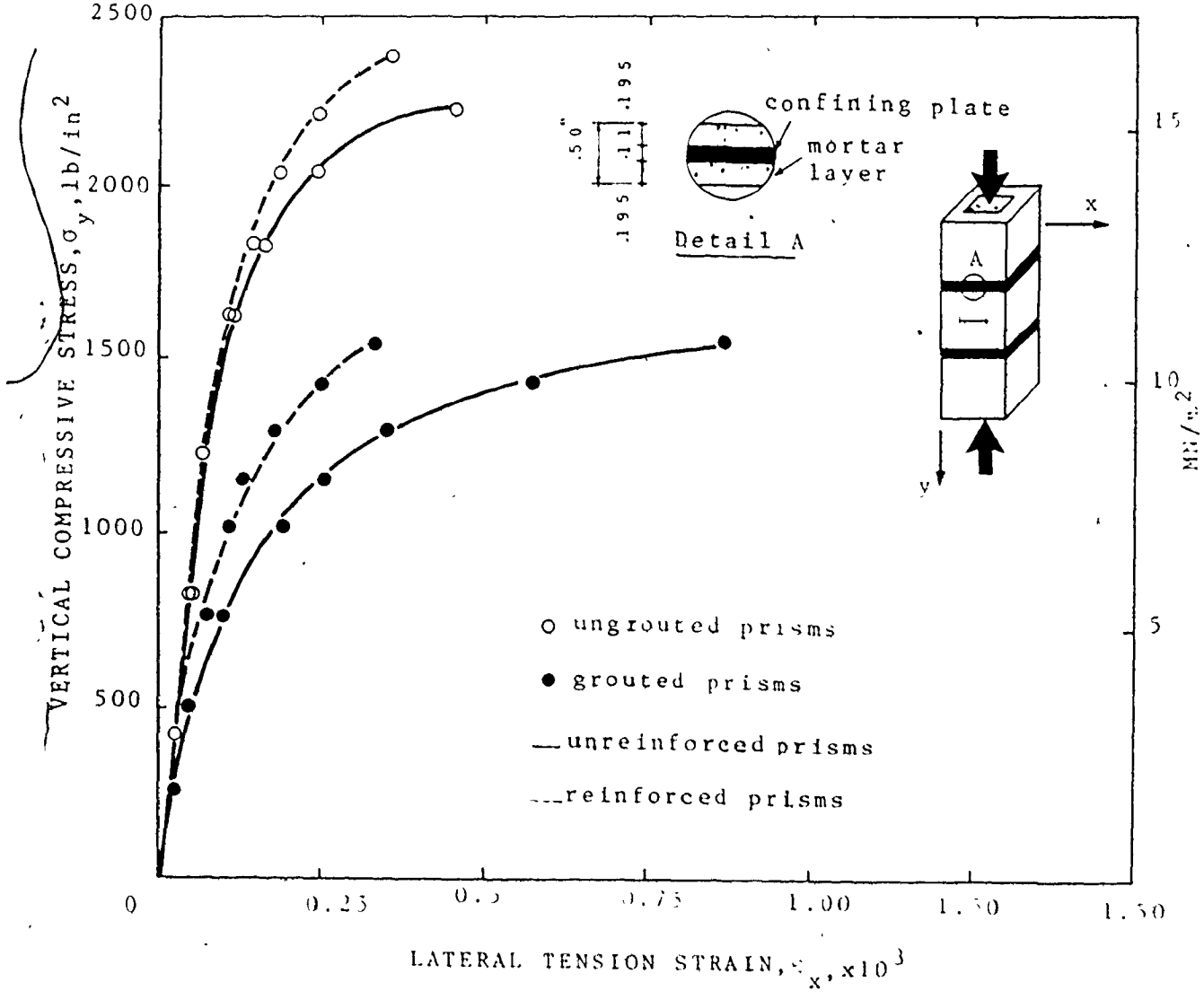

Fig. 3.28 EFFECT OF CONFINING PLATES ON THE DEFORMATION CHARACTERISTICS OF AXIALLY LOADED PRISMS

TABLE 3.4

TEST RESULTS OF AXIALLY LOADED PRISMS HAVING DIFFERENT BOND TYPES (Series C2-1)

Bond Type	Mortar Strength[a] (psi)	Grout Strength[b] (psi)	Prism Strength			$\frac{f'_{mgn}}{f'_{mun}}$
			Individual (psi)	Mean (psi)	C.O.V. (%)	
Ungrouted A	2190		2210 2210 2250 2360 2420	2290	4.2	0.69
Grouted	2190	1870	1710 1590 1480 1570 1480	1570	6.1	
Ungrouted B	2420		2500 2420 2360 2040 2300	2320	7.5	0.70
Grouted	2420	1800	1570 1480 1630 1680 1740	1620	6.3	
Ungrouted C	2500		2300 2250 2300 2260 2440	2310	3.3	0.71
Grouted	2500	1800	1660 1570 1730 1560 1670	1640	4.4	

Note: 1 psi = 6.9×10^{-3} MN/m^2

a - air cured 2-inch cube strength
b - Unconfined strength as calculated from block moulded prisms

specimens as the head joint did not influence either the failure mode or the compressive strength. The results also indicate similar reductions in the compressive strengths of grouted masonry compared to those for ungrouted masonry as was obtained for the 3-half block prisms of Series C1-1.

The mode of failure was splitting failure which initiated mainly in the narrow sides of the prisms regardless of the bond type along the broad sides. The grouted prisms showed tensile splitting of the outer shells as shown in Fig. 3.29 where in many cases it was possible to recover the grout core intact after extensive splitting of the shell. Typical modes of failures of the tested prisms are shown in Fig. 3.30 through Fig. 3.32. Contrary to the widely held view[21,51], in no case did splitting occur along the central vertical joint. The lateral deformations measured across the head joints, which are shown in Figs. 3.33 and 3.34, were unexpectly compressive at early stages of loading and only changed to tensile strain at much higher levels of applied compressive stress. Compared to the lateral strains on the block, it seems that no overstressing existed acorss the head joint. This is consistent with the mode of failure showing no splitting along the vertical joint. The compression strains measured across the joint at early stages of loading may be explained by the tendency of the lateral deformations of the blocks, under vertical compression, on both sides of the joints to confine the vertical joint which is less stiff than the blocks.

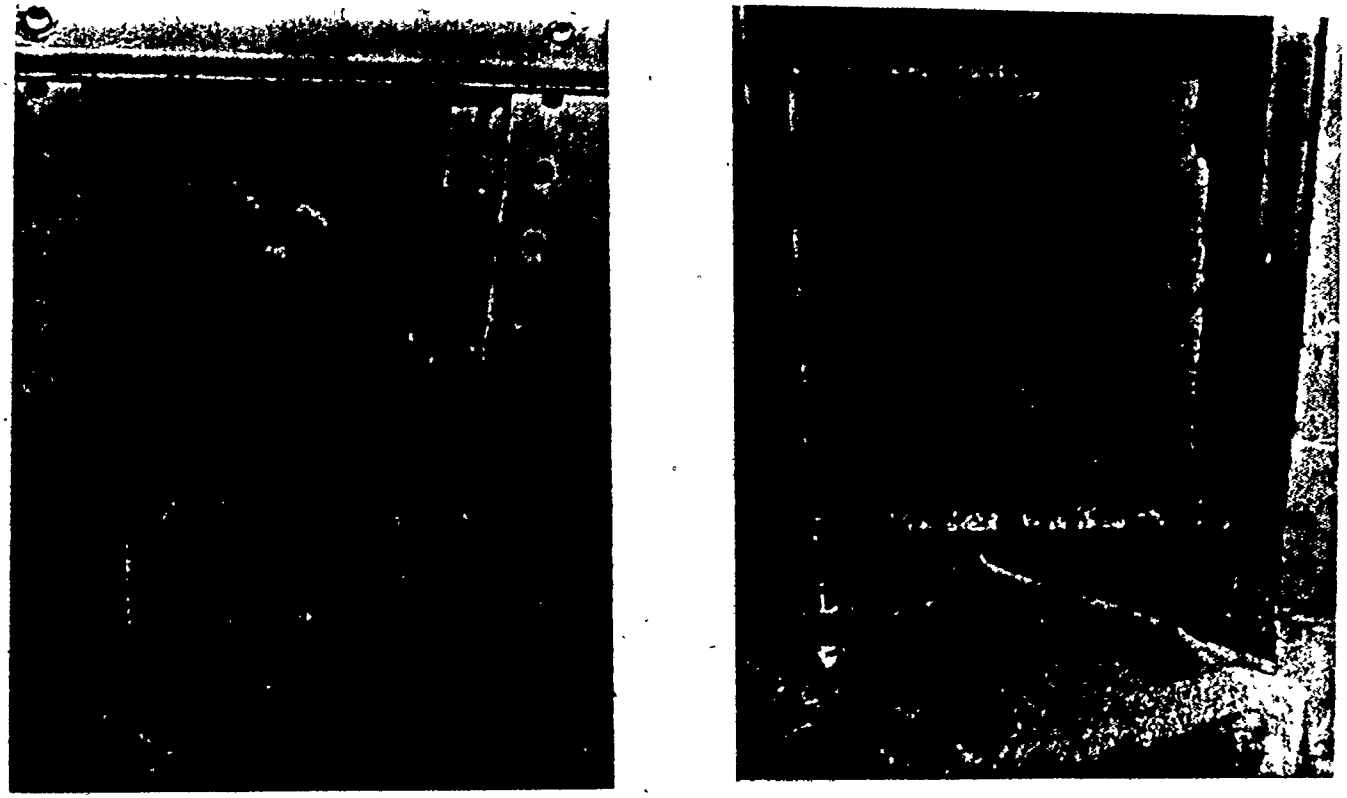

(a) Type A-Bond

(b) Type B-Bond

Fig. 3.29 TYPICAL FAILURE OF THE OUTER SHELLS OF AXIALLY LOADED GROUTED PRISMS

(a) Ungrouted Prism

(b) Grouted Prism

Fig.3.30 TYPICAL FAILURES OF AXIALLY LOADED PRISMS, TYPE A-BOND

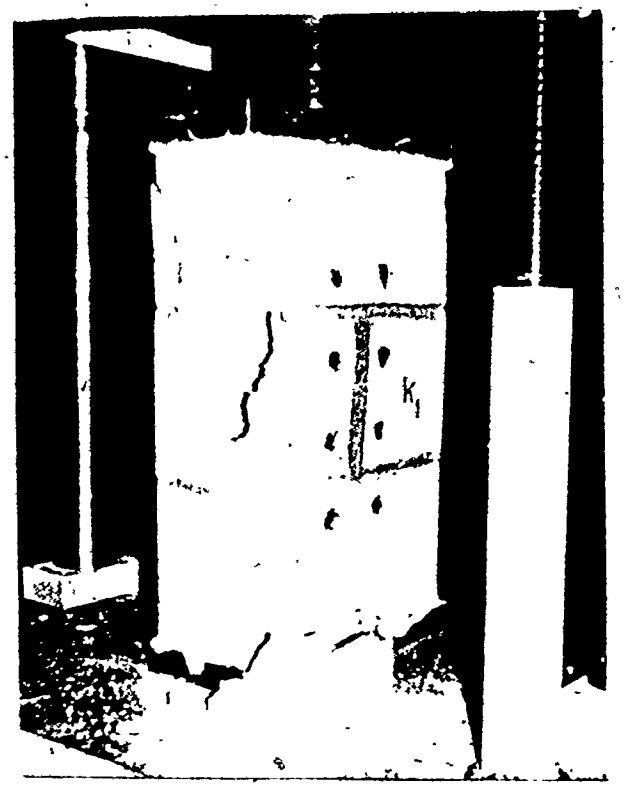

(a) Ungrouted Prism

(b) Grouted Prism

Fig. 3.31 TYPICAL FAILURES OF AXIALLY LOADED PRISMS, TYPE B-BOND

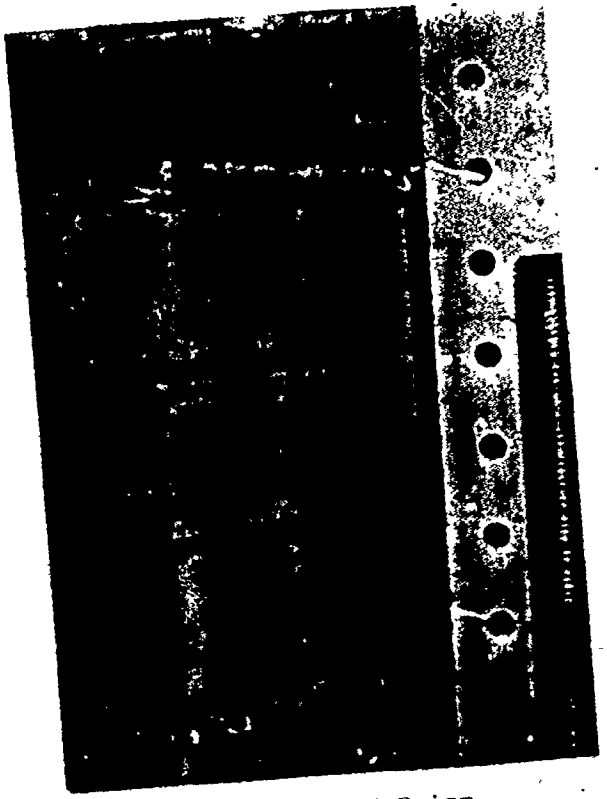

(a) Ungrouted Prism

(b) Grouted Prism

Fig.3.32 TYPICAL FAILURES OF AXIALLY LOADED PRISMS, TYPE C-BOND

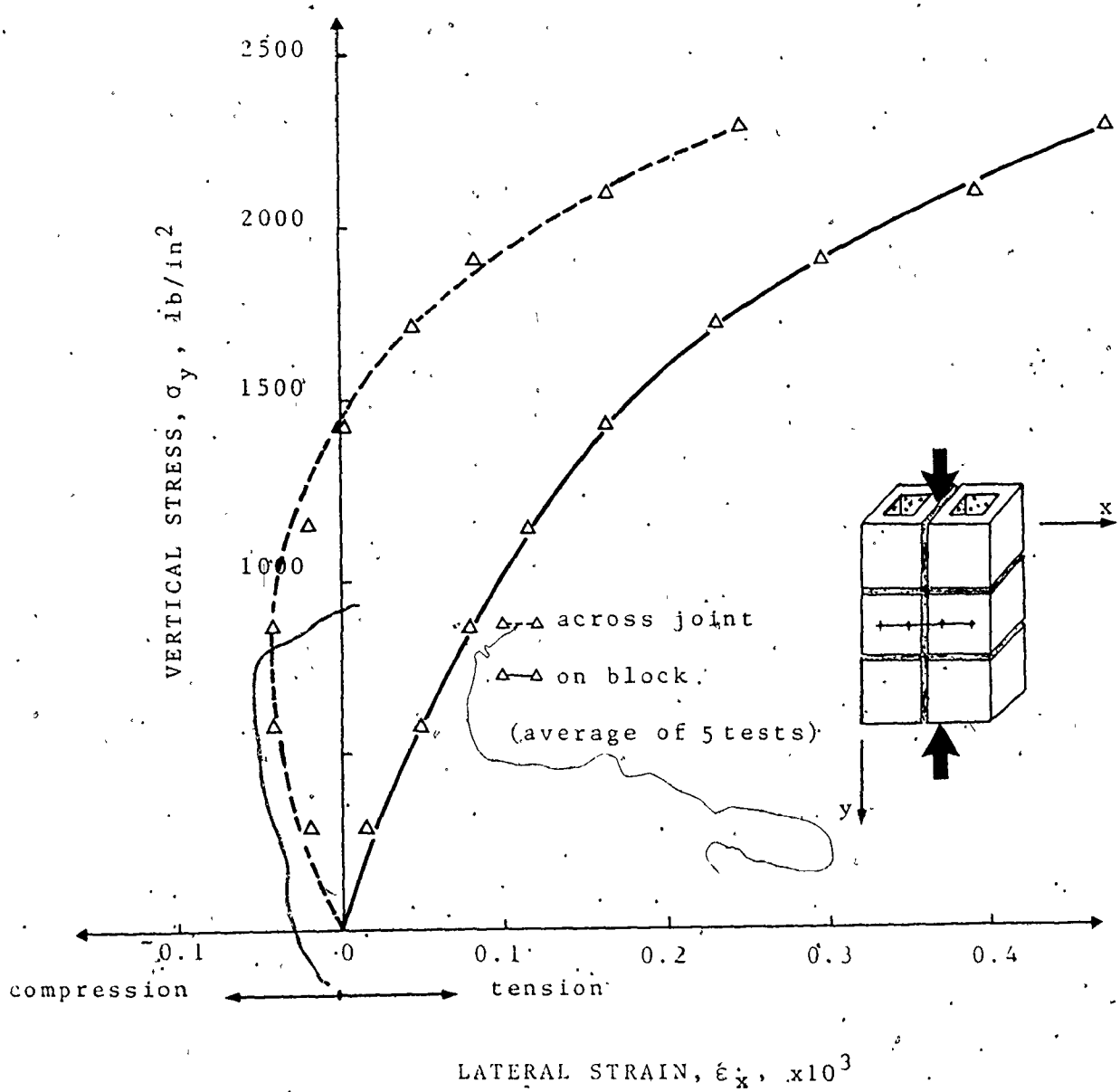

Fig. 3.33 LATERAL DEFORMATIONS ON BLOCKS AND ACROSS THE HEAD JOINTS OF AXIALLY LOADED UNGROUTED PRISMS (TYPE C-BOND)

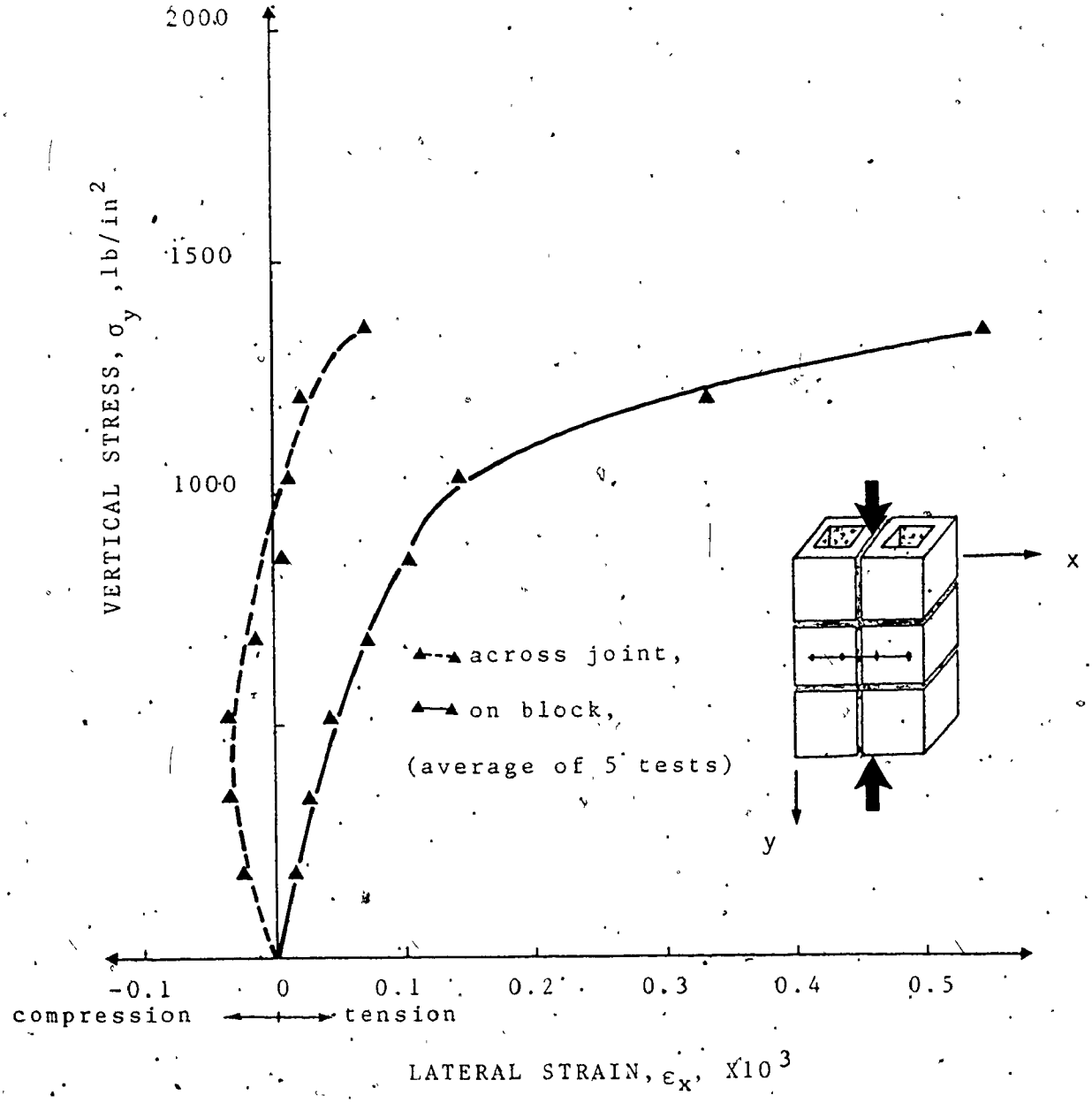

Fig. 3.34 LATERAL DEFORMATIONS ON BLOCKS AND ACROSS THE HEAD JOINTS OF AXIALLY LOADED GROUTED PRISMS (TYPE C- BOND)

Results published by the Structural Clay Product Institute[54] revealed no significant effect of the bond type (common or running bond and stack bond) on the compressive strength of brick masonry prisms. This agrees with the results of this investigation. However, Stafford-Smith and Carter[51], as a result of finite element analyses of brick masonry assemblages under axial compression, indicated that the peak values of the horizontal tensile stresses were associated with vertical joints, and concluded that the vertical joint would decrease the compression capacity. They adopted a two dimensional finite element analysis assuming elastic properties for the components. However, in reality, both brick and mortar are not truly elastic. This is particularly so for mortar near the ultimate stress[31,42]. In fact, it is principally the inelastic behaviour of the mortar as it approaches failure which governs the compressive strength of masonry[31]. Also, considering that the splitting failure of the assemblage, which was initiated in the narrow side of the element under axial compression, could only be predicted using a three dimensional stress analysis, Stafford-Smith's and Carter's conclusion concerning the failure capacity, is questionable. Their conclusion is not applicable to grouted masonry since the lateral inelastic deformations of the grout have a significant effect on the compression capacity which again cannot be predicted using a two dimension elastic finite element model. Hegemier et al[21] tested 3- and 5-course grouted

concrete block prisms under axial compression using stack and running bond. A reduction of only 4% due to the existence of the vertical joints in the 3-course prisms indicates the insignificance of the bond type. This again agrees with the results of the current investigation. However for the 5-course prisms a reduction of 16% was shown for running bond. The authors attributed the difference between the strengths for the two bond types to the nonalignment of the cross webs for running bond and stated that even if the webs are mortared they would not efficiently transmit compression through the joint. This argument is not as applicable to the grouted masonry where the grouted cores will help to efficiently transmit the compression force. It is worth mentioning that the authors adopted full mortar bed for stack bond prisms and face-shell mortar bed for running bond specimens. Also, the repetitions of the test specimens for the two bond types were different (6 for running bond and 3 for stack bond). These discrepancies could make the author's comparison regarding the effect of the bond questionable.

Figures 3.35 and 3.37 show the lateral strains developed in grouted and similar ungrouted prisms under axial comrpession for different bond types. (Each point in the shown curves is the average of at least 16 readings, using 4 per specimen.) The graphs indicate that higher lateral tensile strains were developed for grouted prisms compared to ungrouted prisms for all three bond types. It is suggested that high lateral strains are induced by

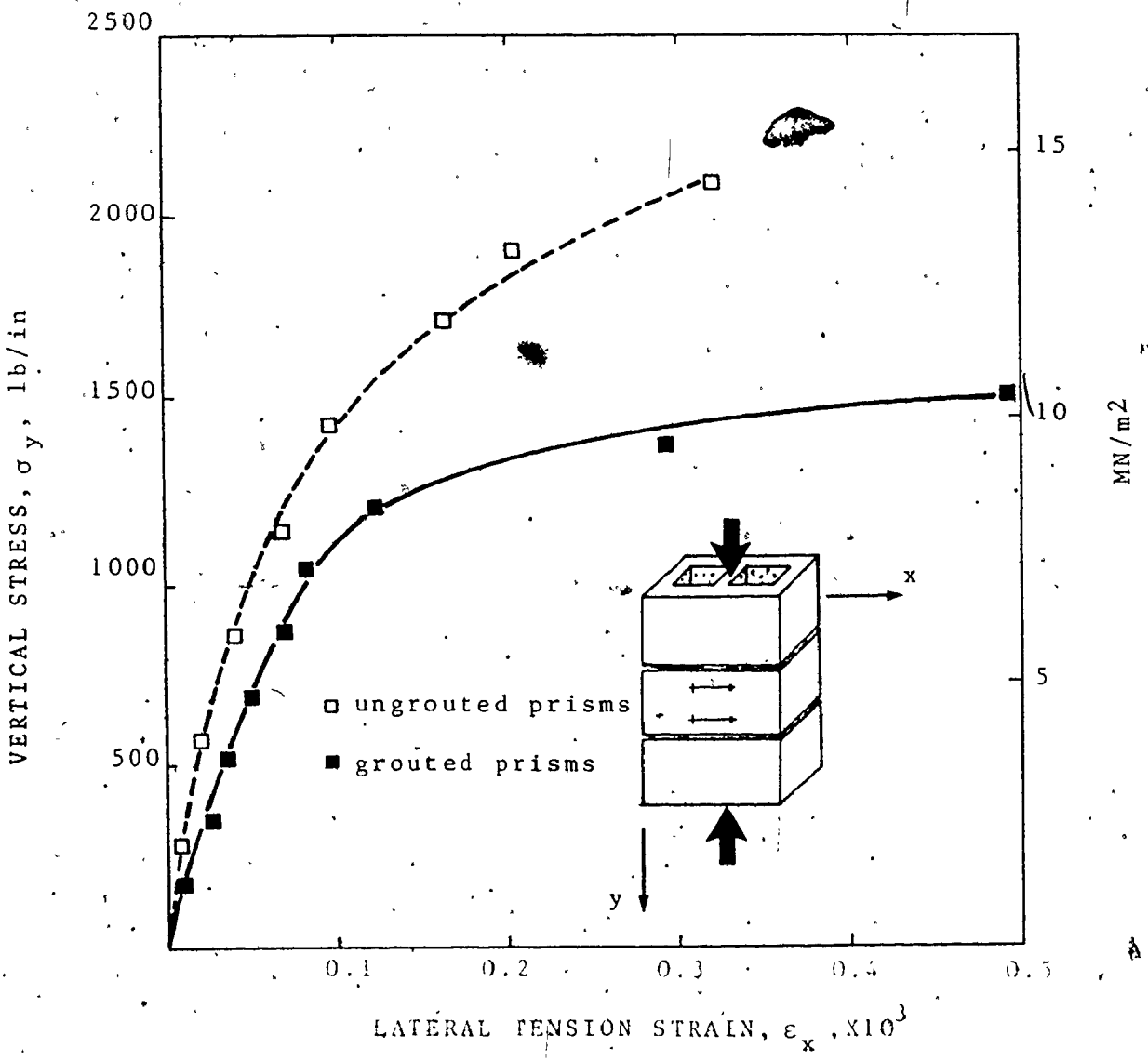

Fig. 3.35 LATERAL DEFORMATIONS OF AXIALLY LOADED PRISMS (TYPE A-BOND)

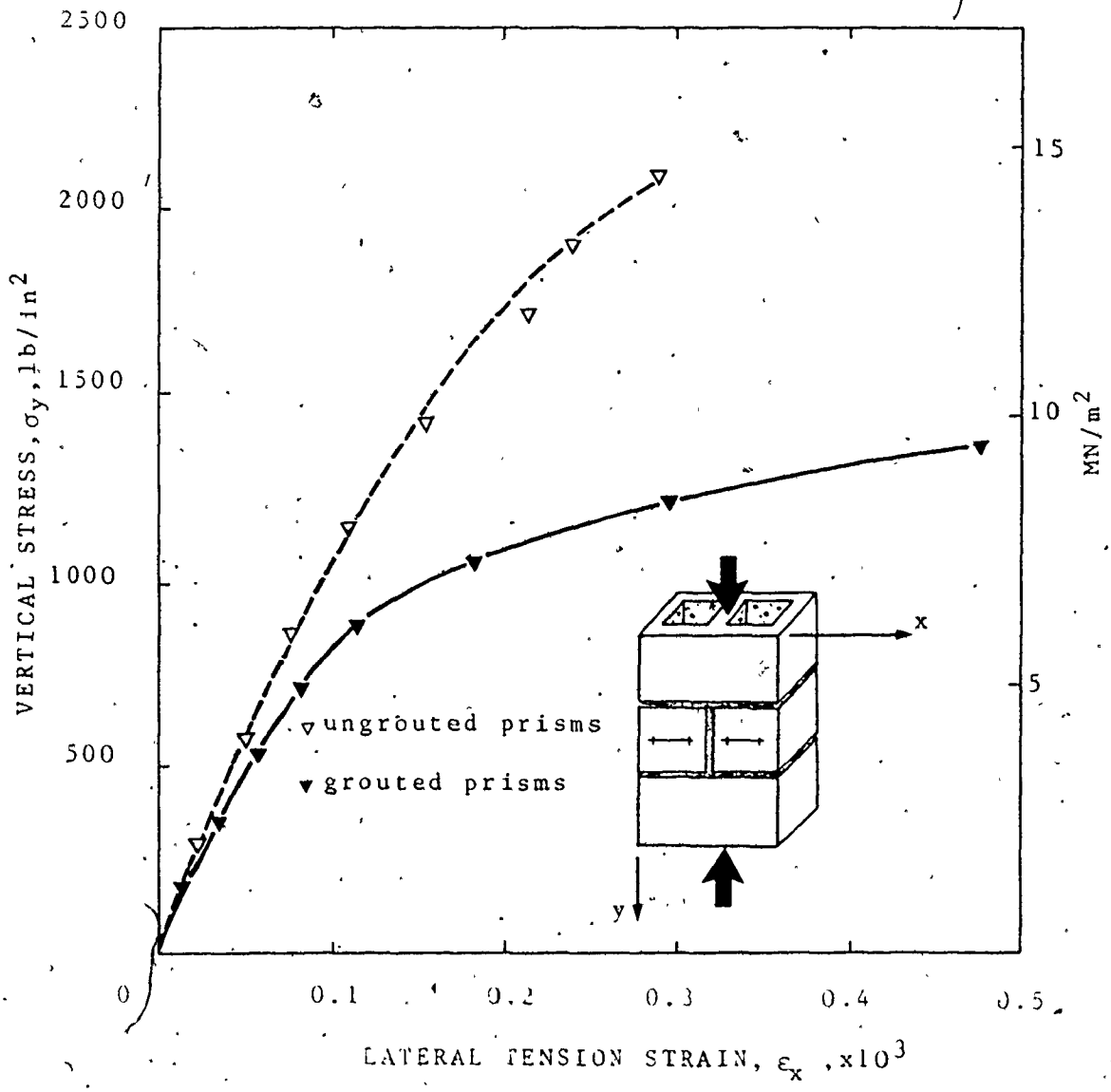

Fig. 3.36 LATERAL DEFORMATIONS OF AXIALLY LOADED PRISMS (TYPE B-BOND)

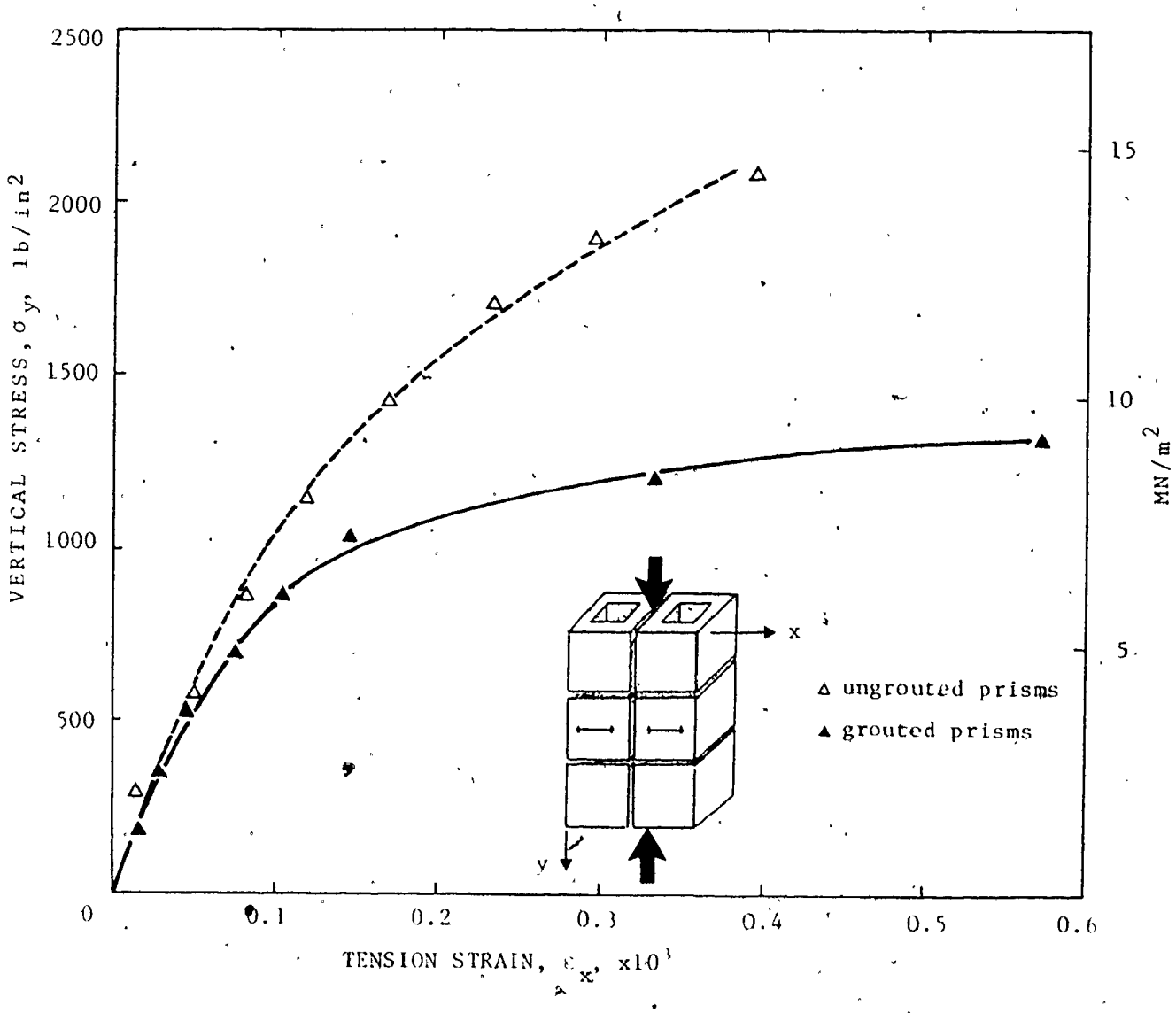

Fig. 3.37 LATERAL DEFORMATIONS OF AXIALLY LOADED PRISMS (TYPE C-BOND)

the lateral expansion of the grout which causes premature splitting failures of the grouted prisms and reductions in their compressive strengths. An average reduction of about 31% was obtained which agrees with the results for the 3-half block prisms discussed in Section 3.2.4.1.

b) Series C2-2: Effect of joint thickness: The results concerning the effect of the joint thickness on the compressive strength of ungrouted and grouted prisms are lsited in Table 3.5 and are displayed graphically in Fig. 3.38. It is shown that the mortar joint thickness had a considerable effect on the compressive strength of ungrouted prisms, but has relatively very little effect on the strength of the grouted prisms. The trend toward increasing compressive strength of ungrouted prisms with decreasing joint thickness confirms the results of earlier investigations[15,48,54] for solid brick or block masonry. For a specified block or brick strength and geometry, thinner joints result in lower lateral strains being imposed in the masonry units due to the mortars expansion, and consequently higher compression load is necessary for failure.

The decrease of the compression capacity for ungrouted concrete prisms with the increase of the joint thickness was proportionally less than that observed for brick masonry. A reduction of about 25% was obtained by increasing the joint thickness of brick masonry prisms from 1/4 inch to 1/2 inch[54]. A significant factor is that for block masonry the joint thickness

TABLE 3.5

TEST RESULTS OF AXIALLY LOADED PRISMS HAVING DIFFERENT JOINT THICKNESSES (Series C2-2)

Type of prism	Joint thick. (in.)	Mortar Strength[a] (psi)	Grout Strength[b] (psi)	Prism Strength, f'_m			$\frac{f'_m}{f'_{mo}}$[c]
				Individual (psi)	Mean (psi)	C.O.V. (%)	
ungrouted	zero			4460 3970 4080	4170	6.1	1.05
	3/8	2060 (5.1%)		3760 3970 4040 4230	4000	4.9	1.00
	3/4	2060 (5.1%)		3390 3340	3370	-	0.84
grouted	zero		2870 (10%)[d]	2390 2640	2520	-	1.03
	3/8	2060 (5.1%)	2870 (10%)[d]	2380 2440 2450 2520	2450	2.3	1.00
	3/4	2060 (5.1%)	2870 (10%)[d]	2370 2300 2300 2560	2380	5.2	0.97

NOTE: 1 in = 25.4 mm 1 psi = 6.9×10^{-3} MN/m^2

a - Compressive strength of air-cured 2-in cubes, average of 10 batches.
b - Unconfined compressive strength from block moulded specimens
c - Compressive strength of prisms having 3/8 inch joint thickness
d - Coefficient of variation based on 3 test repetitions

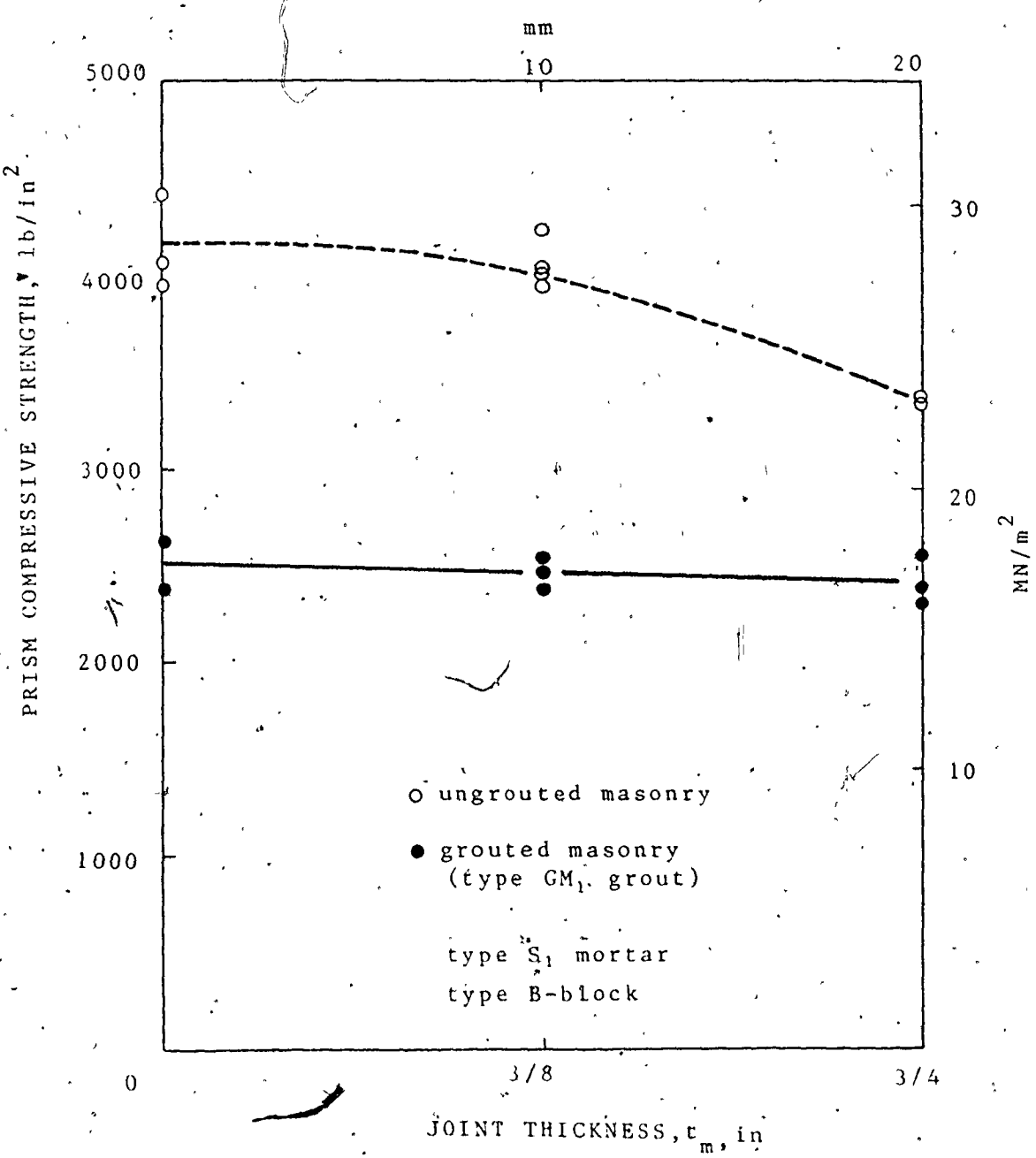

Fig. 3.38 EFFECT OF JOINT THICKNESS ON THE COMPRESSIVE STRENGTH OF UNGROUTED AND GROUTED MASONRY PRISMS

to unit height ratio is much lower than that for brick masonry. A suggested explanation for the larger reduction for brick masonry is that this ratio reflects how much average lateral stresses are imposed on the units which tend to confine the weaker mortar under axial compression (see Section 3.3.3). Higher joint thickness to masonry unit height ratios would result in higher average tensile stresses developed in the units and consequently, lower compressive strength of the assemblage would be expected.

Similar explanations of this characteristic were proposed by other investigators[15,31,48]. This explanation provides a different view of the masonry behaviour under axial compression from that based simply on the absolute value of the joint thickness.

It will also be shown in Section 3.3.3 that the joint thickness for the ungrouted prisms becomes more significant when the strength difference between the mortar and the masonry unit is large. Higher masonry unit to mortar strength ratios result in greater effects of joint thickness provided that the block height is kept constant[33]. Because this strength ratio is lower in block masonry (about 2-3) than in brick masonry (about 3-6), it would be expected that the joint thickness is less significant for block masonry.

It is interesting to observe the small effect of the mortar thickness on the compressive strength of the grouted masonry. This may be attributed to the continuity provided by the grouted

cores which reduces the significance of the mortar joint on the assemblage behaviour. Comparisons of the deformations for ungrouted and grouted prisms having different joint thicknesses shown in Figs. 3.39 and 3.40, respectively, illustrate this. The stress-strain relationships for grouted prisms having different joint thicknesses were closer than in the case of ungrouted prisms. This feature of behaviour seems consistent with the discussion in Section 3.2.4.1 which indicated that the mortar strength is not a significant factor concerning the compressive strength of grouted block masonry.

The mode of failure of grouted prisms having zero mortar joint thickness is shown in Fig. 3.41. A splitting failure of the outer shell was observed while the grouted core was intact and could be recovered after extensive splitting of the shell. Since mortar expansion was eliminated, the splitting failure is attributed to the lateral tension imposed on the shell due to the inelastic lateral deformations of the grouted cores under high compressive stresses.

c) Series C2-3: Effect of Core Geometry: The results concerning the effect of the core shape on the compressive strength of grouted masonry prisms are presented in Table 3.6. The effectiveness of grouting is expressed by the ratio of the compressive strength of the grouted prisms to that of a simialr ungrouted prism. It is shown that grouted prisms having circular cores exhibited a slightly higher compressive strength compared to

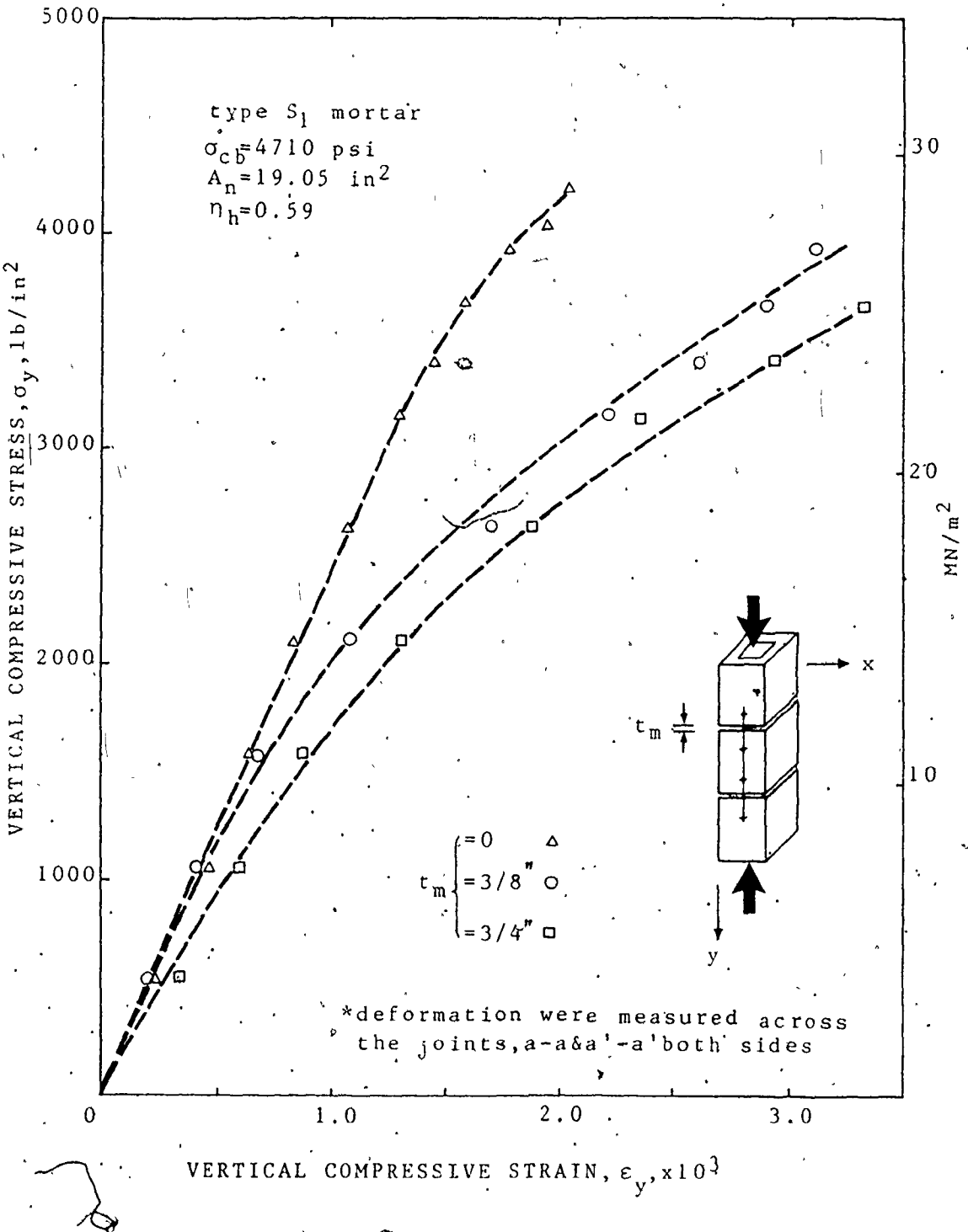

Fig. 3.39 STRESS-STRAIN CURVES OF AXIALLY LOADED UNGROUTED PRISMS HAVING DIFFERENT JOINT THICKNESSES

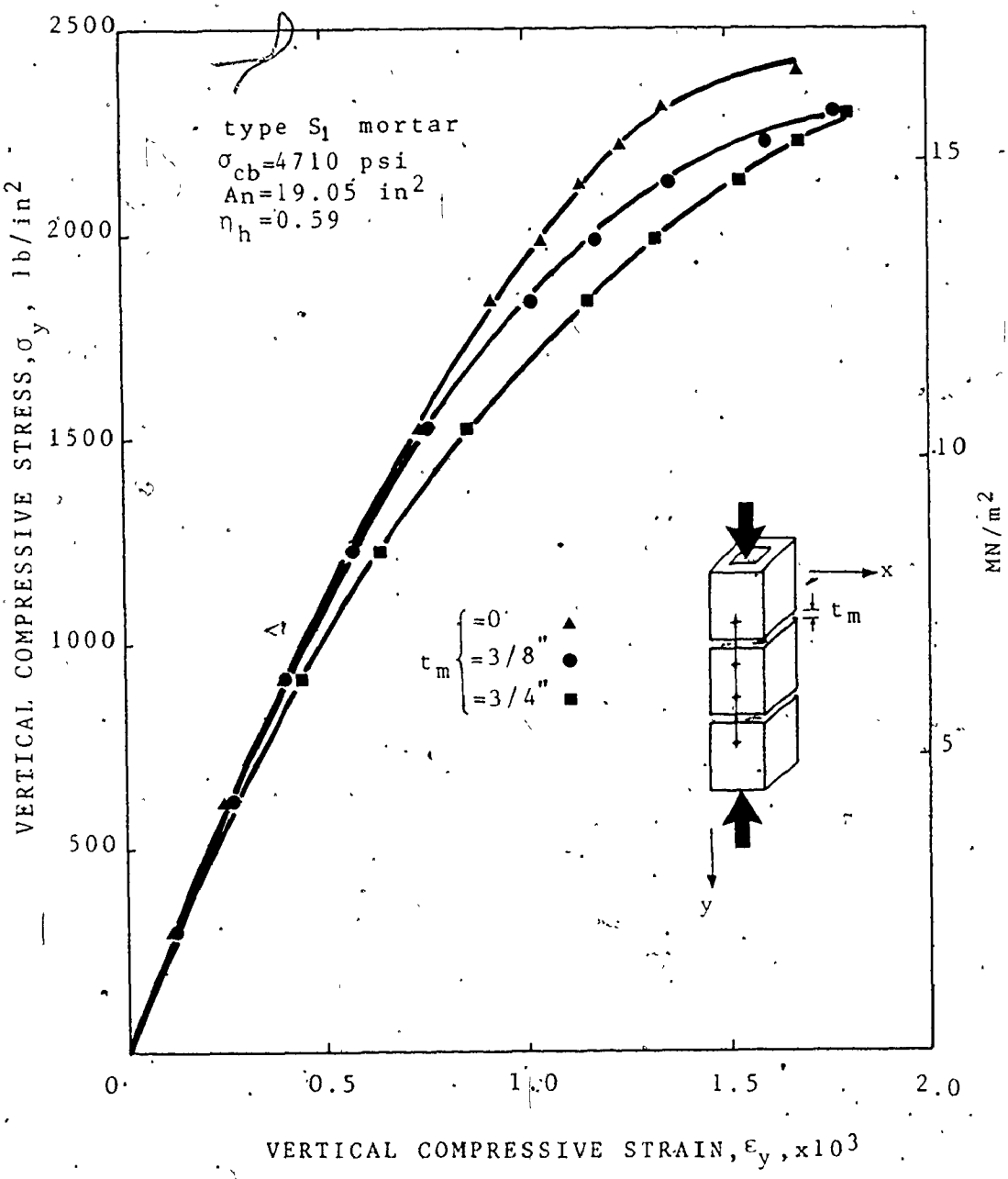

Fig. 3.40 STRESS-STRAIN CURVES OF AXIALLY LOADED GROUTED PRISMS HAVING DIFFERENT JOINT THICKNESSES

Fig. 3.41 TYPICAL SPLITTING FAILURE OF AN AXIALLY LOADED PRISM OF ZERO JOINT THICKNESS

TABLE 3.6

TEST RESULTS OF AXIALLY LOADED PRISMS HAVING DIFFERENT CORE SHAPES

Core Shape	Type of Prism	Mortar Strength[a] (psi)	Grout Strength[b] (psi)	Prism Compressive Strength			$\frac{f'_{mgn}}{f'_{mun}}$
				Ind. (psi)	Mean (psi)	C.O.V. (%)	
rectangular (unitE)[c]	ungrouted	2060		2390 2690 2610 2650	2590	5.1	0.68
	grouted		2870	1760 1780 1781 1730	1760	1.3	
circular (unitG)[c]	ungrouted	2060		1720 1800 2020	1850	8.4	0.72
	grouted		3100	1320 1390 1310	1340	3.3	

Note: 1 psi = 6.9×10^{-3} MN/m^2

a - Compressive strength of air cured 2-inch cubes, average of 10 batches

b - Unconfined compressive strength as calculated from block moulded specimens

c - The blocks properties are shown in Fig. 3.13

those having rectangular cores (the net to gross area ratio was nearly the same). Realizing that the higher grout to block strength ratio in case of prisms of circular cores compared to that for prisms having rectangular cores could be the cause of this slight increase in the strength, the core shape does not seem to be a significant parameter. Probably the rounded corners for the rectangular core shapes help to eliminate stress concentrations which could cause a reduction in strength.

No difference in the failure mode between prisms of the two different core shapes were observed as both exhibited a splitting mode of failure. However, for prisms with circular cores, the major vertical cracks generally initiated near the middle where there is a minimum shell thickness, they were initiated for prisms having rectangular cores near the corners where maximum transverse tensile stresses are expected (see Section 3.3.2). Figures 3.42 and 3.43 show typical failures of ungrouted and grouted prisms having rectangular and circular cores, respectively.

The results listed in Table 3.7 indicates that the shell thickness to width ratio (ts/w) was shown to have no significant effect on the comrpessive strength of grouted masonry as long as the net to gross area ratio is kept the same. This is particularly true for the practical ranges of ts/w ratio where a minimum face shell thickness is limited by the construction requirements.

(a) Ungrouted Prism

(b) Grouted Prism

Fig.3.42 TYPICAL FAILURES OF AXIALLY LOADED PRISMS WITH RECTANGULAR CORE SHAPES

(a) Ungrouted Prism

(b) Grouted Prism

Fig. 3.43 TYPICAL FAILURE OF AXIALLY LOADED PRISMS WITH CIRCULAR CORE SHAPES

TABLE 3.7

TEST RESULTS OF AXIALLY LOADED PRISMS OF DIFFERENT SHELL THICKNESS TO WIDTH RATIOS, ts/w

ts/w	Type of prism	Mortar Strength[a] (psi)	Grout Strength[b] (psi)	Prism Compressive Strength			$\frac{f'_{mg}}{f'_{mu}}$
				Ind. (psi)	Mean (psi)	C.O.V. (%)	
0.22 (Unit C)[c]	ungrouted	2060 (5.1%)[d]		2590 2590 2590 2680	2610	1.7	0.73
	grouted		3190 (2.7%)[d]	1820 1960 1870 1990	1910	4.1	
0.16 (Unit D)[c]	ungrouted	2060 (5.1%)[d]		2860 2780 2800	2810	1.5	0.73
	grouted		3190 (2.7%)[d]	1920 2020 2120 2120	2050	4.7	

NOTE: 1 psi = 6.9×10^{-3} MN/m^2

a - Compresive strength of air cured 2-inch cubes, average of 10 batches

b - Unconfined compressive strength as calculated from block moulded specimens

c - The blocks properties are shown in Fig. 3.13

d - Coefficient of variation

Figure 3.44 presents a comparison of the deformation characteristics of prisms having 100 percent solid units and those having cored units (formed by drilling circular cores from the 100 percent solid units). Nearly similar deformations were displayed. Also, consideration of the fact that the compressive strengths of the two types of prisms (solid and hollow) were nearly the same, as shown in Table 3.8, indicates that the behaviour of ungrouted prisms having different percentage solid are very similar.

TABLE 3.8

TEST RESULTS OF SOLID AND HOLLOW AXIALLY LOADED PRISMS

Type of Prism	Block type[a]	Mortar Strength[b] (psi)	Prism Compressive Strength		
			Individual (psi)	Mean (psi)	C.O.V.[c] (%)
Solid	A	2060 (5.1%)[c]	1850 2000 1960	1940	4.0
Hollow	G	2060 (5.1%)[c]	1720 1800 2020	1940	8.4

NOTE: 1 psi = 6.9×10^{-3} MN/m^2

a - The block properties are shown in Fig. 3.13
b - Compressive strength of air cured 2-in cubes, average of 10 batches
c - Coefficient of variation

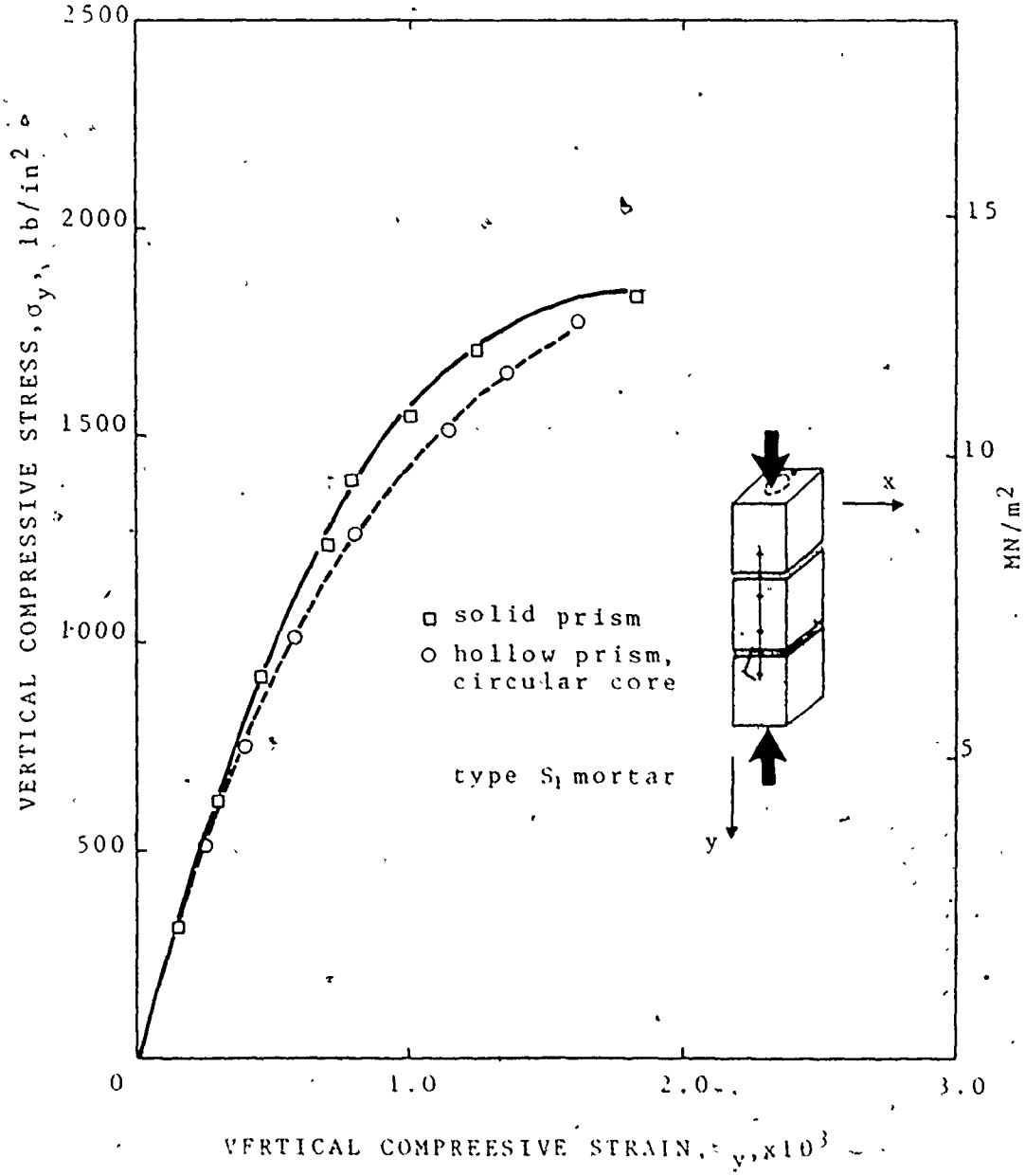

Fig. 3.44 STRESS-STRAIN CURVES OF AXIALLY LOADED HOLLOW AND SOLID MASONRY PRISMS

The results presented in Table 3.9 show the influence of the net to gross area ratio, η_h, on the compressive strength of ungrouted and grouted masonry prisms. A comparison of the strength results for grouted prisms indicates that the η_h ratio could affect the assemblage compressive strength. Higher net to gross area ratios result in higher compressive strengths of grouted prisms. As shown previously, the compressive strengths of grouted prisms were less than those for similar ungrouted prisms. This reduction in the compressive strength seems to decrease as the net to gross area ratio increases. (Eventually, for η_h equals unit (case of 100 percent solid), there would be no reduction in the strength assuming that the strengths of the blocks and the mortar are similar). The lateral strains of grouted prisms having different η_h ratios, shown in Fig. 3.45, indicate the reason more clearly. Greater η_h ratios result in lower lateral stresses imposed on the outer shell (blocks) and consequently, higher compressive stress for failure of the shell under a state of compression-tension is necessary. The failures displayed in Figs. 3.46 and 3.47 for ungrouted and grouted prisms show no difference in the failure mode of prisms having different η_h ratios, as they all failed by vertical splitting.

3.3 Analytical Investigation

3.3.1 Introduction

In the absence of an analytical solution, empirical

TABLE 3.9

TEST RESULTS OF AXIALLY LOADED PRISMS OF DIFFERENT NET TO GROSS AREA RATIOS, η_h

η_h	Type of Prism	Mortar Strength[a] (psi)	Grout Strength[b] (psi)	Prism Compressive Strength			$\frac{f'_{mgn}}{f'_{mun}}$
				Ind. (psi)	Mean (psi)	C.O.V. (%)	
0.63 (UnitE)[c]	ungrouted	2060 (5.1%)[d]		2390 2690 2610 2650	2590	5.1	0.68
	grouted		2870 (10%)[d]	1760 1780 1780 1730	1760	1.3	
0.69 (UnitD)[c]	ungrouted	2060 (5.1%)[d]		2860 2780 2800	2810	1.5	0.73
	grouted		3190 (2.7%)[d]	1920 2020 2120 2120	2050	4.7	
0.73 (UnitF)[c]	ungrouted	2060 (5.1%)[d]		2100 2380 2460 2410	2340	6.9	0.91
	grouted		3190 (2.7%)[d]	1900 2090 2140 2380	2130	9.2	

NOTE: 1 psi = 6.9×10^{-3} MN/m^2

a - Compressive strength of air cured 2-inch cubes, average of 10 batches.
b - Unconfined compressive strength as calculated from block moulded specimens
c - The blocks properties are shown in Fig. 3.13
d - Coefficient of variation

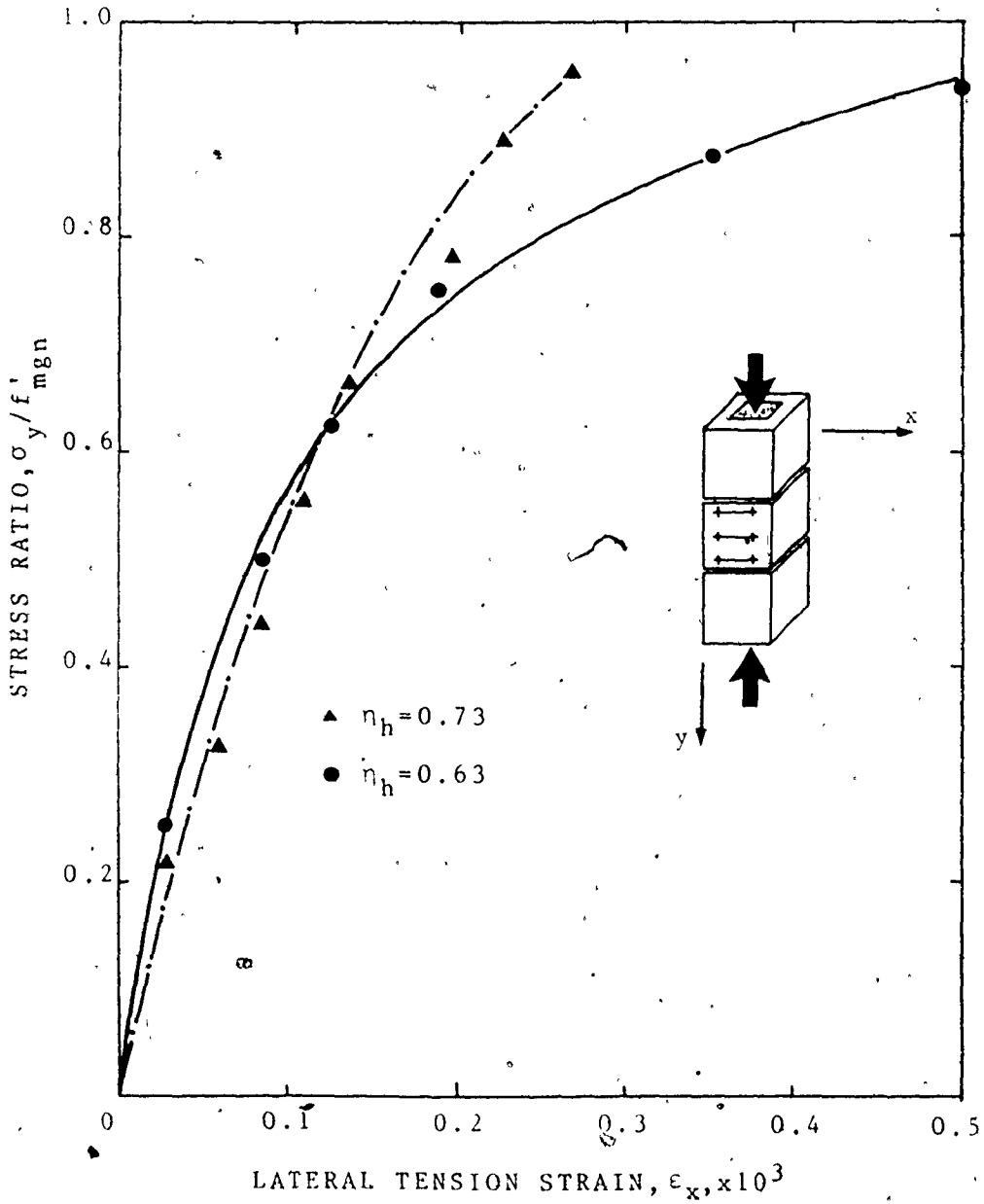

Fig. 3.45 LATERAL STRAINS OF GROUTED PRISMS WITH DIFFERENT η_h RATIOS

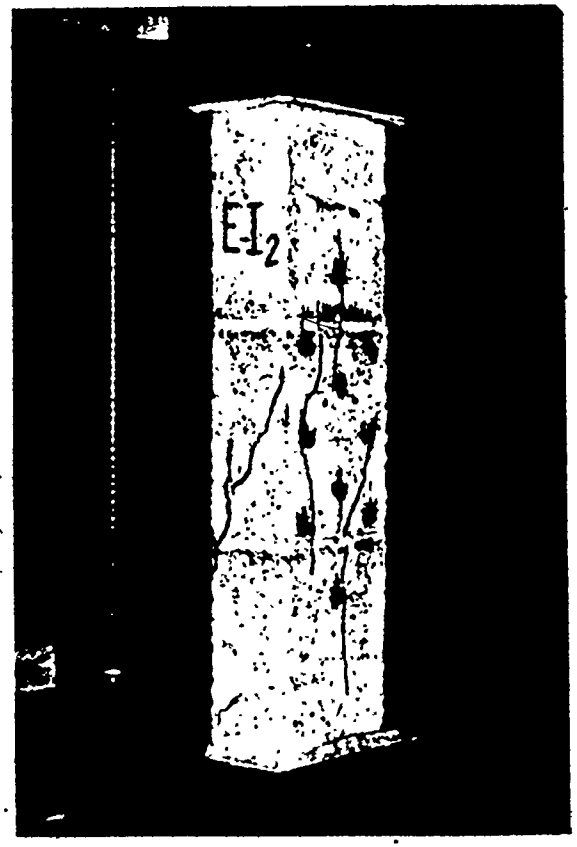

(a) $\eta_h = 0.63$

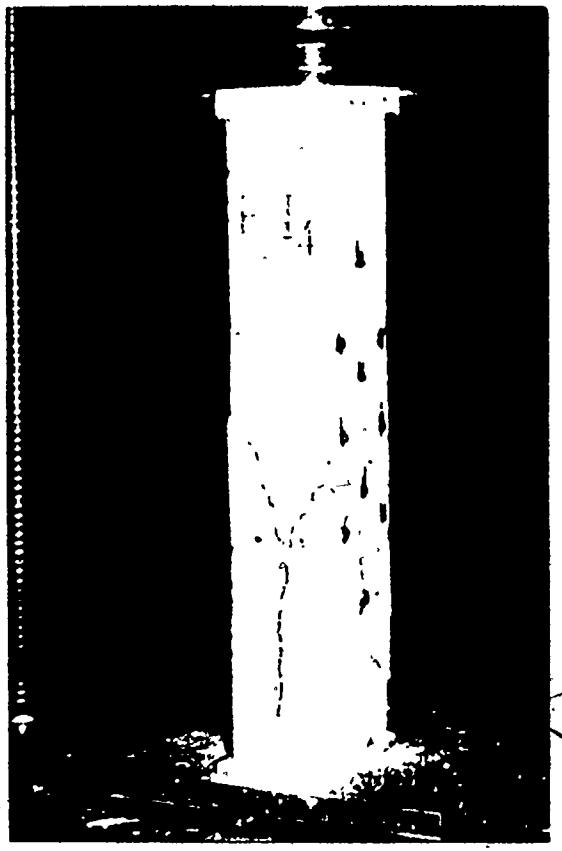

(b) $\eta_h = 0.73$

Fig. 3.46 TYPICAL FAILURES OF AXIALLY LOADED UNGROUTED PRISMS WITH DIFFERENT NET TO GROSS AREA RATIOS, η_h

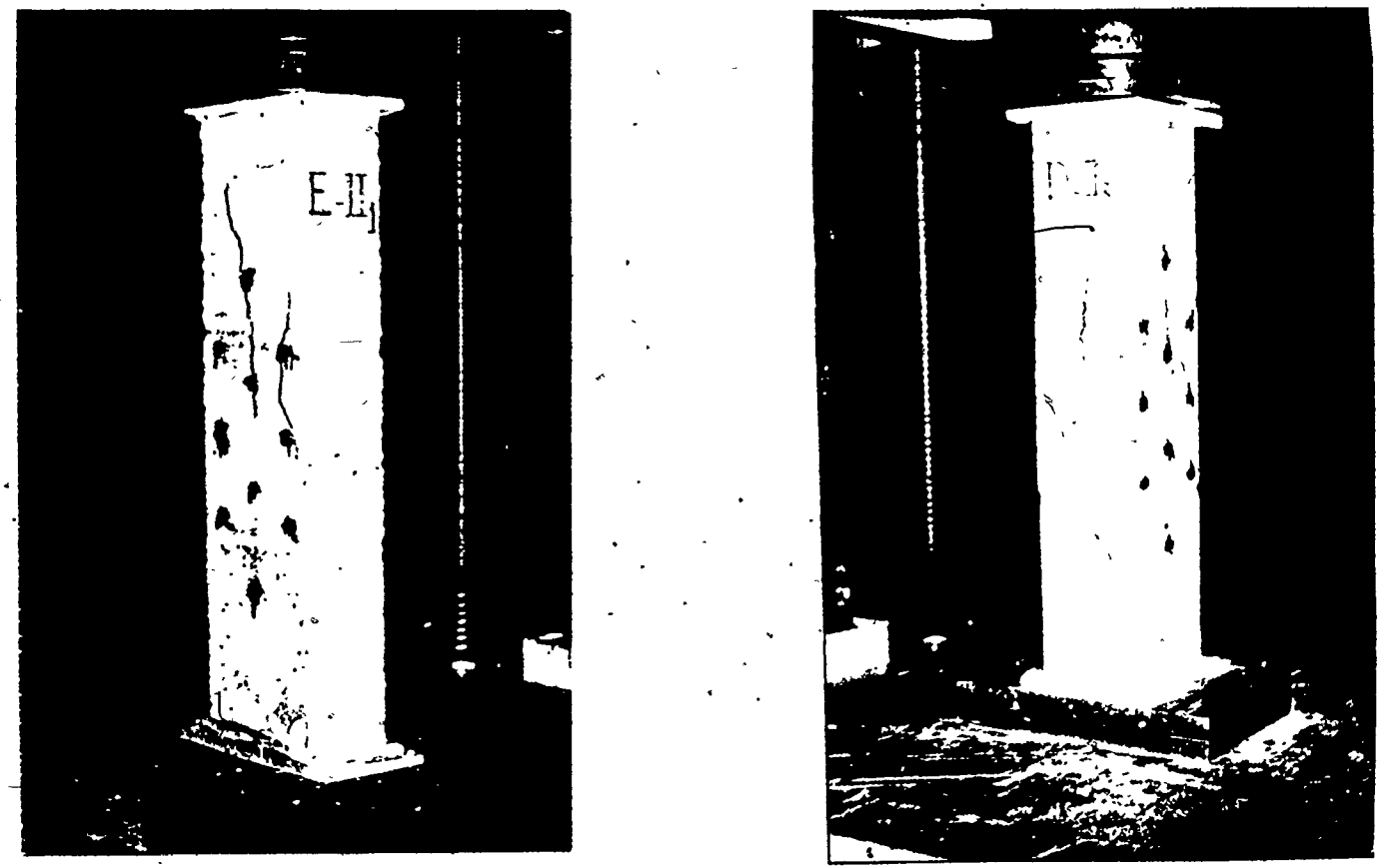

(a) η_h = 0.63

(b) η_h =0.69

Fig.3.47 TYPICAL FAILURES OF AXIALLY LOADED GROUTED PRISMS WITH DIFFERENT NET TO GROSS AREA RATIOS, η_h

relationships[17,47] derived from the experimental results have been put forward to show the variation of masonry compressive strength with given factors. These relationships may only apply to the type of masonry units chosen and to the type of mortar and its joint thickness used in these series of experiments. Whether these relationships could be extended to include other units and mortars with different strengths and geometric characteristics is doubtful. In other words, empirical relationships derived from test data are often limited in scope and before their general applicability could be accepted, they should be checked over different practical ranges of parameters. It does not seem feasible to rely on experiments alone to provide empirical expressions which can allow for the large number of permutations arising from the multitude of factors affecting the compressive strength of brick and block masonry. This is particularly true for grouted masonry where there are three component materials of different geometric and strength characteristics.

Attempts have been made to quantitatively determine the compressive strength of solid brick masonry prisms. In a paper to the International Conference on Masonry Structural Systems, in 1967, Hilsdorf[24] outlined a new approach for the development of a failure criterion based on stress analysis considerations, where the compressive strength of brickwork was determined by the interaction of the strength properties of brick and mortar under their appropriate complex states of stresses. Mohr's theory of

failure was adopted to express the strength of brick under biaxial stresses. It was also assumed that the strength of mortar under triaxial compression is similar to the strength of concrete under triaxial compression.

A second attempt to quantitatively predict the compressive strength of brick masonry was presented by Francis, Hormand and Jerrems[15] in 1970. Their analytical procedure was based on a strain consideration which assumed that both brick and mortar have Hookean behaviour up to failure. This assumption seems to be invalid because it is the inelastic behaviour of mortar as it approaches failure which principally governs the compressive strength of brickwork[31,42]. They also ignored the important fact that the properties of such brittle materials as brick and mortar alter under different states of applied stresses. For example, the values of elastic constants, say for mortar, under uniaxial compression differs from that under triaxial compression[31,36].

In 1972, Khoo[31] presented a failure criterion for brickwork under axial compression which adopted a "strength" approach first proposed by Hilsdorf[24]. The solution was achieved by assigning empirical equations to the failure envelopes for brick under biaxial tension-compression stresses and for mortar under triaxial compression stresses.

The proposed formulas resulting from the three attempts outlined above are considered approximate solutions containing the

following assumptions to simplify the analytical procedure for such a complex problem:

1. The stresses in the two lateral directions are equal.
2. There is perfect bond between the brick and mortar interfaces.
3. There are uniform lateral and vertical stress distributions.
4. The shear stresses at the brick-mortar interfaces (see Section 3.3.2) were ignored and consequently the failure criteria presented are only valid for an element at the centroidal axis.
5. The three methods assumed that failure occurs in the brick and propagates through the mortar joint. The possibility of a failure initiating either in the mortar joint or by bond failure at the mortar-brick interfaces was ignored.

To improve on the quantitative relationships presented by these methods, information on the complex strain distribution over the height of the masonry unit and the mortar joints is needed before a better method can be developed to predict the failure mechanism[33]. It is worth mentioning that no analytical study has been found for the compressive strength of concrete masonry taking into consideration the effect of the grouted cores. The experimental results presented in this chapter show that the behaviour of grouted masonry is appreciably different from ungrouted masonry. For instance, whereas the mortar joint

characteristics are the most significant factors affecting the behaviour characteristics of ungrouted masonry, they are not significant for grouted masonry. The significance in behaviour is attributed to the continuity provided by the grouted cores.

It is the objective of this part of the investigation to:

1 - Study the shear stress distributions along the block-mortar interfaces and the lateral tensile stresses over the height of the block for both ungrouted and grouted masonry. A sensitivity analysis is conducted varying the components' characteristics.

2 - Develop a failure mechanism to predict the compressive strength of the assemblage in terms of the strength and geometric characteristics of its components (block, mortar and grout). The proposed formulas will then be used to examine, in quantitative terms, the contribution of the various factors influencing the compressive strength of ungrouted and grouted concrete masonry.

3 - Formulate an analytical expression to determine the stiffness (elastic modulus) of grouted masonry assemblages under axial compression in terms of the geometry and the elastic moduli of the component materials.

3.3.2 Distribution of Lateral Stresses

Determination of the lateral stress distribution for axailly loaded masonry prisms is a three dimensional stress

problem of an anisotropic nonhomogeneous media. Since the main concern in this part of the investigation is to study comparable behaviour rather than absolute values of stresses, the problem is assumed to be approximated by a two dimensional plane stress condition where the finite element method is adopted to define these stress distributions. A computer program available in the Department of Civil Engineering and Engineering Mechanics, McMaster University was used.

As shown in Fig. 3.48, a total of 238 elements were used to idealize one quarter of the prism. A constant strain triangular element was used. In the discretization of the ungrouted prisms, the element boundaries were made to coincide with the faces of the mortar joints so that the finite elements would always represent a single material. However, for the same discretization the elements will contain two different materials in the case of grouted masonry prisms (block and grout or mortar and grout). Since this feature could only be handled using a three-dimensional analysis, an assumption had to be made regarding the value of the modulus of elasticity of such elements. For a plane stress problem this could be handled approximately by assuming the axial rigidity of the composite element to be the sum of the axial rigidities of its components[2]. The equivalent modulus, E_{eq}, for the composite element having two materials (e.g. block and grout) is obtained as,

$$E_{eq} \; A_g = A_{gr} \; E_g + A_b \; E_b \qquad \ldots\ldots (3.6)$$

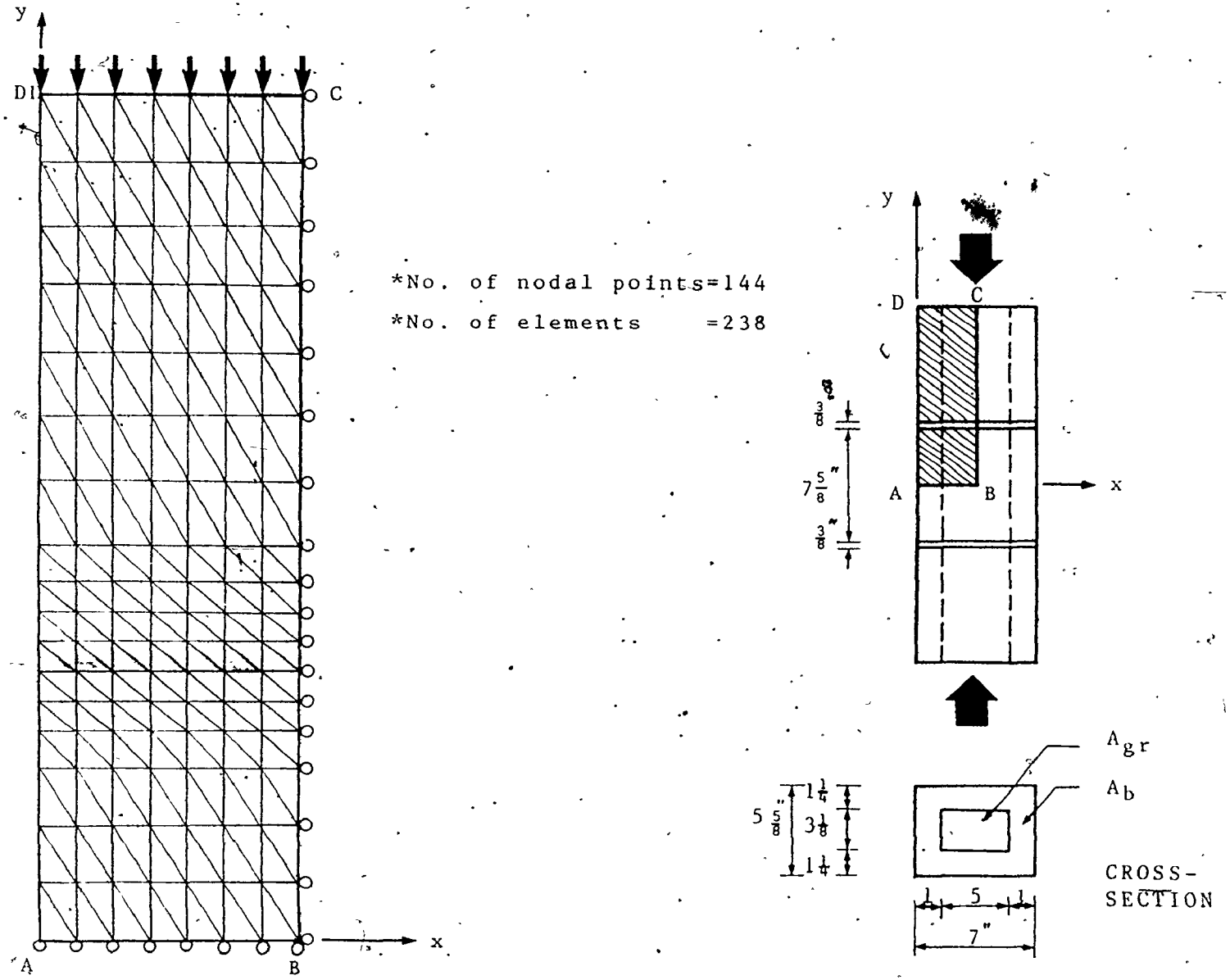

Fig. 3.48 FINITE ELEMENT IDEALIZATION OF AXIALLY LOADED PRISMS

therefore

$$E_{eq} = (1-\eta_h)E_g + \eta_h E_b \quad \ldots\ (3.7)$$

Similarly in the case of a composite element composed of mortar and grout,

$$E_{eq} = (1-\eta_h) E_g + \eta_h E_m \quad \ldots\ (3.8)$$

where E_g, E_b, and E_m denote the grout, block, and mortar moduli and η_h is the net to gross area ratio.

The lateral stress distributions (the shear stresses, τ_{xy}, at the interfaces and the lateral normal stresses σ_x, along the height of the block and the joint) were investigated for different conditions for ungrouted and grouted prisms. Arbitrary representative values of the material constants were assumed. This was satisfactory since the purpose of the analysis is not concerned with absolute values of stresses. The stress distributions resulting from the finite element analysis are displayed in Fig. 3.49 through Fig. 3.56. All the stresses are expressed in lb/in^2 for arbitrary applied uniform vertical stress of 100 lb/in^2.

The significant features to be drawn from the analysis as illustrated in the figures are:

1 - The lateral stress distributions along the height and the width of the block are not uniform but they are sharply concentrated near the interfaces and towards the edges become very small at the mid-height of the block. This finding agrees with

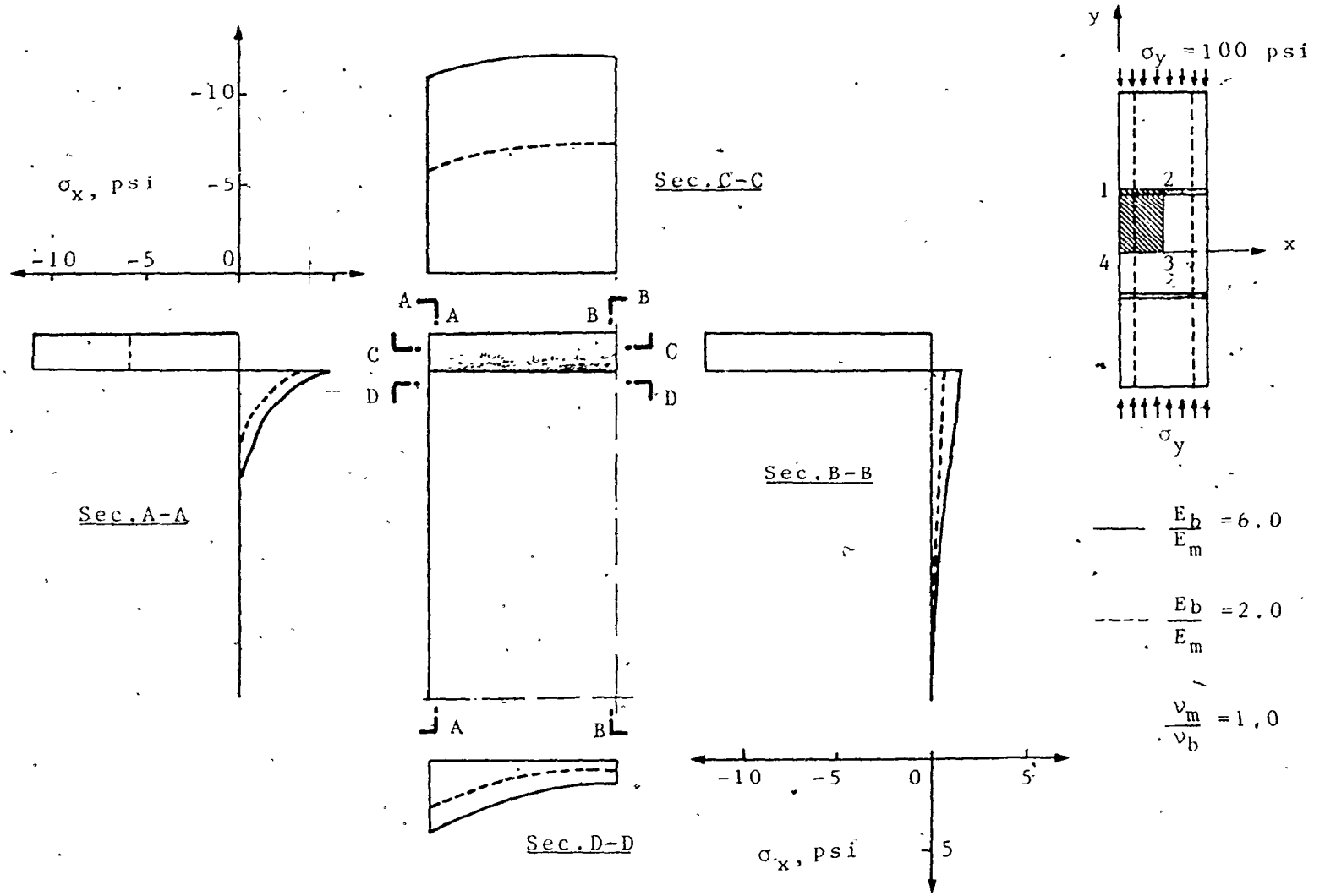

Fig. 3.49 EFFECT OF MORTAR STIFFNESS ON THE LATERAL STRESS DISTRIBUTIONS, σ_x, FOR AXAIALLY LOADED UNGROUTED PRISMS

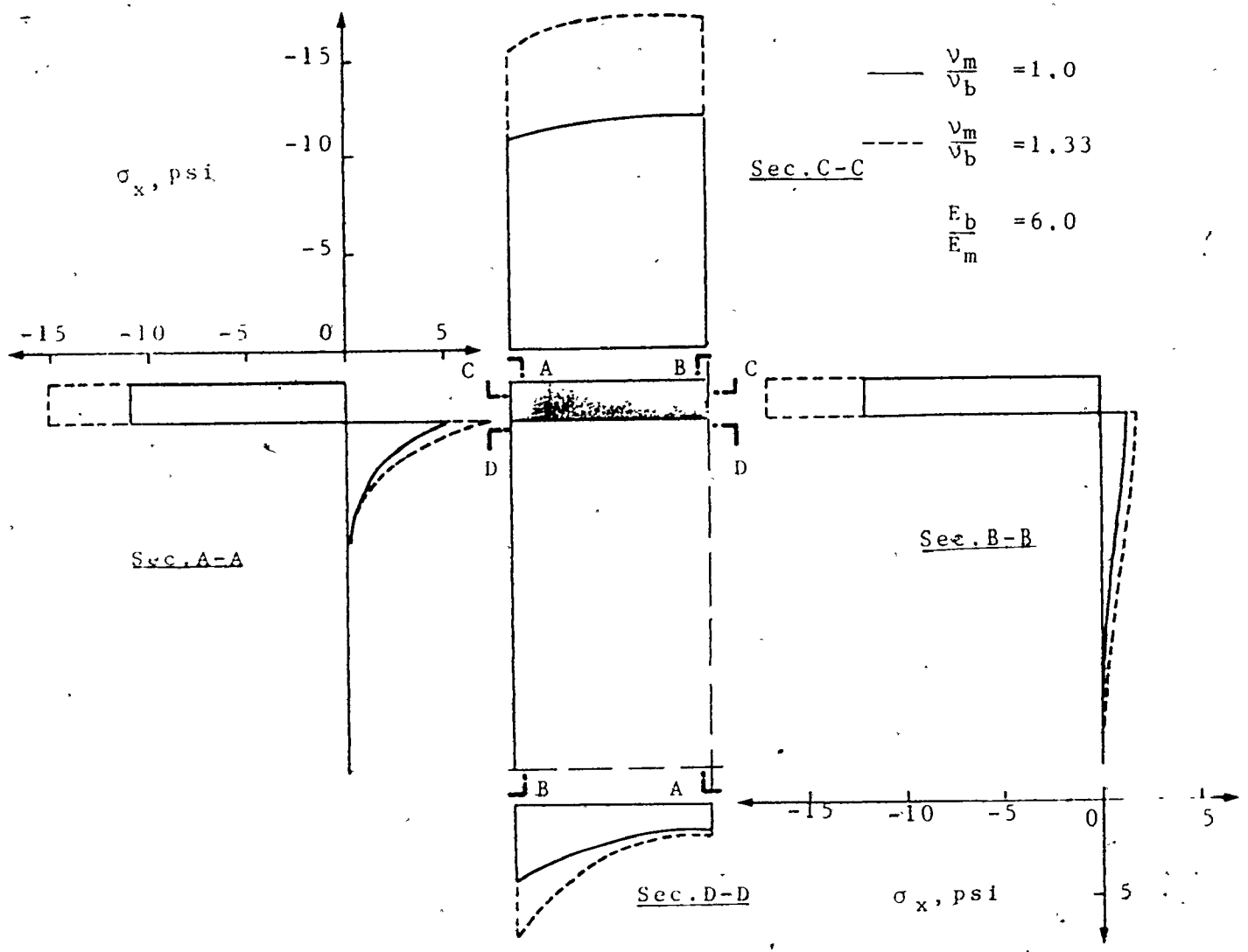

Fig. 3.50 EFFECT OF POISSON S RATIO OF THE MORTAR ON THE LATERAL STRESS DISTRIBUTIONS, σ_x, FOR AXIALLY LOADDED UNGROUTED PRISIMS

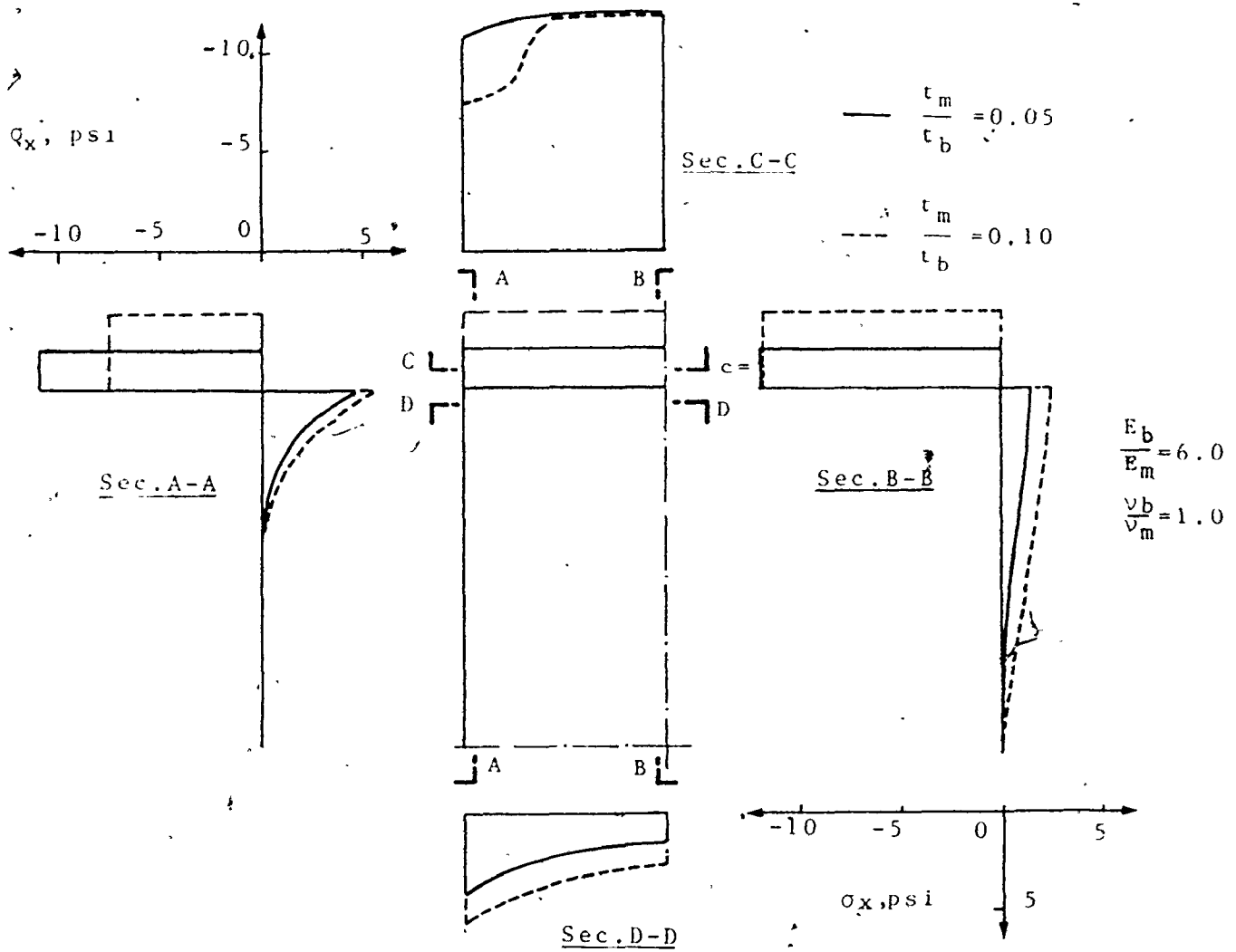

Fig. 3.51 EFFECT OF JOINT THICKNESS ON THE LATERAL STRESS DISTRIBUTIONS, σ_x, FOR AXIALLY LOADED UNGROUTED PRISMS

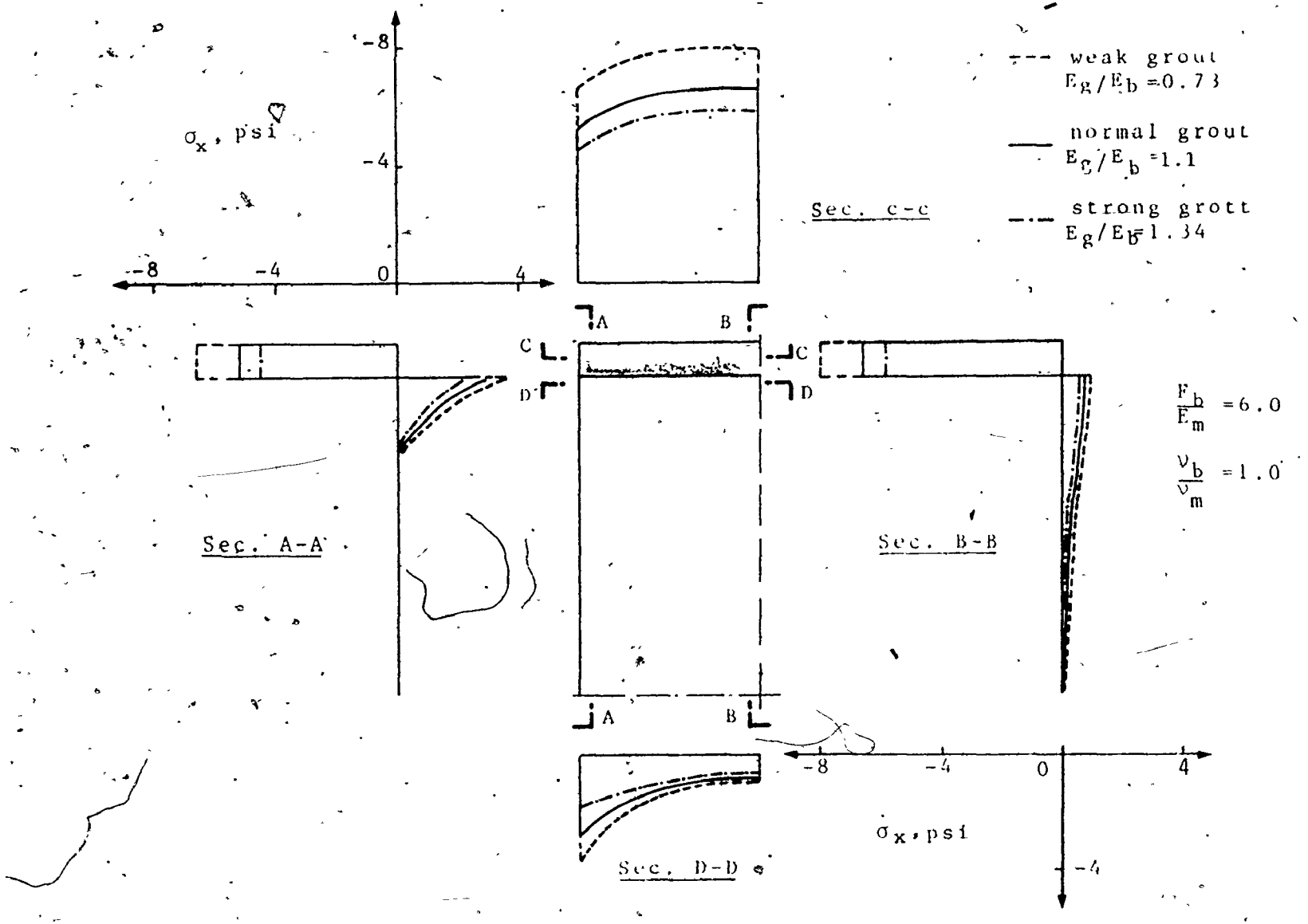

Fig. 3.52 EFFECT OF GROUT STIFFNESS ON THE LATERAL STRESS DISTRIBUTIONS, σ_x, FOR AXIALLY LOADED GROUTED PRISMS

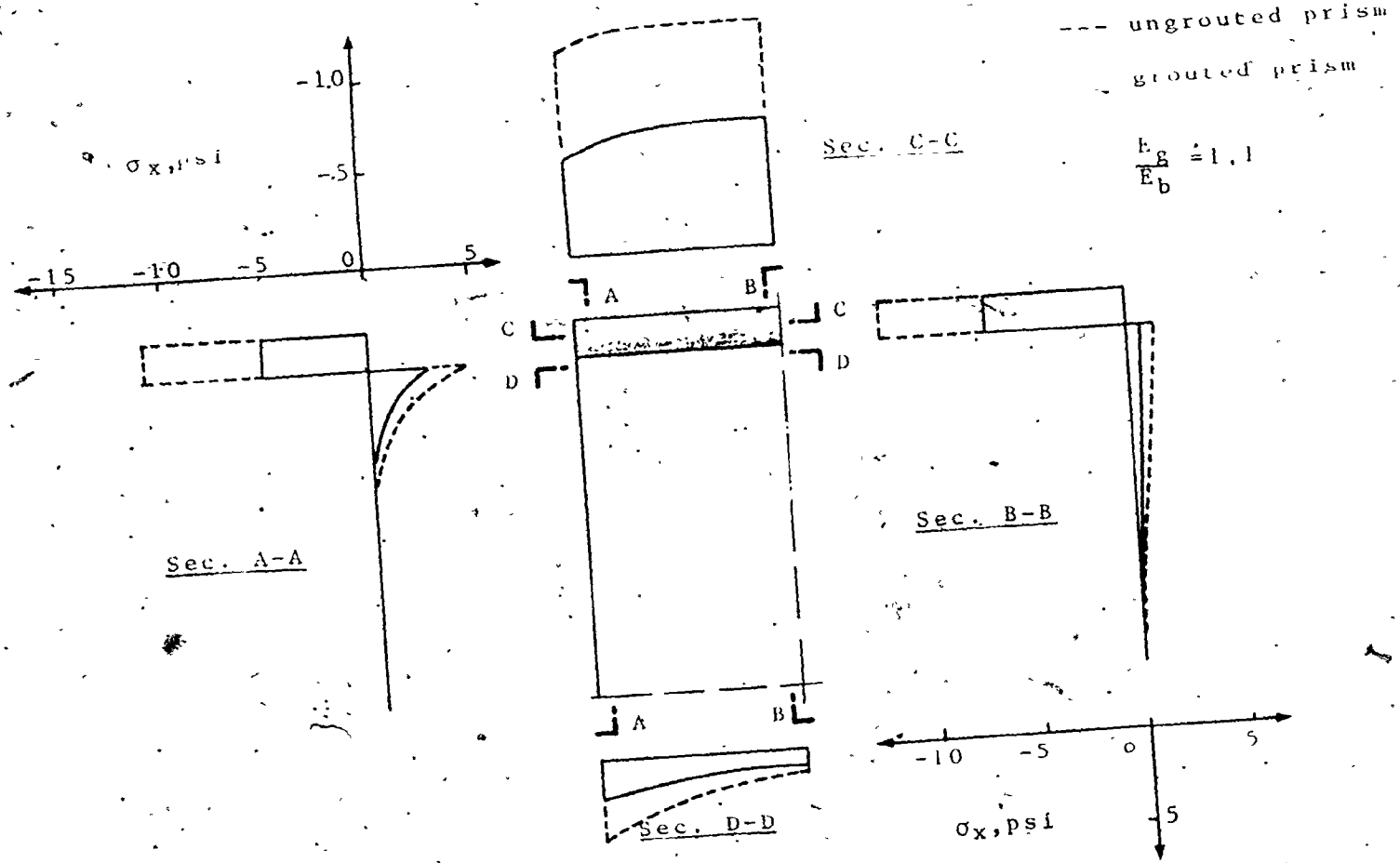

Fig. 3.53 LATERAL STRESS DISTRIBUTION, σ_x, OF AXIALLY LOADED UNGROUTED AND GROUTED PRISMS

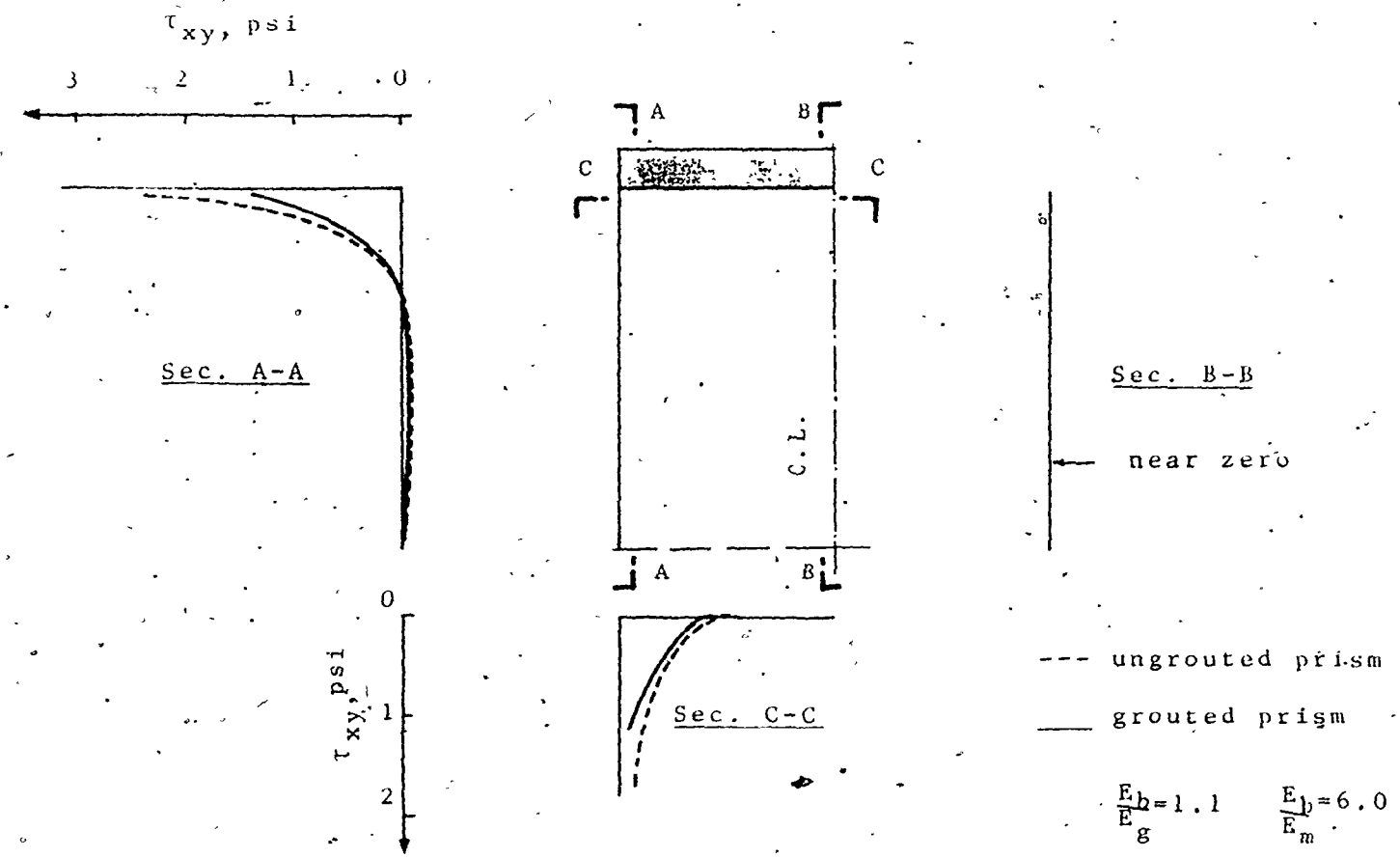

Fig. 3.54 SHEAR STRESS DISTRIBUTIONS, τ_{xy}, FOR AXIALLY LOADED UNGROUTED AND GROUTED PRISMS

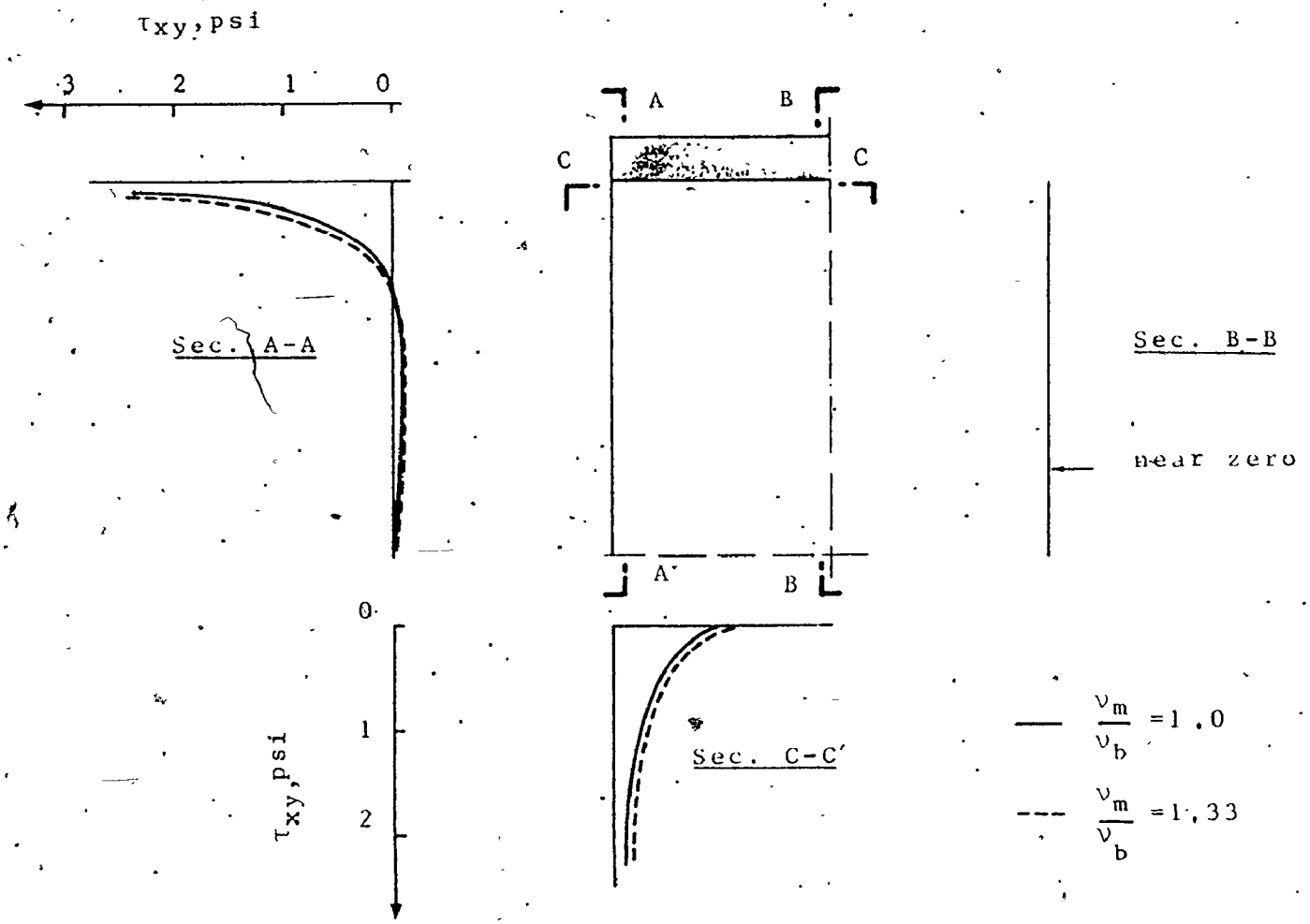

Fig. 3.55 EFFECT OF POISSON'S RATIO OF THE MORTAR ON THE SHEAR STRESS DISTRIBUTIONS, τ_{xy}, FOR AXIALLY LOADED UNGROUTED PRISMS

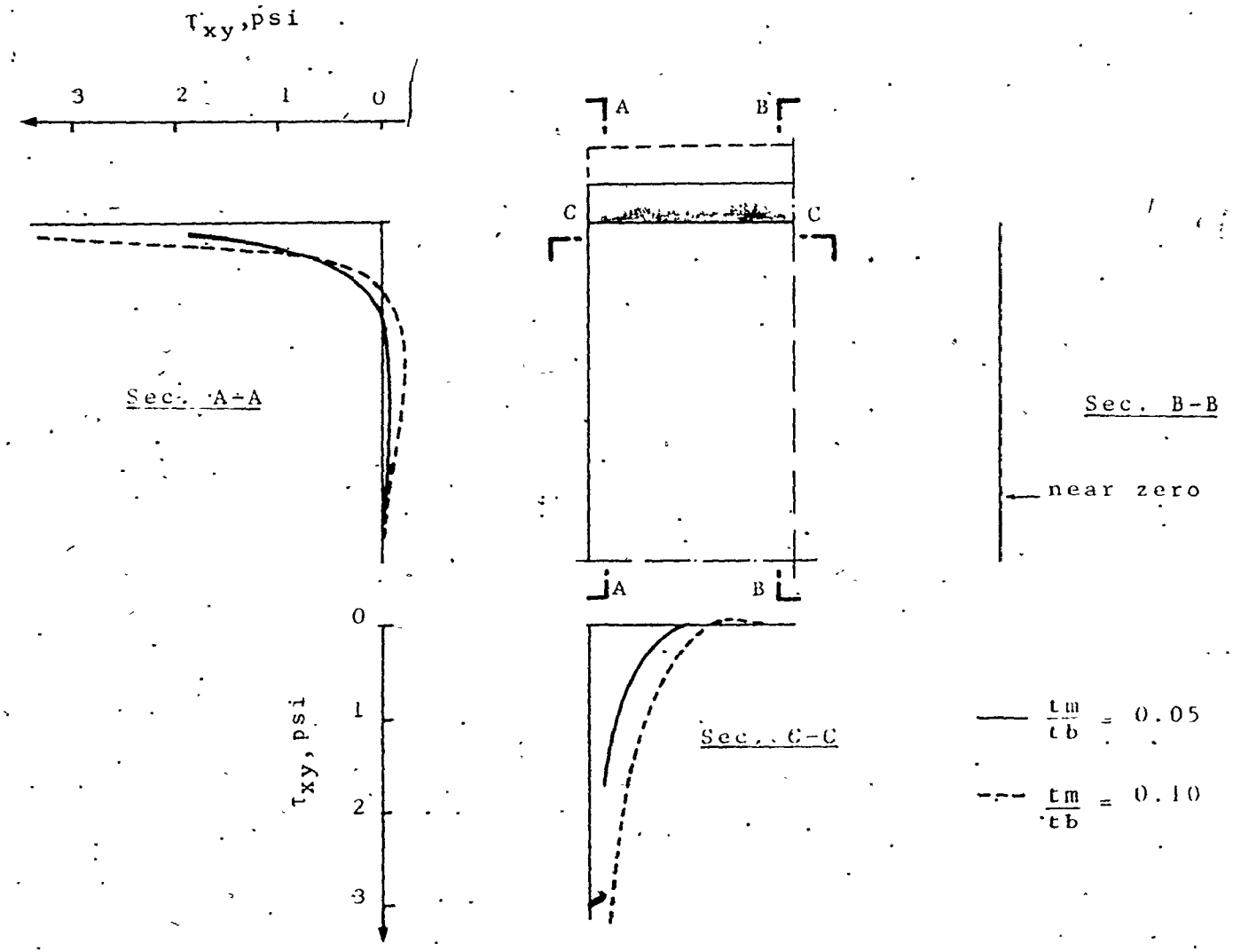

Fig. 3.56 EFFECT OF JOINT THICKNESS ON THE SHEAR STRESS DISTRIBUTIONS, τ_{xy}, FOR AXIALLY LOADED UNGROUTED PRISMS

the experimental observations that the cracks initiated at the corners of the block and not in the middle.

2 - Shear stresses, which were ignored by investigators[15,24,31] who analysed the compressive strength of brick masonry, are created near the block-mortar interfaces and are sharply concentrated at the interfaces and towards the corners especially for ungrouted masonry. This causes a nonuniform distribution of the lateral normal stresses which can be explained by shear lag. As shown in Figs. 3.53 and 3.55, higher values of lateral tensile and shear stresses were obtained for ungrouted masonry prisms compared to similar grouted prisms at the same stress level. The stress concentrations near the corners indicate a higher possibility of the major cracks initiating near the corners of the central block. This phenomenon was shown to exist for most of the prisms tested, as shown in Figs. 3.14, 3.15, 3.16 and 3.41. However, because of the fact that the crack positions could be significantly influenced by local material flaws, in some cases the initial cracks had no preferential location along the interfaces of the block and the mortar. However, without exception, cracks initiated at the interfaces of the central block and the top and bottom mortar joints and propagated after towards the middle.

3 - The greater the flexibility of the mortar (lower modulus of elasticity and/or higher Poisson's ratio), the higher are the tensile stresses imposed on the blocks as shown in Figs.

3.49 and 3.50 for ungrouted prisms. Figure 3.51 shows that higher lateral tensile stresses are imposed on the blocks by increasing the mortar joint thickness. A comparison of the tensile stresses shown in Figs. 3.51 and 3.53 indicates that the joint thickness has less effect in the case of grouted prisms than in the case of similar ungrouted assemblages. This feature of behaviour confirms the experimental finding mentioned in Section 3.2.4.2 which is that for grouted masonry the mortar joint characteristics are less significant in influencing the behaviour of masonry assemblages under axial compression.

4 - The mortar is shown to be more confined near the centre where there are no shear stresses developed at the interfaces. Elements of mortar near the edges are less confined and therefore would probably fail first under compression stresses if the concrete block does not fail under a biaxial compression-tension state of stress. As explained before, the blocks tend to confine the mortar joint as it is less stiff and the failure normally occurs when the blocks are no longer capable of confining the mortar joints. It was observed in the experimental program that spalling of the outer faces of the mortar joints around the edges had occurred immediately before failure and was followed, after very little increase in load, by splitting of the blocks which caused the failure of the prism.

5 - Comparing the maximum shear stresses developed at the interfaces with the limiting friction which could exist due to the

vertical compressive stresses normal to the bed joints adopting a coefficient of internal friction of about 1.0 (see Section 5.2.3.6) indicates that these shear stresses are far below the frictional resistance and the possibility of failure by debonding at the interfaces will not take place under axial compression.

3.3.3 A Failure Criterion For Block Masonry under Axial Compression

3.3.3.1 Introduction: It is pointed out in the concluding part of Section 3.3.1 that the failure theories available to describe the compressive strength of solid brickwork are not applicable to grouted concrete masonry because they have been developed on the basis of the interaction between only two materials, brick and mortar. As shown experimently, the continuity provided by grouting the cores makes the behaviour of grouted masonry much different from ungrouted masonry. A failure criterion for ungrouted and grouted concrete masonry under axial compression is proposed and will be discussed in the following sections:

3.3.3.2 The Approach to the Problem: In this investigation a 'strength' approach, which was first adopted by Hilsdorf[13] in 1967, for the development of a failure criterion is considered. In this approach, the assemblage strength will be determined by the interaction of the strength properties of the block, mortar, and grout in their appropriate complex states of stress.

The adopted strength approach has the distinct advantage

over the strain approach adopted by Francis et al[7] in that it deals with the strength values of the constituent materials and these are readily and accurately measurable quantities. The strain approach requires the determination of the elastic constants of the components, and being inelastic materials, these not only vary according to the level of the applied stress but are difficult to measure near ultimate load. For instance, Poisson's ratio for these brittle materials is shown to increase rapidly[39,56] owing to the development of microcracking which changes the material to a discontinuous media and hence, the use of linear elasticity is no longer applicable. More important however is that, the strength approach accounts for the change in material properties of the components in a state of multiaxial stress. This change in material properties is a typical feature in the behaviour of brittle materials.

3.3.3.3 Assumptions and Considerations: Determination of the compressive strength of ungrouted or grouted concrete masonry is a three dimensional stress problem for a nonhomogeneous media composed of multiphase materials. It is the inelastic behaviour characteristics of the components under multi-axial states of stress which govern their interactions and determine the failure mechanisms. Even the use of a sophisticated numerical method such as a nonlinear three dimensional finite element analysis requires detailed information about the deformational characteristics of the different components under multiaxial states of stresses and

these are rather difficult to determine and apparently not yet available in the literature. Even if this information was available, it is not likely that such a detailed analysis would be feasible because of the iterations resulting from the nonlinearities in three dimensions.

Because of the inherently complex nature of the problem and realizing that the objective is to develop a technique to determine the ultimate capacity of the assemblage, simplifications must be made to make this feasible. Therefore, some assumptions have to be introduced concerning the following features:

1 - Bond at the interfaces: Perfect bond at the interfaces between the block, mortar, and grout is assumed. As it is shown from the finite element analysis (Section 3.3.2), the shear stresses developed at the block-mortar interfaces are far below the frictional resistance due to the normal stresses and hence, a shear slippage failure at the interfaces is not possible. Also, the test conditions (stiff plates to transmit the compressive load to the assemblage) would prevent vertical slip between the blocks and the grout.

2 - Distribution of vertical stresses: The vertical stresses are assumed to be distributed between the shell (blocks and mortar joints) and the infill (grouted cores) in proportion to their relative axial stiffness. This is dictated from the compatability of deformation in the vertical direction assured, experimently, by applying the load through stiff bearing plates.

3 - Distribition of Lateral Stresses: It is shown from the finite element analysis that a nonuniform field of lateral stresses would be developed by the compatibility of deformation between weaker mortars and stronger blocks. The lateral stresses imposed on the shell due to the lateral deformation of tne grout would be distributed more uniformly over the height of the block. Also, in reality, as failure approaches there will probably be considerable redistribution of lateral stresses within the masonry units and mortars since these materials, especially mortar, are inelastic near ultimate stress[31,42]. However, since it is not possible to determine the actual stress distribution at failure, a more or less uniform stress condition could be assumed at failure due to the possible stress redistributions[31]. It is worth mentioning that the assumption of a uniform lateral stress distribution will considerably simplify the analytical formulation of the problem. The shear stresses at the block-mortar interfaces are ignored because using the finite element analysis, it is shown that these stresses are very low compared to the compressive stresses (ranging from 2% to 4%). The lateral stresses in the two transverse directions are assumed to be equal since the experimental results revealed no significance of the shell thickness to width ratio of the block as long as the net to gross area ratio is kept the same. Therefore a square cross section could be employed which, in turn, dictates equal transverse stresses.

4 - Strength of concrete block under biaxial stresses:

Mohr's theory of failure is adopted to express the failure of concrete block under a biaxial state of compression-tension. A linear relationship between the shear stress, τ, at any plane and the corresponding normal stress, p, was found by Brestler and Pister[6] for concrete. It takes the form,

$$\tau = a - bp \qquad \ldots\ldots (3.9)$$

where a and b are material constants determined from tests under uniaxial states of stress. The formula leads to a straight line relationship between the principal stresses[35] as shown in Fig. 3.57.

It is reported[31] that Vile, in his biaxial compression-tension tests on concrete and on mortar, obtained the different shapes of failure envelopes shown in Fig. 3.57, the profiles appear to be affected by the volume fraction, V_f, of the coarse aggregates in the concrete mix. A concavity in the failure envelope exists for mortar having no coarse aggregate, $V_{f=0}$, whereas a convexity in the envelope exists for concrete having coarse aggregates. The change in the profile of biaxial failure envelopes with varying percentage of coarse aggregates was attributed to the stone in the mix functioning as crack-arresters during the phase of major microcracking in the concrete under load past the point of discontinuity. This feature of behaviour, which is well established in the study of microcracking of concrete,

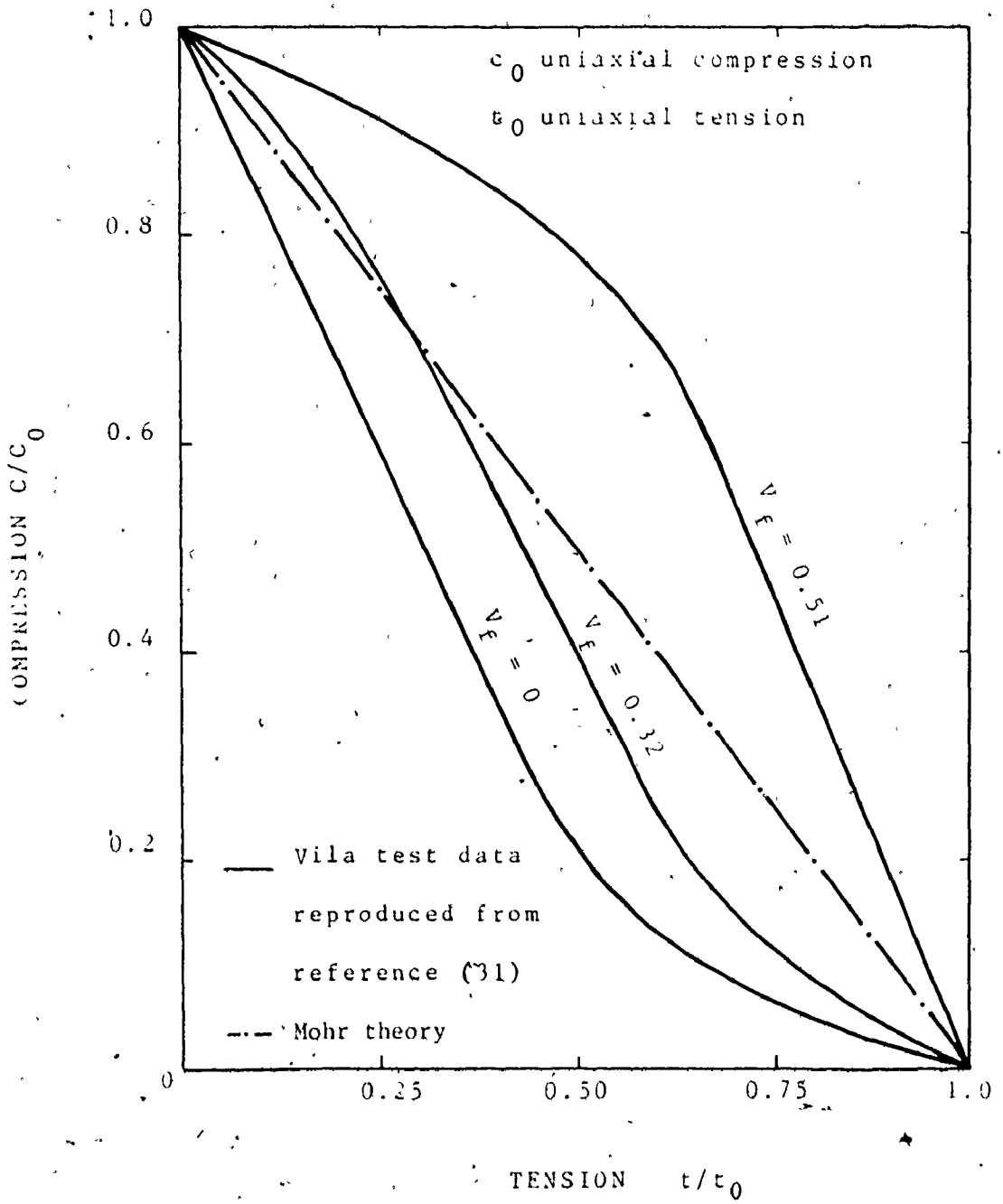

Fig. 3.57 FAILURE ENYELOPES FOR BRITTLE MATERIALS UNDER BIAXIAL TENSION-COMPRESSION

explains the observed increase in the biaxial strength of concrete with increasing percentage of coarse aggregate in the mix. This corresponds to a higher convexity of the biaxial failure envelope. Experimental results by Kupfer et al[32] support the convexity of the failure envelope for normal concrete (having coarse aggregate) while Khoo's[31] experimental results confirm the concavity of the failure envelope for the more homogenous mortar and brick materials.

For concrete blocks having coarse aggregate of moderate size and percentage, it seems to represent an intermediate case between normal concrete having a considerable percentage of coarse aggregate and the brick and mortar having no coarse aggregate. Hence, the adopted straight line relationship seems to be a reasonable representation of the failure envelope of concrete blocks.

5- Strength of mortar and grout under triaxial compression: In his analytical formulation of the compressive strength of brick masonry, Hilsdorf[24] assumed that the strength of the mortar under triaxial compression is similar to the strength of concrete under triaxial compression. The following relationship, which is used for concrete, was adopted by Hilsdorf for mortar:

$$f_1' = f_c' + 4.1\ \sigma_2 \qquad \ldots\ (3.10)$$

where f_1' is the compressive strength of a laterally confined concrete cylinder, f_c' is the uniaxial compressive strength of the

cylinder, and σ_2 is the lateral confining stress. Equation (3.10) is basically Coloumb's theory of internal friction which expresses the relationship between the major stress, σ_3, and the minor stress, σ_1, as[31]:

$$\frac{\sigma_1}{\sigma_0} = 1 + \left(\frac{(\mu^2+1)^{1/2} + \mu}{(\mu^2+1)^{1/2} - \mu}\right) \frac{\sigma_3}{\sigma_0} \qquad \ldots\ldots (3.11)$$

where σ_0 is the uniaxial compressive strength and μ is the coefficient of internal friction. This relation shows that the higher the coefficient of internal friction is, the lower is the confining stress required to increase the compressive strength over the uniaxial strength by a certain percentage. This also indicates that the value 4.1 in Equation (3.10) will be different from one material to another depending on their coefficients of internal friction. Khoo[31] showed, by comparing the failure envelopes for concrete with those for mortar, that the increase in the ultimate strength of concrete caused by increasing the confining pressure is higher than that for mortar. He suggested the following empirical equation to express the strength of mortar under under triaxial compression:

$$\frac{\sigma_1}{\sigma_0} = 1 + 2.91 \left(\frac{\sigma_3}{\sigma_0}\right)^{0.805} \qquad \ldots\ldots (3.12)$$

For the current investigation, and to simplify the formulation of the problem, a linear relationship based on Khoo's experimental results is adopted. His experimental results were

found to be accurately represented using a straight line relationship for the ranges of stresses encountered in the current study. Using a linear regression analysis, Khoo's experimental results yield the following expression:

$$\sigma_1 = \sigma_0 + 3.6\ \sigma_3 \qquad \ldots\ (3.13)$$

For grout under triaxial compression, Equation (3.9) which is used for normal concrete, is adopted in the current investigation. Comparing Equation (3.9) for concrete and Equation (3.13) for mortar indicates that the compressive strength of the grout will be influenced by the confining stresses more than the mortar is. This could be attributed to the higher internal friction coefficient of the grout (having coarse aggregates).

3.3.3.4 Formulation of the Problem: Two failure conditions are possible for grouted concrete masonry under axial compression depending on which is going to first reach its unconfined compressive strength; the shell (the blocks and the mortar joints) or the grouted core. This is mainly governed by the strain at maximum stress for each. In the first condition, which is probably the most frequent case in practice, the grout is stiffer than the shell and has a lower strain level at maximum stress (see Section 3.2.4.1). Hence, its unconfined compressive strength would be reached first and the shell would tend to confine the grout. Failure will occur in the shell when it is no longer capable of confining the grout (and the mortar as well). In the

other case, the shell stiffness is equal or higher than the grout and the ultimate strength of the shell would be reached first. Hence, failure would be controlled by the unconfined strength of either the shell or the grout.

Case I:

If a grouted masonry prism is loaded under axial compression the vertical stress will be shared by the shell and the grouted core in proportion to their axial stiffnesses. When the compressive stresses acting on the mortar and/or the grout approach their uniaxial compressive strengths, they will tend to expand laterally due to the high inelastic deformations caused by the creation of the microcracking. The shell will tend to confine the mortar and the grout. These confining stresses are counterbalanced by tensile stresses developed in the shell which will cause, along with the vertical stress, a premature splitting failure of the shell under a state of compression-tension stresses.

The prisms shown in Fig. 3.58, under an average uniform vertical stress, σ_y, will be considered using an equivalent square cross section.

Considering that the load will be shared by the shell and the grouted core in proportion to their relative axial stiffness, the compatibility of deformation in the vertical direction yields,

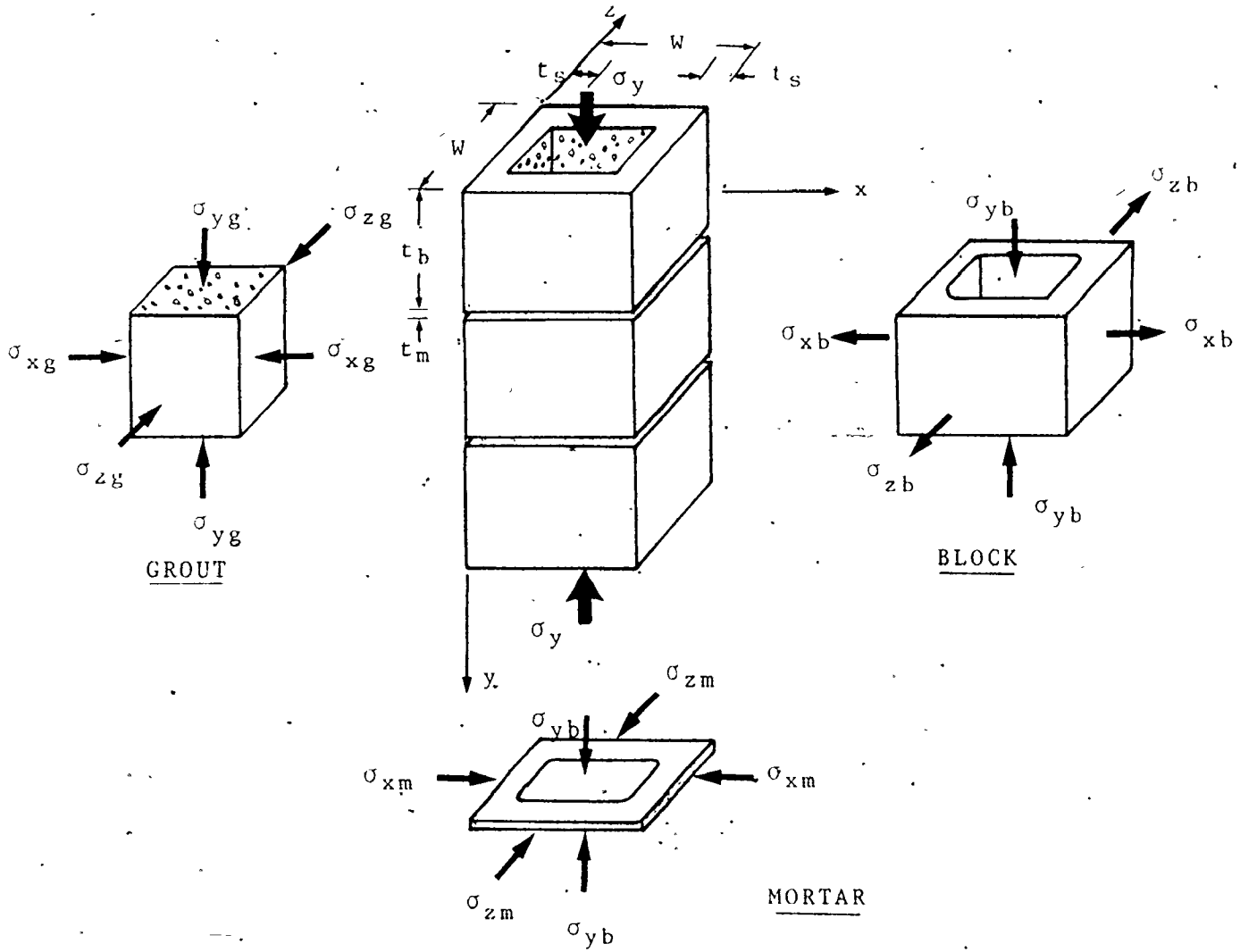

Fig. 3.58 ILLUSTRATION OF THE STRESSES DEVELOPED IN THE COMPONENTS OF A GROUTED MASONRY PRISM LOADED UNDER AXIAL COMPRESSION

$$\frac{\sigma_{yb}}{E_{bs}} = \frac{\sigma_{yg}}{E_g} \qquad \ldots\ldots (3.14)$$

where σ_{yb} and σ_{yg} denote the vertical stresses apply on the shell and the grouted core and E_{bs} and E_g denote the respective secant moduli of elasticity at the same strain level.

From the equilibrium of the stresses in the vertical direction:

$$\sigma_y A_g = \sigma_{yb} A_b + \sigma_{yg} A_{gr} \qquad \ldots\ldots (3.15)$$

where A_g, A_b and A_{gr} denote the gross sectional area, the block sectional area (net area), and the grouted core sectional area. The equation can be rewritten in the form:

$$\sigma_y = \sigma_{yb} \cdot \eta_h + \sigma_{yg} (1-\eta_h) \qquad \ldots\ldots (3.16)$$

where η_h is the net to gross area ratio of the block. Substituting Equation (3.14) into Equation (3.16) yields:

$$\sigma_{yb} = \frac{n}{1+n\eta_h-\eta_h} \sigma_y = n\gamma\, \sigma_y \qquad \ldots\ldots (3.17)$$

$$\sigma_{yg} = \frac{1}{1+n\eta_h-\eta_h} \sigma_y = \gamma\, \sigma_y \qquad \ldots\ldots (3.18)$$

where:

$$n = \frac{E_{bs}}{E_g} \qquad \eta_h = \frac{A_b}{A_b+A_{gr}} \qquad \gamma = \frac{1}{1+(n-1)\eta_h}$$

The failure criterion of the block under biaxial stresses

is represented by Mohr's theory of failure yielding a straight line relationship between the principal stresses as shown by line A in Fig. 3.59. It can be expressed analytically in the form:

$$\sigma_{xb} = \sigma_{zb} = \sigma_{tbl}(1 - \frac{\sigma_{yb}}{\sigma_{cb}}) \quad \ldots\ (3.19)$$

where σ_{tbl} and σ_{cb} are the uniaxial tensile and compressive strengths of the block and σ_{xb} and σ_{zb} are the lateral tensile stresses acting on the shell (see Fig. 3.58).

The state of stress of the mortar under triaxial compression (see Fig. 3.57) can be expressed as:

$$\sigma_{ym} = \sigma_{yb} = \sigma_{cm} + 3.6\ \sigma_{xm} \quad \ldots\ (3.20)$$

where σ_{cm} is the unconfined compressive strength of the mortar and $\sigma_{xm} = \sigma_{zm}$ are the confining stresses necessary for the mortar to develop compressive stress, σ_{ym}, exceeding its unconfined compressive strength. Equation (3.20) can be rewritten in the form:

$$\sigma_{xm} = \sigma_{zm} = 1/3.6\ (\sigma_{yb} - \sigma_{cm}) \quad \ldots\ (3.21)$$

From Equation (3.10) the strength of the grout under the triaxial compression state of stress, shown in Fig. 3.59, can be expressed as:

$$\sigma_{yg} = \sigma_{cg} + 4.1\ \sigma_{xg} \quad \ldots\ (3.22)$$

or

$$\sigma_{xg} = \sigma_{zg} = 1/4.1\ (\sigma_{gy} - \sigma_{cg}) \quad \ldots\ (3.23)$$

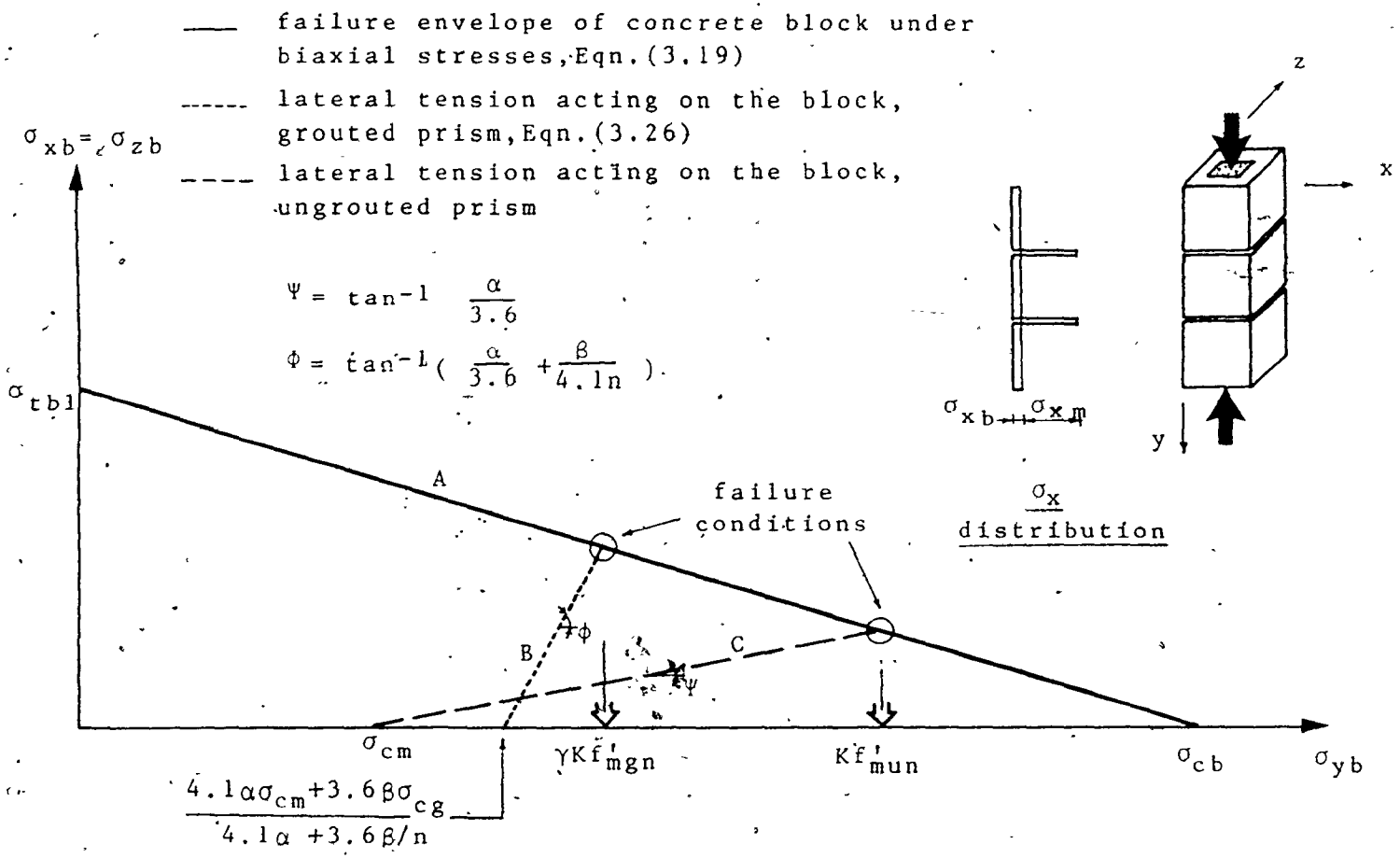

Fig. 3.59 FAILURE CONDITION FOR UNGROUTED AND GROUTED MASONRY UNDER AXIAL COMPRESSION

where σ_{cg} is the unconfined compressive strength of the grout and σ_{yg} is the grout strength under confining lateral stress σ_{xg} ($\sigma_{xg}=\sigma_{zg}$). These confining stresses acting on the mortar and the grout are counterbalanced by tensile stresses acting on the block. From the equilibrium condition in the lateral direction (see the sketch in Fig. 3.59), it follows that

$$2\, t_s t_b \cdot \sigma_{xb} = 2\, t_s t_m \cdot \sigma_{xm} + (W-2t_s) t_b \cdot \sigma_{xg} \quad \ldots\ (3.24)$$

therefore

$$\sigma_{xb} = \alpha\, \sigma_{xm} + \beta\, \sigma_{xg} \quad \ldots\ (3.25)$$

where

$$\alpha = t_m/t_b \qquad \beta = \frac{W-2t_s}{2t_s} = \frac{\sqrt{1-\eta_h}}{1-\sqrt{1-\eta_h}}$$

Substituting Equations (3.21) and (3.23) in Equation (3.25), one obtains an expression of the lateral tensile stresses acting on the block for line B in Fig. 3.59,

$$\sigma_{xb} = \frac{\alpha}{3.6}(\sigma_{yb} - \sigma_{cm}) + \frac{\beta}{4.1}\left(\frac{\sigma_{yb}}{n} - \sigma_{cg}\right) \quad \ldots\ (3.26)$$

From substitution of Equations (3.17) and (3.19) into Equation (3.26) the magnitude of the maximum compressive stress, σ_{yb}, accommodated by the block at failure can be determined. It corresponds to the point of interseotion of lines A and B in Fig. 3.59,

$$\sigma_{yb} = \frac{4.1\ \sigma_{tbl} + 1.14\ \alpha\ \sigma_{cm} + \beta\ \sigma_{cg}}{4.1\ \sigma_{tbl} + (1.14\ \alpha + \beta/n)\ \sigma_{cb}}\ \sigma_{cb} \qquad \ldots\ (3.27)$$

The modular ratio, n, is to be calculated on the basis of the secant modulus of the shell and the grout at the strain corresponding the the maximum unconfined strength of the grout. This strain is nearly equal to 0.002 in/in for the types of grout considered in this investigation as indicated from the stress-strain curves of the grouts shown in Fig. 3.19.

Realizing the fact that a redistribution of the vertical stresses between the shell and the grouted cores will take place near failure due to the expected variation of their stiffnesses from those calculated at 0.002 in/in strain, a coefficient "K" is introduced. This coefficient was determined experimentally from the measurements of the strains on the block near failure. It can be defined as:

$$K = \frac{\sigma_{ybe}}{n\gamma\sigma_{ye}} \qquad \ldots\ (3.28)$$

where σ_y is the average vertical stress calculated near 0.95 of the ultimate load and σ_{ybe} is the block stress calculated from the measured strain at the same load using the stress-strain curve shown in Fig. 2.4. Fig. 3.60 show the variation of the coefficient "K" with the modular ratio "1/n". Using a linear regression analysis, the following expression relating the two parameters is yielded,

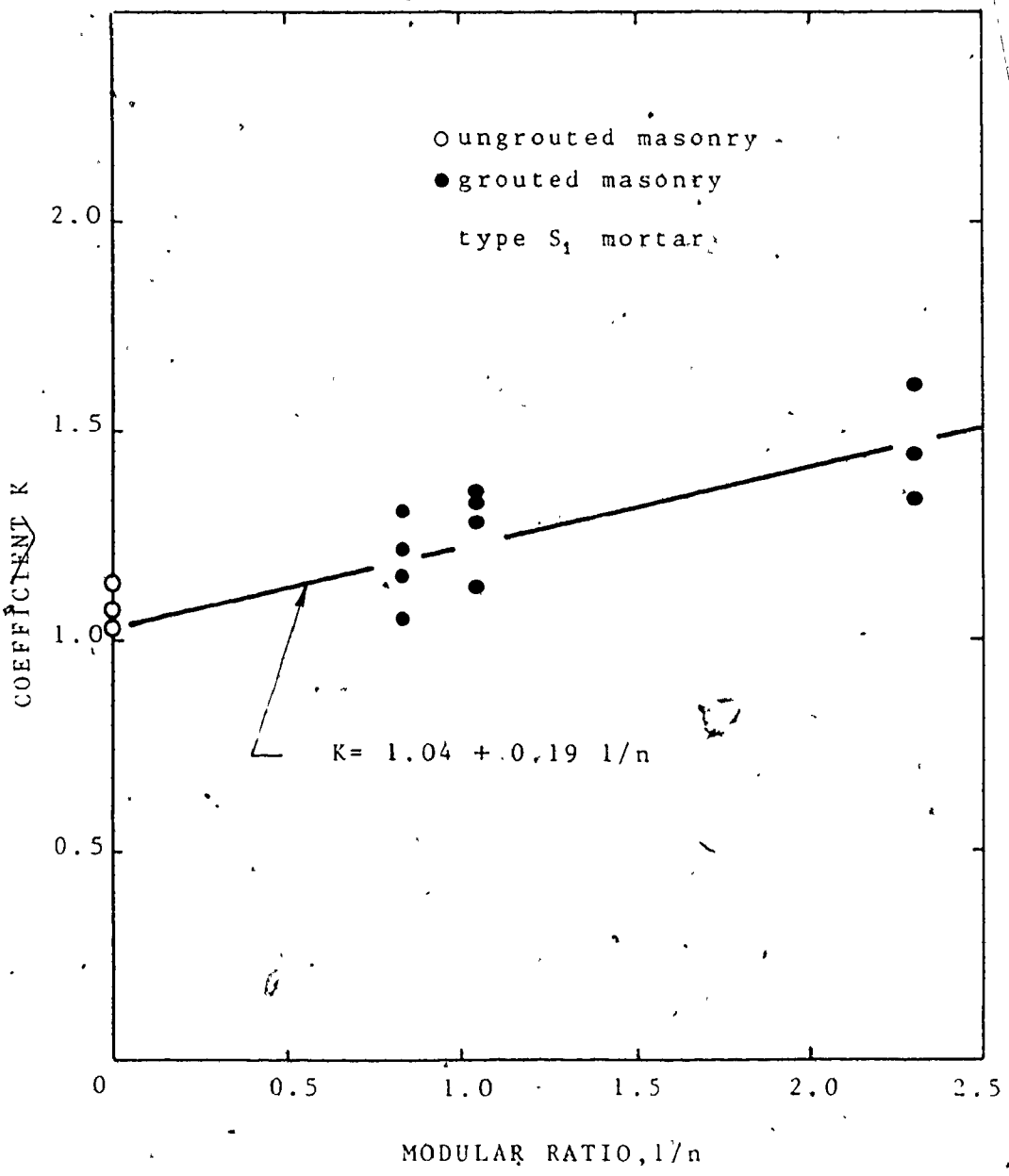

Fig. 3.60 THE COEFFICIENT K VERSUS THE MODULAR RATIO $\frac{1}{n}$

$$K = 1.04 + 0.19\ 1/n \qquad \ldots\ (3.29)$$

considering that Equation (3.28) is applicable at failure, it can be rewritten in the form,

$$K = \frac{\sigma_{yb}}{n\gamma f'_{mgn}} \qquad \ldots\ (3.30)$$

where f'_{mgn} is the average compressive stress of grouted prisms at failure. Substituting Equation (3.30) into Equation (3.27), the prism compressive strength can be expressed in terms of the strength and geometric characteristics of its components as follows:

$$f'_{mgn} = \frac{4.1\ \sigma_{tbl} + 1.14\ \alpha\ \sigma_{cm} + \beta\ \sigma_{cg}}{4.1\ \sigma_{tbl} + (1.14\ \alpha + \beta/n)\ \sigma_{cb}} \frac{\sigma_{cb}}{n\gamma K} \qquad \ldots\ (3.31)$$

It has to be noted that Equation (3.31) is valid as long as the vertical stress acting on the grout at failure is higher than its unconfined compressive strength which insures that the following condition is satisfied:

$$\sigma_{yg} > \sigma_{cg}$$

or

$$\gamma K\ f'_{mgn} > \sigma_{cg} \qquad (3.32)$$

In cases where the above condition is not satisfied, the expressions presented in Case II should be employed.

Case II:

In this case the grout is no longer confined by the shell at failure and the capacity will be controlled by either the capacity of the shell under a compression-tension state of stress or by the capacity of the core under axial compression after failure of the shell.

In this case, the shell will be under vertical compressive stresses, σ_{yb}, in proportion to the relative axial stiffnesses of the shell and the core, as expressed in Equation (3.14). The shell will act to confine the mortar only and these confining stresses have to be counterbalanced by tensile stresses, σ_{xb}, acting on the block which can be expressed using Equation (3.26) and omitting the second term (concerning the effect of grout). Adding the failure criterion for block under tension-compression, expressed by Equation (3.19), the maximum stress, σ_{yb}, at failure can be calculated by substitution from Equations (3.17) into Equation (3.26) which yields

$$\sigma_{yb} = \frac{3.6\ \sigma_{tbl} + \alpha\ \sigma_{cm}}{3.6\ \sigma_{tbl} + \alpha\ \sigma_{cb}} \cdot \sigma_{cb} \qquad \ldots\ (3.33)$$

Substituting Equation (3.33) into Equation (3.30), one obtains an expression for the compressive strength of grouted masonry (Case II) in the form

$$f'_{mgn} = \frac{3.6\ \sigma_{tbl} + \alpha\ \sigma_{cm}}{3.6\ \sigma_{tbl} + \alpha\ \sigma_{cb}} \cdot \frac{\sigma_{cb}}{n\gamma K} \qquad \ldots\ (3.34)$$

If the core capacity is high enough to sustain higher loads, then the average compressive strength (based on the gross area) can be expressed as

$$f'_{mgn} = (1-\eta_h)\ \sigma_{cg} \qquad \ldots\ (3.35)$$

The greater compressive strength, f'_{mgn}, predicted by either Equation (3.34) or (3.35) is the governing strength for Case II.

3.3.3.5 Significance of the Proposed Formulas: The proposed expressions can be used to predict the compressive strength of grouted concrete masonry using the properties of its constituents, (block, mortar, and grout) which are relatively easy to evaluate by simple standard tests (see Chapter 2). These formulas can be also used to examine the effect of the various strength and geometric parameters on the assemblage compression capacity.

The expressions are derived in a general form so that they can also be used for hollow masonry having any percent solid. Substituting $\sigma_{cg} = 0$ (i.e. $n\gamma = 1/\eta_h$) for ungrouted (hollow) masonry in Equation (3.31) or even in Equation (3.34) yields the following expression:

$$f'_{mun} = \eta_h \cdot \frac{3.6\ \sigma_{tbl} + \alpha\ \sigma_{cm}}{3.6\ \sigma_{tbl} + \alpha\ \sigma_{cb}} \cdot \frac{\sigma_{cb}}{K} \qquad \ldots\ (3.36)$$

The above equation can predict the compressive strength of ungrouted masonry (based on the gross area) using the appropriate K value. The compressive strength can be calculated on the basis of the net area as follows:

$$f'_{mun} = \frac{3.6\ \sigma_{tbl} + \alpha_1 \sigma_{cm}}{3.6\ \sigma_{tbl} + \alpha\ \sigma_{cb}} \cdot \frac{\sigma_{cb}}{K} \qquad \ldots\ (3.37)$$

Substituting $\eta_n=1$ and $n=1$ in Equation (3.31) or in Equation (3.34) yields the following expression for plain masonry having 100 percent solid units:

$$f'_{msn} = \frac{3.6\ \sigma_{tbl} + \alpha\ \sigma_{cm}}{3.6\ \sigma_{tbl} + \alpha\ \sigma_{cb}} \cdot \frac{\sigma_{cb}}{K} \qquad \ldots\ (3.38)$$

It is interesting to note that Equation (3.38) is somewhat similar to Hilsdorf's[13] expression for predicting the compressive strength of solid brick masonry despite incorporating different features in the development of the proposed expressions.

It has to be noted that Case I represents the common case for the practical ranges of the strengths and deformation characteristics of the component materials. It also represents the interaction of the components in a more complex situation. Fig. 3.59 illustrates graphically this case. It is shown that the compressive strength of grouted masonry could be less than that for ungrouted masonry. This is attributable to the higher lateral tensile stress imposed in the block in the case of grouted masonry due to the grout's lateral expansion when its unconfined compressive strength is exceeded. Line B, which representing the lateral stresses imposed on the block in the case of grouted masonry, has a higher slope, ϕ, than the slope, ψ, for Line C which represents the lateral tension in the case of ungrouted

maonsry. A higher slope for either line B or C results in a lower compression caapcity. This indicates that, for a specified block characteristics, the compressive strength of ungrouted masonry increases with the decrease of the joint thickness to block's height ratio, α (decreasing α decreases the angle ψ) which agrees with the results of earlier investigators[15,48]. For grouted masonry, the compressive strength increases with a decrease of the ratio "β" (increasing the net to gross area ratio), an increase of the "n" value (increasing the strength and/or the stiffness of the grout), and a decrease of the "α" ratio. These features agree with the experimental results presented in this chapter.

Examining the proposed expressions indicate that the most significant parameter influencing the compressive strength of either ungrouted or grouted masonry is the block strength. This phenomenon has been shown to be valid for solid brick masonry[31]. A comparison of the current results for the compressive strengths of ungrouted an grouted masonry using two different block strengths (see sections 3.2.4.1 and 3.2.4.3) supports this statement.

To verify the proposed formulas, comparisons between the analytical predictions using the suggested expression and the compression tests results described earlier in Section 3.2.4.1 for ungrouted and grouted prisms were made. The experimental results are only applicable to the Case I failure condition where the failure is initiated by reaching the grouts' capacity first.

However, this is the most interesting and should be the controlling condition for most practical combinations of materials.

In Fig. 3.61, the compressive strengths of grouted masonry prisms, computed from Equation (3.31) for different grout strengths, are compared with the experimental results. It is shown that the analytical results compare reasonably well with the experimental results. The extent of the influence of the mortar strength on the compressive strength of grouted and ungrouted masonry is shown in Fig. 3.62 using both the analytical and the experimental results. Again, a reasonably good agreement is achieved. However, the comparisons presented in these figures indicate the tendency of the analytical expressions to predict slightly high strengths. This unconservative prediction could be attributed to having assumed a uniform stress distribution in the lateral direction. Also, the K values were calculated on the basis of the strain measurmeents at about 0.95 the ultimate load. Their values might be slightly increased at failure because of the possible redistribution of the vertical stresses at the onset of failure.

Not withstanding that the proposed expressions are approximate and contain some semi-empirical features, the suggested approach for predicting the compressive strength of

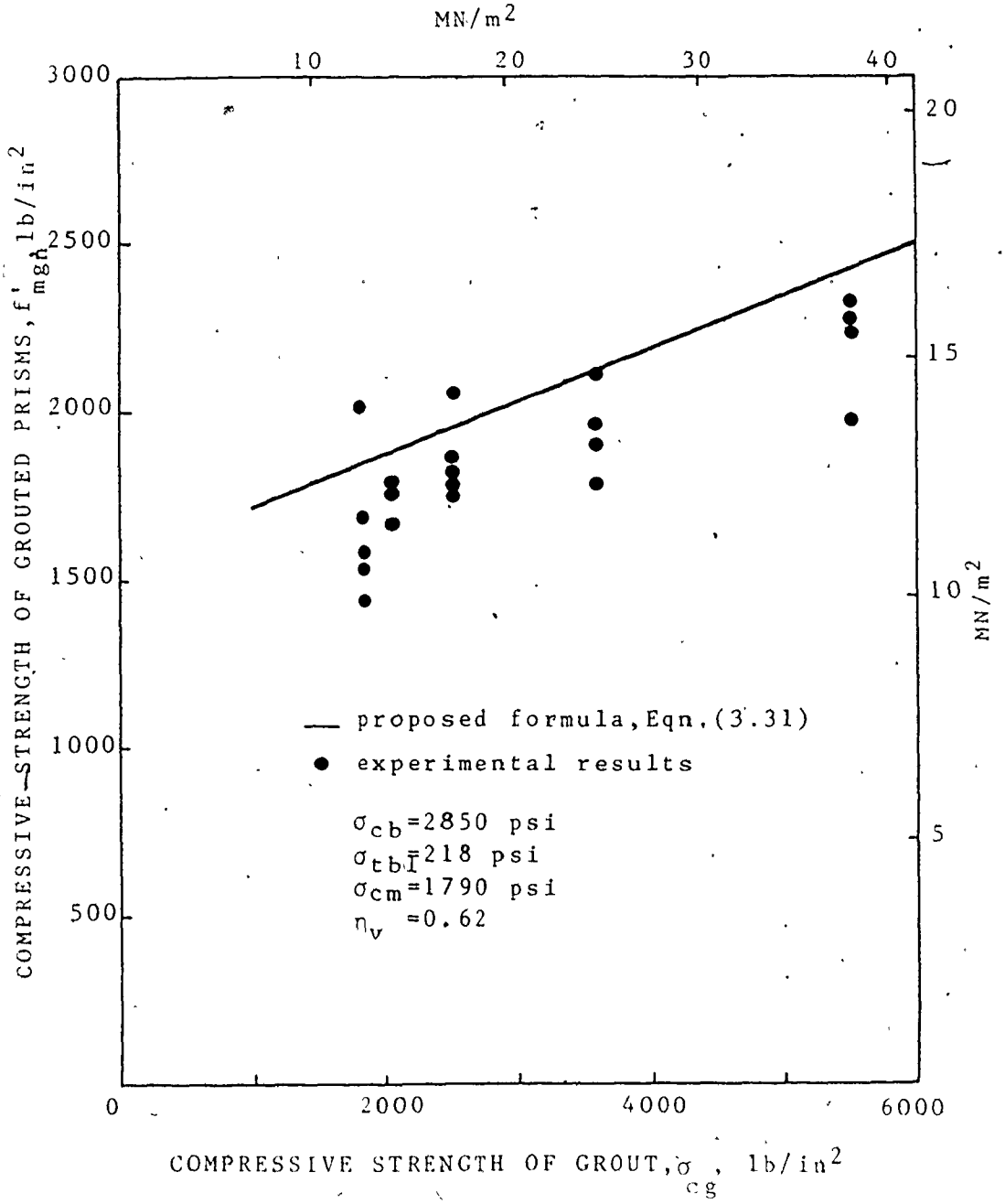

Fig. 3.61 COMPARISON OF MEASURED AND COMPUTED STRENGTH VALUES OF AXIALLY LOADED PRISMS HAVING DIFFERENT GROUT STRENGTHS

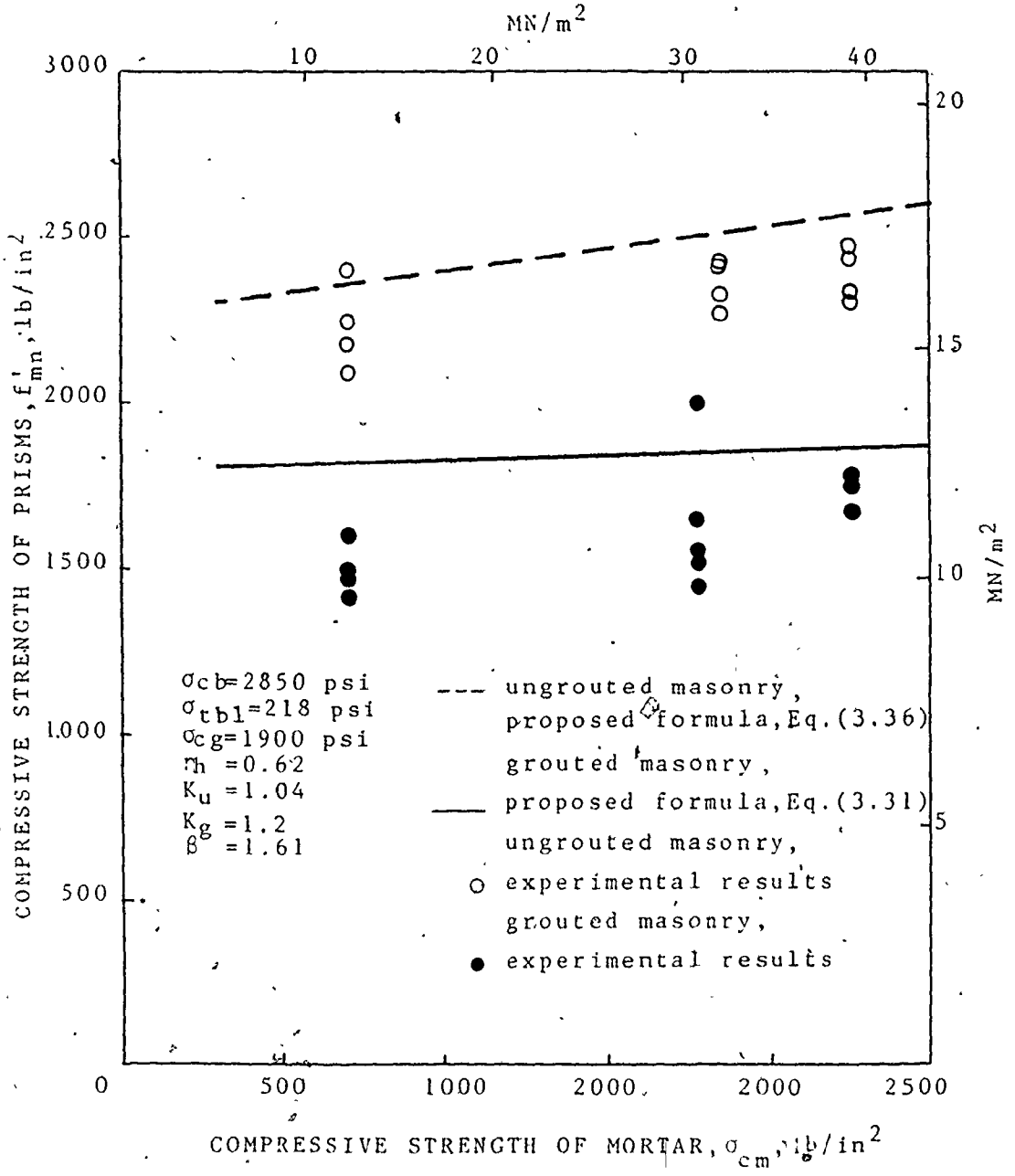

Fig. 3.62 COMPARISONS OF MEASURED AND COMPUTED STRENGTH VALUES OF AXIALLY LOADED PRISMS HAVING DIFFERENT MORTAR STRENGTHS

ungrouted and grouted concrete masonry appears to be rational and is reasonably representative of observed behaviour. It takes into consideration the relevant factors and expresses the components' behaviours in their appropriate complex states of stresses. This formulation provides the capability of predicting, in quantitative terms, the assemblage strength from the characteristics of its components. The proposed expressions are recommended to be used to assess the compressive strength of concrete masonry as long as the strength and the geometric parameters of its constituents are in the same ranges as those used in this investigation. Before the general applicability of the proposeed formulas could be recommended, the values of the coefficient "K", which is intended to account for the redistribution of the vertical stresses between the shell and the cores at the onset of failure, should be established for different ranges of block strengths and for various geometric characteristics.

3.3.4 Modulus of Elasticity of Concrete Masonry under Axial Compression

As shown in Fig. 3.25, the correlation between the stiffnesses of ungrouted and grouted masonry and their strengths under axial compression is poor. This can be attributed to the fact that the complex states of stress developed at failure due to the interaction of the component materials (under inelastic conditions) are quite different from those at early stages of

loading.

The following presentation is an attempt to express the elastic stiffness of the assemblage (the modulus of elasticity) as a function of the geometric and deformation characteristics of the block, mortar, and grout. It is assumed tht the components follow Hooke's Law which is reasonable because the prime concern here is to establish the modulus of elasticity of the assemblage for the elastic range. It has been shown that for stress below 50% of the strength of the component materials, they behave nearly elastically. Also a perfect bond at the interfaces is assumed.

The equivalent modulus of elasticity for an element consisting of either block and grout or mortar and grout is obtained by assuming that the axial rigidity of the composite is the sum of the axial rigidities of its components so that

i.e. $$E_{bg} A = E_g \cdot A_{gr} + E_b \cdot A_b, \quad \ldots\ldots (3.39)$$

$$E_{bg} = (1-n_h) E_g + n_h E_b \quad \ldots\ldots (3.40)$$

Similarly

$$E_{mg} = (1-n_h) E_g + n_h E_m \quad \ldots\ldots (3.41)$$

where E_{bg} and E_{mg} are the equivalent moduli of elasticity for composite elements of either block and grout or mortar and grout, respectively, n_h, is the net to gross area ratio of the block, and E_b, E_m, and E_g denote the modulus of rigidity of block, mortar, and grout, respectively.

The total axial deformation of the assemblage, Δ_a, between

the centre lines of two successive blocks can be expressed as the sum of the deformations of the two composite elements; block and grout, Δ_{bg}, and mortar and grout, Δ_{mg},

Hence $\Delta_a = \Delta_{bg} + \Delta_{mg}$ .... (3.42)

which can be rewritten as:

$$\frac{\sigma_y}{E_a}(t_b + t_m) = \frac{\sigma_y}{E_{bg}}(t_b) + \frac{\sigma_y}{E_{mg}}(t_m) \quad \text{.... (3.43)}$$

and substituting Equations (3.40) and (3.41) in Equation (3.43) yields

$$\therefore \quad \frac{1}{E_a} = \frac{\frac{t_b}{t_b+t_m}}{(1-\eta_h)E_g+\eta_h E_b} + \frac{\frac{t_m}{t_b+t_m}}{(1-\eta_h)E_g+\eta_h E_m} \quad \text{.... (3.44)}$$

Considering $\delta = t_b/(t_b+t_m)$, Equation (3.44) can be rewritten as:

$$E_a = \frac{1}{\frac{\delta}{(1-\eta_h)E_g+\eta_h E_b} + \frac{1-\delta}{(1-\eta_h)E_g+\eta_h E_m}} \quad \text{.... (3.45)}$$

Equation (3.37) can be used to determine the modulus of elasticity of the assemblage from the elastic properties and the geometric characteristics of the block, mortar and grout. This equation can also be used to 100% solid masonry by substituting $\eta_h = 1$ which yields,

$$E_a = \frac{1}{\frac{\delta}{E_b} + \frac{1-\delta}{E_m}} \qquad \ldots\ldots(3.46)$$

This last equation is similar to that derived by Sahlin[47] for solid brick masonry. It is also valid for ungrouted masonry with any percent solid.

Figure 3.63 shows a comparison between the moduli of elasticity for prisms having different grout strengths calculated using Equation (3.45), and those obtained experimentally (the secand modulus for the stress strain curves was obtained by a least square fit at 0.5 of the ultimate load). The average strain at this stress level was nearly 0.0005 in/in and since the components should undergo the same vertical strain (compatability of deformation), their moduli of elasticity were calculated at the same strain. The block, mortar, and grout moduli of elasticity were determined from the stress-strain curves shown respectively in Figs. 2.4, 3.25, and 3.19. It is shown that the proposed expression can reasonably pedict the assemblage stiffness from the characteristics of its components.

Figure 3.64 shows the variation of the assemblage modulus of elasticity with the variation of the mortar's modulus of elasticity. It is shown that while the mortar stiffness has a significant effect on the stiffness of ungrouted masonry, it is less significant for grouted masonry. The figure also indicates that the mortar joint thickness has relatively little influence on

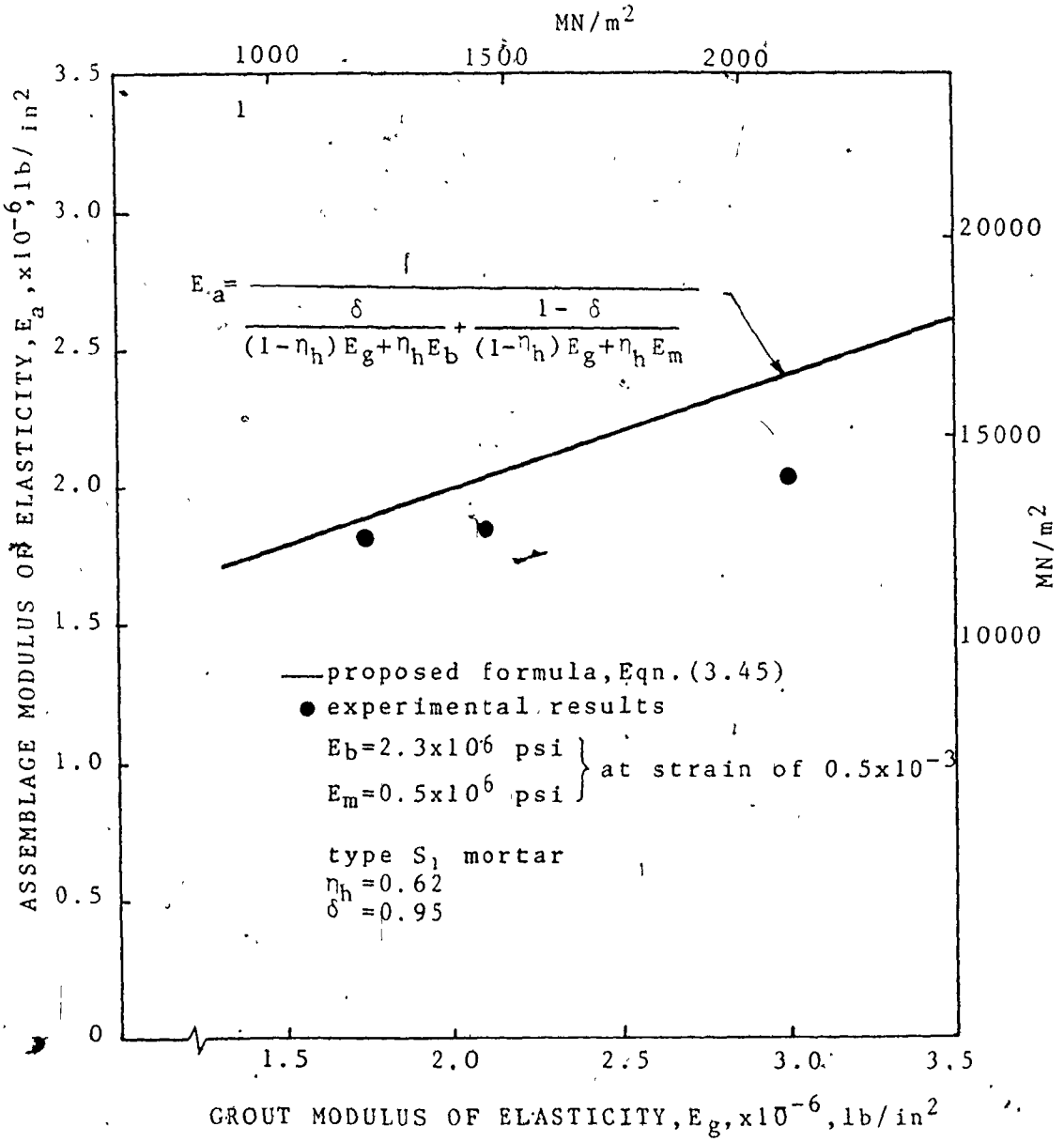

Fig. 3.63 COMPARISON OF THE COMPUTED AND MEASURED VALUES OF PRISMS MODULI OF ELASTICITY

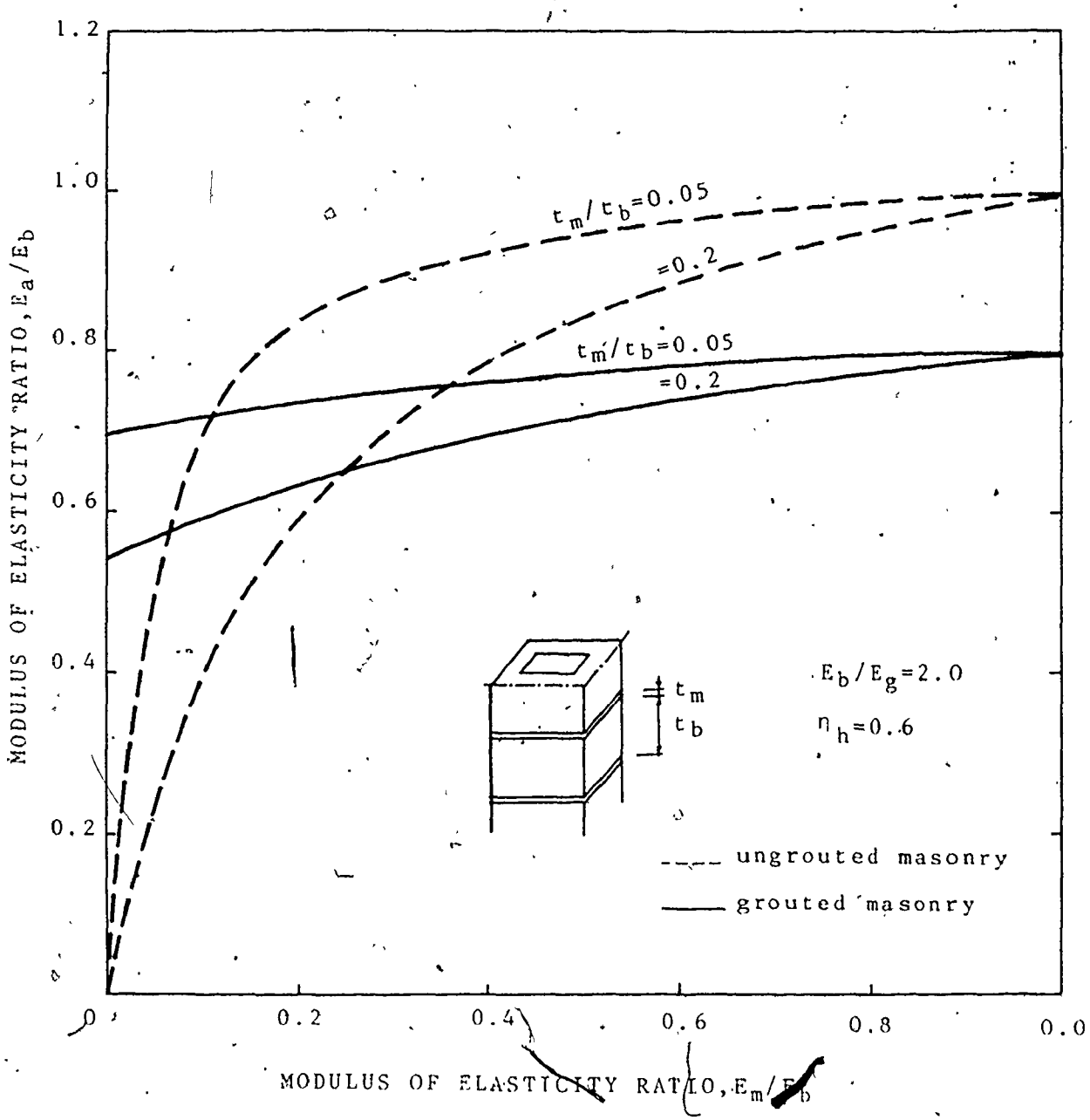

Fig. 3.64 ASSEMBLAGE MODULUS OF ELASTICITY VERSUS MORTAR MODULUS OF ELASTICITY FOR AXIALLY LOADED PRISMS

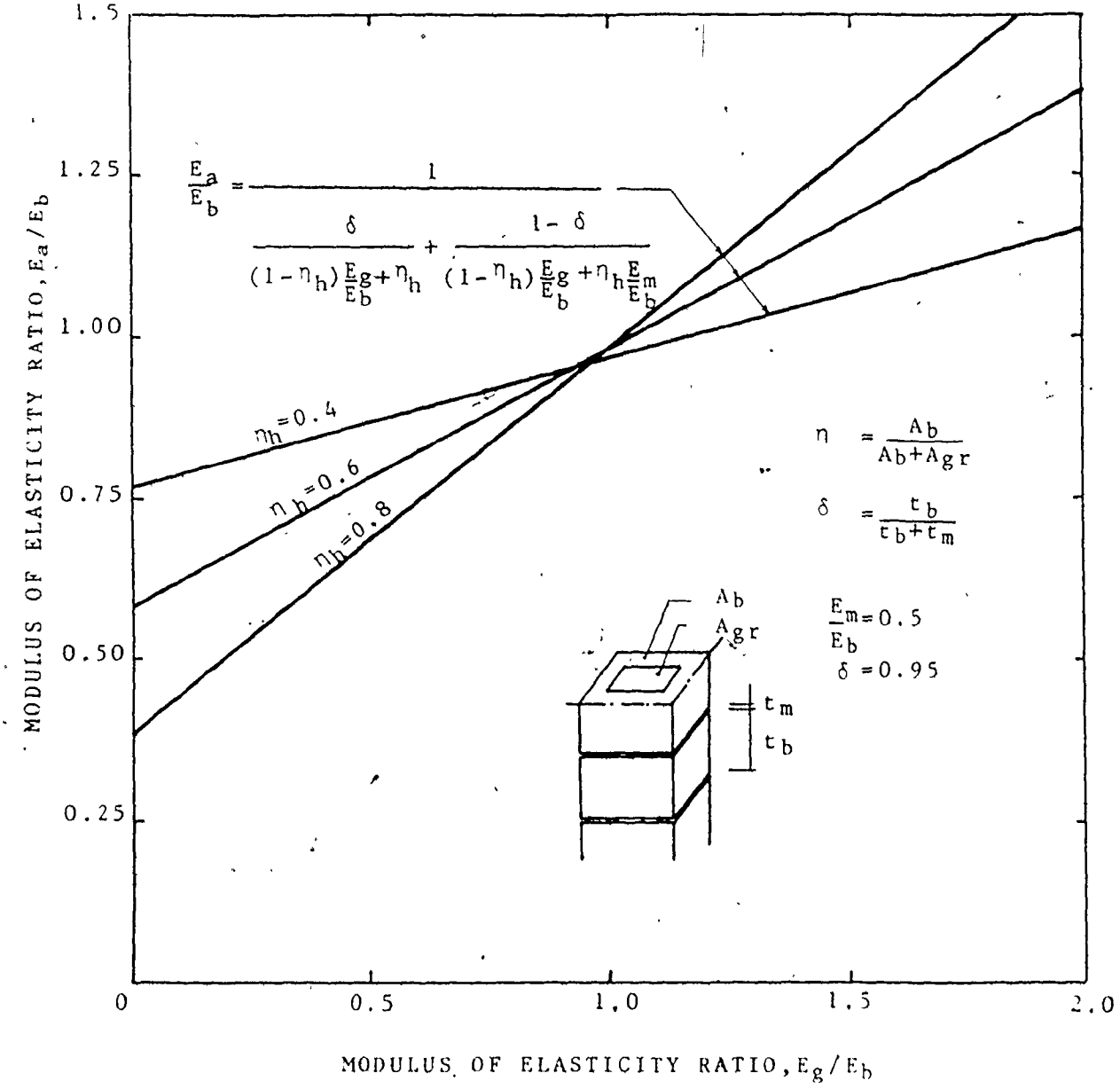

Fig. 3.65 ASSEMBLAGE MODULUS OF ELASTICITY VERSUS GROUT MODULUS OF ELASTICITY OF AXIALLY LOADED GROUTED PRISMS

the assemblage's axial stiffness for grouted masonry compared to its influence for ungrouted masonry. This feature of behaviour supports the conclusion previously drawn from the experimental results which suggested that the mortar properties have comparatively little effect on the behaviour of grouted masonry assemblages under axial compression. Figure 3.65 shows the significance of the net to gross area ratio of the block, η_h, on the assemblage's modulus of elasticity for different grouts. For a grout which is less stiff than the block, higher η_h ratios result in higher assemblage stiffnesses, while for a stiffer grout higher η_h ratios lead to lower assemblage stiffnesses under axial compression.

3.4 Review of the Code Provisions:

Utilizing the results of the current experimental and analytical investigations, the provisions of CSA Standard S 304[12] concerning the compressive strength of ungrouted and grouted concrete masonry and their moduli of elasticity are reviewed as follows:

1 - The code assigns a compressive strength for grouted masonry similar to that for solid masonry provided that the grout strength is at least equal to that of the masonry units. The current experimental results showed strength values for grouted masonry which were less than those for ungrouted masonry even for high strength grout. They also indicated that the

strength superposition concept is not applicable and that the requirement for matching the compressive strength of the block and the grout, which is adopted by the code, is not sound and may lead to nonconservative results. It seems that matching the deformational characteristics of the two components would be more efficient.

2 - The compression capacities predicted using the proposed strength formula (Equation (3.38) for solid masonry) and the code's strength values for f'_m are compared in Fig. 3.66 for types S and N mortars. The block tensile strength σ_{tbl} was calculated from the block compressive strength, σ_{cb}, using the strength ratios considered for concrete[40]. These ratios are presented in the figure. The unconfined compressive strength of the mortar, σ_{cm}, was taken equals to 0.85 of the cube compressive strength[39]. It is shown that the code's values for f'_m agree reasonably well with the analytical results for unit strengths up to about 3000 psi. For higher block strengths, the code values drastically underestimate the masonry compression capacity. This conclusion applies for ungrouted masonry having any percent solid.

3 - The code values show a significant difference between the compressive strengths of masonry using type S and type N mortar. A reduction of about 40% results when changing from type S to type N mortar. The current experimental and analytical results indicate relatively little effect of the mortar compressive strength on the assemblage capacity, especially for

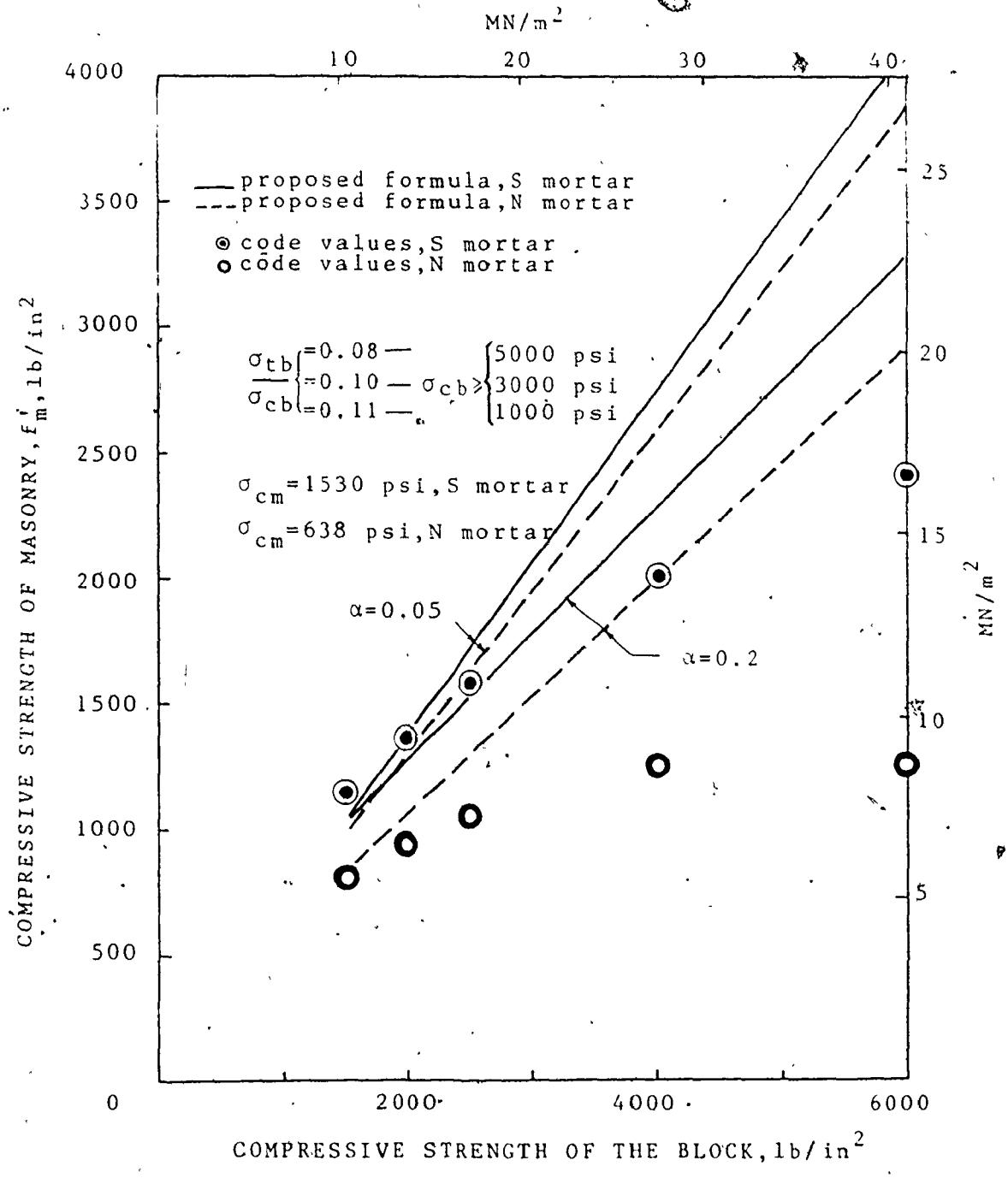

Fig. 3.66 MASONRY COMPRESSNE STRENGTH VERSUS BLOCK COMPRESSNE STRENGTH CALCULATED FROM THE PROPOSED EXPRESSION AND THE CODE PROVISIONS

grouted masonry (see Section 3.3.3.6). Other investigators[48,56] arrived at the same conclusion for 100 percent solid block masonry. The code's strength values indicate that the mortar strength has a greater influence than the block strength. This is contrary to the current results and to those of other investigators[15,45]. The values assigned by the code will lead to inconsistent safety factors for concrete masonry under axial compression. (It should be noted that the code does permit use of prism tests to determine the compression capacity of masonry).

4 - The code classifies the compressive strength values according to the mortar strength and ignores the mortar thickness to block height ratio, α. It is evident from the current experimental anad analytical investigation for ungrouted and grouted masonry and from the results of other investigators[15,31,48] for solid masonry, that the α ratio has a more significant influence on the capacity than does the mortar strength. It is reasonable to conclude that the code values were based on the nominal joint thickness of 3/8 of an inch. However, the generally held view that the mortar joint thickness (as an absolute value) is the basic parameter is not sound. In fact, within practical limits of strength and geometric characteristics of the block and the mortar, it is likely that the joint thickness to the block height ratio has a more direct correlation with the compressive strength than the absolute value of the joint thickness[15,47,48]. As indicated in the proposed failure

expressions, the α ratio governs the amount of lateral tensile stress induced on the blocks. These stresses cause the splitting failure of the assemblage under axial compression.

5 - Figure 3.25 shows that the moduli of elasticity obtained experimentally from the stress-strain curves do not conform closely to the code formula, $E_a = 1000\ f'_m$. No strong correlation between the stiffness and the strength of masonry is apparent. As previously discussed, this may be because the complex states of stresses developed at failure (influencing f'_m), due to the interaction of the constituent materials, are basically different from those developed at early stages of loading (influencing E_a).

3.5 Summary and Conclusions

The behavioural characteristics of ungrouted and grouted masonry prisms under axial compression are presented and discussed in this chapter. The effects of the strength and geometric characteristics of the block, mortars, and grouts on the assemblage compressive strength are investigated. A failure mechanism for ungrouted and grouted prisms under axial compression is proposed to analytically predict the compressive strength of the assemblage using the properties of its component materials.

The following are the conclusion drawn from the experimental and analytical results presented in this chapter:

1 - The 2-course prism, currently used as a standard test

to determine the compressive strength of masonry, f'_m, does not properly represent the strengtn of a masonry wall under axial compression, as it fails in a shear mode whereas the wall usually fails in a tensile splitting mode. It is shown that a 3-course half block prism is representative as it exhibits a similar tensile splitting mode of failure.

2 - The compressive strength of grouted masonry, based on gross area, is less than that of ungrouted masonry, based on net area, even for high strength grout. The lateral expansion of the grout when approaching its unconfined strength imposes lateral tensile stresses in the outer shell causing a premature splitting failure of the prism. Relatively little increase of the strength was achieved with a large increase in the grout strength indicating that the strength superposition concept is not applicable. The results indicate that the concept of matching the compressive strength fof the grout to that of the masonry units, as currently recommended by the codes, is not sound and it is suggested that matching the deformational characteristics would be more efficient.

3 - The mortar joint characteristics (strength and thickness) have no significant influence on the strength and the deformation of grouted masonry under axial compression. This is attributed to the influence of the continuity provided by the grouted cores.

4 - Reinforcing the mortar joints, by using confining steel

plates, helps to eliminate the lateral expansion of the mortar and consequently changes the failure mode for ungrouted prisms from a tensile splitting (exhibits by nonreinforced prisms) to a shear mode of failure. For grouted prisms, similar reinforcing of the joints helps to confine the grouted cores and to reduce the lateral tension imposed on the outer shell and hence increases the prism compressive strength. (An increase of about 17% was achieved).

5 - Dur-O-Wal reinforcement embedded in the mortar joints does not seem to have any significant influence on either the mode of failure or the strength capacity of ungrouted and grouted masonry under axial compression.

6 - The bond type (stack and running bond) has no significant effect on the compressive strength of either ungrouted or grouted concrete masonry prisms.

7 - The shell thickness to width ratio of the block has no pronounced effect on the compressive strength of grouted masonry provided that the net to gross area ratio is kept constant.

8 - The lateral stress distribution along the height of the block for axially loaded ungrouted prisms are not uniform. They are large near the interfaces and become very small at the mid-height of the block. For grouted masonry, these lateral stresses are relatively uniform over the block's height.

9 - Shear stresses are created at the block to mortar interfaces and are concentrated near the edges of the blocks and

towards their corners, causing a nonuniformity of the lateral stress distribution along the block height. This is particularly true for ungrouted masonry. These shear stresses are far below the frictional resistance at the interfaces and hence there will be no possibility of failure by debonding at the interfaces under axial compression.

10 - The mortar joints in axially loaded prisms are shown to be under confining stresses (a state of triaxial compression). Elements of mortar near the edges are less confined (the degree of confinement varies along the mortar layers) and thereby they would fail first under compression loading.

11 - There is no significant effect of the percent solid on the behaviour characteristics (strength and deformations) of plain masonry.

12 - No strong correlation exists between the stiffness (or the modulus of elasticity) and the strength for axially loaded maonsry assemblages.

13 - The code's[12] approach in assigning compressive strengths for grouted masonry similar to solid masonry is not appropriate. The continuity provided by the grouted cores dictates different characteristic behaviour for grouted masonry. The code provisions will lead to inconsistent design value for grouted masonry under axial compression.

CHAPTER 4

TENSILE BEHAVIOUR OF CONCRETE MASONRY

4.1 General

The tensile strength of masonry is an important parameter in the behaviour of structural masonry elements such as shear walls, where the masonry is subjected to forces which produce tensile and/or shear stresses. One of the possible modes of failure of masonry shear walls is the diagonal tension failure which is governed, mainly, by the tensile strength characteristics of masonry.

Because of its significance for the structural behaviour of masonry, numerous studies on the diagonal tensile strength of masonry have been done, but mostly for brick masonry. Many investigators[2,18,19,49,55] considered the diagonal tension capacity, f_{td}, to be a constant value directly proportional to the square root of the compressive strength of masonry, f'_m, as follows:

$$f_{td} = R\sqrt{f'_m} \qquad \ldots\ (4.1)$$

Square panels (Wallette Test), circular discs (splitting test) and masonry piers have been tested to establish, experimentally, the proportionality constant, R. For brickwork, R values ranging from 2.5 to 4.5 have been reported[17]. While Balanchandran[2]

suggested a R value of 3.8 for grouted concrete masonry piers, he was not able to provide a physical explanation relating the diagonal tension capacity to the compressive strength of masonry piers. Because different test techniques and different shapes of specimens have been proposed in various test programs, the diagonal tension capacities were evaluated under compressive stresses normal to the bed joint which varied significantly from one program to another. It seems that this latter parameter would appreciably affect the capacity of the assemblages[29] and, consequently, result in the lack of correlation between the different studies. The orientations of the applied loads and, consequently, the resulting stresses normal to the bed joints were shown to appreciably influence the tensile strength of brick masonry[28].

Based on a linear finite element analysis of masonry discs loaded at 45 degrees to the bed joint and utilizing the experimental data obtained in the Structural Clay Products Small Specimen Test Program, Stafford-Smith et al[52] concluded that the diagonal tensile strength of the brickwork is approximately equal to either the tensile strength of the mortar or the tensile strength of the brick whichever is less. Balachandran[2] assumed that the tensile cracking of ungrouted concrete masonry occurs if the maximum principal tensile stress exceeds the tensile strength of the block or mortar, whichever is less.

Yokel and Fattal[58], in an attempt to propose a failure

hypothesis for brick masonry under combined stresses, adopted the tensile strength as the apparent major stress at failure when the principal compressive stress is equal to zero. Mohr's theory of failure for isotropic materials was considered in their investigation of brick masonry which is characterized by its anisotropic nature of behaviour. The authors stated that for a more general application of their hypothesis, the directional variation of the splitting strength should be considered so that:

$$\sigma_1 = f(\sigma_3, \alpha) \qquad \ldots\ (4.2)$$

where σ_1 and σ_3 are the principal tensile and compressive stresses, respectively, and α is the angle between the principal tensile stress and the bed joint.

Information concerning the effect of grouting on the behaviour of hollow concrete masonry under tensile stresses having different orientations with respect to the bed joint is not available. This may have led to the assignment of design stress values for grouted masonry similar to those for solid masonry in typical masonry codes[12,27] provided that the grout strength is at least equal to that of the block. This design approach ignores the influence of the continuity provided by the grouted cores which may significantly affect the capacity, especially under tensile stresses parallel to the core direction.

It is the objective of this section of the program to investigate the behaviour characteristics of ungrouted and grouted concrete masonry assemblages under tensile stress of different

orientations relative to the bed joint direction. The effect of grout strength, mortar type, and joint reinformcement on the tension capacity are considered in this investigation. The results of the experimental and the analytical study are presented along with a review of the code[12] provisions concerning tensile strength of concrete masonry.

4.2 Experimental Program

The test results for ungrouted and grouted masonry assemblages under tensile stresses are presented and discussed in this section. Particular attention is paid to the effect of grouting which is investigated through a comparison between the behaviour of grouted and similar ungrouted specimens.

4.2.1 Rationale for Choosing the Testing Technique and Interpretation of Data

A promising method for testing brickwork to establish its tensile strength was developed by Johanson and Thompson[28]. Circular discs, 15 inch in diameter, were tested to failure by loading in compression along the diameter as shown in Fig. 4.1. The typical mode of failure was by splitting along the loaded diameter as a result of induced transverse tensile stresses which are approximately constant for about 65% of the diameter. This testing technique is similar to the indirect method for determining the tensile strength of concrete where a cylinder is

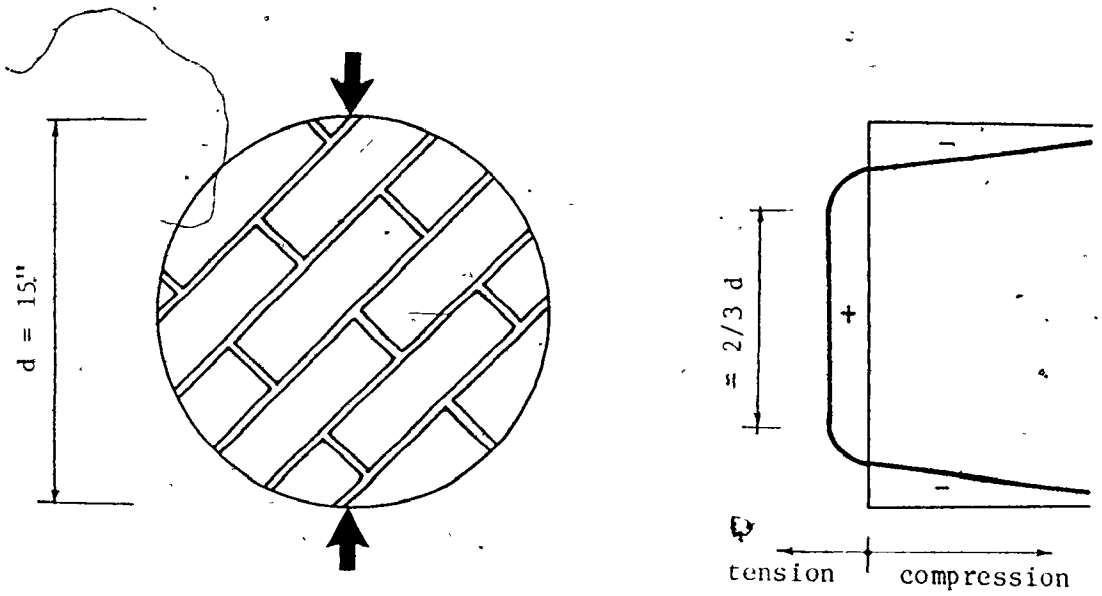

a - Splitting Test Specimen

b - Stress Distribution Along the Loaded Plane

Fig. 4.1 SPLITTING TEST FOR TENSILE STRENGTH OF BRICKWORK

split under loads applied along its generatrix[57]. If a concentrated line load is applied along the generatrix of a thin circular plate, as shown in Fig. 4.2, then an element on the vertical diameter is subjected to a vertical compressive stress, σ_y, expressed as:

$$\sigma_y = \frac{2P}{\pi td}\left(\frac{d^2}{r(d-r)} - 1\right) \quad \ldots\ldots (4.3)$$

and a horizontal tensile stress, σ_x, expressed as

$$\sigma_x = \frac{2P}{\pi td} \quad \ldots\ldots (4.4)$$

where P = the compressive load,

t = the plate thickness,

d = the diameter, and

r and (d-r) are the distances of the element from upper and lower points of the application of the load, respectively.

Theoretically, high compressive stresses, σ_y, would be induced immediately under the concentrated load which would cause local compression failure. In practice, the load is distributed over a band of appreciable width. If the width of the loading strip is "c", and the load is assumed to be uniformly distributed over this width as indicated in Fig. 4.3, it is reported[57] that if c<d/10, the stresses on the vertical diameter can be accurately expressed

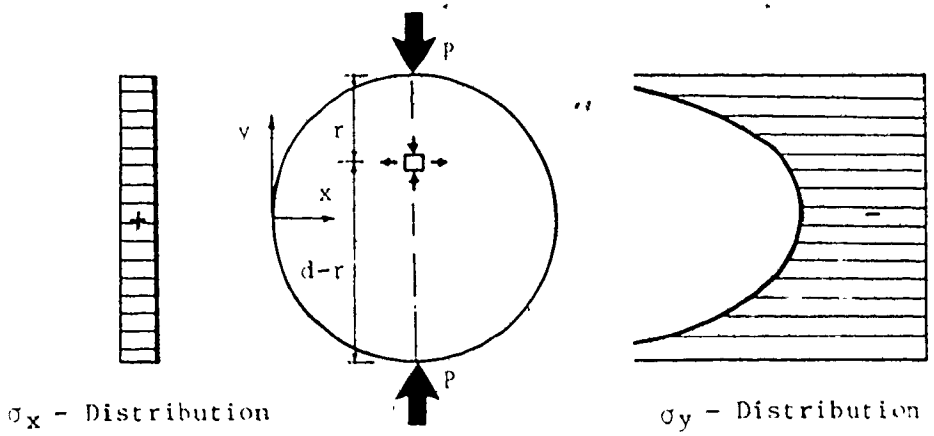

Fig. 4.2 CIRCULAR DISC UNDER CONCENTRATED LINE LOADS

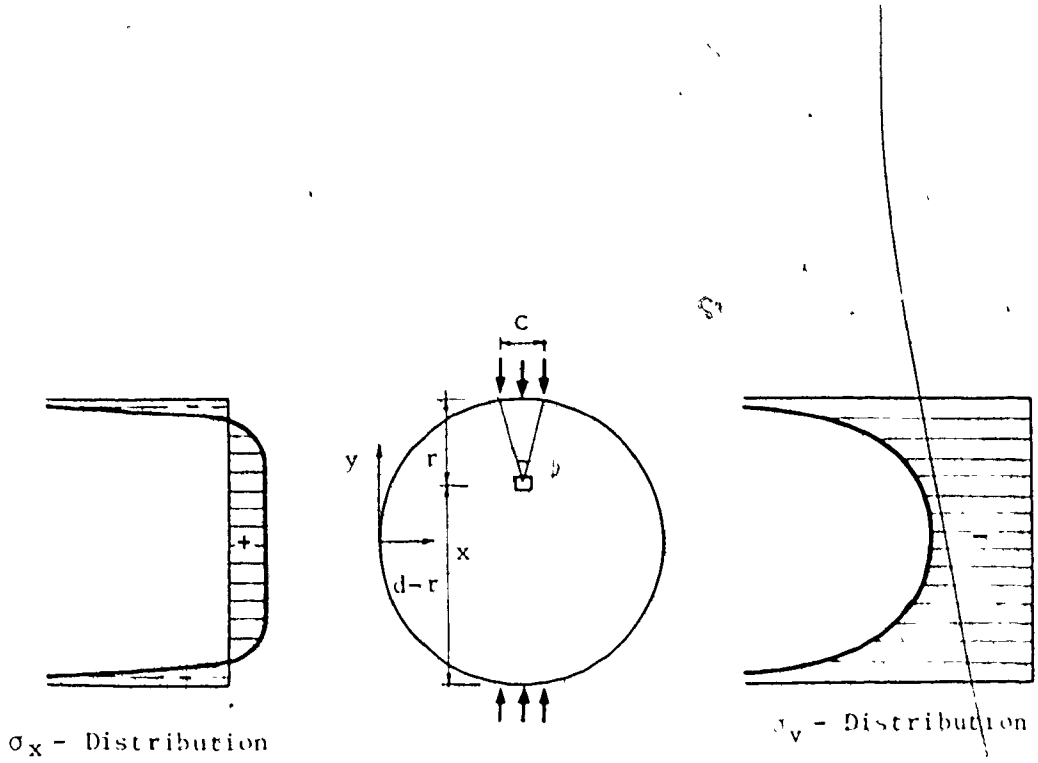

Fig. 4.3 CIRCULAR DISC UNDER LOADS DISTRIBUTED OVER A WIDTH "c"

as:

$$\sigma_y = \frac{2P}{\pi td}\left(\frac{d}{2c}(\psi + \sin\psi) + \frac{d}{d-r} - 1\right) \quad \ldots\ldots (4.5)$$

and

$$\sigma_x = \frac{2P}{\pi td}\left(1 - \frac{d}{2c}(\psi - \sin\psi)\right) \quad \ldots\ldots (4.6)$$

where ψ is the angle subtended by the loaded width to the point considered, as shown in Fig. 4.3. Under the latter case, high compressive stresses exist in the vicinity of the loads (Fig. 4.3), but, as this is accompanied by vertical compressive stress of comparable magnitude, biaxial stresses are produced and failure in compression does not take place[40].

The splitting test, as a technique for determining the tensile strength of brittle materials, has the following advantages over other techniques such as the direct tension and the flexural tension tests: (Note: these types of tests were discussed more fully in Section 2.2.1)

1 - The test procedure and the preparation of the test set-up are simple.

2 - It enables similar specimens and the same testing machine to be used for both tensile and compressive strength tests.

3 - The test results are influenced less by stress concentration compared to the situation for direct tension tests.

4 - The friction resistance, usually present at the contact interfaces between the test specimen and the machine plate, is

kept to a minimum and therefore the influence of confinement is insignificant[36].

5 - Splitting failure occurs through the central portion of the specimen and it is less likely to be affected by surface imperfections and multidirectional drying of the test specimens.

6 - The rate of loading has little effect on the test results[9].

7 - It leads to smaller testing errors and to less variation in the results than for either the direct tensile test or the flexural test[9,28,36].

Because of the above-mentioned merits and adding the principal advantage of the splitting test for measonry assemblages which is that it facilitates testing of identical specimens under tensile stresses at different orientations from the mortar bed joints, a similar test technique was adopted for the current program with the circular shape being modified to the hexagonal shape shown in Fig. 4.4. The suggested shape is more convenient for preparation of the concrete masonry discs which are rather heavy and less easily handled compared to brickwork discs. The corner blocks were cut first and then the discs were built arranging the blocks to provide the final hexagonal shape.

The finite element method was used to investigate the stress distribution along the loaded plane of the suggested hexagonal shape. The details of the analysis are presented in Appendix B. The longitudinal and transverse stresses along the

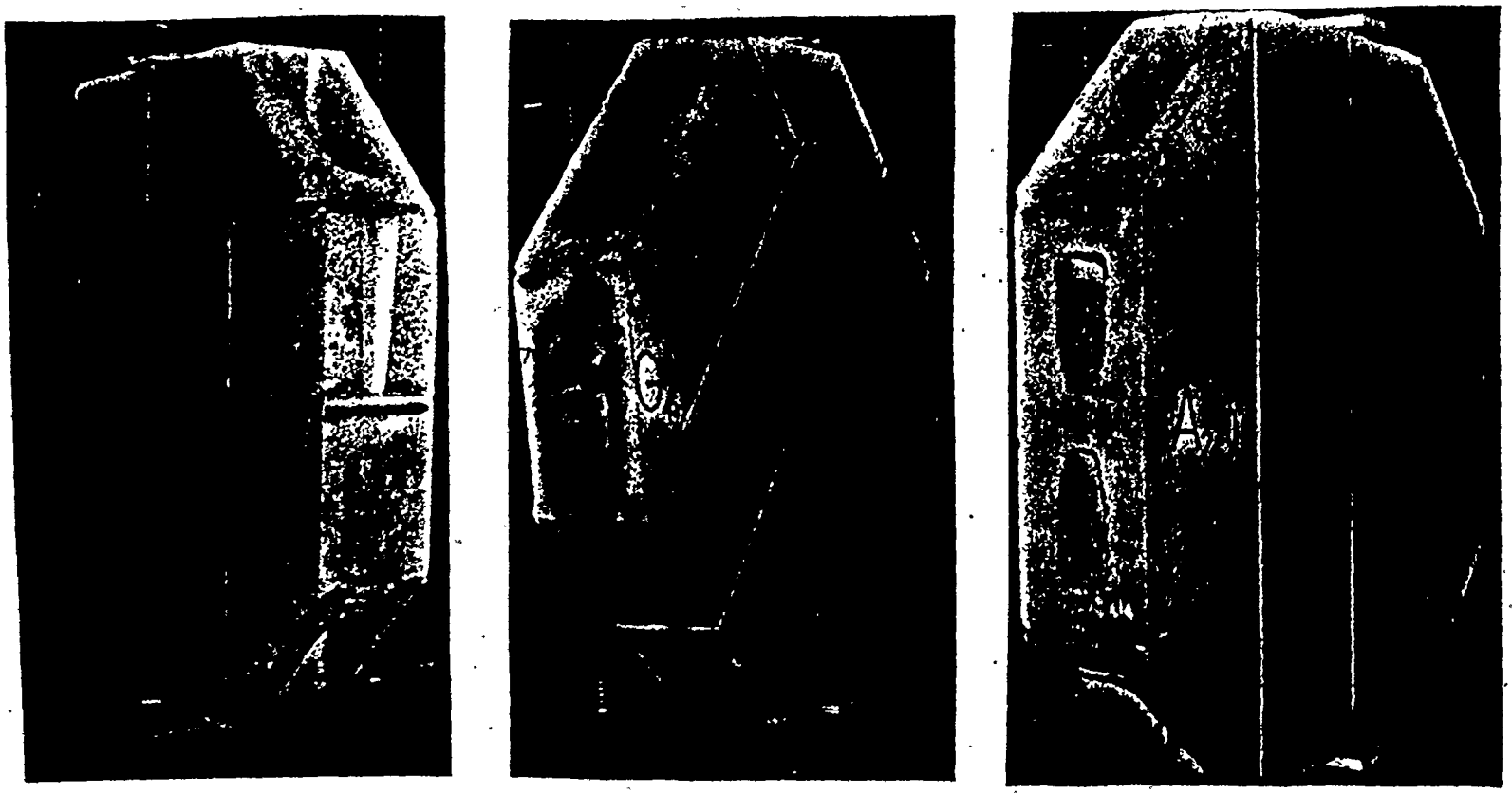

$\theta = 90^{\circ}$ $\theta = 45^{\circ}$ $\theta = 0^{\circ}$

Fig. 4.4 SPLITTING TESTS OF MASONRY DISCS UNDER LOADS HAVING THREE DIFFERENT ORIENTATIONS WITH RESPECT TO THE BED-JOINTS

loaded plane of the hexagonal disc from the finite element analysis are compared to those for a thin circular plate analyzed using elasticity theory. This comparison is also presented in Appendix B. It is shown that the suggested hexagonal shape provides a very good approximation to the stresses for the conventional circular shape, and the formula

$$f_t = \frac{2P}{\pi A}, \qquad \ldots\ (4.7)$$

where P is the splitting load and A is the area of the splitting plane, could be used to accurately calculate the maximum tensile stress, f_t, at the centre of the disc at failure for a homogenous material.

Using the finite element method, Stafford-Smith et al[52] analyzed nonhomogenous circular brickwork discs under splitting loads oriented at 45° from the bed joint. Different brick to mortar modular ratios were tried. The results demonstrated that when the brick is stiffer than the mortar, concentrations of high principal tensile stresses are induced in the mortar layers. Higher brick to mortar ratios result in higher local tensile stresses. These localized stresses may be of particular interest where the interaction of the constituent materials is examined on a microscopic scale. However, in the current investigation, the macromechanics concept was adopted as it is more applicable to the practical application of the test results[30]. The material is presumed homogenous (globally homogenous) and the effect of the

constituent materials is detected only in the averaged properties of the composite[30]. Consequently, Equation (4.7) is adopted to calculate the average tensile strength of the tested masonry discs.

4.2.2 Construction of the Masonry Discs

A total of 63 ungrouted and grouted masonry discs were constructed in running bond with full bed and head joints. The mortar joints were tooled on both faces of the specimens. Types S_1 mortar and type N mortar were used. The proportions and the properties of these mortars are presented in Section 2.2.2. All discs were constructed by the same experienced mason using techniques representative of good workmanship. Upon completion of each panel, two blocks were placed on top of the panel to provide some weight on the bed joints of the upper courses. After a minimum of 24 hours, grout was poured into the cells and puddled using a steel rod. The proportions of the grout mixes are presented in Section 2.2.3.

4.2.3 Control Specimens

Control specimens were made along with the masonry discs and were air cured in the laboratory under the same conditions as the discs.

For mortar, the following are the adopted control specimens:

1 - three 2 inch cubes per batch tested under axial compression

2 - Six 3x6-in. cylinders per batch tested under both axial compression and splitting tension (3 specimens per test)

3 - Masonry couplets tested under splitting tension (Section 2.2.2). The two units were stacked both flatwise and endwise to determine the tension bond strength of the bed and head joints, respectively.

For grout, the following are the adopted control specimens:

1 - Six 3x6-in. cylinders per batch, cast in nonabsorbent moulds, tested under both axial compression and splitting tension.

2 - Six 2 1/2 x 5 5/8 x 7 5/8-in. block moulded prisms per batch tested under both axial compression and splitting tension. For the splitting test, compressive loads was applied along the width of the prism through plywood strips of 1/2 in. width and 1/8 in. thickness as shown in Fig. 4.5.

The finite element method was used to investigate the transverse stresses along the loaded plane of grout prisms under splitting loads and to examine the validity of applying Equation (4.7), derived for circular plates, to the rectangular prisms under study. The details of the analysis and discussion of the results are presented in Appendix B. The results indicate that Equation (4.7) can reasonably predict the tensile stress at failure at the centre of the grout prism.

Fig. 4.5 SPLITTING TEST OF A BLOCK MOULDED PRISM

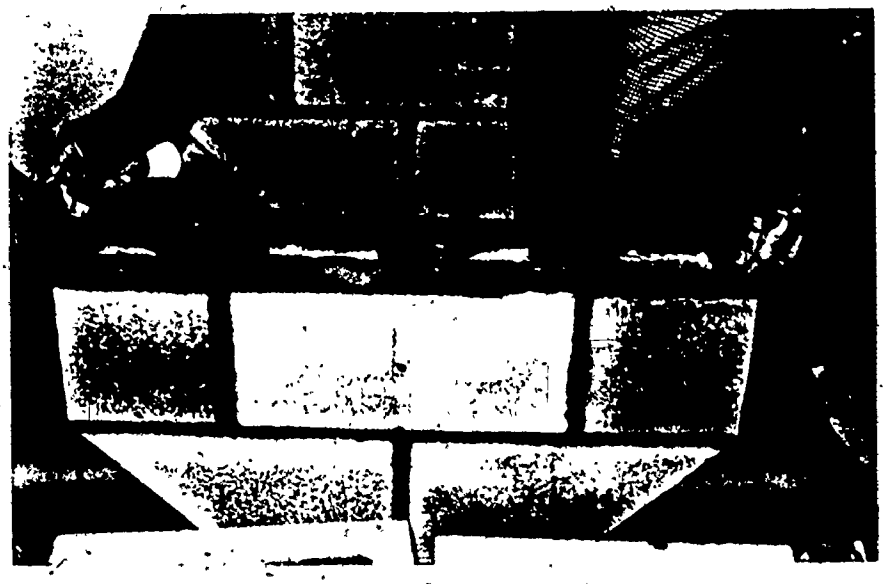

Fig.4.6 A MASONRY DISC WITH DUR-O-WAL STEEL AS BED JOINT REINFORCEMENT

4.2.4 Testing Procedure

The discs were tested under splitting loads having three different orientations, θ, with respect to the bed joint direction as shown in the photographs in Fig. 4.4. These orientations are:

1 - $\theta = 0^{\circ}$. This allows the measurement of the tensile strength, f_{tn}, normal to the bed joint (tensile bond strength of the mortar in the case of ungrouted specimens).

2 - $\theta = 45^{\circ}$. This allows the measurement of the diagonal tensile strength, f_{td}.

3 - $\theta = 90^{\circ}$. This allows the measurement of the tensile strength, f_{tp}, parallel to the bed joint.

The program comprises three groups of discs, each concerned with one parameter:

Group T1: The effect of the mortar type on the tension capacity of ungrouted masonry under loads having orientations of 0°, 45° and 90° from the bed joint was studied. Type S_1 mortar and type N mortar were considered. A minimum of three repetitions for each test type were adopted in order to be better able to analyze the results on a statistical basis. For ungrouted discs loaded at 45° with the bed joint, the cells of the bearing block adjacent to the load were filled with gypsum-cement compound to prevent local compression failure of the face shells.

Group T2: The effect of the grout strength on the tension capacity of masonry assemblages under loads having orientations of 0°, 45°, and 90° from the bed joint was studied. Three different

grout mixes were used; weak grout, GW, medium grout, GM_1, and strong grout, GS. Type S_1 mortar was adopted for all of these specimens.

Group T3: The effect of providing bed joint reinforcement (Dur-O-Wal) as shown in Fig. 4.6, on the cracking load and the tension capacity under splitting loads having orientations of 45° and 90° from the bed joints for ungrouted discs and of 45° from the bed joint for grouted discs was studied. Type GM_1 grout and type S_1 mortar were adopted from this test series.

Mechanical gauge points were mounted on both faces of the discs using a 4 inch gauge length, so that the deformations in the transverse direction along the loaded plane and in the vertical directon at the centre of the discs could be measured. The arrangements of the gauge points are shown in Fig. 4.4 for the three different load directions. Strain measurements were taken at regular load increments up to about 90% of the failure load.

Strips of 1/2 in. plywood along with 1/2 in. steel plates provided the bearing surface top and bottom. The strips were 2 in. wide which assumed a distribution of the applied load over an area equal to 1/16 of the height of the disc. The dimensions and the test set-up are shown in Fig. 4.7. This c/d ratio gives a deviation of tensile stresses from those calculated on the basis of line loads ($f_t = 2P/\pi dt$) of about 2% (see Appendix B). This small deviation is ignored in the strength calculation.

Each masonry disc was carefully aligned in the testing

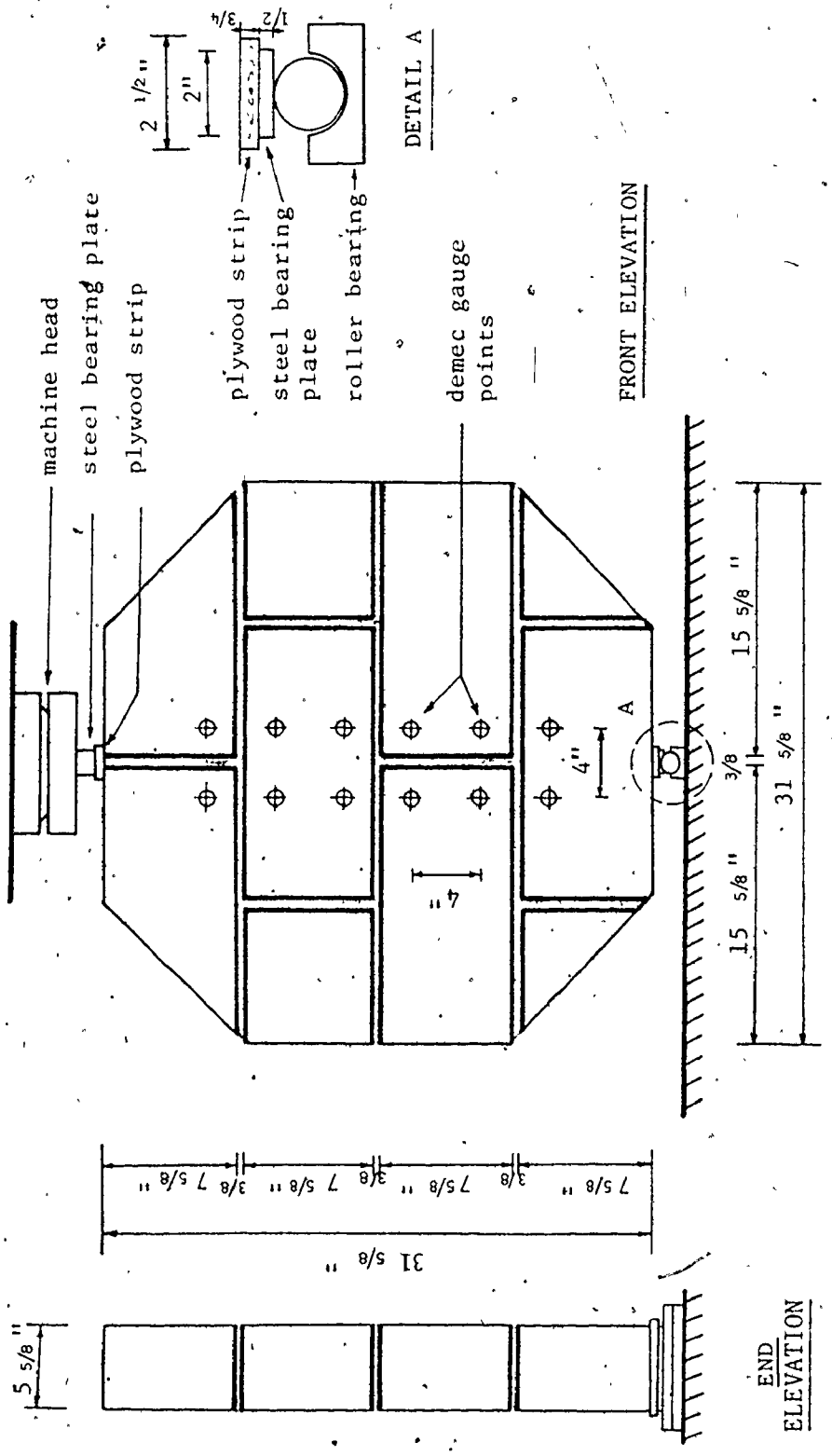

Fig. 4.7 SPLITTING TENSION TEST SET-UP FOR CONCRETE MASONRY DISCS

machine by centering and plumbing the points of bearing with the vertical axis of the machine head. The load was slowly applied taking strain measurements at each load increment until failure occurred. The patterns of the failure cracks were recorded. The control specimens for mortar and grout were tested at approximately the average age of the assemblages. (The discs were tested at the age of 28-56 days)

4.2.5 Discussion of the Test Results

4.2.5.1 Modes of Failure: The mode of failure for most of the tested discs was that of splitting along the central portion due to the induced transverse tensile stresses. All discs with the bed joints perpendicular to the load plane failed in the same ideal tension mode with the failure plane passing through the intercepted blocks face shells and along the mortar-block interfaces at the head joints, in the most direct line between the load points. It was interesting to observe exactly the same mode of failure for ungrouted and grouted specimens. In the latter case, the fracture plane crossed the blocks' shells and the head joints since the minimum path did not cross the grouted cores. A mode of failure typical for both ungrouted and grouted discs under tensile stress parallel to the bed joint is shown in Fig. 4.8. A somewhat similar mode of failure occurred in the masonry discs where the loaded plane was parallel to the bed joints. In these cases, the failure plane was along the mortar-block interfaces for

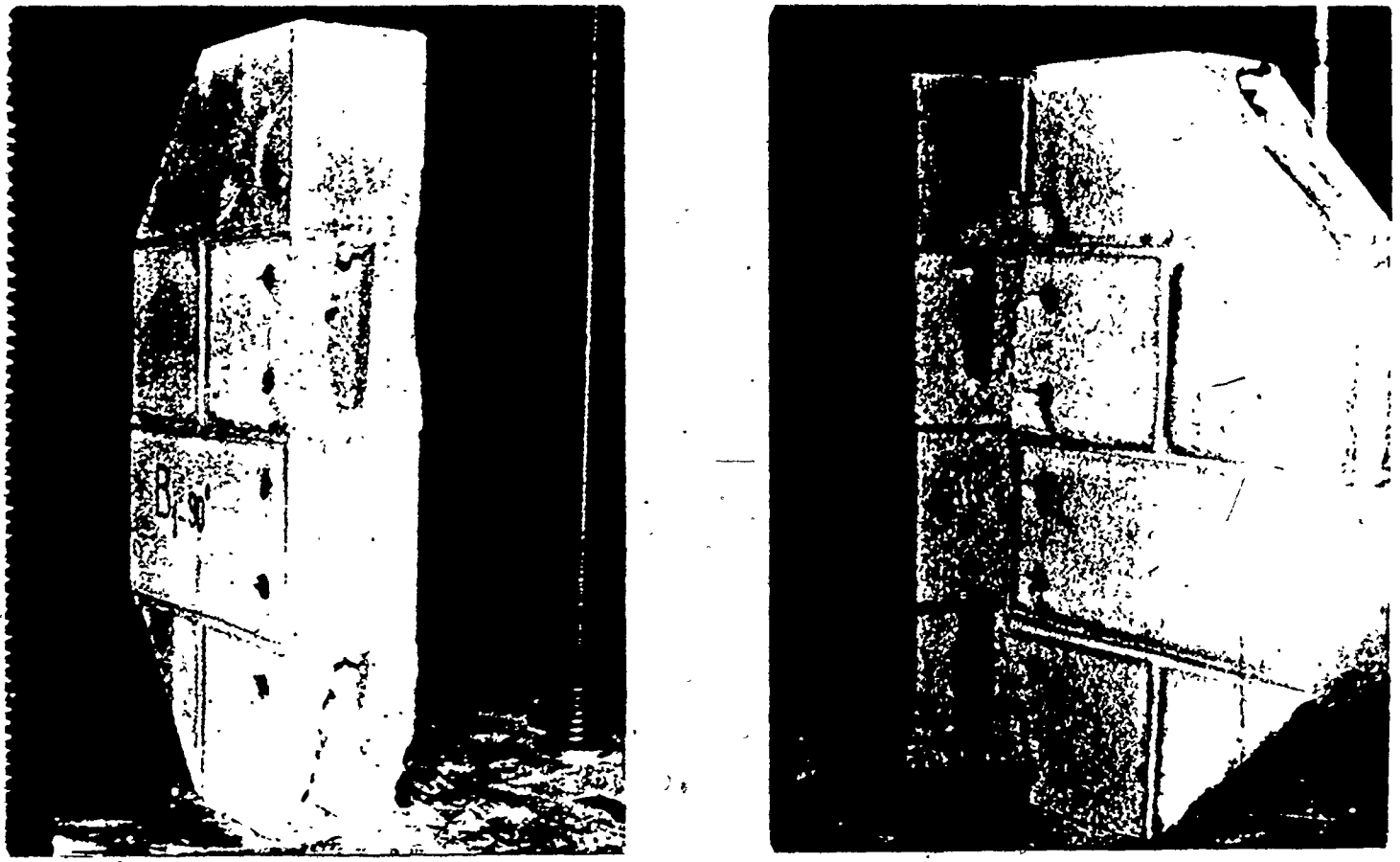

(a) Ungrouted Prism

(b) Grouted Prism

Fig.4.8 TYPICAL FAILURES OF MASONRY DISCS UNDER TENSION PARALLEL TO THE BED JOINTS

ungrouted discs and, for grouted discs, included splitting tension failure of the grouted cores. Because the blocks have flared webs and shells at their top surfaces, failure occurred along the weakest plane which had the minimum grouted areas (see Fig. 4.9(b)). As will be discussed in more detail in Section 4.3.2, the grout capacity is the dominant factor influencing the assemblage capacity. In this group, the failure mode was consistently the typical ideal splitting failure.

Differences in the failure patterns for tests with the bed joints at 45° were evident for a high strength mortar (type S_1), the failure mode of ungrouted discs approached the ideal tension failure with the fracture crack extending through the blocks and the mortar joints in the most direct path between the load points (see Fig. 4.10(a)). For a low strength mortar (type N), the fracture crack did not pass through the blocks all along the loaded plane, but sometimes followed the mortar-block interfaces along part of the fracture planes as shown in Fig. 4.10(b). This latter case was a mixed shear (slip at the block-mortar interfaces), tension (splitting of the block, mortar, and/or grout) mode of failure. For grouted discs, a similar mixed mode of failure was also observed as shown in Fig. 4.11, where the failure crack again did not always follow the most direct path.

The results showed that the joint reinforcement had no effect on the patterns of the failure cracks. However, the reinforcing steel helped to prevent the sudden collapse exhibited

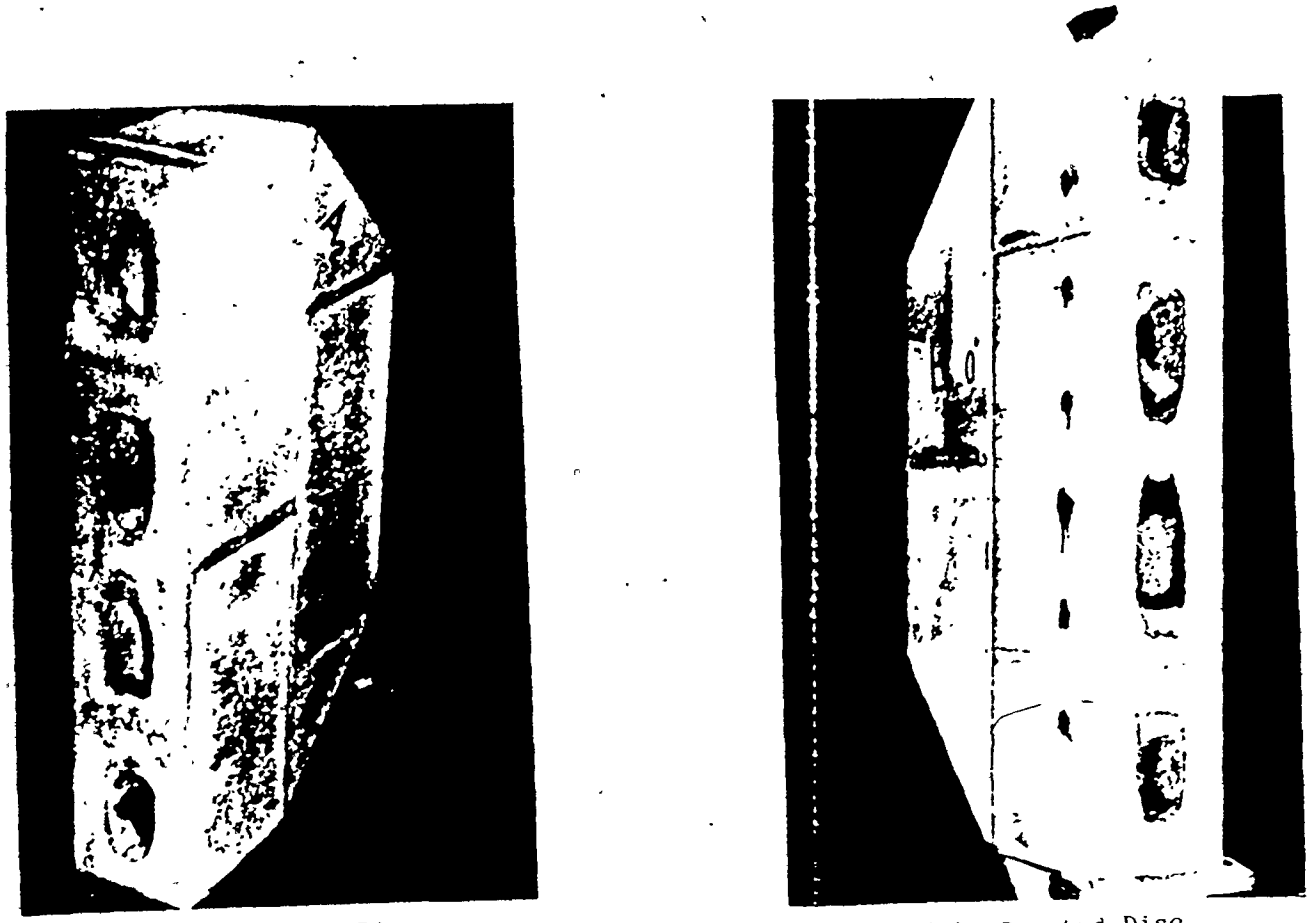

(a) Ungrouted Disc

(b) Grouted Disc

Fig. 4.9 TYPICAL FAILURES OF MASONRY DISCS UNDER TENSION NORMAL TO THE BED JOINTS

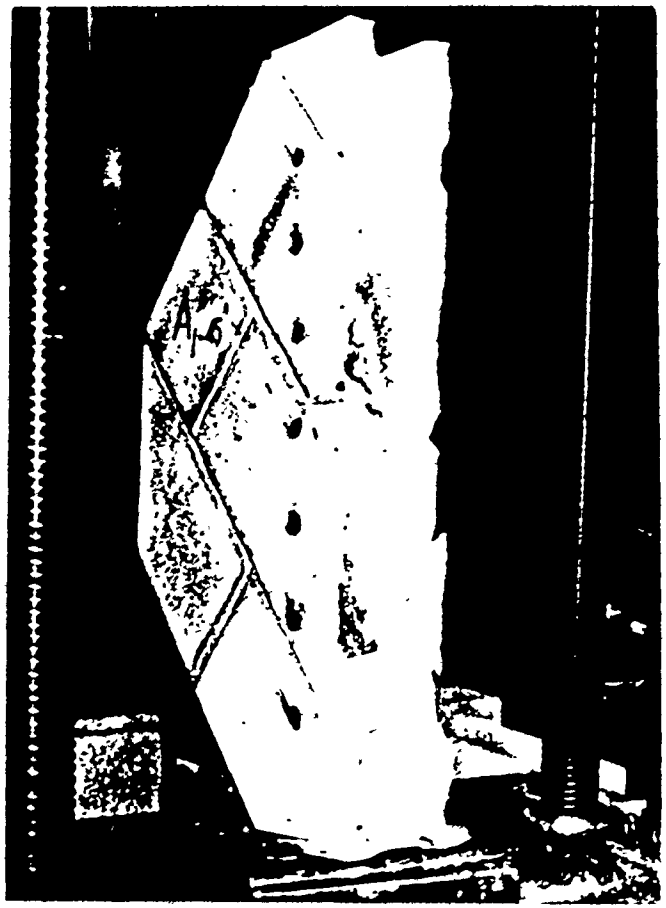

(a) Type S_1 Mortar

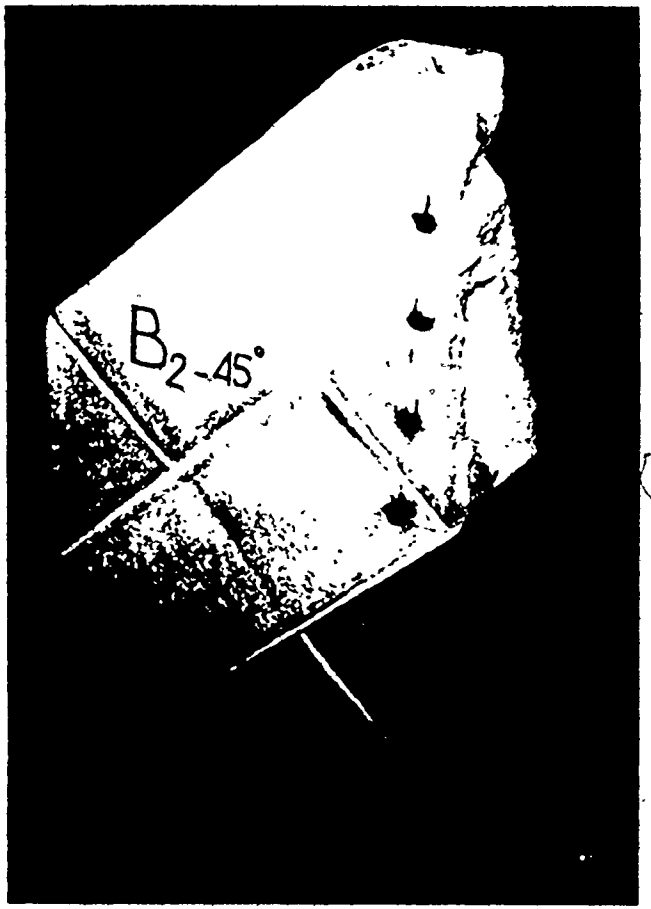

(b) Type N Mortar

Fig. 4.10 TYPICAL FAILURES OF UNGROUTED DISCS UNDER TENSION ORIENTED AT 45° FROM THE BED JOINTS

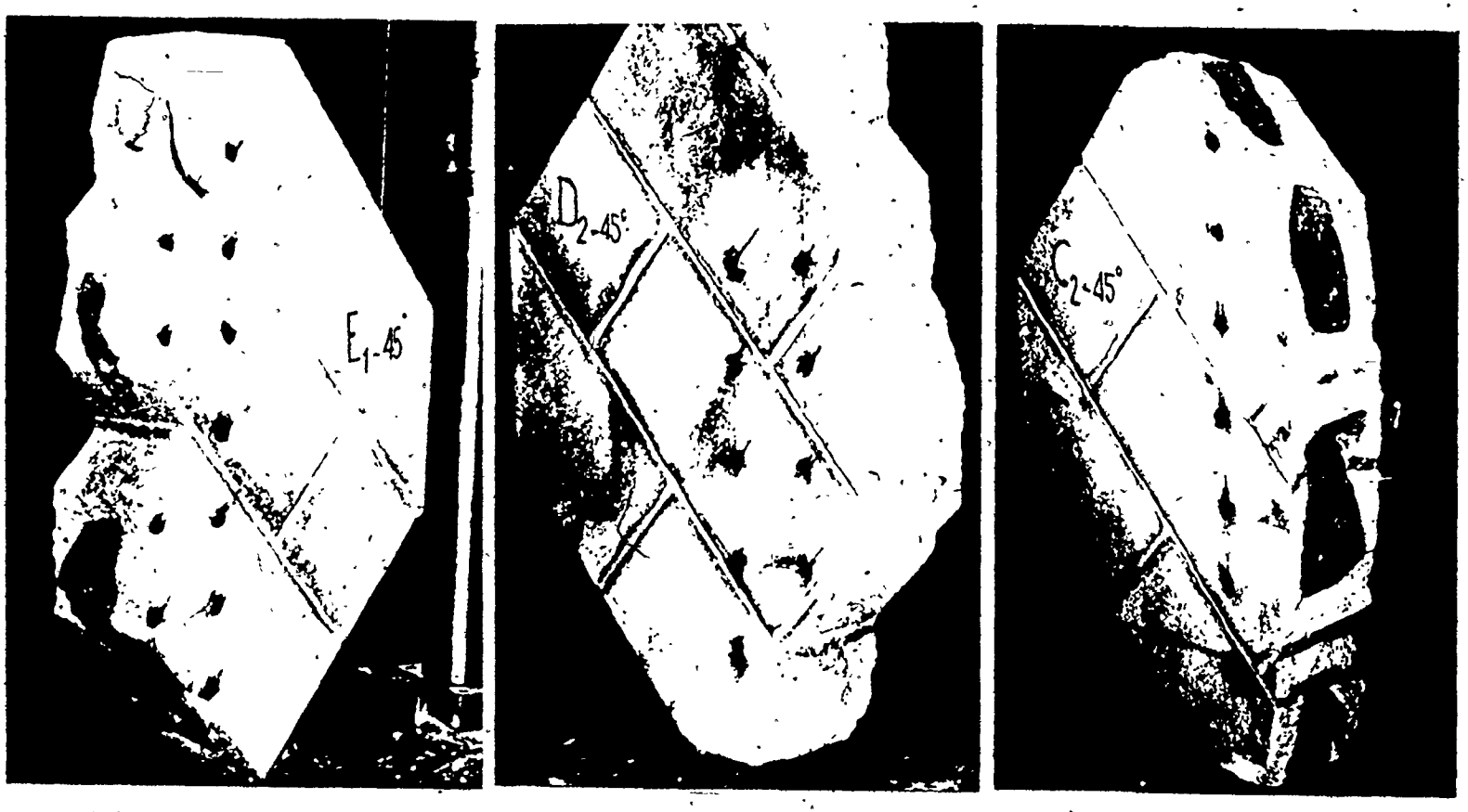

(a) Weak Grout, GW (b) Medium Grout, GM, (c) Strong Grout, GS

Fig. 4.11 TYPICAL FAILURES OF GROUTED DISCS UNDER TENSION ORIENTED AT 45° FROM THE BED JOINTS

TABLE 4.1

RESULTS OF SPLITTING TESTS ON UNGROUTED MASONRY DISCS
(Group T1)

Type of Mortar	Mortar Strength		Tensile strength, f_{tp}, α=0			Tensile strength, f_{td} α = 45°			Tensile strength, f_{tn}, α = 90°		
	comp.[a] psi	Tension[b] psi	Individ. (psi)	Mean (psi)	C.O.V.[c] (%)	Individ. (psi)	Mean (psi)	C.O.V. (%)	Individ. (psi)	Mean (psi)	C.O.V. (%)
1	3000 (12.3%)[c]	314 (5.5%)[c]	108 118 114 122	116	5.2	117 118 106 115	114	4.9	58 50 36 50	48	18.9
4	1180 (9.7%)[c]	136 (6.8%)[c]	105 101 94	100	5.4	96 108 106	103	6.3	43 51 36	43	17.8

Note: 1 psi = 6.9×10^{-3} MN/m^2

a. Cube compressive strength, air cured, based on an average of 17 batches for type S, mortar

b. Mortar tensile strength as calculated from splitting tests of 3 x 6 in cylinders

c. Coefficient of variation

TABLE 4.2

RESULTS OF SPLITTING TESTS ON GROUTED MASONRY DISCS
(Group T2)

Type of grout	Mortar strength[a] (psi)	Grout strength		Tensile strength, f_{tp}, $\alpha=0$			Tensile strength, f_{td}, $\alpha=45^{\circ}$			Tensile Strength, f_{tn}, $\alpha=90^{\circ}$		
		σ^{b}_{cg} (psi)	σ^{c}_{tg} (psi)	Individual (psi)	Mean (psi)	C.O.V.[d] (%)	Individual (psi)	Mean (psi)	C.O.V.[d] (%)	Individual (psi)	Mean (psi)	C.O.V.[d] (%)
Weak grout (GW)	3000 (12.3%)[d]	1710 (10.6%)[d]	170 (4%)[d]	114 121 117	117	2.3	134 158 141	144	8.6	107 107 102	106	3.1
Med. grout (GM_1)	3000 (12.3%)[d]	3250 (7.9%)[d]	300 (2.5%)[d]	122 133 114	123	7.7	141 159 151	151	6.5	114 111 112	112	1.3
Strong grout (GS)	3000 (12.39%)[d]	5240 (11.1%)[d]	400 (7%)[d]	115 115 108	113	3.6	178 167 158	168	5.9	144 138 135	139	3.3

Note: 1 psi = 6.9×10^{-3} MN/m^2

a. Cube compressive strength, air cured, based on an average of 17 batches (3 cubes per batch)

b. compressive strength as calculated from block moulded prisons

c. coefficient of variation

by the unreinforced specimens. Fig. 4.12 shows the reinforced discs after failure.

4.2.5.2 Effect of Load Orientation on the Tensile Strength: the tensile stress at failure at the centre of the specimen, f_t, is calculated as:

$$f_t = 2P/\pi A_g \qquad \ldots\ldots (4.8)$$

where P is the failure load in pounds and Ag is the gross area of the splitting plane in square inches for either ungrouted or grouted discs. The results for ungrouted and grouted specimens are listed in Tables 4.1 and 4.2, respectively. The results of the corresponding control specimens are also presented. Fig. 4.13 illustrates the influence of the orientations of the principal tensile stresses with respect to the bed joints (measured by the angle α) on the splitting tensile strength of the masonry discs. It is quite obvious that the tensile strength of either ungrouted or grouted masonry is not constant and that it varies with the orientation of the principal tensile stress. This behaviour is expected for a nonisotropic, nonhomogenous material such as masonry where the basic strength characteristics in tension should be evaluated in the principal material directions. This phenomenon was first observed by Johanson and Thompson[28] from tests on brickwork discs under splitting loads.

For ungrouted discs the minimum capacity was obtained when the tensile stress was normal to the bed joints. In this case,

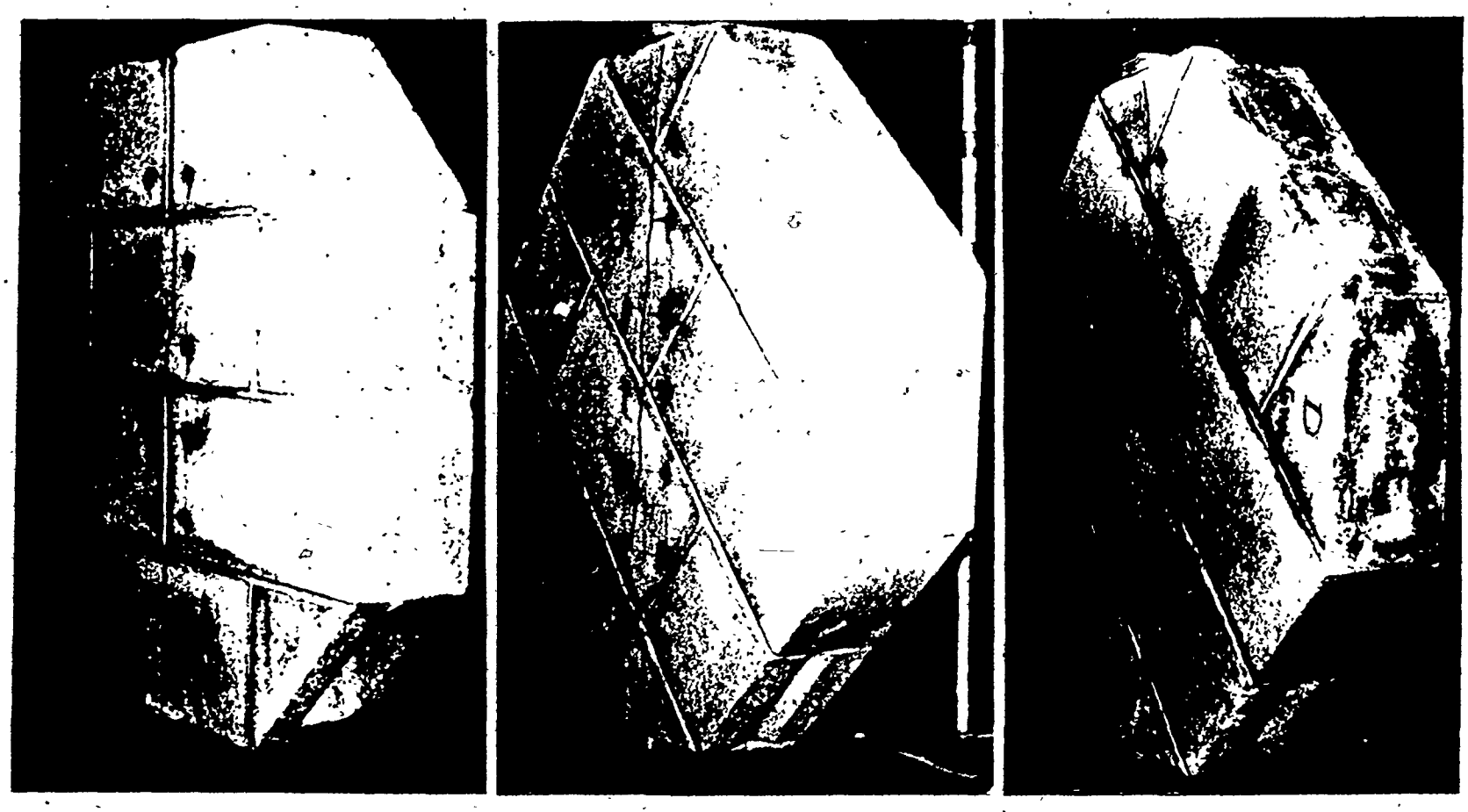

(a) Ungrouted, $\theta = 90^{\circ}$ (b) Ungrouted, $\theta = 45^{\circ}$ (c) Grouted, $\theta = 45^{\circ}$

Fig. 4.12 TYPICAL FAILURES OF REINFORCED MASONRY DISCS

the capacity was only influenced by the mortar bond strength as the block strength made no contribution to the capacity. Under tensile stresses parallel to the bed joints, both the block splitting tensile strength and the tensile bond strength of the head joints contributed to the capacity. For $\alpha = 45^{o}$, the capacity was governed by the block and mortar tensile strengths for a tension mode of failure, or the block tensile strength and the mortar tension and shear bond strengths for a mixed shear-tension failure. Because the tensile strength of the block is much greater than the tensile bond strength of the mortar, the higher the contribution of the block, the higher the tension capacity of the specimen. Examination of the normal stress applied on the bed joint, shown in Fig. 4.14 in conjunction with the tension capacity, shown in Fig. 4.13, indicates that a correlation between increased normal compressive stress and increased tension capacity of ungrouted masonry disc exists. The normal compressive stresses applied on the bed joints seem to increase the resistance of the assemblage to debonding failure at the block-mortar interfaces which forces splitting to occur in the block and hence increases the tension capacity of the assemblage. (The influence of the compressive stresses normal to the bed joint on the joint shearing capacity will be discussed in more detail in Section 5.2.4.6).

For grouted specimens, the anisotropic nature of behaviour of the assemblage was also evident (Fig. 4.13). However, it is

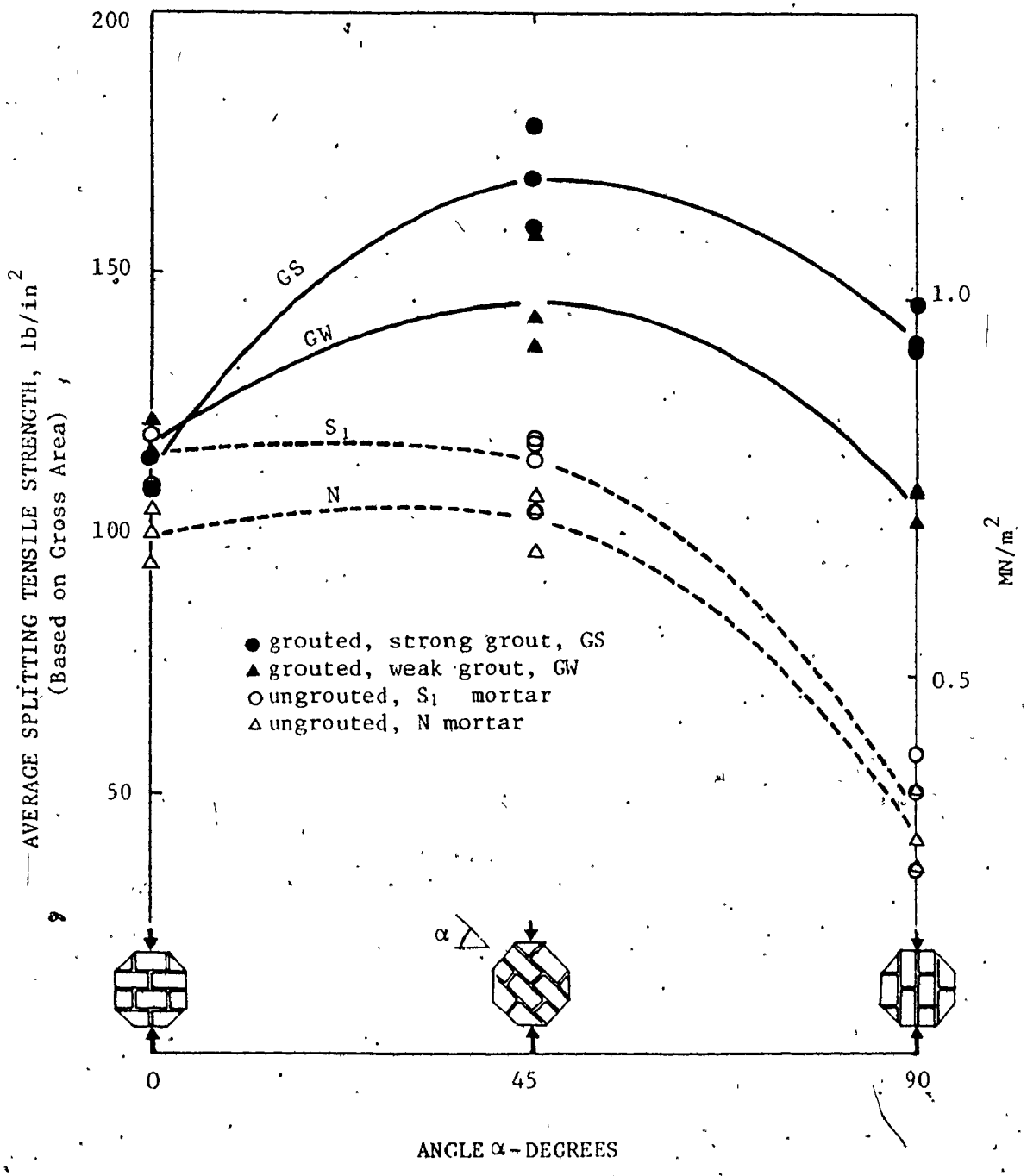

Fig. 4.13 EFFECT OF STRESS ORIENTATION ON THE SPLITTING TENSILE STRENGTH OF MASONRY DISCS

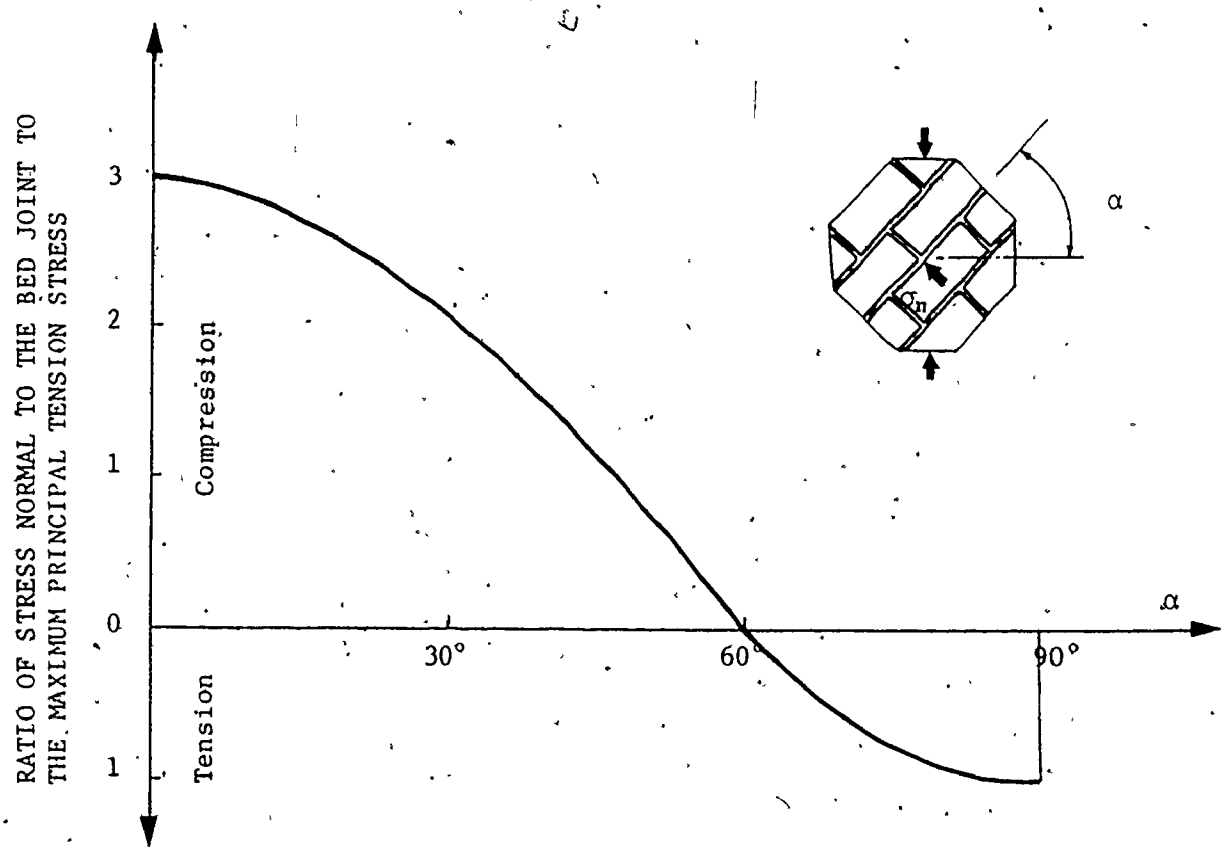

Fig. 4.14 VARIATION OF THE NORMAL STRESSES, σ_n, AT THE CENTRE OF THE DISC WITH THE ANGLE, α

less pronounced compared to the case of the ungrouted specimens. This behaviour indicates that the grouted cores provide some continuity to the media which may help to give masonry the tendency towards a more isotropic behaviour.

4.2.5.3 Effect of Mortar Type: The test results for the ungrouted discs shown in Fig. 4.13 indicate that the mortar type had very little effect on the tensile strength of ungrouted masonry. A decrease in the compressive strength of the mortar by about 60% reduced the capacity of the assemblage by approximately 11% (an average of the three loading conditions). The relatively insignificant effect of the mortar strength on the tensile strength can be attributed to the fact that the mortar bond strength is not predominately a function of its compressive or tensile strength[7]. The mortar bond strength is mainly influenced by both the plastic behaviour of the mortar, measured by its initial flow and water retentivity, and the block's surface condition, measured by its roughness and initial rate of absorption. Utilizing the experimental results of ungrouted concrete masonry piers tested under shear and precompression, Balachandran[2] concluded that, within the ranges of strengths of mortar adopted, the mortar strength does not appreciably affect the shear (diagonal tension) capacity.

4.2.5.4 Effect of Grout Strength on the Tension Capacity: Fig. 4.15 shows that the grouted cores significantly affected the tensile strength of masonry discs. Their contribution towards

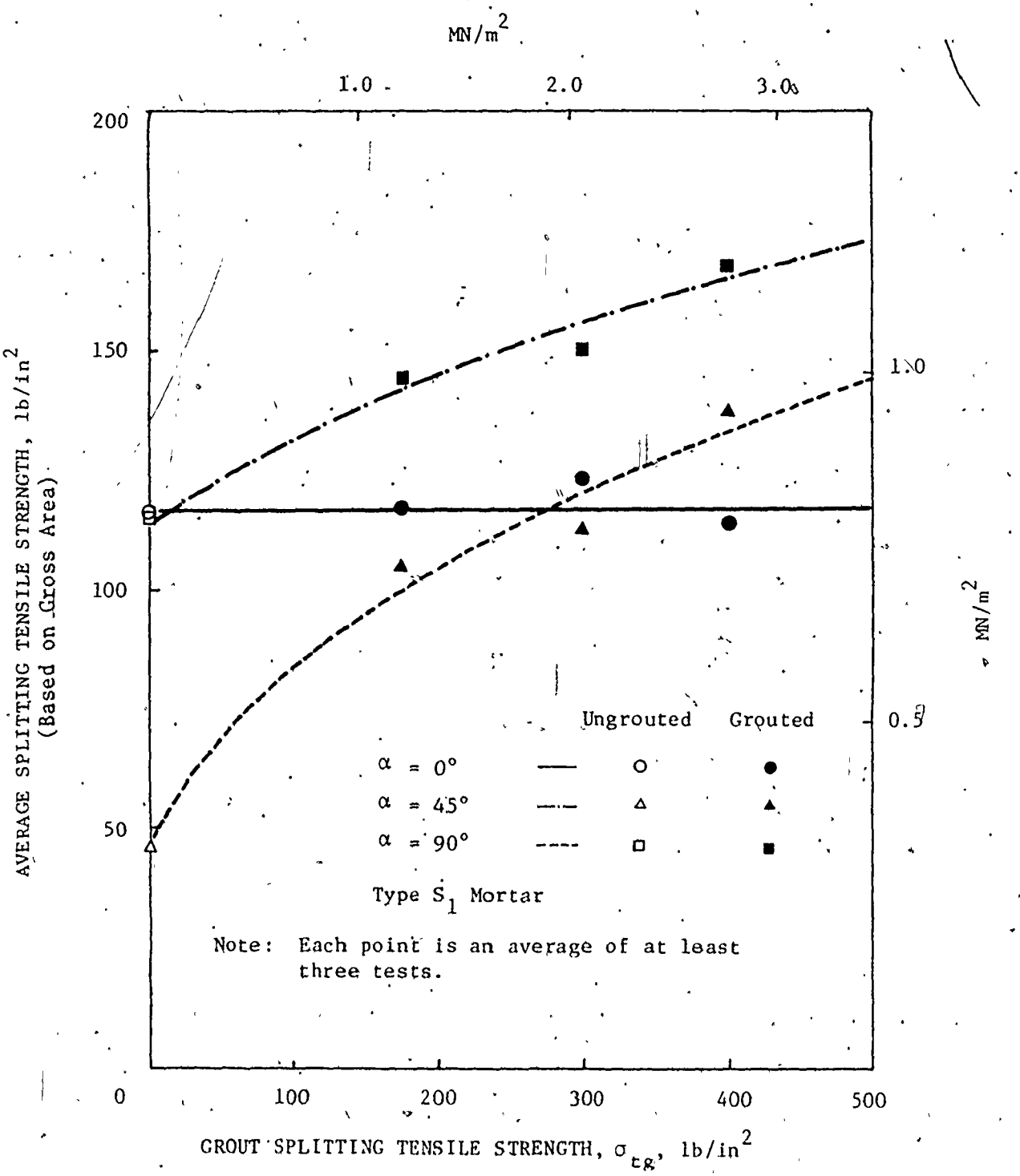

Fig. 4.15 EFFECT OF GROUT STRENGTH ON THE ASSEMBLAGES SPLITTING TENSILE STRENGTHS

increasing the tensile strengths, relative to those of ungrouted masonry, varied with the stress orientation. It had a maximum contribution when the tensile stresses were normal to the bed joints (i.e. in the core direction) as the grouted cores contributed by their tensile strengths which were much higher than the tension bond strength of the mortar. It is interesting to observe that grouting had no effect on the capacity for tensile stresses parallel to the bed joints regardless of the grout strength. The discs split along the blocks face shells and the head joints and the crack did not cross the grouted cores as shown in Fig. 4.8. It seems that the tension bond between the blocks and the grouted cores had a negligible contribution.

It is worth noting in Fig. 4.13 that, for the grouted discs, the maximum tensile capacity was achieved under stresses at $\alpha = 45^{o}$ (the diagonal tension case) where there is no appreciable contribution of the mortar bond strength which is quite small compared to the block or the grout tensile strength. The capacity in this case is mainly influenced by the contribution of the tensile strengths of the blocks, mortar, and grout.

4.2.5.5 Discussion of Using Net Area Versus Gross Area of the Block: The tensile strength of the assemblage versus the orientation of the maximum tensile stress with respect to the bed joint (measured by the angle α) are displayed in Fig. 4.16, using the net area for ungrouted masonry and the gross area for grouted masonry. The use of the net area for the calculation of the

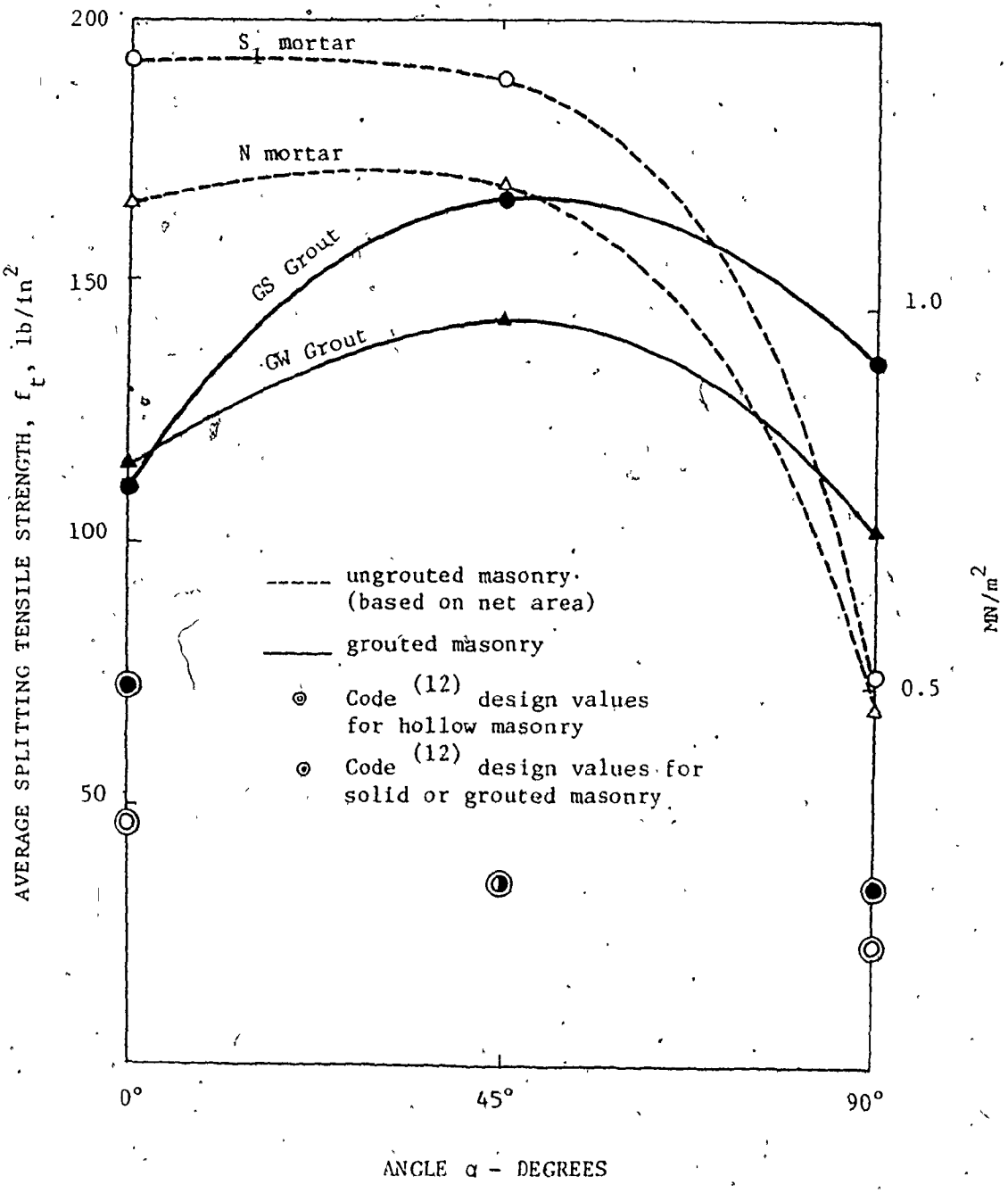

Fig. 4.16 EFFECT OF LOAD ORIENTATION ON THE SPLITTING TENSILE STRENGTH, BASED ON NET AREA FOR UNGROUTED MASONRY

stresses for ungrouted masonry is a widely adopted practice[2,12,27]. The current results indicate that calculating the tensile strength of ungrouted masonry on the basis of the net area for assemblages under stresses oriented at $\alpha = 0^{\circ}$ and $\alpha = 45^{\circ}$ may lead to higher tension capacities than for similar grouted assemblages. It seems that using the tensile strength of ungrouted masonry, calculated on the basis of the net area, could lead to assigning tensile strengths for grouted masonry which are too high. Except for tensile stresses normal to the bed joints, the use of the net area to calculate the tensile strength may not be a realistic or appropriate approach. For the other orientations (i.e. for $\alpha = 0^{\circ}$ and $\alpha = 45^{\circ}$), the fracture surfaces of the tested discs showed that the areas along the splitting planes were different from the net area of the blocks in the horizontal cross-section. It seems that a single definition for the net area is not feasible for the calculation of the tensile stresses of ungrouted masonry under loads having different orientations with respect to the bed joint direction.

4.2.5.6 Effect of Joint Reinforcement: Eleven discs, having Dur-O-Wal Steel as the bed joint reinforcement, were tested under tensile stresses oriented at $\alpha = 0^{\circ}$ and $\alpha = 45^{\circ}$ from the bed joints to study the effect of joint reinforcement on the tensile capacity of masonry. The test results are listed in Table 4.3. These reults are plotted in Fig. 4.17 along with the results for similar unreinforced specimens. No tests were done for the

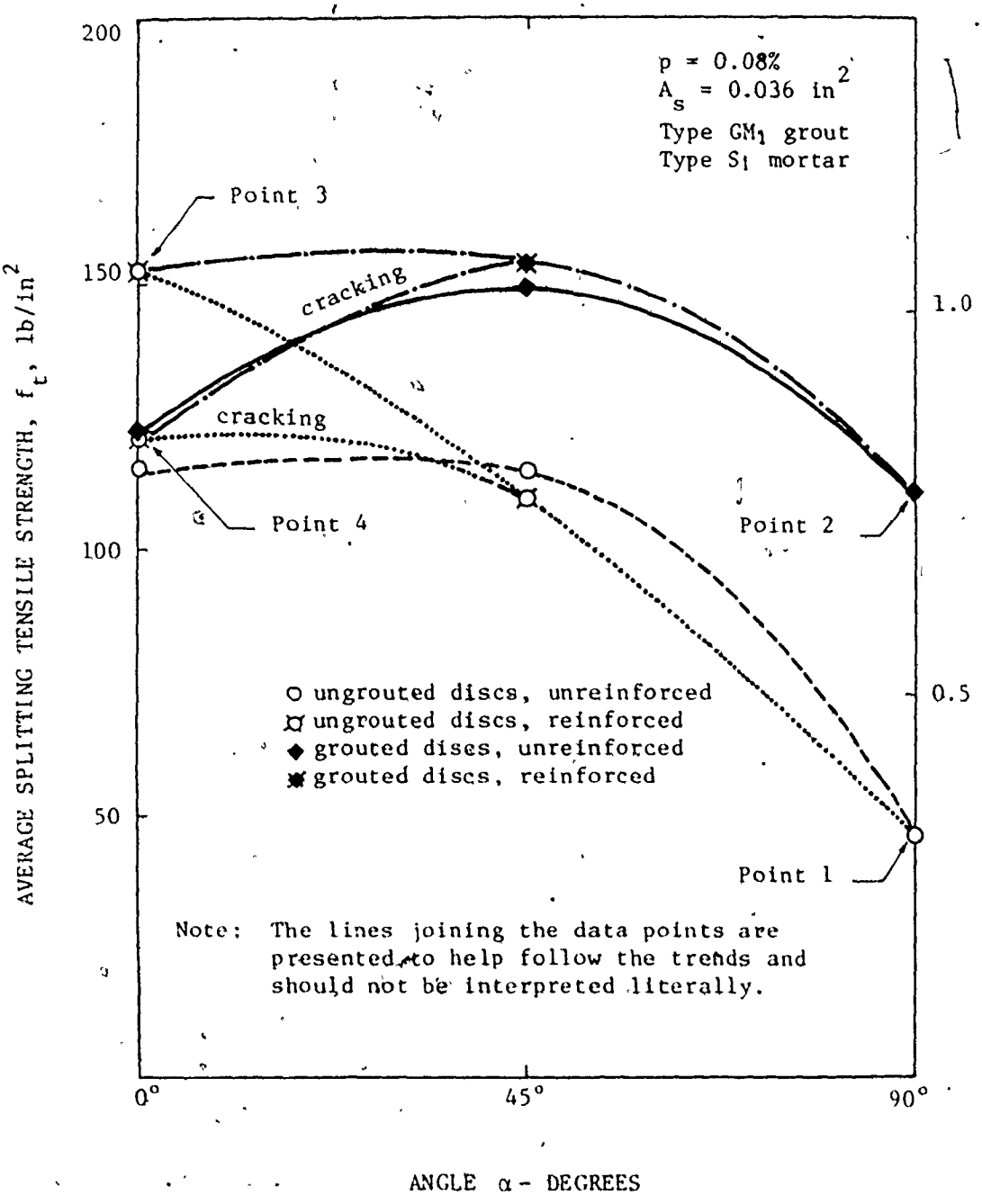

Fig. 4.17 EFFECT OF BED JOINT REINFORCEMENT ON THE SPLITTING TENSILE STRENGTH OF CONCRETE MASONRY

TABLE 4.3

RESULTS OF SPLITTING TESTS ON REINFORCED MASONRY DISC
(Group T3)

Type of specimen	Mortar strength[a] (psi)	Grout Strength, psi		Tensile strength, f_{td}, $\theta=45^{o}$			Tensile strength, f_{tp}, $\theta=90^{o}$		
		σ^{b}_{cg}	σ^{c}_{tg}	Individual (psi)	Mean (psi)	C.O.V.[d] (psi)	Individual psi	Mean (psi)	C.O.V.[d] (%)
ungrouted, type S_1 mortar	3000 (12.3%)[d]			115 116 100 98 112	108	8.0	153 157 149	153	2.8
Grouted, GM_1 grout, type S_1 mortar	3000 (12.3%)[d]	3250 (7.9%)[d]	300 (9.5%)[d]	160 144 163	155	9.4			

Note: 1 psi = 6.9 x 10-3 MN/m^2

a. Cube compressive strength, air cured, based on an average of 17 batches. Three cubles per batch were used

b. Compressive strength as calculated from block moulded prisms

c. Prison splitting tensile strength

d. Coefficient of variation

reinforced case with the principal tensile stress normal to the bed joint, because it was logical to assume that the reinforcing steel would have no effect on the tensile strength in this direction. Therefore, the reinforced case was considered to coincide with the previously tested unreinforced case (points 1 and 2 in Fig. 4.17) for this particular orientation of the tensile stresses. For the case of tensile stresses parallel to the bed joints, only ungrouted specimens were tested with joint reinforcement. This decision was based on the behaviour of the unreinforced specimens which indicated very little influence of the grout on the tensile capacity parallel to the bed joints. Therefore, point 3 in Fig. 4.17 is actually the stress at failure for the ungrouted reinforced specimens. It is assumed to also represent the grouted case. For $\alpha = 0^{o}$, cracking occurred at stress represented by point 4 in the figure which was about the same stress at failure for the unreinforced specimens. The reinforcement increased the tension capacity by about 25%.

The results show that under a diagonal tension loading, $\alpha=45^{o}$, reinforcing the bed joints with Dur-O-Wal Steel ($p = 0.08\%$) had no significant effect on the splitting strength. Because of the low steel percentage used, the component of the steel tension force after cracking, assuming that the steel had reached its yield stress, was less than the tensile capacity of the unreinforced specimens. Jolley [29] observed experimentally that the small amount of horizontal steel embedded in the bed joints of

ungrouted concrete masonry shear walls had no significant effort on the shear (diagonal tension) capacity of the walls. From the failure modes observed in the current experimental program, it was obvious that the joint reinforcement helped to prevent the sudden brittle failure exhibited by the unreinforced discs.

4.2.5.7 Effect of Load Orientation on the Deformation Characteristics: Fig. 4.18 shows the stress-strain relationships at the centre of typical ungrouted and grouted discs under tensile stresses oriented at 0°, 45°, and 90° from the bed joints. It is shown that the deformation characteristics of grouted masonry were different from those of ungrouted masonry. Under the same load levels, ungrouted discs exhibited higher tensile strains than grouted ones. Ungrouted discs exhibited low deformation under tensile stresses normal to the bed joints as failure was very brittle due to debonding at the block-mortar interfaces, whereas comparatively higher deformation capability was displayed under stresses parallel to the bed joints. Grouted discs exhibited similar deformations under stresses normal and parallel to the bed joints, indicating that the continuity provided by the grouted cores helped to give masonry a tendency to a more isotropic behaviour.

If the masonry discs are presumed to be globally homogeneous, the modulus of elasticity could be determined from the principal strains measured in the centre of the disc. The modulus of elasticy, E_a, assumed equal for tension or compression,

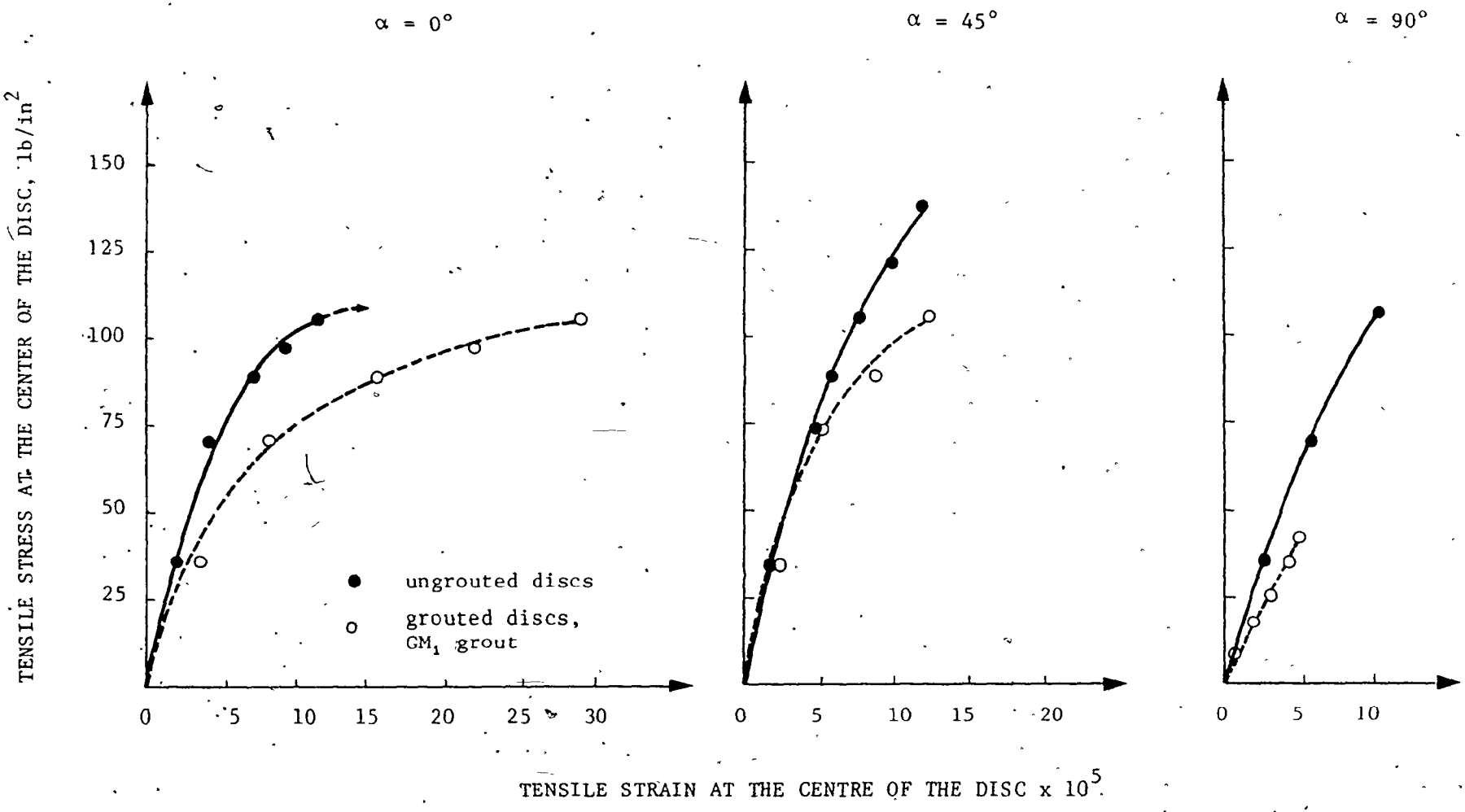

Fig. 4.18 STRESS-STRAIN RELATIONSHIPS FOR MASONRY DISCS UNDER SPLITTING LOADS

could be expressed[36] for circular disc under splitting load, P, as:

$$E_a = 5.095 \frac{P}{dt} \frac{.1}{\epsilon_x + 3\epsilon_y} \quad \ldots\ldots (4.9)$$

where d and t are the diameter and thickness of the disc, and ϵ_x and ϵ_y are the strains measured at the centre in the horizontal and vertical directions, respectively. For comparison purposes, rather than as absolute values, the above expression was adopted to calculate the moduli of elasticity of ungrouted and grouted discs under different stress orientations. These values are presented in Fig. 4.19. It is shown that while the moduli of elasticity of ungrouted discs varied with the principal tensile stress orientations, they were about the same under different orientations for grouted discs. This behaviour supports the previous conclusion that grouting the cores tends to cause a more isotropic behaviour. The results also indicate that if the calculation of stresses for ungrouted masonry is based on the net area, its modulus of elasticity could be higher than that for grouted masonry.

4.3 Formulation of an Analytical Model for Tensile Strength of Masonry

4.3.1 Introduction

The experimental results presented in the previous section show clearly that the tensile strength of masonry assemblages

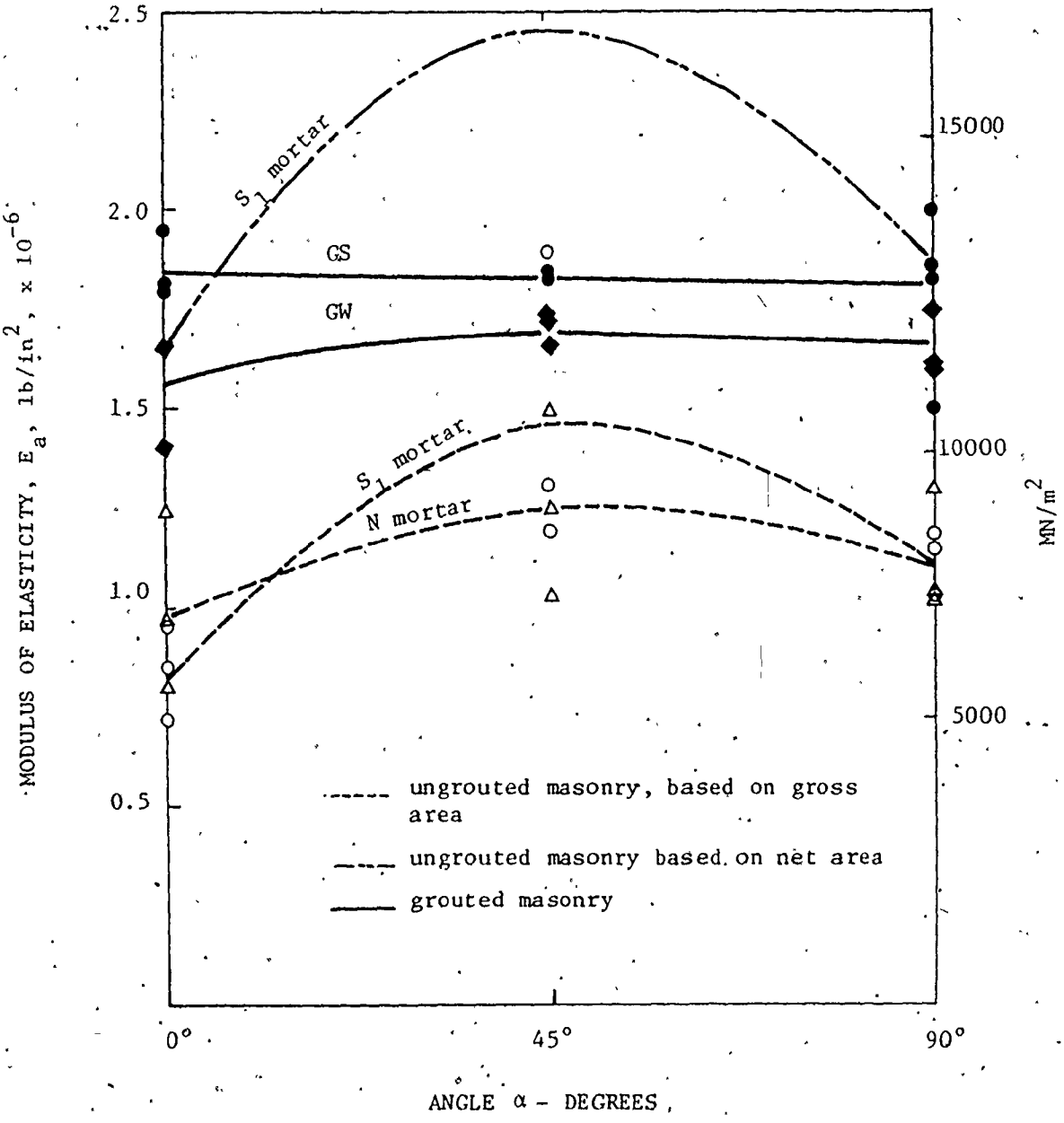

Fig. 4.19 EFFECT OF LOAD ORIENTATION ON THE DEFORMATION CHARACTERISTICS OF MASONRY DISCS UNDER SPLITTING LOADS

varies with the load orientation. This inherent anisotropy of masonry as a composite having two or three phase materials leads to mechanical behaviour characteristics quite different from those of conventional isotropic material and, consequently, there is no single value of the tensile strength, but different values for different directions of the tensile stresses.

4.3.2 Assumptions

As shown experimentally, the bed joint is the weakest plane when the tensile stresses are normal to it, and because of its continuous nature in the horizontal direction, it divides the assemblage into equal horizontal layers. The bed joint direction and the direction normal to it are considered to be the principal material directions in terms of which the tensile strengths will be formulated.

In the current study, the strength will be investigated from the macromechanics point of view as it is more readily adaptable to incorporating the important analytical features for design than the micromechanics approach[30]. In this concern, the material is presumed to be globally homogenous and the effect of the constituent materials is detected only as averaged apparent properties of the composite material. The apparent strength of the assemblage will be described by a linear combination of the resistances of the constitutent materials.

4.3.3 Masonry Tensile Strength Normal to the Bed Joints, f_{tn}

Under tensile stresses normal to the bed joints, separation occurs at the block-mortar interfaces including tensile failure of the cores for the case of grouted assemblages. This mode of failure was observed from the split discs discussed in the previous section (see Fig. 4.8).

For ungrouted masonry the capacity is governed by the tensile bond strength of the mortar acting along the block-mortar contact area, while for grouted masonry the grout will contribute to the tensile strength of the assemblage by its tensile capacity which is a function of the core area and the grout tensile strength. The apparent tensile strength of the assemblage can be described by incorporating the resistance of the component materials (mortar and grout) as follows:

$$A_g f_{tn} = A_{nm} \sigma_{tbm} + (A_g - A_{nm}) \sigma_{tg} \quad \ldots\ (4.10)$$

therefore

$$f_{tn} = \eta_{nm} \sigma_{tbm} + (1-\eta_{hm}) \sigma_{tg} \quad \ldots\ (4.11)$$

where f_{tn} = average tensile strength of masonry assemblage under load normal to the bed joints,

σ_{tbm} = tensile bond strength of mortar,

σ_{tg} = grout tensile strength (equal to zero for ungrouted masonry),

A_{nm} = maximum net area of the block cross-section (in the horizontal plane),

A_g = gross sectional area, and

n_{hm} = maximum net to gross area ratio (in a horizontal plane).

A comparison between the strength predicted from the proposed formula, Equation (4.11), and the experimental results is presented in Fig. 4.20. The grout tensile strength, σ_{tg}, was calculated from the splitting tensile strength of block moulded grout prisms and σ_{tbm} was determined from the splitting test of masonry couplets. A reasonable agreement is achieved. Fig. 4.21 indicates that the splitting tensile strengths could be predicted analytically to within ±20% of the actual values obtained experimentally with the trend being on the conservative side. This degree of accuracy for masonry as a nonhomogenous nonisotropic material where larger variability is expected because of the multitude of parameters involved, seems to be quite acceptable[17].

Equation (4.11) expresses the average tensile strength of the assemblage in terms of both the strengths (σ_{tbm}, σ_{tg}) and geometric characteristics (n_{hm}) of the block, mortar, and grout. The proposed simple formula indicates the following features of behaviour of masonry under tensile stresses normal to the bed joints:

1 - The mortar contributes to the tensile strength of masonry normal to the bed joints by its tensile bond strength which is a characteristic of the physical properties of the mortar

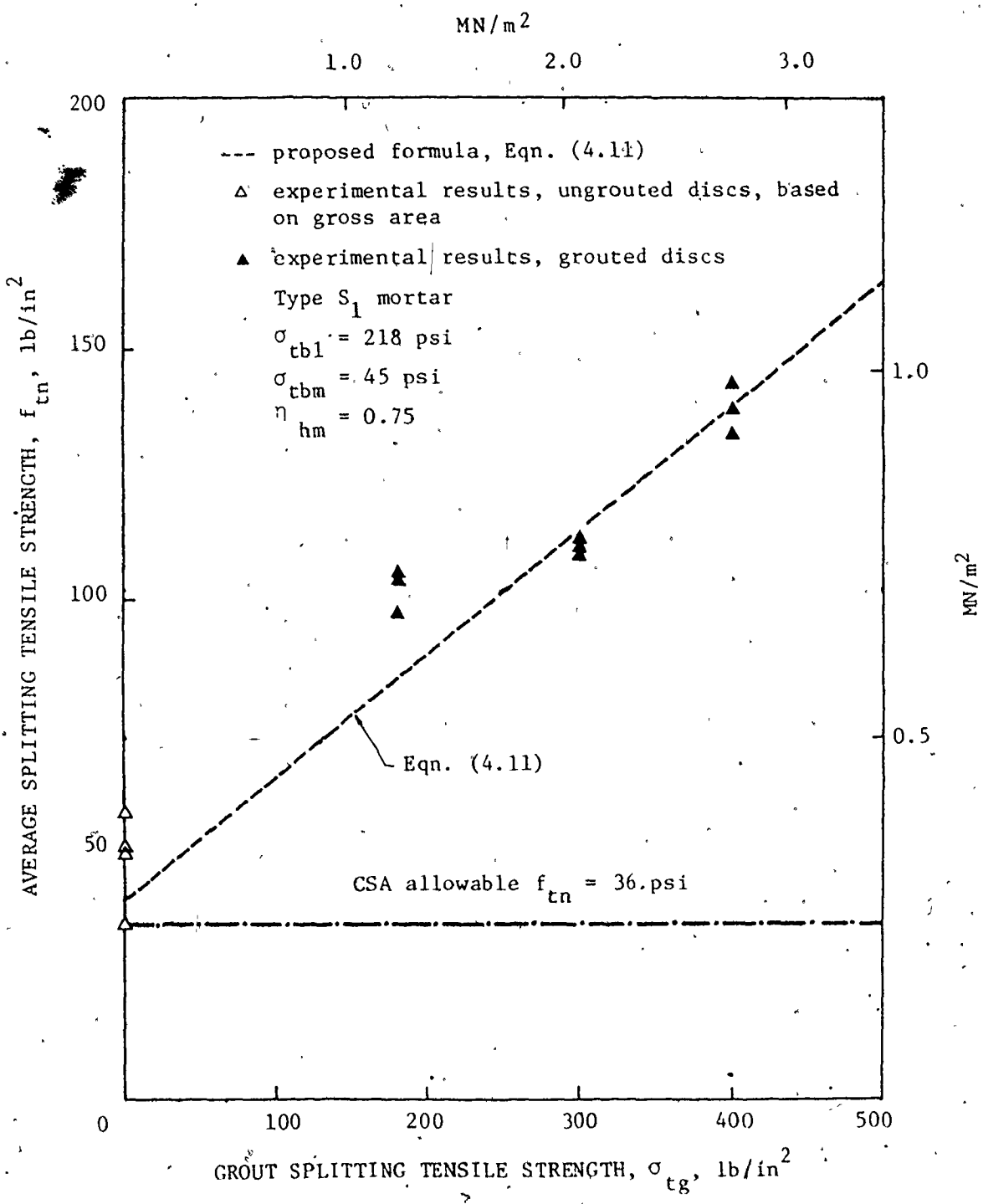

Fig. 4.20 ASSEMBLAGE TENSILE STRENGTH NORMAL TO THE BED JOINTS VERSUS GROUT STRENGTH

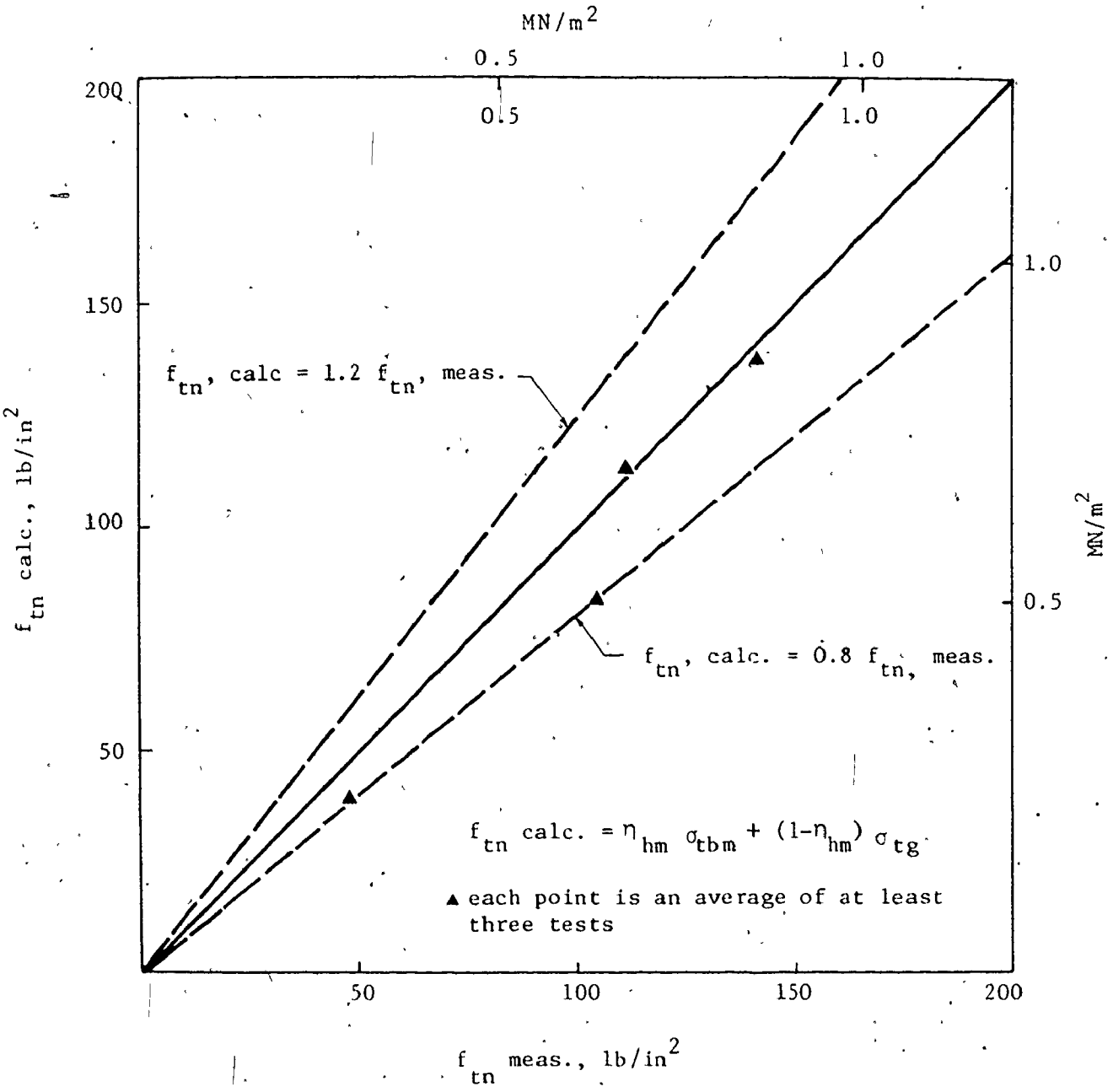

Fig. 4.21 COMPARISON OF MEASURED AND CALCULATED VALUES OF MASONRY TENSILE STRENGTH NORMAL TO THE BED JOINTS

and the block. Higher tension bond results in higher tension capacity of the assemblage especially for ungrouted masonry where it is the only influencing strength parameter. It has less significance for grouted masonry where the grout tensile strength (much higher than the bond strength) is the dominant parameter. This is particularly true for a lower net to gross area ratio, η_{hm}, as shown in Fig. 4.22.

2 - The grout significantly affects the assemblage tensile capacity normal to the bed joints, especially for lower values of the net to gross area ratios. Higher grout tensile strengths result in higher assemblage capacities, as shown in Fig. 4.22. This behaviour indicates that the units having flared top sections (see the sketch in Fig. 4.22) are not appropriate from this strength viewpoint. The grout area is decreased in the top section which would be the critical area governing the capacity of the assemblage. In cases where the net to gross area ratio is increased from 0.6 to 0.75, due to the flared shape, the capacity would be decreased by about 25% for medium grout strength (σ_{tg} = 300 psi).

3 - The block's mechanical properties have no effect on the masonry tensile strength normal to the bed joints. It is the block physical properties which affect the capacity. Its surface roughness and initial rate of absorption (IRA) affect the tensile bond strength of the mortar, and its net to gross area ratio, η_{hm}, affects the contribution of the mortar and the grout.

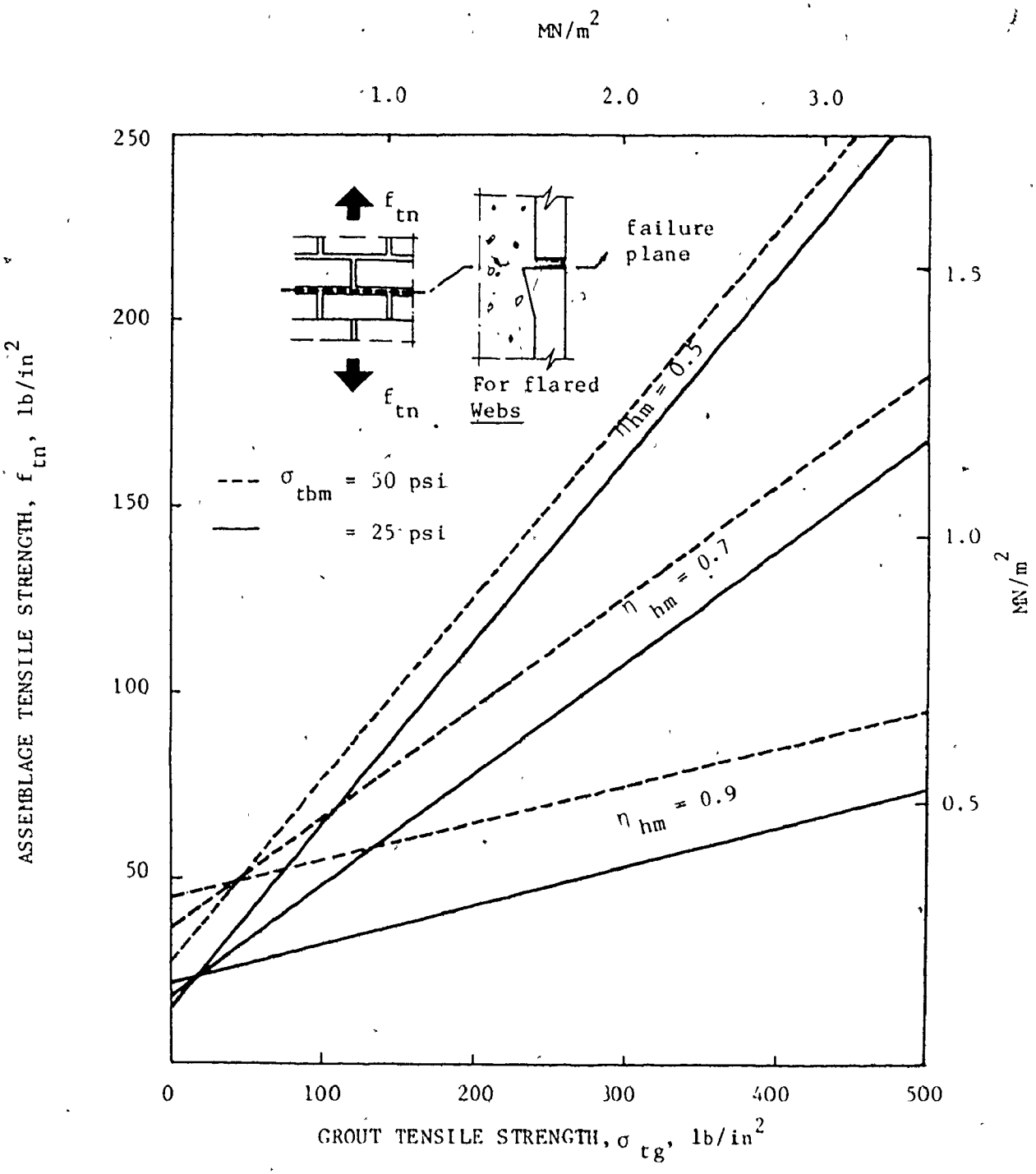

Fig. 4.22 TENSILE STRENGTH OF MASONRY NORMAL TO THE BED JOINTS VERSUS GROUT TENSILE STRENGTH

4.3.4 Masonry Tensile Strength Parallel to the Bed Joints, f_{tp}

Under tensile stresses parallel to the bed joints, there are two possible modes of failure:

Mode-I is distinguished by splitting failure along a plane passing through the head joints and the block's face shells even for grouted masonry as shown in Fig. 4.23(a). The effect of any tension bond between the block and the grout is very small and can be neglected in the present analytical formulation. The failure plane is identical for both ungrouted and grouted masonry as it passes between the columns of grout. The capacity is governed by the tensile strength of the blocks and the tensile bond strength of the head joints. Because the mortar thickness is quite small compared to the block height (about 5%) and its tensile strength is not far from that of the block, the joint thickness is added to the block height and the analytical formulation is based on the nominal height of the block. For the minimum path of the failure plane associated with Mode-I (see Fig. 4.23), the apparent tensile strength of the assemblage can be described by incorporating the resistance of the component materials (block and grout) as follows:

$$2 A_g f_{tp-I} = A_g \sigma_{tbm} + \eta_v A_g \sigma_{tbl} \quad .... (4.12)$$

therefore

$$f_{tp-I} = 1/2 (\sigma_{tbm} + \eta_v \sigma_{tbl}) \quad .... (4.13)$$

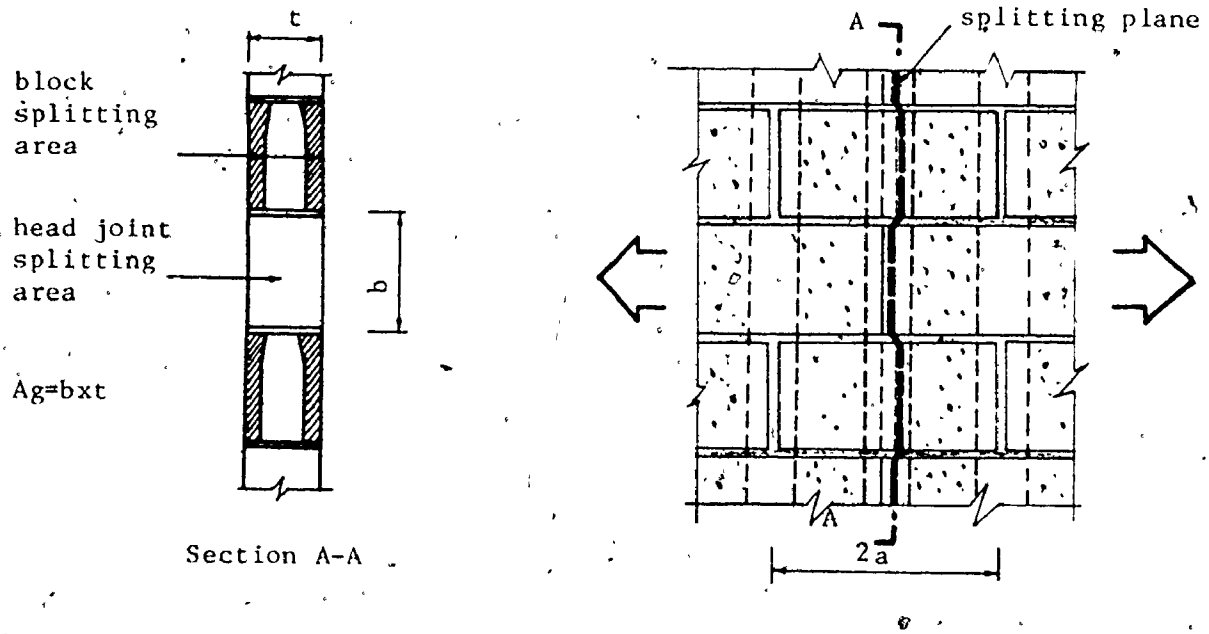

a - Failure Mode - I

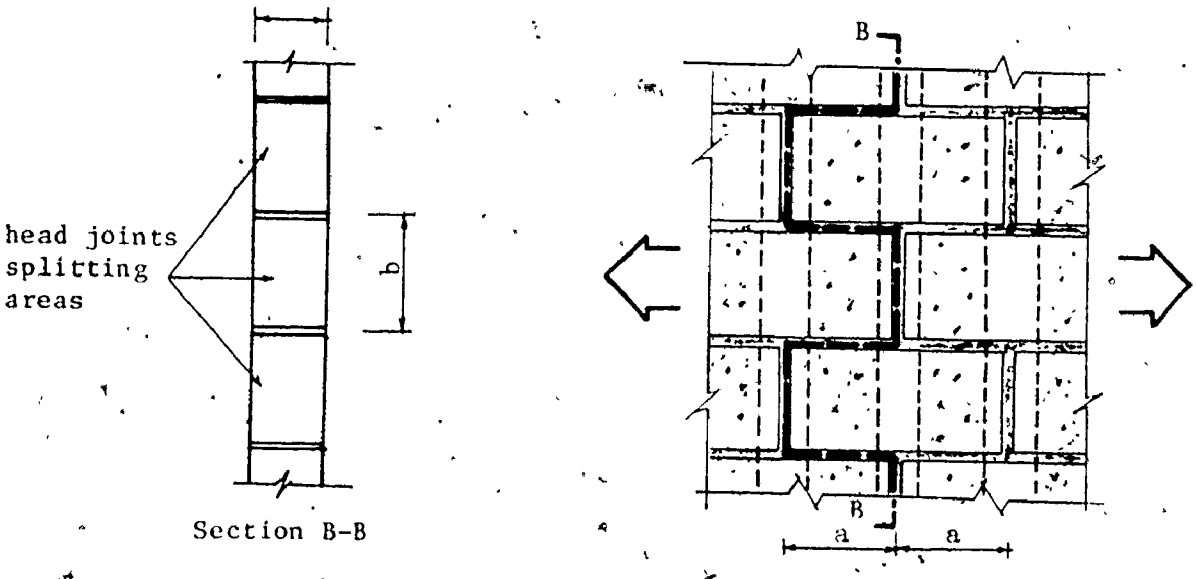

b - Failure Mode - II

Fig. 4.23 FAILURE MODES OF MASONRY ASSEMBLAGES UNDER TENSILE STRESSES PARALLEL TO THE BED JOINTS

where f_{tp-I} = average tensile strength of the assemblage parallel to the bed joints, mode-I of failure

σ_{tbm} = tensile bond strength of the head joints

σ_{tbl} = splitting tensile strength of the block

η_v = net to gross area ratio for vertical section crossing the face shells just beside the middle web (see Fig. 4.23)

The above strength formula, shown graphically in Fig. 4.24 for different block characteristics, indicates the following features of behaviour of ungrouted and grouted masonry under tensile stresses parallel to the bed joints where failure mode-I is the governing mode:

1 - The block tensile strength significantly affects the tension capacity of the assemblage especially for higher η_v values.

2 - The mortar bond strength does not appreciably affect the relative capacity particularly for high block strength.

3 - Since the block's tensile strength is the dominant parameter, it seems appropriate to try to correlate the tensile strength of either ungrouted or grouted masonry to the block tensile strength.

4 - The grout strength has no influence on the tensile capacity of grouted masonry under tensile stresses parallel to the bed joints where failure mode-I is the governing mode.

5 - The net to gross area ratio of the block for a vertical

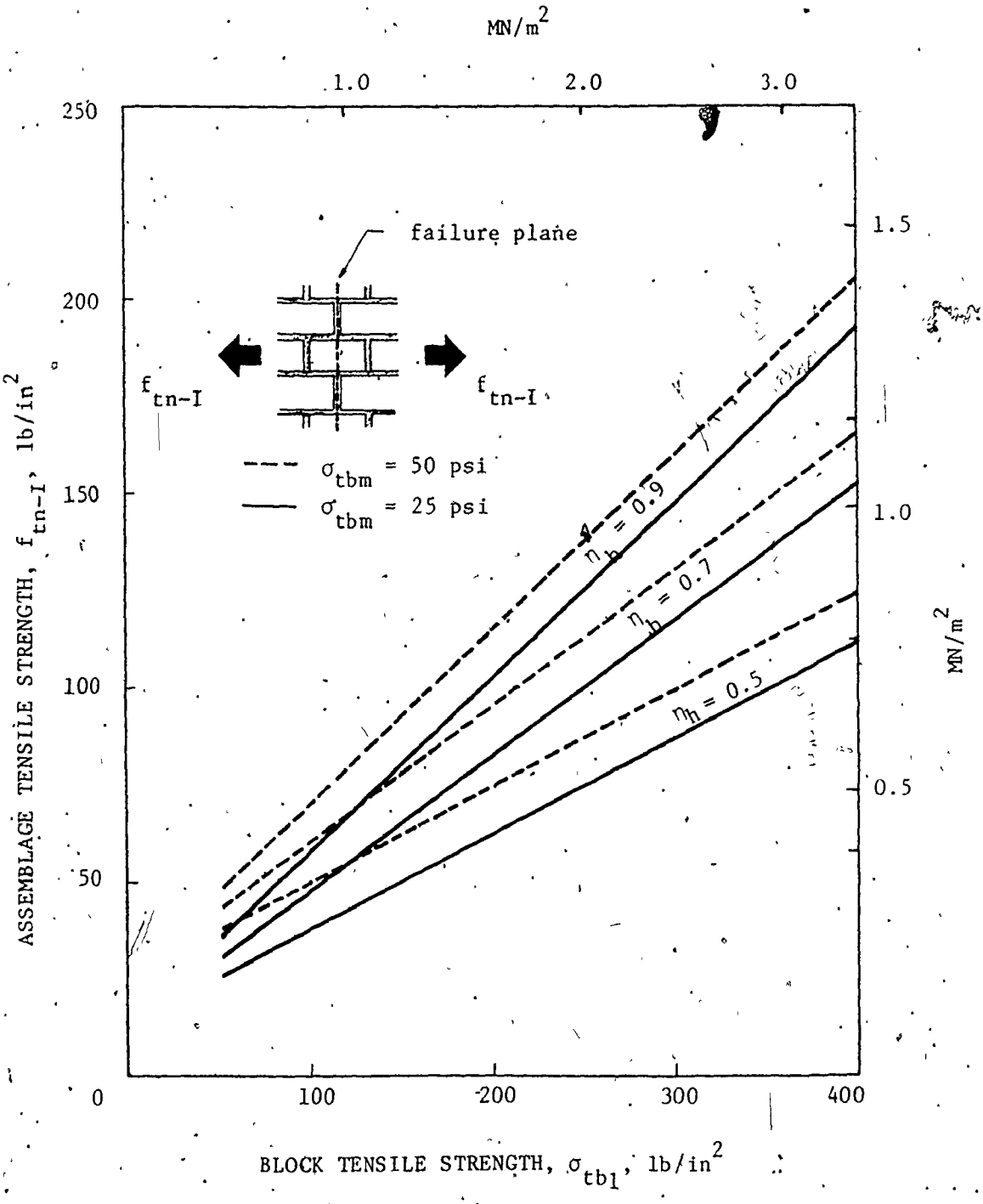

Fig. 4.24 EFFECT OF BLOCK TENSILE STRENGTH ON THE TENSILE STRENGTH OF MASONRY PARALLEL TO THE BED JOINTS (FAILURE MODE-I)

cross section passing through the face shells just beside the middle web, has a significant effect on the tensile strength. The trend of current practice to taper the face shells to increase their thickness towards the middle web (see Fig. 2.1), may appreciably increase the tension capacity because it increases the block's area normal to the applied stresses. For the blocks chosen for the current experimental program, the increase of the face shell thickness (see Fig. 2.1) helped, by increasing η_v from 0.46 to 0.7, to increase the overall capacity by about 30%.

Mode-II is distinguished by a stepped failure surface passing through the head and bed joints as shown in Fig. 4.23(b). It is a joint failure as the blocks suffer no distress. For ungrouted masonry, failure occurs at the block-mortar interfaces, whereas the failure of grouted masonry is similar but with shearing of the cores at the horizontal section of minimum grout area (of maximum η_h). The shearing capacity of the grouted cores is governed by their principal tensile strength, which is considered equal to their splitting tensile strength, σ_{tg}. The apparent tensile strength of the assemblage can be described by incorporating the resistance of the component materials (mortar and grout) as follows:

$$(2bt) f_{tp-II} = (2bt)\sigma_{tbm} + (2at\ \eta_{hm})\sigma_{sbm} + 2(1-\eta_{hm})(at)\sigma_{tg} \quad .... (4.14)$$

therefore

$$f_{tp-II} = \sigma_{tbm} + (a/b.\eta_{hm})\sigma_{sbm} + (a/b(1-\eta_{hm}))\sigma_{tg} \quad .... (4.15)$$

where f_{tp-II} = average tensile strengtn of the assemblage parallel to the bed joints, mode-II of failure

σ_{tbm} = tensile bond strength of the head joints.

σ_{sbm} = shear bond strength of the bed joints

σ_{tg} = splitting tensile strength of the grout (equal zero for ungrouted masonry)

η_{hm} = maximum net to gross area ratio of the block in the horizontal direction

$2a/b$ = aspect ratio of the block.

Equation (4.15), presented graphically in Fig. 4.25 for several different conditions, indicates the following features of behaviour of masonry under tensile stresses parallel to bed joints where failure mode-II is the governing mode:

1 - The mortar strength has a considerable effect on the tensile capacity of both ungrouted and grouted masonry.

2 - The tensile strength of the grout has a pronounced effect on the assemblage tension capacity especially for lower values of η_{hm} (higher core areas).

3 - The net to gross area ratio of the block in the horizontal direction has an appreciable effect on the tensile capacity, particularly for grouted masonry. The flared shape of the block reduces the area of grout in the critical section thereby causing a reduction in the horizontal shear resistance and consequently in the average tensile strength of the assemblage.

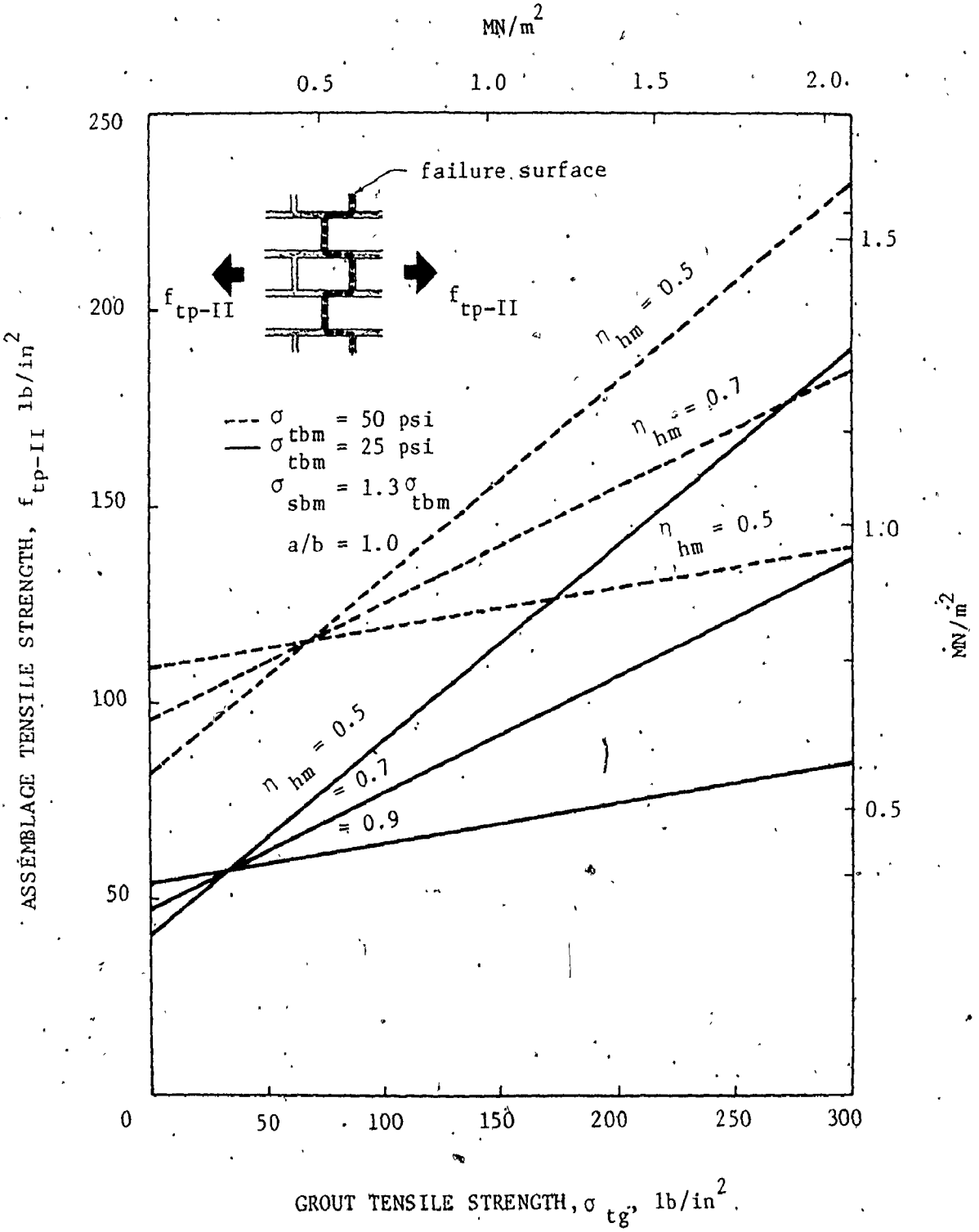

Fig. 4.25 EFFECT OF GROUT TENSILE STRENGTH ON THE TENSILE STRENGTH OF MASONRY PARALLEL TO THE BED JOINTS (FAILURE MODE - II)

Equations (4.13) and (4.15) express the tension capacity of either ungrouted or grouted masonry under tensile stresses parallel to the bed joints for failure modes I and II, respectively. The governing formula is the one giving the lower capacity. Hence, the mode of failure could be determined for various strength and geometric characteristics of the components. This is shown in Fig. 4.26 for representative constant conditions concerning the grout strength and the net to grosss area ratios of the block. It seems that the two major parameters influencing the mode of failure and consequently the tensile capacity are as follows:

1.- The aspect ratio of the block, which is a geometric characteristic of the assemblage. The possibility of failure mode-I is greater for higher aspect ratios particularly for grouted masonry as shown in Fig. 4.26. For lowen values of a/b, where failure mode-II governs, higher aspect ratios result in relatively greater tension capacities because the failure path will be longer thereby providing greater resistance along the horizontal joints. This is particularly true for grouted masonry where the core area has a significant effect.

2 - The block tensile stength to mortar bond strength ratio, which is a strength characteristic of the assemblage. Figs. 4.26 and 4.27 show that higher strength ratios increase the possibility of failure mode-II occurring especially for ungrouted masonry where the mortar is the only media joining the blocks.

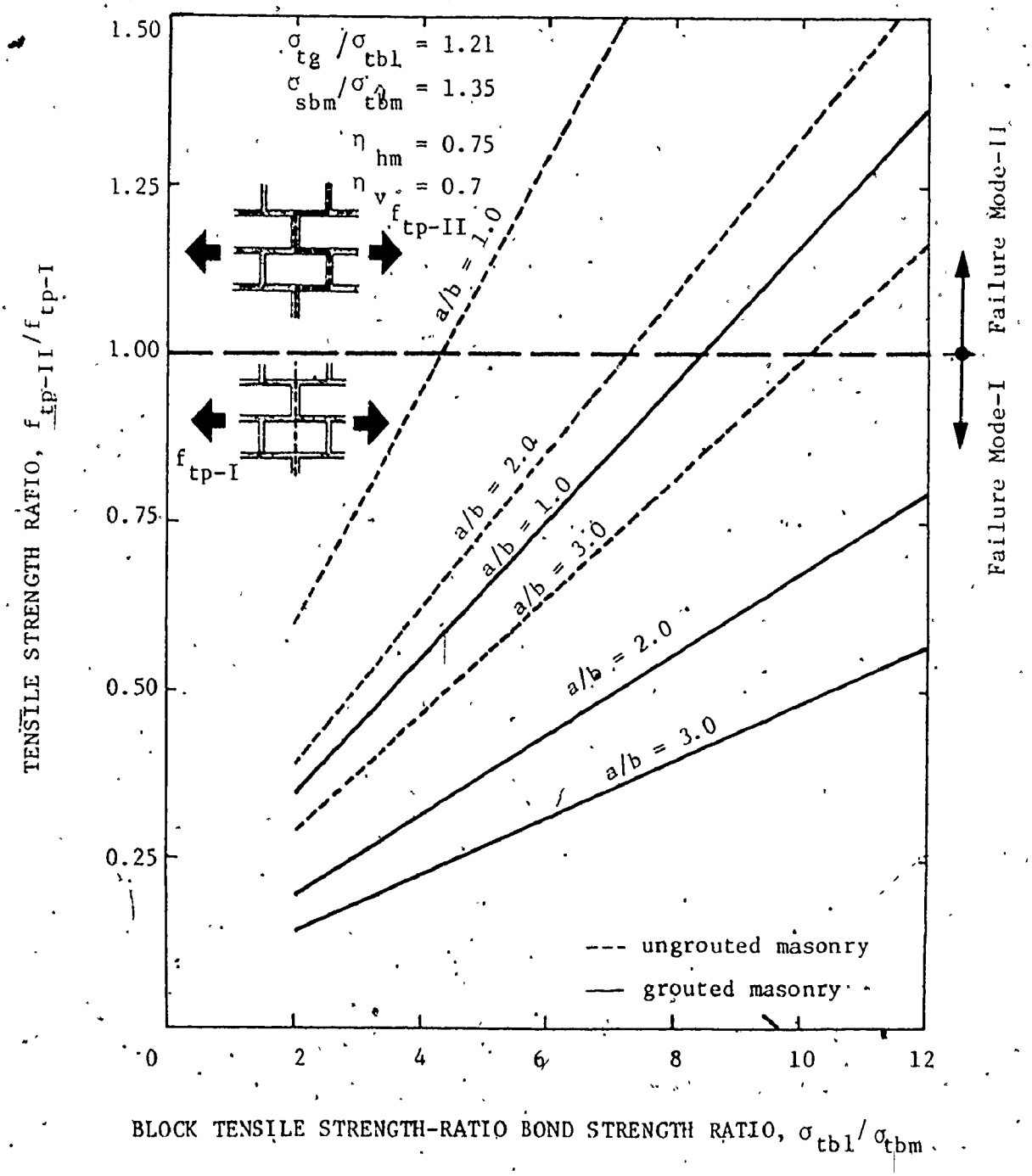

Fig. 4.26 INFLUENCE OF COMPONENTS' CHARACTERISTICS ON THE MODE OF FAILURE UNDER TENSILE STRESSES PARALLEL TO THE BED JOINTS

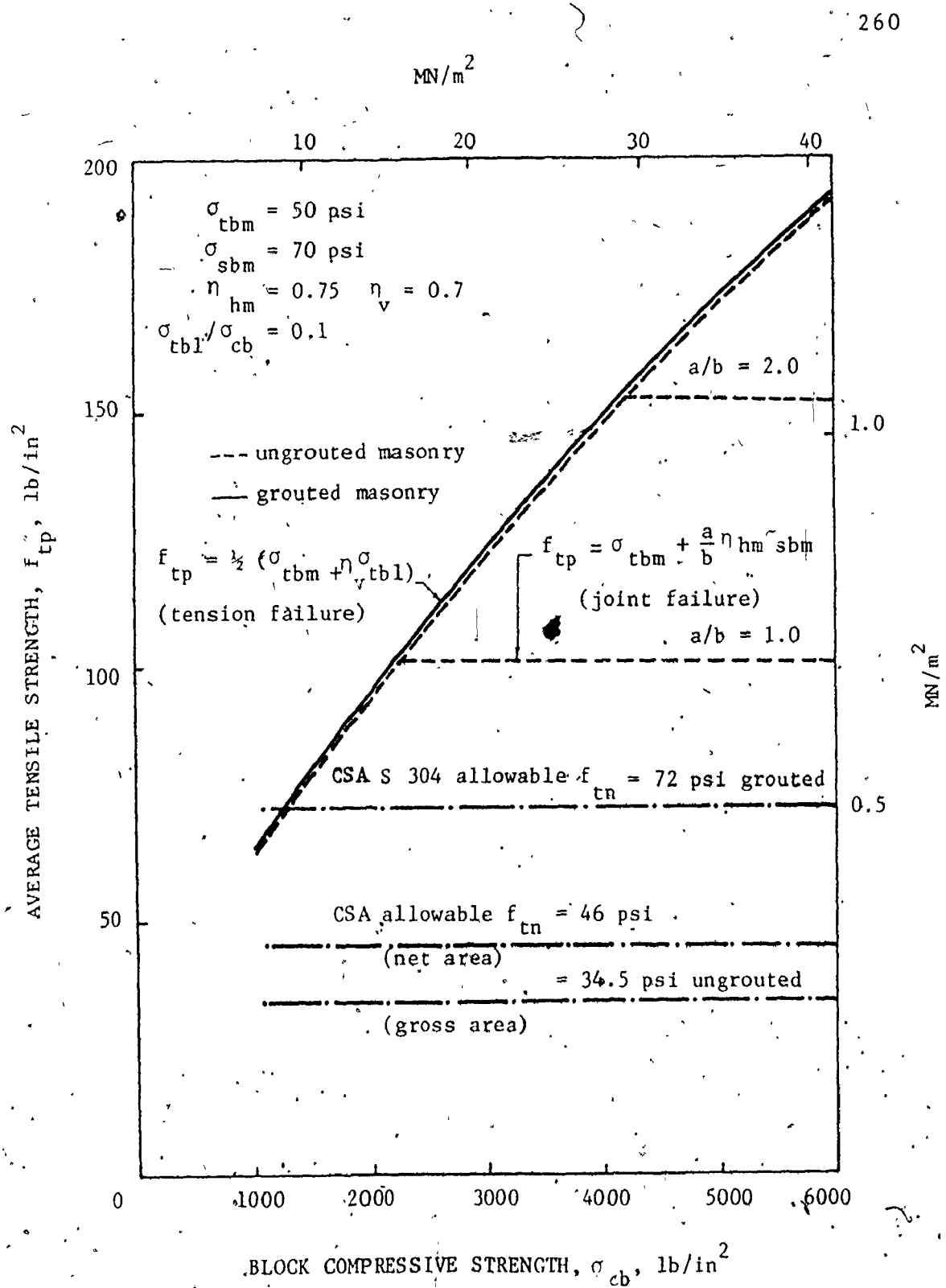

Fig. 4.27 TENSILE STRENGTH OF MASONRY PARALLEL TO THE BED JOINTS VERSUS BLOCK COMPRESSIVE STRENGTH

These figures also indicate that for grouted masonry, Failure mode-I (splitting along vertical plane passing between the columns of grout) is the expected mode for most practical cases where the a/b ratio is greater than one and the grout and block strengths are about the same.

A comparison between the experimental results and Equation (4.13) for the tensile strength of masonry parallel to the bed joints (failure mode-I) is presented in Fig. 4.28. The splitting tensile strength of the block was adopted for σ_{tbl} and the couplet test results were used for the tensile bond strength of the head joints. There is reasonably good agreement between the proposed expression and the experimental results. Fig. 4.28 also indicates that the splitting tensile strength of the discs could be predicted analytically to within 20% of the experimental results with the trend of being on the conservative side.

4.3.5 Diagonal Tensile Strength of Masonry, f_{td}

When the angle between the principal tensile stress and the bed joint is 45°, the results of the tested masonry discs can be considered as a measure of the shear strength of a masonry assemblge which is applicable to masonry beams and shear walls[28].

Under loads applied in directions other than the principal material directions (parallel and normal to the bed joints), the most probable mode of failure is a mixed shear (debonding at the

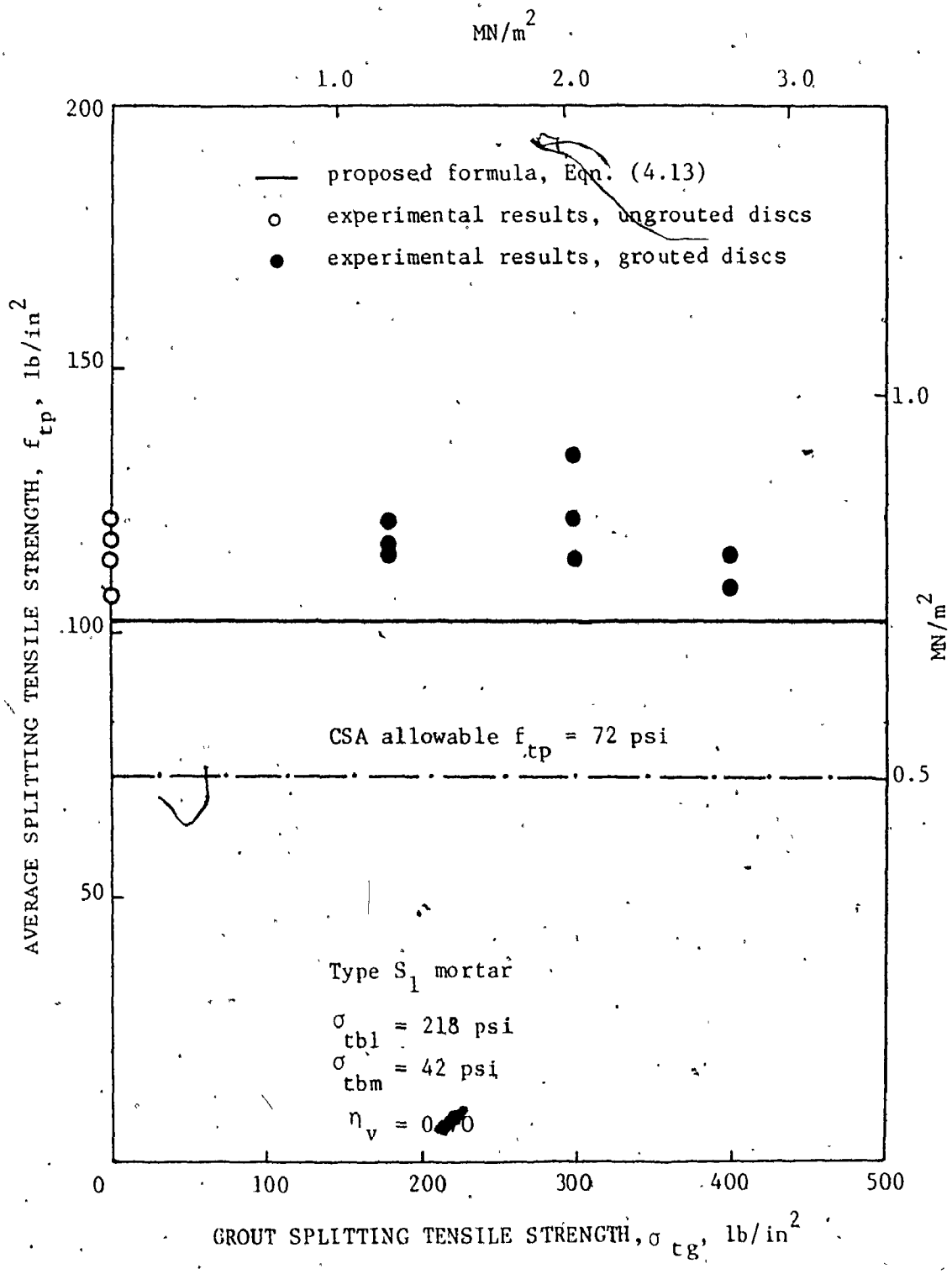

Fig. 4.28 COMPARISON OF MEASURED AND CALCULATED VALUES OF MASONRY TENSILE STRENGTH PARALLEL TO THE BED JOINTS (FAILURE MODE-I)

interfaces) - tension (splitting of the units and the mortar joint) mode of failure. This is due to the fact that the failure crack does not follow the most direct path especially for grouted masonry as is indicated in Fig. 4.11. The tension capacity under tensile stresses oriented at 45° from the bed joints might reasonably be assumed to be a function of the average strengths in the two orthogonal directions (normal and parallel to the bed joints) as follows:

$$f_{td} = f\left(\frac{f_{tn}+f_{tp}}{2}\right) \qquad \ldots\ (4.16)$$

Utilizing the experimental results, a strong correlation was found between the diagonal tension capacity and the average strengths, as shown in Fig. 4.29. A simple linear relationship of the form given below (Equation 4.17) is shown to adequately represent this assumed relationship.

$$f_{td} = 2/3\ (f_{tn} + f_{tp}) \qquad \ldots\ (4.17)$$

Substituting the values of f_{tn} and f_{tp} from Equations (4.11), (4.13), and (4.15) into Equation (4.17) yields the following two semi-empirical equations (i.e. two different failure modes related to f_{tp});

$$f_{td} = 2/3[(0.5+\eta_{hm})\sigma_{tbm}+0.5\eta_{v}\ \sigma_{tbl}+(1-\eta_{hm})\ \sigma_{tg}] \qquad \ldots\ (4.18)$$

for failure mode-I (splitting tension failure) and,

$$f_{td} = 2/3[(1+\eta_{hm})\sigma_{tbm}+(a/b.\eta_{v})\sigma_{sbm}+((1-\eta_{hm})a/b+(1-\eta_{v}))\sigma_{tg}] \qquad \ldots\ (4.19)$$

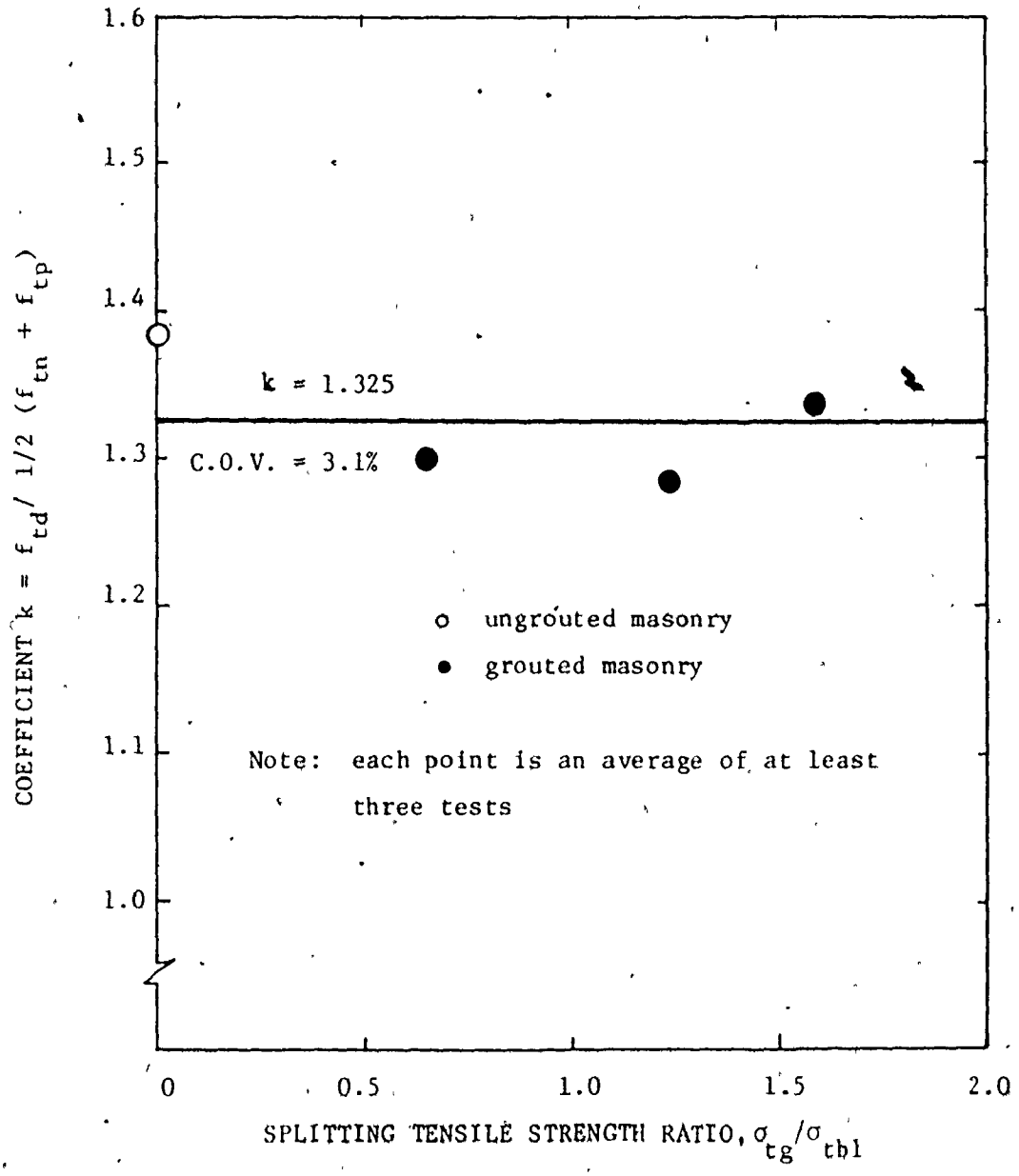

Fig. 4.29 CORRELATION BETWEEN THE DIAGONAL TENSION CAPACITY AND THE TENSILE STRENGTHS IN THE PRINCIPAL DIRECTIONS

for failure mode-II (debonding failure). The minimum strength calculated from the above two equations governs. The mode of failure as well as the strength could be predicted using these proposed formulas.

Fig. 4.30 presents the average diagonal tensile strength of ungrouted masonry, as calculated from the proposed formulas, versus the block tensile strength to mortar bond strength ratio, $\sigma_{tbl}/\sigma_{tbm}$. It is shown that there are two distinct modes of failure possible under diagonal tension stresses:

1 - A splitting tension failure is distinguished by failure crack passing mainly through the blocks and the mortar bed joints. It occurs in cases of blocks of lower tensile strength and mortars of high bond strength.

2 - A shear-tension failure (debonding failure) is distinguished by a step crack occurring mostly along the mortar bed and head joints. It occurs in cases of blocks of higher tensile strengths and mortars of lower bond strengths. It is indicated in Fig. 4.30 that the aspect ratio of the block has a significant effect on the mode of failure and the tension capacity, especially for cases of high strength ratios $\sigma_{tbl}/\sigma_{tbm}$.

Sinha and Hendry[49] suggested the following empirical formula to relate the diagonal tensile strength of solid brick masonry, f_{td}, to its compressive strength f'_m:

$$f_{td} = 2\sqrt{f'_m} \qquad \ldots\ (4.20)$$

The formula suggested in Section 3.3.3.4 (Equation 3.38)) was

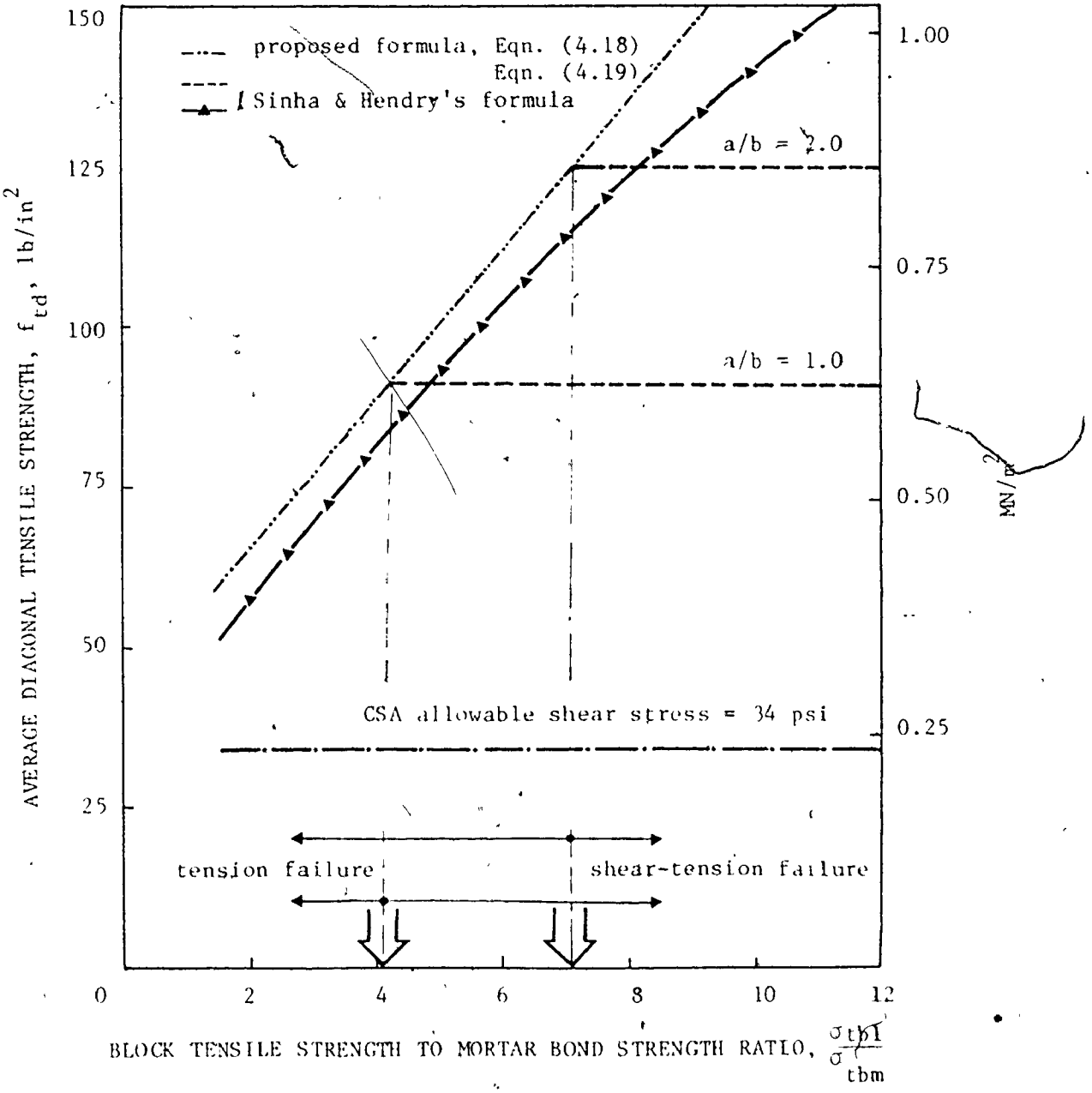

Fig. 4.30 EFFECT OF THE CHARACTERISTICS OF THE COMPONENTS ON THE DIAGONAL TENSILE STRENGTH OF UNGROUTED MASONRY

adopted to relate the prism compressive strength to the geometric and strength characteristics of the components. Using this relationship, Sinha and Hendry's formula is plotted in Fig. 4.30. Their empricial equation predicts results close to the proposed formula in cases where splitting tension is the governing mode of failure. It is important to mention that their formula was developed for brick masonry where the aspect ratio of the units is greater than 2. However, when debonding failure is the governing mode (i.e. as shown for a/b ratios of 1 and 2), Sinha and Hendry's formula overestimates the tension capacities. This can be attributed to the fact that the tension and the shear bond strengths of the mortar significantly affect the resistance to a debonding failure which is not directly related with the compression capacity. Hence, there is not necessarily any physical correlation between the two strength parameters (f_{td} and f'_m) in this case.

Stafford-Smith et al[52], by comparing some experimental results with their analytical values, suggested that the diagonal tensile strength of brickwork equals either the tensile strength of the mortar or the tensile strength of the brick whichever is less. The current experimental results presented in Table 4.1 show a reduction in the diagonal tension capacity of only 10% for a reduction in the mortar strength of about 60%. This indicates that no direct proportionality exists between the diagonal tension and the mortar strength contrary to the suggestion of

Stafford-Smith et al[52]. Balachandran[2] also concluded, as a result of extensive experimental and analytical investigations on block masonry piers, that increasing the mortar strength does not appreciably increase the shear strength. It seems that the proposal of Stafford-Smith et al[52] is a conservative approach to approximately predict the diagonal tension capacity of brickwork and as such may highly underestimate the tensile capacity. Also, it may only be applicable in cases where the tension mode of failure is the governing criterion. In cases where debonding is the governing mode of failure, the tensile strength of either the block or the mortar seems to have very little effect on the diagonal tension capacity of the assemblage. This is attributed to the fact that the bonding strength of the mortar is not predominatly a function of its compressive or tensile strength[7].

Up to this point in this section, only the results for ungrouted masonry have been compared. Fig. 4.31 shows the average diagonal tensile strength of grouted masonry, as calculated from the proposed formulas (Eqautions (4.18) and (4.19)), versus the block tensile strength to mortar bond strength ratio, $\sigma_{tbl}/\sigma_{tbm}$, for two grout strengths (relative to the block strength). It is shown that there are two possible modes of failure (as the curves expressing the governing two equations intersect at point A) in cases of an aspect ratio $a/b \leq 1$ and strength ratio $\sigma_{tg}/\sigma_{tbl} \leq 0.5$. For lower values of $\sigma_{tbl}/\sigma_{tbm}$, tension failure will control (expressed by Equation (4.18)), whereas shear-tension failure will

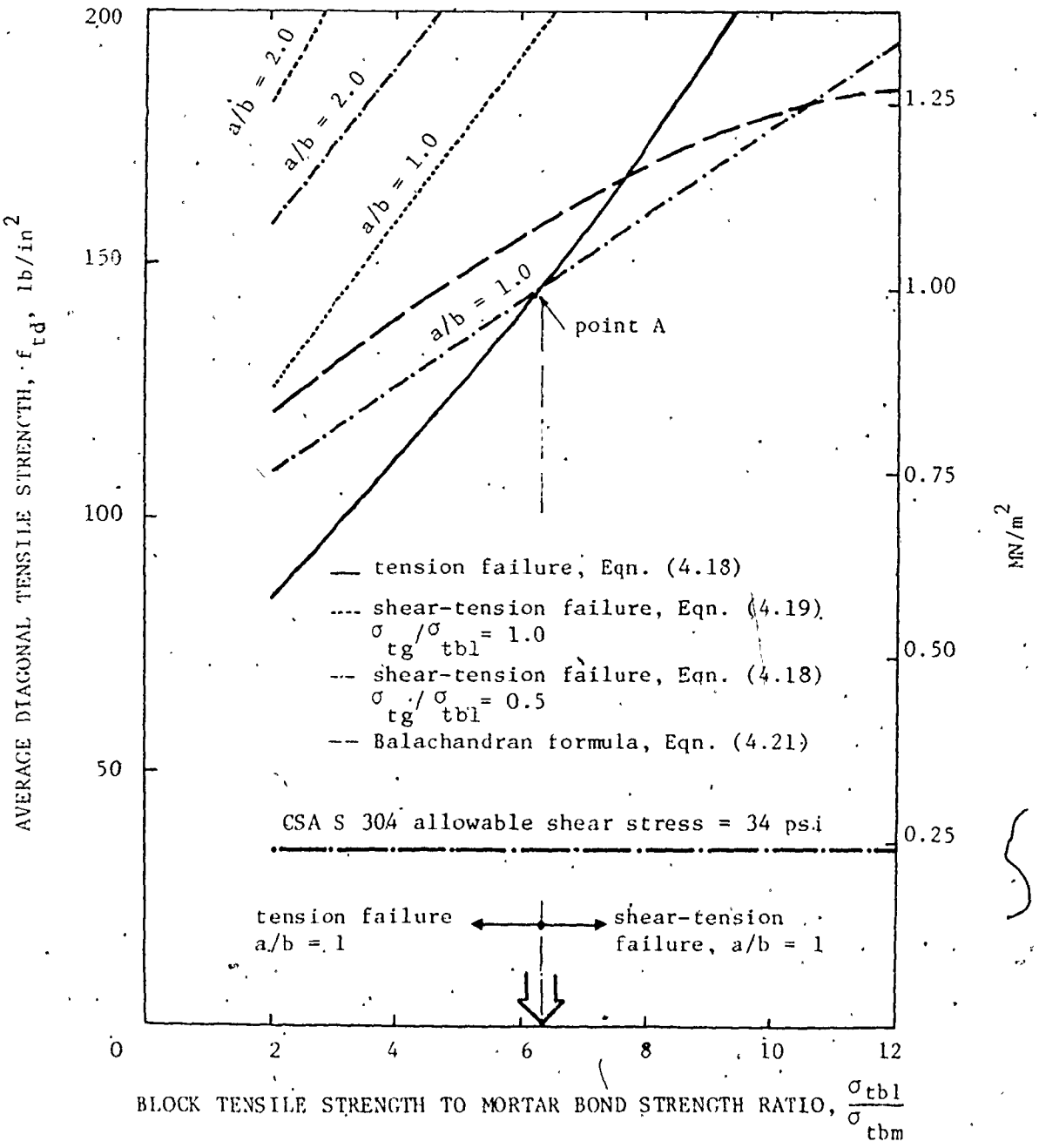

Fig. 4.31 EFFECT OF THE CHARACTERISTICS OF THE COMPONENTS ON THE DIAGONAL TENSILE STRENGTH OF GROUTED MASONRY

govern (expressed by Equation 4.19)) for higher values of $\sigma_{tbl}/\sigma_{tbm}$. In other cases of high aspect ratios (a/b > 2) and or higher grout strengths ($\sigma_{tg} \geq \sigma_{tbl}$), only the tension failure mode, expressed by Equation (4.18), will control.

Balachandran[2] used the method of least squares to relate f_{td} and f'_m values from his experimental data by a straight line. The best fit yielded the following relation:

$$f_{td} = 3.8\sqrt{f'_m} \quad \ldots\ldots (4.21)$$

where f_{td} is the average shear strength of a grouted concrete masonry pier as governed by its diagonal tension capacity, and f'_m is the compressive strength of the corresponding grouted prism. The above formula is compared with the proposed formulas, (Equations (4.18) and (4.19)) in Fig. 4.32. The compressive strengths of the grouted prisms are related to the geometric and strength characteristics of the components using Equation (3.31) which is proposed in Section 3.3.3.4. There is relatively poor agreement, especially for the extreme values of strength ratio $\sigma_{tbl}/\sigma_{tbm}$. However, as shown in Fig. 4.32, a reasonable agreement is achieved between the formulas and the test results.

Trying to correlate the diagonal tension strength of masonry to its compressive strength may not be sound because the parameters influencing these are not the same, particularly for grouted masonry where a more complex interaction of the component materials (block, mortar, and grout) exists. Balachandran[2] pointed out that it was not possible to attribute any physical

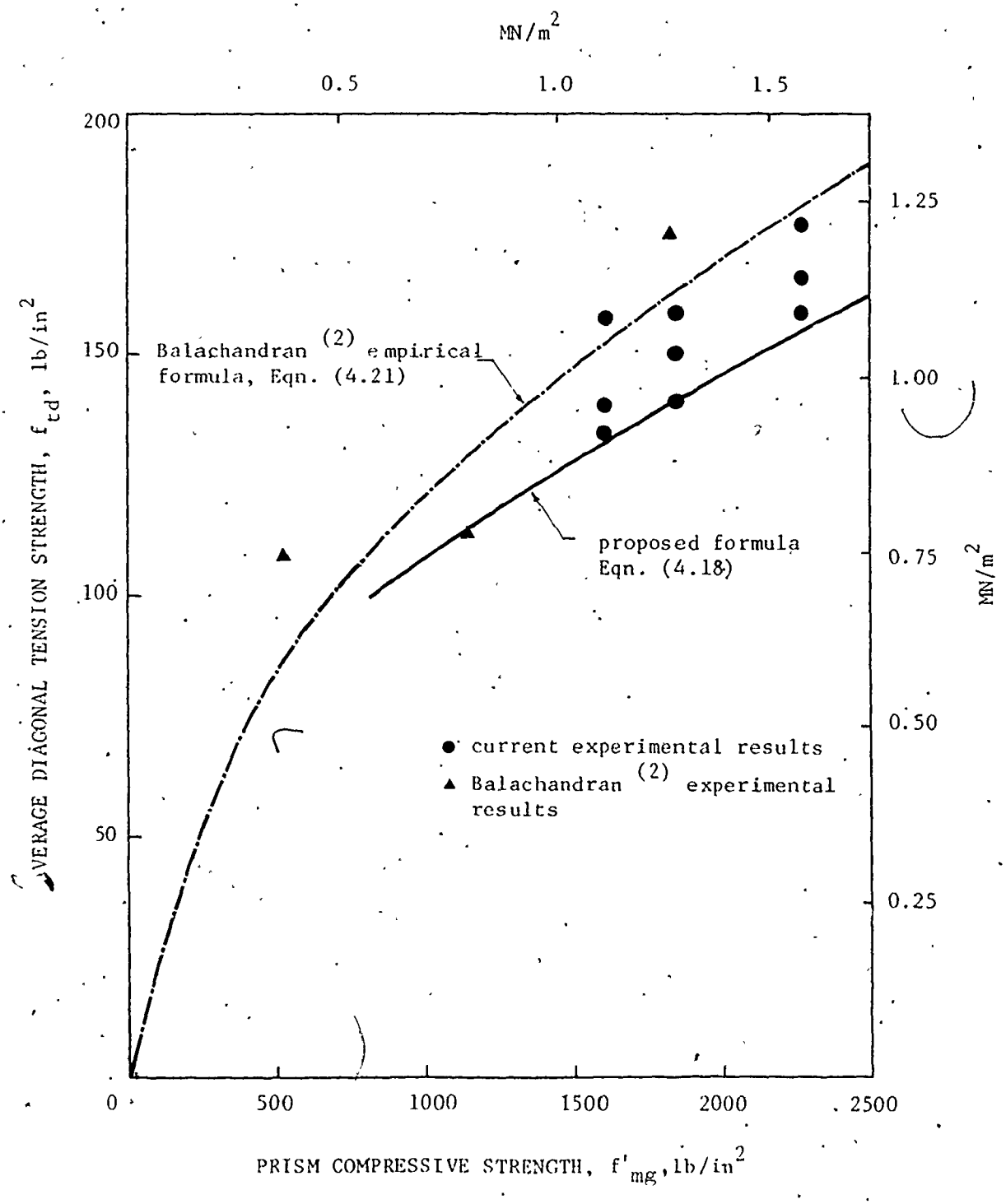

Fig. 4.32 DIAGONAL TENSILE STRENGTH OF GROUTED MASONRY VERSUS PRISM STRENGTH

relationship between the failure of a grouted prism in axial compression and a grouted pier in diagonal tension, and concluded by stating that his Equation (4.21) could only be used to empirically assess the diagonal tensile strength of grouted masonry piers as long as the mortar and the grout strengths are similar to those used in his investigation.

It has to be noted that before the general application of the proposed strength formulas (used to assess the tensile strength of both ungrouted and grouted masonry under different stesss oreientations) could be recommended, their validity over different geometric and block characteristics should be examined.

4.4 Review of the Code Provisions

The CSA Standard S304[12] assigns allowable tensile stresses normal and parallel to the bed joints for grouted masonry similar to those for solid masonry provided that the grout strength is at least equal to that of the block. The only parameter considered for the classification of the allowable stresses is the mortar type. This ignores the strength and geometric characteristics of both the block and the grout.

The code provisions, based on the observed behaviour of ungrouted and grouted masonry under tension stresses, which was discussed previously, are evaluated below:

1 - The code design values for ungrouted masonry under tension normal to the bed joints is classified on the basis of the

mortar type. The experimental results indicated that, for one type of block, the mortar type has no pronounced effect on the tension capacity (Fig. 4.13). The tensile bond strength of the mortar, which is the dominant parameter, depends not only on the mortar properties but also on the physical properties of the block (surface roughness and initial rate of absroption).

2 - The code assigns design values for grouted masonry under tension normal to the bed joints similar to those for solid masonry. These values depend only on the mortar type ignoring the continuity provided by the cores in the direction of the tensile stresses. Because of the fact that the tensile strength of the grout is much higner than the tensile bond strength of the mortar, the code values substantially underestimate the capacity of grouted masonry for tensile stresses normal to the bed joints. Figs. 4.20 and 4.22 indicate that the effect is even greater for high strength grout. The current experimental results showed an increase of tne tensile strength of grouted specimens of about 100% to 200% over the ungrouted specimens. Fig. 4.22 indicates that the grout strength significantly affects the assemblage tensile strength and seems to be the governing parameter especially for lower values of net to gross area ratio. Grout strength should be considered in the code provision as a major parameter in the assignment of design strengtn values for masonry under tension normal to the bed joint. It should be noted that the bond strength of mortar has a secondary effect on the tensile

capacity of grouted masonry under tensile stresses normal to the bed joints except in cases where the net to gross area ratio is greater than about 0.90 which is not a practical case for grouted masonry.

3 - The code assigns similar design values for tensile stresses parallel to the bed joints for both ungrouted and grouted masonry. This provision is based on the net area for ungrouted masonry and the gross area for grouted masonry. The experimental results showed similar strengths on the basis of gross area for both ungrouted and grouted masonry, whereas based on the above criterion, they showed much high strength for ungrouted masonry compared to grouted masonry (see Section 4.2.4.5). Also, the code classifies the allowable stresses parallel to bed joints as a function of only the mortar type no matter what the block strength is. Fig. 4.24 indicates that the block tensile strength is the most significant parameter influencing the tension capacity under tensile stresses parallel to the bed joints. The code should consider the block stength when assigning design values for both ungrouted and grouted masonry under tension parallel to bed joint. Fig. 4.27 indicates the nonuniformity of safety of the code provision concerning tension parallel to the bed joints for either ungrouted or grouted concrete masonry particularly for cases where tension failure is the governing modee. This is attributed to the code approach in ignoring the block tensile strength which is shown to be a significant parameter influencing the tension

capacity. It is worth noting in Fig. 4.27 that the code values for grouted masonry yield safety factors less than 2 under tension parallel to the bed joints where the presence of grout is not significant.

4 - The code states that design values for ungrouted masonry are to be based on the net area. Under tensile stresses normal to the bed joints, the net area is that of the block but under stresses parallel to the bed joint, the net area of the block in its horizontal cross-section bears no physical relationship to the failure plane which is mainly in the vertical direction passing through the head joints and the face shells of the blocks for the case of the tension mode of failure (see Section 4.3.4). Under tensile stresses, which are not applied in the principal material directions (normal and parallel to the bed joints), the net area is rather difficult to determine. The calculation of the average tensile strength of the assemblage based on the gross area, as adopted in the proposed formulas, is recommended as being appropriate.

5 - The current results indicate that the diagonal tensile strength of ungrouted or grouted masonry is different from the strength in the principal material directions. The code provisions do not assign design values for diagonal tension which is an important strength characteristic for the design of masonry elements under critical combinations of compression and shearing forces. The code values for the allowable shear stresses, v_m,

were probably assigned for design against joint slip failure along the bed joints. No distinction is made between the possible modes of failure under combined stress conditions. If v_m is used for design of diagonal tension conditions, it substantially underestimates the assemblage capacity, especially for grouted masonry.

4.5 Summary and Conclusions

The behavioural characteristics of ungrouted and grouted masonry under tensile stresses at different orientations from the bed joint direction are presented and discussed in this chapter. The effects of grout strength, mortar type, and bed joint reinforcement on the assemblage tensile strength are investigated. Strength formulas to predict the assemblage tensile strengths under different stress orientations are proposed in terms of the geometric and strength characteristics of its components.

The following conclusions are drawn from the experimental and analytical results presented in this chapter:

1 - The tensile strength of either ungrouted or grouted masonry varies with the stress orientation. This is attributed to the anisotropic nature of masonry.

2 - The tensile strength of block masonry for a specified direction, is not only a function of the strength characteristics of the component materials but also a function of their geometric characteristics. The block geometric parameters such as the

aspect ratio and the net to gross area ratio in the horizontal and vertical directions have significant effect on the tensile strength of both ungrouted and grouted masonry.

3 - There are two possible modes of failure under tension parallel to the bed joints. These are a splitting mode distinguished by a failure crack passing through the head joints and the block face shells, and a shear-tension mode distinguished by stepped-wise crack at the block-mortar interfaces. The component's geometric and strength characteristics determine which one of the two is the governing mode.

4 - The block strength and its geometric characteristics significantly influence the tensile strength of masonry assemblages. The code's consideration that the mortar type is the only parameter affecting masonry tensile strength, seems to be unrealistic and may lead to a substantial underestimation of masonry capacity especially under tensile stresses parallel to the bed joints.

5 - The mortar type is the governing parameter for the tensile strength of ungrouted masonry normal to the bed joints whereas it has only a secondary influence under tensile stresses parallel to the bed joints.

6 - Calculating the tensile stresses of ungrouted masonry under stresses parallel to the bed joints, on the basis of the net area, seems to be an inappropriate approach. The net area of the block, in a horizontal cross-section, does not relate to the

failure plane.

7 - Grouting contributes differently to the tensile strength of block masonry depending upon the direction of the applied stresses. It has a maximum contribution when the tensile stresses are applied in the direction of the grouted cores (i.e. normal to the bed joints). It has no contribution when these stesses are applied normal to the direction of the grouted cores (i.e. parallel to the bed joints).

8 - The continuity provided by the grouted cores in the vertical direction, which is ignored by the code, has a significant effect on the deformational and strength characteristics of concrete masonry under stresses normal to the bed joints.

9 - The code's consideration of grouted masonry being similar to solid masonry, provided that the grout strength is at least equal to that of the blocks, may lead to inconsistency and nonuniformity of safety. It underestimates the contribution of grouting for tensile stresses normal to the bed joints, whereas it overestimates the contribution of grouting for tensile stresses parallel to the bed joint.

CHAPTER 5

SHEAR BEHAVIOUR OF MASONRY JOINTS

5.1 General

Masonry shear walls are commonly used to resist horizontal forces in buildings. These walls are usually subjected to some combination of gravity loads and lateral loads. Gravity loads from upper level floors, walls and the roof and horizontal loads caused by wind, earthquake or explosion are the principal forces considered in shear wall design. For shear forces in the plane of the wall where failure is not controlled by tension caused by the combination of axial load and bending, the possibility of a shear failure must be examined. This shear failure may take the form of a slip along the bed joints at one or more courses. Even for a stepped diagonal crack caused by the combination of normal and shear stresses, there would be some proportion of failure along some of the bed joints. As will be discussed in Chapter 6, the assemblage capacity under biaxial stresses would be governed by the strength characteristics in the critical bed and head joint directions.

A criterion for shear failure of a joint, reported by many investigators[19,29,43,46,58], assumes that the joint resistance is attributed to the initial bond strength between the mortar and

the masonry units and to the shear friction capacity which is said to be proportional to the compressive stresses normal to the slip plane (precompression). This criterion can be formulated as:

$$\tau = \tau_o + \mu \sigma_n \qquad (5.1)$$

where

τ = the average shear stress at failure

τ_o = the shear bond strength expressed as the average shear stress at failure when $\sigma_n = 0$

σ_n = precompression stress, based on the net area of the slip plane

μ = a coefficient attributed to friction.

Equation (5.1) is basically Coulomb's theory of internal friction which is a special case of Mohr's theory of failure when the envelope curves consist of two straight lines, as shown in Fig. 5.1.

Since this criterion is stated in terms of the average stresses, it is implicitly assumed that the failure load is not sensitive to the shear stress distribution[52]. Also, it is not contemplated that this formulation would be applicable to failure modes other than slip along the mortar joints[47].

It has been reported[53] that experiments to establish separate values for τ_o and $\mu \sigma_n$ (Equation (5.1)) have shown that, for similar brick and mortar specimens, the values of μ appears to decrease substantially with increasing normal compressive

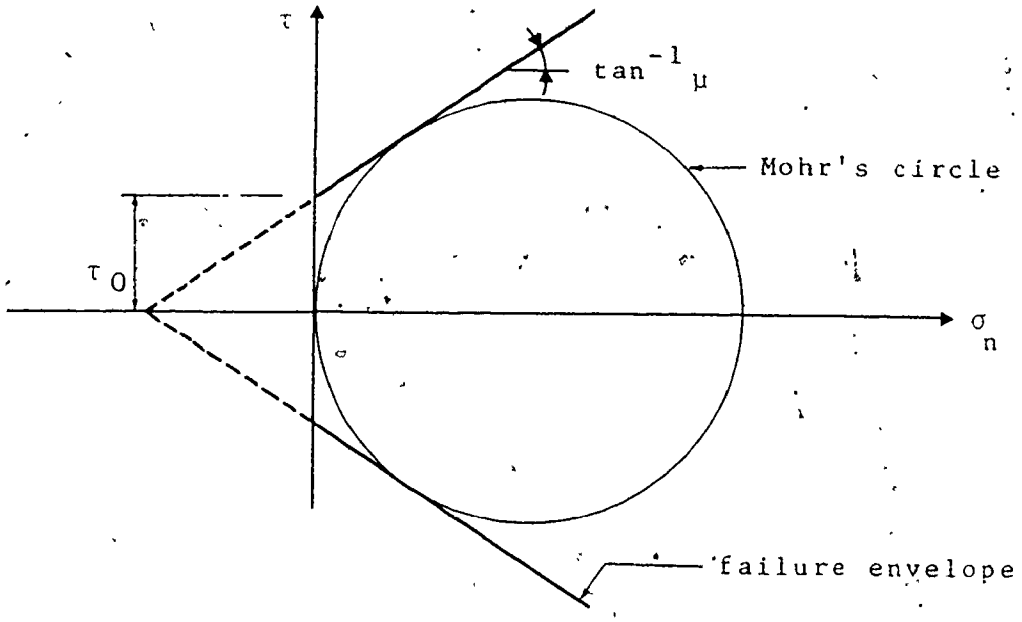

Fig. 5.1 COLOUMB THEORY OF INTERNAL FRICTION (11)

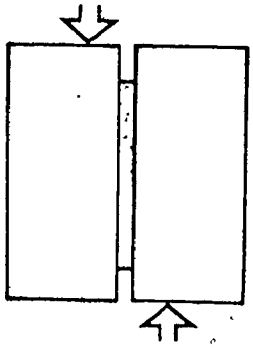

Fig. 5.2 COUPLET SHEAR TEST ADOPTED BY BENJAMIN AND WILLIAMS (Reproduced from Reference 4)

stresses, σ_n, and in order to support the friction theory, it has been necessary to adopt an average value of μ. It seems that evaluation of a real internal friction from the resistance of a failed surface may not appropriate as it represents more an apparent external friction. Apparently, there is no physical explanation of the superposition of the internal cohesion (initial bond) and the friction resistance. However, Equation (5.1) has been used, as an empirical expression, to reasonably predict the shear strength for both solid brick masonry joints[29,43,49] and hollow concrete masonry joints[29] for the range of precompression, σ_n, up to 20% of the masonry compressive strength. Above this level, Equation (5.1) no longer applies because of the observed change in the failure mode from joint slip to a combined shear-tension mode[47].

Stafford-Smith and Carter[53] proposed that shear failure may be due to a tensile failure in the mortar layer and, therefore, may be predicted by a comparison of the actual tensile stresses in the mortar layer with its tensile strength, rather than due to the combined initial bond and friction resistance. The well established observation that the shear capacity of the joint is not proportional to the tensile strength of the mortar[2,29] makes the authors proposal questionable.

No research on the effect of grouting on the shear resistance of concrete masonry joints has been found. This lack of information may account for the situation where typical masonry

codes[12,27] assign similar shear design values for grouted masonry and solid masonry provided that the grout strength is at least equal to that of the units. For most practical cases, this simple approach incorporates the untrue assumption that the shear strength of the grouted cores is only equal to the shear bond strength of the mortar.

An aim of this part of the investigation is to study the effect of grouting on the shear capacity of masonry joints under shear and precompression loading. The validity and adequacy of the code[12] provisions concerning the shear strength of grouted masonry will also be checked. To meet these objectives, an experimental and analytical investigation is reported in this chapter.

5.2 Description of the Experimental Investigation

The effect of grouting on the shear strength of masonry joints is demonstrated through a comparison study between the behaviour of grouted and ungrouted specimens. The effects of the mortar type and joint reinforcement on the shear capacity of ungrouted masonry have also been considered. The investigation was carried out under three different levels of compressive stress normal to the bed joint.

5.2.1 Test Specimens

Different shapes of specimens associated with different test techniques have been adopted by various researchers to investigate the shearing capacity of masonry joints. Benjamin and Williams[4] and Huizer[26] carried out tests on shear couplets composed of two bricks and a mortar joint as illustrated in Fig. 5.2. The test set-up shown in Fig. 5.3 was adopted by Haller[18] to determine the capacity of the joints in solid brick masonry under shearing along with precompression (stresses normal to the bed joints) loading. Jolley[29] used the three unit specimen (triplet) shown in Fig. 5.4 to evaluate the shear bond strength of brick masonry joints. A similar triplet specimen was adopted by Stafford-Smith and Carter[53]. These techniques have the disadvantage of developing flexural stresses over the mortar joint and hence do not representing a state of pure shear over the joint. Balachandran[2] showed, experimentally, that the flexural stresses developed from the external bending moments could considerably reduce the shear capacity of the joints.

To avoid creating bending moments at the mortar joints Balachandran[2] adopted a triplet specimen supported and loaded in such a way, Fig. 5.5, that the joints were at the points of contraflexure. [A similar test technique was adopted before by Mostafa[37] to determine the shearing capacity of the joints connecting the units of a segmental precast concrete bridge.] For such proportions (the depth to span ratio was about 1), the

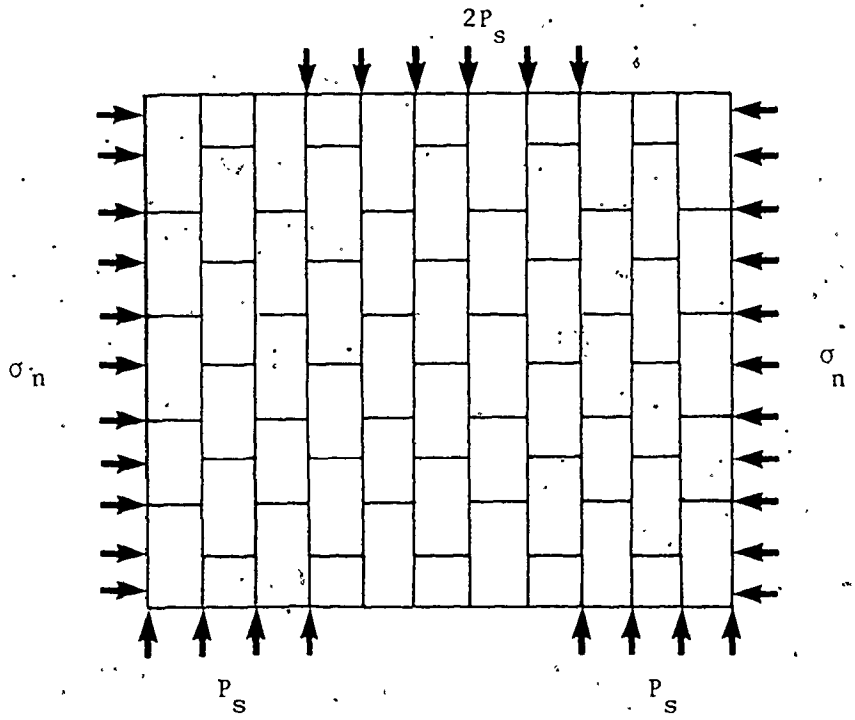

Fig. 5.3 TEST SPECIMEN ADOPTED BY HALLER (18)

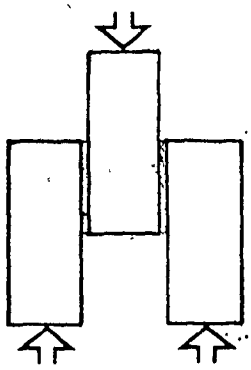

Fig. 5.4 TRIPLET SHEAR SPECIMEN USED BY JOLLEY (29)

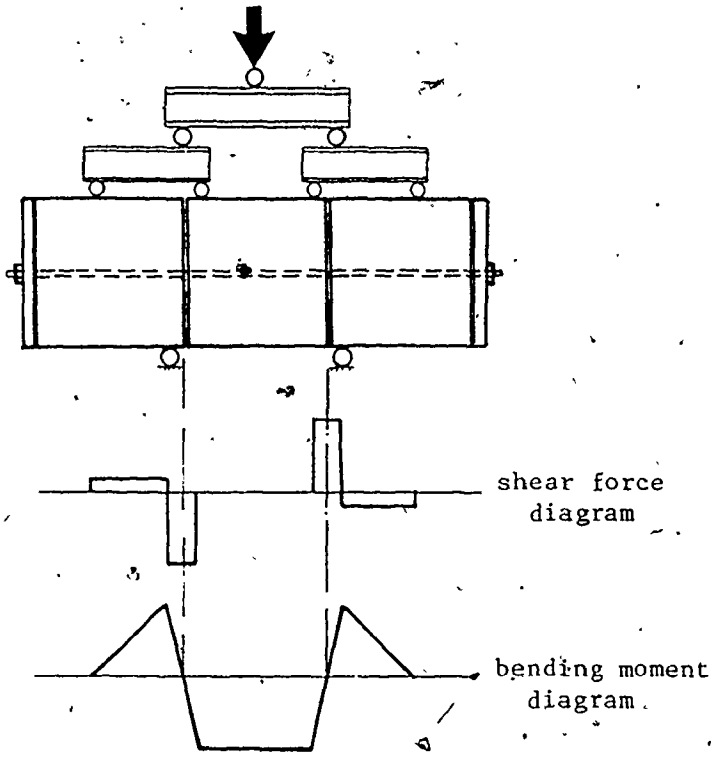

Fig. 5.5 SHEAR TEST SET-UP ADOPTED BY BALACHANDRAN (2)

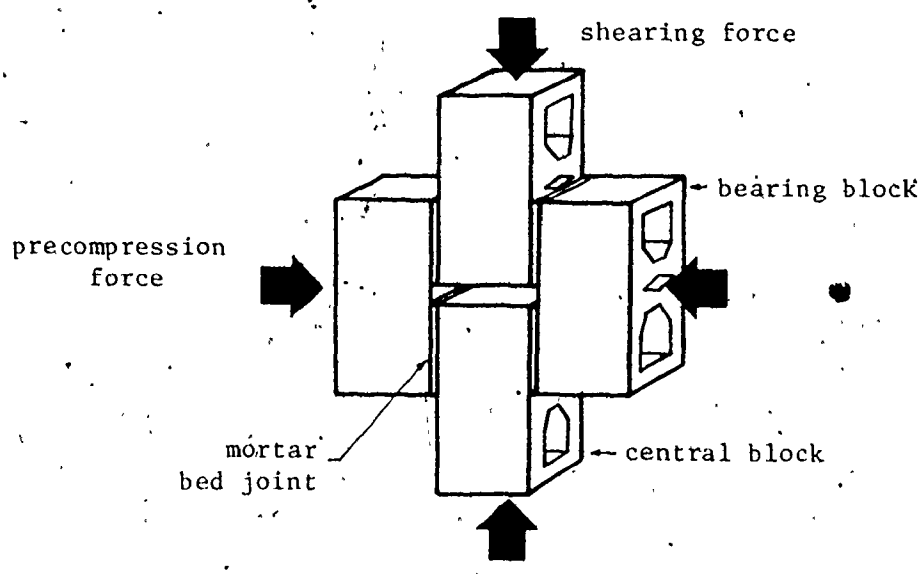

Fig. 5.6 THE SHEAR TEST SPECIMEN USED IN THE CURRENT PROGRAM

concept of plane sections remaining plane is not valid and a complex stress pattern would be developed for this specimen (deep beam action). This leads to combined shear and flexural stresses being developed along the joints. The specimen would also be affected by stress concentrations near the joints since the supports and the two point loading were close to the mortar joints. In addition, the system seems to be very sensitive to any slight variation in the position of the applied loads which could be expected for this type of multiple load mechanism (flexural stresses of about 15% of the average shear stresses could be developed for a shift of the support by about 1/8 of an inch). The test technique was designed to provide zero bending moment at the centre of the joint. However, at the interfaces where the joint failure is expected, flexural stresses of about 15% of the average shear stresses would be developed.

For the current experimental program, the four unit assemblage shown in Fig. 5.6 was adopted for the shear tests. This specimen has the following advantages over those mentioned above:

1 - The flexural stresses at the joints are eliminated (the load is transferred by shear through these joints).

2 - The test is relatively easy to set up and simple to perform.

3 - No stress concentration occur because the load is applied uniformly over an area far from the joints.

4 - The shear deformation of the joint can be easily measured.

It has been reported[2] that Meli and Reyes adopted similar specimen for testing mortar joints under shear and precompression loading. Rostampour[46] also used similar assemblages to evaluate the shear bond strength of solid brick masonry.

A total of 52 specimens were constructed using kerfed blocks (see type B-block, Fig. 2.1) which provided two continuous cores for grouting and created the intermediate gap between the central blocks, as shown in Fig. 5.6. The joints were tooled on both sides of the specimen. Temporary supports were provided for the two central blocks, as shown in Fig. 5.7, and these were moved upon completing construction of the specimen. After 24 hours, for 32 of the 52 specimens, grout mixes GW, GM_1, or GS having the properties described in Chapter 2, were poured into the cores and puddled with a steel rod.

As was the case for previously described tests, control specimens were made along with the masonry assemblages and were air cured in the laboratory under the same conditions as the shear specimens. The adopted control specimens were similar to those used for the masonry discs and were presented in Section 4.2.2.

5.2.2 Testing Procedure

At the age of 28-42 days, the ends of the central blocks were capped using gypsum-cement compound. The specimens were

Fig. 5.7 CONSTRUCTION OF SHEAR ASSEMBLAGES

(REINFORCED SPECIMENS)

tested under shear (with no precompression) using a hydraulic testing machine. Each specimen was carefully aligned in the testing machine by centering the bearing plates with the vertical axis of the machine head. Slip at the joint was established at different load levels by measuring the relative movement between the central blocks and the side ones using dial gauges mounted at both sides as shown in Fig. 5.8. The load was slowly applied, taking deflection mesurements at each load increment until failure occurred. The control specimens were tested at approximately the average age of the assemblages.

For the precompression case, the compressive load normal to the bed joints was first applied and maintained constant while the shear force was incrementally increased until failure. A sketch of the test set-up for providing precompression along with shear loading is shown in Fig. 5.9. A series of steel plates connected by four 1 inch in diameter rods, together with a 40 kip hand operated hydraulic jack were used to apply precompression loading. This load was measured using a commerical load cell located at the centre of the bearing block. Two 1 1/2 inch thick bearing plates were used to provide a uniform distribution of the precompression load over the contact areas of the bearing blocks. After failure of the joint, the precompression level was increased by 100 psi and the vertical load was incrementally increased to the maximum attainable capacity. This loading pattern was repeated so that the friction resistance and the proportionality constant μ (in

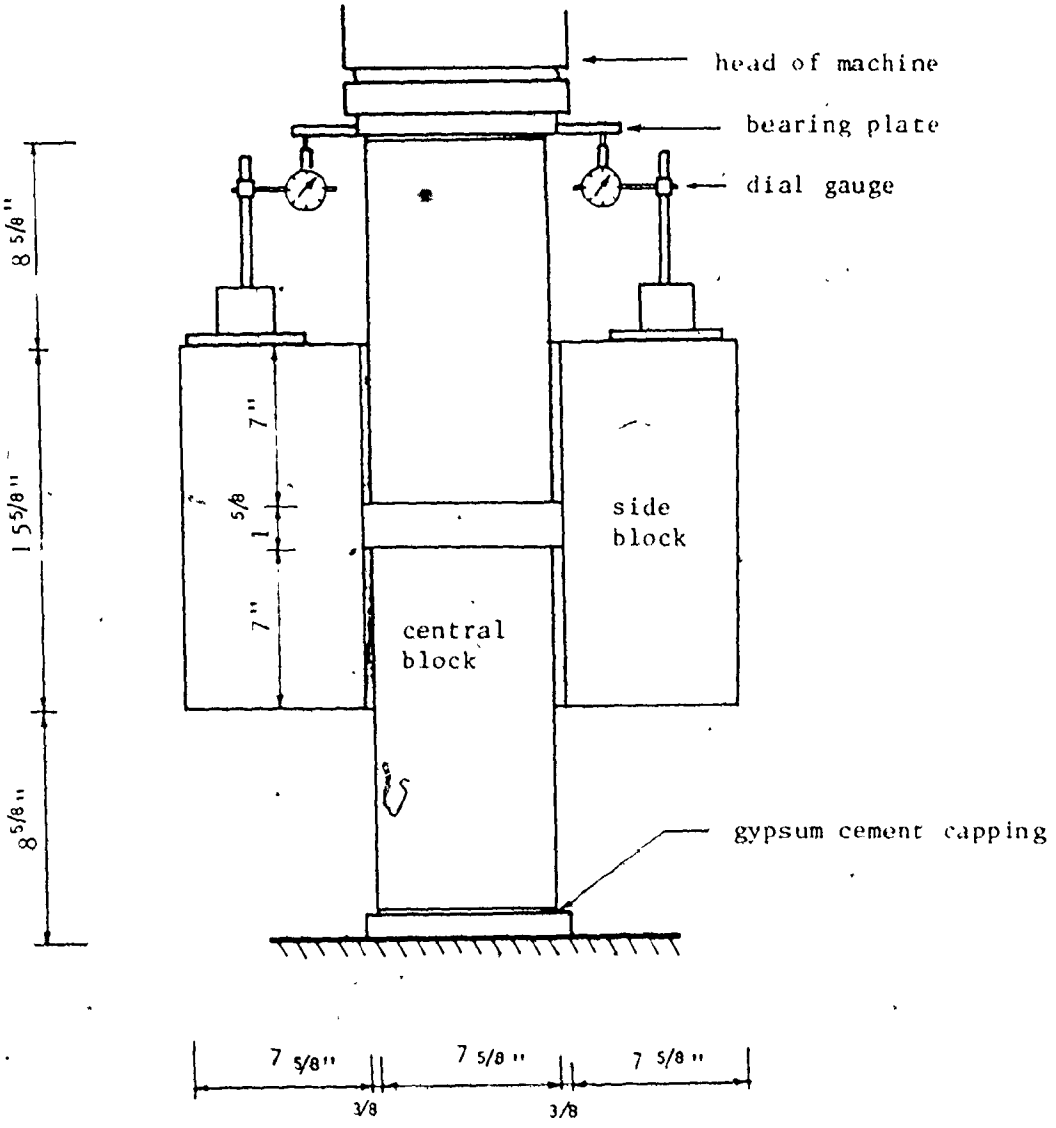

Fig. 5.8 TEST SET-UP FOR SHEAR WITH NO PRECOMPRESSION

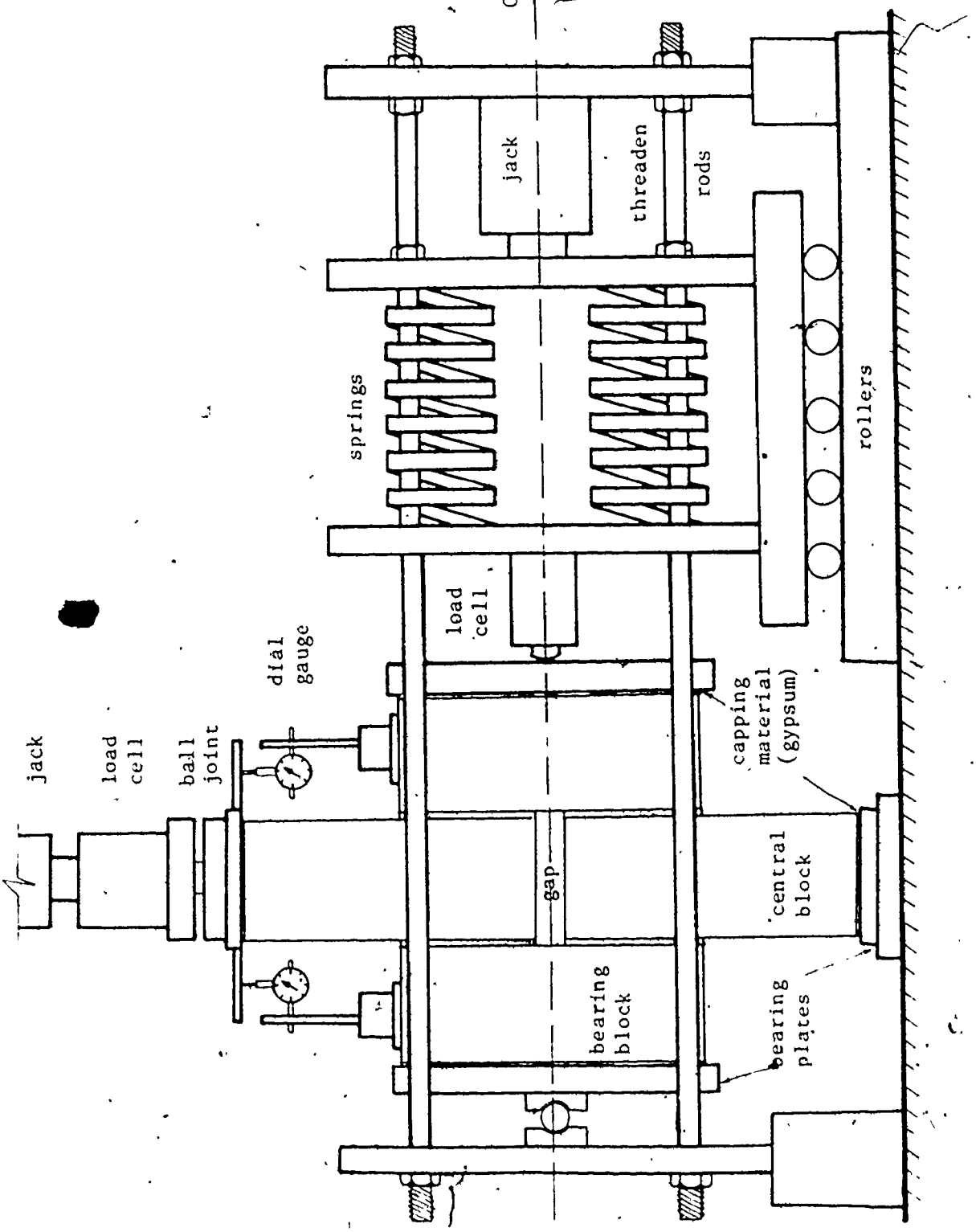

Fig. 5.9 SKETCH OF THE SET-UP FOR THE SHEAR TEST WITH PRECOMPRESSION LOADING

Equation (5.1)) could be evaluated.

For the specimens grouted with strong grout, GS, the extreme cores of the central blocks were filled with a gypsum-cement compound for the tests under high precompression (200 psi). This guarded against the possibility of a compression failure of the central blocks before the full capacity of the joints was achieved.

This experimental program was comprised of five groups of assemblages, each concerned with one parameter at a time, while the other parameters were kept constant. These groups are:

Group S1 was designed to study the effect of the type of mortar on the shear bond strength of ungrouted masonry joints without precompression stresses. Types S_1, and N mortars were chosen. Their properties were presented in Section 2.2.2. Four test repetitions for each type of mortar were adopted to facilitate a statistical analysis of the results.

Group S2 was used to study the effect of grout strength on the shear capacity of joints under zero precompression. Three different grout mixes were used; weak grout, GW; medium grout, GM_1, and strong grout, GS. (For the properties of the mixes, see Section 2.2.3.) Only type S_1 mortar was used for all of these specimens and four test repetitions for each grout type were arranged.

Group S3 studied the effect of grouting the cores on the joint strength. In order to eliminate the effect of the mortar,

the specimens were built without mortar joints. Sheets of polyethylene were placed between the blocks to eliminate the friction resistance at the interface. The blocks were temporarily held together by a small precompression force until the grout had hardened. The two types of grout mixes adopted were; weak grout, GW, and strong grout, GS.

Group S4 investigated the effect of providing bed joint reinforcement (Dur-O-Wal steel placed as shown in Fig. 5.7) on the shear bond strength of ungrouted masonry joints under zero precompression. The cross bars of the reinforcement were relocated to fit the contact area of the mortar joints for ~~kerfed~~ blocks. Type S_1 mortar was used.

Group S5 was initiated to study the effect of the compressive stresses normal to the bed joint (precompression) on the joint capacity of ungrouted and grouted masonry assemblages. The 2 levels of precompression considered were 100 psi and 200 psi based on the net contact area for the ungrouted specimens and the gross area for the grouted ones. For the grouted assemblages, both weak grout, GW, and strong grout, GS, were used.

5.2.3 Discussion of Test Results

5.2.3.1 Modes of Failure: The mode of failure was consistently a shear failure of the joints. The failure was initiated by a debonding at the block and mortar interfaces for the ungrouted masonry assemblages. In the case of grouted masonry, failure

occurred instantaneously with the formation of the visible crack at the mortar and block interfaces. The failure surface of the grout had the typical conical shape associated with diagonal tension failure conditions. It was interesting to observe that even for precompression loading, in most cases, only two joints failed. For cases of zero precompression, the grouted specimens having no mortar joints failed in a staggered manner, whereas for specimens with mortar joints, the failed joints were mostly in one plane which was at the interface between the mortar and the uppermost block layed during fabrication. Figures 5.10 and 5.11 show the failure mode in the two cases. This observation indicates the sensitivity of the mortar's bond, at early stages, to any pressure normal to the bed joint even if it is the result of only the self weight of the upper courses. Under precompression, this preferential failure pattern did not exist for either ungrouted or grouted specimens. In the second cycle of loading after increasing the precompression stress following initial failure, one or two other joints usually failed also. A typical mode of failure under precompression loading is shown in Fig. 5.12(b).

For the grouted specimens under zero precompression, it was always observed that the failure plane was the one containing the minimum area of grout or conversely having the higher net to gross area ratio. This aspect occurs because the thickness of the outer shells and the middle web of the block increase at its top in a

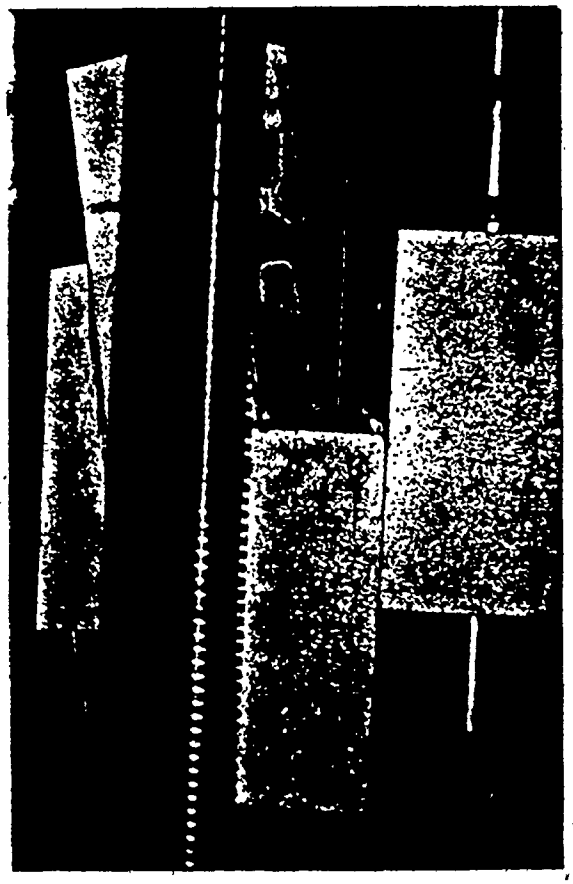

Fig. 5.10 GROUTED SPECIMENS WITHOUT MORTAR JOINTS TESTED UNDER SHEAR WITH NO PRECOMPRESSION

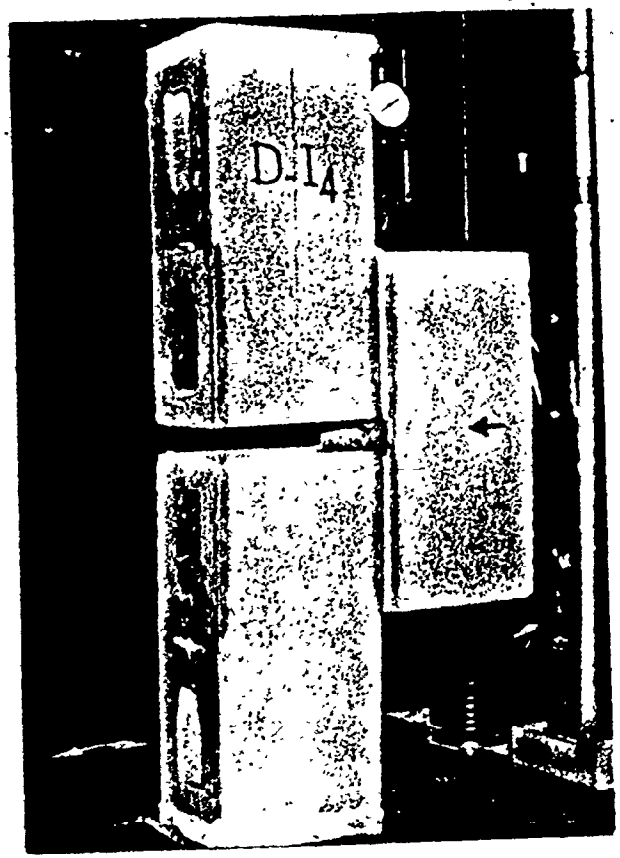

(a) Weak Grout, GW

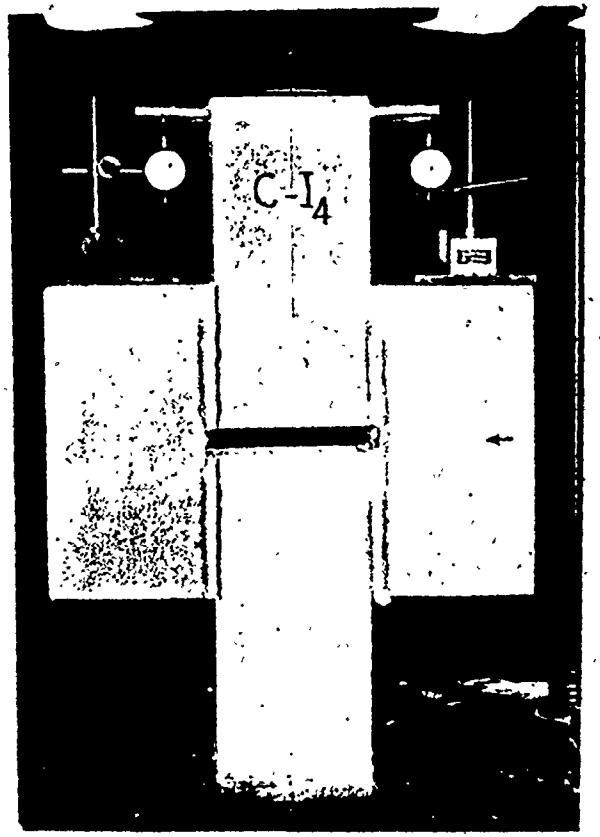

(b) Strong Grout, GS

Fig. 5.11 TYPICAL FAILURES OF GROUTED SPECIMENS UNDER SHEAR WITH NO PRECOMPRESSION

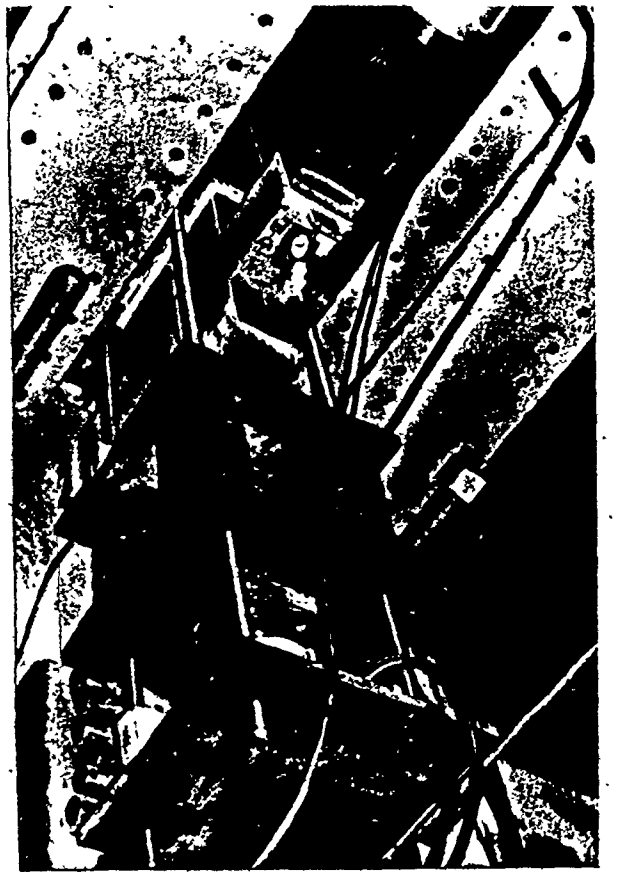

(a) During Testing

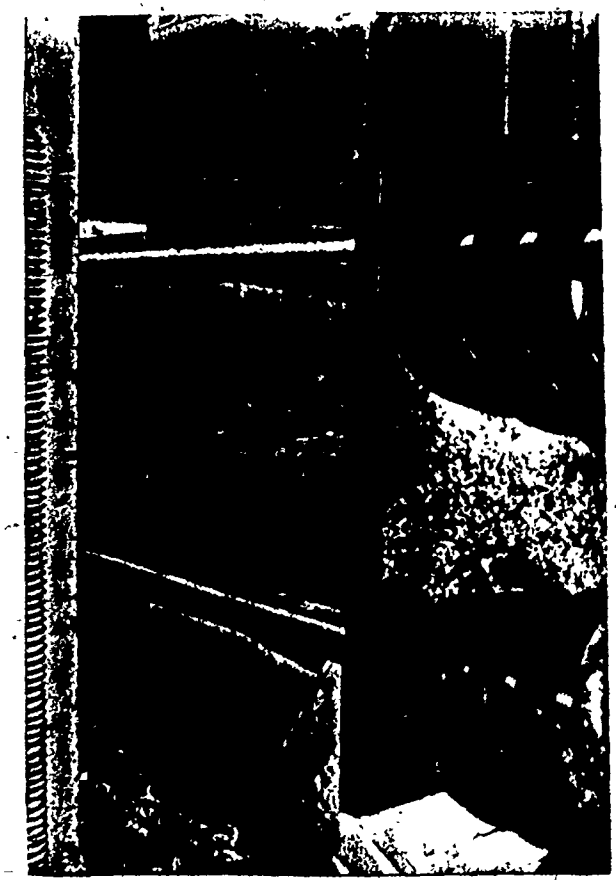

(b) After Failure

Fig. 5.12 GROUTED SPECIMEN TESTED UNDER SHEAR AND PRECOMPRESSION

flared shape as shown in Fig. 2.2. This may be attributed to the fact that the grout shear strength (governed by its diagonal tension capacity) is much higher than the mortar shear bond strength and consequently, the grout's capacity, which is a function of the core area, will be the dominant factor in the shear capacity of the joint. This feature of behaviour indicates that blocks with flared shapes would not be preferred from the strength viewpoint, because they reduce the core areas and consequently the shear capacity of the joints. Fig. 5.11 shows that the failure occurred at the weakest plane, having the minimum grout area.

5.2.4.2 Effect of Mortar Type: The average shear stress at failure, τ_a, is calculated as:

$$\tau_a = \frac{P}{2A} \qquad (5.2)$$

where P is the applied vertical load and A is the area of contact between two blocks. (It is the net area for ungrouted specimens and the gross area for grouted specimens.) The test results for ungrouted specimens (Group S1) listed in Table 5.1 indicate that the shear bond strength of the masonry joints was not proportional to the compressive strength of the mortar cubes. A decrease of the compressive stength of the mortar by 70% reduced the shear capacity of the joint by only 24%. This behaviour supports the contention that the mortar bonding value is not simply a function of its compressive strength[7] and hence it is unlikely that any

TABLE 5.1
SHEAR TEST RESULTS FOR UNGROUTED SPECIMENS
WITHOUT PRECOMPRESSION
(Group S1)

Mortar type	Mortar cube strength (psi)	Assemblage Shear Strength		
		Individual (psi)	Mean (psi)	C.O.V. (%)
S_1	3110	70 70 57 61	70	21.0
N	820	59 54 43 58	53	14.3

Note: 1 psi = 6.9×10^{-3} MN/m^2

TABLE 5.2
SHEAR TEST RESULTS FOR GROUTED SPECIMENS
WITHOUT PRECOMPRESSION
(Group S2)

grout type	Mortar cube strength (psi)	Grout Strength		Assemblage shear strength		
		comp.[a] (psi)	tension[b] (psi)	Individual (psi)	Mean (psi)	C.O.V. (%)
GW	3110	2080	220	98 110 99 108	106	9.4
GM_1	3110	3350	300	122 108 108 102	110	7.8
GS	3110	5350	500	147 158 141 166	153	7.4

Note: 1 psi = 6.9×10^{-3} MN/m^2

a. Equivalent cylinder strength of block moulded prisms
b. Splitting tensile strength of grout prism

direct correlation between the two parameters would exist. This is because the shear bond strength is not only a function of the mortar properties, but is also a function of the physical properties of the block such as its surface roughness and initial rate of absorption. Utilizing the experimental results of ungrouted concrete masonry piers tested under lateral loads, Balachandran[2] concluded that within the ranges of mortars considered, the mortar strength did not appreciably affect the shear strength of the piers.

It is worthwhile noting that the above shear bond strength results exhibited a relatively high variability compared to most other parts of this study. The maximum coefficient of variation was 21%. This variation may be quite normal and may be attributable to the multitude of parameters influencing the shear bond strength such as:

1. The block surface condition in terms of its roughness and cleanliness from dust,
2. The initial rate of absorption of the block,
3. The composition of the mortar,
4. The air content of the mortar,
5. The initial flow and flow after suction of the mortar,
6. The curing of the assemblage, and
7. The pressure applied by the mason during the alignment and construction of the assemblage and in general the consistency of good workmanship.

The small number of repetitions may also contribute to the high variability obtained[41]. Most publications report average results without supplying their standard deviations or coefficients of variation. However, a coefficient of variation for shear bond tests exceeding 20% is reported[26].

5.2.3.3 Effect of Grout Strength: The results of the Group S2 tests, concerning the effect of grouting on the shear strength of the joints under zero precompression, are listed in Table 5.2. The test results for ungrouted specimens using type S_1 mortar from Table 5.1 can be used as a reference point when the strengths are converted to being based on gross area. The lowest curve in Fig. 5.13 shows the variation of the average shear strength with the variation of the grout tensile strength as calculated from the splitting test of the block moulded grout prisms (see Section 4.2.2). It is shown that grouting appreciably increased the average shear strength of masonry joints with higher grout strengths resulting in higher shear strengths for the assemblages. An increase of about 100% was achieved by grouting the cores with grout of nearly the same strength as the block.

It is interesting to observe that grouting helped to significantly decrease the variability of the shear test results. The coefficient of variation was reduced from 21% for ungrouted specimens to an average of 8% for grouted specimens. This variability is similar to that expected for ordinary concrete[40] and would tend to confirm that the shear capacity of the grouted

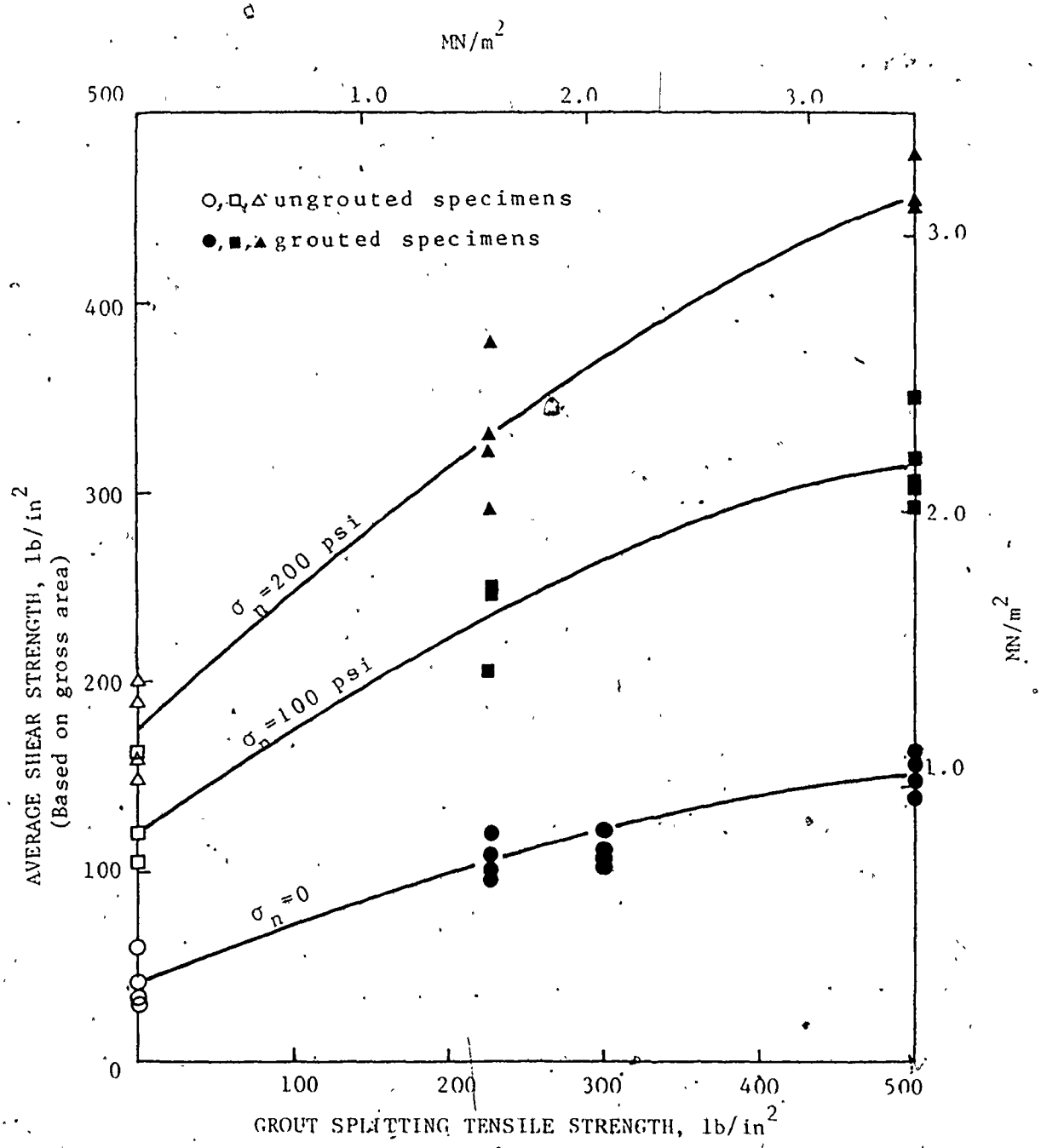

Fig. 5.13 EFFECT OF GROUT STRENGTH ON THE SHEAR CAPACITY OF MASONRY JOINTS

cores is the predominant factor influencing the shear strength of concrete masonry assemblages.

5.2.3.4 Combination of the Individual Strengths of the Mortar and Grout: The shear strengths of grouted assemblages not having mortar joints (Group S3) are listed in Table 5.3. Comparable results for the shear strength of grouted specimens having mortar joints (Group S2) and the shear strengths obtained by adding the shear strength from the ungrouted specimens, having only mortar joints, to those of grouted specimens without mortar joints are presented in Fig. 5.14. In the latter case the average shear strength, τ_{ags}, based on gross area, A_g, was calculated as:

$$\tau_{ags} = \frac{1}{A_g} \left(Q_{au} \frac{A_{nm}}{A_n} + Q_{ag} \right) \qquad (5.3)$$

where Q_{au} and Q_{ag} are the failure loads of ungrouted specimens with mortar joints and grouted specimens without mortar joints, respectively and A_{nm} and A_n are the maximum and minimum net contact areas of the block, respectively. The adjustment of the first term of the above equation concerning the shear capacity of the ungrouted specimens was introduced to account for the shift of the failure plane from that passing through the minimum net area for ungrouted specimens to that passing through the maximum net area for grouted specimens. This is true as long as the grout shear strength is at least equal to the shear bond strength of the mortar (this case is presented by point A in Fig. 5.14). For most

TABLE 5.3

SHEAR TEST RESULTS FOR GROUTED SPECIMENS WITHOUT MORTAR JOINTS AND NOT SUBJECTED TO PRECOMPRESSION LOADING (Group S3)

Grout type	grout strength		Assemblage shear strength[b]		
	comp.[a] (psi)	tension (psi)	Individual (psi)	Mean (psi)	C.O.V. (%)
GW	2100	200	286 228 270	261	11.1
GS	6010	480	314 456 371	380	18.8

Note: 1 psi = 6.9×10^{-3} MN/m^2

a. Equivalent cylinder strength as calculated from block moulded prisms
b. Calculated on the basis of the minimum core area

TABLE 5.4

SHEAR RESULTS FOR REINFORCED UNGROUTED SPECIMENS WITHOUT PRECOMPRESSION (Group S4)

Mortar type	Mortar cube strength (psi)	Assemblage shear strength		
		Individual (psi)	Mean (psi)	C.O.V. (%)
S_1	3110	71 87 89 61	77	17.3

Note: 1 psi = 6.9×10^{-3} MN/m^2

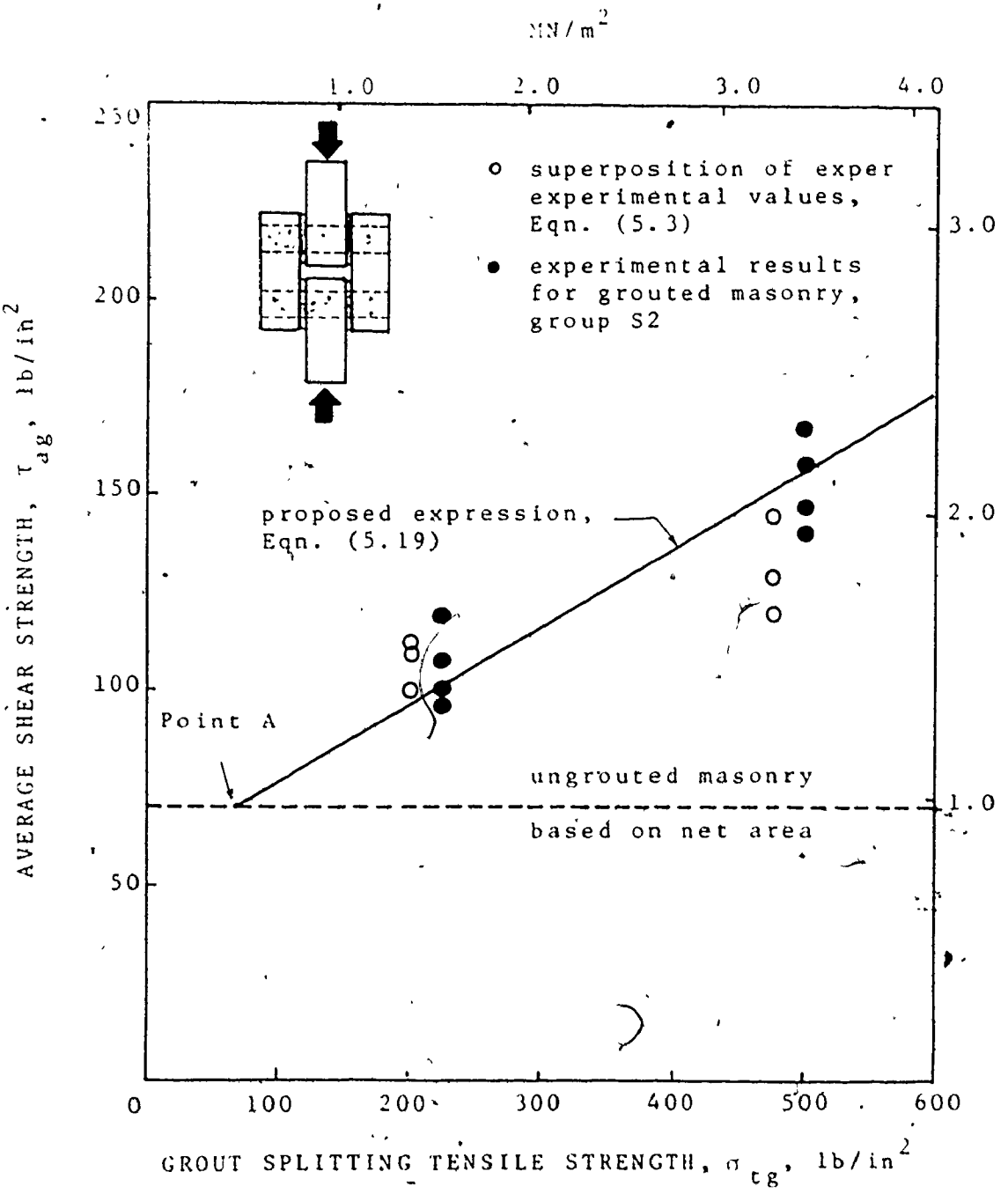

Fig. 5.14 SHEAR CAPACITY AS CALCULATED FROM LINEAR COMBINATION OF THE COMPONENTS' CAPACITIES

practical cases this condition is quite valid. Equation (5.19), which represents a linear combination of the strengths of the component materials to predict the assemblage strength (see Section 5.3.3), is also displayed in the figure. It is shown that a linear combination of the strengths of ungrouted assemblages and the grouted specimens without mortar joints (i.e. strength superpostion) gives reasonably good agreement with the strength of the grouted assemblages.

5.2.3.5 Effect of Joint Reinforcement: Comparison of the shear strength results for the reinforced joints (Group S5) listed in Table 5.4 with those of similar unreinforced joints listed in Table 5.1 indicates that the joint reinforcement did not significantly affect the shear bond strength of the joint. This behaviour supports the previous discussion (Section 5.2.4.2) which suggested that the shear bond strength of the joint is not a function of its strength characteristics, and as long as the mortar contact at the block to mortar interface is not interrupted by the reinforcement, no significant influence on the shear bond strength would be expected. The small increase of the shear capacity of the reinforced joints compared to the unreinforced ones (about 10%) may be attributed to the effects of the natural variability found for ungrouted assemblages.

Jolley[29] reports tests of horizontally reinforced concrete masonry shear walls under racking and precompression loading. The walls failed by joint separation in a stepped

diagonal pattern (horizontal joint sliding and vertical joint separation). His results showed that the presence of the horizontal joint reinforcement did not increase the panel shear strength.

5.2.3.6 Effect of Compressive Stresses Normal to the Bed Joint: The test results for Group S4, concerning the effect of the precompression loading on the shear strength of ungrouted and grouted masonry joints are listed in Table 5.5. Using these results along with the results from Tables 5.1 and 5.2 for the case of zero precompression, the variation of the average shear stresses at failure for various levels of precompression is presented graphically in Fig. 5.15. The results show that the precompression stresses significantly increased the shear capacity of both ungrouted and grouted maasonry joints. A strong correlation between the increased precompression stresses and the increased shear strengths of the joints is shown to exist and the linear relationship, suggested in Equation (5.1), could be used to empirically predict the shear strengths for both ungrouted and grouted concrete masonry joints for low levels of precompression. Using a linear regression analysis, the following empirical expressions were obtained:

For ungrouted masonry,

$$\tau_{au} = 76 + 1.07\ \sigma_n \qquad (5.4)$$

TABLE 5.5

SHEAR TEST RESULTS OF UNGROUTED AND GROUTED SPECIMENS WITH PRECOMPRESSION LOADING (GROUP S5)

Specimen	Mortar Cube Strength (psi)	Grout Strength		Shear Strength σ_n = 100 psi			Shear Strength σ_n = 200 psi		
		Comp.[a] (psi)	Tension[b] (psi)	Individual (psi)	Mean (psi)	C.O.V. (%)	Individual (psi)	Mean (psi)	C.O.V. (%)
ungrouted S_1-mortar	3110			240 172 172 195	195	16.5	323 260 247 307	284	12.9
grouted G_W	3110	2080	220	250 209 250	237	10.0 10.0	292 330 384 322	332	11.6
grouted G_S	3110	5350	500	305 319 293 349	316	7.7	479 452 450	461	3.5

Note: 1 psi = 6.9×10^{-3} MN/m^2

a Equivalent cylinder strength as calculated from the block-moulded prisms, see Chapter 3
b Obtained from the splitting tension test of block-moulded prisms.

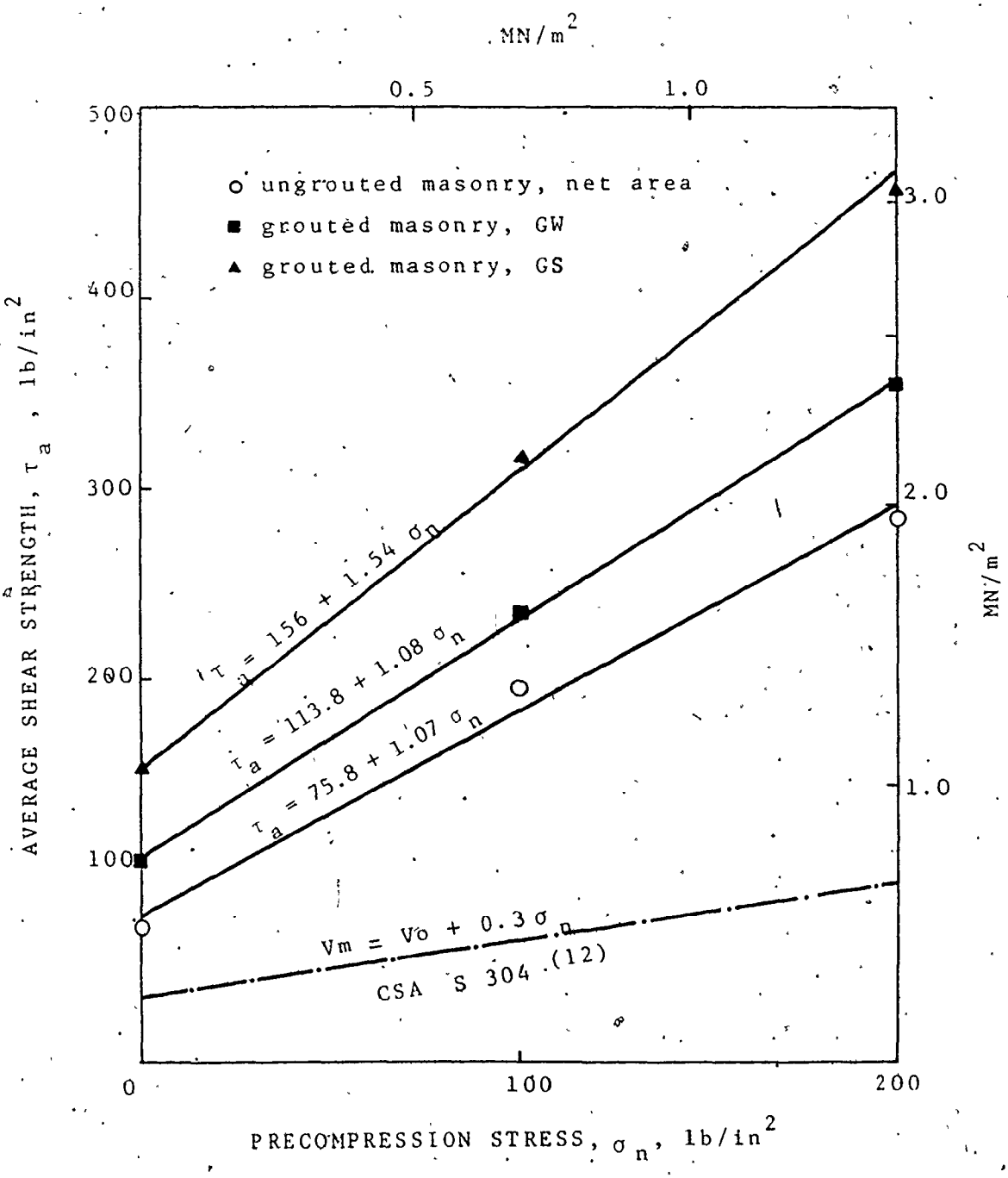

Fig. 5.15 EFFECT OF PRECOMPRESSION ON THE SHEAR STRENGTH OF MASONRY JOINTS

For masonry with weak grout, σ_{tg} = 223 psi,

$$\tau_{ag} = 114 + 1.08\,\sigma_n \qquad (5.5)$$

For masonry with strong grout, σ_{tg} = 500 psi,

$$\tau_{ag} = 156 + 1.54\,\sigma_n \qquad (5.6)$$

where τ_{au} and τ_{ag} are the average shear stresses (psi) at failure for ungrouted (based on net area) and grouted masonry (based on gross area), respectively and σ_n is the precompression stress (psi) calculated on a similar basis for the shear stresses.

It has been reported[29,46,47,49] that the increase of the shear resistance of masonry joints to debonding failure with the increase of the compressive stresses normal to them is attributed to the increase of the friction resistance which is considered to be proportional to the stress level (Coulomb's theory of internal friction). For grouted masonry, in addition to the increase of the resistance of the mortar to debonding, the capacity of the grouted cores would also increase with the increase of the precompression stress, as the shearing stress required to produce a shear failure of the core should be higher under the shear-compression state of stress. [This is only true up to a certain level of precompression, after which compression failure would control and the increase of the compression stress would lead to a decrease in the shear resistance (see Section 6.2.2.3)].

The relative contribution of grouting towards increasing the shear strength, considering the shear strength of ungrouted

masonry as a reference, is plotted versus the level of precompression in Fig. 5.16. It is interesting to observe that the relative contribution of grouting, measured by the shear strength of grouted specimens over that of ungrouted specimens, decreased appreciably with the increase of the precompression stress. It would appear that the resistance of the mortar at the interfaces to debonding shear failure is much more influenced by the precompression stresses than the shear strength of the grouted cores under a compression-tension state of stress.

The load which could be sustained dropped for ungrouted specimens after debonding had occurred. Subsequently, the precompression stress was increased by 100 psi and then the shearing forces increased until the maximum load was reached. The precompression stress was then increased by 100 psi and the loading process repeated. The test results for ungrouted specimens for this post-failure loading are listed in Table 5.6 and similar results for grouted assemblages are listed in Table 5.7. The shear capacity of the failed joints, τ_{af}, subjected to precompression loading could be attributed to the frictional resistance which may be considered proportional to the precompression stress, σ_n. It can be formulated as:

$$\tau_{af} = \mu \sigma_n \qquad (5.7)$$

where μ is the proportionality constant (coefficient of friction) which could be determined for different levels of precompression

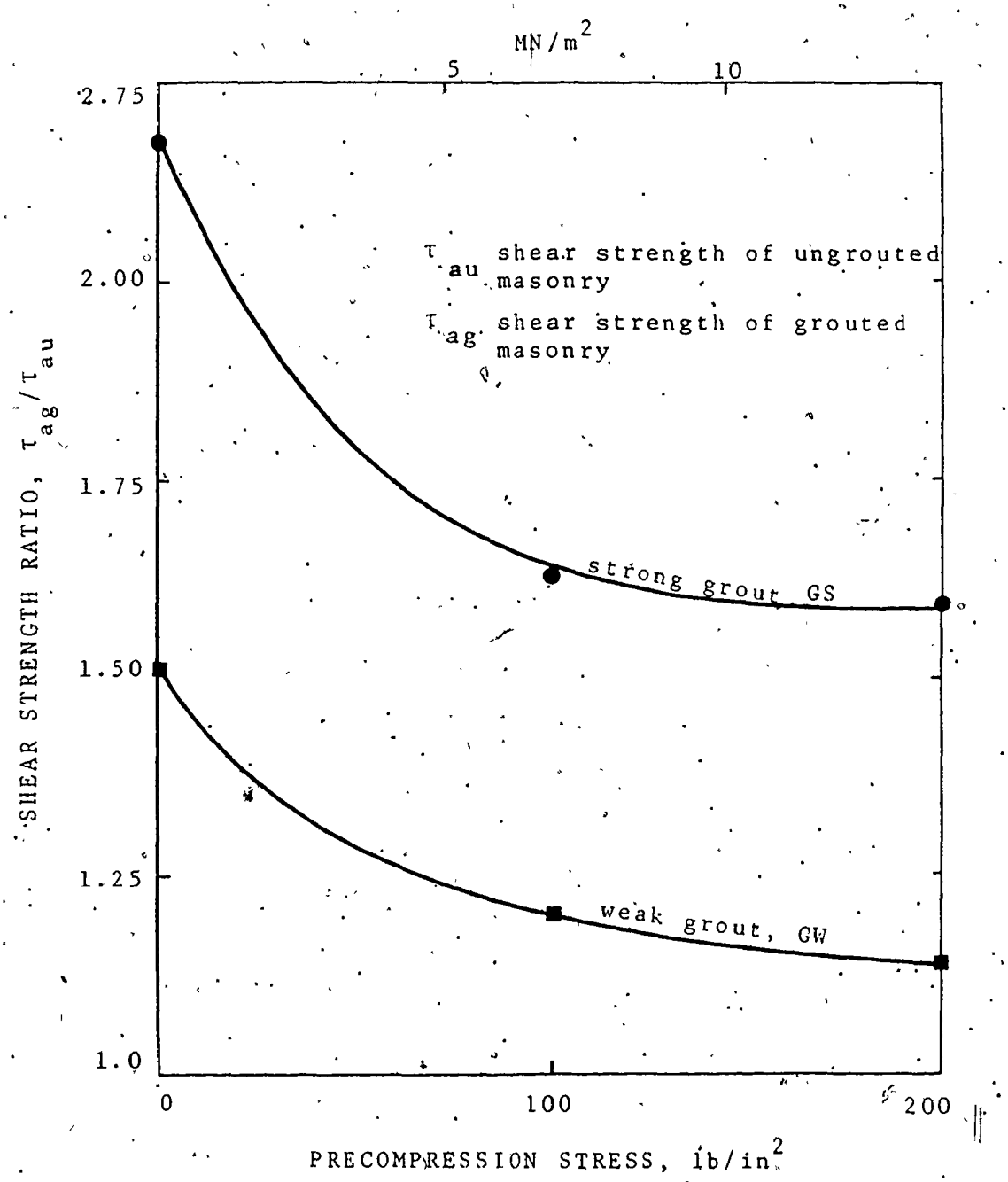

Fig. 5.16 EFFECT OF PRECOMPRESSION ON THE CONTRIBUTION OF GROUTING TOWARDS INCREASING THE SHEAR STRENGTH

TABLE 5.6

COEFFICIENT OF FRICTION FROM SHEAR TESTS OF FAILED JOINTS OF UNGROUTED SPECIMENS UNDER INCREASED LEVELS OF PRECOMPRESSION

Case	Precompression = 200 psi				Precompression = 300 psi				Precompression = 400 psi			
	Joint Shear Strength				Joint Shear Strength				Joint Shear Strength			
	Individual (psi)	Mean (psi)	C.O.V. (%)	μ	Individual (psi)	Mean (psi)	C.O.V. (%)	μ	Individual (psi)	Mean (psi)	C.O.V. (%)	μ
(1)[a]	263 253 226	247	8.0 8.0	1.24	273 297 277	282	5.0	0.94	320 374	347		0.93
(2)[b]					255 247 256	253	2.0	0.84	316 294 362	324	11.0	0.81

Note: 1 psi = 6.9×10^{-3} MN/m^2

a. Initial precompression = 100 psi

b. Initial precompression = 200 psi

TABLE 5.7

COEFFICIENT OF FRICTION FOR FAILED JOINTS OF GROUTED SPECIMENS

UNDER INCREASED LEVELS OF PRECOMPRESSION

Grout Type	Case	Precompression Stress = 200 spi				Precompression Stress = 300 psi			
		Joint Shear Strength				Joint Shear Strength			
		Individual (psi)	Mean (psi)	C.O.V. (%)	μ	Individual (psi)	Mean (psi)	C.O.V. (%)	μ
GW	(1)[a]	247 247 205	233	10.0	1.17	319 281	300	-	1.00
	(2)[b]					374 406 399 361	385	5.5	1.28
GS	(1)[a]	299 357 311 302	317	9.0 9.0	1.59 1.59	367 433 386 353	385	9.0	1.28
	(2)[b]					384 489 439	537	12.0	1.36

Note: 1 psi = 6.9×10^{-3} MN/m^2

a. Initial precompression = 100 psi
b. Initial precompression = 200 psi

as shown in Tables 5.6 and 5.7. The results show that the coefficient of friction decreased with the increase of the precompression stress. The grouted specimens yielded coefficients of friction considerably higher than those for ungrouted specimens especially for stronger grout. This may be attributed to the coarse aggregate in the grout mixes. Also, the mechanical interlocking of the failed cores may contribute in increasing the shear resistance of the joint.

5.2.3.7 Significance of Joint Strength Characteristics: The results concerning the effects of the mortar type, presented in Table 5.1, and the joint reinforcement, presented in Table 5.4, indicate that the strength characteristics of the joint did not appreciably influence its shear bond strength. This observation raises questions concerning the suggestion[53] that the shear failure of masonry joints is attributed to the tensile failure of the mortar layer rather than to the breakdown of the combined shear and friction resistance.

5.2.3.8 Deformation Characteristics of the Assemblages: The average stress-slip relationships of ungrouted and grouted specimens under shear without precompression are plotted in Fig. 5.17. Slip was calculated as the relative vertical movement between the side blocks and the central blocks. It is shown that grouted masonry exhibited higher deformation capability compared to ungrouted masonry at the same average stress levels. In addition, grouted specimens seemed to have a more gradual failure

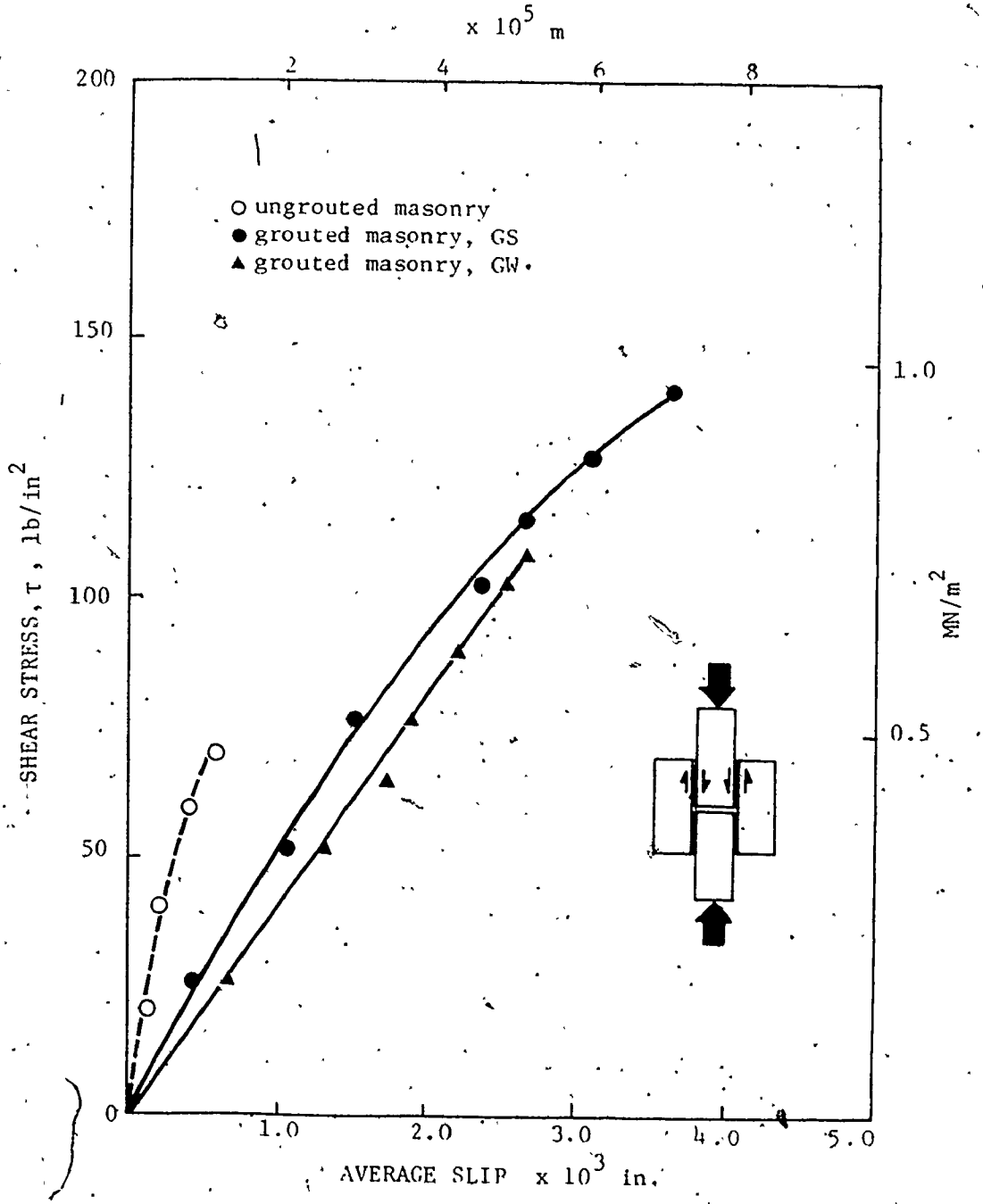

Fig. 5.17. SHEAR STRESS SLIP RELATIONSHIPS FOR CONCRETE MASONRY JOINTS

compared to ungrouted masonry which was very brittle (it is a characteristic of a debonding type of failure). The grouted cores afforded some mechanical interlocking which tended to hold the specimen together. Fig. 5.18 shows the effect of precompression loading on the deformation characteristics of ungrouted masonry joints. It indicates that the precompression stress significantly increased the deformation of the assemblage necessary to produce a joint shear failure which, in turn, gives the tendency for a less brittle nature of behaviour of masonry assemblage. It is interesting to also observe that precompression stress led to an increase of the joint stiffness under shearing loads, and if the joint failure is the governing mode, then the joint stiffness will be representative of the assemblage stiffness. (This aspect will be discussed in more detail in Section 6.2.2.3.)

5.3 Analytical Formulation of the Shear Strength of Masonry Joints

5.3.1 Introduction

The experimental results showed that, for a specified block geometry, the grout strength and the level of precompression are the most significant parameters influencing the shear strength of masonry joints. However, for different blocks having different strength and geometric characteristics other parameters related to those characteristics should be introduced. In the remainder of this section, an attempt was made to analytically express the

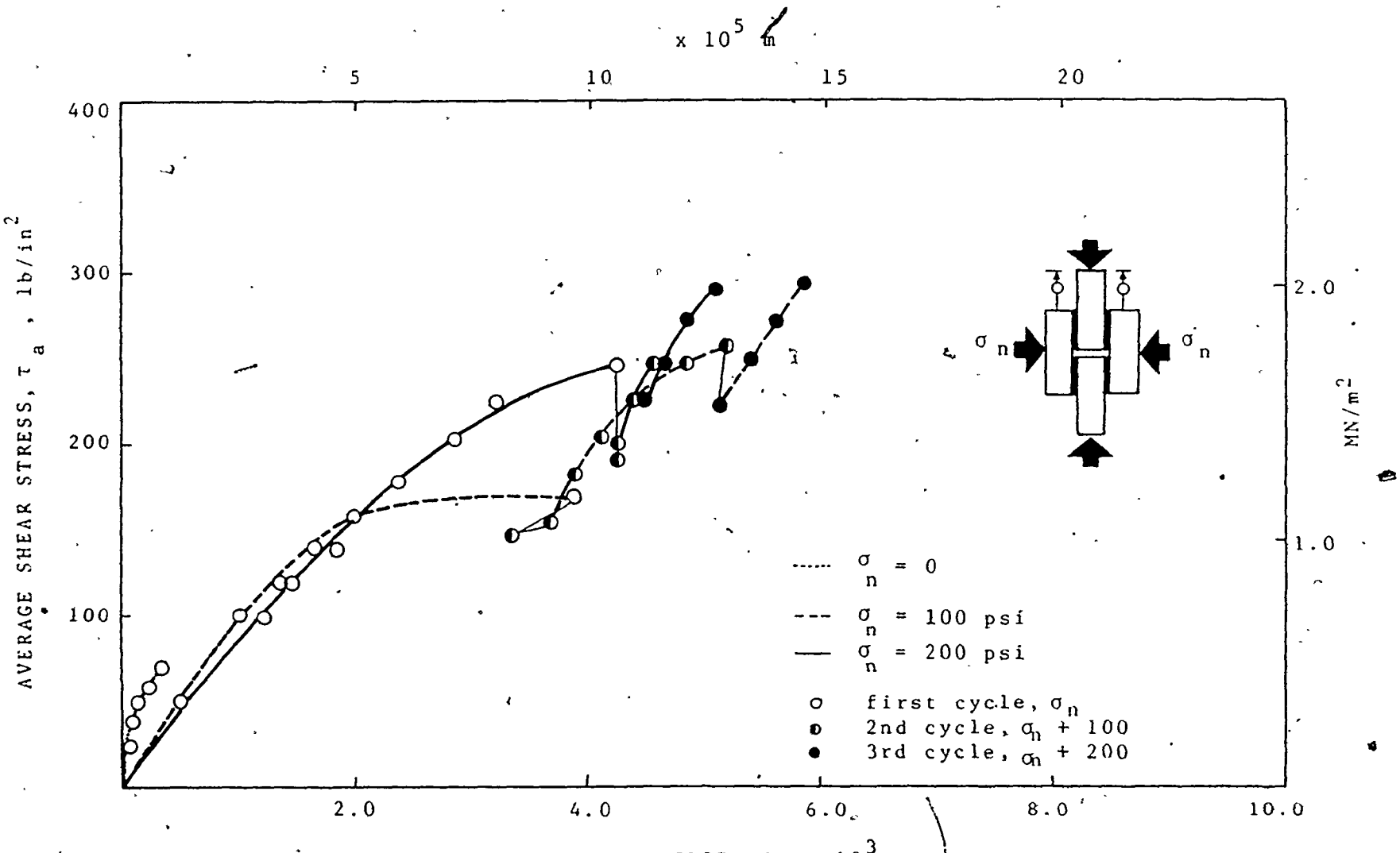

Fig. 5.18 SHEAR STRESS-SLIP RELATIONSHIPS FOR UNGROUTED SPECIMENS UNDER PRECOMPRESSION LOADING

average shear strength of the masonry joints in the assemblage in terms of the strength and geometric characteristics of the block, mortar, and grout.

5.3.2 Assumptions

The following assumptions were made:

1 - The shear bond strength relationship of the mortar joint under shear and normal stresses can be empirically described by Coulomb's theory of friction (Equation (5.1)). The experimental results of the current program concerning the shear strength of ungrouted masonry and those from other investigators[19,29,43,46] as well showed that a linear relationship in the form expressed by Equation (5.1) could reasonably predict the shear strength of joints for low levels of precompression.

2 - The shear strength is expressed as the average shear stress at failure which implies that the failure load is not sensitive to the stress distribution producing the average stress[58].

3 - The apparent average shear strength of the joint in the assemblage will be described by incorporating the resistance of the mortar and the grout. A linear combination of the strength of the constituent materials was shown to reasonably express the assemblage capacity (see Section 5.2.4.4).

4 - The behaviour of grout under a combined state of stress is similar to that of ordinary concrete. Mohr's theory of failure

for biaxial (compression-tension) stresses is adopted as a simplified form of the octahedral shear stress failure criterion[38]. It provides a lower bound solution which gives a conservative prediction of the strength.

5.3.3 Formulation of the Shear Strength Relationships

The shear strength of the mortar joint, τ_m, under shear and normal stress, σ_n, can be expressed, using Coulomb's theory of friction as:

$$\tau_m = \tau_{mb} + \mu \sigma_n \qquad (5.8)$$

where τ_{mb} is the initial shear bond strength (under zero precompression) and μ is the coefficient of friction.

Due to the external shear and precompression the core will be under combined shear and compression stresses which create a biaxial state of tension and compression principal stresses as shown in Fig. 5.19. Using the octahedral shear stress criterion, and adopting a linear expression to relate the octahedral shear stress, τ_{oct}, with the octahedral normal stress, σ_{oct}, in the form[35]:

$$\tau_{oct} = a - b\,\sigma_{oct} \qquad (5.9)$$

where a and b are the material constants and

$$\tau_{oct} = \frac{1}{3}\sqrt{(\sigma_1-\sigma_2)^2 + (\sigma_2-\sigma_3)^2 + (\sigma_3-\sigma_1)^2} \qquad (5.10)$$

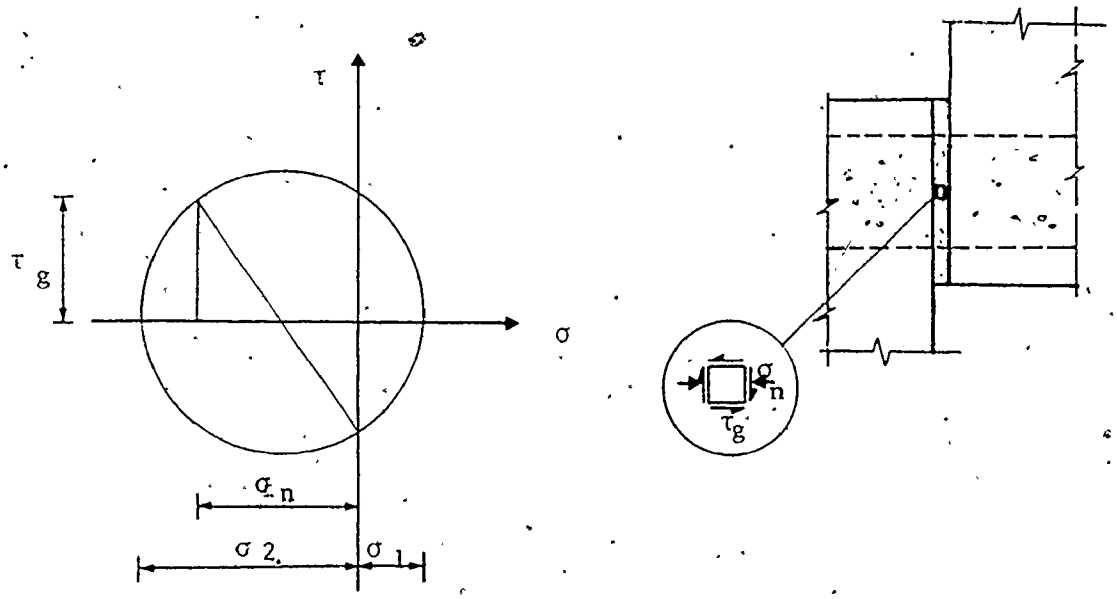

Fig. 5.19 STRESSES ACTING ON AN ELEMENT OF GROUT

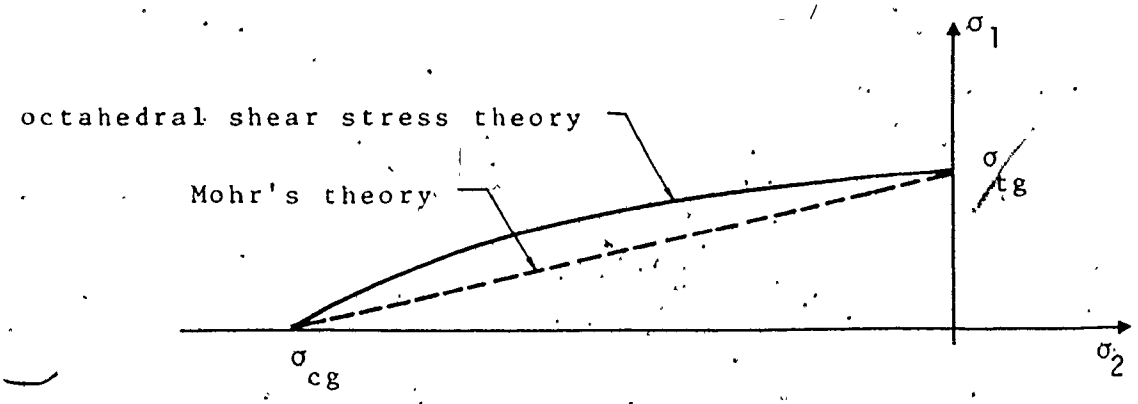

Fig. 5.20 FAILURE ENVELOPES FOR GROUT UNDER A TENSION-COMPRESSION STATE OF STRESS

and

$$\sigma_{oct} = \frac{1}{3}(\sigma_1+\sigma_2+\sigma_3) \tag{5.11}$$

the yielding surface (fracture surface in case of brittle materials) can be expressed, for a biaxial state of stress ($\sigma_3=0$), in the form:

$$\frac{1}{3}(2\sigma_1^2+2\sigma_2^2-2\sigma_1\sigma_2)^{1/2} + \frac{\sqrt{2}}{3}\frac{1-r}{1+r}(\sigma_1+\sigma_2) - \frac{2\sqrt{2}}{3}\frac{r}{1+r}\sigma_{cg} = 0 \tag{5.12}$$

$$(\text{for } \sigma_1 > 0 \text{ or } \sigma_2 > 0)$$

where σ_{cg} is the compressive strength of the grout, and r is the ratio of the tensile strength of the grout to its compressive strength, σ_{tg}/σ_{cg}. Equation (5.12) may be simplified using Mohr's function for biaxial state of stress[35] to be:

$$\frac{1}{2}(\sigma_1-\sigma_2) = \frac{r}{1+r}\sigma_{cg} - \frac{1}{2}\frac{1-r}{1+r}(\sigma_1+\sigma_2) \tag{5.13}$$

Obviously, the two principal stresses, σ_1 and σ_2, can be expressed as a function of the applied shear, τ_g, and the normal stress, σ_n, acting on an element of grout (Fig. 5.19) so that:

$$\sigma_{\substack{1\\2}} = -\frac{\sigma_n}{2} \pm \sqrt{\left(\frac{\sigma_n}{2}\right)^2 + \tau_g^2} \tag{5.14}$$

substituting the σ_1 and σ_2 values from Equation (5.14) into Equation (5.13) yields,

$$\tau_g = \sqrt{\left(\frac{r}{1+r}\sigma_{cg} + \frac{1-r}{2(1+r)}\sigma_n\right)^2 - \left(\frac{\sigma_n}{2}\right)^2} \tag{5.15}$$

Considering that the assemblage capacity could be expressed by a linear combination of the capacities of the mortar and grout components,

Then $$\tau_a A_g = \tau_m \cdot A_n + \tau_g (A - A_n) \quad (5.16)$$

so that $$\tau_a = \tau_m \cdot \eta_h + \tau_g (1-\eta_h) \quad (5.17)$$

Substituting Equations (5.8) and (5.15) into Equation (5.17) yields,

$$\tau_a = (\tau_{mb} + \mu \sigma_n)\, \eta_h + \sqrt{\left(\frac{r}{1+r}\,\sigma_{cg} + \frac{1-r}{2(1+r)}\,\sigma_n\right)^2 + \left(\frac{\sigma_n}{2}\right)^2}\,(1-\eta_h) \quad (5.18)$$

where τ_a is the average shear stress at failure, based on the gross area, and η_h is the ratio of the net to gross area of the block at the critical failure plane. As discussed previously, the critical plane occurs at the minimum core area (maximum η_h).

As shown in Fig. 5.20, it should be noted that adopting the Mohr theory as a failure criterion to express the failure envelope under a biaxial state of tension-compression leads to a conservative solution compared to the octahedral shear stress theory.

5.3.4 Parameters Influencing the Shear Capacity

Equation (5.18) is presented graphically in Fig. 5.21. It illustrates the effect of varying the grout strength, the net to gross area ratio, η_h, and the mortar type on the shear strength of masonry joints under zero precompression. It is apparent that the

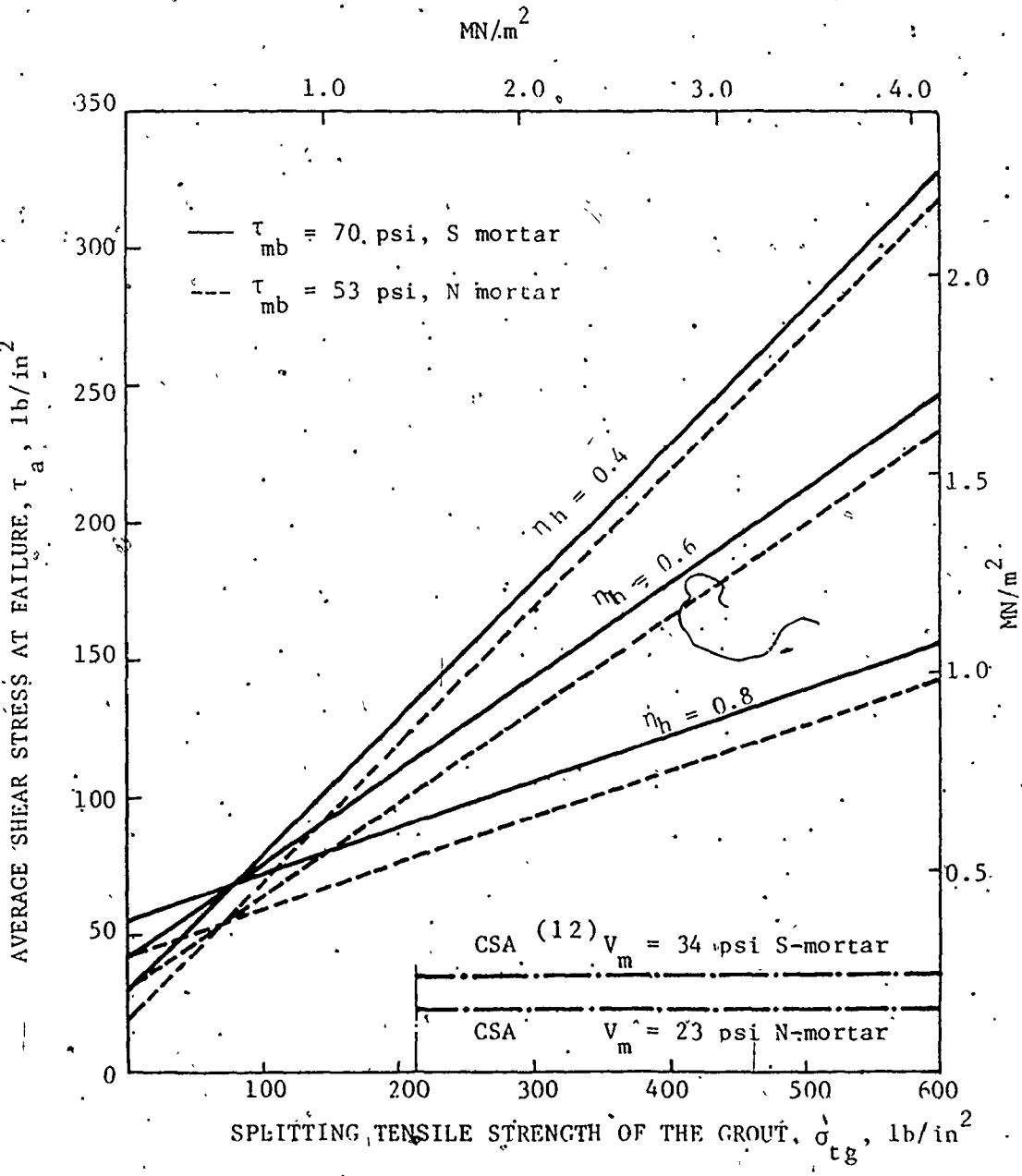

Figure 5.21 SHEAR STRENGTH RELATIONSHIPS FOR VARIOUS GROUT STRENGTHS, MORTAR TYPES, AND NET TO GROSS AREA RATIOS (η_n)

grout strength and the η_h ratio (block geoemtric characteristics) are the most significant parameters whereas the mortar type does not seem to have much effect. Higher grout tensile strengths and lower η_h ratios result in higher shear strengths. This indicates that the tension capacity of the grouted cores, which increases with increased strength of the grout and/or increased core area, is the governing parameter influencing the shear strength of grouted masonry joints.

In Fig. 5.22, Equation (5.18) was used again to graphically illustrate the influence of the precompression stress on the shear strength of the joint. The graph indicates the following two distinct aspects of behaviour:

1 - Ungrouted masonry is influenced more by precompression than is the grouted masonry, especially compared to higher strength grout. It seems that the representative frictional resistance strength component at the block/mortar interface is highly sensitive to the normal stress because it is taken to be directly proportional to it, whereas the grout shear capacity under biaxial stresses is not as significantly affected by these normal stresses.

2 - The net to gross area ratio, η_h, is more significant under low levels of precompression than under high levels, especially for weaker grout. Also, for a particular level of precompression, the influence of the η_h ratio is higher for stronger grout.

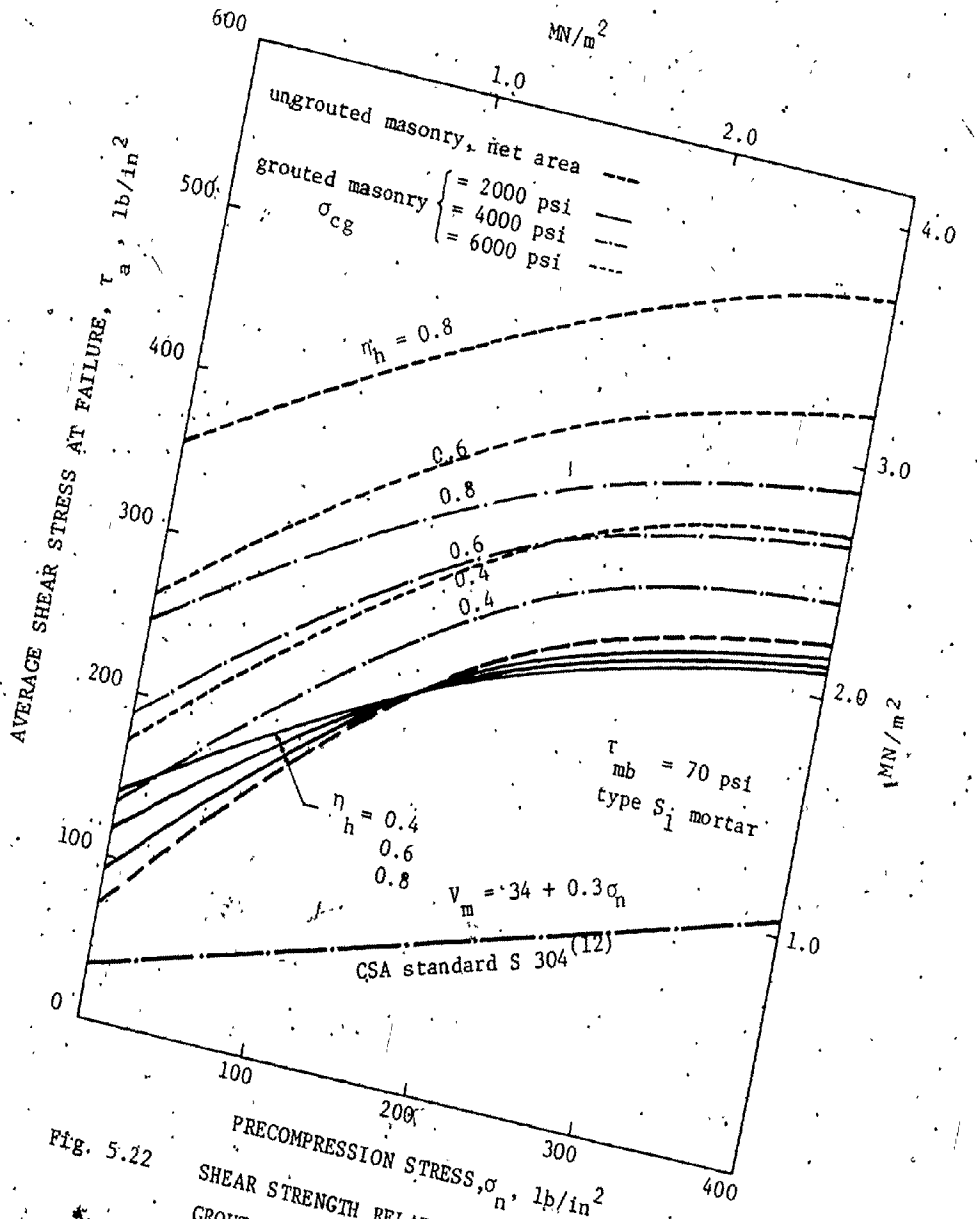

Fig. 5.22 SHEAR STRENGTH RELATIONSHIPS FOR VARIOUS GROUT STRENGTHS AND NET TO GROSS AREA RATIOS UNDER PRECOMPRESSION LOADING

5.3.5 Comparison of the Proposed Expression with the Experimental Results

For comparison, the measured and computed values of the shear strength of grouted assemblages under zero precompression are presented in Fig. 5.23. The analysis using Equation (5.18) gives very good agreement with the experimental results. However, as shown in Figs. 5.24 and 5.25, under precompression loading the agreement does not seem to be quite as good. The shear stresses developed along the joints would be accompanied by compressive stresses - parallel to the bed joint direction (i.e. in the x-direction). These σ_x stresses are simply developed from the equilibrium condition of the external and internal forces in the x-direction. It seems that these σ_x stresses would be significant for cases where high shear stresses are accommodated before failure occurs (case of precompression loading). Apparently, ignoring the σ_x stresses could be a cause of the observed difference between the measured and computed results in the precompression case. No information concerning the effect of the σ_x stresses on the shear capacity of masonry joints has been found in the literature. However, it has been reported[47] that the shear strength of a masonry joint can depend upon not only the normal compressive stresses perpendicular to the joint, but also on the stresses parallel to it. This thought was based on assuming similar behaviour with concrete which has been shown[32] to be influenced by the stresses in the two principal directions.

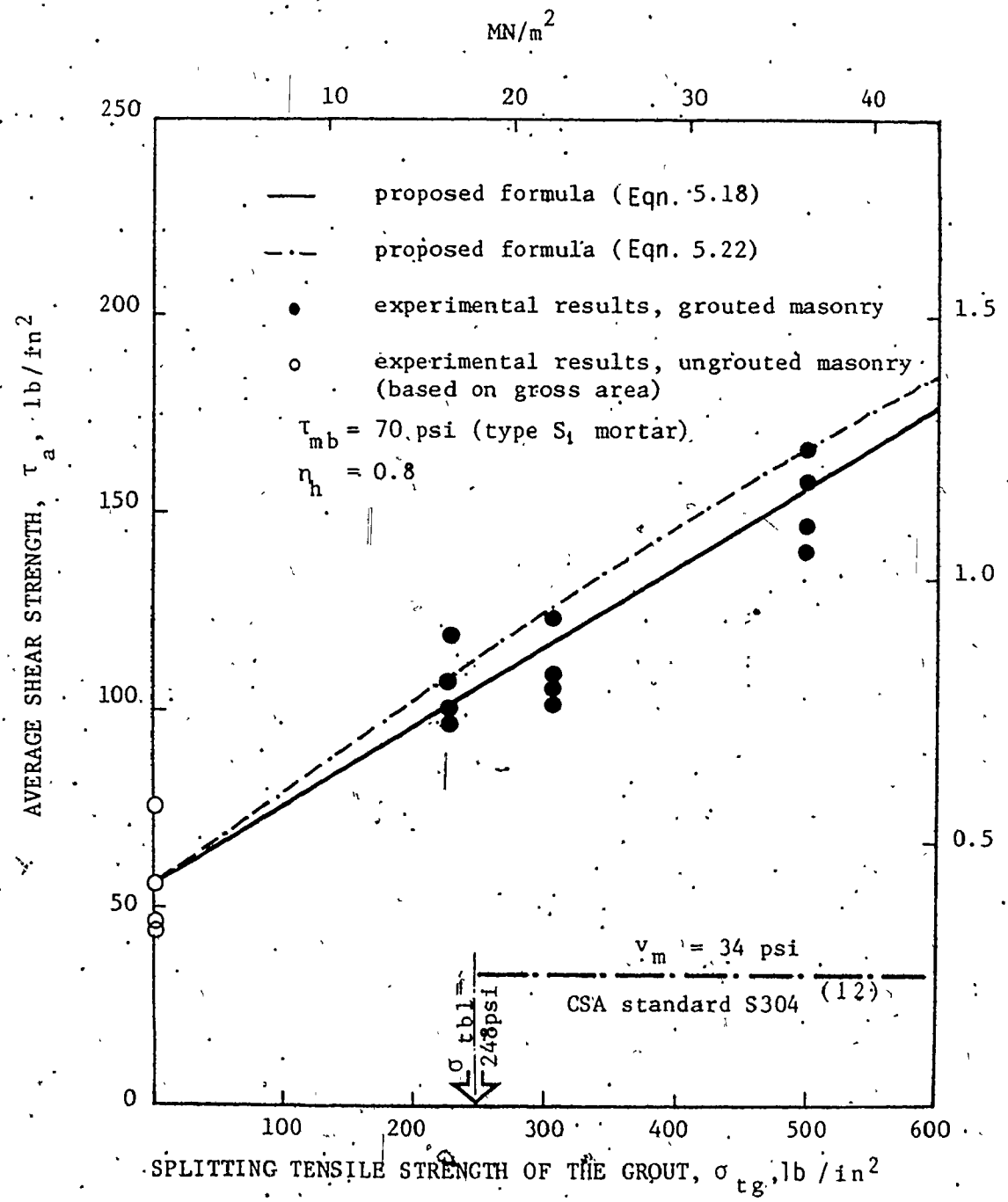

Fig. 5.23 COMPUTED AND MEASURED SHEAR STRENGTHS VERSUS GROUT STRENGTHS WITH NO PRECOMPRESSION

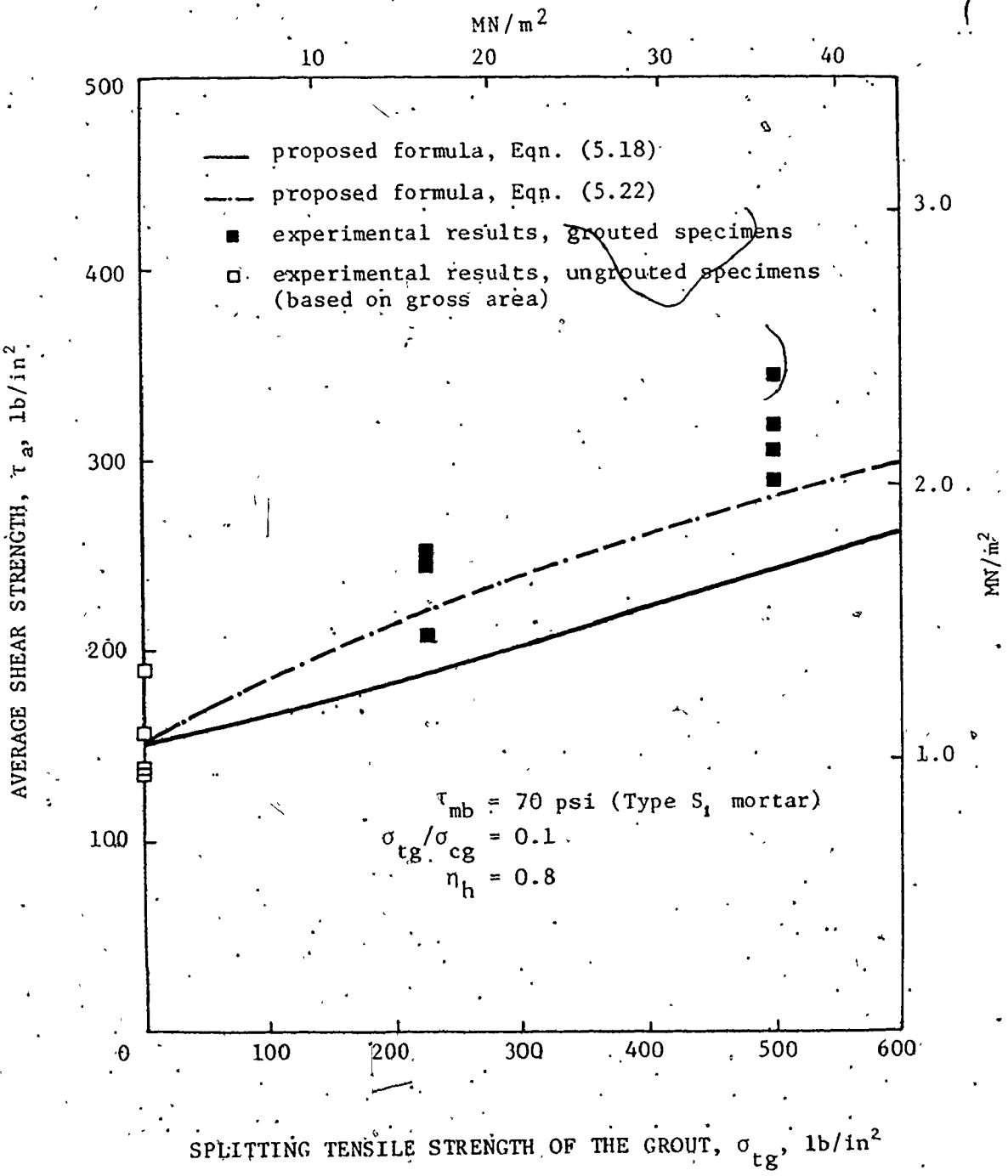

Fig. 5.24 MEASURED AND COMPUTED SHEAR STRENGTHS VERSUS GROUT STRENGTHS FOR ASSEMBLAGES UNDER PRECOMPRESSION STRESSES OF 100 psi

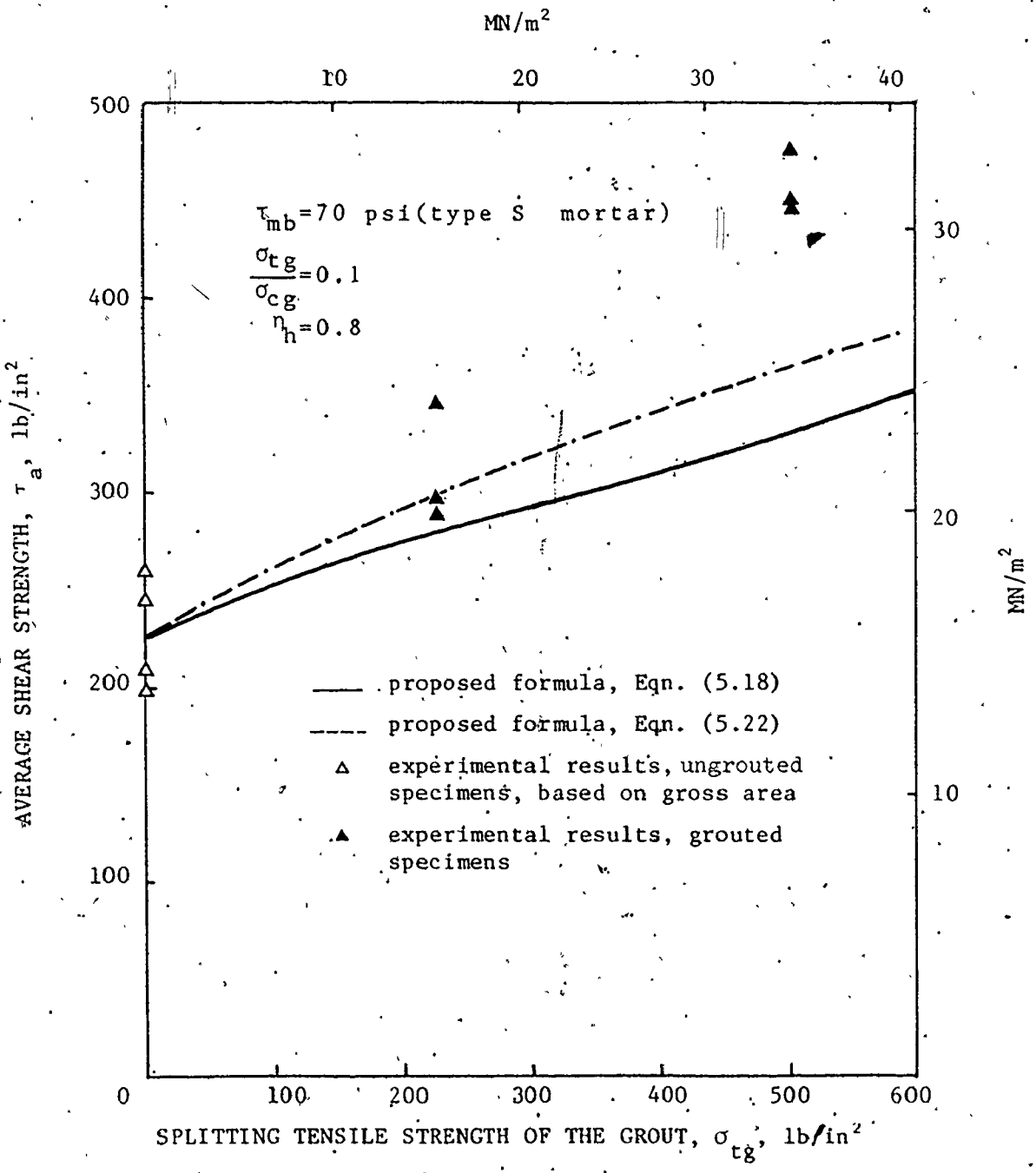

Fig. 5.25 MEASURED AND COMPUTED SHEAR STRENGTHS VERSUS GROUT STRENGTHS FOR ASSEMBLAGES UNDER PRECOMPRESSION STRESSES OF 200 psi

In the current program, an attempt has been made to include the effect of the σ_x stresses on the formulation of the shear capacity of grouted masonry assemblages. It is assumed that the resistance of the mortar joint to debonding failure would not be influenced by the σ_x stresses and that it is only the grout's shearing capacity which is influenced by these stresses.

An elastic analysis using the finite element method was done to investigate the distribution of the σ_x stresses for the four unit assemblages adopted in the experimental study. The analysis was carried out for both ungrouted and grouted specimens for the condition of plane stress using constant strain triangular elements. A total of 358 elements were used to idealize one quarter of the specimen, as shown in Fig. 5.26. For elements representing two materials, which is the case for grouted specimens, equivalent element thickness was considered on the basis of the modular ratio. The resulting σ_x stress distributions are shown in Fig. 5.27 for both the ungrouted and the grouted (medium grout) cases. The stress values are expressed as functions of the average shear stress over the joint. It is shown that the distributions of the σ_x stresses are not constant along the y_1-y_1 plane and also along the joint x_1-x_1 plane.

Adopting a representative value of the σ_x stresses (average of stresses along the joint shown by curve A in Fig. 5.27), equal to 1.5 τ_a, Equation (5.14) is rewritten in the form:

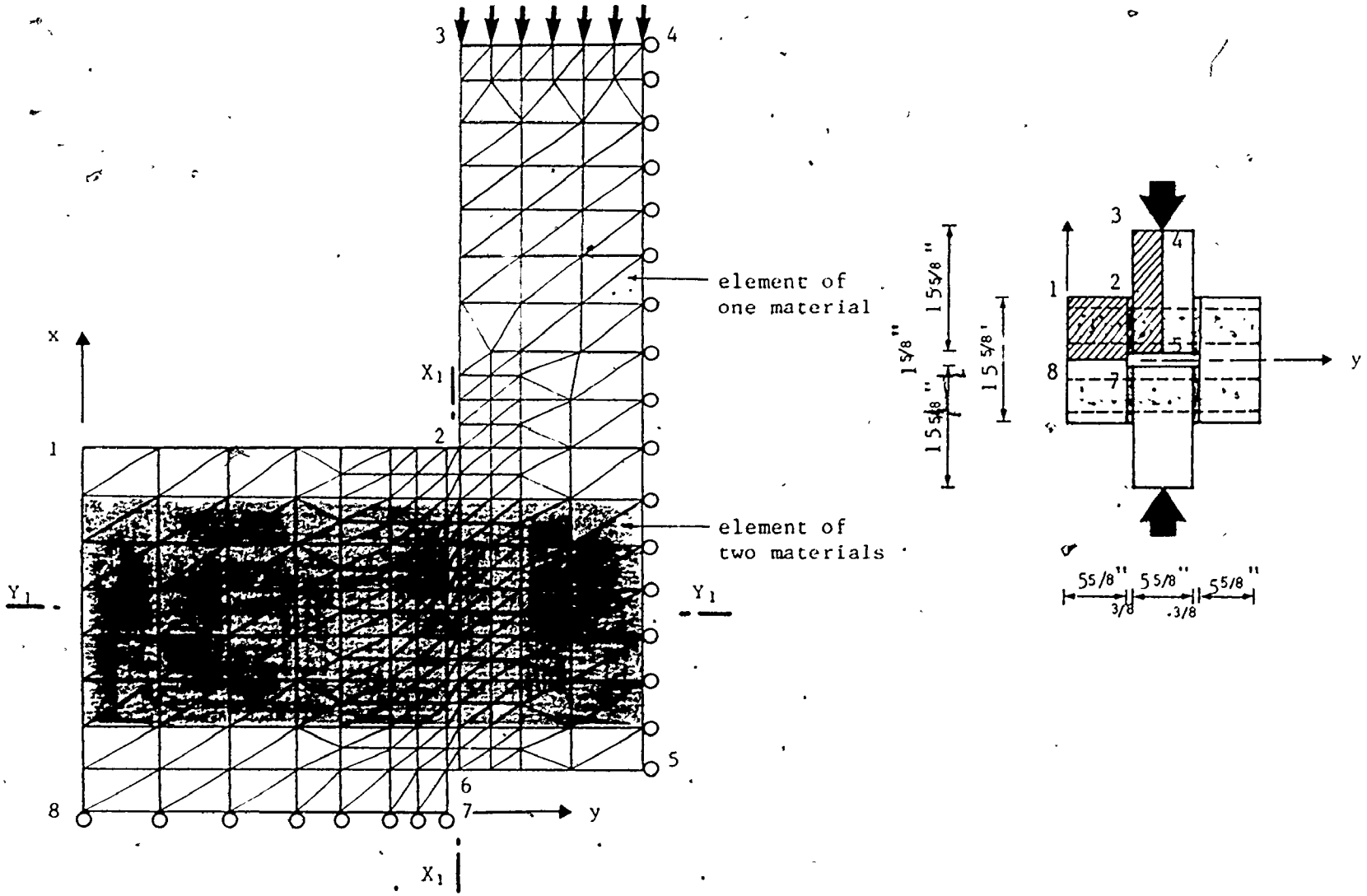

Fig. 5.26 FINITE ELEMENT IDEALIZATION OF THE SHEAR SPECIMEN

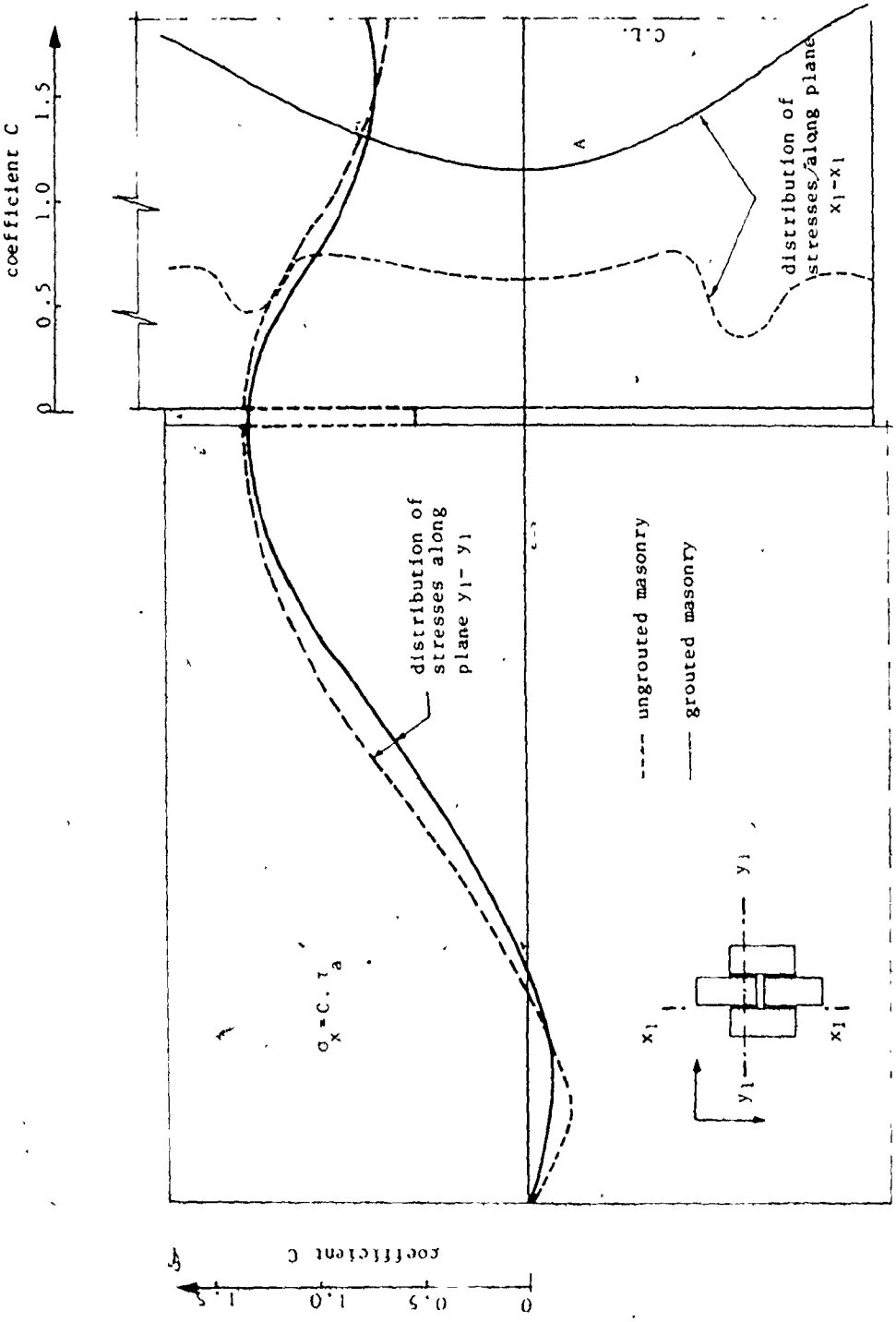

Fig. 5.27 DISTRIBUTION OF THE σ_x STRESSES FROM THE FINITE ELEMENT ANALYSIS

$$\sigma_{1,2} = -\frac{\sigma_n+1.5\tau_a}{2} \pm \sqrt{\tau_g^2 + \left(\frac{\sigma_n-1.5\tau_a}{2}\right)^2} \qquad (5.19)$$

Substituting the σ_1 and σ_2 values from Equation (5.19) into Equation (5.13) yields,

$$\tau_g = \sqrt{\left(\frac{r}{1+r}\,\sigma_{cg} + \frac{1-r}{2(1+r)}\,(\sigma_n+1.5\tau_a)\right)^2 - \left(\frac{\sigma_n+1.5\tau_a}{2}\right)^2} \qquad (5.20)$$

Assuming that the shear capacity of the assemblage could be expressed by a linear combination of the components' capacities,

$$\text{i.e.,} \qquad \tau_a = (\tau_{mb} + \mu\,\sigma_n)\,\eta_h + \tau_g\,(1-\eta_h) \qquad (5.21)$$

and substituting τ_g from Equation (5.18), into Equation (5.19) yields,

$$\tau_a = (\tau_{mb} + \mu\,\sigma_n)\,\eta_h + \sqrt{\left(\frac{r}{1+r}\,\sigma_{cg} + \frac{1-r}{2(1+r)}\,(\sigma_n+1.5\tau_a)\right)^2 - \left(\frac{\sigma_n+1.5\tau_a}{2}\right)^2}\,(1-\eta_h) \qquad (5.22)$$

Solving the above equation for τ_a, one can determine the shear capacity of grouted masonry under shearing forces along with precompression, taking into consideration the effect of the stresses parallel to the joint (σ_x stresses). The results using Equation (5.22) are plotted in Figs. 5.24 and 5.25. It is shown that taking the σ_x stresses into consideration improves the agreement between the computed and the experimental values. However, for the case of high precompression, the agreement was not as good as might be desired. It seems that the confining

effect of the mortar joint under high precompression could lead to an increase of the joint shear capacity.

It should be noted that the adopted representative value of the σ_x stresses is valid for the assemblages used in the current program and may not be applicable to other shapes of assemblages. However, Equation (5.22) could be rewritten in a more general form in terms of the compression stresses perpendicular, σ_n, and parallel, σ_p, to the bed joint direction as follows:

$$\tau_a = (\tau_{mb} + \mu \sigma_n) \eta_h + \sqrt{\left(\frac{r}{1+r} \sigma_{cg} + \frac{1-r}{2(1+r)} (\sigma_n+\sigma_p)\right)^2 - \left(\frac{\sigma_n+\sigma_p}{2}\right)^2}$$

$$(1 - \eta_h) \qquad (5.23)$$

The proposed expressions can only be applied as long as the failure mode is by slip along the joints (shear failure of the joint) which seems to be the governing criterion for low precompression levels (less than 0.1 of the compressive strength normal to the bed joint). Under higher precompression, the mode of failure will probably be changed to a mixed shear-tension failure or a shear failure, as discussed in Chapter 6, and hence Equations (5.18) and (5.23) will no longer be applicable.

It should be noted that the proposed simplified expressions provide conservative results and could be used to give a lower bound prediction of the shear strength of ungrouted and grouted concrete masonry joints as long as the physical and mechanical properties of the components are similar to those used in this investigation. It is anticipated that the proposed expressions

will have general applicability but before recommending it, tests should be done with blocks having different geometric and strength characteristics.

5.4 Review of Code Design Provisions

Possibly because of the lack of information concerning the shear strength of grouted masonry, the North American codes[12,27] assign strength values for grouted masonry similar to solid masonry provided that the grout strength is at least equal to that of the units. Utilizing the investigation presented in this chapter, the CSA S 304[12] design provisions concerning the shear values for plain concrete masonry have been reviewed and lead to the following observations:

1 - The codes' shear values do not distinguish between the shear failures controlled by slip or by diagonal tension. It is presumed, in the following discussion, that the assigned values relate to the joint slip mode of failure under zero precompression. The code allows different shear values for different levels of precompression when assigning the maximum allowable horizontal shear stress for masonry shear walls.

2 - The codes' allowable shear stress values for ungrouted masonry for types S and N mortars seem to be compatible with the experimental results. The code values provide a safety factor of about 2 for the two mortar types. (34 versus 70 and 23 versus 53 psi, respectively.).

3 - The current investigation clearly shows the significance of the compressive stresses normal to the bed joint (precompression) in increasing the shear resistance of masonry joints. However most of the present masonry codes do not allow for the increase in the shear strength with the increase of the precompression level[29], the Canadian code[12] does allow for such an increase in the shear values and the following relationship is recommended for shear walls:

$$v = v_m + 0.3\, f_{cs} \tag{5.24}$$

where v = maximum allowable shear stress

v_m = allowable shear stress at zero precompression

f_{cs} = compressive stress due to dead load

Comparing the experimental results with the code values for the precompression cases indicates a safety factor ranging from about 2 to 3 over precompression stress from zero to 200 psi (see Fig. 5.15). The approach of the Canadian code[12] seems to be appropriate and more realistic in considering the effect of the precompression which, certainly, exists due to the dead loads. However, the code does not explicitly assign any limitation to the compressive stresses, f_{cs}, for the applicability of the recommended equation. Therefore it must be assumed that it is intended to be applicable up to the allowable compressive stress for masonry, f_m. At higher levels of normal compressive stresses, the failure mode will be changed to a mixed shear-tension failure or a shear failure, and the recommended Equation (5.24) will no

longer be applicable as it will highly overestimate the shear capacity and lead to nonconservative results.

4 - Considering grouted masonry to be similar to solid masonry as designated by the code, (i.e. equating the shear bond strength of the mortar and the shear strength of the grout) seems to be unrealistic. This is attributed to the fact that, in most practical cases, the diagonal tensile strength of the grout (governing its shear strength) is much higher than the shear bond strength of the mortar. Therefore, this approach adopted by the code, leads to a substantial underestimation of the shear capacity of grouted masonry, especially for high strength grout and low net to gross area ratios, as shown in Fig. 5.21.

5 - The code classifies the shear values according to the mortar type without reference to the properties of the block. For concrete masonry, the block's surface roughness and its initial rate of absorption may significantly affect the shear bond strength of the mortar. As has been shown in Figs. 5.21 and 5.22, the block's net to gross area ratio appreciably affects the contribution of grouting towards the increase of the shear strength of grouted masonry joints.

5.5 Summary and Conclusions

The behaviour characteristics of ungrouted and grouted concrete masonry joints under shear and normal stresses are presented and discussed in this chapter. The effects of the

mortar type, grout strength, and joint reinforcement on the joint capacity are experimentally investigated. Formulas to predict, in quantitative terms, the shear strength of the joints in terms of the strength and geometric characteristics of the block, mortar, and grout are proposed.

The following conclusions can be made based on the contents of this chapter:

1 - The shear bond strength of ungrouted masonry is not directly proportional to the compressive strength of the mortar joint because of the fact that the bonding value of the mortar is not mainly a function of its strength. It is likely to be influenced by the properties of both the mortar and the blcoks.

2 - The variable most significantly affecting the shear strength of ungrouted masonry is the level of normal stress (precompression). A strong correlation between the shear strength and the normal stress was shown to exist. Significantly higher shear strengths were obtained for the assemblages which were loaded with higher values of precompression. The nature of the shear strength, τ, and normal stress, σ_n, relationship can be represented by the form of the following equation:

$$\tau = a + b\,\sigma_n \qquad (5.25)$$

where a and b are constants depending on the components' characteristics (a is referred to the initial bond strength, whereas b is referred to the coefficient of internal friction).

This relationship seems to be applicable on an empirical basis for both ungrouted and grouted masonry where the material constants a and b would vary for different materials and different geeometric characteristics.

3 - Grouting is shown to significantly increase the shear strength of masonry joints. Its contribution towards the increase of the shear capacity is influenced by the tensile strength of the grout and the percent of the core area. Higher grout strengths and lower net to gross area ratios result in higher shear capacities of the assemblage. For practical cases, an increase of the shearing strength, ranging from 50% to 150%, could be achieved by grouting the cores with medium strength grout ($\sigma_{cg} \approx 3000$ psi). Therefore, grouting the cores would help to decrease the possibility of debonding failure of the bed joint which frequently occurs for ungrouted masonry shear walls under racking loads with low levels of compressive normal stresses.

4 - The net to gross area ratio of the block, which is a geometric characteristic of the block, seems to be a significant parameter for the shear strength of grouted masonry. Its influence has been ignored by the code when assigning shear values for grouted masonry.

5 - The test results indicate that the relative contribution of grouting (based as a ratio of the comparable strength of grouted and ungrouted masonry) to the shear strength decreases as the level of precompression increases. This may

support the suggestion that the precompression stress (normal to the bed joint) affects the shearing strengths of ungrouted and grouted masonry in different ways.

6 - The shear analysis using the proposed expression (Equation 5.23) indicates that the compressive stresses parallel to the bed joint can have a noticable effect on the shear capacity of grouted masonry joints, especially at high levels of precompression. This aspect should be taken into account when interpreting test data as well as for design situations.

7 - The variability of the shear results for grouted masonry are much less than those for ungrouted masonry. The grouted cores provide partial continuity to the masonry assemblage which may increase the reliability of the composite as a construction material. Therefore, it could be that the safety factors can be reduced in the future which would lead to more economical masonry structures using grouted masonry.

8 - The code's philosophy in assigning the same allowable shear stresses for grouted and ungrouted masonry does not take advantage of the benefits of grouting which leads to a substantial underestimation of the shear strength of grouted masonry, especially in case of high strength grout.

CHAPTER 6

BEHAVIOUR OF CONCRETE MASONRY UNDER BIAXIAL STRESSES

6.1 Introduction

Masonry assemblages such as shear walls are frequently designed to withstand horizontal forces from earthquakes or wind loading in their own planes. These horizontal forces are accompanied by vertical forces (dead loads,, etc.) of different magnitudes. In a masonry building, walls loaded in this way are also affected by surrounding concrete frames and other confining parts of the building structure. Hence, these assemblages will be under normal stresses parallel and perpendicular to the bed joints as well as shearing stresses along these joints. In other words, a state of biaxial stress is common.

Most experimental determinations of the strengths of materials are based on uniaxial stress states. However, the general practical problem involves at least a biaxial if not a triaxial state of stress. Thus, a logical method of using uniaxial strength information in the analysis of multiaxial loading problems is required.

For concrete, it is known that the strength in one direction is to some extent affected by the stress in the perpendicular direction[32]. Different failure theories for isotropic materials

such as Mohr's theory of failure[38] and the octahedral shear stress theory[38] have been used successfully to express tne fracture condition for concrete under biaxial stresses in terms of its uniaxial tension and compressive strengths[35,59].

Because masonry is an anisotropic material, the elastic properties and the strength characteristics will vary with the stress orientation relative to the bed and head joints planes (see Section 4.2.5.2). Therefore, the failure theories for isotropic materials, used currently for masonry[8,49,58], are not applicable as they are basically derived on the concept of an invarient state of stresses[38]. They deal with a material having only one strength characteristic under compression, tension, or shear, where, by definition, the direction of stress has no significance for this isotropic material.

For masonry, since it is impractical to obtain the strength characteristics for all directions, a means must be found for determining the characteristics at any orientation in terms of the characteristics in the principal material directions (planes of material property symmetry).

Information about the variation of the strength and deformation characteristics of masonry assemblages with the variation of the stress orientation is not documented yet[58] in the masonry literature.

The objective of this chapter is to investigate the following two points:

1 - The anisotropic nature of behaviour of ungrouted and grouted masonry as a composite material under different stress orientations with respect to the bed joint direction.

2 - The available failure hypotheses for masonry and the applicability of the failure theories of composite materials to ungrouted and grouted concrete masonry.

This investigation should help in the development of an appropriate failure criterion for masonry under biaxial stresses taking into consideration its inherent anisotropic nature. To meet these objectives, experimental and theoretical, studies nave been conducted and will be presented in the following sections:

6.2 Effect of Stress Orientation on the Behavioural Characteristics of Concrete Masonry Assemblages

In Chapter 3, the behaviour of ungrouted and grouted masonry prisms under compressive stresses normal to the bed joint ($= 90^{o}$) was discussed, while in chapters 4 and 5, the strength characteristics of ungrouted and grouted masonry assemblages under tensile stresses parallel and normal to the bed joints and under shear stresses along with precompression were presented, respectively. In this chapter, an experimental investigation conducted mainly to study the behavioural characteristics in directions other than the principal material directions (the bed and head joints directions) is reported.

6.2.1 Behaviour of Masonry Prisms under Compression Normal to the Head Joint

6.2.1.1 Experimental Details and Testing Procedure: Ten 3 course prisms were used for this test series. Three half blocks, similar to those used in the prisms loaded normal to the bed joint (Section 3.2.1), were laid in stack bond, end-to-end as shown in Fig. 6.1. The mortar joints represent the head joints. For grouting, the prisms were positioned horizontally (using temporary prestressing to avoid the possibility of a joint separation failure) and the grout was poured into the cores and puddled with a steel rod. Type S_1 mortar and types GW, GM_1, and GS grouts were used. Three 2-inch cubes per batch, were used as control specimens for the mortar and 6 block moulded prisms, per batch, were used for the grout. They were all air cured in the laboratory under the same conditions as the prisms. The properties of the mortar and the grouts were presented in Chapter 2.

The prisms were capped using a sulphur compound and tested (in a vertical direction) under axial compression. Mechanical gauge points were mounted on both faces and sides of the prisms so that the deformations in the vertical and horizontal directions could be measured. Fig. 6.1 shows the test set-up and the arrangements of the gauge points. The control specimens were tested (mortar cubes under axial compression and grout prisms under axial compression and splitting tension) at approximately

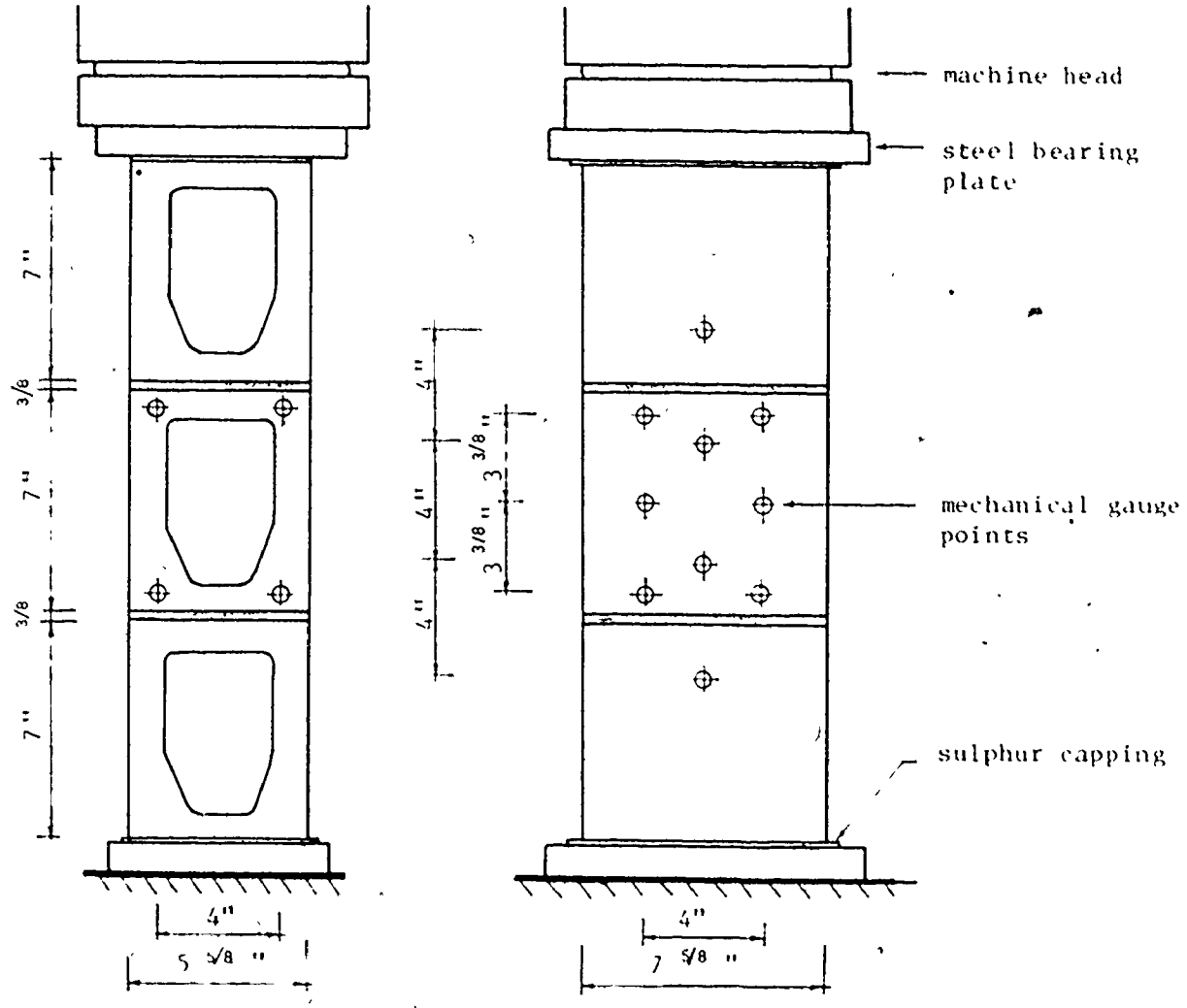

Fig. 6.1 TEST SET-UP FOR PRISMS TESTED UNDER COMPRESSION NORMAL TO THE BED JOINTS

the same average age as the assemblages.

6.2.1.2 Discussion of Test Results: Ungrouted prisms failed in an ideal vertical splitting failure crossing the intermediate webs at the minimum vertical cross section as shown in Fig. 6.2(a). There were no signs of fracture cracks along the faces of the prisms. This splitting failure is attributed to the lateral tensile stresses developed within the blocks, which has previously been subscribed to the different lateral strain characteristics of the blocks and their mortar joints. Grouted prisms exhibited a similar mode of splitting failure where the fracture plane crossed the intermediate webs at a section passing through the grout-block interfaces which seems to be the minimum resisting section under lateral tensile stresses. Figure 6.2(b) shows the typical mode of failure of a grouted prism. The type of grout had no influence on the mode of failure.

Table 6.1 presents the results of the prism tests along with the control specimen results. The influence of the grout strength on the prism strength is shown graphically in Fig. 6.3. It is interesting to observe that there is very little effect of the grout strength on the compressive capacity of the prisms loaded normal to the head joints. This phenomenon seems consistent with the exhibited mode of failure since the fracture surface did not cross the grout which in this case acts mainly as a filler to distribute the stresses over the full contact area between the blocks and the mortar joints.

(a) Ungrouted Prism

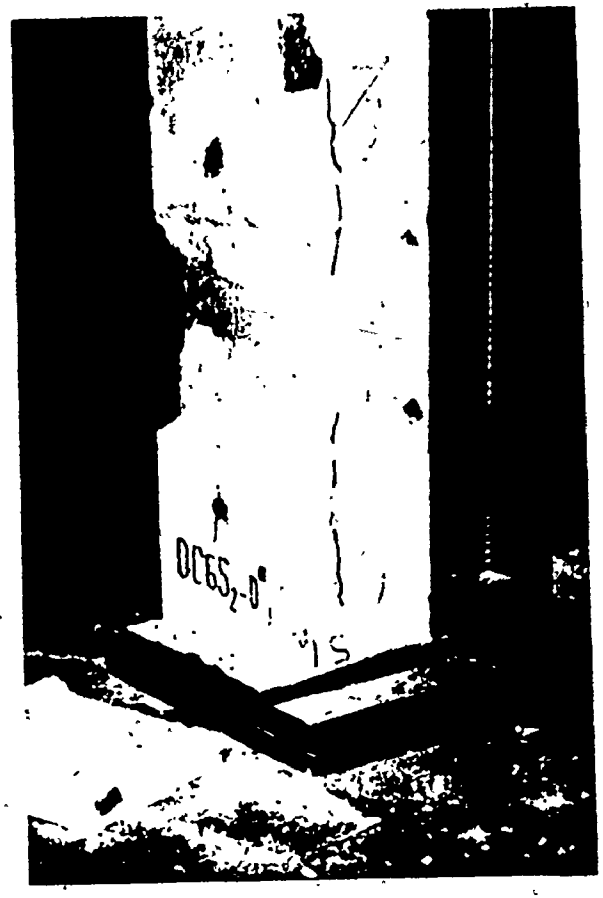

(b) Grouted Prism

Fig. 6.2 TYPICAL FAILURES FOR PRISMS TESTED UNDER COMPRESSION NORMAL TO THE HEAD JOINTS

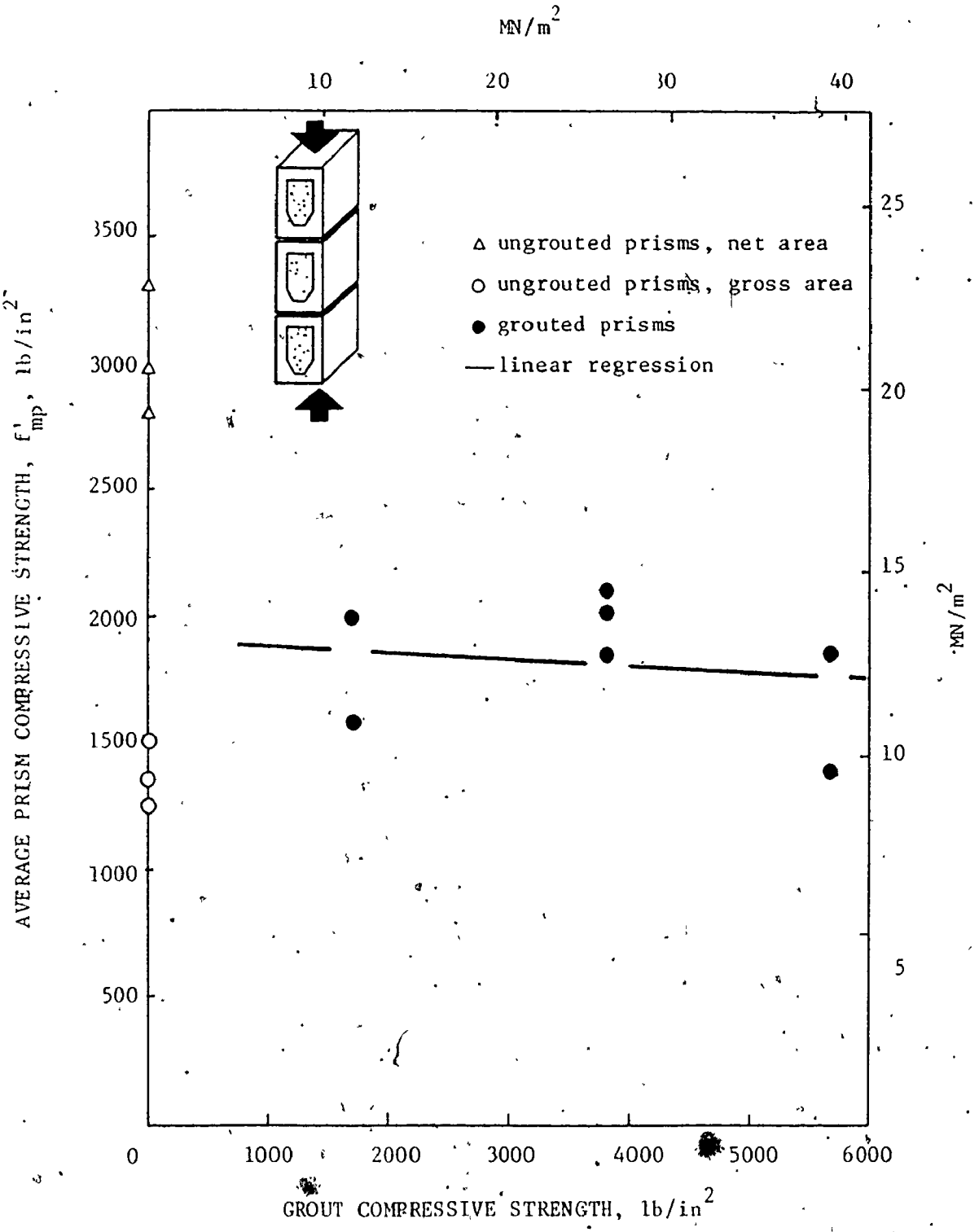

Fig. 6.3 EFFECT OF GROUT STRENGTH ON THE COMPRESSIVE STRENGTH OF MASONRY PARALLEL TO THE BED JOINT

TABLE 6.1

COMPRESSION RESULTS FOR UNGROUTED AND GROUTED PRISMS TESTED UNDER LOADS NORMAL TO THE HEAD JOINTS

Type	Mortar Strength[a]	Grout Strength[b]	Prism Compressive strength[c]		
			Individual (psi)	Mean (psi)	C.O.V. (%)
ungrouted	2630		1360 1520 1280	1390	8.8
Grouted GW	2630	1700	2000 1590	1800	-
Grouted GM_1	2630	3800	1850 2020 2100	1990	6.4
Grouted GS	2630	5680	1400 1850	1630	-

Note: 1 psi = 6.9×10^{-3} MN/m^2

a. Compressive strength of 2 in. mortar cubes, average of 10 batches, 3 cubes per batch (C.O.V. = 15%)

b. grout compressive strengths calculated from block moulded prisms

c. based on gross area for both ungrouted and grouted prisms

Figure 6.4 shows the vertical stress-lateral strain relationships for the ungrouted prisms and a typical set of grouted prisms. Higher tensile strains were developed on the sides rather than on the faces of the prisms at high stress levels. This behaviour is consistent with the mode of failure as the fracture surface crossed the intermediate webs where the tensile strains were maximum.

Figure 6.5 displays the different stress-strain relationships for deformations measured on the block compared to those measured across the joints for ungrouted and grouted masonry prisms (type GM_1 grout). The vertical strains measured across the joint using a 4 inch gauge length were greater than the corresponding strains taken within the height of the block for both types of prisms. Considering the greater cross-sectional area of the block in the vicinity of the joint, this result dramatically indicates the significance of the mortar joint on the behaviour of both ungrouted and grouted masonry under compression normal to the head joints. For grouted prisms, there is no continuity provided by the grouted cores. This differs from the case of prisms loaded normal to the bed joint and hence, the mortar joint is the only media connecting the blocks. Here, the mortar joint will have a significant effect on the compression capacity whereas it has been shown that the mortar bed joint has an insignificant effect on the behaviour of grouted prisms loaded normal to the bed joints (see Section 3.2.4.1). Figure 6.5 also

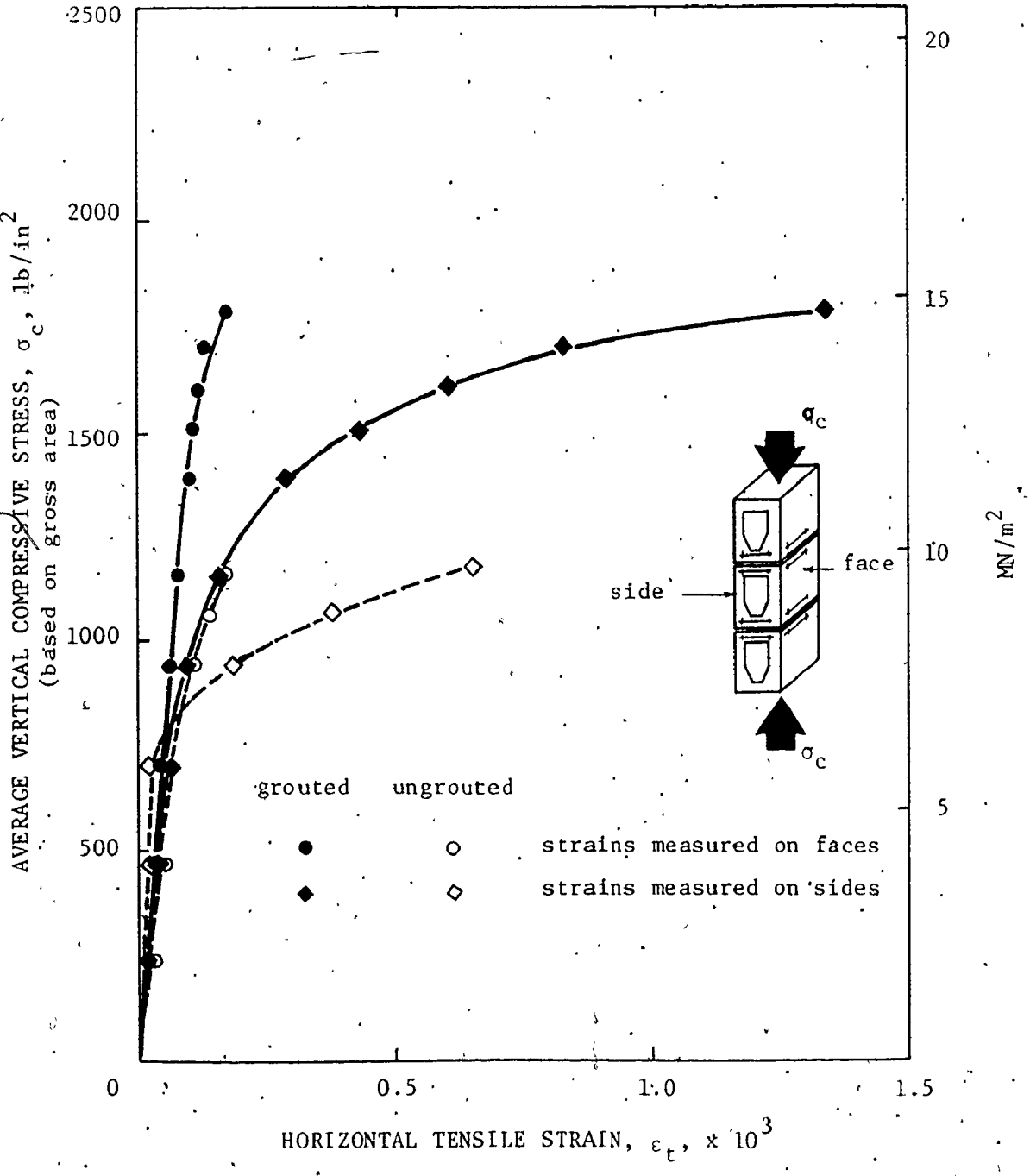

Fig. 6.4 VERTICAL STRESS VERSUS LATERAL STRAIN FOR PRISMS LOADED NORMAL TO THE HEAD JOINTS

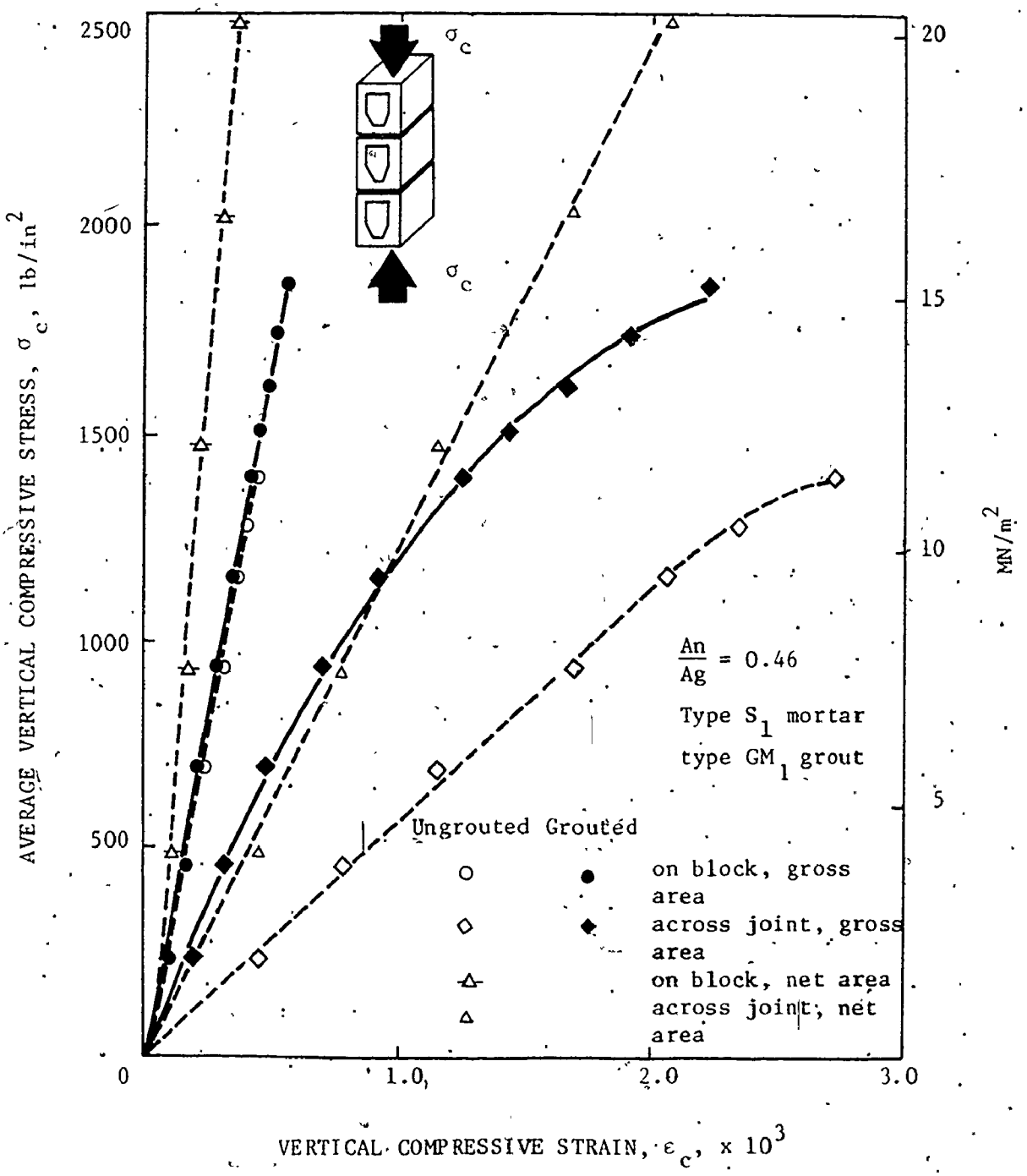

Fig. 6.5 DEFORMATIONS ON THE BLOCKS AND ACROSS THE JOINTS OF PRISMS LOADED NORMAL TO THE HEAD JOINTS

indicates that the deformations measured across the joint for ungrouted prisms (based on net area) and for grouted prisms (based on gross area) were about the same. Also, the difference between the deformations across the joints and on the blocks was higher in the case of ungrouted prisms compared to the case of grouted prisms. This may be because of the reduction of the compressive strain measured on the blocks of ungrouted prisms due to the possible out of plane bending of the face shells under compressive stresses (frame action).

6.2.2 Behaviour of Masonry Prisms under Compression having Different Orientations from the Bed Joints (Off-Axis Compression)

6.2.2.1 Test Technique: It was desirable to devise a method for evaluating the behaviour of masonry under any combination of shear and normal stresses on the critical bed and head joints planes. This condition can be induced by the application of a compressive load on the top and bottom of an assemblage where the bed joints are oriented at different angles from the direction of the load (see Fig. 6.6). Different compression stress components normal to the bed joints (for different load orientations), which seems to significantly influence both the assemblage's mode of failure and the strength could be employed using this test technique. [Considering the bed and head joints directions, the axes of material symmetry (principal material directions), the application

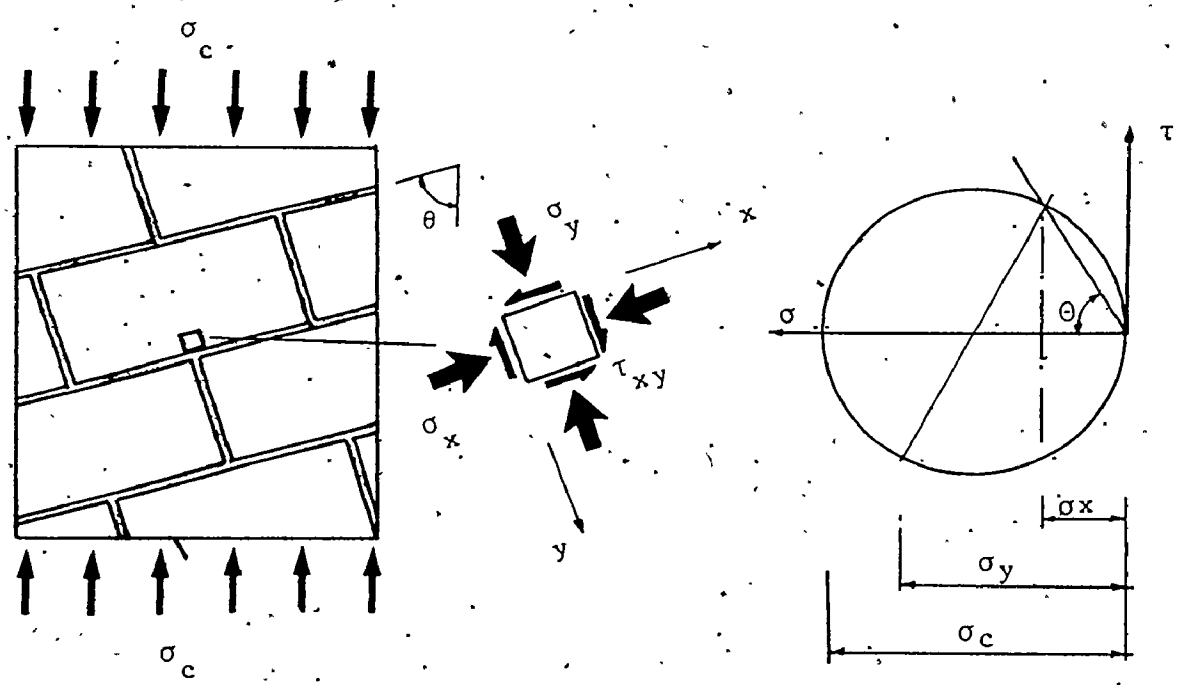

Fig. 6.6 MASONRY ASSEMBLAGE TESTED UNDER OFF-AXIS COMPRESSION

of external compression loads inclined to these axes will be referred as "Off-axis compression".]

In the case of a uniform load applied to the panel's edges; as shown in Fig. 6.6, the resulting stress distribution is globally homogenous, and hence statically determinate. Figure 6.6 illustrates the basic concept of testing masonry assemblages under inclined loads. If x and y are the principal stress directions (parallel and normal to the bed joints), then for a particular orientation, θ, of the applied stress, σ_c, with respect to the x-axis, the stress resultants can be expressed as:

$$\sigma_x = \sigma_c \cos^2\theta \qquad (6.1)$$

$$\sigma_y = \sigma_c \sin^2\theta \qquad (6.2)$$

$$\tau_{xy} = \sigma_c \sin\theta \cos\theta \qquad (6.3)$$

6.2.2.2 Experimental Details and Testing Procedure: The ungrouted and grouted test specimens were cut from 32 by 32 in. masonry walls constructed in running bond with full bedded 3/8-in. mortar joints. The cutting was done with a 12-in. diameter diamond edge saw. Each panel was cut into 3 prisms as shown in Fig. 6.7. The 3 layup angles adopted were 15^o, 45^o, and 75^o.

Six panels were constructed using the standard 8x6x16-in. blocks and type S_1 mortar. Half blocks, obtained by splitting of kerfed blocks, were used with their unsplit sides facing the mortar head joints. (This assured consistency of the bonding

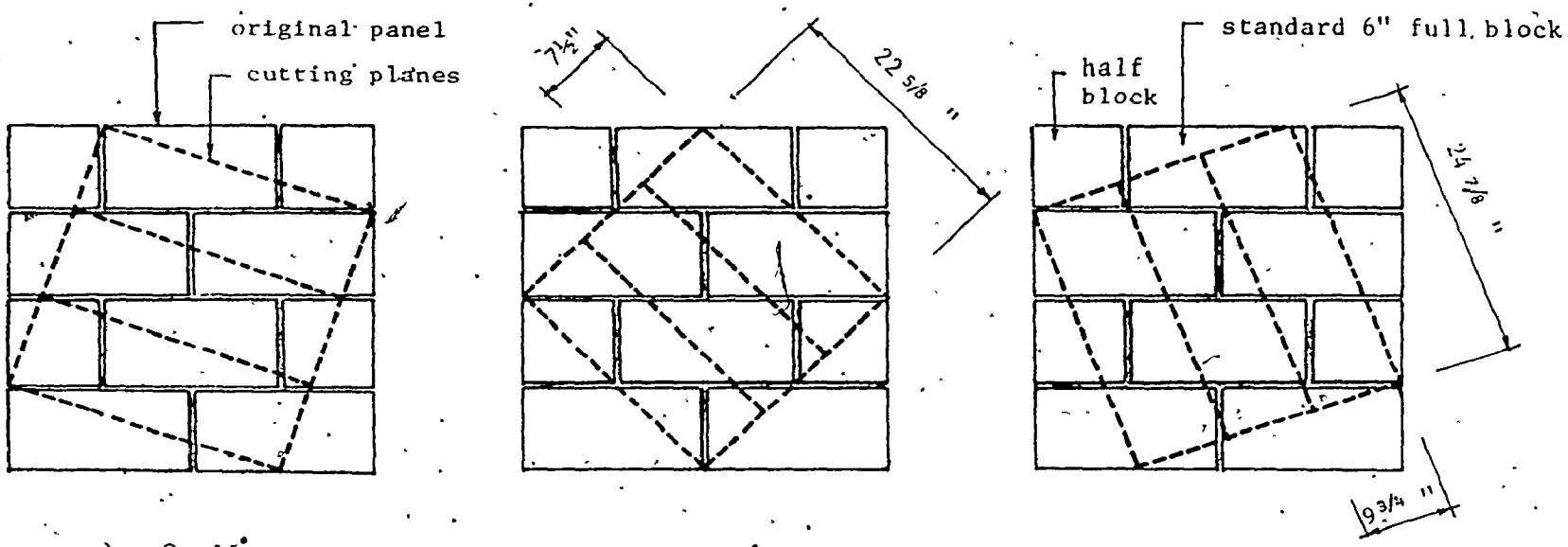

Fig. 6.7 PREPARATION OF THE MASONRY PRISMS BY SAW-CUTTING OF SQUARE PANELS

surfaces of the joints in the panels.) Prior to cutting, medium grout, GM_1, was poured into the cores of 3 panels and puddled with a steel rod. Three 2 inch cubes per batch, were used as control specimens for mortar and 6 block moulded prisms (2 1/2 x 5 5/8 x 7 5/8 in.) per batch were adopted as representatives of the grout in the assemblages. The material properties of the mortar and grout mixes were presented in Chapter 2. Equiangular rosettes for mechanical gauges were used to measure the principal strains at the centre of the two faces for each test prism. A 4 in. gauge length was used.

6.2.2.3 Discussion of Test Results: The results will be discussed under the following headings:

Failure modes: Figure 6.8 shows sketches of the failure patterns of the ungrouted and grouted prisms for different orientations of the applied compressive stress with respect to the bed joint measured by the angle, θ. For $\theta = 15^{\circ}$, both the ungrouted and the grouted prisms showed the expected shear failures along the bed joints. These were characterized by debonding failures at the block-mortar interfaces for ungrouted prisms and by debonding failures accompanied by shear failures of the cores for grouted prisms. No signs of distress of the blocks were observed as the failure was a joint slip failure. This is expected for the high shear stresses along with low normal stresses developed along the bed joint for this small angle of the applied stress relative to the bed joint. Therefore, the joint

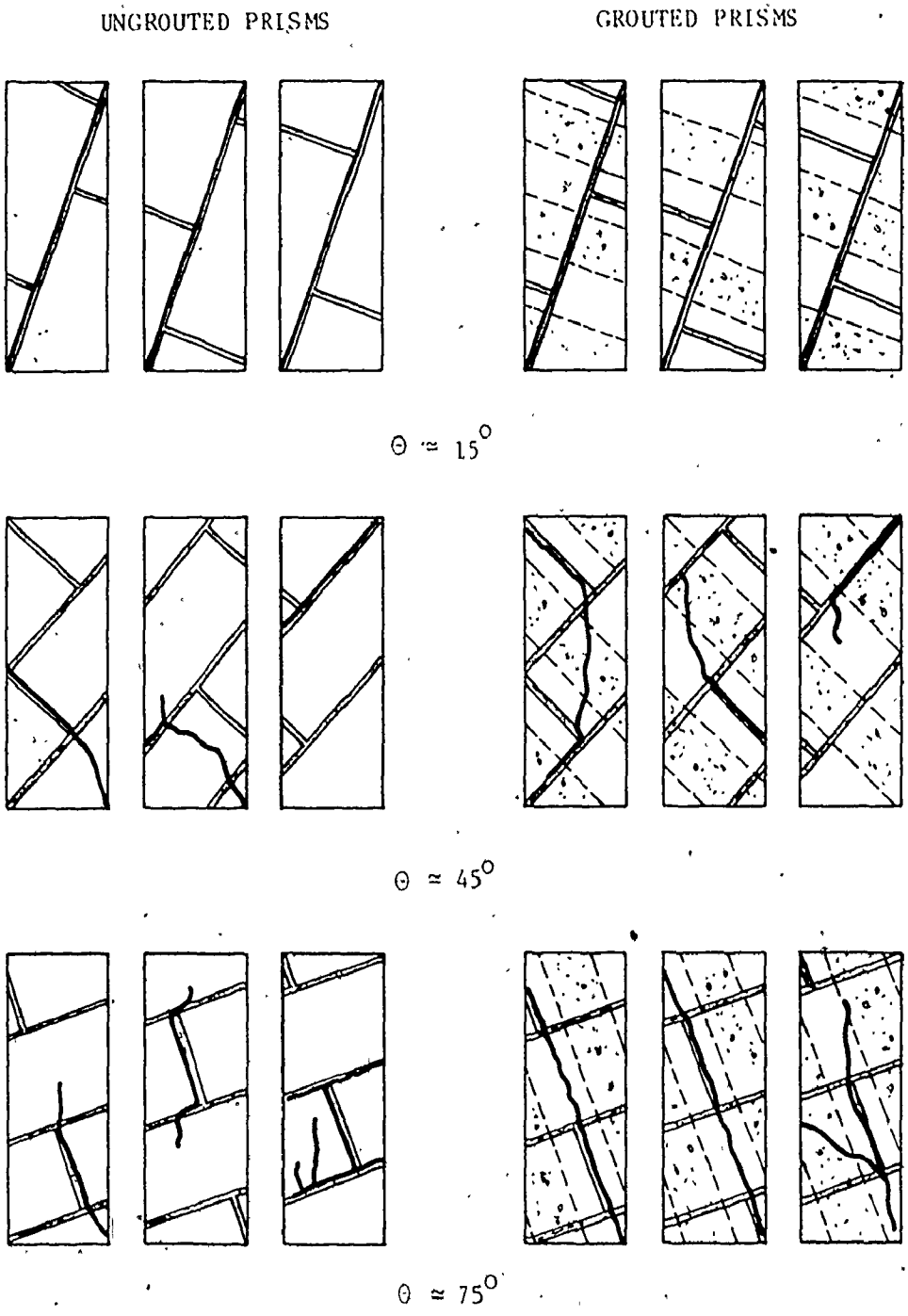

Fig. 6.8 FAILURE PATTERNS OF UNGROUTED AND GROUTED MASONRY PRISMS UNDER OFF-AXIS COMPRESSION

shear strength was the major parameter governing the assemblage capacity. Figures 6.9(a) and 6.9(b) show typical joint failures for ungrouted and grouted prisms, respectively.

Ungrouted prisms, tested with $\theta = 75^{\circ}$, exhibited a splitting mode of failure near the head joints as shown in Fig. 6.10(b). For similar grouted prisms, shear failure was shown to occur where the fracture planes followed the head joints and sheared off the face shells of the blocks inbetween the columns of grout as shown in Fig. 6.8. It is interesting to observe a similarity between the fracture planes of these prisms and those for discs tested under splitting tension parallel to the bed joints (see section 4.2.4.1). Comparison of the failure of the prism shown in Fig. 6.10(b) with the splitting failure of the disc shown in Fig. 4.15 indicates this similarity clearly. For this load orientation, the shear applied on the bed joint, τ, was relatively small compared to the normal stress, σ_n. Therefore the frictional resistance (proportional to the normal stress) was high enough to prevent shear debonding failures of the bed joints. However, high shears accompanied by low normal compression developed along the head joint planes causing shearing of the head joints and the blocks. The capacity in this case is mainly governed by the capacity of the blocks under biaxial stresses and by the shear bond strength of the head joints. This behaviour indicates the significance of the head joints when the assemblage is under biaxial stresses.

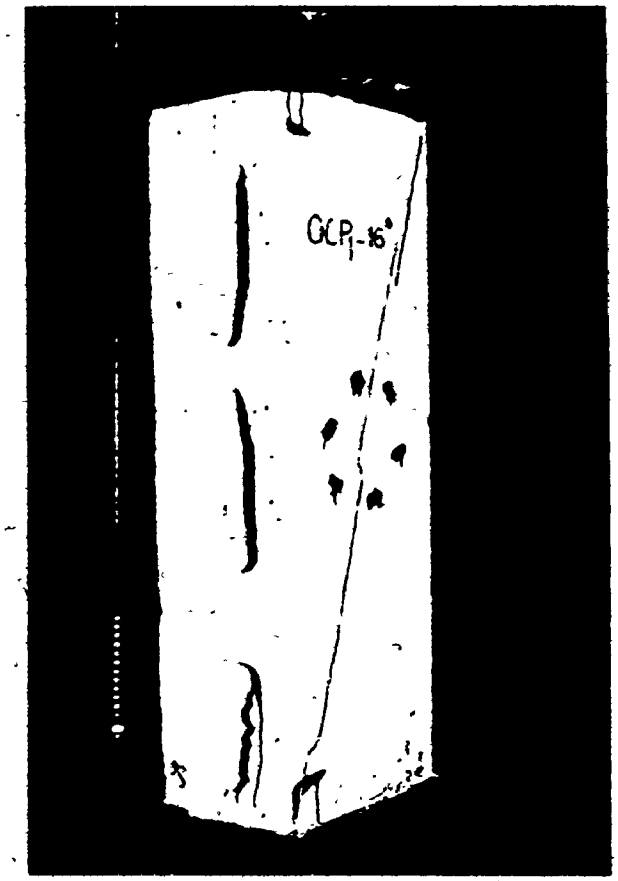

(a) Ungrouted Prism

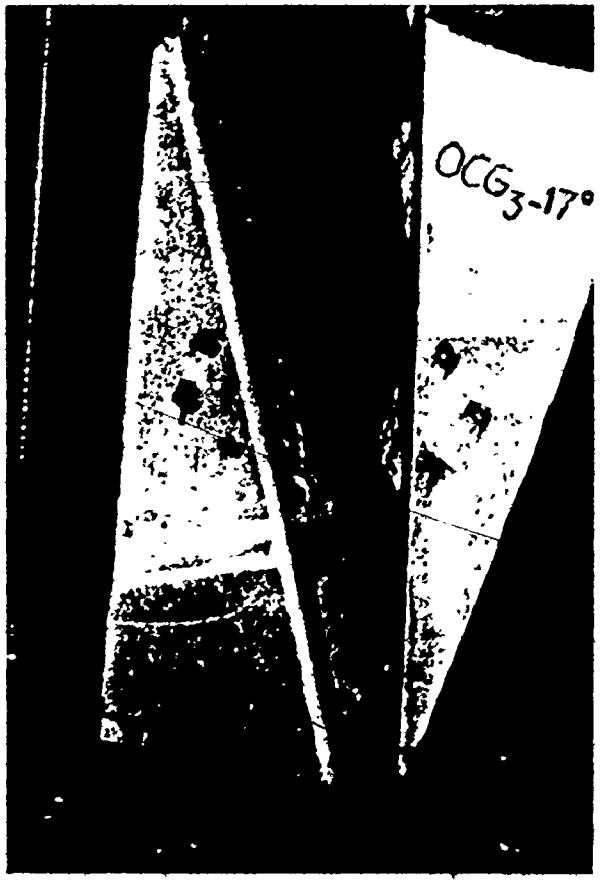

(b) Grouted Prism

Fig. 6.9 TYPICAL FAILURES OF PRISMS TESTED UNDER OFF-AXIS COMPRESSION ($\theta \simeq 15^{\circ}$)

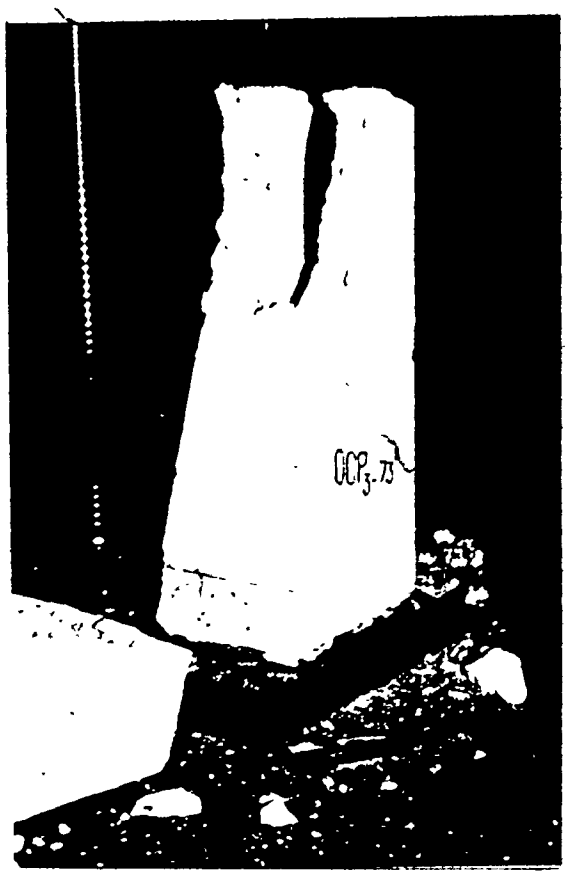

(a) Ungrouted Prism

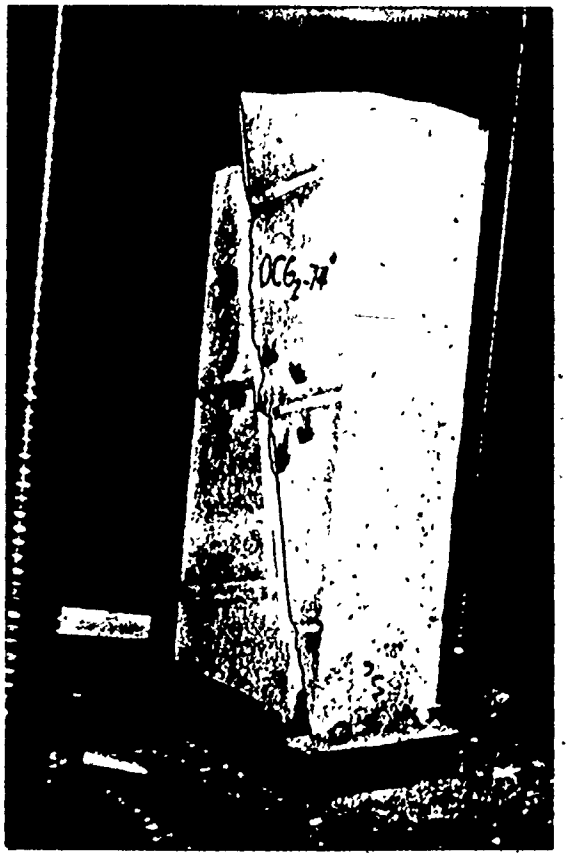

(b) Grouted Prism

Fig.6.10 TYPICAL FAILURES OF PRISMS TESTED UNDER OFF-AXIS COMPRESSION ($\phi \approx 75^{\circ}$)

For $\theta \simeq 45^{\circ}$, where nearly equal shear and normal stresses occur on the bed and head joints, the failure mode was essentially a mixed shear-tension mode of failure. This case represents a somewhat intermediate state between the shear failure at $\theta \simeq 15^{\circ}$ and the tension-shear failure at $\theta \simeq 75^{\circ}$. Typical failures of ungrouted and grouted prisms under compressive stresses oriented at $\theta \simeq 45^{\circ}$ from the bed joints are shown in Figs. 6.11(a) and 6.11(b), respectively.

Assemblage Capacity: The test results of the ungrouted and grouted prisms and their control specimens are presented in Table 6.2. The strengths were calculated on the basis of the gross area for both ungrouted and grouted prisms, since the net area has no practical definition under stress orientations other than normal to the bed joint. (The net area of a horizontal cross-section of a block is only meaningful for stresses normal to the bed joints.) Figure 6.12 shows the variation of the average compressive strengths with the stress orientation, θ, with respect to the bed joint direction. The strengths for the case of $\theta = 90^{\circ}$ were taken from the results of the axially loaded prisms presented in Section 3.2.4.1. The figure clearly indicates the anisotropic nature of behaviour of masonry, as the strength varied considerably with the stress orientation, particularly for ungrouted masonry. It appears that the continuity provided by the grouted cores helped to reduce the degree of anisotropy exhibited by the ungrouted assemblages where the mortar bed joints create relatively weak

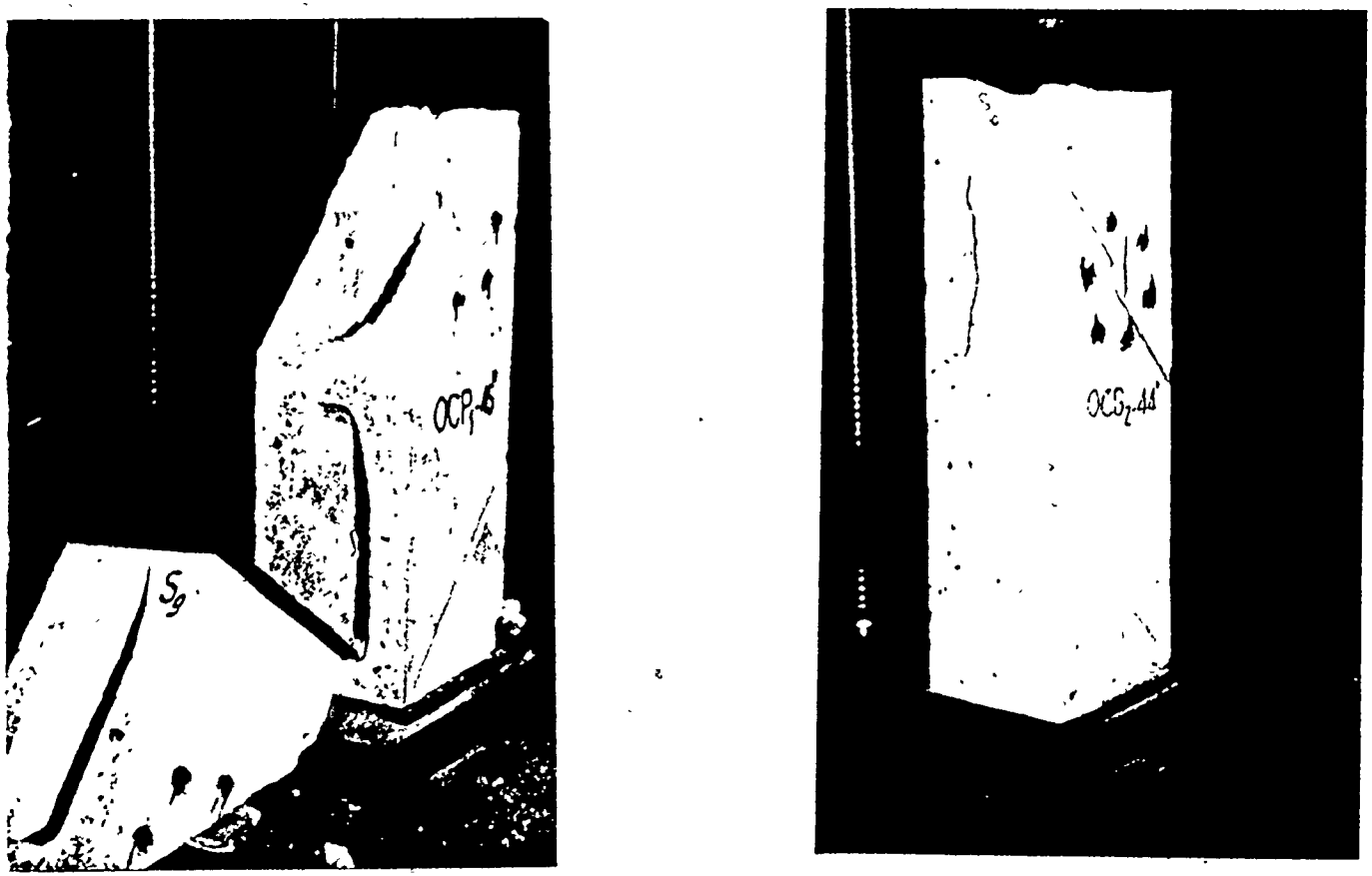

(a) Ungrouted Prism

(b) Grouted Prism

Fig. 6.11 TYPICAL FAILURES OF PRISMS TESTED UNDER OFF-AXIS COMPRESSION ($\theta = 45^{\circ}$)

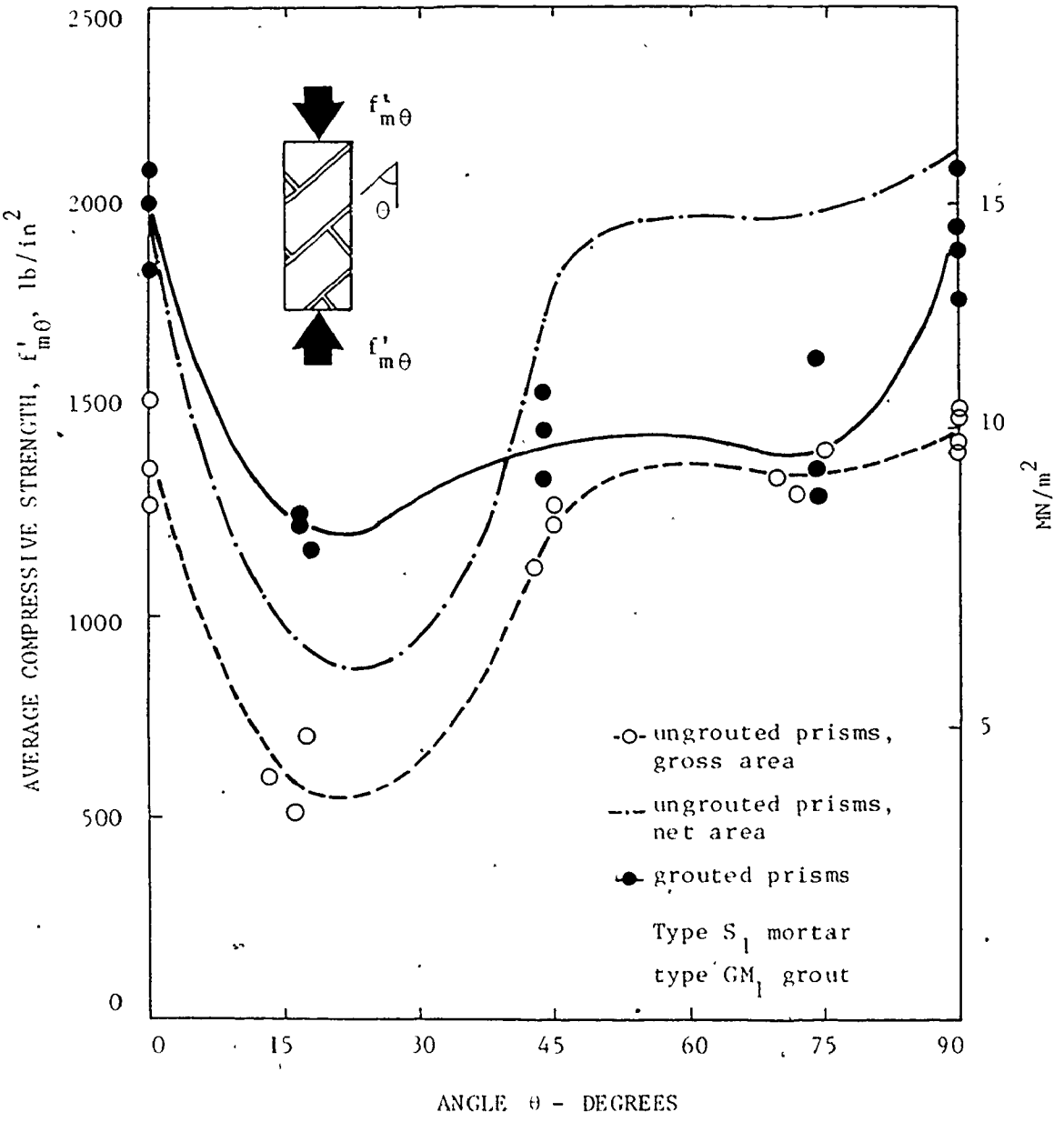

Fig. 6.12 EFFECT OF ORIENTATION OF THE LOAD RELATIVE TO THE BED JOINT, θ, ON THE COMPRESSIVE STRENGTH OF MASONRY PRISMS

TABLE 6.2

TEST RESULTS FOR PRISMS UNDER OFF-AXIS COMPRESSION

Type	Mortar Strength[a] (psi)	Grout Strength[b] (psi)	Prism Strength, $\theta = 15^{o}$			Prism Strength, $\theta = 45^{o}$			Prism Strength, $\theta = 75^{o}$		
			Individual (psi)	Mean (psi)	C.O.V. (%)	Individual (psi)	Mean (psi)	C.O.V. (%)	Individual (psi)	Mean (psi)	C.O.V (%)
Ungrouted[c]	2630		720 590 510	610	17.0	1120 1230 1280	1210	6.7	1330 1280 1380	1330	3.7
Grouted (GM_1)	2630	2800	1240 1220 1160	1210	3.0	1560 1360 1460	1460	7.0	1350 1280 1640	1420	13.0
Efficiency Coefficient[d]				1.97			1.2			1.07	

Note: 1 psi = 6.9×10^{-3} MN/m^2

a. Compressive strength of 2 in. cubes, average of 10 batches (C.O.V. = 15%)
b. Compressive strength of the grout as calculated from block moulded prisms
c. Based on gross area.
d. The strength ratio of the grouted and similar ungrouted specimens.

planes. In these ungrouted assemblages the interaction depends only on the bonding strength of the mortar which is relatively very small compared to the strength of the block or the mortar, especially for low levels of stresses normal to the bed joint. This explains the low capacity exhibited by the ungrouted prisms under compressive streseses oriented at approximately 15^{o} from the bed joint.

The contribution of grouting towards the increase of the compressive strength is presented in Table 6.2 as an efficiency coeffficient (the ratio of the strength for a grouted prism compared to a similar ungrouted prism). It is shown that this contribution varied with the stress orientation and consequently with the failure mode. The grout had a maximum contribution when shear (joint slip) was the governing mode as the fracture surface crossed the cores which contributed to the overall capacity by their shearing (diagonal tension) strength. This was the case for $\theta \simeq 15^{o}$. However, for the case where shearing along the head joint plane occurred no significant contribution was observed because the fracture plane did not cross the grouted cores. This feature of behaviour is somewhat similar to that of ungrouted and grouted masonry discs under tensile stresses parallel to the bed joint where the failure plane did not cross the columns of grout and consequently no contribution of the grouted cores was developed (see Section 4.2.5.1). The bond strength between the grout and the blocks seems to have a negligible effect.

Figure 6.12 also shows the strengths of the ungrouted prisms calculated on the basis of an arbitrarily defined net area, A_{nr}, calculated as:

$$A_{nr} = \frac{V_n}{V_g} \cdot A_g = 0.67\ A_g \qquad (6.8)$$

where A_g is the gross area of the prism and V_n and V_g are the net and the gross volume of the block, respectively. It is shown that the compression capacity of ungrouted masonry could be higher than that of grouted masonry for the cases of θ between 45^o and 90^o. This finding is consistent with the observed behaviour for the prisms tested under compression normal to the bed joints where the failure mode involves a complex interaction between the shell (blocks and mortar) and the grouted cores as discussed in Section 3.2.4.1.

Figure 6.13 presents the relationships between the ultimate shear stress, τ_a and the normal compressive stress, σ_n, acting along the bed joint at fialure for both ungrouted and grouted masonry. It is shown that up to a certain point, the normal stress helped to increase the shear strength by increasing the joint capacity. At stresses above about 30% of the compressive strength normal to the bed joint, a decrease in the shear capacity occurred. This is attributable to the change of the failure mode from joint slip failure along the bed joint to a shear failure along the head joint plane or to a tensile splitting of the outer shell.

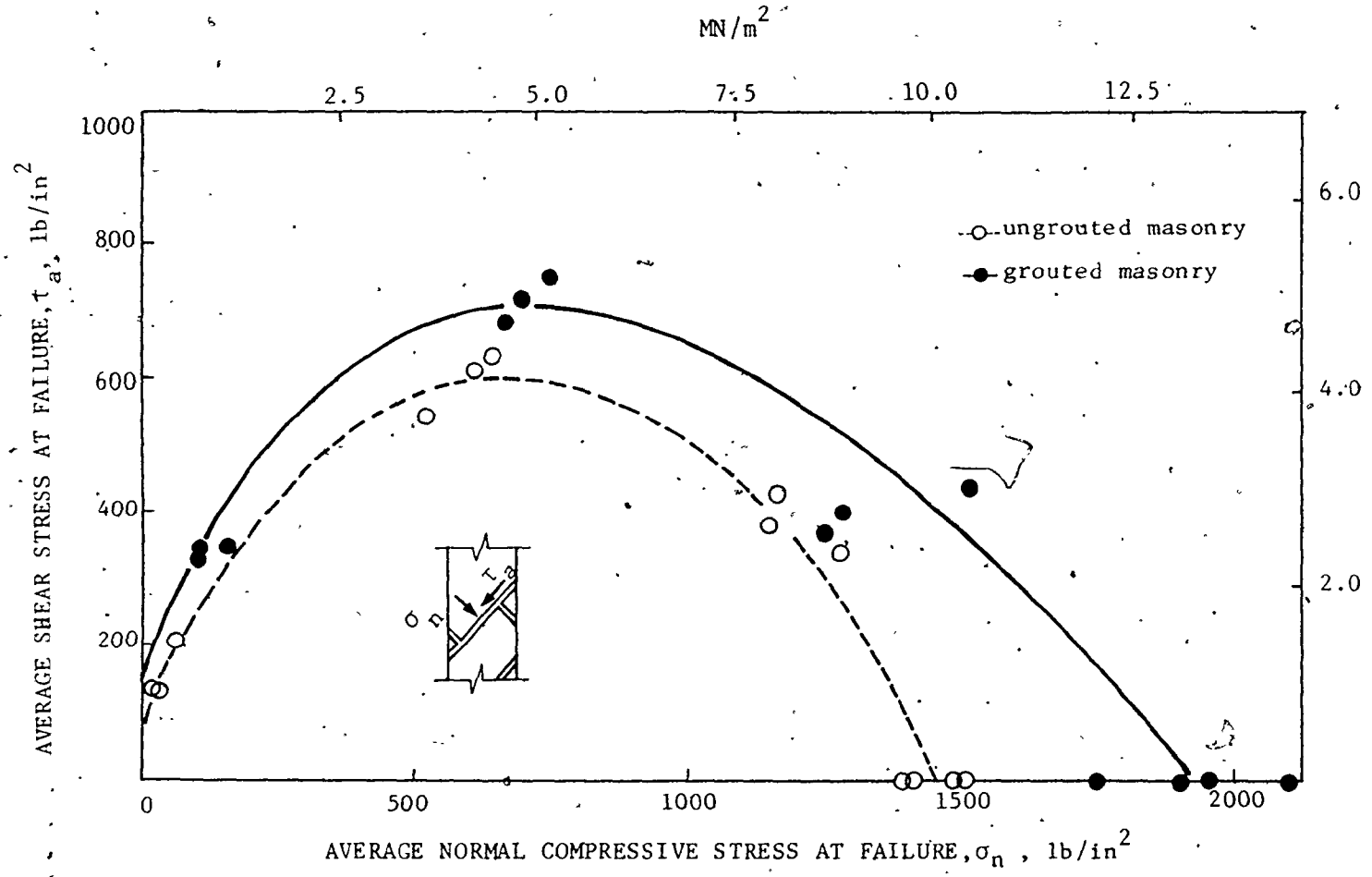

Fig. 6.13 RELATIONSHIPS BETWEEN SHEAR STRESSES AND NORMAL COMPRESSIVE STRESSES ALONG THE BED JOINTS AT FAILURE FOR CONCRETE MASONRY

Hedstrom[20] reported load tests of ungrouted concrete masonry walls with constant wall dimensions, but with the mortar bed joints in 90°, 45° and 0° inclinations from the axial load. The failure for the diagonal patterned walls (45°) built using type S mortar was due to shear along the bed joints. A splitting mode of failure under loads normal and parallel to the bed joints was observed. The strengths of the walls for $\theta = 0^{\circ}$ and $\theta = 45^{\circ}$ were about 75% of those for the $\theta = 90^{\circ}$ case. Hedstrom's results agree with the current observations regarding the failure mode for ungrouted prisms. However, in the current study the strengths of prims having θ equal to 0° and 45° were respectively about 100% and 85% of the strength of prisms having $\theta = 90^{\circ}$. This discrepancy may be due to the fact that the blocks used in Hestrom's walls had a compressive strength parallel to the bed face of 60%-70% of the strength normal to the bed face, whereas for the blocks used in the current investigation the compressive strength was nearly the same in both directions.

Deformation Charactertistics: Figures 6.14 and 6.15 show the stress-strain relationships for ungrouted and grouted masonry prisms respectively under different stress orientations. (The strains in the vertical direction were calculated from the principal strains obtained from analyses of rosette readings.) The curves for $\theta = 90^{\circ}$ were reproduced from Fig. 3.19. The graphs indicate the anisotropic nature of the deformation characteristics of ungrouted and grouted assemblages. However, grouted prisms

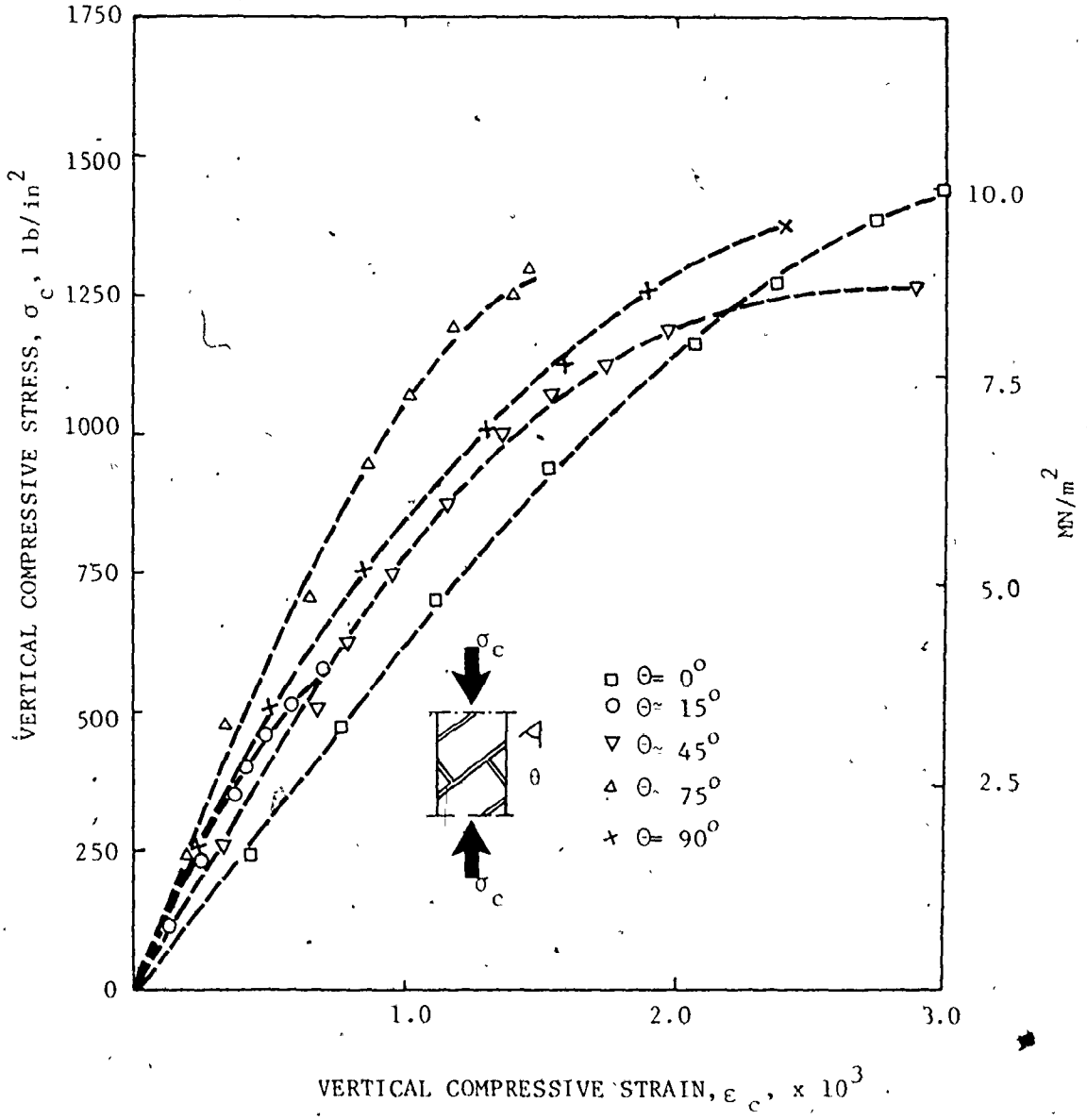

Fig. 6.14 STRESS-STRAIN CURVES FOR UNGROUTED MASONRY PRISMS UNDER OFF-AXIS COMPRESSION

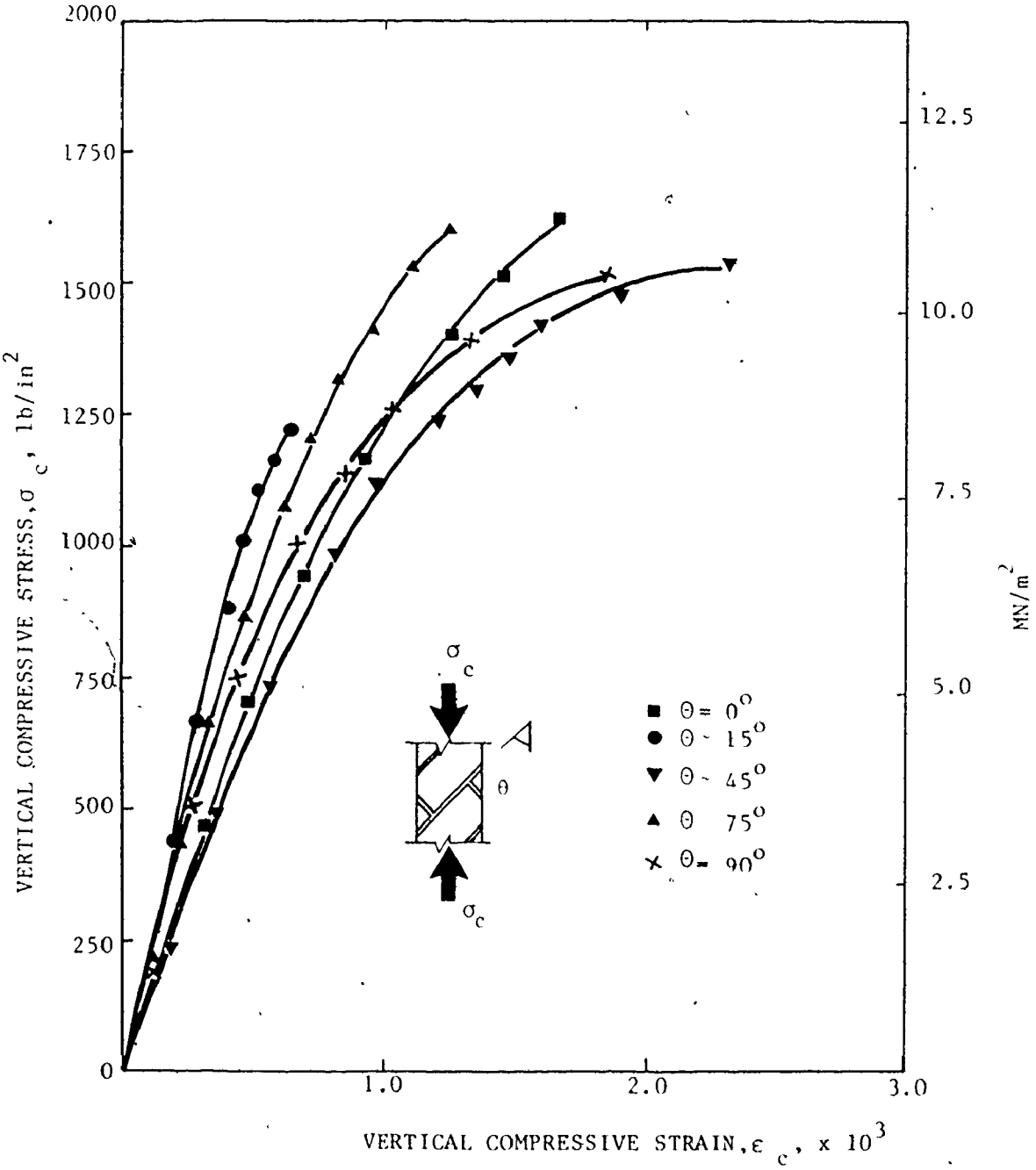

Fig. 6.15 STRESS-STRAIN CURVES FOR GROUTED MASONRY PRISMS UNDER OFF-AXIS COMPRESSION

showed less anisotropy compared to the ungrouted prisms. This is consistent with the strength results presented in Fig. 6.12 where the strengths of the grouted prisms were influenced less by the stress orientation. The results also indicate that grouted assemblages had higher stiffnesses than the ungrouted assemblages. (Stresses were calculated on the basis of the gross area for both types of prisms.)

Figure 6.16 presents the shear stress-shear strain relationships for ungrouted and grouted prisms for diffeerent stress orientations, expressed by the amount of the normal stress, σ_n, developed perpendicular to the bed joints. The shear strains were calculated from the strain rossette readings taken at the centre of the prisms. It is interesing to observe that the compressive stresses normal to the bed joints, σ_n, did tend to influence the shear deformation characteristics of masonry assemblages. This tendency is shown more clearly in Fig. 6.17 which displays the influence of the normal stress, σ_n, on the assemblage modulus of rigidity, G_a. The variation of the modulus of rigidity with the normal stress, σ_n, was more apparent for ungrouted masonry. This indicates a higher degree of anisotropy for ungrouted masonry compared to grouted masonry. These results seem to be consistent with those concerned with the variation of the stiffness as presented previously in Figs. 6.14 and 6.15. Using a linear regression analysis, the shear moduli of ungrouted and grouted masonry, G_{au} and G_{ag}, (lb/in^2), can be expressed as:

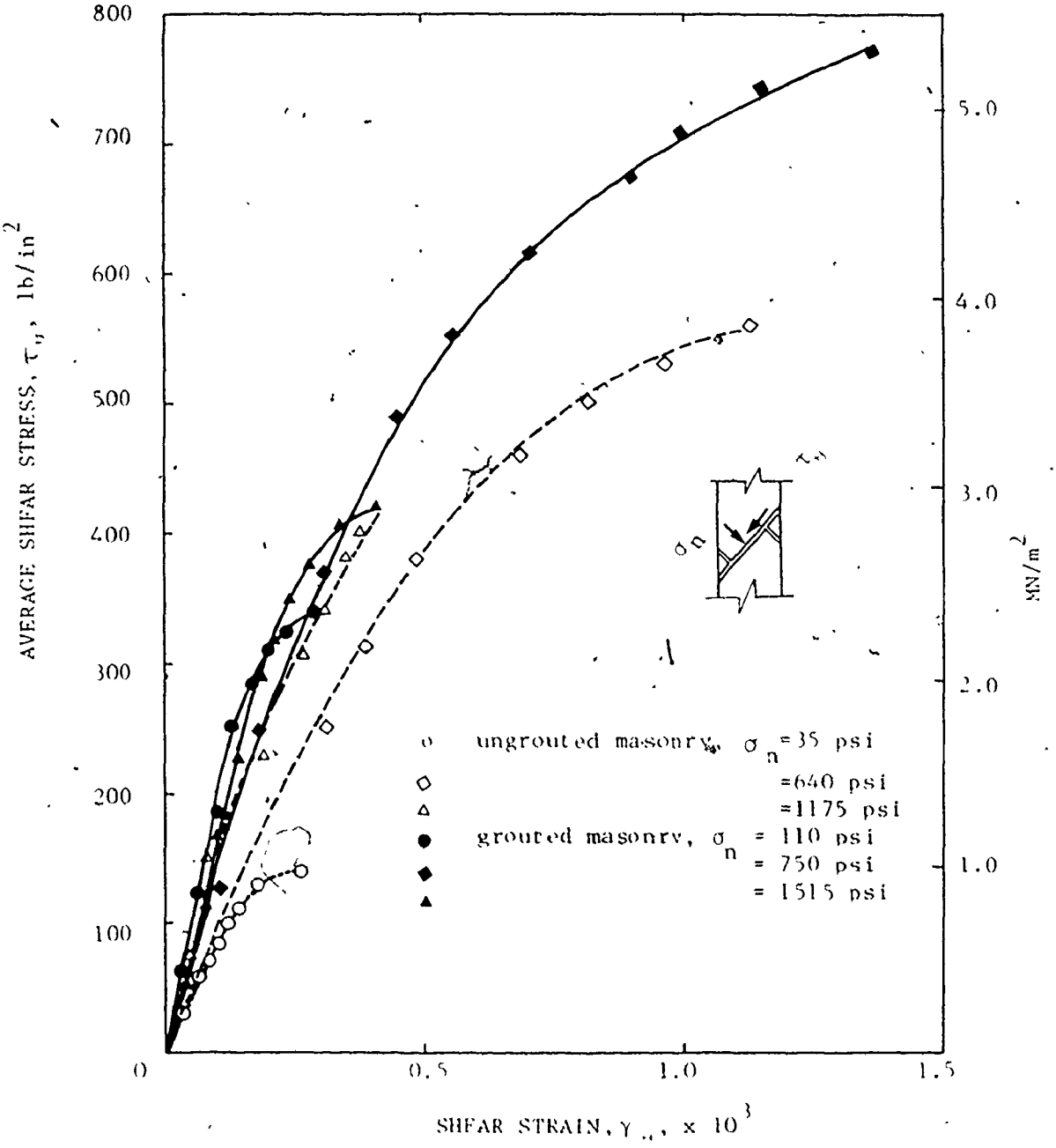

Fig. 6.16 SHEAR STRESS-SHEAR STRAIN RELATIONSHIPS FOR MASONRY PRISMS UNDER OFF-AXIS COMPRESSION

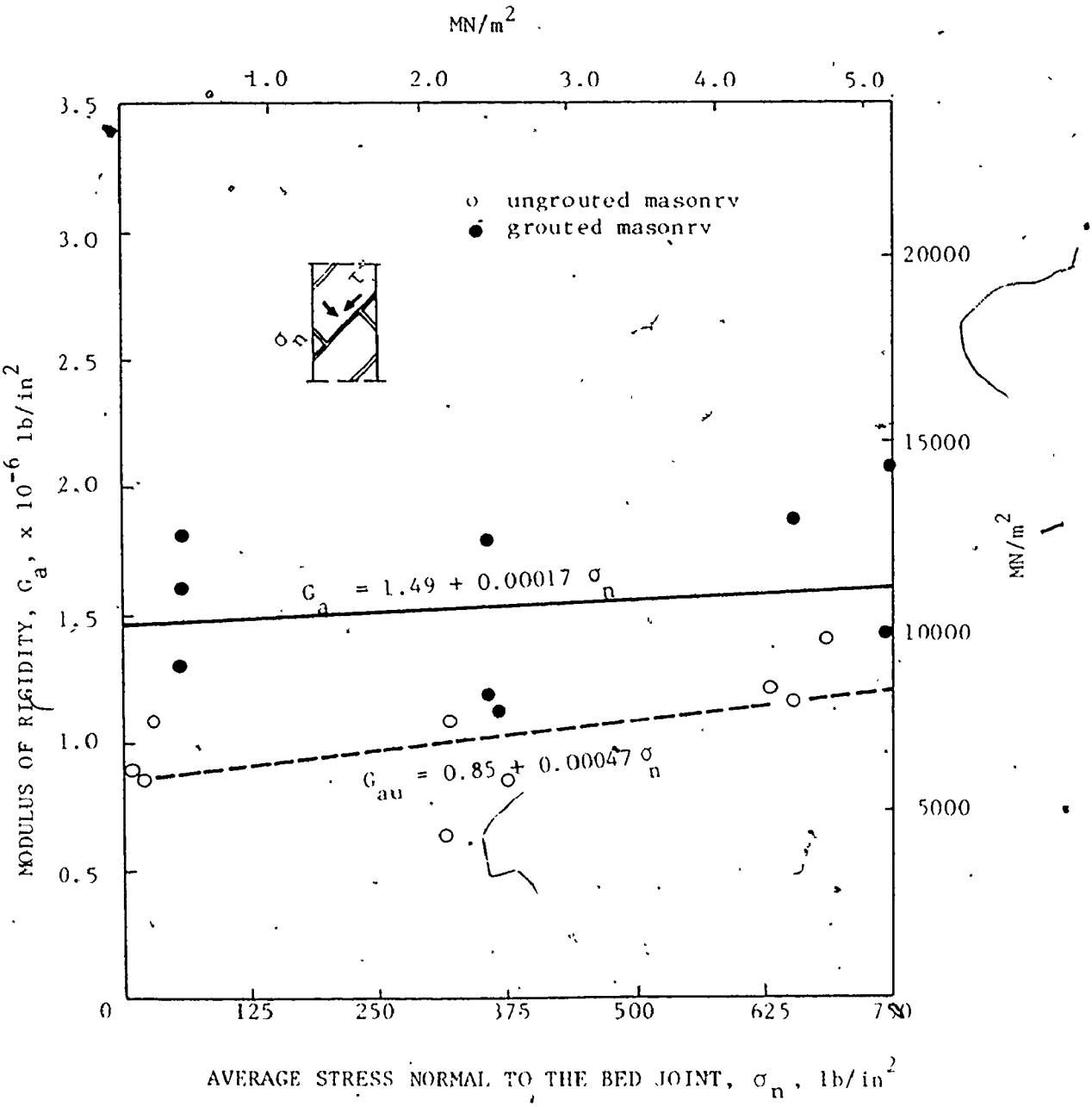

Fig. 6.17 EFFECT OF THE STRESS NORMAL TO THE BED JOINTS ON THE MODULUS OF RIGIDITY OF CONCRETE MASONRY

$$G_{au} = (0.85 + 0.00047\ \sigma_n) \times 10^6 \qquad (6.4)$$

and

$$G_{ag} = (1.49 + 0.00017\ \sigma_n) \times 10^6 \qquad (6.5)$$

where σ_n is the compressive stress normal to the bed joints in lb/in^2. The above expressions indicate that grouted assemblages have a considerably higher shear stiffness compared to ungrouted masonry. (The calculation of shear stresses was based on the gross area for both ungrouted and grouted masonry.) Also, a constant modulus of rigidity for grouted masonry would seem to be reasonable. Sinha and Hendry[49], utilizing experimental results from racking tests of brick shear walls, concluded that the modulus of rigidity increases with the level of precompression (compressive stresses normal to the bed joints). This evidence supports the current results.

More recently, in 1977, Hegemier et al.[21] adopted a similar technique (testing under off-axis compression) to investigate the behaviour of concrete masonry walls under biaxial stresses. No documented test results have been reported yet.

6.2.3 Strength of Ungrouted and Grouted Prisms under Off-Axis Tension Loading

Two panels, 32 by 32 in., were constructed in running bond using the standard blocks and type S_1 mortar. Medium grout, GM_1, was poured into the cores of one panel. From each panel, 3 prisms were made by saw-cutting at 45° from the orthogonal directions as

shown in Fig. 6.7(b). Control specimens were similar to those adopted for the prisms tested under off-axis compression (section 6.2.2.2).

The prisms were tested under tension oriented at 45^{o} from the bed joints using the same technique as the direct tension test of the concrete blocks presented in Section 2.2.1.3. The test set-up and the failures of typical ungrouted and grouted prisms are shown in Fig. 6.18.

The prisms exhibited a tension mode of failure where the fracture surface passed through the head and/or the bed joints a shown in Fig. 6.19. This failure mode indicates the significance of the head joints on the tension capacity of masonry under a biaxial tension state of stress. For grouted masonry, the continuity provided by the grouted cores strengthened the tension capacity normal to the bed joints and hence the head joint became the weakest plane governing the assemblage's capacity (the head joint capacity depends partially on the bonding strength of the mortar which is quite small compared to the tensile strength of the block, mortar, or grout).

Table 6.3 lists the capacities of the ungrouted and grouted prisms along with their control specimens. The strength calculations were based on the gross area for both ungrouted and grouted specimens. The results indicate a considerably higher tension capacity for grouted prisms compared to ungrouted prisms.

(a) Test Set-Up

(b) A Typical Failure of Ungrouted Prisms

(c) A Typical Failure of grouted Prisms

Fig. 6.18 PRISMS TESTED UNDER OFF-AXIS TENSION ($\theta = 45^{\circ}$)

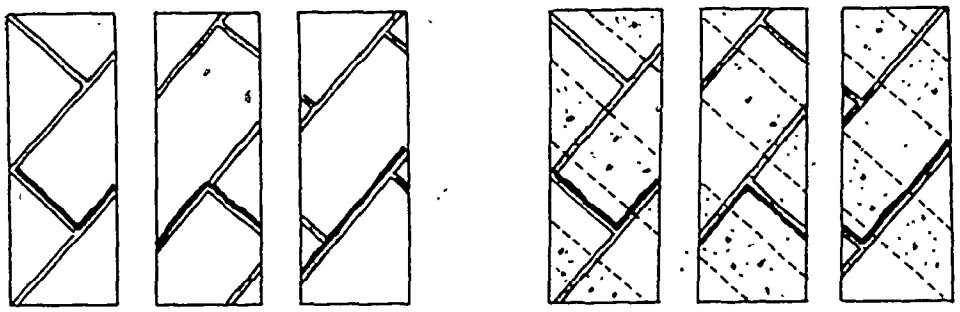

a - ungrouted prisms b - grouted prisms

Fig. 6.19 FAILURE PATTERNS OF UNGROUTED AND GROUTED MASONRY PRISMS UNDER OFF-AXIS TENSION

Table 6.3 TEST RESULTS FOR PRISMS UNDER OFF-AXIS TENSION

Mortar strength[a] psi	Grout Strength		Ungrouted Prisms[d]			Grouted Prisms		
	compression[b] (psi)	tension[c] (psi)	individual (psi)	mean (psi)	c.o.v. (%)	individual (psi)	mean (psi)	c.o.v. (%)
2630	3800	343	15 28 24	22	29.8	60 74 82	72	15.5

Note: 1 psi = 6.9×10^{-3} MN/m^2

a. compressive strength of 2-in cubes, average of 4 batches (c.o.v. = 7.6%)

b. compressive strength of grout as calculated from block moulded prisms

c. Tensile strength of grout as calculated from splitting of prisms

d. based on the gross area

Comparison of these capacities with those under splitting along the diagonal obtained from tests of the masonry discs, presented in Tables 4.1 and 4.2, shows higher capacities for the latter case compared to the former. This is attributed to the different stress conditions which resulted at the critical bed and head joints for the two cases. Under tensile loading oriented at 45^{o} from the bed joints (off-axis tension), equal tension and shear stresses were developed along the critical planes whereas under diagonal tension (splitting test of discs at 45^{o}), equal compressive and shear stresses were developed along these joints. The compressive stresses normal to the critical planes increased the shear capacities along these planes and hence prevented joint slip failure from occuring and thereby increased the assemblage's capacity. In the case of off-axis tension, the tensile stresses developed normal to the bed joints caused a decrease in the shear strength of the joints[2] and consequently a reduction in the overall capacity. This comparison of behaviour illustrates the important feature which is that the principal tensile strength concept is not valid for masonry assemblages and that the governing stress condition should depend on the relative magnitudes of the normal and shear stresses acting along the critical head and bed joints. This is a typical characteristic of a composite material.

6.3 Failure Hypotheses for Masonry Assemblages

6.3.1 Possible Modes of Failures

The results presented in the previous section indicated a strong relationship between the mode of failure and the assemblage's capacity. The failure modes of masonry assemblages are primarily dependent upon the relative magnitudes of the normal and shear stresses along the critical bed and head joints.

Based on the current investigation, the assemblage failures could be classified in one of the following three general categories:

1 - A tension mode of failure whhich is distinguished by:

a) splitting of the outer shell under high compression normal to the bed joints (see Section 3.2.4.1), or splitting along the head joints and the face shells under tension normal to the head joints. (The capacity in this case will be mainly governed by the strength of the block as the grout strength has no significant influence.)

b) diagonal tension failure under critical combinations of normal and shear stresses acting on the critical head and bed joints. (The capacity will be mainly governed by the splitting tensile strength of the block, mortar, and grout), and

c) separation failure at the block-mortar interfaces along the bed joint under tensile stresses normal to it with or without shear stresses. (The strength is governed by the tensile bond strength of the mortar and the tension capacity of the grout.)

2 - A shear mode of failure which is distinguished by:

a) debonding or joint slip failure at the block-mortar interfaces occurring under zero or low compression stresses normal to the bed joints and accompanied by high shear stresses. (The capacity is governed by the shear bond strength of the mortar and the shearing capacity of the grout.)

b) shearing along the head joint direction so that the crack crosses the face shells of the blocks and the head joints. (The overall capacity is determined from the block strength and the mortar bond strength. The grout strength has no significant influence on the assemblage's capacity in this case.)

3 - A mixed shear-tension mode of failure which probably occurs for medium levels of shear stresses accompanied by similar values of normal stresses acting along the head and bed joints..

6.3.2 Existed Failure Hypotheses for Masonry Assemblages

The failure hypotheses for masonry[8,49,58] are related to the failure theories for isotropic materials such as Coulomb's theory of interenal friction, the maximum stress theory, and Mohr's theory of failure[38]. These theories have been proposed to predict failures under particular stress conditions. No general failure theory has been published to describe failure envelopes for masonry assemblages under combined stresses.

For a joint slip failure, it has been shown that Coulomb's thoery of internal friction in the form of Equation (5.1) can

reasonably predict the joint capacity of solid brick[29,49] and block[29] masonry. The current investigation indicates the validity of this equation for ungrouted and grouted concrete masonry as well (see Section 5.2.3.6). It should be noted that this equation is only valid for cases of low precompression, σ_n, (i.e. up to about 0.1 of the compressive strength of the assemblage normal to the bed joint, f'_m). For higher values of normal stress, this expression no longer applies because of the change of the failure mode[47].

For a joint slip failure under a state of shear-tension stresses, Coulomb's theory is not applicable because of the limited capacity of the material under tension normal to the bed joint where the tension mode is the governing criterion. Cowan's theory and the modified Cowan theory were proposed to express the failure envelope of brittle materials under a state of shear tension stresses[11] (see Fig. 6.20). Balachandran[2], utilizing experimental results for masonry joints under combined stresses, suggested the circular relationship shown in Fig. 6.20 to express the joint capacity for ungrouted and grouted masonry under a shear-tension state of stress.

When the tension or the tension-shear mode of failure is the governing mode, the problem becomes rather complicated because the fracture plane is not predetermined and the influence of the blocks, mortar, and grout characteristics should be considered. The assemblage capacity will be governed by the different

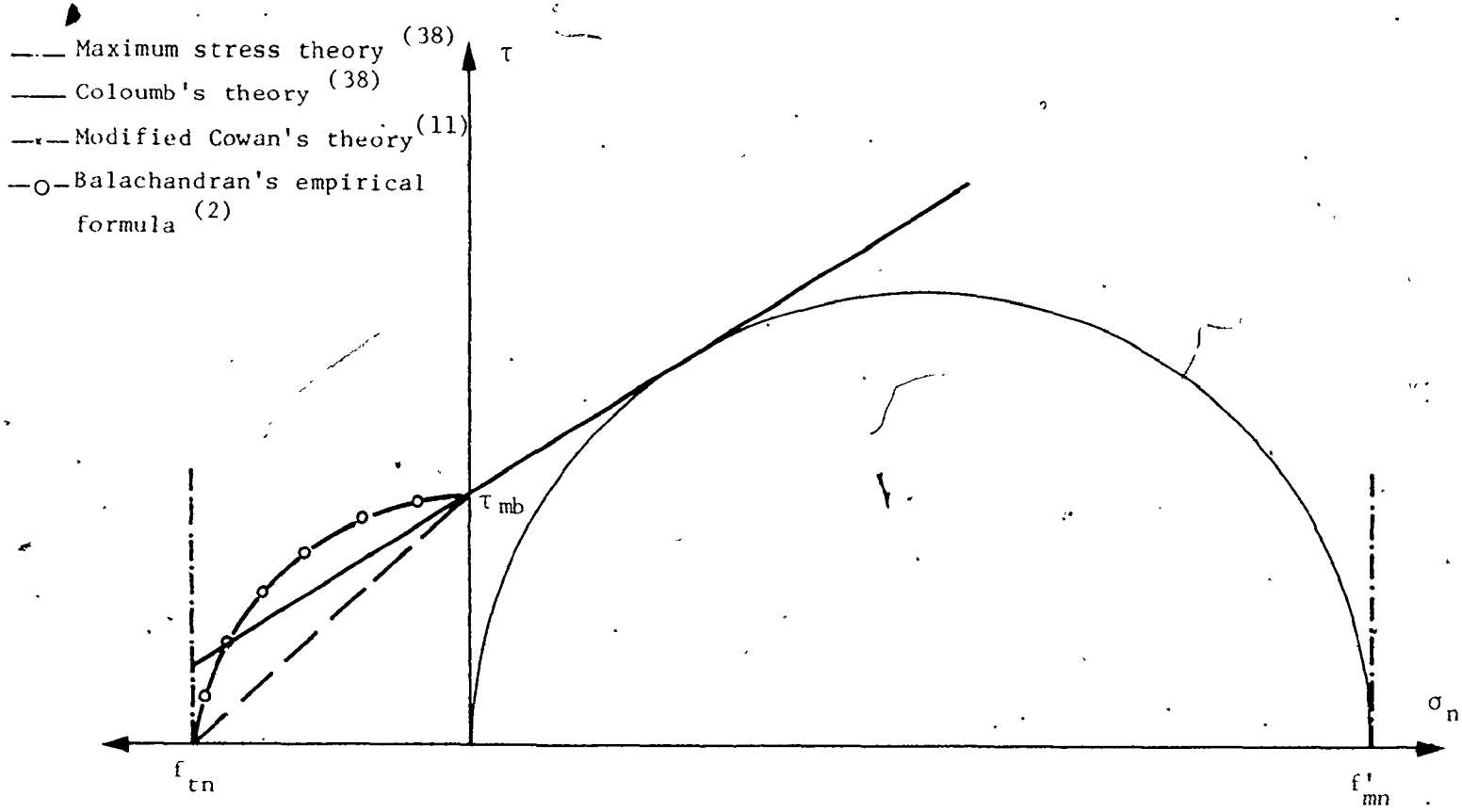

Fig. 6.20 ILLUSTRATION OF DIFFERENT FAILURE THEORIES FOR SHEAR AND NORMAL STRESS ALONG THE FRACTURE PLANE (BED JOINT DIRECTION)

combinations of normal and shear stresses along the critical head and bed joints.

Sinha and Hendry[49] adopted the criterion of maximum tensile stress to determine the capacity of brick masonry shear walls under shear, τ, and precompression, σ_n. They used a constant tensile strength value,

$$f_t = \sqrt{\frac{\sigma_y^2}{4} + \tau^2} - \frac{\sigma_y}{2} = 2\sqrt{f'_{mn}} \qquad (6.6)$$

where f_t is the principal tensile stress and f'_{mn} is the brick compressive strength normal to the bed joint. Two values of τ were considered and Equation (6.6) was rewritten as:

$$f_t = \sqrt{\frac{\sigma_{y1}^2}{4} + (\tau_0 + \mu\ \sigma_{y1})^2} - \frac{\sigma_{y1}}{2} \qquad (6.7)$$

for $\tau = \tau_0 + \mu\ \sigma_{y1}$, and

$$f_t = \sqrt{\frac{\sigma_{y2}^2}{4} + (\mu\ \sigma_{y2})^2} - \frac{\sigma_{y2}}{2} \qquad (6.8)$$

for $\tau = \mu\ \sigma_{y2}$

Knowing τ_0, f_t, and μ, σ_{y1} and σ_{y2} can be calculated. It was assumed that failure would occur by reaching the maximum tensile strength for compression stress values between σ_{y1} and σ_{y2}. Below and above this range failure would be governed by shear at the brick-mortar interfaces. It was stated that precompression

greater than σ_{y2} would suppress the inherent diagonal tension failure. The authors assumed a constant value for the maximum tensile strength. It has been shown that this assumption is not valid for masonry when it is considered as a composite material[28]. The proportionality constant in Equation (6.6) relating f_t and $\sqrt{f'_m}$ would vary with the various states of stresses developed by different test techniques along the critical bed and head joints. Values ranging from 2 to 4.5 were reported for brick masonry[17]. The proposed approach predicts the shear capacity of the joint for $\sigma_y \geq \sigma_{y2}$, but it does not predict the capacity of the assemblage. The authors proposal could be applied to predict the shear strength of masonry shear walls where shear and normal stresses acting along the bed joint will be developed, but the proposed criterion can not be applied to a general biaxial state of stress. Brochelt[6] also adopted the maximum tensile stress theory to express the failure of brick masonry assemblages.

Yokel and Fattal[58], in an attempt to propose a failure criterion for brick masonry under combined stresses, adopted Mohr's theory of failure which was developed for isotropic materials. A linear relationship between the major and minor stresses (principal stresses) was considered. The material constants for Mohr's envelope are the strengths under uniaxial compression and uniaxial tension. Because masonry is an anisotropic material, the strengths for both compression and tension vary with the orientations of the stress with respect to

the principal material directions. The authors adopted the tensile strength as the apparent major stress at failure when the principal compressive stress is equal to zero. From the stresses developed at the centre of masonry walls at failure, point B in Fig. 6.21(a) was established. By considering f'_m to be a constant value, (point A in the figure), the intersection of the straight line joining points A and B with the vertical axis provides the apparent tensile strength, σ_1. However, the authors stated that for a more general application of their hypothesis, the directional variation of the splitting tensile strength should be considered. The authors' proposal is a very approximate approach having the following drawbacks:

1 - Mohr's theory of failure, like other failure theories for isotropic materials, was derived on the basis of the invarient state of stress concept where the principal stresses at any orientation will express the stress condition[38]. This concept, which was the basis for the authors' approach, is not valid for composite materials[30], where there are critical planes (weak planes) which will influence the location of the failure plane and consequently the assemblage capacity.

2 - Mohr's theory assumes that a material (isotropic and homogenous) may fail either through slip or fracture when either the shearing stress, τ, in the plane of the slip has increased to a certain value which will depend on the normal stress, σ_n, acting across the same plane or when the largest stress has reached a

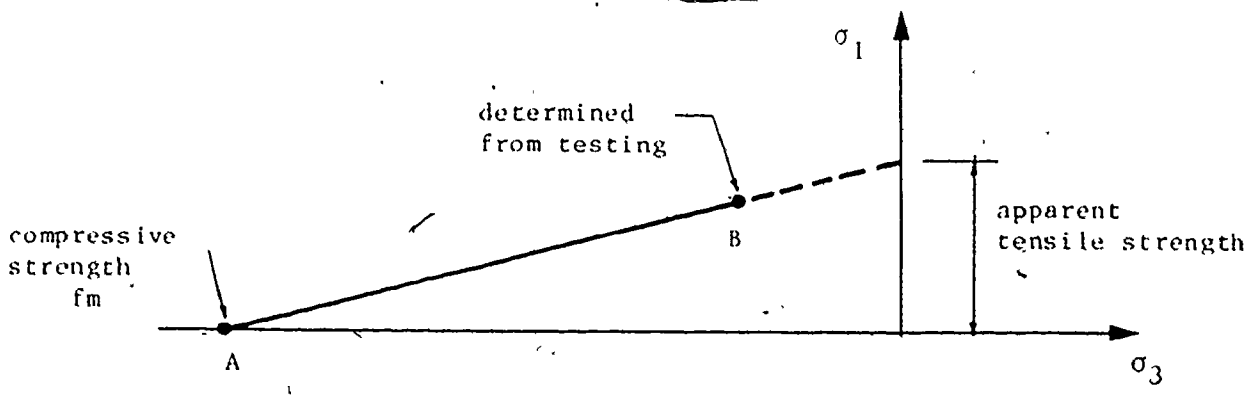

a - Failure Envelope Adopted by Yorkel and Fattal [58] using Mohr's Theory

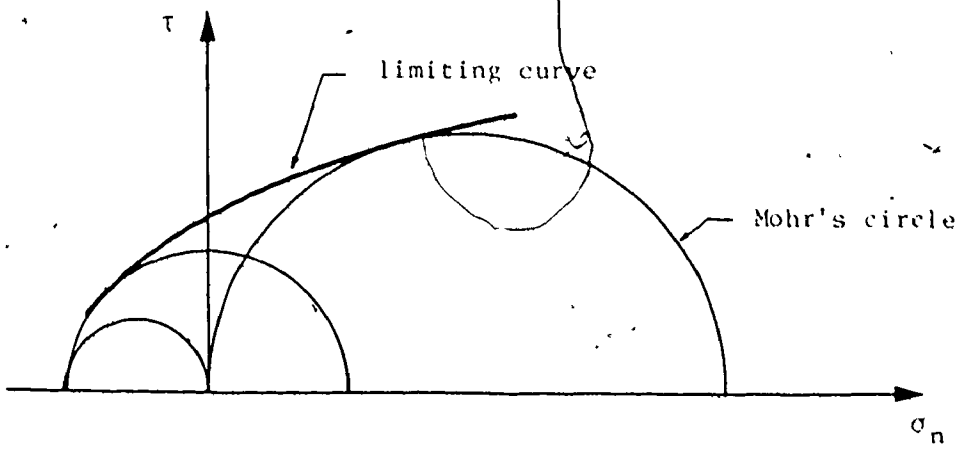

b - Limiting Curve for Mohr's Theory [32]

Fig. 6.21 MOHR'S THEORY OF FAILURE

limiting value which is dependent on the properties of the material. The limiting curve, shown in Fig. 6.21(b), is expressed as:

$$\tau = f(\sigma_n) \qquad (6.9)$$

The actual shape of the limiting curve can vary considerably according to the ratio of the uniaxial compressive strength to the uniaxial tensile strength of the material. It has been shown[6], experimentally, that this curve can be approximated by a straight line for concrete. However, for masonry, the strength ratio is not constant but varies with the stress orientations. Therefore, the assumption of a straight line relationship is questionable.

3 - The compressive strength, f'_m, which was taken as a constant value, has been shown to vary with the stress orientation (see Section 6.2). Therefore, the directional variation of both the compression and tension strengths should be considered.

6.3.3 Failure Theories for Composite Materials.

6.3.3.1 Introduction: Composite materials have many characteristics that are different from more conventional engineering materials which are usually characterized by their homogenous and isotropic nature. In contrast, composite materials are often both inhomogenous (or hetrogenous) and nonisotropic (orthotripic or, more generally, anisotropic). An orthotropic body has material properties which are different in three mutually perpendicular directions at a point in the body and, further, have

three mutually perpendicular planes of material symmetry (principal material directions). thus, the properties are function of the stress orientation at a point in the body. An anisotropic body has material properties which are different in all directions and there are no planes of symmetry for material properties. Again, the properties are a function of the stress orientation at a point in the body.

For orthotropic material, and since it is physically impossible to obtain the strength characteristics for all possible directions, theoretical failure envelopes have been proposed to express the strength of the material for any state of stress in terms of its strength characteristics in the principal material directions, X, Y, and Z. When the strength characteristics in the principal material directions are considered, the well-known concepts of principal stresses and principal strains are of no value[30]. Moreover, because the strength of orthotropic material is lower in one direction than another, the highest stress may not be the governing failure stress.

The following are some of the more commonly used failure theories for orthotropic materials:

6.3.3.2 Maximum Stress Theory[30]: In the maximum stress theory, the stresses in the principal material directions must be less than the respective strengths. Otherwise fracture is said to have occurred when for tensile stresses,

$$\sigma_x > F_{tx}$$
$$\sigma_y > F_{ty} \qquad \ldots\ (6.10)$$

For compressive stresses,

$$\sigma_x < F_{cx}$$
$$\sigma_y < F_{cy} \qquad \ldots\ (6.11)$$

and for shear stresses

$$|\tau_{xy}| > F_{sxy} \qquad \ldots\ (6.12)$$

where σ_x and σ_y are the normal stresses acting in the principal material directions, τ_{xy} is the applied shear stress, F_{tx} and F_{ty} and F_{cx} and F_{cy} are the tensile and compressive strength characteristics in compression and tension, respectively, and F_{sxy} is the shear strength in the principal material directions.

If any one of the foregoing inequalities is not satisfied, then it is considered that the material has failed. It should be noted that there is no interaction between the modes of failure in this criterion and that there are actually three independent subcriteria.

6.3.3.3 Hill-Tasia Theory[30]: Hill proposed a yield criterion for anisotropic material in the form:

$$(G+H)\,\sigma_x^2 + (F+H)\,\sigma_y^2 + (F+G)\,\sigma_z^2 - 2H\,\sigma_x\sigma_y - 2G\,\sigma_x\sigma_z$$
$$- 2F\,\sigma_y\sigma_z + 2L\,\tau_{yz}^2 + 2M\,\tau_{xy}^2 + 2N\,\tau_{xy}^2 = 1 \qquad \ldots\ (6.13)$$

This anisotropic yield criterion was also used by Tasia in the spirit of being the limit of linear elastic behaviour. Thus, Hill's yield strengths F, G, H, L, M, and N will be regarded as failure strengths. Hill's theory is an extension of Von Mises' isotropic yield criterion.

The failure strength parameters F, G, H, L, M, and N were related to the strength characteristics F_x, F_y and F_{xy} by Tsai as follows:

$$G + H = 1/F_x^2$$

$$F + H = 1/F_y^2 \qquad \ldots\ldots (6.14)$$

$$F + G = 1/F_z^2$$

$$2L = 1/F_{yz}^2 \qquad 2M = 1/F_{xz}^2 \qquad 2N = 1/F_{xy}^2 \qquad \ldots\ldots (6.15)$$

then, upon combination of the Equations in (6.14), the following relationships between F, G, and H and F_x, F_y, and F_z result:

$$2H = 1/F_x^2 + 1/F_y^2 - 1/F_z^2$$

$$2G = 1/F_x^2 + 1/F_z^2 - 1/F_y^2 \qquad \ldots\ldots (6.16)$$

$$2F = 1/F_y^2 + 1/F_z^2 - 1/F_x^2$$

substituting Equation (6.14) through Equation (6.16) in Equation (6.13) yields the following Hill-Tsia fracture criterion for orthotropic material:

$$(1/F_x^2)\,\sigma_1^2 + (1/F_y^2)\,\sigma_2^2 + (1/F_z^2)\,\sigma_3^2 - (1/F_x^2 + 1/F_y^2 - 1/F_z^2)$$

$$\sigma_1\sigma_2 - (1/F_x^2 + 1/F_z^2 - 1/F_y^2)\,\sigma_1\sigma_3 + 1/F_{yz}^2\,\tau_{23}^2 + 1/F_{xy}^2\,\tau_{12}^2 = 1 \quad \ldots\ldots (6.17)$$

This criterion has an advantage over the maximum stress theory in that it considers the interaction between the failure strengths. In addition, it provides a continuous smooth failure envelope rather than possessing cusps. However, this criterion does not take into cosnideration the difference between the tensile and compressive strengths which characterizes the brittle materials, and consquently it is not applicable for a tension-compression biaxial state of stress wherein this characteristic is of prime importance. It can be applied for either a biaxial compression or a biaxial tension state of stress.

6.3.3.4 Hoffman Theory[25]: Hoffman proposed a phenomenological fracture condition to predict the strength of brittle orthotropic materials under multiaxial states of stress.

In developing his fracture condition, Hoffman followed the pattern of yield condition adopted by Hill for orthotropic material in the form:

$$F(\sigma_x - \sigma_z)^2 + G(\sigma_z - \sigma_x)^2 + H(\sigma_x - \sigma_y)^2$$

$$+ 2L\,\tau_{yz}^2 + 2M\,\tau_{zx}^2 + 2N\,\tau_{xy}^2 = 1 \quad \ldots\ldots (6.18)$$

where F, G, H, L, M, and N are the material parameters. To account for the variously differing tension and compression strengths that characterize brittle behaviour, Hoffman introduced linear terms in Equation (6.18) which are odd functions of σ_x, σ_y, and σ_z. This leads to the following fracture condition:

$$c_1 (\sigma_y - \sigma_z)^2 + c_2 (\sigma_z - \sigma_x)^2 + c_3 (\sigma_x - \sigma_y)^2 + c_4 \sigma_x + c_5 \sigma_y + c_6 \sigma_z + c_7 t_{yz}^2 + c_8 \tau_{zx}^2 + c_9 \tau_{xy}^2 = 1 \quad \ldots\ (6.19)$$

where $C_1 \ldots C_9$ are nine material parameters, which are uniquely determined from the nine basic strength characteristics, namely:

The three uniaxial tensile strengths: F_{tx}, F_{ty}, F_{tz}

The three uniaxial compressive strengths: F_{cx}, F_{cy}, F_{cz}

The three pure shear strengths: F_{syz}, F_{szx}, F_{sxy}

The following expressions can be readily verified as follows:

$$C_1 = \frac{1}{2} ((F_{ty} F_{cy})^{-1} + (F_{tz} F_{cz})^{-1} - (F_{tx} F_{cx})^{-1})^{-1} \quad (6.20)$$

C_2 and C_3 by permutation of x, y, z

$$C_4 = (F_{tx})^{-1} - (F_{cx})^{-1} \quad (6.21)$$

C_5 and C_6 by permutation of x, y, z

$$C_7 = (F_{syz})^{-1} \quad (6.22)$$

C_8 and C_9 by permutation of x, y, z

6.3.4 Applicability of the Failure Theories for Composite Materials to Masonry Assemblages

6.3.4.1 Introduction: It has been shown in the current experimental study that the bed and head joint directions are the critical planes where failure will probably be initiated. The mortar bed joints, because of their continuous nature, divide the media into layers of equal thickness and hence give masonry the appearance of a laminated composite material.

The bed and head joint directions are assumed to be the planes of strength symmetry (orthogonal principal materials directions, x and y) where the strength characteristics have to be determined. However, because there is no transverse symmetry, the strength characteristics should also be evaluated in the z-direction (see Fig. 6.22) to be able to fully express the behaviour of the composite under a multiaxial state of stress (in the Hill-tsia theory and the Hoffman theory, the strength characteristics in the z-direction were shown to be part of the boundary conditions).

6.3.4.2 Strength Characteristics of Masonry in the z-Direction: It is assumed that the mortar head joint will have very little effect on the compressive and tensile strengths in the z-direction for either ungrouted or grouted masonry since the joint dimension normal to the applied load is quite small (about 5% of the cross-sectional area) and thus it can be considered as part of the block.

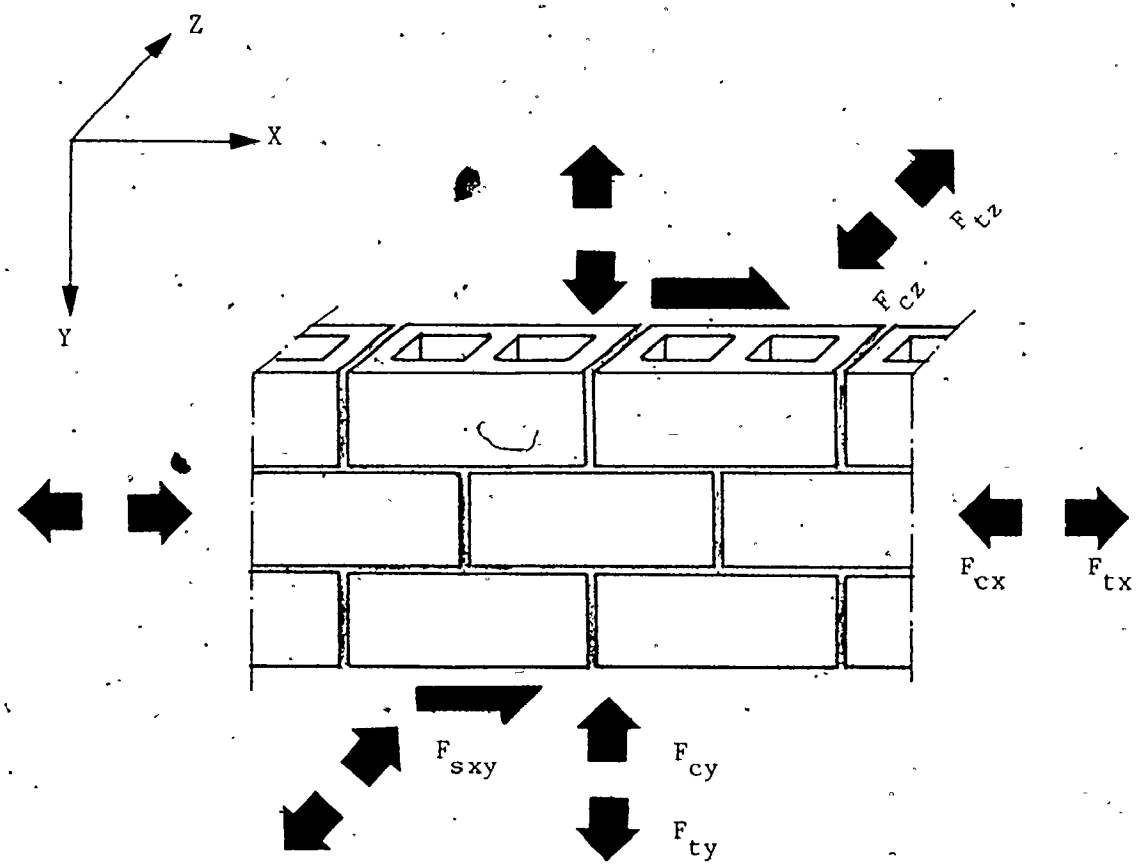

Fig. 6.22 ILLUSTRATION OF STRENGTH CHARACTERISTICS FOR MASONRY AS A COMPOSITE MATERIAL UNDER MULTIAXIAL STATES OF STRESS

An experimental program was conducted, in conjunction with that of prisms tested under off-axis loading, to investigate the compressive strength of ungrouted and grouted masonry in the z-direction. Since the influence of the mortar joints was assumed to be insignificant in this case, the assemblage was modelled by half blocks cut from kerfed units and tested normal to the faces under axial compression as shown in Fig. 6.23. Medium grout, GM_1, was used for grouted specimens.

Ungrouted specimens failed by shearing of the side shells across their thicknesses. For grouted specimens, a similar shear failure of the shells was observed (see Fig. 6.23). The failure planes passed through the block-grout interfaces which seem to be the weakest planes. The grout in this case acts mainly as a filler to distribute the stresses over the gross loaded area.

The test results are listed in Table 6.4. It is shown that even when the grout was stronger than the block, the strengths of the grouted specimens, based on the gross area, were less than those for ungrouted specimens, based on the net area (in this direction, the net to gross area ratio is equal to 0.29). This behaviour may be attributed to the possible lack of full interaction between the block and the grout at high stress levels due to the weak bond at their interfaces. This reduction in the strength of grouted specimens seems consistent with the mode of failure where the fracture planes passed through the interfaces. It has to be noted that the strengths in the z-direction for both

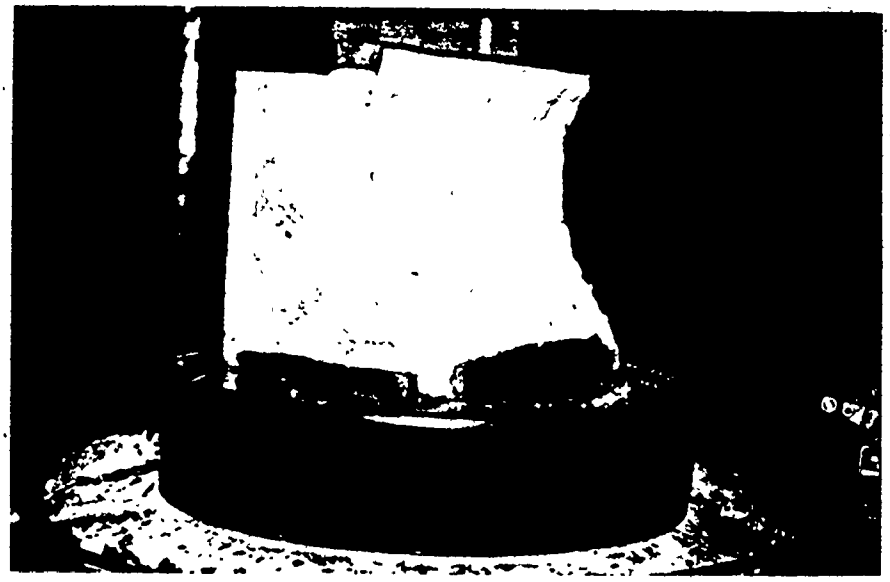

Fig. 6.23 A TYPICAL FAILURE OF GROUTED SPECIMENS TESTED UNDER COMPRESSION IN THE Z-DIRECTION

TABLE 6.4

COMPRESSIVE STRENGTH RESULTS IN THE Z-DIRECTION

Type	Grout Strength[a]	Assemblage strength[b]		
		Individual (psi)	Mean (psi)	C.O.V. (%)
ungrouted		1290 1150 1230	1220	5.7
grouted	3800	2530 2940 3300	2920	13.1

Note: 1 psi = 6.9×10^{-3} MN/m^2

a. grout compressive strength as calculated from block moulded prisms

b. based on gross area

ungrouted and grouted masonry are higher than those in the x and y directions. This increase in the strength is due to the insignificant effect of the mortar joints and the confining stresses introduced in the test specimens.

The tensile strength of ungrouted masonry was considered to be equal to the block tensile strength since the mortar joint's influence was ignored. It was shown in the splitting tests of masonry discs that the grouted cores did not provide any significant contribution to the assemblage tensile strength since the fracture plane did not cross the grouted cores. Therefore, the tensile strength of grouted masonry in the z-direction was

also considered to be equal to the block tensile strength (calculated on the basis of gross area). The splitting tensile strength of the block was adopted to represent its tensile strength.

6.3.4.3 Comparison between the Theoretical Failure Envelopes and the Experimental Results for Prisms under Off-Axis Loading: The prism test results for off-axis compression and tension loading, presented in Section 6.2, provide the capacities of ungrouted and grouted masonry assemblages under different combinations of biaxial stresses applied in the principal material directions (the bed and head joint directions). This data will be used to examine the applicability of the different failure theories for composite materials (presented in Section 6.3.3) to predict the strength of masonry assemblages under biaxial stresses.

The experimental results for prisms under axial compression normal and parallel to the bed joints (presented in Sections 3.2.4.1 and 6.2.1, respectively), discs under splitting loads (presented in Section 4.2.5.2), and assemblages under shearing along the joints (presented in Section 5.2.3.3) provide the strength characteristics of ungrouted and grouted masonry in the orthogonal directions, x and y. These strength characteristics along with those in the z-direction (presented in the previous section) are listed in Table 6.5 for ungrouted and grouted masonry.

Figures 6.24, 6.25, and 6.26 are presented to facilitate

TABLE 6.5

STRENGTH CHARACTERISTICS OF MASONRY IN THE PRINCIPAL MATERIAL DIRECTIONS

Type[a]	principal material direction	Compression[b] (psi)	Tension[b] (psi)	Shear[b] (psi)
ungrouted	x	1390	113	44
	y	1480	33	
	z	1220	53	
grouted	x	1990	123	134
	y	1940	113	
	z	2920	53	

Note: 1 psi = 6.9×10^{-3} MN/m^2

a. Type S_1 mortar and GM_1 grout

b. based on gross area

comparisons between the experimental results for ungrouted and grouted prisms under off-axis compression and the theoretical failure envelopes predicted by the maximum stress theory, the Hill-Tsai theory, and the Hoffman theory, respectively. There is poor agreements between the theoretical failure envelopes and the experimental results, particularly for the applied stress oriented at 45° from the bed joint. This is probably attributable to the very low values of the shear strengths of the assemblages along the mortar bed joints compared to the compressive strengths in the orthogonal direction, considering that these failure theories do not take into account the interaction between the shear capacities of the joints and the normal compressive stresses perpendicular to

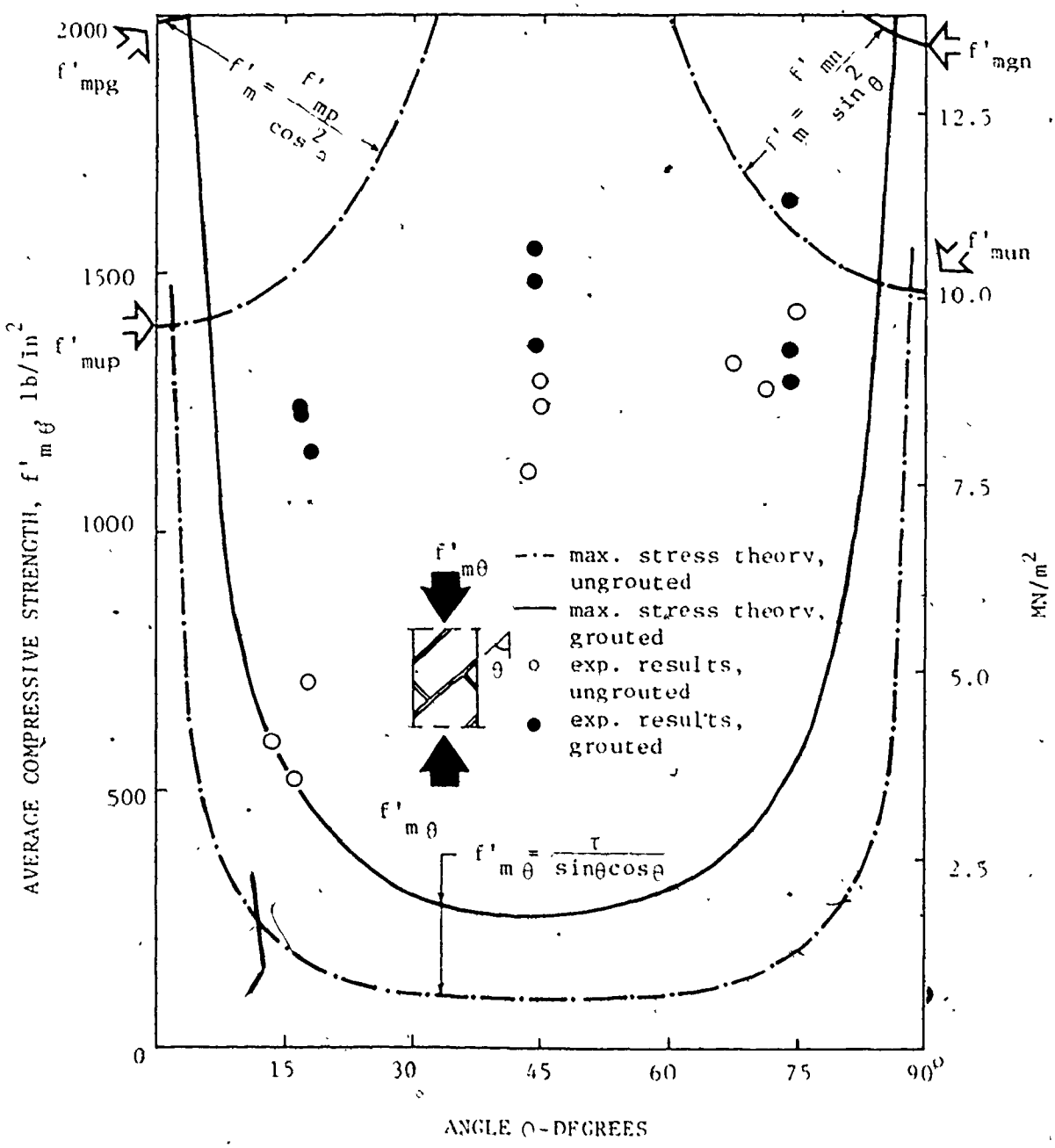

Fig. 6.24 COMPARISON BETWEEN THE MAXIMUM STRESS THEORY OF FAILURE AND THE EXPERIMENTAL RESULTS FOR PRISMS UNDER OFF-AXIS COMPRESSION

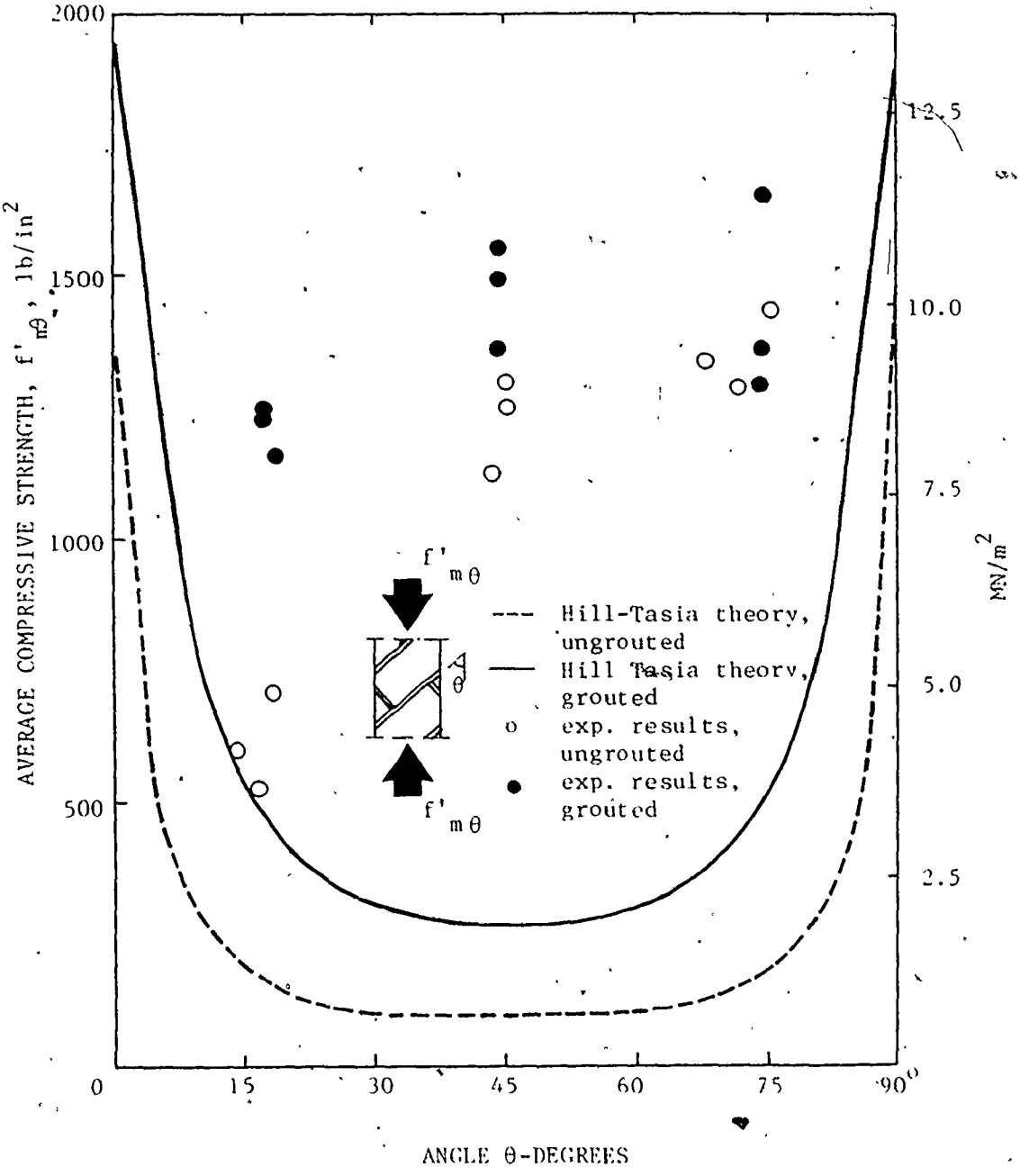

Fig. 6.25 COMPARISON BETWEEN THE HILL-TASIA THEORY OF FAILURE AND THE EXPERIMENTAL RESULTS FOR PRISMS UNDER OFF-AXIS COMPRESSION

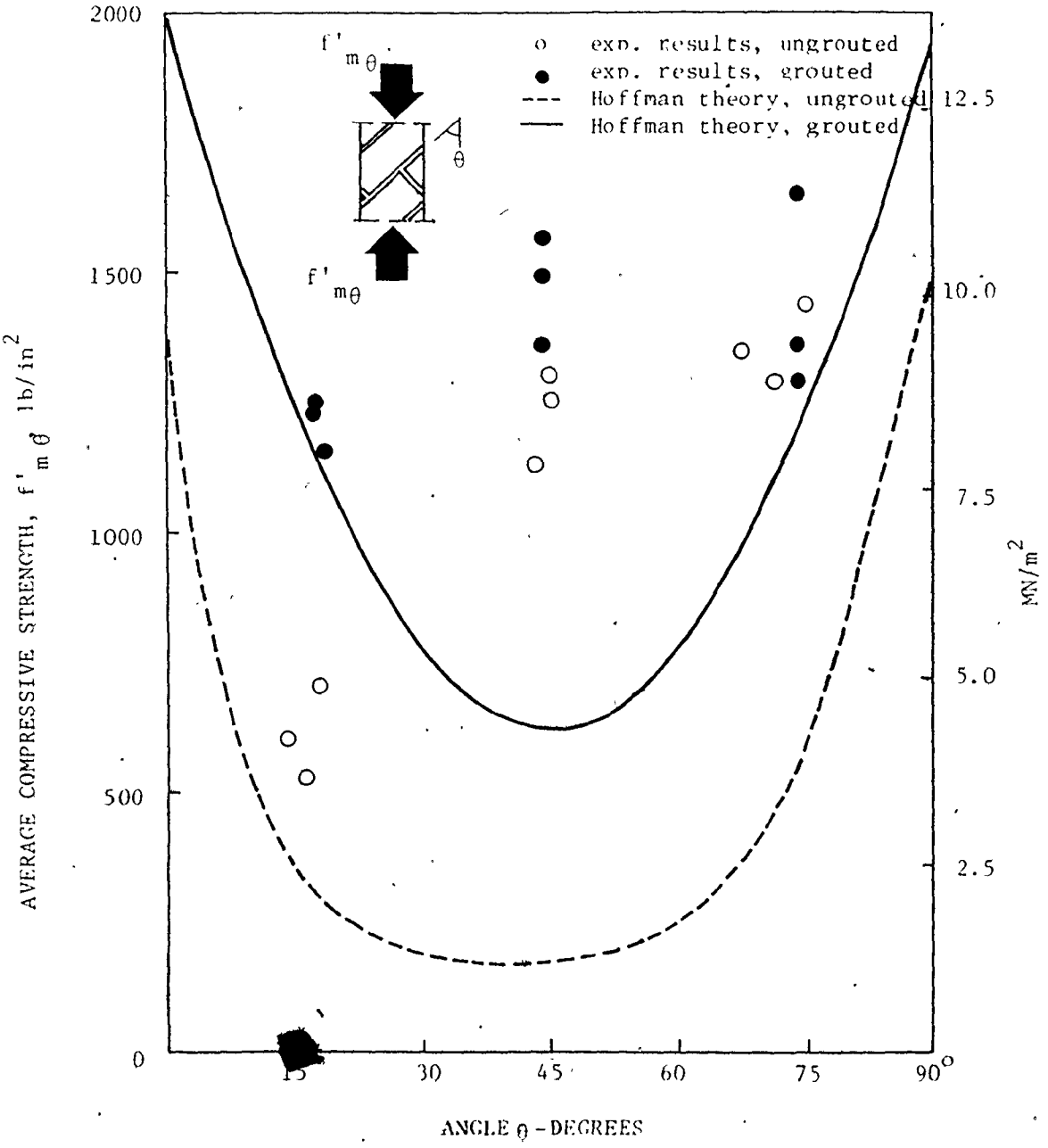

Fig. 6.26 COMPARISON BETWEEN THE HOFFMAN THEORY OF FAILURE AND THE EXPERIMENTAL RESULTS FOR PRISMS UNDER OFF-AXIS COMPRESSION

them. As discussed in Section 5.2.3.6, a strong correlation exists between the shear strengths of the bed joints and the normal compressive stresses. The results of the prisms tested under off-axis compression indicated that for the case of $\theta = 45^{\circ}$, and because of the increase of the compressive stresses normal to the bed joints compared to the case of $\theta = 15^{\circ}$, the joint capacity was substantially increased. This obviously prevented the joint slip failure and increased the assemblage capacity. It does not seem to be feasible to express the failure condition by using a single criterion where there are more than one failure mode.

Figures 6.27 and 6.28 exhibit the different failure envelopes along with the experimental results for ungrouted and grouted prisms, respectively under off-axis tension. It is shown that the maximum stress theory seems to highly overestimate the assemblage capacity. This may be because it does not take into account the interaction between the shear and the tension stresses along the critical bed joint which was shown to decrease the joint capacity[2] and consequently the overall strength. Considering both ungrouted and grouted masonry, the Hoffman theory agrees best with the experimental results. In addition, it provides a single smooth failure envelope.

6.3.4.4 Proposed Failure Criterion: To formulate a failure condition for a composite material like masonry, it seems to be necessary to account for the possible modes of failures under biaxial stresses. These may produce shear failure along the

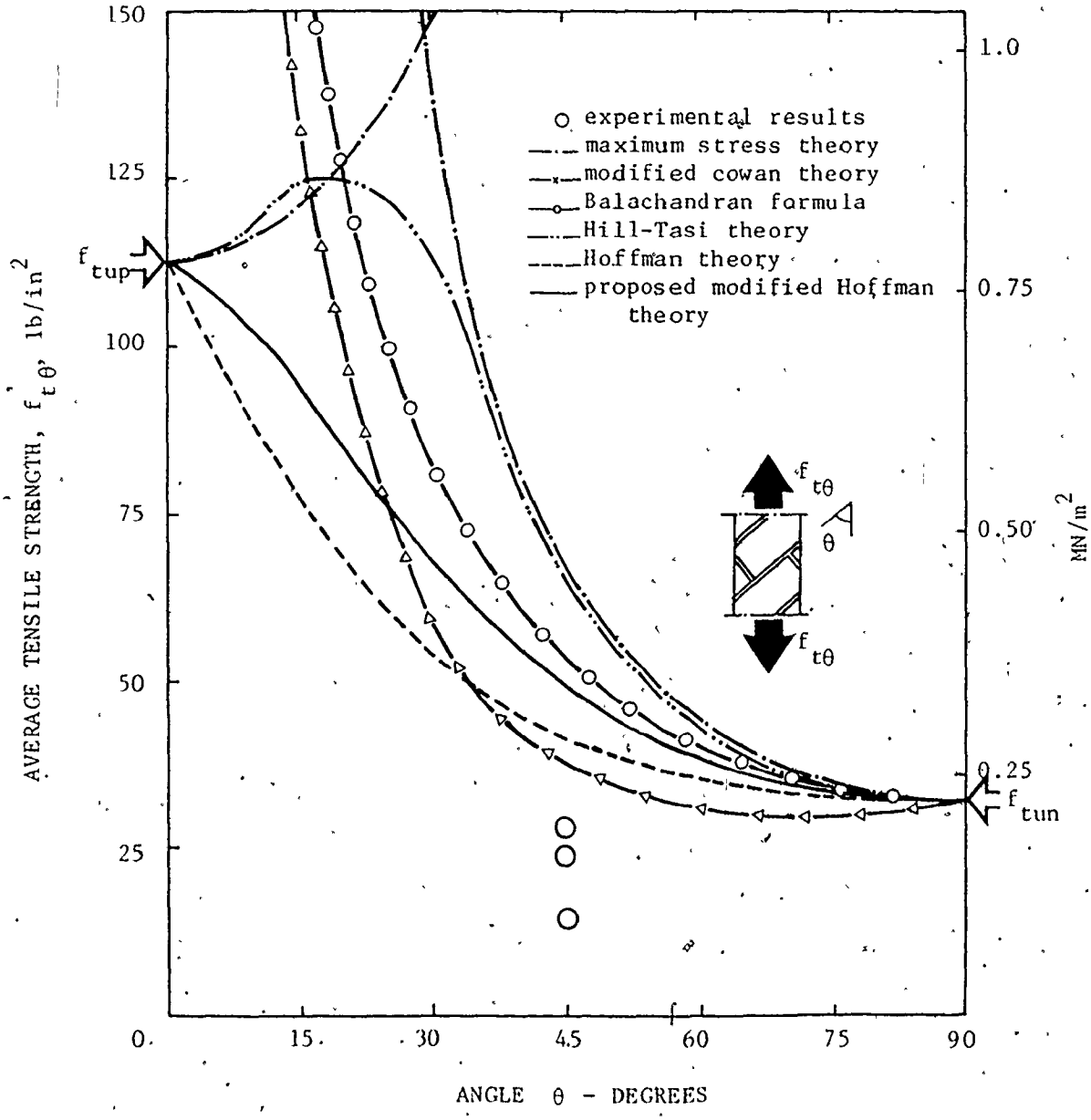

Fig. 6.27 FAILURE THEORIES AND EXPERIMENTAL RESULTS FOR UNGROUTED PRISMS UNDER OFF-AXIS TENSION

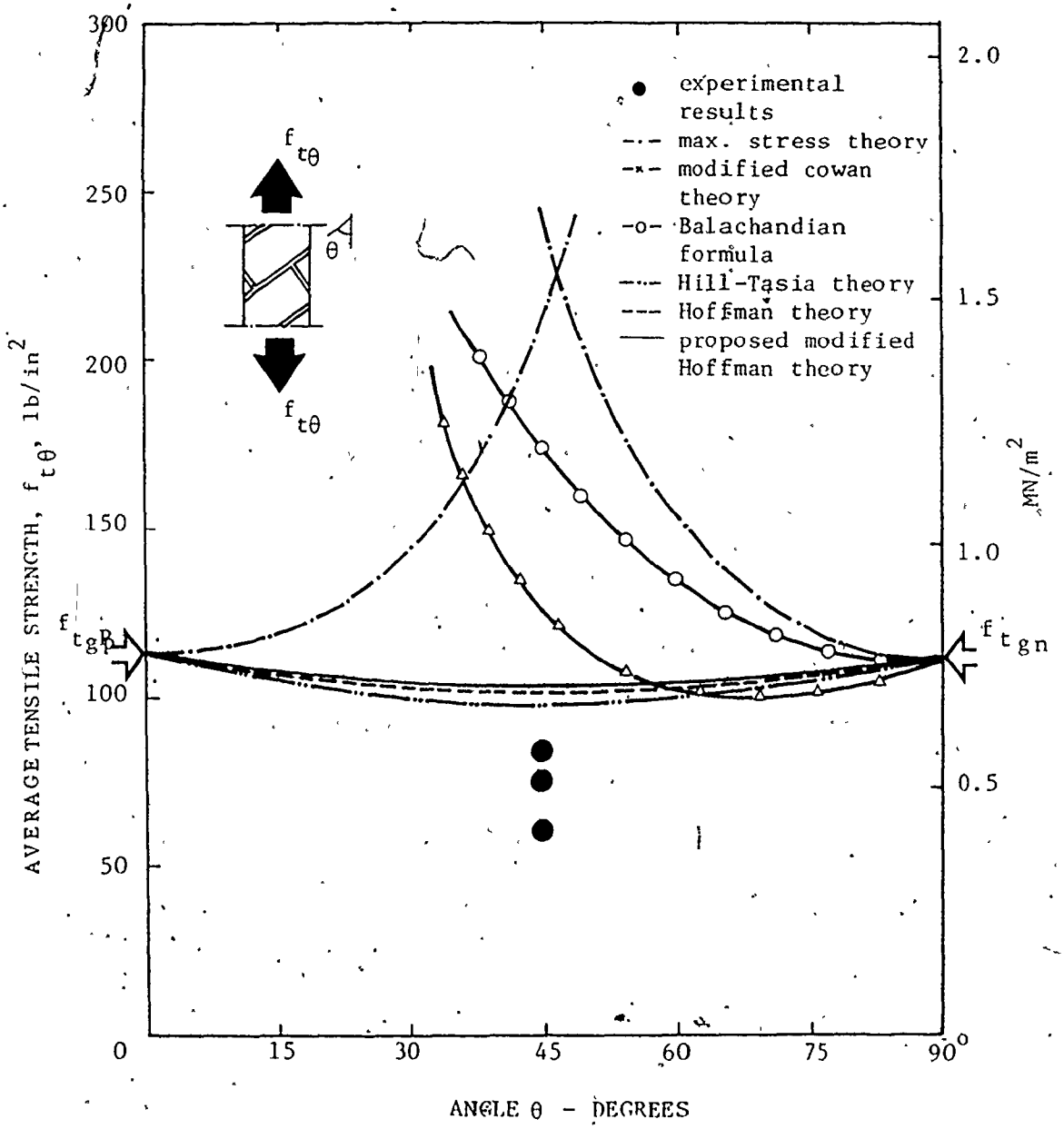

Fig. 6.28 FAILURE THEORIES AND EXPERIMENTAL RESULTS FOR GROUTED PRISMS UNDER OFF-AXIS TENSION

critical bed and head joints and/or tension failure of the block, grout or mortar. Shear failures should take into account the normal compressive stress, σ_n, perpendicular to the slip plane as this parameter was shown previously to have a significant influence on the shear capacity.

As indicated previsouly, it was not possible to provide an appropriate single failure envelope to predict the strength for more than one mode of failure. Therefore, it was decided to adopt two subcriteria with each describing a single mode of failure; either a shear failure along one of the critical principal material planes or a tension failure incorporating the interaction of the block, mortar, and grout.

To express the shear capacity of the bed joint under shear along with normal compressive stress, σ_y (acting on the bed joints), the proposed empirical formulas (Section 5.2.3.6) will be used. They are rewritten based on gross area for both ungrouted and grouted masonry as:

For ungrouted masonry, $$\tau_{xyb} = 44 + 1.08\,\sigma_y \qquad (6.23)$$

For grouted masonry, $$\tau_{xyb} = 110 + 1.1\,\sigma_y \qquad (6.24)$$

where type S_1 mortar and medium grout (GM_1), as described in Chapter 2, have been used.

The average apparent shear capacity along the head joint for zero normal stress, τ_{oh}, is assumed to be a combination of the mortar shear bond strength, τ_{mh}, and the shear strength of the

face shells of the blocks, τ_b. It can be expressed as:

$$\tau_{oh} = \frac{1}{2} (\tau_{mh} + \eta_v \cdot \tau_b) \qquad (6.25)$$

The experimentally determined shear bond strengtn for type S_1 mortar, presented in Section 5.2.3.2, will be used for the τ_{mh} value. The block shear strength, τ_b, for σ_n equal to zero, is calculated on the basis of a straight line relationship for the limiting curve, $\tau = f(\sigma_n)$, shown in Fig. 6.21(b). This is illustrated graphically in Fig. 6.29. It has to be noted that the straight line relationship, adlopted for concrete[6], provides conservative shear strength values.

The shear capacity along the head joint, including the effect of the normal compressive stess, σ_x, will be expressed by Coulomb's shear failure theory. A proportionality constant of 1.1, which is similar to that found for shear along the bed joint, is adopted and using Equation (6.25) for the capacity under zero normal stress yields the following expression:

$$\tau_{xyh} = 165 + 1.1\ \sigma_x \qquad (6.26)$$

Under off-axis compression, the shear stress, τ_{xy}, along the principal material directions can be expressed in terms of the applied vertical stress, σ_c (see Section 6.2.2.1). Substituting Equations (6.23), (6.24), and (6.26) into Equation (6.1) yields, respectively, the following expressions relating the external stress at failure, $f'_{m\theta}$, with the orientation of the bed joint, θ,

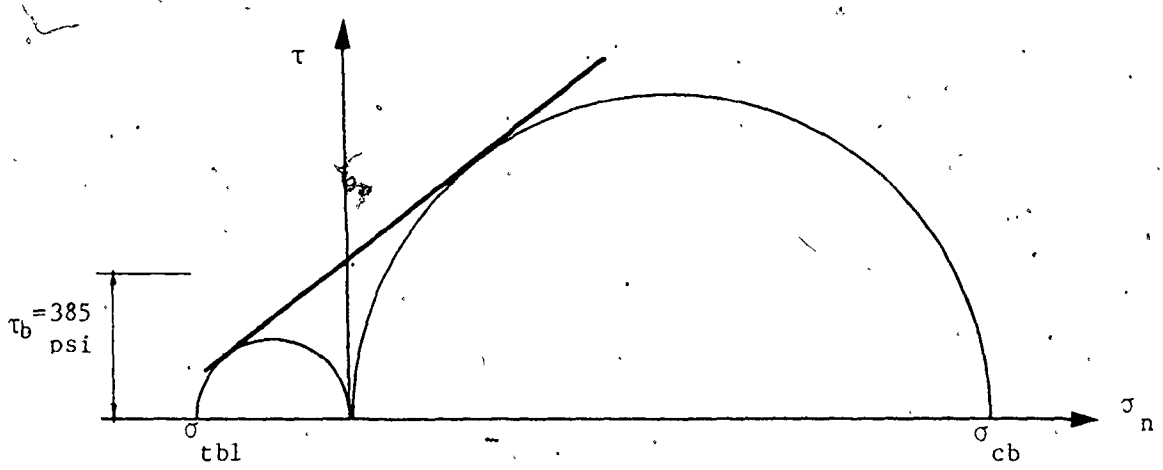

Fig. 6.29 SHEAR STRENGTH OF THE CONCRETE BLOCK

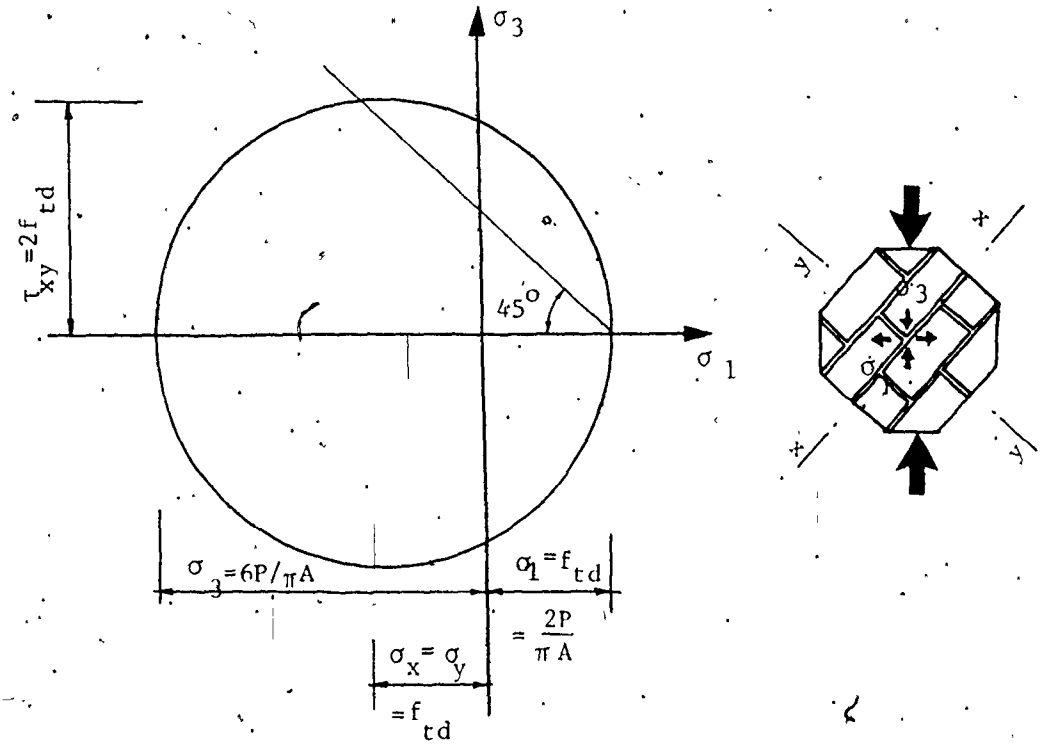

Fig. 6.30 STRESSES DEVELOPED AT THE CENTRE OF A MASONRY DISC LOADED AT 45° FROM THE BED JOINT

for different shear failure conditions:

a) Shear failure along the bed joint for ungrouted masonry;

$$f'_{m\theta} = \frac{88}{\sin^2 2\theta + 1.08(\cos 2\theta - 1)} \qquad (6.27)$$

b) Shear failure along the bed joint for grouted masonry,

$$f'_{m\theta} = \frac{220}{\sin 2\theta + 1.1(\cos 2\theta - 1)} \qquad (6.28)$$

c) Shear failure along the head joint for either ungrouted or grouted masonry,

$$f'_{m\theta} = \frac{330}{\sin 2\theta + 1.1(\cos 2\theta - 1)} \qquad (6.29)$$

The above shear failure criteria ((a)&(c) and (b)&(c)) are illustrated for ungrouted and grouted masonry in Figs. (6.31) and (6.32), respectively. It should be noted that these failure criteria are not continuous over the whole rangle of θ from 0^o to 90^o because they represent the failure conditions only when shear is the governing failure mode. To complete tne failure criterion for the full range, the other tension failure subcriterion has to be considered.

The failure condition proposed by Hoffman[25] for brittle orthotropic materials will be used to provide the tension subcriterion. However, it will be modified to take into account the interaction between the shear strength and the normal compression stress, σ_n. This modification is employed when

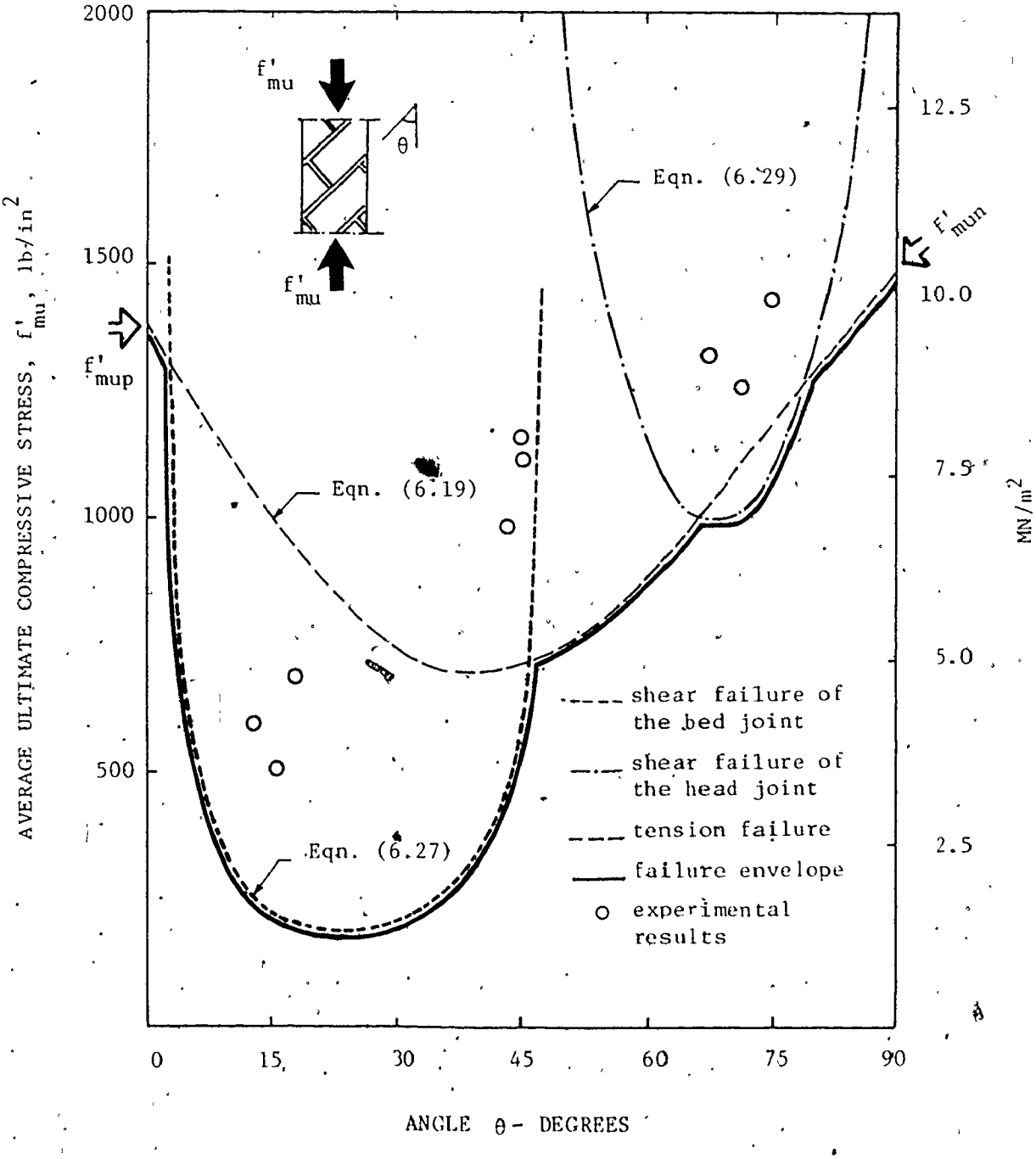

Fig. 6.31 PROPOSED FAILURE CRITERIA FOR UNGROUTED MASONRY UNDER OFF-AXIS COMPRESSION

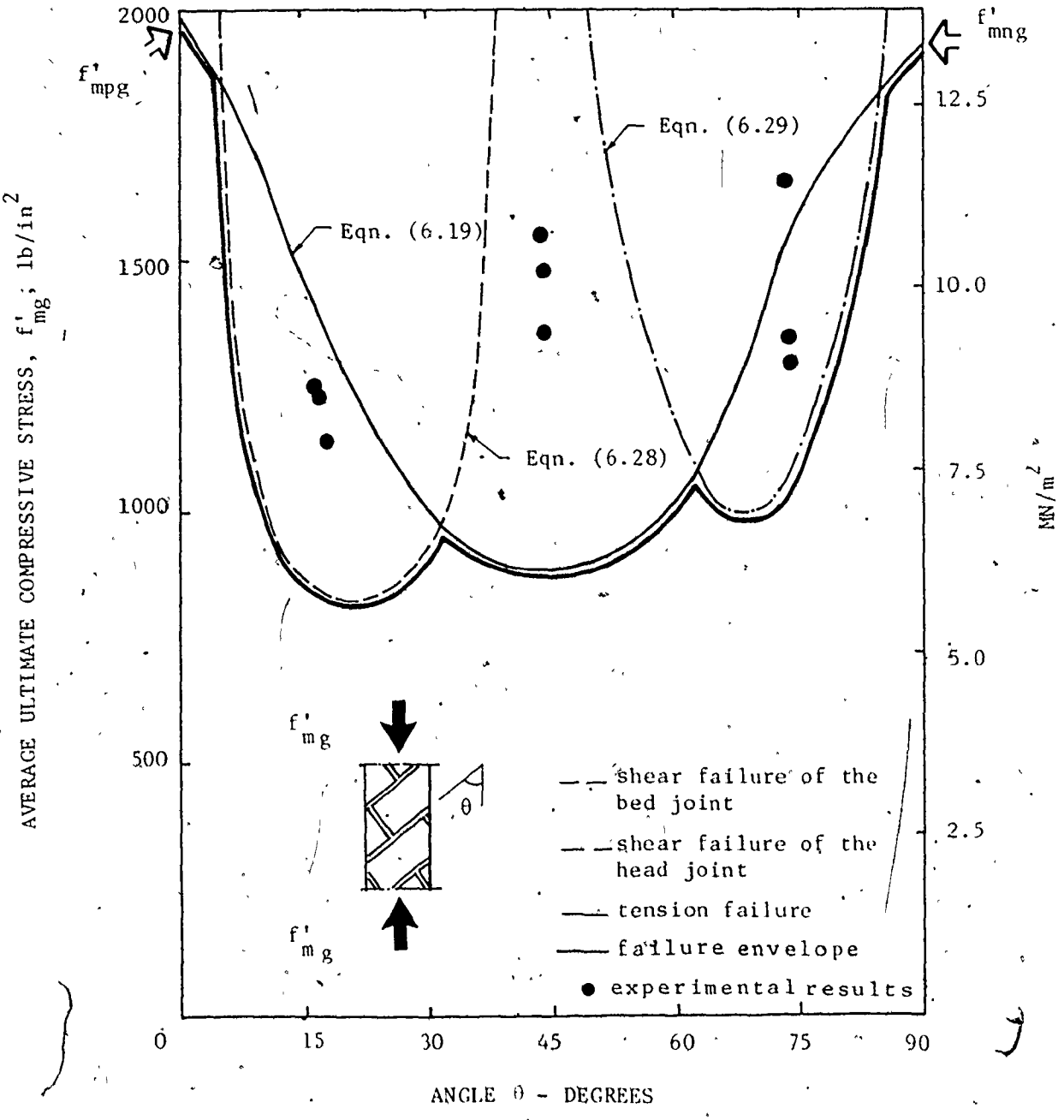

Fig. 6.32 PROPOSED FAILURE CRITERION FOR GROUTED MASONRY PRISMS UNDER OFF AXIS COMPRESSION

evaluating the shear constant, c_9, in Equation (6.19). The tension failure stress conditions found by testing ungrouted and grouted masonry discs under splitting loads, oriented at 45° from the bed joint, (presented in Section 4.2.5.2) will be used to evaluate the constant c_9. As shown in Fig. 6.30, under this test condition, the state of normal stresses at the centre of the disc along the bed and head joints can, empirically, be expressed using Equation (4.17) as:

$$\sigma_x = \sigma_y = f_{td} = \frac{2}{3} (F_{tx} + F_{ty}) \qquad (6.30)$$

and the shear stress along the bed joint can be expressed as:

$$\tau_{xy} = 2 f_{td} = \frac{4}{3} (F_{tx} + F_{ty}) \qquad (6.31)$$

Substituting the values of σ_x, σ_y, and τ_{xy} from Equations (6.30) and (6.31) and the values of C_1 .... C_8 from Equations (6.20) and (6.21) into Equation (6.19), the shear constant c_9 can be determined in terms of the tensile strength characteristics of masonry in the principal material directions. The resulting failure criterion (Equation (6.19)) for ungrouted and grouted masonry are also presented in Figs. 6.31 and 6.32, respectively.

As shown in Figs. 6.31 and 6.32, the two criteria for shear and tension failures were used to predict the failure condition for any stress combination; the minimum of which would be the governing criterion. The proposed failure criteria led to a better agreement with the experimental results for both ungrouted

and grouted masonry compared to the other failure theories. The proposed failure criteria not only predict the capacity of masonry under biaxial stresses, but also predict the mode of failure. The proposed criteria are based on a physical interpretation rather than being strictly phenomenological.

The modified Hoffman theory, which was adopted as a criterion for the proposed failure criteria when tension is the governing mode, is also shown in Figs. 6.27 and 6.28 to reasonably predict the tensile capacity of ungrouted and grouted masonry prisms, respectively, for off-axis loading.

Although the predicted capacities using the proposed failure criteria are better than other criteria, they are not as close to the experimental results as might be desired. However, the failure modes were predicted accurately and in general it is suggested that the proposed criteria are promising since the inherent anisotropic characteristics of masonry as a composite material have been rationally considered. It should be noted that as they now stand, these criteria provide a conservative (lower bound) prediction of the strength under biaxial stresses.

The proposed criteria were only checked against the experimental results for off-axis loaded prisms having relatively small dimensions. Before the general application of the proposed failure criteria can be recommended, results of testing larger masonry assemblages under different combinations of biaxial stresses should be checked.

6.4 Summary and Conclusions

The behavioural characteristics of ungrouted and grouted masonry prisms under compression normal to the head joints are presented. Using different orientations of the bed joint from the applied loads, other masonry prisms were tested under off-axis compression and tension wherein biaxial states of stresses were developed along the critical bed and head joints planes. The strengths and deformational characteristics of these prisms are presented and discussed. Different failure theories for isotropic materials, which have been used for masonry by many investigators, are reviewed. Also, failure theories for composite materials and their applicability to masonry are investigated. Finally, failure criteria for masonry under biaxial stresses, taking into consideration its anisotropic nature, are proposed.

The following are the conclusions drawn from the investigation presented in this chapter:

1 - For practical ranges, the strength of the grout has very little effect on the compressive strength of grouted masonry under compression normal to the head joint.

2 - For grouted masonry, the mortar joint, while not having a significant influence on the strength and the deformation characteristics under compression normal to the bed joint, has a pronounced effect under compression normal to the head joint. The mortar strength is a governing parameter influencing the compressive strength of both ungrouted and grouted masonry under

compression normal to the head joint.

3 - There are two distinct modes of failures of masonry assemblages under biaxial stresses; a shear mode of failure along the bed or head joint planes and a tension mode of failure mainly distinguished by tensile failure of the component materials. There is also a possibility of mixed shear-tension mode of failure.

4 - The contribution of the grouted cores towards increasing the masonry strength under biaxial stresses varies with the failure mode or, in other words, with the location of the failure plane. The maximum contribution occurs when shear failure of the bed joint is the governing mode, whereas no contribution is evident when shear failure along the head joint plane is the mode of failure. In the latter case, the failure plane would not cross the grouted cores, which is similar to the behaviour of grouted masonry under axial tension parallel to the bed joint.

5 - The mortar head joint has a significant effect on the strength of grouted masonry under biaxial stresses as it represent a weak plane where failure could be initiated. The continuity provided by the grouted cores strengthens the bed joint and consequently make the head joint plane more critical.

6 - The strength and the deformation characteristics of masonry assemblages vary with the stress orientation (relative to the critical bed or head joint planes) indicating the anisortropic nature of masonry. This is particularly true for ungrouted masonry whereas the continuity provided by the grouted cores helps

to decrease the degree of anisotropy for grouted masonry.

7 - The shear modulus of masonry increases with increased compressive stress normal to the bed joint, particularly for ungrouted masonry.

8 - The failure theories for isotropic material are not applicable for masonry because they were derived on the basis of the invarient state of stress concept where the stress orientation has no effect on the strength. It was shown that masonry strength is highly sensitive to the orientation of the stress with respect to the critical head and bed joint directions. The failure criterion based on principal tensile stress is not valid for masonry because it has more than one tensile strength characteristic.

9 - To provide a realistic failure criterion for masonry, the possible shear and tension modes of failure should be taken into account. For the shear slip along the head or the bed joint directions, the effect of the compressive stresses normal to the failure plane should also be considered.

10 - The CSA standard S 304[12] assigns constant values for the deformation characteristics of masonry (Modulus of elasticity and modulus of rigidity). As an anisotropic material, the properties of masonry vary with the stress orientation and hence, this inherent characteristic, particularly for ungrouted masonry, should be considered for the development of a more rational basis for design for masonry assemblages.

CHAPTER 7

SUMMARY AND CONCLUSIONS

7.1 Summary

The behaviour characteristics of ungrouted and grouted concrete masonry under compression, tension, shear, and biaxial stresses acting along the principal material directions (parallel and normal to the bed joints) were investigated. The effect of stress orientation on the strength and deformation characteristics of concrete masonry was studied.

An experimental investigation was initiated to study the behaviour of concrete masonry under different loading conditions. Effect of grouting on the behaviour characteristics was investigated through comparisons of the behaviour of ungrouted and similar grouted assemblages. A total of 323 masonry assemblages were built using standard 6 inch concrete blocks. The test variables were mortar type, grout strength, and bed joint reinforcement. Other factors, such as block geometric and strength characteristics, were standardized and held constant. The specimens were tested under compression normal and parallel to the bed joints, splitting tension normal, diagonal, and parallel to the bed joints, shear with different levels of precompression acting along the bed joints, and combined normal and shear

stresses acting along the bed and head joints. The experimental results provide detailed information on the strength and deformation characteristics of ungrouted and grouted masonry under different stress orientations.

An analytical investigation was employed to develop expressions for the assemblage ultimate strength in terms of the strength and geometric characteristics of the component materials (block, mortar, and grout). Based on a "strength" approach, proposed strength formulas were derived to express the assemblage compressive, tensile, and shear stresses.

The applicability of the different failure theories for isotropic and anisotropic materials to masonry was examined. Failure criteria were proposed to predict the strength and the failure mode of concrete masonry under biaxial stresses, taking into consideration the inherent anisotropic nature of masonry as a brittle composite material.

7.2 Conclusions

Conclusions concerning the behaviour characteristics under axial compression, tension, shear, and biaxial stresses were presented by the end of Chapters 3, 4, 5, and 6, respectively. However, general conclusions are also presented below to help gain an overall understanding of the behaviour of concrete masonry.

1. The strength and deformation characteristics of concrete masonary vary with the stress orientations (with respect to the

bed joint direction). This is a typical behaviour of anisotropic composite material. The continuity provided by the grouted cores in the direction normal to the bed joints helps to decrease the degree of anisotropy of concrete masonry. Grouted masonry exhibits a more isotropic behaviour compared to ungrouted masonry either from a strength or a deformation viewpoint.

2. For the combination of materials used in this investigation, failure of plain concrete masonry can occur in one of the following three general categories:

a. A tension mode of failure which is distinguished by: (i) splitting of the outer shell under high compression normal to the bed joints or splitting along the head joints and the face shells under tension normal to the head joints, (ii) diagonal tension failure under critical combinations of normal and shear stresses acting on the critical head and bed joints, and (iii) separation failure at the block-mortar interfaces along the bed joint under tensile stress normal to it with or without precompression.

b. A shear mode of failure which is distinguished by: (i) debonding or joint slip failure at the block-mortar interfaces occurring under zero or low compression stresses normal to the bed joints and accompanied by high shear stresses, and (ii) shearing along the head joint direction so that the crack crosses the face shells of the blocks and the head joints.

c. A mixed shear-tension mode of failure distinguished by

stepped-wise cracks. It occurs for medium levels of shear and normal stresses acting along the bed and head joints.

3. Grouting contributes differently to the strength of concrete masonry depending on the stress condition. Under axial compression, it results in a reduction of the compressive strength due to inducing lateral tensile stresses on the outer shell caused by lateral inelastic deformation of the grouted cores. Under shear along the bed joints, grouted cores significantly increase the joint shear capacity. The relative contribution towards increasing the shear strength (compared to ungrouted masonry) decreases as the level of compressive stresses normal to the bed joints increases. The grouted cores have a maximum contribution towards increasing the tensile strength under loads normal to the bed joints, whereas they have no contribution under tensile loads parallel to the bed joints. Block moulded prisms seems to be representative of the grout in the assemblage.

4. Mortar strength has relatively little effect on the compressive strength of concrete block masonry. This is particularly true for grouted masonry where the continuity provided by the grouted cores reduces the significance of the mortar joint in influencing either the strength or the deformation characteristics of concrete masonry. Also, mortar strength shows no significant effect on the shear and tensile strength of the joints. This is attributed to the fact that the shear or bond strength of mortar is not predominately a function of its

strength. The compressive strength of air cured mortar cubes is not a representative test for the mortar in the assemblage. Shear and bond strengths of the mortar have to be determined directly from testing of masonry assemblages.

5. The block strength and geometric characteristics have a pronounced effect on the behaviour of concrete block masonry. The block tensile strength is the most significant parameter influencing the compressive strength and the tensile strength parallel to the bed joint for either ungrouted or grouted masonry. The block geometry governs the area of the grouted cores and consequently the contribution of grouting towards increasing the shear strength and the tensile strength normal to the bed joints. The flared shape of the block reduces the core area which causes a reduction in the benefits of grouting, for shear strength and for tensile strength normal to the bed joints. This shape is not recommended from the strength viewpoint, but may be necessary for the practical requirements. Tapering the shells of the blocks towards the central web increases the cross-sectional area of the failure plane under tensile loads parallel to the bed joints and therefore, helps to increase the tensile strength of both ungrouted and grouted masonry parallel to the bed joints.

6. Dur-O-Wal steel embedded in the mortar bed joints has no effect on the compressive strength, the shear strength along the bed joints, or the diagonal tension strength. Confining the mortar joints and the grouted cores, using confining steel plates

embedded in the bed joints, helps to reduce the lateral tensile stresses imposed on the blocks and consequently increases the compressive strength of masonry. This is particularly true for grouted masonry where a reduction in the compressive strength occurs due to the lateral expansion of the grout. Generally, reinforced masonry exhibits a more gradual and less explosive type of failure compared to unreinforced masonry.

7. The failure theories for isotropic materials are not suitable for predicting the strength of masonry under biaxial stresses. These failure theories are based on the concept of the invarient states of stress which is not valid for masonry where the strength characteristics vary with the stress orientation.

8. The Canadian code's (CSA S 304[12]) approach in considering grouted masonry to be similar to solid masonry ignores the continuity provided by the grouted cores which is shown to have a pronounced effect on both the strength and the deformation characteristics of grouted concrete masonry. The code design values are inconsistent as in some cases they either significantly overestimate or underestimate the contribution of grouting. The code recommendation for matching the compressive strengths of the block and the grout to allow higher design values is not sound. It has been shown that matching the deformation characteristics of the components would be more efficient. The block tensile strength and its geometric characteristics and the grout strength are the most significant parameters influencing the tensile and

shear strengths of masonry. They are ignored by the code and the design values for shear and tension are classified only according to the mortar type. However, the test results indicate that the mortar strength has a secondary effect on the strength of grouted concrete masonry. The strength and the geometric characteristics of the block and the grouted cores should be considered as controlling parameters in assigning design values for grouted masonry under shear and tension stresses.

APPENDIX A

RATIONALE FOR THE EXPERIMENTAL SCHEME

A.1 Test Repetitions

Replication, the repetition of the basic experiment, is of utmost importance in the design of an experiment in that it provides an estimate of the experimental error. Basically the random errors caused by errors of experimentation, material variation, observations and measurements which can not be avoided[41]. This experimental error acts as a "basic unit of measurement" for assessing the significance of the observed differences or for determining the length of the confidence interval[41]. It also helps to obtain a more precise estimate of the mean effect of any factor which is one of the objectives of the experimental investigation.

A decision on the number of specimens per test for a given experiment depends, statistically[23] on:

1 - How large a shift or a difference in a parameter is to be detected? (The tolerable error permitted.)

2 - How much variation is expected? (The expected standard deviation.)

3 - What size of risks are to be tolerated? (Confidence level required.)

To determine the number of replicates, numerical values are required to be estimated in answering the above questions. In practice, the number of replicates is usually determined as a compromise between the statistical and economical requirements.

Because in structural engineering problems the number of replicates (samples) is usually small (less than 30), the normal probability distribution is not necessarily applicable[34]. In the current study, the student's t-distribution is adopted as it seems applicable[34] to the small number of samples likely to be used.

To have some idea about the expected variability of masonry assemblages, three trial 3-course prisms were built and tested under axial compression. A coefficient of variation of 13% was acnieved (the workmanship level was not good as the specimens were built by this investigator). Unfortunately, most publications produce average results without supplying their standard deviations or variation coefficient. However, it has been reported[17] that the average coefficient of variation for the compressive strength of conventional brick masonry prisms tested in a National Survey of Commerical Laboratories made in the United States in 1963 was 9.4% with a range from 5% to 24% depending on the level of the quality control.

Based on this information and assuming a very good quality control would be achieved in the Laboratory since construction of the specimens will be performed by an experienced mason using

techniques representitive of good workmanship, the expected variation was assumed to be ±10%. Adopting a confidence level of 95% and using the tables for the student t-distribution[34], 5 replicates provide a tolerable error of 10.7% whereas 4 replicates provide an error of 13.6%. Considering that about a 10% tolerable error is acceptable for a composite material consisting of two or three component materials such as ungrouted or grouted masonry, 5 repetitions were adopted in the current program. However, results of the first group of tested prisms (Section 3.2.4.1) revealed an average coefficient of variation of less than 8%. This low variation allows the possibility of only 4 repetitions which provide the same level of acceptable accuracy (about 10%). Therefore it was decided to adopt only 4 repetitions for the other series of tests.

A.2 Grouping and Time of Testing of the Specimens

Specimens were constructed using different batches of similar mortar mixes over a period of two or three days for each of the five sets of experiments: 1) Axial compression, strength parameters, 2) Axial compression, geometric parameters, 3) shear along with percompression, 4) splitting tension, and 5) Off-axis compression and tension. Different grout mixes were poured into the cores of some specimens. For each grout mix (concerning with one series or group of experiments), specimens from different mortar batches were chosen at random to eliminate the effect of

the errors arising from the natural variation of the mortar characteristics due to reproducing the mixes.

The specimens for each set of experiments were tested within a period of time ranging from 14 to 21 days. The time schedule was designed to test each series (concerning with one parameter) over the whole range of the test period so that the average time for each series coincided with those for the other series. This average time was designed to be in the mid period at which time the control specimens were tested.

APPENDIX B

TENSILE SPLITTING TESTS

The splitting test of cylinders are widely adopted to determine the tensile strength of concrete. Equation (4.4), derived from the elastic theory of a thin circular plate, is used to determine the maximum tensile stress at failure at the centre of the circle. As mentioned in the main text, the finite element method was adopted to check the validity of this equation to predict the tensile strength of the hexagonal masonry discs and the grout prisms:

a) Masonry Discs

A total of 294 constant strain triangular elements were used to idealize one quarter of the disc, as shown in Fig. B.1 (the disc is presumed homogeneous). Two types of splitting loads were considered; line loads and loads uniformly distributed over a distance "c" ranging from 5% to 15% of the disc's height.

In Figs. B.2 and B.3 the longitudinal and transverse stresses over the loaded plane of the hexagonal disc using the finite element method are compared to those for a thin circular plate using the theory of elasticity (Equations (4.5) and (4.6)). Comparisons of the distribution and magnitude of stresses shown in these figures indicate clearly that the suggested hexagonal

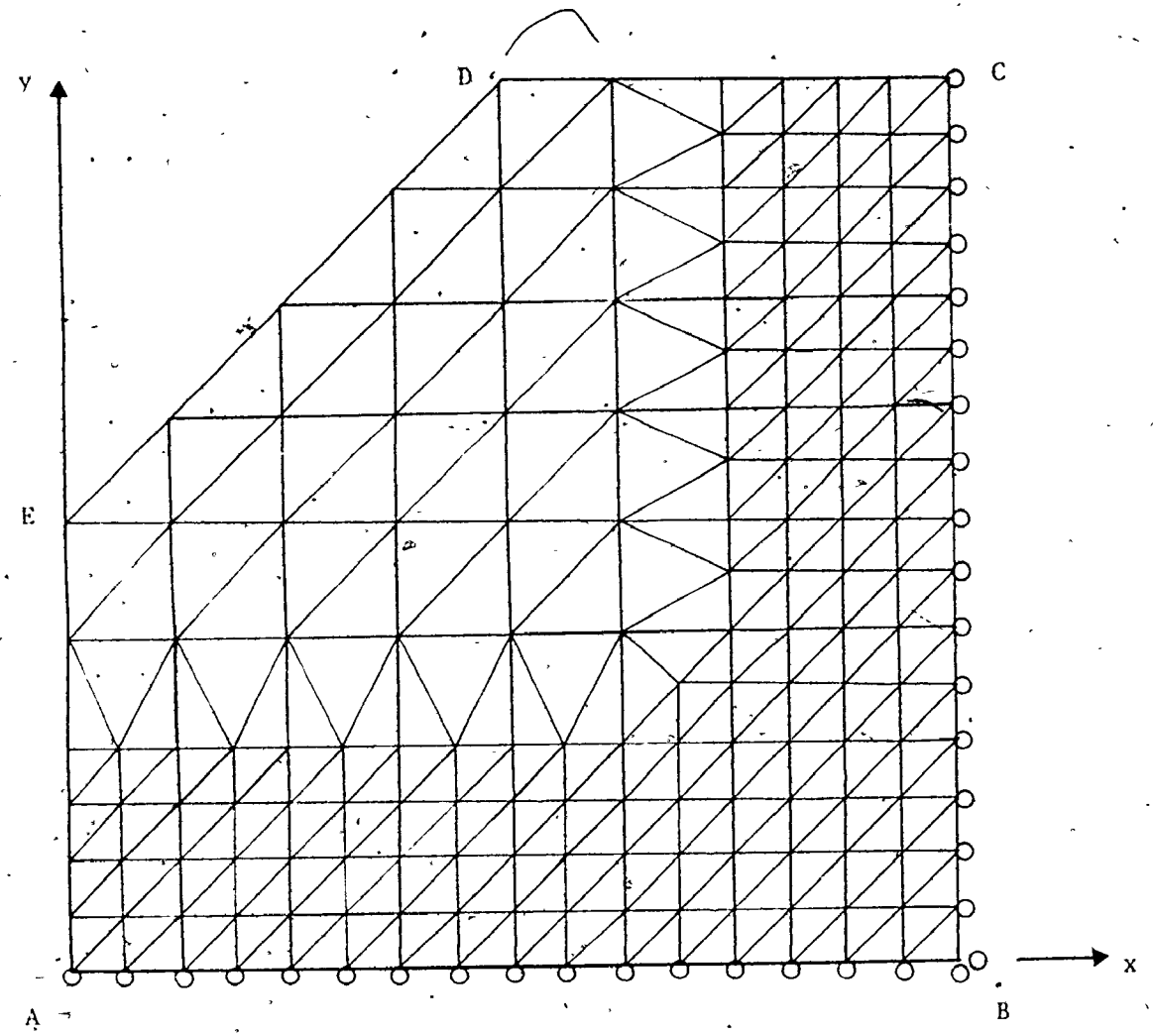

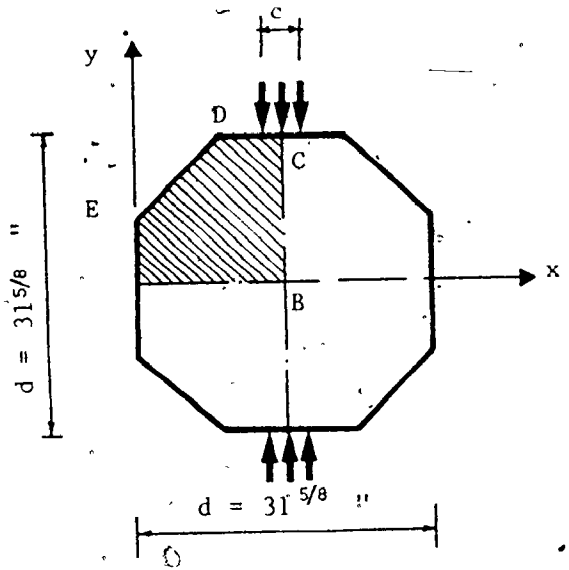

Fig. B.1 FINITE ELEMENT IDEALIZATION OF THE HEXAGONAL DISC UNDER SPLITTING LOADS

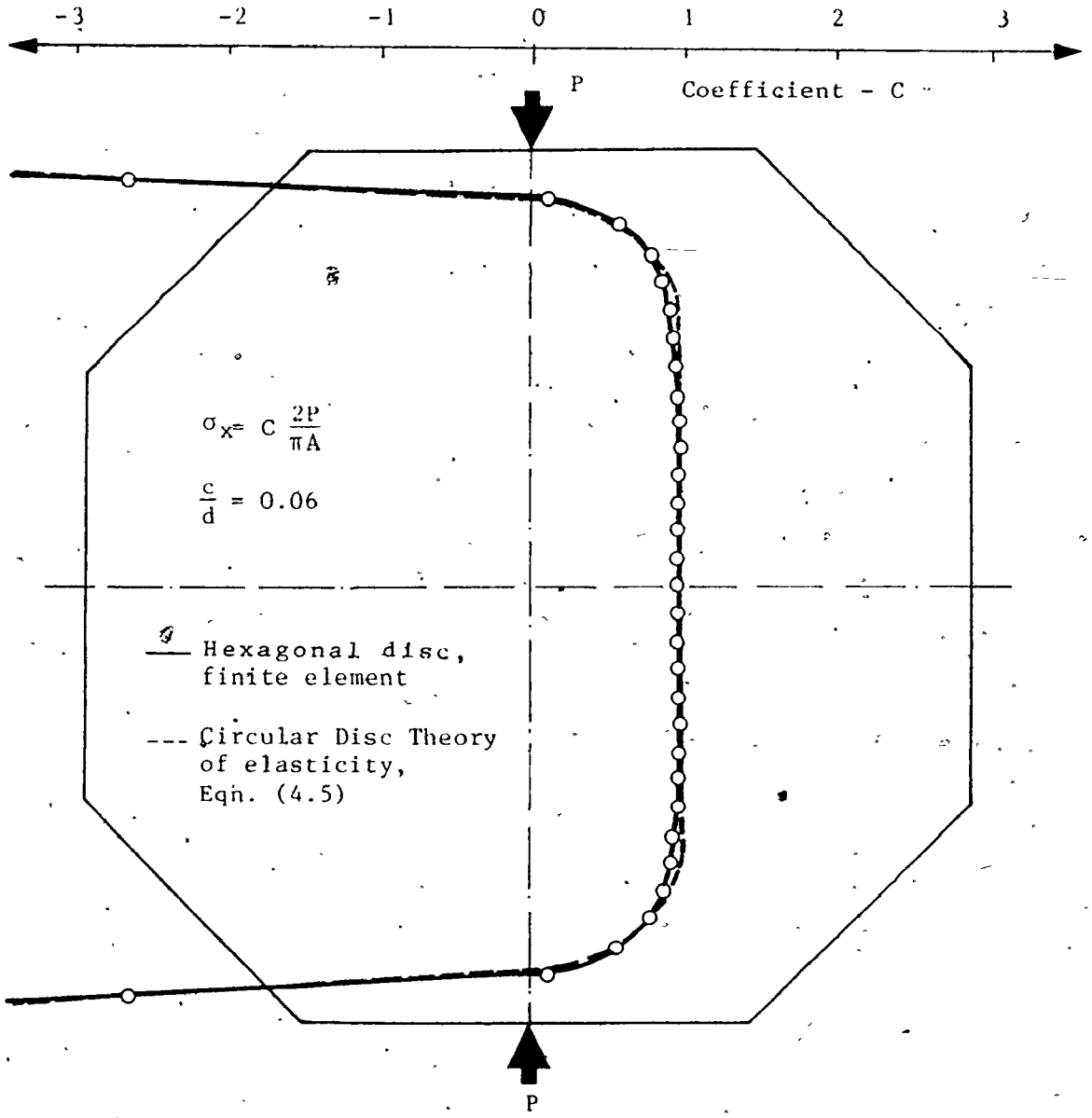

Fig. B.2 DISTRIBUTION OF THE TRANSVERSE TENSILE STRESSES ALONG THE LOADED PLANE OF A HEXAGONAL DISC UNDER SPLITTING LOAD

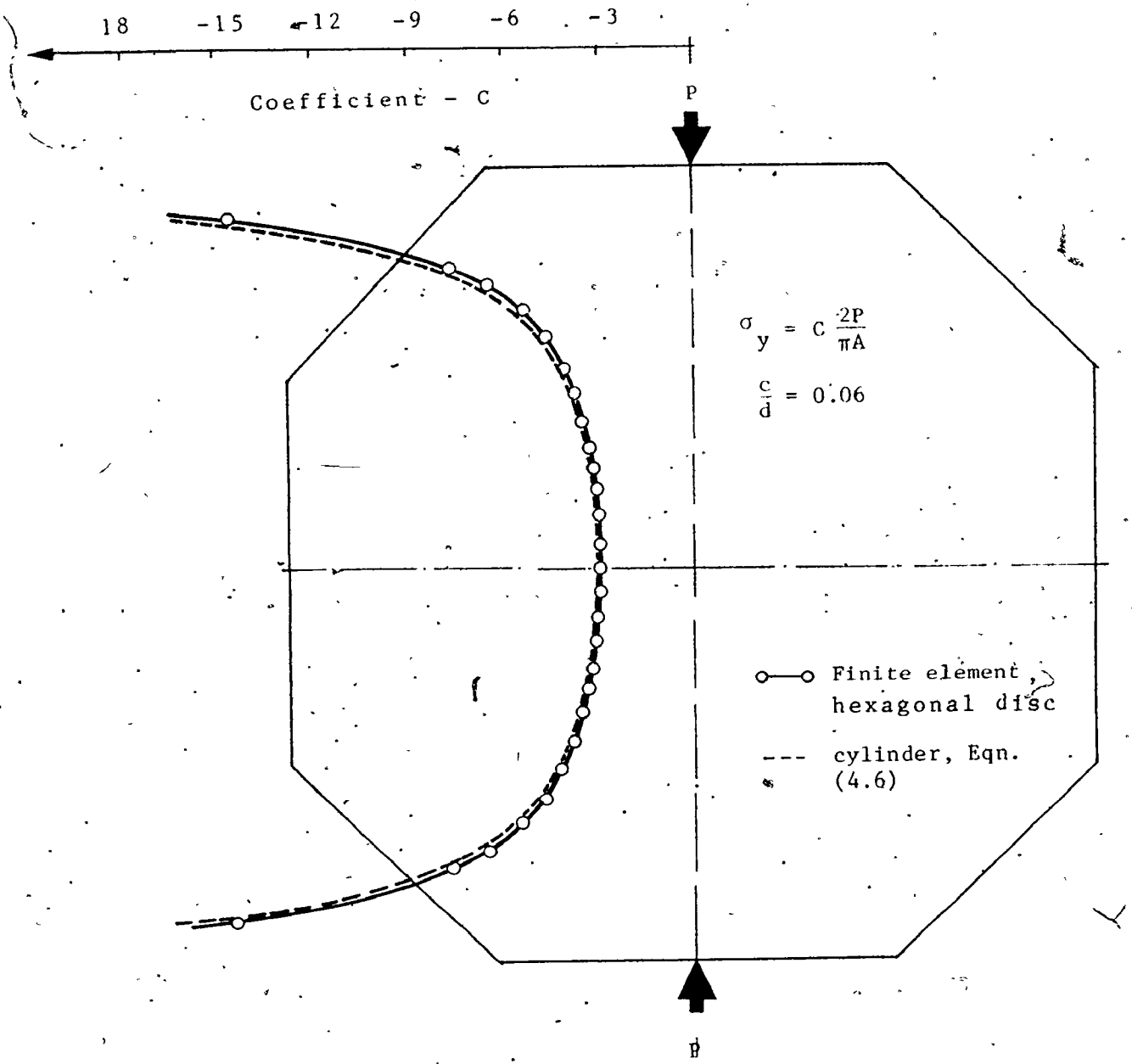

Fig. B.3 DISTRIBUTION OF VERTICAL COMPRESSIVE STRESSES ALONG THE LOADED PLANE OF A HEXAGONAL DISC UNDER SPLITTING LOAD .

shape is a very good approximation to the conventional circular shape of the concrete cylinders and the brickwork discs. Figure B.2 shows that the formula,

$$\sigma_t = \frac{2P}{\pi A} \qquad (B.1)$$

where P is the splitting load and A is the area of the split plane can be used to accurately calculate the maximum tensile stress at the centre of the disc at failure, σ_t.

Figure B.4 shows the effect of load distribution on the splitting tensile stress developed at the centre of the disc. It is indicated that increasing the loaded area up to about d/10 reduces the tensile stress by only about 3%. The reduction in the stress associated with a c/d ratio of 0.06 is neglected in the stress analysis of the masonry discs (presented in Chapter 4).

b) Grout Prisms

A total of 105 constant strain triangular elements were used to idealize one quarter of the prism as shown in Fig. B.5. A condition of plane stress was considered.

Comparisons of the stresses along the principal orthogonal directions for the prism using the finite element method and for a circular plate using the elasticity theory are presented in Figs. B.6 and B.7. The comparison of the tensile stresses shown in Fig. B.6 indicates that the formula, Equation (B.1), can reasonably predict the tensile stress at failure over the central portion of the prism. It is also shown in Figs. B.6 and B.7 that the aspect

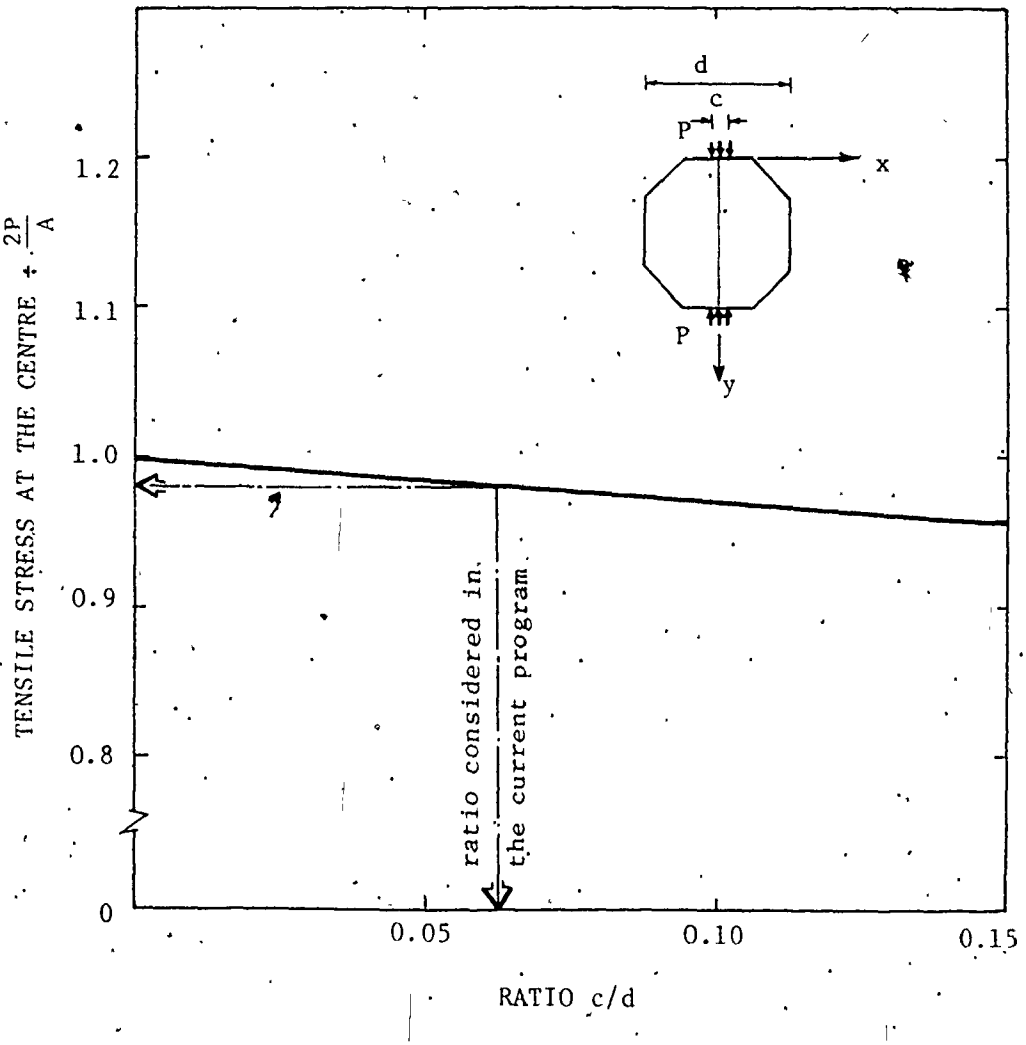

Fig. B.4 EFFECT OF LOAD DISTRIBUTION ON THE SPLITTING TENSILE STRESS DEVELOPED AT THE CENTRE OF THE DISC

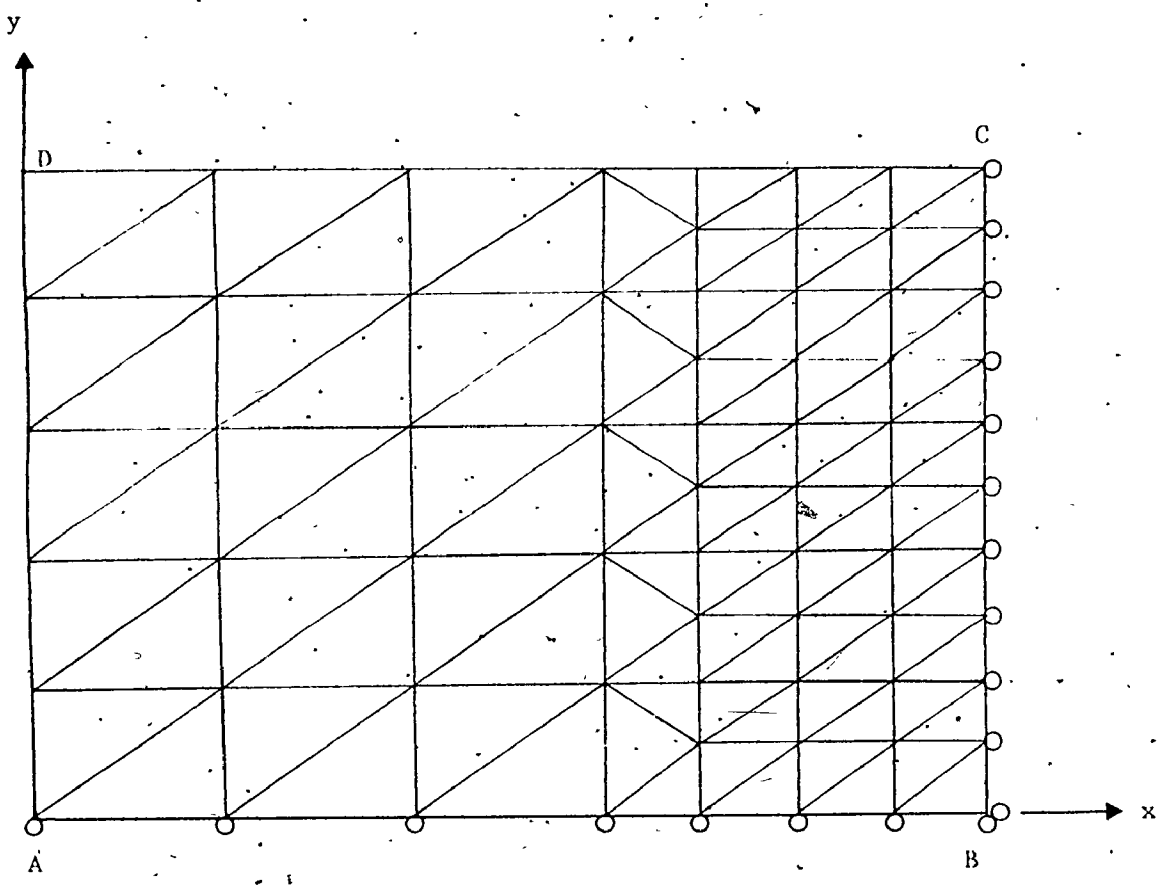

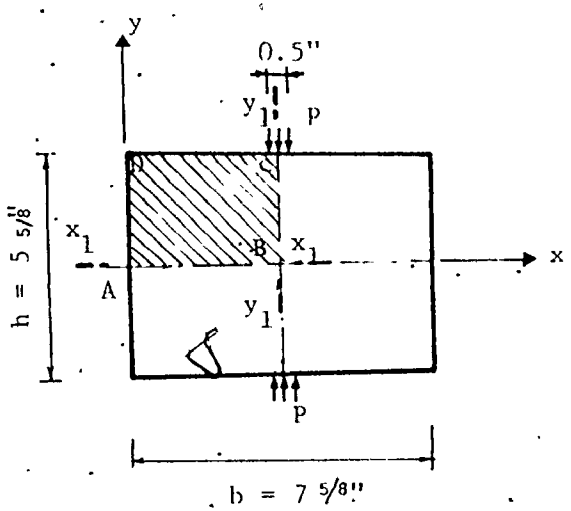

Fig. B.5 FINITE ELEMENT IDEALIZATION OF A GROUT PRISM UNDER SPLITTING LOAD

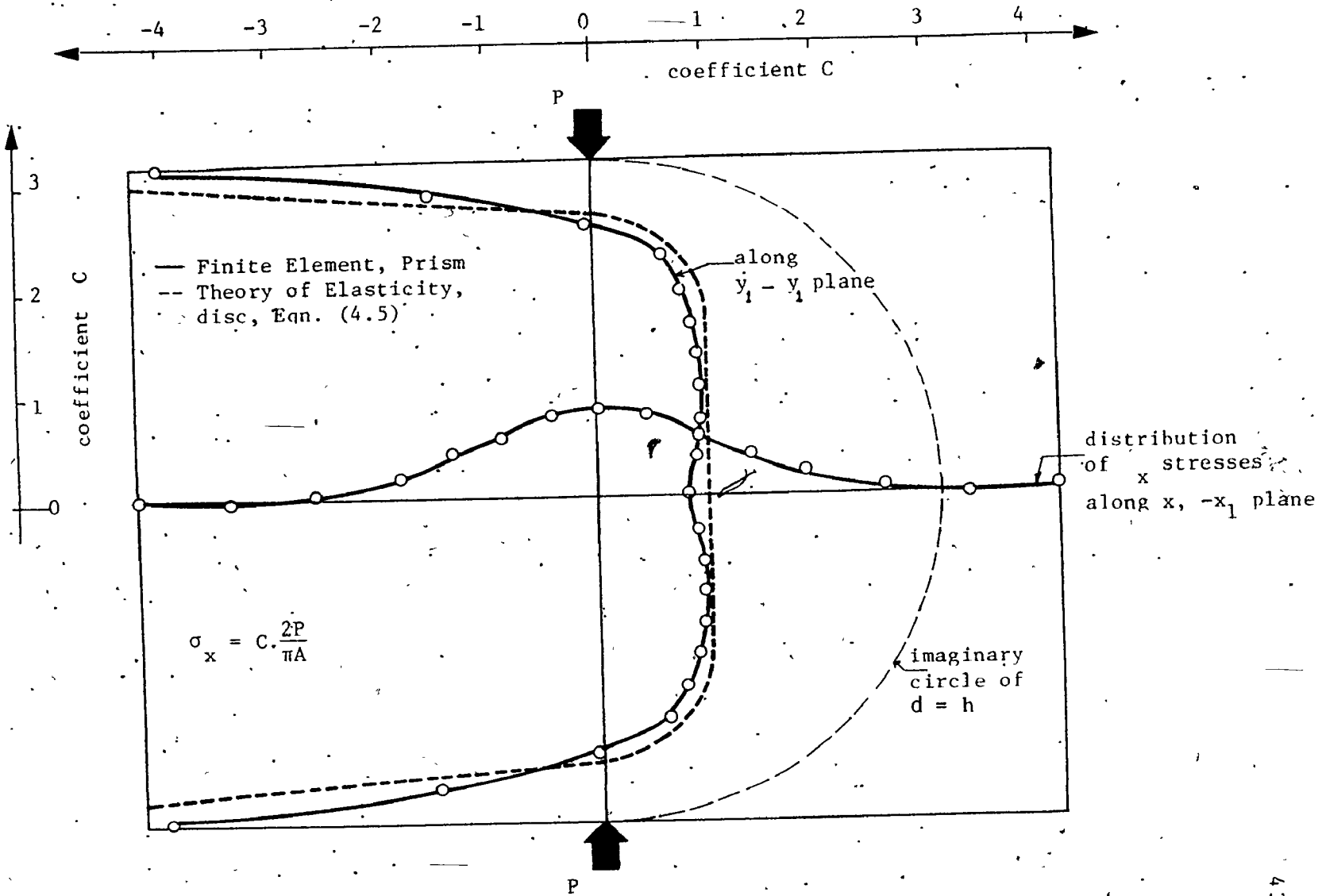

Fig. B.6 DISTRIBUTION OF A TRANSVERSE TENSILE STRESSES, σ_x, ALONG THE PRINCIPAL PLANES OF A GROUT PRISM UNDER SPLITTING LOAD

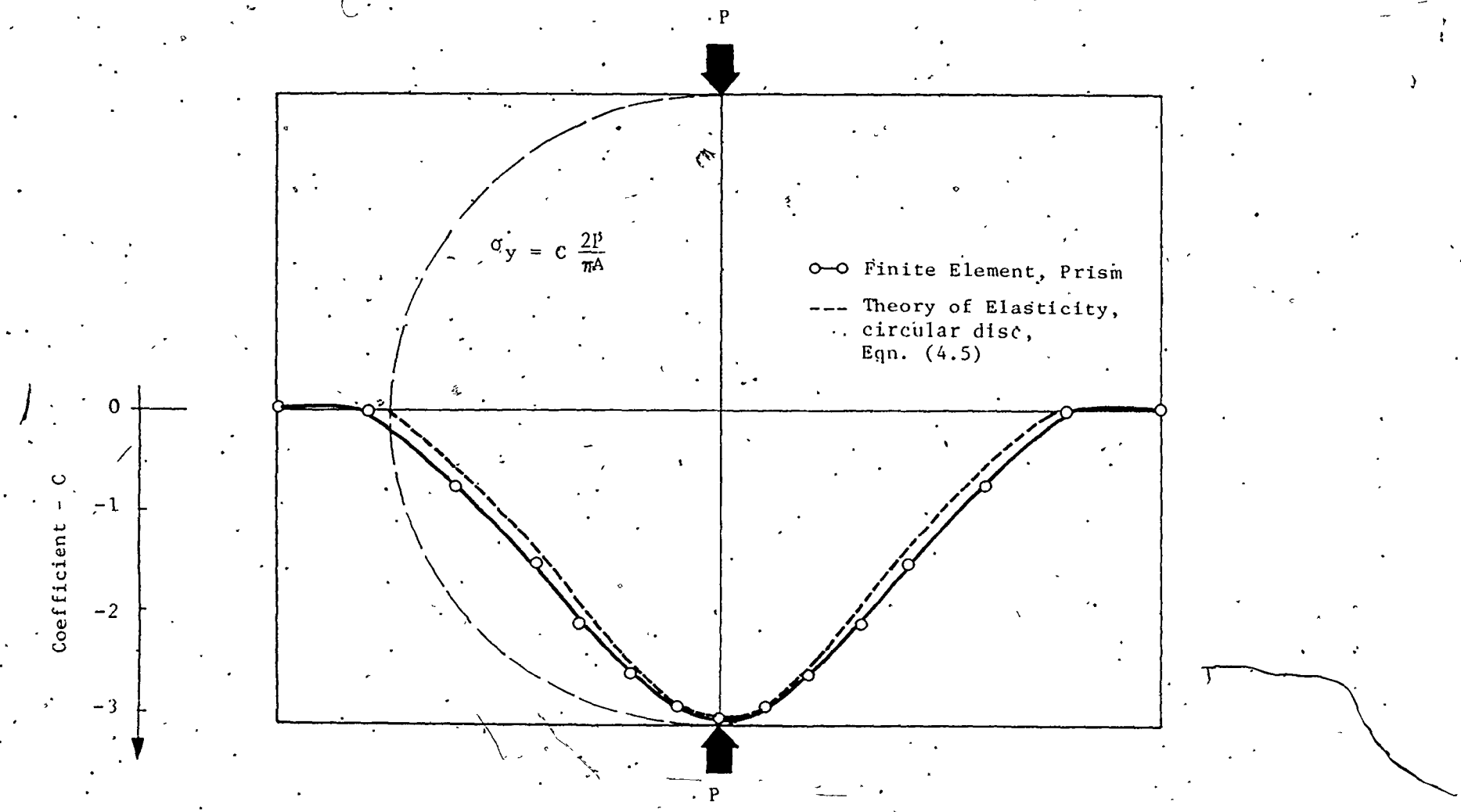

Fig. B.7 DISTRIBUTION OF VERTICAL COMPRESSIVE STRESSES, σ_y, ALONG X_1-X_1 PLANE OF A GROUT PRISM UNDER SPLITTING LOAD

ratio of the prism (b/h) does not seem to have any effect on the stress field provided that it is higher than unity. The end regions outside the imaginary circle of a diameter equal to the prism height exhibit very small vertical and lateral stresses indicating their insignificant influence on the prism capacity under splitting load.

From this comparison study it is suggested that for the determination of the indirect tensile strength of brittle materials, square specimens can be employed rather than circular ones. This shape has the advantage of a simpler laboratory technique. Based on a theoretical investigation of the stress distribution in a square plate under a pair of line loads, Goddier[16] concluded that the magnitude of the tensile stress at the center of the plate is nearly the same as in a circular disc under the same loading.

REFERENCES

1. American Society for Testing and Materials, 1974 Annual Standards, Part 16, April 1974.

2. K. Balachandran, "An investigation of the strength of concrete masonry shear wall structures", Ph.D. Thesis, The University of Florida, 1974.

3. E.M. Bartee, Engineering Experimental Design Fundamentals, Prentice-Hall, 1963.

4. J.R. Benjamin and H.A. Williams, "The behaviour of one-story brick shear walls", Proc. ASCE, Journal of Structural Division, vol. 84, no. ST4, 1958.

5. J.A. Blume and J. Proulx, "Shear in grouted brick masonry wall elements", Western States Clay Products Assoc., San Francisco, CA, 1968.

6. B. Brestler and K.S. Pister. "Strength of concrete under combined stresses", ACI Journal Proc., vol. 55, Sept. 1958, pp. 321-345.

7. Brick Institute of California, Handbook on Reinforced Grouted Brick Masonry Construction, 8th Ed., Los Angeles, CA, 1974.

8. J.G. Brochelt, "Analysis of snear walls subject to axial compression and in-plane shear", Proc. Second Int. Brick Masonry Conf. (Stoke-on-Trent, Apr. 1970) pp. 263-265.

9. J.G. Brochelt and R.H. Brown, "An indirect tensile test for masonry units", ASTM, Journal of Testing and Evaluation, vol. 6, March 1978, pp. 134-143.

10. W.B. Cranston and J.J. Roberts, "The structural behaviour of concrete masonry - reinforced and unreinforced", The Structural Engineeer, vol. 54, Nov. 1976, pp. 423-436.

11. H.J. Cowan, "The strength of plain. reinforced and prestressed concrete under the action of combined stresses, with particular reference to the combined bending and torsion of rectangular sections" Magazine of Concrete Research, No. 14, 1953, pp. 75-86.

12. CSA Standard S304 - 1977, Masonry Design and Construction for Buildings, Canadian Standards Association, Rexdale, Ontario, 1977.

13. R.G. Drysdale, A.A. Sallam and E. Karaluk, "Design of masonry walls and columns for combined axial load and bending moment", Proc. First Canadian Masonry Symp. E.L. Jessop and N.A. Ward, Eds. (Calgary, Canada, June 1976) pp. 394-408.

14. Dur-O-Wal Products, Catalogue for Ties and Reinforcement, published by Dur-O-Wal National, Inc., Canada, 1977.

15. A.J. Francis, C.B. Horman and L.E. Jerrems, "The effect of joint thickness and other factors on the compressive strength of brickwork", Proc. Second Int. Brick Masonry Conf. (Stoke-on-Trent, Apr. 1970) pp. 31-37.

16. J.N. Goodier, "Comparison of rectangular blocks and the bending beams by non-linear distribution of bending forces", Trans. of ASME, vol. 24, 1932, pp. 173-196.

17. C.T. Grimm, "Strength and related properties of brick masonry", Journal of the Struction Division, ASCE, vol. 101, no. ST1.

18. P. Haller, "Load capacity of brick masonry", Designing Engineering and Constructing wth Masonry Products, F.B. Johnson, Ed., Gulf Publishing Co., Houston, Texas, May 1967, pp. 138-145.

19. M. Hatzinikolas, "Shear behaviour of masonry walls subdivided by floor slabs", Proc. First Canadian Masonry Symp. E.L. Jessop and N.A. Ward, Eds. (Calgary, Canada, June 1976) pp. 304-323.

20. R.O. Hedstrom, "Load tests of patterned concrete masonry walls", ACI Journal Proc., vol. 57, April 1961, pp. 1265-1286.

21. G.A. Hegemier, R.O. Krishnamoorthy, R.O. Nunn and J.V. Moorthy, "Prism tests for the compressive strengtn of concrete masonry", Report No. AMES-NSF TR-77-1, Univ. of CA, San Diego, CA, Nov. 1977.

22. G.A. Hegemier, R.O. Krishnamoorthy and R.O. Nunn, "An experimental study of concrete masonry under seismic-type loading", Proc. National Workshop Earthquake Resistant Masonry Construction, National Bureau of Standards, Boulder, CO, Sept. 1976.

23. C.R. Hicks, Fundamental Concepts in the Design of Experiments, Holt, Rinehart and Winston, Inc., 1973.

24. H.K. Hilsdorf, "Investigation into the failure mechanism of brick masonry under fixed compression", Designing, Engineering and Construction with Masonry Products, F.B. Johanson, Ed. Gulf Publishing Co., Houston, Texas, May 1969, pp. 34-41.

25. O. Hoffman, "The brittle strength of orthotropic materials", Journal of Composite Materials, vol. 1, no. 2, Apr. 1967, pp. 200-206.

26. A. Huizer, "Effect of mortar properties on compression prism-, shear bond- , and bending bond control tests for clay brick masonry", Research Report CE 75-6, Department of Civil Engineering, University of Calgary, Canada, December 1975.

27. International Conference of Building Officials, "Uniform Building Code", 1973 Ed., Chapter 24, Whittier, CA.

28. F.B. Johanson and J.N. Thompon, "Development of diametric testing procedures to provide a measure of strength characteristics of masonry assemblages", Designing, Engineering, and Construction with Masonry Products, F.B. Johanson, Ed. Gulf Publishing Co., Houston, Texas, May 1969, pp. 51-57.

29. R. Jolley, "Shear strength: A predictive technique for masonry walls", Ph.D. Thesis, Brigham Young University, 1976.

30. R.M. Jones, Mechanics of Composite Materials, 1st Ed. McGraw-Hill, 1975.

31. C.L. Khoo, "A failure criterion for brickwork in axial compression", Ph.D. Thesis, Univ. of Edinburgh, Scotland, 1972.

32. H. Kupfer. H.K. Hilsdorf and H. Rush, "Behaviour of concrete under biaxial stresses", AIC Journal Proc., vol. 66, Aug. 1969, pp. 656-665.

33. R.L. Mayes and R.W. Clough, "A literature survey: compressive tensile, bond and shear strength of masonry", Report No. ELPC 75-15, College of Engineering, Univ. of California, Berkeley, CA, June 1975.

34. S.L. Meyer, Data Analysis for Scientists and Engineers, John Wiley and Sons, 1975.

35. M.J. Mikkola and W.C. Schnobrich, "Material behaviour characteristics for reinforced concrete shells stressed beyond the elastic range", Civil Engineering Studies, Structural Research Seeries No. 347, Univ. of Illinois, 1970.

36. E. Morsy, "An investigation of mortar properties influencing brickwork strength", Ph.D. Thesis,, University of Edinburgh, Scotland, 1966.

37. S. Moustafa, "Ultimate load test of a segmentally constructed prestressed concrete I beam", Journal of Prestressed Concrete Institute, vol. 19, no. 4, 1974, pp. 54-75.

38. A. Nadai, Theory of Flow and Fracture of Solids, vol. 1, McGraw-Hill, 1950.

39. A.M. Neville, "General relation for strengths of specimens", ACI Journal Proc., vol. 63, no. 52, Oct. 1966, pp. 1095-1108.

40. A.M. Neville, Properties of Concrete, 2nd Ed. . Pitman Pub., 1973.

41. B. Ostle, Statistic in Research, The Iowa University Press, 1963.

42. A.W. Page, "A model for the in-plane deformation and failure of brickwork", Engineering Bulletin CE8, Australia, March 1978.

43. K. Pieper and W. Trautsch, "Shear tests on walls", Proc. Second Int. Brick Masonry Conf. (Stoke-on-Trent, Apr. 1970) pp. 140-143.

44. M.J.N. Priestly and D.O. Bridgeman, "Seismic resistance of brick masonry walls", Bulletin of the New Zealand National Society for Earthquake Engineering, vol. 7, no. 4, Dec. 1974.

45. J.B. Read and S.W. Clements, "The strength of concrete block walls, Phase II; under uniaxial loading", Cement and Concrete Association, Technical Report 42-475, London, 1972.

46. M. Rostampour, "Aspects of the design of multistory buildings in light-weight concrete blockwork", Ph.D. Thesis, University of Edinburgh, Scotland, July 1975.

47. S. Sahlin, Structural Masonry, Prentice-Hall, 1971.

48. M.W. Self, "Structural properties of loadbearing concrete masonry", in Masonry: Past and Present, STP 589, American Society for Testing and Materials, Philadelphia, PA, 1975.

49. B.P. Sinha and A.W. Hendry, "Parking tests on storey height shear wall structures with openings. subject to precompression", Designing, Engineering and Construction with Masonry Products, F.B. Johanson, Ed. Gulf Publishing Co., Houston, TX, May 1969, pp. 192-199.

50. T. Sneck "Winter masonry construction", Proc. First Canadian Masonry Conference, E.L. Jessop and M.A. Waid, Ed. Calgary, Canada, June 1976, pp. 238-246.

51. B. Stafford-Smith and C. Carter, "Distribution of stresses in masonry walls subjected to vertical loading", Proc. Second Int. Brick Masonry Conf. (Stoke-on-Trent, April 1970), pp. 119-124.

52. B. Stafford-Smith, C. Carter and J.R. Choudhery, "The diagonal tensile strength of brickwork", The Structural Engineer, vol. 48, no. 4, June 1970, pp. 219-225.

53. B. Stafford-Smith, C. Carter, "Hypothesis of shear failure of brickwork", Journal of the Structural Division, Proc. of ASCE, ST4, vol. 97, April 1971, pp. 1055-1062.

54. Structural Clay Products Research Foundation. "Compressive, transverse and racking strength tests of four-inch brick walls", Research Report No. 9, Geneva, IL, 1965.

55. V. Turnsek and F. Cacovic, "Some experimental results on the strength of brick masonry walls", Proc. Second Int. Brick Masonry Conf. (Stoke-on-Trent, April 1970) pp. 149-156.

56. D. Williams, "Seismic behaviour of reinforced masonry shear walls", Ph.D. Thesis, University of Canterbury, Christchurch, New Zealand, 1971.

57. P.J.F. Wright, "Comments on an indirect tensile test on concrete cylinders", Magazine of Concrete Research, July 1955, pp. 87-95.

58. F. Yokel and G. Fattal, "Failure hypothesis for masonry shear walls", Journal of the Structural Division, Proc. of ASCE, ST3, vol. 102, March 1976, pp. 515-532.

59. P. Zia, "Torsional strength of prestressed concrete members", ACI Journal Proc., vol. 57, April 1961, pp. 1337-1359.